The role of calcium signalling in plant-aphid interactions

Thomas Robert Vincent

University of East Anglia

A thesis submitted for the degree of Doctor of Philosophy

September 2016

This page is intentionally left blank

Blank pages are used throughout to allow legends to appear opposite display items in the paper copy of this document

Abstract

Myzus persicae is one of the most successful insects on the planet. It is the world's most pesticide-resistant insect, feeds on hundreds of plant species and acts as a vector for over 100 viruses. Upon perception of *M. persicae* feeding, plants activate pattern-triggered immunity (PTI), a pivotal part of which is believed to be calcium signalling. The aim of this thesis is to uncover the role that calcium signalling might be playing in the interaction between *M. persicae* and one of its hosts: the model plant Arabidopsis.

Using a fluorescent calcium sensor (GCAMP3), *in vivo* imaging of calcium dynamics was performed on leaves infested with *M. persicae*. There is a rapid and highly localised calcium burst around the feeding site in the epidermal and mesophyll cells, making it as one of the first plant responses to aphid attack. This calcium burst is triggered after perception of the aphid by the defence co-receptor BRASSINOSTEROID INSENSITIVE-ASSOCIATED KINASE 1 (BAK1), establishing it as part of PTI. Calcium is released from the extracellular space into the cell by GLUTAMATE-LIKE RECEPTORS 3.3 and 3.6 (GLR3.3 and GLR3.6), in combination with the release of intracellular calcium from the vacuole by TWO-PORE CHANNEL 1 (TPC1). Loss of *BAK1*, *GLR3.3*/*GLR3.6* or *TPC1* significantly attenuates the aphid-induced calcium burst and has an effect on the induction of anti-aphid defence responses.

Downstream of the burst, CBL-INTERACTING PROTEIN KINASES 3, 9, 23 and 26 are activated by calcium and together mediate plant resistance to aphid attack. Furthermore, the *M. persicae* effector Mp10 partially suppresses the feeding site calcium burst, suggesting that the aphid is manipulating this pathway as part of its successful colonisation of the plant. Together, the data presented in this thesis provide evidence for the significant involvement of calcium signalling in the plant response to aphid attack.

“No amount of experimentation can ever prove me right; a single experiment can prove me wrong.” - Albert Einstein

Translated by Alice Calaprice (ISBN 0-691-12074-9)

Table of Contents

Acknowledgements

First and foremost I must thank my incredible supervisory team for their support, suggestions and encouragement over the past four years. I am grateful to Dale Sanders and Tony Miller for allowing me to conduct a PhD with them and for giving me the freedom to pursue a project that I have enjoyed enormously. I am also grateful to Saskia Hogenhout for the expertise and opportunities she has shared with me over the course of this project and Sam Mugford for tolerating my "lurking" when I needed advice. Likewise, the guidance and experimental work of Simon Gilroy and colleagues has been instrumental to this PhD. I must also thank Nick Brewin, George Lomonossoff and Michael McArthur for the experience and training I received during my rotation year at the JIC.

In addition to my supervisory committee, I have to acknowledge the huge support I have received from every member of Dale, Tony and Saskia's groups, both professionally and personally, during this PhD. I am especially indebted to Paloma Menguer and Claire Drurey for their time and patience whilst training me in the lab, as well as Chrissy Wilson and Nicola Capstaff for their friendship and humour during my time here. I have also been lucky enough to supervise several excellent students, with the work of Marieta Avramova, James Canham, Magda Steele, Peter Higgins and Natasha Bilkey contributing significantly to this thesis.

Outside of the lab, life in Norwich has been immensely enjoyable. My sanity has been maintained by an incredible cohort of peers, including my fellow brunch, lunch and wine enthusiasts, especially Leonie, Jan, Daniel, Ben, Jon, Alex, Lizzie, Emily, Sibyl, and Dash, as well as many others I don't have space to list here.

Finally, I have to acknowledge my parents for their unwavering support over the last 25 years, and my sister for hers over the last 23. Nothing would have been possible without it.

List of figures

List of tables

List of videos

The data presented in this thesis is supported by videos from the calcium microscopy assay. These files are included with the electronic copy of this document.

Video 3.1: GCAMP3 can be used to detect aphid-induced calcium signals around the feeding site in whole Arabidopsis plants. GFP fluorescence (represented by a heat map) in a 35S::GCAMP3 plant during *Myzus persicae* treatment. Inset: Abaxial leaf surface showing location of aphid settling. Video recorded over a 20 min period.

Video 3.2: GCAMP3 can be used to detect aphid-induced calcium signals around the feeding site in whole Arabidopsis plants. GFP fluorescence (represented by a heat map) in a 35S::GCAMP3 plant during *Myzus persicae* treatment. Video recorded over a 10 min period.

Video 3.3: Cold water induces rapid biphasic calcium bursts in isolated Arabidopsis 35S::GCAMP3 leaves. GFP fluorescence represented by a heat map. Point of treatment indicated on video.

Video 3.4: GCAMP3 can be used to detect aphid-induced calcium signals in isolated leaves. GFP fluorescence represented by a heat map. Left: 35S::GCAMP leaf treated with *Myzus persicae*. Right: non-treated control 35S::GCAMP3 leaf.

Video 3.5: Wounding of Arabidopsis expressing 35S::YCNano-65. FRET ratio represented by a heat map. Point of wounding indicated on video. Recorded over a 7 min period.

Video 3.6: Cold water treatment of Arabidopsis expressing 35S::YCNano-65. FRET ratio represented by a heat map. Point of treatment indicated on video. Recorded over a 5 min period.

Video 3.7: The FRET reporter 35S::YCNano-65 is unable to detect aphid-induced calcium signals in isolated leaves. FRET ratio represented as a heat map. Recorded over a 20 min period from a representative sample (n=10).

Video 3.8: The FRET reporter 35S::YCNano-65 is unable to detect aphid-induced calcium signals in isolated leaves. FRET ratio represented as a heat map. Recorded over a 20 min period from a representative sample (n=10).

Video 3.9: GCAMP3 localised to the phloem using the *SUC2* promoter does not detect aphid-induced calcium signals in isolated leaves. GFP fluorescence represented by a heat map. Top left: 35S::GCAMP leaf treated with *Myzus persicae*. Top right: non-treated control 35S::GCAMP3 leaf. Bottom left: SUC2::GCAMP leaf treated with *Myzus persicae*. Bottom right: non-treated SUC2::GCAMP3 leaf.

Video 3.10: GCAMP3 can be used to visualise systemic wound-induced calcium signals in the phloem. GFP fluorescence represented by a heat map. Left: 35S::GCAMP3 plant wounded with forceps. Right: SUC2::GCAMP3 plant wounded with forceps.

Video 3.11: GFP fluorescence in 35::GCAMP3 and 35S::GCAMP3 x *bak1-5* isolated leaves treated with *Myzus persicae*. GFP fluorescence represented by a heat map. Top left: 35S::GCAMP leaf treated with *Myzus persicae*. Top right: non-treated control 35S::GCAMP3 leaf. Bottom left: 35S::GCAMP3 x *bak1-5* leaf treated with *Myzus persicae*. Bottom right: non-treated 35S::GCAMP3 *bak1-5* leaf.

Video 3.12: GFP fluorescence in 35::GCAMP3 leaves treated with dsGFP and dsMP10 aphids. GFP fluorescence represented by a heat map. Top left: 35S::GCAMP leaf treated with dsGFP *Myzus persicae*. Top right: non-treated control 35S::GCAMP3 leaf. Bottom left: 35S::GCAMP3 leaf treated with dsMp10 *Myzus persicae*. Bottom right: non-treated 35S::GCAMP3 leaf.

Video 4.1: GFP fluorescence in 35::GCAMP3 and 35S::GCAMP3 x *tpc1-2* isolated leaves treated with *Myzus persicae*. GFP fluorescence represented by a heat map. Top left: 35S::GCAMP leaf treated with *Myzus persicae*. Top right: non-treated control 35S::GCAMP3 leaf. Bottom left: 35S::GCAMP3 x *tpc1-2* leaf treated with *Myzus persicae*. Bottom right: non-treated 35S::GCAMP3 x *tpc1-2* leaf.

Video 4.2: GFP fluorescence in 35::GCAMP3 and 35S::GCAMP3 x 35S::TPC1 5.6 isolated leaves treated with *Myzus persicae*. GFP fluorescence represented by a

heat map. Top left: 35S::GCAMP leaf treated with *Myzus persicae*. Top right: non-treated control 35S::GCAMP3 leaf. Bottom left: 35S::GCAMP3 x 35S::TPC1 5.6 leaf treated with *Myzus persicae*. Bottom right: non-treated 35S::GCAMP3 x 35S::TPC1 5.6 leaf.

Video 4.3: GFP fluorescence in 35::GCAMP3 and 35S::GCAMP3 x *fou2* isolated leaves treated with *Myzus persicae*. GFP fluorescence represented by a heat map. Top left: 35S::GCAMP leaf treated with *Myzus persicae*. Top right: non-treated control 35S::GCAMP3 leaf. Bottom left: 35S::GCAMP3 x *fou2* leaf treated with *Myzus persicae*. Bottom right: non-treated 35S::GCAMP3 x *fou2* leaf.

Video 4.4: GFP fluorescence in 35::GCAMP3 and 35S::GCAMP3 x *glr3.3/3.6* isolated leaves treated with *Myzus persicae*. GFP fluorescence represented by a heat map. Top left: 35S::GCAMP leaf treated with *Myzus persicae*. Top right: non-treated control 35S::GCAMP3 leaf. Bottom left: 35S::GCAMP3 x *glr3.3/3.6* leaf treated with *Myzus persicae*. Bottom right: non-treated 35S::GCAMP3 x *glr3.3/3.6* leaf.

List of common abbreviations

Ca^{2+}	calcium ion
$[Ca^{2+}]$	free calcium ion concentration
$[Ca^{2+}]_{cyt}$	cytosolic free calcium ion concentration
4MI3M	4-methoxyindol-3-yl-methylglucosinolate
ABA	abscisic acid
AEQ	aequorin
CaM	calmodulin
CBL	calcineurin B-like protein
CC	companion cell
CDPK/CPK	calcium-dependent protein kinase
CFP	cyan fluorescent protein
CICR	calcium-induced calcium release
CIPK	CBL-interacting protein kinases
CNGC	cyclic nucleotide gated channel
DAMP	damage-associated molecular pattern
EDTA	ethylenediaminetetraacetate
EPG	electrical penetration graph
ER	endoplasmic reticulum
ET	ethylene
ETI	effector-triggered immunity
FAC	fatty acid conjugate
FRET	fluorescence resonance energy transfer
GFP	green fluorescent protein
GLM	generalised linear model
GLR	glutamate receptor-like channel
H_2O_2	hydrogen peroxide
HAMP	herbivore-associated molecular pattern
HR	hypersensitive response
IR	induced resistance
JA	jasmonic acid
K_d	dissociation constant
RLK	receptor-like kinase
ROI	region of interest

MAPK	mitogen-activated protein kinase
MeJA	methyl jasmonate
OS	oral secretions
PAMP	pathogen-associated molecular pattern
PM	plasma membrane
PPI domain	protein phosphatase interacting domain
P-protein	phloem protein
PRR	pattern-recognition receptor
PTI	PAMP-triggered immunity
R-gene	resistance-gene
RNAi	RNA interference
ROS	reactive oxygen species
SA	salicylic acid
SAA	systemic acquired acclimation
SAR	systemic acquired resistance
SE	sieve element
SEM	standard error of the mean
Single-FP	single fluorophore
V_m	membrane potential
VOC	volatile organic compound
YFP	yellow fluorescent protein

Chapter 1: Introduction

1.1 Calcium Signalling

1.1.1 Calcium signalling: an overview

There are few signalling components as ubiquitous as calcium ions (Ca^{2+}). In plants, Ca^{2+} signals are generated by the release of Ca^{2+} into the cytosol, altering the Ca^{2+} concentration ($[Ca^{2+}]$) and resulting in transient increases in cytosolic free Ca^{2+} ($[Ca^{2+}]_{cyt}$). This release is coordinated by Ca^{2+}-permeable membrane channels and the resulting change in $[Ca^{2+}]_{cyt}$ is decoded by a complex network of proteins. However, despite its ubiquity, we are still relatively naïve about the molecular components that underlie Ca^{2+} signalling.

High levels of Ca^{2+} are toxic to cells. As such, throughout evolution there has been selective pressure to keep $[Ca^{2+}]_{cyt}$ low by active removal into the extracellular space and, in the case of eukaryotes, intracellular organelles. This has provided the context for a simple and effective signalling mechanism whereby there is a steep electrochemical gradient between the cytosol and its surroundings, allowing efficient and rapid rises in $[Ca^{2+}]_{cyt}$ to be achieved [1]. These increases act in a wide range of plant processes, including responses to abiotic stress, pathogens and insects, as well as participating in the regulation of carbon dioxide sensing, symbiosis, tip growth and the circadian clock [1, 2].

1.1.2 The Ca^{2+} signature

$[Ca^{2+}]$ increases have defined amplitudes, durations and patterns that are determined by the stimulus and are termed the 'Ca^{2+} signature' [3]. $[Ca^{2+}]$ elevations are often asymmetric; the rise is faster than the decline. They also show a degree of attenuation upon repeated application of a stimulus [4, 5]. Specificity in Ca^{2+} signalling is achieved through a combination of the Ca^{2+} signature and the Ca^{2+}-binding proteins that decode the signature.

Part of the signature-encoded specificity is spatial. This includes localising $[Ca^{2+}]$ elevations to specific cells or tissues. For example *Arabidopsis thaliana* (thale cress - henceforth referred to as Arabidopsis) roots exposed to salt stress exhibit $[Ca^{2+}]_{cyt}$ elevations specifically in the endodermis and cortex [6, 7]. Spatial specificity can also be achieved within a single cell. Rises in $[Ca^{2+}]$ can be observed within various organelles, including the nucleus ($[Ca^{2+}]_{nuc}$), endoplasmic reticulum (ER -

$[Ca^{2+}]_{ER}$), mitochondria ($[Ca^{2+}]_{mit}$) and chloroplast ($[Ca^{2+}]_{chl}$) (Figure 1.2). For instance, rises in $[Ca^{2+}]_{nuc}$ can be observed in *Medicargo truncatula* (barrelclover) in response to symbionts, with different microorganisms generating different $[Ca^{2+}]_{nuc}$ oscillatory patterns [8]. Fluxes in $[Ca^{2+}]_{mit}$ have a resting baseline concentration twice that of $[Ca^{2+}]_{cyt}$ and transient increases can be stimulated by touch, mannitol, cold and hydrogen peroxide. Interestingly, these signals do not reach the same amplitude as those seen in the cytosol [9] (Figure 1.2). $[Ca^{2+}]_{chl}$ oscillations have been linked to circadian rhythms [10, 11]. Moreover, spatial specificity may also be introduced by heterogeneity in $[Ca^{2+}]_{cyt}$ within a cell [4, 12, 13]. Different stimuli can induce Ca^{2+} release into the cytosol from specific locations: for example the apoplast in response to blue light [14], the vacuole in response to abscisic acid (ABA) [15] or the ER upon stimulation with inositol trisphosphate ($InsP_3$) [16].

The duration of the Ca^{2+} signature can also introduce specificity. Differences in the length of $[Ca^{2+}]$ elevation have been found between different cell types in response to the same stress, as seen with osmotic stress in Arabidopsis [6]. Moreover, durations can vary within the same cell in response to the same stimulus. For example the pathogen elicitor harpin can induce long Ca^{2+} transients in the nucleus (~120 min) whilst generating shorter transients in the cytosol (~5 min) [17].

Frequency and amplitude are also critical to encoding specificity. $[Ca^{2+}]_{nuc}$ oscillates with a characteristic frequency during symbiosis [8], whilst artificially increasing the number of $[Ca^{2+}]_{cyt}$ transients in guard cells can significantly alter stomatal aperture [3]. Furthermore, the concentration of sodium chloride (NaCl) is correlated with amplitude of the $[Ca^{2+}]_{cyt}$ elevation in the root [18].

1.1.3 Energised Ca^{2+} transporters

Energised Ca^{2+} transporters are required to maintain the strong electrochemical gradient between $[Ca^{2+}]_{cyt}$ and its surroundings. In plants this is achieved through hydrolysis of adenosine triphosphate (ATP) by ATP-powered Ca^{2+} pumps or by a proton motive force generated through Ca^{2+}/proton (H^+) antiporters. These two forms of active transport are directed by P_2-type ATPases and the Cation eXchange (CAX) families respectively [1, 2]. These transporters are not merely the background machinery required to maintain resting $[Ca^{2+}]_{cyt}$; many also have specific physiological functions in the plant [19].

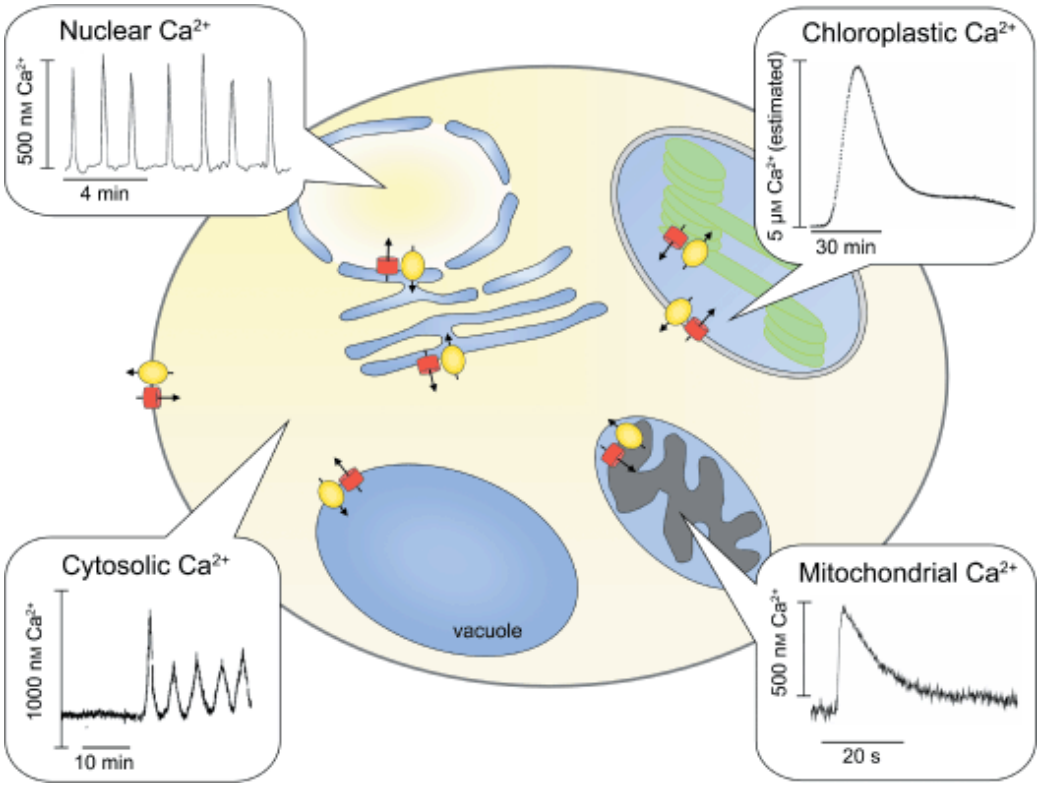

Figure 1.1: Ca^{2+} signatures in the different compartments of a plant cell.

Signatures are mediated by the influx of Ca^{2+} through channels (red cylinders) and efflux by active transporters (yellow circles). The amplitude and duration of these signatures varies between the cytosol, nucleus, mitochondria and chloroplast. In this example, cytosolic Ca^{2+} oscillations were stimulated by external Ca^{2+} application, nuclear oscillations by Nod factor application, chloroplast elevations by dark treatment and mitochondrial elevations by touch. Adapted from McAinsh et al. [19] and references within.

Ca^{2+}-specific ATPases

Ca^{2+}-specific P_2-type ATPases can be divided into two groups based on amino acid sequence; the P_{2A}/ER-TYPE Ca^{2+}-ATPases (ECAs) and the P_{2B}/AUTO-INHIBITED Ca^{2+}-ATPases (ACAs). There are important structural differences between ATPase classes. First, there are differences in their Ca^{2+}-binding membrane-localised residues [20, 21]. Second, the ACAs contain a calmodulin (CaM)-regulated auto-inhibitory domain [22]. In Arabidopsis, there are four known ECAs and ten known ACAs [23].

As their name suggests, ECAs are localised to the ER [24], whilst ACAs can be found in the plasma membrane (PM) [25] and the membranes of the ER [26] and the tonoplast [27]. Abolishing transcription of ECAs leads to Ca^{2+} and Mg^{2+} toxicity phenotypes due to disrupted sequestration of these ions [28-30]. Conversely, ACAs are implicated directly in signalling, during both abiotic [31-33] and biotic [21, 34] stress. Furthermore, the N-terminal auto-inhibitory domain allows for easy regulation of ACAs by other proteins during Ca^{2+} signalling [35].

CAX antiporters

CAX antiporters are localised to the tonoplast and act primarily as cytosolic Ca^{2+} export systems to the vacuole. These antiporters use the energy flux from the flow of H^+ ions down their thermodynamic potential into the cytosol to drive the active transport of Ca^{2+} against it's potential in the opposite direction [36, 37]. There are six members in Arabidopsis, but their functions are largely unknown [38].

CAXs have a low affinity for Ca^{2+} compared to the ACAs [35, 36], leading some to speculate that ACAs act to fine-tune Ca^{2+} around the vacuole, whilst CAXs play a role in reducing the high $[Ca^{2+}]_{cyt}$ at the end of a Ca^{2+} signalling event [38]. Like ACAs, CAXs have an N-terminal auto-inhibitory domain [39, 40] resulting in a requirement for additional components to activate them, such as CAX-INTERACTING PROTEIN 1 (CXIP1) [41].

As with the Ca^{2+}-ATPases, the role of CAX transporters in specific processes remains unclear. *CAX1* transcripts are increased during cold stress, and *cax1* mutants show increase freezing tolerance [42]. Furthermore, *CAX1, CAX2, CAX3 and CAX4* are all induced during salt stress [43, 44]. This implies a potential role in abiotic stress tolerance. However, *cax* mutants display growth and development phenotypes typical of plants disrupted in Ca^{2+} homeostasis [45], making it difficult to differentiate between this and a direct role in signalling [1].

1.1.4 Ca^{2+}-permeable channels

The two major regions of high [Ca^{2+}] in plants are the apoplast and the vacuole [2], and release of Ca^{2+} from these locations dominates most cytosolic Ca^{2+} signatures. Extracellular Ca^{2+} is released into the cell through PM-localised channels, whilst vacuolar Ca^{2+} is released via tonoplast-localised channels. Electrophysiological and molecular characterisation has been used to identify Ca^{2+}-permeable channels in both membranes and these channels can be voltage-dependent or independent.

Electrophysiological characterisation identified the Hyperpolarisation-Activated Ca^{2+} Channels (HACCs) which are activated at negative membrane potentials above -120mV [46], and one of their best characterised roles is during stomatal closure, where a hydrogen peroxide (H_2O_2)-dependent hyperpolarisation and the resultant HACC-mediated Ca^{2+} influx is required for the response [47, 48]. Conversely, Depolarisation-Activated Ca^{2+} Channels (DACCs) are activated at less negative membrane voltages, peaking in activity at around -80mV [49]. However, their identity and function in plants is controversial due to their inherent instability and potentially non-specific ion conductance [50, 51]. Nevertheless, various examples of DACCs have been reported [52]. In addition, there are also Voltage-Independent Ca^{2+} Channels (VICCs), that are only minimally affected by membrane voltage, and have been implicated in various responses from sodium uptake [53] to pathogen defence [54].

Molecular characterisation has mainly focused on three families of channels, all of which homologous to Ca^{2+} channels found in animals and are thought to be the most likely source of the genes that encode HACCs, DACCs and VICCs; the CYCLIC NUCLEOTIDE GATED CHANNELS (CNGCs) and the GLUTAMATE RECEPTOR-LIKE channels (GLRs) in the PM, and TWO-PORE CHANNEL 1 (TPC1) in the tonoplast [1, 51] (Figure 1.2).

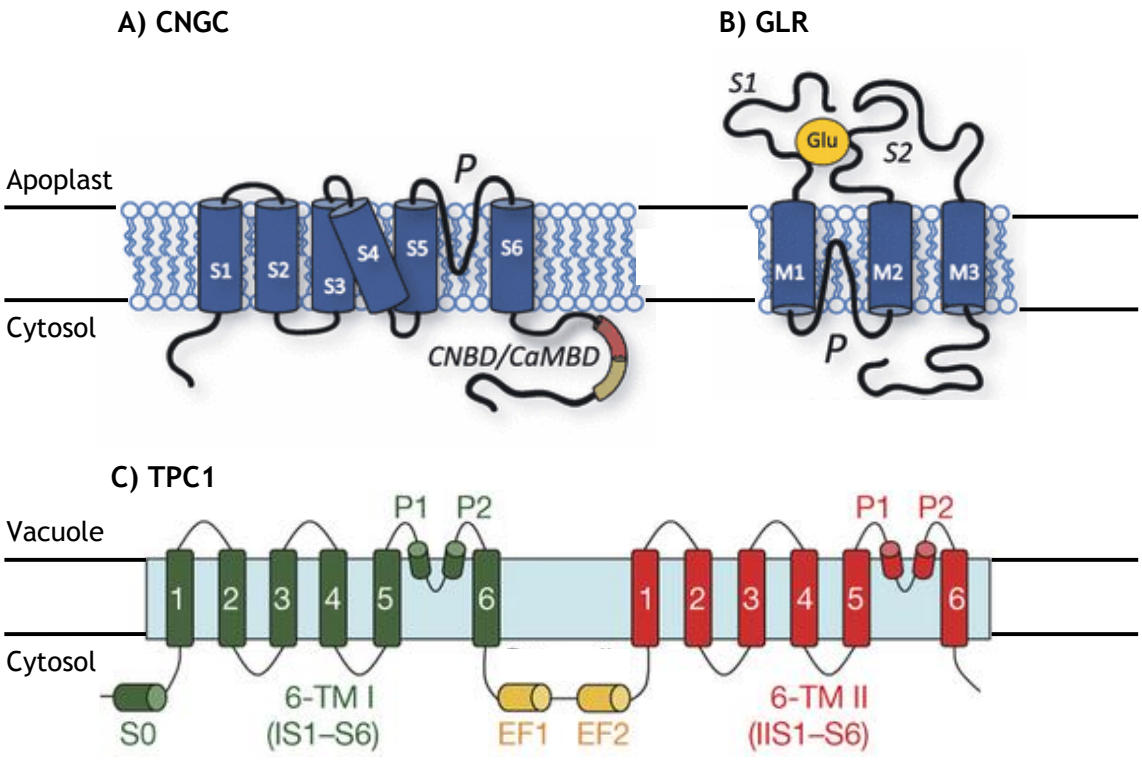

Figure 1.2: Structural comparison of Ca^{2+}-permeable channels in plants.

A) CNGCs contain 6 transmembrane domains (S1-S6), an extracellular pore helix (P) and C-terminal overlapping intracellular binding domains for cyclic nucleotides (CNBD, red) and calmodulin (CaMBD, yellow). **B)** GLRs contain three transmembrane domains (M1-3), an intracellular pore helix (P) and two extracellular glutamate (Glu) binding sites (S1 & S2). **C)** TPC1 is composed of twelve transmembrane domains (IS1-6, IIS1-6) in two groups (6-TM I & 6-TM II) each containing two pore domains (P1 & P2) and separated by cytosolic EF hands (EF1 & EF2). Adapted from Dietrich et al. [75], Chiu et al. [55] and Guo et al. [114].

CNGCs

First identified in *Hordeum vulgare* (barley) [56], genome sequencing has revealed 20 CNGCs in Arabidopsis [57]. CNGCs mostly localise to the PM [58-61] although recent evidence has suggested that CNGC7, CNGC8, CNGC19 and CNGC20 localise to the tonoplast, and CNGC18 to post-golgi vesicles [62, 63]. Furthermore, CNGC15 from *M. truncatula* was recently localised to the nucleus [64]. CNGCs have six transmembrane domains and assemble in tetramers to form the ion pore [1] (Figure 1.2a). This pore is permeable to Ca^{2+} [60, 65], but can also be permeable to potassium (K^+), sodium (Na^+) and other monovalent ions [66, 67].

In animals, binding of cyclic nucleotides to Cyclic Nucleotide Gated (CNG) channels is required for channel activation [68, 69]. However, such binding was not confirmed unequivocally in plants until recently [70]. The existence of cyclic nucleotide-based signalling is supported by the presence of cyclic nucleotides [71, 72] and nucleotide cyclases [73, 74] in plant cells. Furthermore, CNGCs are capable of binding calmodulin (CaM) [56] (Figure 1.2a) and this acts as part of a negative feedback system, in which Ca^{2+}-dependent CaM binding to CNCGs inhibits cyclic nucleotide binding [75, 76].

CNGCs have been heavily implicated in pathogen defence and the hypersensitive response, outlined in more detail in Section 1.3.3. In addition, CNGCs are suggested to play roles in heavy metal uptake [77], cation uptake [59, 78], pollen tube development [61, 79, 80], salt stress [59, 81], light signal transduction [82, 83], temperature sensing [70] and jasmonic acid (JA) signalling [84].

GLRs

The other family of Ca^{2+}-permeable channels at the PM that have been characterised at the molecular level are the GLRs. These are homologues of non-selective ionotropic glutamate receptors (iGluRs) in animals which are involved in neuronal signalling [85]. There are 20 GLR homologues in Arabidopsis [86] and functional channels are composed of multimeric units, as discovered through the use of C-terminal antibodies [87]. Subunits can form homo- and hetero-multimers that can be composed of various GLR family members [88-90], and different GLRs are co-expressed in the same cell to achieve this [91]. GLRs share some domains with high homology to iGluRs; two extracellular domains (S1 and S2) and three transmembrane domains (M1-3) (Figure 1.2b). S1 and S2 are hypothesised to act in ligand binding,

whilst domains M1-3 are involved in ion conductance [92]. As with CNGCs, the GLRs are not specific for Ca^{2+}. The GLR pore region (P – Figure 1.2b) shows the least similarity to iGluRs [93, 94], making it difficult to infer GLR ion selectivity from iGluRs [92]. The study of GLR (and CNGC) selectivity has been limited by the difficulty in expressing them in heterologous systems [76]. This problem is starting to be addressed, with GLRs shown to be capable of conducting Ca^{2+}, barium ions (Ba^{2+}), Na^{+} and K^{+} [88, 91, 95, 96].

Very little is known about the physiological role of GLRs in plants. They have been suggested to act in glutamate sensing [93, 97-99], as well as during cold and mechanical signalling [100] and ABA signalling [101, 102]. A recent breakthrough by Farmer and colleagues demonstrated that *GLR3.2*, *GLR3.3* and *GLR3.6* are required for systemic electrical signalling in Arabidopsis upon wounding [103]. *GLR3.5* also acts in this pathway as negative regulator [104]. Unlike the CNGCs, that have an intracellular ligand binding site (Figure 1.2a), the putative ligand binding site in GLRs is believed to be extracellular (Figure 1.2b) [105]. This potentially allows GLRs to act in the transduction of signals from the extracellular space, which is essential during systemic signalling. As a result, the function of GLRs in plants is now starting to be unravelled.

TPC1

The vacuole is the main intracellular store of Ca^{2+} in mature plant cells. Some Ca^{2+} is bound to chelating agents, whilst the remaining free Ca^{2+} is available for Ca^{2+} signalling [106]. As with the PM, little is known about the molecular identity of vacuolar Ca^{2+} channels. Although many have been characterised electrophysiologically [2], the only one with an established molecular identity is TPC1 [15], a DACC originally designated the slow-voltage (SV) channel [107].

Ubiquitous across plants and animals, in plants TPC1 is localised to the tonoplast membrane [15]. TPC1 conducts Ca^{2+} [15, 108-111], as well as K^{+} and Na^{+} [112, 113]. It is a homodimer in which each monomer consists of two sets of 6 transmembrane domains, two EF hand domains and a total of 4 pore domains (Figure 1.2c) [114, 115]. Interestingly, these EF hand domains allow TPC1 to be activated by Ca^{2+} [112, 116], allowing for a positive feedback mechanism termed Ca^{2+}-induced Ca^{2+}release (CICR) [108]. Indeed, recent structural analysis of TPC1 revealed that the

conformational change required for full channel opening is dependent on Ca^{2+} binding to the EF-hand domains [114, 115].

Historically, CICR has been the subject of controversy, with some authors suggesting that the [Ca^{2+}] required for CICR is greater than that found *in vivo* [113, 117, 118]. Refinement of the CICR theory has led to reactive oxygen species (ROS) being added as an additional component, in which ROS act to potentiate the CICR systemically between cells via the apoplast [119-121]. As such, TPC1 might be acting to produce local hot spots of Ca^{2+} around the vacuole that then activate nearby TPC1 channels and the ROS producing enzyme RESPIRATORY BURST OXIDASE HOMOLOGUE D (RBOHD) to potentiate systemic signals (more details in Section 1.3.6) [121].

A physiological role for TPC1 has been hard to identify [122], although it was originally characterised as playing a role in stomatal closure and germination [15]. However, recent evidence clearly shows a vital role for TPC1 in systemic signalling during stress (see Section 1.3.6) [7, 123], with the significance of TPC1 in plants is becoming apparent.

Other channels

There is electrophysiological evidence pointing to the existence of several more Ca^{2+}-permeable channels in plants. In the PM, mechanosensitive channels exist that are thought to be permeable to Ca^{2+} or at least related to Ca^{2+} signalling [124]. Furthermore, it has been suggested that annexin membrane proteins might act in Ca^{2+} transport, with a *Zea mays* (maize) annexin preparation capable of increasing Ca^{2+} import into Arabidopsis protoplasts [125].

The vacuole is also thought to house additional channels [126]. These include a HACC named the fast vacuolar channel [112], a Ca^{2+}-insensitive channel [122] and ligand-gated channels that are activated by cyclic ADP Ribose (cADPR) or inositol phosphates [127, 128]. In addition, Ca^{2+} release can be triggered from the ER by $InsP_3$ [16], cADPR [129] and nicotinic acid adenine dinucleotide phosphate (NAADP) [130], suggesting the presence of ligand-gated channels on this membrane as well.

1.1.5 Decoding the Ca^{2+} signal

In order to translate the rise in [Ca^{2+}] into a molecular or biochemical response, decoding mechanisms that directly bind Ca^{2+} are required. Conceptually, these decoders can be classified into sensor relays and sensor responders [2] (Figure 1.3). Some of these decoders are found across eukaryotes, whilst others are plant- or protist-specific [131].

Sensor relays are proteins that bind Ca^{2+}, often causing a conformational change, but that lack other functional domains or enzymatic activity. Examples include CaM, CaM-Like proteins (CMLs) and Calcineurin B-Like proteins (CBLs). Sensor responders incorporate both Ca^{2+} binding and functional activity, and include the Ca^{2+} -Dependent Protein Kinases (CDPK/CPKs), the Ca^{2+} and CaM-dependent protein Kinases (CCaMKs) and the CBL-interacting protein kinases (CIPKs) (Figure 1.3) [2, 132].

CaMs & CMLs

CaMs in plants share 89% identity with those found in animals [133]. There are seven genes in Arabidopsis that encode CaMs, but these give rise to only four protein isoforms [134]. As in animals, plant CaMs bind Ca^{2+} through a 12-amino acid loop in the EF hand motif, with each CaM composed of two globular domains each with a pair of EF hands (Figure 1.3) [135, 136]. Ca^{2+} binding results in a conformational change that allows CaMs to bind a diverse range of downstream targets. These include enzymes and ion channels [137, 138], as well as a specific set of CaM-binding transcription factors (CAMTAs) that are thought to act as one of the main intermediaries in signal transduction during stress [139, 140].

CMLs are a group of 50 genes that have diverged from CaMs both genetically and functionally, but which share at least 16% amino acid identity with them [133]. CMLs have a variable number of EF hand motifs, although the majority (31/50) are predicted to have four in total (Figure 1.3) [133, 134]. Substitutions in the Ca^{2+} binding loop account for some of the divergence between CaMs and CMLs and this might have an effect on ion selectivity, affinity or the ability of CMLs to undergo conformational changes [134]. A meta-analysis by McCormack et al. [134] found a striking difference between CaM and CML expression profiles. Whilst the CMLs were

differentially regulated in responses to a many stimuli (including biotic, chemicals, hormones and light), the CaMs were remarkably unresponsive in comparison.

CDPKs

CDPKs, also known as CPKs, are a 34-member family in Arabidopsis capable of both binding Ca^{2+} and phosphorylating downstream proteins. CDPKs contain a serine/threonine kinase domain, a CaM-like domain harbouring four EF hands and an auto-inhibitory domain (Figure 1.3) [141]. The auto-inhibitory domain suppresses CDPK activity and upon Ca^{2+} binding a conformational change occurs in the protein that removes this inhibition [142]. Activation is further enhanced by auto-phosphorylation [141].

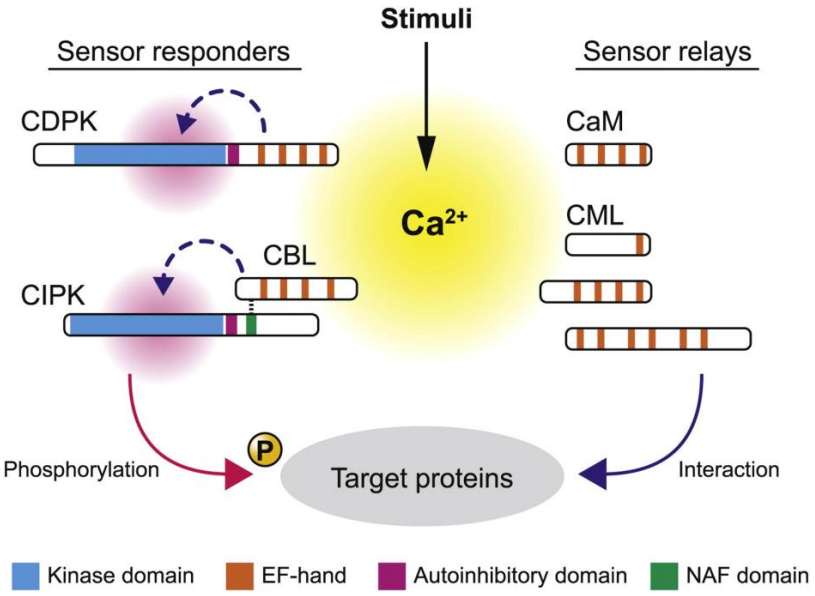

Figure 1.3: Ca^{2+} decoding mechanisms in plants.
Sensor responders (left) can bind Ca^{2+} and possess inherent kinase activity, whilst sensor relays (right) can bind Ca^{2+} but have no functional domains. Sensor responders convey signals through phosphorylation of downstream targets, whilst sensor relays mediate signalling by directly interacting with targets. Taken from Hashimoto & Kudla [132].

In Arabidopsis, CDPKs exhibit a diverse range of subcellular locations, from those that are anchored in the PM (e.g. CPK 7, CPK8), ER (e.g CPK2) or the peroxisome (e.g. CPK1), to those that are found soluble in the cytosol and nucleus (e.g. CPK3, CPK4) [143, 144]. A wide range of CDPK targets have been found in these locations too. Membrane-bound targets include ion channels [145], Ca^{2+}-dependant ATPases [146], and ROS-producing enzymes [147]. This implies that CDPKs can act as part of feedback loops within signalling cascades. In the cytosol and nucleus, CDPKs have been shown to target transcription factors vital in ABA and gibberellin signalling [148-150].

Furthermore, the CDPK pathway has been linked to another major class of plant kinases, the Mitogen-Activated Protein Kinases (MAPKs). MAPK cascades are an essential component of stress signalling, including during plant defence (Section 1.3.3) [151]. There appears to be crosstalk between the CDPK and MAPK networks, with CDPK signalling inhibiting MAPK activity [152]. Thus, CDPKs mark the entry point of Ca^{2+} into vast protein phosphorylation networks that we are only just beginning to unravel.

CCAMKs

Similar to CDPKs, CCaMKs have an auto-inhibitory domain, a kinase domain responsible for protein function and EF hand domains responsible for Ca^{2+} binding [141]. CCaMK activity is also regulated by auto-phosphorylation sites in the protein [153]. CCaMKs are plant-specific, but absent from green algae and the Brassicaceae. As such, the model plant Arabidopsis does not have CCaMK and this might explain why CCaMKs are less-well characterised than other sensor responders. Despite this, CCaMKs have been extensively implicated in legume symbiosis, where they act as convergence point for signalling between plants and both mycorrhizal fungi and nitrogen-fixing rhizobia [8, 154].

CBLs and CIPKs

CBLs and CIPKs function in pairs to transduce Ca^{2+} signals [155]. The CBL acts as sensor relay, binding Ca^{2+} [156], whilst the CIPK acts as a sensor responder, phosphorylating downstream targets [157, 158] (Figure 1.3). CBLs directly target CIPKs through a conserved NAF domain in the CIPK C-terminal region [159]. This releases the CIPK from auto-inhibition caused by an interaction between the NAF and

kinase domains [160], as well as releasing CIPKs from external inhibition by protein phosphatases that also target the C-terminus of CIPKs [161].

There are 26 CIPKs and 10 CBLs in Arabidopsis [162]. For both CBLs and CIPKs, redundancy between closely related proteins is found *in planta* [163-166]. In addition, CBLs and CIPKs show overlapping interactions with each other *in vitro*, allowing for a possible "mix and match" of different components that might underlie the specificity in Ca^{2+} decoding [136, 167]. CBL/CIPK combinations have been implicated in a diverse range of responses to abiotic stress through mediation of ion transport (Figure 1.4). This network consists of many interconnected nodes, some of which act as highly connected hubs. Loss of hubs will generate measurable effects, whilst the loss of individual nodes might not [1]. This is supported by experimental data from the clade 1 CIPKs that act as a hub required for magnesium ion (Mg^{2+}) sequestration (Figure 1.4) [165, 166].

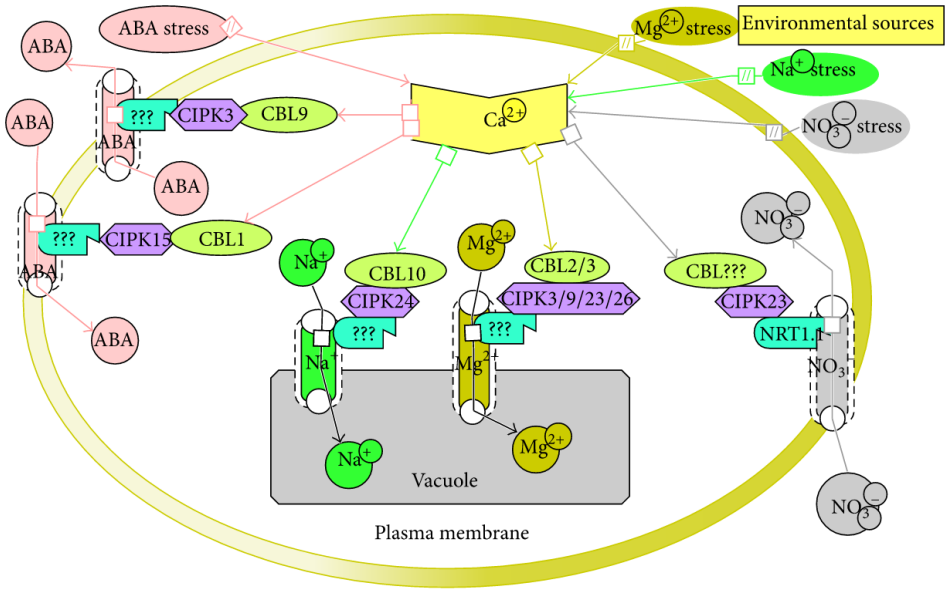

Figure 1.4: CIPKs mediate ABA and ion uptake, export and sequestration.
CIPKs and CBLs regulate a range of ion channels and transporters in the PM and the tonoplast that govern ABA (salmon), Na^{2+} (green), Mg^{2+} (yellow) and NO_3 (grey) homeostasis. Regulation is mediated by phosphorylation of the target channels and transporters by the CIPK. ??? indicates components that have not yet been identified. NRT1.1 = NITRATE TRANSPORTER 1.1. Taken from Manik et al. [168].

1.1.6 Ca^{2+} signalling during abiotic stress

It is essential during times of stress that the plant is able to perceive the threat and react quickly, and Ca^{2+} signalling plays a role in both biotic (Section 1.3.3) and abiotic stress responses. One of the best studied models for Ca^{2+} signalling is the stomatal guard cell [13]. Guard cells exhibit stimulus-specific Ca^{2+} oscillations in response to many stimuli, including drought, cold and carbon dioxide [4, 5, 169]. Stomata are a useful model as their aperture is sensitive to a wide range of abiotic stimuli and can be readily studied in a wide range of plant species and mutant lines.

The plant hormone ABA plays a central role in the plant response to abiotic stresses, including during osmotic stress [170], thermotolerance [171] and mechanical wounding [172, 173]. Moreover, ABA is intricately linked to Ca^{2+}. ABA application can stimulate $[Ca^{2+}]_{cyt}$ oscillations in guard cells [3, 174], and many of the same physiological responses to stress that ABA regulates are also modulated by Ca^{2+}. Furthermore, many of the genes in the Ca^{2+} "toolkit" play a central role in ABA-dependent responses to abiotic stress, including Ca^{2+} transporters [32] and Ca^{2+} decoders [175, 176].

In the root, cold, salt, touch and H_2O_2 can all induce $[Ca^{2+}]_{cyt}$ increases [7]. Sodium chloride (NaCl) application results in large Ca^{2+} transients in roots [18] that can travel systemically to the shoots [7]. *ACA10* and *CAX1* are differentially regulated upon cold and play a role in freezing tolerance [31, 42]. Interestingly, cold-stimulated root Ca^{2+} oscillations are dependent on the rate of cooling rather than the absolute temperature. Indeed, when the rate of cooling is sufficiently slow, no change in $[Ca^{2+}]_{cyt}$ can be measured [177]. Touch also elicits $[Ca^{2+}]_{cyt}$ increases in plants [178], as does wounding [123].

Several Ca^{2+}-permeable channels are implicated in abiotic stress responses. CNCCs are involved in the response to various abiotic stimuli, including lead and boron stress [77, 179], heat shock [70] and salt tolerance [59, 78, 81]. *GLR3.4* plays a role in touch signalling [100], whilst *GLR3.3*, *GLR3.4* and *GLR3.6* have a clear role during wounding [103, 104]. TPC1 has roles in ABA-mediated germination [15], salt stress [7] and wounding [123].

There is considerable evidence linking Ca^{2+} decoding proteins to abiotic stress. CaMs and CMLs are responsive to heat, cold, salt, ABA, drought and heavy metals [140] whilst CDPKs have been linked to cold, salt, ABA and drought [180]. Whilst CDPKs appear to positively regulate ABA-dependent signalling during stress, CIPKs

and CBLs have been implicated in the negative regulation of such responses [181]. For example CBL9, CIPK3 and CIPK23 null mutants show enhanced ABA accumulation and ABA hypersensitivity [175, 176, 182, 183]. Furthermore, CIPK and CBLs have roles in the sequestration of Mg^{2+} [165, 166], salt tolerance [157, 184, 185], K^+ homeostasis [163, 183, 186-188], nitrate deficiency [189] as well as during wounding, drought and the cold [175].

1.1.7 Genetically-encoded Ca^{2+} sensors

Properties of Ca^{2+} sensors

The only way to investigate Ca^{2+} signals directly is to measure them *in vivo*. Traditionally, Ca^{2+}-selective microelectrodes have been used to achieve this [190, 191]. More recently, bioluminescent and fluorescent sensors have become increasingly popular. These sensors bind Ca^{2+} and produce light, and have allowed un-paralleled opportunities to study Ca^{2+} dynamics in both cells and whole tissues (Figure 1.5).

First developed in the animal field [192], many Ca^{2+} sensors are now being used in plant biology. Such sensors can either be injected into plant tissue as dyes, or genetically encoded. Genetically-encoded sensors have the major advantage of being easy to express in live tissue and localise to subcellular compartments, whilst dyes offer a good option for plants that cannot be transformed [193].

The ideal Ca^{2+} sensor will exhibit four key qualities: high fluorescent yield (brightness), sensitivity, selectivity and responsiveness [193]. The fluorescent yield of the fluorophores used in a Ca^{2+} sensor greatly affects the $[Ca^{2+}]$ changes they can report and is dependent on two factors. The first is the extinction coefficient, a measure of how well the fluorophore absorbs light. The second is the quantum yield, the amount of the absorbed energy that emitted as light [194].

Sensitivity can be measured in terms of two properties, the dynamic range and affinity of the sensor [195]. Dynamic range is a ratio that expresses how many times brighter the Ca^{2+}-bound sensor is relative to the Ca^{2+}-free sensor. The affinity of the sensor describes the concentration range over which the sensor produces a measurable output and depends on the dissociation constant (K_d) of the sensor. The K_d represents the strength of binding between the sensor and Ca^{2+}. Consequently, the

dynamic range and the affinity determine resolution of the [Ca^{2+}] measurements that can be achieved.

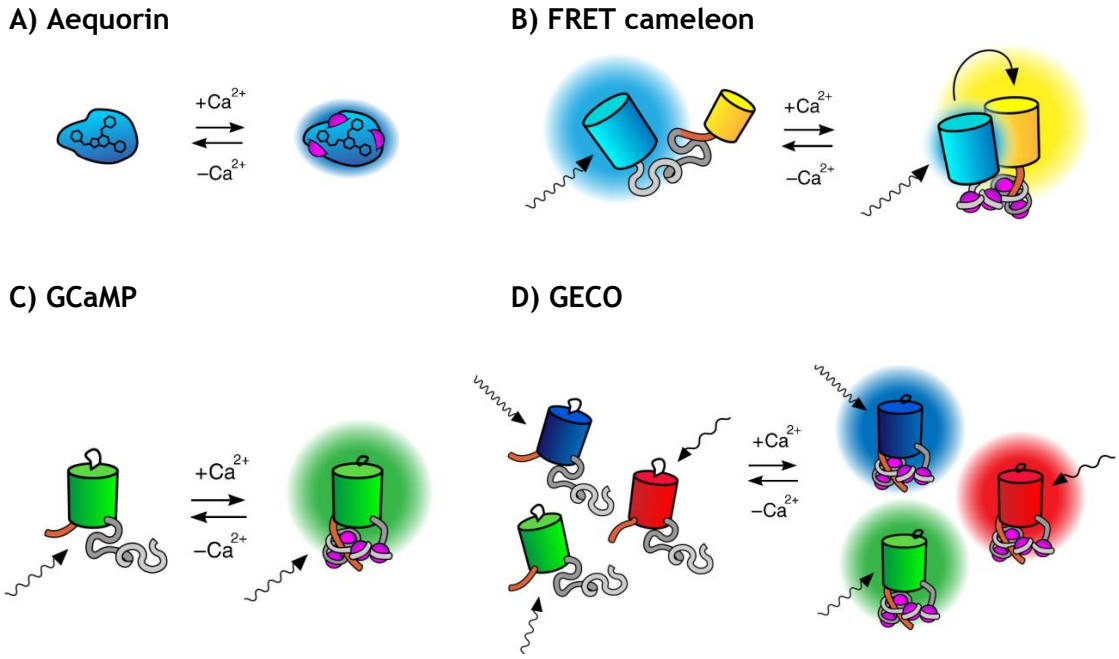

Figure 1.5: Genetically-encoded Ca^{2+} sensors.
Ca^{2+} is represented as purple circles and sensors are coloured according to their most common emission wavelength. **A)** Aequorin is a bioluminescent sensor that produces light in the presence of Ca^{2+} and coelenterazine. **B)** FRET cameleons are fluorescent sensors, typically composed of CFP and YFP. FRET sensors require CFP excitation and upon binding of Ca^{2+} the two fluorophores are brought into close contact and FRET occurs, exciting YFP. **C)** GCAMPs are fluorescent sensors composed of a circularly-permutated GFP molecule. Upon binding of Ca^{2+} GFP becomes protonated, resulting in an increase in fluorescence. **D)** GECOs are genetically-encoded fluorophore sensors based on GCAMP that have an expanded colour range. Adapted from Koldenkova & Nagai [195].

Selectivity is a measure of the reliability of the sensor at accurately reporting changes in [Ca^{2+}]. Selectivity can be assessed by comparing the fluorescent response of the sensor to non-target ions. In order to bind Ca^{2+}, CaM is often used as part of the sensor. However, Mg^{2+} can compete with Ca^{2+} for this site [196]. In addition, selectivity is liable to alterations caused by the pH, ionic strength and ionic composition of the system [195].

The responsiveness of a sensor describes the speed at which it reports changes in [Ca^{2+}]. This will be based on the sensor's kinetic properties and is based on the [Ca^{2+}] in the environment of the sensor, the K_d and the Hill coefficient of the sensor, where the Hill coefficient indicates the degree of cooperativity of binding of each subsequent Ca^{2+} ion. In addition, the association kinetics, the time it takes Ca^{2+} to bind the sensor at different concentrations, are also important [195]. Thus, responsiveness is a description of the temporal resolution one can achieve with a Ca^{2+} sensor.

The relationship between the Hill coefficient and K_d of the sensor, and the [Ca^{2+}] in the environment, is described by the Hill Equation (Equation 1.1). The Hill equation (Ø) describes the fraction of the sensor that is bound to Ca^{2+} at a given [Ca^{2+}], where n = the Hill coefficient. It therefore allows one to assess the suitability of a given sensor at reporting [Ca^{2+}] under different physiological conditions, for example by helping to predict how the brightness of a sensor will respond when the [Ca^{2+}] changes, and identifying when saturation of the sensor will occur.

$$\Theta = [Ca^{2+}]^n / ([Ca^{2+}]^n + K_d) \quad (1.1)$$

Various genetically-encoded Ca^{2+} sensors are now being used in plants and each has different biochemical and biophysical properties based on the attributes above that determines their utility in different systems.

Aequorin

The aequorin (AEQ) protein, isolated from *Aequorea victoria* (crystal jelly) was the first genetically-encoded Ca^{2+} sensor to be used in plants [192]. It is an EF hand-containing photoprotein that in the presence of Ca^{2+} acts as an oxygenase to excite the chemical substrate coelenterazine. As the excited coelenterazine returns to its ground state, it emits blue light (λ = 469 nm) (Figure 1.5a) [197]. This has been exploited by expressing this sensor in model organisms, including Arabidopsis, to allow visualisation Ca^{2+} dynamics [178].

The major advantage of AEQ over traditional dyes is the comparative ease of use and the ability to target AEQ to specific tissue or cellular locations. Furthermore, since AEQ is bioluminescent, it does not require external stimulation by light (as is required for fluorescent sensors). This can be a major advantage as it avoids

chromophore bleaching and autofluorescence [198]. However, a major disadvantage is the requirement of coelenterazine treatment for the sensor to function, as well as the relatively poor signal generated by individual AEQ-expressing cells [193]. Additionally, there are some limitations to the quantification of [Ca^{2+}] associated with the use of non-ratiometric signals. Despite this, AEQ has been successfully deployed to measure plant [Ca^{2+}] changes in a range of processes, including temperature regulation [199], pathogen defence [200-202] salt stress [6, 203] and wounding [123] .

FRET cameleons

The first ratiometric fluorescent Ca^{2+} sensor to be developed was the cameleon, which is based on the principle of fluorescence resonance energy transfer (FRET) between two fluorophores. FRET occurs when fluorophores come into close contact, with the donor fluorophore (typically cyan fluorescent protein – CFP) exciting the acceptor fluorophore (typically yellow fluorescent protein – YFP). In addition to the fluorophores, FRET sensors contain a CaM domain, a glycylglycine linker and a CaM-binding M13 protein. Ca^{2+} binding to CaM leads to an altered interaction between CaM and M13 that results in a conformational change of the whole sensor. This conformational change brings CFP and YFP in close contact and allows FRET to occur (Figure 1.5b). One can then use the ratio between CFP and YFP fluorescence to determine the change in [Ca^{2+}] in a cell or cellular compartment [204]. As the FRET ratio is directly related to Ca^{2+} binding, this system allows accurate quantification of [Ca^{2+}]. FRET sensors offer superiority over AEQ and non-ratiometric fluorescent dyes as they are not affected by the expression level of the protein [195] and they have a much greater dynamic range, allowing analysis of (sub-)cellular Ca^{2+} signalling [195].

Having been used in Arabidopsis for 17 years [174], FRET sensors are constantly undergoing improvements to their dynamic range, affinity, and stability *in vivo* [195]. One major breakthrough has been the use of a circularly-permutated form of YFP to develop yellow cameleon 3.6 (YC3.6) [205]. YC3.6 and derivatives (e.g YCNano-65 [206]) have been used to advance studying of cellular Ca^{2+} signalling, from the identification of new components to the discovery of long-distance signalling between the root and shoot [7, 121, 207].

Single-fluorophore sensors

Genetically-encoded single fluorophore (single-FP) sensors were developed relatively recently, and consist of circularly-permutated GFP linked to a CaM and M13 [208, 209]. The permutated GFP is more accessible to protons outside of the protein and protonation is known to modulate GFP fluorescent emission [210]. Upon Ca^{2+} binding to CaM, CaM and M13 interact and this results in a water-mediated reaction between CaM and GFP. This reaction alters the protonation state of GFP by blocking solvent access and thus increases GFP florescence intensity [211].

Single-FP sensors have several advantages over cameleons. Firstly, they are easier to use as data is collected from only one fluorophore. The recording of a single set of measurements also allows an increase in the temporal resolution of the experiment [212]. Another major advantage of single-FP sensors is that they have a much greater dynamic range, in some cases 5-fold greater than FRET cameleons [195]. Moreover, single-FP sensors have in a range of emission spectra and therefore can be combined in cells to allow simultaneous imaging of several organelles [205, 213]. Taken together, these advantages make single-FP sensors well suited to studying a dynamic system like Ca^{2+} signalling.

A major disadvantage of single-FP sensors is that they cannot measure the precise [Ca^{2+}] as reliably as FRET sensors. This is because it is difficult to distinguish changes in fluorescence that are due to the experimental variables (e.g. changes in pH, motion or expression level), from changes mediated by Ca^{2+}. During FRET, the transfer of energy from CFP to YFP only occurs upon Ca^{2+} binding; other conditions that alter the fluorescent properties of the individual sensors are unlikely to mimic the opposing changes in intensity of CFP and YFP [195, 212].

One of the most established single-FP sensor varieties are the GCaMPs, based on GFP and first developed by Nakai et al. [209] (Figure 1.5c). GCAMPs have undergone major revisions over the last few years, including GCaMP 1.6 [214] GCAMP2 [215], GCAMP3 [216] and GCAMP5 [217]. Each iteration resulted in more stable sensors with greater dynamic ranges, higher affinities for Ca^{2+} and better signal-to-noise ratios. The GCaMPs have been used in a variety of animal systems, from *Danio rerio* (zebrafish) motor neurones [218] to *Drosophila melanogaster* (common fruit fly) neuromuscular junctions [217]. Furthermore, a new type of single-FP sensors, the GECOs, have been developed from GCAMP3 by random mutagenesis.

GECOs can fluoresce in various colours to allow multi-sensor imaging within the same cell (Figure 1.5d) [213].

In plants, single-FP sensors are not yet extensively used. However, R-GECO was recently expressed in Arabidopsis. Comparison between R-GECO and YC3.6 found that in response to various stimuli, including ATP, fungal chitin and bacterial Flg22, R-GECO out-performed YC3.6 in terms of maximal signal change and signal-to-noise ratio [219]. Consequently, R-GECO can measure [Ca^{2+}] changes not detectable with FRET cameleons. Thus, it is clear that single-FP sensors offer a golden opportunity to identify plant Ca^{2+} dynamics that have remained elusive until now.

1.2 Aphids

1.2.1 Aphids: an overview

Aphid biology

Aphids (Hemiptera: Aphididae) are one of the most successful insects on the planet, having colonised every continent except mainland Antarctica. Composed of over 4000 species, aphids feed exclusively on plant phloem sap [220]. Most aphid species, including biotypes of the model aphid *Acyrthosiphon pisum* (the pea aphid – Figure 1.6a), are specialists that feed on a subset of related plant species (monophagous or oligophagous). In the case of *A. pisum*, these are the legumes. Other species such as *Myzus persicae* (green peach aphid - Figure 1.6b), are highly successful generalists that can colonise hundreds of plant species (polyphagous). For example, *M. persicae* is capable of feeding on over 400 species from 40 different families [221], thought to be achieved partly through transcriptional plasticity [222].

The success of aphids is partly due to their asexual production of live young during the summer months (Figure 1.6c). During the winter, aphids undergo sexual reproduction, allowing for the introduction of genetic diversity (Figure 1.6c). In the case of *M. persicae*, sexual reproduction occurs on its primary hosts, trees of the Prunus genera, whilst the aphid becomes highly polyphagous during the asexual stage [221]. Despite this asexuality, large behavioural variation is observed between clones [223]. Indeed, in the absence of a primary host, some aphid species can survive exclusively asexually [224].

All Hemiptera harbour symbiotic microorganisms and essential to the survival of aphids is the obligate bacterial symbiont *Buchnera aphidicola* [225]. Phloem sap is an unbalanced source of amino acids [226] and symbionts such as *B. aphidicola* synthesise essential amino acids for the host [227-230]. Genomic analysis of *A. pisum* and *B. aphidcola* revealed that the machinery required for the synthesis of certain amino acids is shared between the two [231]. Furthermore, several amino acid transporters are expressed at the aphid-bacteria interface [232].

Aphids are predated on by a wide range of other insects, including ladybirds (Coleoptera: Coccinellidae) and lacewings (Neuroptera: Chrysopidae). They are also parasitized by various entomopathogenic fungi and several insects, including parasitic wasps (Hymenoptera: Braconidae) [233].

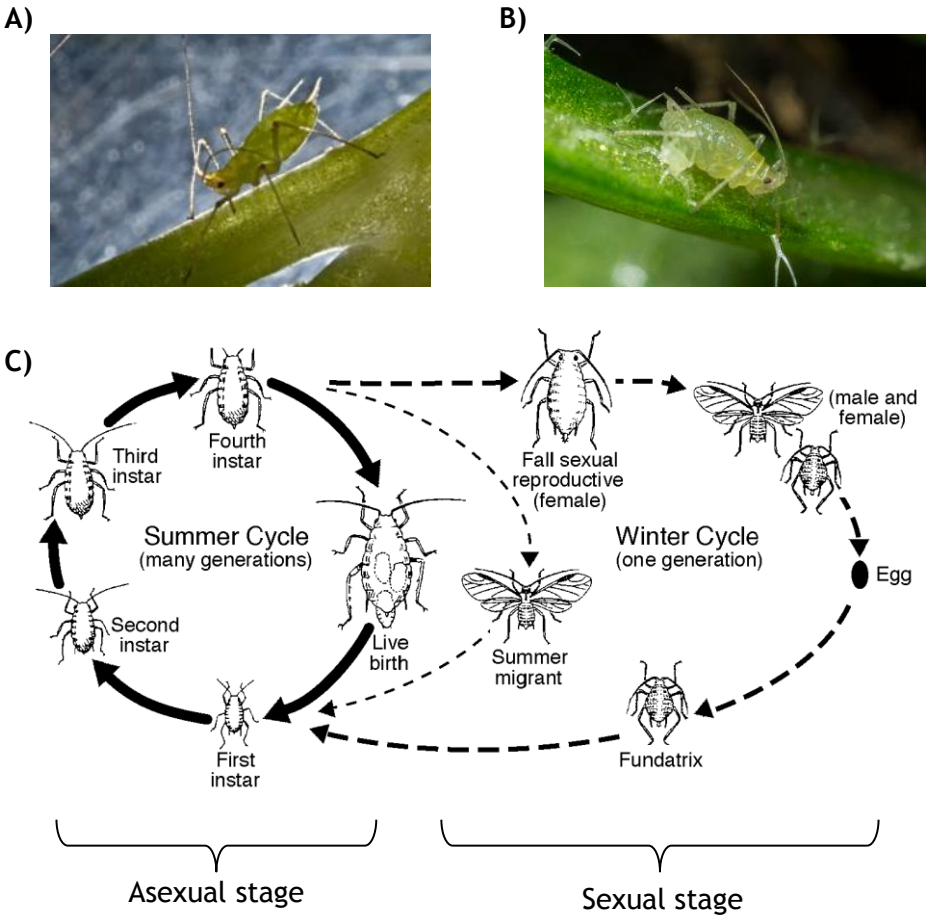

Figure 1.6: The model aphids.

A) *A. pisum* feeding on a legume. Photo: Andrew Davis (JIC). **B)** *M. persicae* feeding on Arabidopsis. Photo: Andrew Davis (JIC). **C)** The life cycle of *M. persicae* generally consists of an asexual summer cycle on multiple hosts, followed by a sexual winter cycle on its primary host; trees of the genus Prunus. Illustration adapted from Davidson & Lyon [234] and taken from http://ipm.ucanr.edu/PMG/PESTNOTES/pni7404-2.html.

***M. persicae* is a major plant pest**

The huge number of aphid species and the extraordinary host range of some of these species results in aphids presenting a serious threat to world agriculture. *M. persicae* can feed on hundreds of species, including vegetables (including potato, sugar beet, pea and carrots), fruits (including apple, citrus, peach and tomato) grains (including barley, wheat and maize) and ornamental plants (including rose and lily) [221, 233, 235]. Although aphid infestation reduces plant growth [236], the main agricultural damage resulting from aphid feeding is the transmission of plant viruses. *M. persicae* is capable of transmitting over 100 different types of viruses, including *Potato leafroll virus* and *Cauliflower mosaic virus* [237]. Through a combination of feeding and virus transmission, aphid infestation results in significant decreases in crop yield and quality [238-240].

Managing aphid populations is one of the great challenges of modern agriculture. One of the main forms of control is the use of chemical insecticides [241]. However, insecticide resistance is now a major issue [242-244]. *M. persicae* has developed resistance to 77 active ingredients [245] and at one point this was more than any other insect, leading to a Guinness World Record [246]. Additional control strategies include biological control using natural enemies [247, 248] and adjusting fertiliser application [249]. Genetic engineering may also offer a novel control strategy. For example, plants were recently created that synthesised the aphid alarm pheromone (E)-ß-farnesene (EBf). Whilst EBf expressed in Arabidopsis successfully repelled *M. persicae* in the lab [250], this effect was not seen with wheat (Triticum spp, henceforth referred to as wheat) in the field [251], which highlights the difficulty of translating research in the lab into successful crop protection strategies.

1.2.2 Aphid feeding behaviour

Before settling

Before an aphid can settle, it has to choose a plant. For this to occur, a winged fundatrix (Figure 1.6c) must find and select a host. If a chosen host is not of sufficient quality the aphid might reject it [252]. Differentiating between host-finding a host-selecting is difficult and is most likely based on a similar set of cues

[253]. Such cues include the visual properties of the target. For example, yellow traps are widely used for aphid control as aphids find this colour attractive [254]. In addition, odours are used in host selection. This includes both those emitted from plants as volatile compounds and those emitted by other aphids as pheromones [255, 256]. Abiotic factors such as wind and temperature also affect aphid dispersal, as do biotic factors including predators and parasitoids [253].

Once a plant has been chosen, there are several barriers to establishing successful feeding with the aphid needing to decide where on a leaf to feed. *A. pisum* fecundity is not affected by feeding location, however there is an increased risk of predation when feeding near the petiole, but this does not appear to deter feeding from this area [257]. Stimuli such as gravity can help some species, including *Euceraphis betulae* (silver birch aphid), to orientate themselves on the underside of leaves [258]. Various chemical and physical features of the plant will also influence feeding site selection, including allelochemicals and trichomes [259]. Indeed, physical barriers are one of the first layers of plant defence that an insect must overcome to establish successful feeding [260].

Pathway phase

Once settled, feeding can commence. Aphids feed from plants using needle-like mouth parts called stylets that penetrate the plant tissue. This begins with probing of the upper cell layers of the leaf (epidermis and mesophyll) before long-term feeding is established from the phloem sieve elements (SEs) (Figure 1.7) [261]. The cues that govern aphid behaviour as it probes the plant are largely unknown.

The electrical penetration graph (EPG) technique pioneered by Freddy Tjallingii and others [262-265] has allowed detailed analyses of aphid feeding behaviours on plants. This technique makes the aphid part of an electrical circuit by attaching electrodes to the aphid and the plant host. Upon cellular penetration by the stylets, a voltage change can be recorded and the pattern of this change is dependent on the cell type. The stylets will travel through the apoplast of the plant, occasionally penetrating surrounding cells (Figure 1.7). EPG has revealed that cell punctures can occur within 10 s of the aphid beginning a probe and many punctures will occur in the epidermal and mesophyll cells as the aphid attempts to find the phloem. This behaviour is called the pathway phase [266, 267].

During the pathway phase, the aphid both salivates and ingests, as demonstrated by elegant experiments analysing virus acquisition and inoculation by aphids as they feed on plants [268, 269]. The aphid secretes two types of saliva into the plant; sheath saliva and watery saliva [270]. Sheath saliva protects the stylets as they move through the plant tissue [267], whilst watery saliva is secreted into plant tissue in order to suppress host defence responses (Figure 1.7) [271].

Watery saliva is injected into the cells probed by the aphid during the pathway phase [268] and proteomic studies on the watery saliva have identified that it contains various proteins that are hypothesised to suppress plant defence [272-274]. Such molecules are referred to as effectors [275]. Various putative aphid effectors have been discovered, often identified through aphid genes expressed in the salivary glands [276-278], and some can be found in the cytoplasm of cells adjacent to the stylet track [279].

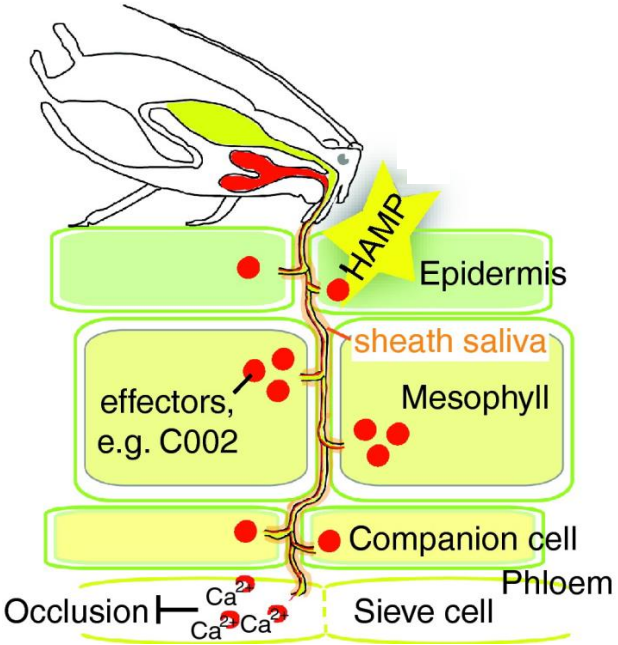

Figure 1.7: Aphids feed from plants using specialised mouthparts called stylets.
The stylets probe epidermal, mesophyll and companion cells until establishing long-term feeding from the SEs. The stylets are covered in sheath saliva and secrete watery saliva, containing effector molecules that modulate host physiology, into the cells. Phloem occlusion is inhibited during aphid feeding, and this is hypothesised to be achieved through the chelation of Ca^{2+}. Taken from Hogenhout & Bos [275].

During incompatible interactions (non-host resistance), where an aphid is not capable of successfully feeding from a specific plant species, probing still occurs. Evidence for this includes the observation that incompatible aphids are still capable of transmitting viruses [280], as well as direct demonstration of feeding on non-host plant species by EPG [281, 282] and histochemical staining [283]. Furthermore, when *M. persicae* feeds on a susceptible genotype of peach, less probing of upper cell layers is observed than on a resistance variety [282]. Thus, during the pathway phase host suitability (such as susceptibility or resistance) is determined and this information is being relayed to the aphid.

Phloem phase

Once the aphid reaches the phloem, two distinct behaviours have been identified by EPG (Figure 1.8a). Upon reaching the SE, the aphid will inject watery saliva into the cell (E1 phase – Figure 1.8b). Subsequently, the aphid will begin ingesting the phloem sap (E2 phase – Figure 1.8c). These two phases are characteristic of phloem feeding by aphids [270, 284].

The phloem allows continuous flow of photo-assimilates in the form of sap [285, 286], thus when a wound or puncture occurs in the sieve tubes the plant acts to seal the breach. In most angiosperms this is achieved by occlusion via phloem (P)-proteins [287, 288] and callose production [289] that plug these gaps. In legumes this manifests itself as the formation of crystalline protein bodies called forisomes [290, 291]. Forisome-dependent occlusion is activated by the presence of Ca^{2+} and inhibited by Ca^{2+} chelators such as ethylenediaminetetraacetate (EDTA) [287, 291]. Synthesis of callose might also be Ca^{2+}-dependent [292-295], although *in vivo* evidence has been lacking thus far. In order for aphids to feed continuously from the phloem, occlusion must be inhibited [296] and it has been suggested that this is achieved by Ca^{2+}-binding proteins present in the saliva [297] (Figure 1.7).

An aphid might not accept the first SE it finds [267] and the degree of phloem feeding depends on the aphid's compatibility with the host [298, 299]. During incompatible interactions, the aphid can complete the pathway phase normally but can exhibit difficulties in establishing ingestion (E2) once reaching the SE. This is can manifest itself as long E1 salivations coupled with shorter E2 ingestions or periods of isolated E1 behaviours [300-303]. Resistance appears to be correlated with the

amount of salivary excretion into the phloem [282], and therefore aphid-derived effectors are also likely to play a role during phloem phase feeding.

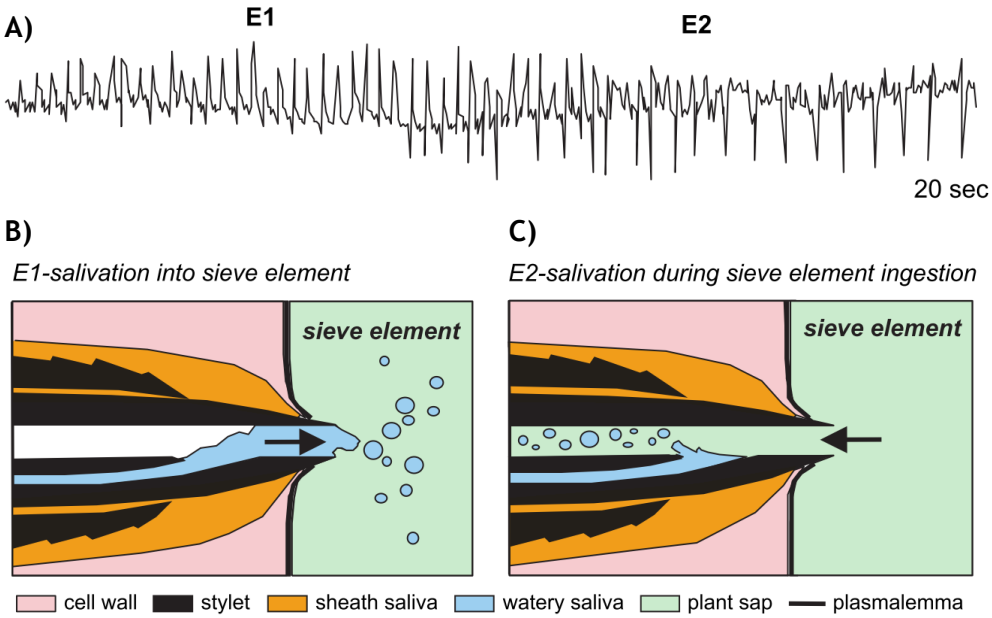

Figure 1.8: Phloem feeding involves salivation (E1) followed by ingestion (E2).
A) EPG trace showing the waveform patterns typical of E1 and E2 feeding. **B)** E1 involves salivation of watery saliva into the sieve element, thought to help modulate plant defence responses. **C)** E2 involves ingestion of the phloem sap. Although salivation continues during E2 no saliva reaches the SE due to the bulk transport of sap into the aphid stylets. Taken from Tjallingii [270].

1.3 Plant defence

1.3.1 Plant defence: an overview

Despite our relatively well informed knowledge of the ecology of aphids, the molecular details that underpin their huge success remain largely unknown. As with the continuing elucidation of Ca^{2+} "toolkit" in plants (Section 1.1), we are only now beginning to identify the mechanisms involved in the aphid colonisation of hosts and the plant responses required to prevent this.

Arabidopsis has a wide selection of anti-aphid defences at its disposal. These include callose production [304], toxic substances such as glucosinolates [305] and camalexins [306], defence hormones such as JA and salicylic acid (SA) [307, 308], as well as the production of natural enemy-attracting volatiles [309]. Many insects feed on plants by herbivory that results in large tissue damage, such as chewing insects like lepidopteran larvae. Consequently, there are many parallels between the plant response to chewing insects and wounding stress [310]. However, hemipterans are subtle feeders, piercing phloem cells and sucking the sap. They also establish long-term feeding and reproduction on the same leaf, unlike chewing insects where feeding and reproduction are temporally separated. Thus, the hemipteran feeding style is more akin to plant-pathogen interactions, in which far fewer cells are damaged [275]. This difference in feeding style between chewing and piercing insects can result in the activation of different plant defence responses [311].

Interactions between plants and pathogens or insects can be thought of as a multi-stage process [312]. The plant recognises the pathogen or insect through conserved pathogen-associated molecular patterns (PAMPs) or herbivore-associated molecular patterns (HAMPs) which activate PAMP-triggered immunity (PTI) (Figure 1.9a). Successful activation of PTI results in an incompatible interaction between the insect and the plant. However, in certain cases the pathogen or insect suppresses PTI using effector molecules, leading to a compatible interaction (Figure 1.9b). To counter this, it is possible for the plant to develop the capacity to recognise these effectors through resistance (R)-genes and activate a second wave of defences known as effector-triggered immunity (ETI) (Figure 1.9c).

It is worth noting that the PTI/ETI model has some limitations. The distinction between PAMPs and effectors is not always clear and it can be difficult to apply the PTI/ETI model to mutualists and necrotrophs that use similar mechanisms of invasion

[313]. This led Cook et al. [313] to propose a simplified model in which the plant recognises general invasion patterns (IPs) by IP receptors, and invaders use effectors that suppress (compatible biotrophs), fail to suppress (incompatible biotrophs) or utilise (necrotrophs/mutualists) IP-triggered defence responses. However, the PTI/ETI model still remains the favoured representation of plant defence and will form the conceptual framework within which the present work is discussed.

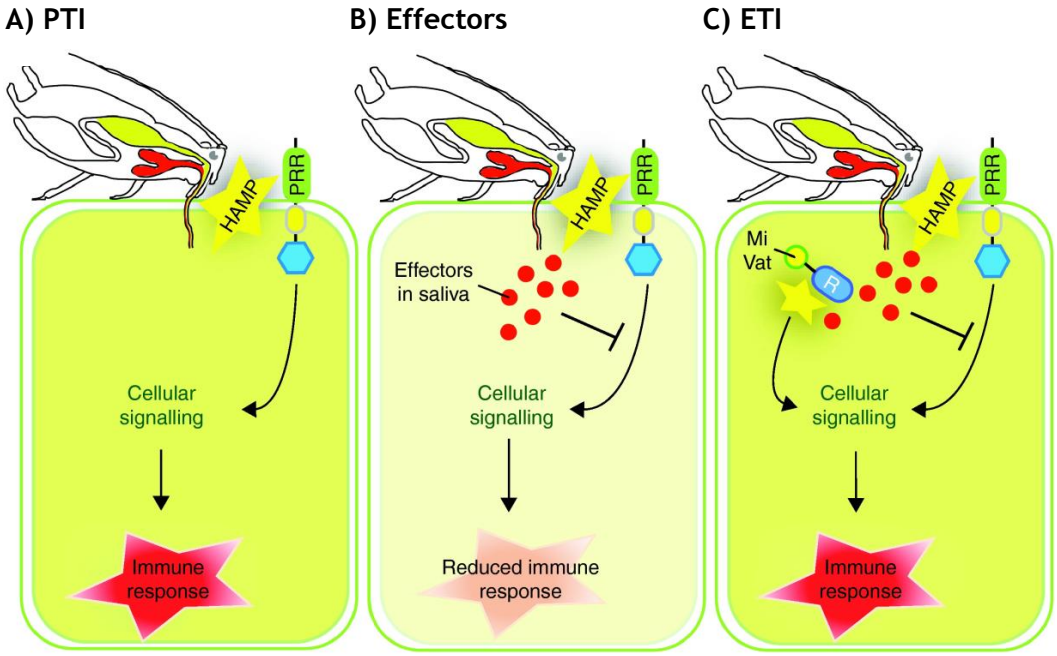

Figure 1.9: The three stages of molecular plant-aphid interactions.

A) PTI is activated in a plant cell after perception of conserved PAMPs or HAMPs by pattern recognition receptors (PRRs). **B)** Compatible pathogens and insects secrete effector molecules into the cell to suppress PTI, often by modulating intracellular signalling pathways. **C)** ETI is activated when the plant detects effectors through R-genes, re-establishing immunity. Examples of aphid R-genes include *Mi-1* from tomato and *Vat* from melon. Figure taken from Hogenhout & Bos [275].

1.3.2 Perception of pathogens and insects

Pathogen and insect elicitors

Attackers are recognised by plants through pathogen- or insect-derived elicitors. These are slowly-evolving conserved molecular fingerprints termed PAMPs [312, 314], or in the case of insects HAMPs [315] (Figure 1.9). Evolution and diversification of PAMPs/HAMPs might contribute to developing increased virulence although this is not directly accounted for in the PTI/ETI model [313, 316]. Various PAMPs have been identified, with the two best characterised from bacteria being flg22 from flagellin [317] and elf18 from elongation factor EF-Tu [318]. Flg22 perception results in many of the hallmarks of plant defence, outlined in detail in sections 1.3.3 and 1.3.4 [317, 319, 320]. Fungi also contain PAMPs [321], the best studied of which is chitin [322, 323].

Conversely, very few HAMPs have been identified. This is partly because chewing insects cause large amounts of internal damage that can itself elicit plant defence responses [324]. Thus, wound-induced damage represents an effective way for a plant to identify such insects. Plant-derived molecules produced during wounding that result in defence activation are termed damage-associated molecular patterns (DAMPs). DAMPs can include cell wall fragments [325-327], cutin monomers [328], and specific peptides such as the JA-responsive systemin and the Arabidopsis wound peptide ARABIDOPSIS THALIANA PEPTIDE 1 (PEP1) [329-331]. Despite the elicitation of defence by DAMPs, application of insect oral secretions (OS) to wounds can elicit plant responses distinct from wounding alone, which suggests there are additional methods of insect-specific detection. For example, applying OS to wounds can increase JA [332] and plant volatile [333] production.

At the interface of DAMPs and HAMPs is inceptin. Inceptin is composed of fragments of the chloroplast ATP synthase, broken down in the insect gut and is present in the OS from *Spodoptera frugiperda* (fall armyworm). Inceptin activates defence responses in *Vigna unguiculata* (cowpea) including ethylene (ET) and JA production, as well as volatile organic compounds (VOCs) [334, 335]. However, the best studied class of insect HAMPs are fatty acid conjugates (FACs) [336-342]. These include volicitin, a lepidopteran FAC that can elicit plant defence [337, 343]. FAC-based elicitors have also been identified in members of the order Orthoptera, such as *Schistocerca americana* (American bird grasshopper) [344]. Whilst inceptins only

function like PAMPs in the Fabaceae, volicitin can elicit responses across angiosperms [345]. In addition to FACs, other HAMPs of lepidopterans include oviposition elicitors [346, 347] and ß-glucosidase [348].

Application of whole-body aphid extract to plants can initiate defence responses [349]. However, the specific aphid HAMP(s) involved has remained elusive until recently. Chaudhary et al. [350] discovered that the GroEL chaperonin protein from the symbiont *B. aphidicola* was capable of stimulating plant defence and that heterologous expression of GroEL in Arabidopsis and *Solanum. lycopersicum* (tomato) significantly reduced *M. persicae* fecundity. To date this is the only known aphid HAMP.

Plant receptors

Several plant cell-surface pattern recognition receptors (PRRs) for PAMPs and DAMPs have been identified. During bacterial infection, FLAGELLIN-SENSITIVE 2 (FLS2) directly binds flg22 [351] and activates plant defence responses [352]. Consequently, loss of FLS2 results in flg22-insensitivity [353]. The receptor for elf18 has been identified as EF-Tu RECEPTOR (EFR) and loss of EFR in Arabidopsis results in higher susceptibility to *Agrobacterium tumefaciens* [354]. For DAMPs, the PEP1 receptor has been identified in Arabidopsis and characterised as PEP1 RECEPTOR 1 (PEPR1) [355]. Furthermore, it has been suggested that GLRs could act as DAMP receptors by sensing changes in amino acids levels during wounding and herbivory [356], although no evidence of this has been presented yet. FLS2, EFR and PEPR1 all belong to the receptor-like kinases (RLKs) and are capable of transducing a phosphorylation signal to downstream components. In plant-fungal interactions, PAMP receptors include CHITIN ELICITOR RECEPTOR KINASE 1 (CERK1) which mediates fungal chitin perception [357, 358], but not perception of aphid chitin [349].

The receptors for HAMPs are not yet known. The Lepidopteran HAMP volicitin has been demonstrated to bind the PM in *Z. mays* [343], suggesting that like PAMPs, HAMPs bind cell-surface receptors. Indeed, many of the downstream responses to HAMP perception are similar to those elicited by PAMPs, implying a common signalling mechanism.

BAK1

Despite containing kinase domains capable of transducing intracellular signalling, many RLKs appear to require other RLKs for full function [314]. In plant immunity, *BRI1-ASSOCIATED RECEPTOR KINASE* (*BAK1*), a gene originally identified by its role in brassinosteroid signalling [359], is required for the full activation of FLS2- and EFR-dependant pathways [360, 361]. Within minutes of flg22 treatment *in vivo*, FLS2 and BAK1 form a complex, making this a very early event in plant defence. Plants lacking BAK1 still exhibit normal flg22 binding and BAK1 is not a direct PAMP receptor, rather a co-receptor required for full signal propagation. Furthermore BAK1 null mutants are still capable of some defence signalling, suggesting that PAMP receptors are capable of some inherent signalling or that additional co-receptors might be present [314, 360, 361]. BAK1 is also involved HAMP-perception during PTI against *Manduca sexta* (goliath worm) [362]. and *M. persicae* [349]. However, the role of BAK1 in plant-aphid interactions is independent of known PRRs including FLS2, EFR or PEPR1 [349].

Activation of PTI

Once a plant perceives PAMPs, HAMPs or DAMPs, PTI will be activated. PTI involves a multitude of processes, characterised from both the pathogen and insect literature. These can be divided into early and late PTI responses. The early responses include ion fluxes, kinase activation, and ROS production, whilst the late responses include hormone biosynthesis, gene transcription and secondary metabolite production. PTI is rapidly activated upon perception of a biotic threat, with the early events occurring within seconds of perception (Figure 1.10).

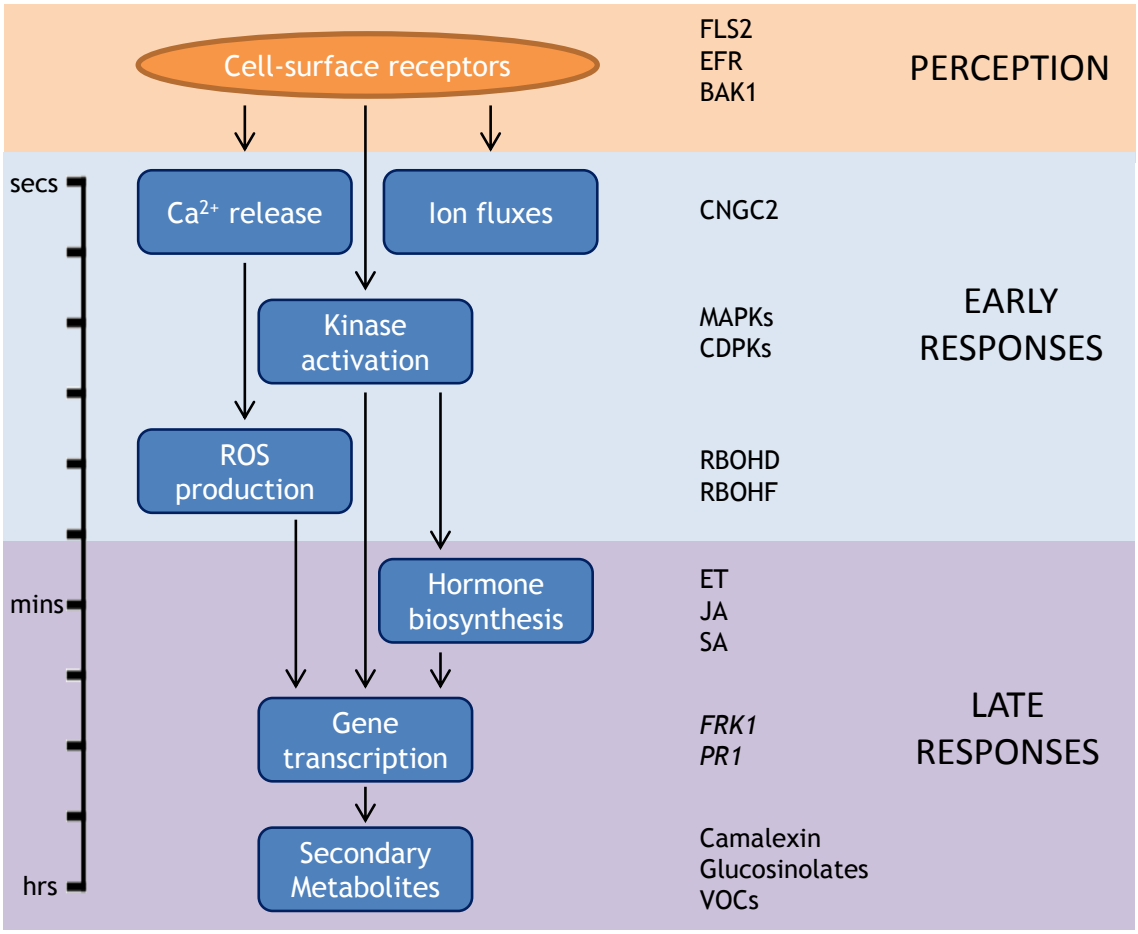

Figure 1.10: Early and late events in PTI against pathogens and insects.

Approximate timing of events indicated on the left. Arrows indicate direct molecular connections between responses. Examples of proteins and chemicals involved in the response are given on the right. Based on information in Maffei et al. [406], Boller et al. [331], Zipfel & Robatzek [363] and Wu & Baldwin [310].

1.3.3 Early events in PAMP-triggered immunity

Ion fluxes and electrical signalling

Plant stress often results in ion fluxes, ultimately causing changes in the PM electrical potential (V_m) [364]. V_m changes caused by biotic stresses result in changes in gene transcription, including those involved in defence [365]. These electrical signals are one of the first plant responses to pathogen and insect attack (Figure 1.10), with Ca^{2+}, K^+, H^+ and nitrate (NO^{3-}) all potentially playing a role [366, 367]. In *Phaseolus lunatus* (lima bean), *Spodoptera littoralis* (African cotton leafworm) attack causes membrane depolarisation around the bite zone and throughout the attacked leaf. Wounding alone is not sufficient to generate a V_m change, application of OS to wounds is required [368] and the strongest elicitation occurring in response to live biting [369]. Interestingly, volicitin cannot induce V_m changes [369]. In *Glycine max* (soybean) membranes, OS from eight different lepidopteran species resulted in ion fluxes, with the activated channels responsible demonstrating a preference for cations over anions [370].

In Arabidopsis, wounding alone induces V_m changes that can be detected with surface electrodes [103]. *S. littoralis*, *M. persicae* and *Pseudomonas syringae* can all induced V_m changes, as recorded by Bricchi et al. [365]. All three induce V_m depolarisations with a similar magnitude, but the timing of the peak depolarisation was variable between the attackers. *S. littoralis* induced a 35 mV depolarisation within 30 min, whilst *M. persicae* took 4 h to reach this level and *P. syringae* 16 h. This appears to reflect the amounts of cellular damage caused by each organism, and suggests that mechanical wounding is the primary cause of V_m changes during such interactions with Arabidopsis. Furthermore, Ca^{2+} channel blockers significantly reduce the V_m changes seen upon insect attack [369] and this implies that Ca^{2+} might be acting as one of the ions directly involved in V_m changes, and/or there is crosstalk between Ca^{2+} and other ions during this signalling.

Ca^{2+} elevations

Interactions with microorganisms often involve $[Ca^{2+}]$ oscillations in the plant. However, unlike symbioses in which $[Ca^{2+}]_{nuc}$ oscillatory patterns lead to a response [8, 64], PAMP-triggered signals generally result in transient $[Ca^{2+}]_{cyt}$ elevations, the amplitude and duration of which are pathogen-specific. For example flg22 induces higher amplitude, shorter duration Ca^{2+} bursts relative to bacterial harpin [17]. Various elicitors induce $[Ca^{2+}]_{cyt}$ elevations, including those from bacteria [17, 122, 219, 371], oomycetes [17, 372] and fungi [122, 219, 373]. The role of Ca^{2+} in pathogen defence is not entirely clear, with Ca^{2+} elevations capable of both activating [374] and suppressing [375] defence. $[Ca^{2+}]$ changes have also been measured in response to chewing insects. OS can induce a transmembrane ion flux in cell cultures [370] and feeding by lepidopteran larvae also induces $[Ca^{2+}]_{cyt}$ elevations in Arabidopsis that are distinct from mechanical damage or OS alone [376].

The Ca^{2+}-permeable channels that mediate PTI-induced $[Ca^{2+}]_{cyt}$ elevations have not yet been identified; however there are several promising candidates. The *CNGC2* null-mutant *defence no death 1* (*dnd1*) displays a strong defence phenotype, showing clear upregulation of the hormone SA and increased resistance to a range of pathogens [79, 377]. This mutant also exhibits reduced $[Ca^{2+}]_{cyt}$ elevation in response to Pep3, but not flg22, implying it mediates Ca^{2+} release upon DAMP perception [378]. Furthermore, *CNGC4* is expressed in response to pathogens and leaves of the *CNGC4* mutant *hml1* develop spontaneous lesions [66]. Interestingly, both *dnd1* and *hml1* have a reduced hypersensitive response (HR), a hallmark of ETI (section 1.3.5) [66, 377]. As such, CNGC2 and CNGC4 could be forming heterotetramers to mediate the same defence pathway [379] and this might be ETI-specific. CNGC11 and CNGC12 have also been implicated defence, as when combined as a chimeric protein they confer enhanced resistance to pathogens [374]. Evidence for GLR involvement in PTI is lacking, however overexpression in Arabidopsis of a putative *Raphanus sativus* (radish) *GLR* resulted in defence gene upregulation and increased resistance to the fungal pathogen *Botrytis cinerea* [380]. Downstream of $[Ca^{2+}]$ elevations, many of the decoders have been implicated in defence against insects and pathogens, including CAMTAs [381, 382], CDPKs (see below) [383, 384] and CIPKs [385].

Kinase activation

MAPKs and CDPKs play a central role in early signal transduction during PTI and there is considerable crosstalk between the two kinase classes. MAPKs can regulate CDPK transcript abundance [386], whilst CDPKs can inhibit MAPK activation through ET-mediated crosstalk [152].

In Arabidopsis, MAPK activation begins minutes after flg22 application [387] (Figure 1.10) in a BAK1-dependant manner [360] and modulates SA production [388], PTI marker gene expression [389] and the HR [390]. MAPK activation is also part of the defence response to fungi [354] and nematodes [391]. Moreover, MAPKs including the wound-induced protein kinases (WIPKs) and SA-induced protein kinases (SIPKs) are activated upon wounding and are required for JA production and defence gene induction [392-396]. Consequently, herbivory by *M. sexta* results in a rapid upregulation of the WIPKs and SIPKs that mediate JA and ROS production during this interaction [386], whilst silencing of *MPK1* and *MPK2* in *S. lycopersicum* results in a much higher susceptibility to herbivory [397]. The role of MAPKs in aphid-induced PTI has not been clearly elucidated, however the MAPK marker gene FLG22-INDUCED RECEPTOR-LIKE KINASE 1 (*FRK1*) is induced by whole-body extract from several aphid species [349] and silencing MAPKs in *S. lycopersicum* significantly reduces ET-mediated resistance to *Macrosiphum euphorbiae* (potato aphid) [398].

CDPKs have also been shown to play an essential role in PTI directly downstream of [Ca^{2+}] elevations. Flg22 can stimulate CDPK activity, whilst loss of *CPK4*, *CPK5*, *CPK6* and *CPK11* results in reduced defence responses and increased susceptibility to *P. syringae* [399]. In agreement with this, over-activating CDPK2 by removing the auto-inhibitory domain induces strong defence responses in *Nicotiana benthamiana* [152] and transcript levels of CDPKs peak significantly earlier in response to wounding if *M. sexta* OS are added [386]. Upregulation of CDPKs in defence is not restricted to dicots; in maize *CPK11* is up-regulated upon wounding [400, 401]. Ten different *G. max* CDPKs were recently shown to be upregulated by infestation with the *Aphis glycines* (soybean aphid) [402], suggesting CDPKs might also play a role in plant-aphid interactions.

CDPKs can also negatively regulate PTI. For example, CPK28 mediates turnover of BIK1, a plasma-membrane enzyme that mediates signalling by multiple RLKs [403] and the PAMP-induced Ca^{2+} burst in Arabidopsis [384]. Furthermore, CDPKs regulate other defence signals, including H_2O_2 production [119], SA accumulation

[404] and increased expression of the JA marker gene *PLANT DEFENSIN 1.2* (*PDF1.2*) [405].

ROS production

A detectable increase in ROS can be measured within minutes of exposure to PAMPs/HAMPs, with ROS acting directly as an anti-microbial substance and as a signalling molecule (Figure 1.10). Bacteria [316, 317, 353, 360, 371, 406], fungi [318, 354, 360], caterpillars [407] and aphids [304, 349, 408] all elicit the production of ROS in plants.

FLS2 is required for this burst in response to flg22, whilst ROS produced in response to elf18 is EFR-dependent [354]. Furthermore, in the case of flg22, elf26 and aphid extract, this burst is also mediated by BAK1 [349, 360]. It is worth noting the ROS burst in response to aphid extract peaks 180 min post-exposure, a much slower response than that observed with flg22. This aphid extract-induced burst is also ten times lower in magnitude [349]. However, the two are not comparable as aphid extract contains all the proteins from the insect's body, not just the isolated HAMP. Indeed, when GroEL was incubated alone with Arabidopsis leaves, the ROS burst was much more rapid, peaking within 14 minutes [350].

For both pathogens and aphids, the PM-localised enzyme RBOHD appears to be the source of the ROS [349, 409-411]. Furthermore, the closely related enzyme RBOHF is also required for pathogen-induced ROS accumulation [409, 412], and *rbohD* and *rbhoF* mutants show reduced resistance to *M. persicae* [283, 413]. Moreover, ROS production mediates host-compatibility, with incompatible aphids inducing greater ROS production than compatible species [283].

There is a clear link between ROS production and Ca^{2+} signalling (Figure 1.10). RBOHD is Ca^{2+}-regulated [414] and required for long-distance Ca^{2+} signalling [121]. Furthermore, RBOHC regulates Ca^{2+} influx during root hair expansion [415] and damaged-induced Ca^{2+} elevations are enhanced by H_2O_2 application [407].

1.3.4 Late events in PAMP-triggered immunity

Hormone biosynthesis

After the initial defence signalling responses, biosynthesis of plant hormones occurs. The four main hormones implicated in defence are JA, SA, ABA and ET. The antagonism and crosstalk between them is not fully understood, and therefore a comprehensive understanding of their individual roles is not yet possible.

JA is a chloroplast- and peroxisome-synthesised hormone that accumulates in response to wounding [392, 395, 416] and in response to herbivory by chewing insects, where it is detrimental to insect fitness [308, 332, 334, 335, 417-420]. It also accumulates in response to some microbial pathogens [421]. JA accumulation peaks about an hour after elicitation (Figure 1.10) [345] and inhibition of the JA pathway results in increased insect performance [422]. JA regulates defence-related genes [421, 423] and its accumulation is regulated by CDPKs [424], MAPKs [392, 393, 395, 425] and BAK1 [362]. Despite the lack of strong differential regulation of JA-related genes upon aphid feeding [426, 427], high levels of JA are detrimental to aphids [307, 426, 428-430]. Furthermore, compatible aphids induce and repress different subsets of JA-related genes [304] further suggesting that regulation of JA is important.

SA accumulates in response to microbial pathogens [431] and phloem-feeding insects [417, 426], and is vital for effective defence [79, 432]. SA-related genes are upregulated in response various aphid species, including *Brevicoryne brassicae* (cabbage aphid) [304], *M. euphorbiae* [433] and *M. persicae* [308]. It has been proposed that aphids upregulate SA and this antagonises JA-mediated defence signalling in order to allow successful colonisation of the plant [426, 427, 434-436]. However, the role of SA in anti-aphid defence remains unclear; for example *M. persicae* displays a range of contradictory fitness phenotypes on different Arabidopsis SA mutants [434].

ABA is now also emerging as a biotic stress hormone, in addition to its role in abiotic signalling (Section 1.1.6). ABA is produced in response to wounding [172, 173] and aphid feeding [437] and plays a role in defence against pathogens [438]. In these responses it is hypothesised that ABA is also acting to antagonise JA [432, 439-441]. As with SA, the extract role of ABA in plant-insect interactions is still unclear, with

both chewing insects and aphids displaying contradictory phenotypes on different ABA mutants [418, 437, 442].

ET signalling is involved in defence against bacteria [443], fungi [318, 444], and chewing insects [334]. This is one of the fastest responses to PAMPs, occurring within 10 min and regulated by l-aminocyclopropane-1-carboxylate (ACC) synthase [445]. Very few ET-related genes are differentially regulated by aphid attack in Arabidopsis [304, 427], however Kerchev et al. [442] found that several ET response factors are upregulated by *M. persicae* infestation. It is unclear if this forms part of a plant defence response or aphid manipulation of the host. Likewise, the biological role of ET in aphid defence is unclear and has been related to both resistance [446, 447] and susceptibility to aphids [448-450] in various plant species.

Gene transcription

Ions, ROS, MAPKs, CDPKs, and plant hormones all regulate gene expression during defence. PTI-regulated genes can be identified from those differentially regulated by direct PAMP/HAMP application. Flg22 application results in rapid differential regulation of 966 genes within 30 min (Figure 1.10) and this is reduced to just 6 genes if *FLS2* is mutated [320]. Elf18 elicits a similar response [354] and in both cases the majority of genes are upregulated. In addition there is the potential for significant feedback, with over 40 RLKs changing in expression, as well as genes regulating Ca^{2+} (e.g. *CNGC1*, *GLR1.1*), ROS (e.g. *RBOHD*), hormones (e.g *LOX, ACC6*) and MAPKs (e.g. *MPK17*) [320].

Wounding and the production of DAMPs also upregulates a wide array of genes, especially those related to JA signalling and water stress [451, 452], as well as those found during PTI such as the *WRKY DNA-BINDING PROTEIN3* (*WRKY3*) [453]. Indeed, many PAMPS and DAMPs regulate a similar set of genes, implying that the responses to these diverse stimuli converge at the point of gene transcription [331].

The lack of characterised HAMPs makes it difficult to identify genes directly involved in PTI against insects and studies performed with whole insects or their derivatives do not easily allow us to distinguish between PTI- and ETI-mediated resistance. However, GroEL upregulates several genes known to be involved in PTI against pathogens, including *FRK1*, and *WRKY29* 3 h post-treatment, and *PATHOGENESIS-RELATED GENE 1* (*PR1*) 24 h post-treatment [350]. *FRK1* and *WRK29* form part of the early signalling response to pathogens and are also upregulated

within 30 min of flg22 application [151], whilst *PR1* is a well-characterised late-responding PTI gene [454]. Prince et al [349] showed that *M. persicae* extract can induce further pathogen-identified PTI marker genes including *CYTOCHROME P450, FAMILY 81* (*CYP81F2*), involved in glucosinolate production [305] and *PHYTOALEXIN DEFICIENT 3* (*PAD3*), involved in camalexin production [455].

Secondary metabolites

The successful activation of defence against insects and pathogens concludes in secondary metabolite biosynthesis and callose production. Callose production was described previously in section 1.2.2 and is a common response that prevents phloem nutrients from reaching pathogens [319, 456] and insects [296, 297, 457]. Secondary metabolites produced in defence include lignin to impede entry, toxic substances (e.g. flavonoids, tannins and lectins) and protease inhibitors that act against insect gut [458].

Camalexin and glucosinolates are two tryptophan derivatives believed to play a key role in defence against insects. Camalexin biosynthesis is mediated by the enzyme PAD3 [455, 459] and plays role in defence against fungi [460, 461], bacteria [462, 463] and aphids [304, 306, 349, 464]. Glucosinolates are also part of PTI against pathogens [465]. Despite constitutive production of glucosinolates in many plants [466], a wide variety of insects from various orders stimulate increased glucosinolates production within a few days, and this has negative effects on insect fitness [467]. Furthermore, at least 120 glucosinolates have been identified across plant species [467], and different classes are detrimental to different insects [468]. In Arabidopsis, 4-methoxyindol-3-yl-methylglucosinolate (4MI3M) is induced by *M. persicae* feeding, enhancing plant resistance and its loss correlates with improved aphid performance [305, 437, 464, 469, 470].

In addition to metabolite production within tissues, plants also release VOCs into the surroundings. The composition of VOCs is altered by herbivory and these act as cues to attract the natural enemies of the attacker [348, 471, 472], as well as for priming defence in systemic tissue and other plants [473, 474]. Some herbivores, including *M. persicae*, can perceive VOCs and this deters them from settling on a host [309]. VOCs include plant hormone derivatives and in turn are regulated by hormones, primarily JA [475-479]. Thus, the plant uses secondary metabolites in a combination of direct toxicity and indirect defence to protect itself from harm.

1.3.5 Effector-triggered immunity

Effectors

In order to survive successfully on a host, microbes and insects need to overcome PTI. This is achieved through the use of effectors (also known as avirulence proteins), molecules that are secreted into plant tissue that attenuate plant defence. Bacteria use needle-like type III secretion systems to deliver up to 30 effectors at once into host cells, targeting a range of cellular processes including vesicle transport, protein degradation and kinase cascades [312, 480]. For example, *P. syringae* secretes AvrPto and AvrPtoB to target BAK1 [481], AvrE to target SA signalling [482] and HopX1 to target JA [483].

Eukaryotic pathogens such as fungi and oomycetes use specialised infection structures (haustoria) to enter plants through openings (e.g. stomata, wounds) or by direct penetration. Consequently, they deliver both extracellular and cytoplasmic effectors to suppress defence [484, 485]. The mode of action for fungal effectors is often through direct binding of chitin to prevent chitin perception by the plant [486-489]. In the case of oomycetes, multiple effectors have been characterised that target host proteases involved in defence [490-493].

For chewing insects, the application of OS to wounds alters wound-induced defence responses and this is believed to be achieved by effectors in the salvia [451, 472, 494, 495]. However, relatively few of these effectors have been identified. Glucose oxidase (GOX), one of the most abundant proteins in lepidopteran saliva [420] has effector properties. GOX is secreted in response to sugars [496] and acts as the active ingredient in OS that suppresses wound-induced defence [497]. Furthermore, GOX activity is higher in generalist species relative to specialists, implying it might have a role in adjusting to different hosts [498].

Aphid infestation results in the differential expression of many genes [283, 308, 442, 499]. In the case of compatible interactions, it is likely that the expression of some of these genes is manipulated by the insect through effectors. The first aphid effector identified was C002, an *A. pisum* salivary protein. C002 is secreted into plants and is required for *A. pisum* survival on its host *Vicia faba* (fava bean). Furthermore, knock-down of the transcript prevents phloem feeding from being established [276, 500]. The *M. persicae* C002 homologue *MpC002* can also increase aphid fecundity when heterologously expressed in *N. benthamiana* [277] or

Arabidopsis [501], and knock-down by RNA interference (RNAi) reduces aphid fecundity [502]. This is a species-specific effect, with C002 from *A. pisum* having no effect on *M. persicae* performance on Arabidopsis [501]. In addition, *MIGRATION INHIBITORY FACTOR 1* (MIF1) from *A. pisum* saliva was recently shown to induce plant defences and was crucial for aphid survival and fecundity [278].

Several *M. persicae* effectors have been identified through an aphid genomic screen selecting for salivary-gland expression and signal sequence similarity to known effectors [277]. This screen identified Mp1 (PIntO1) and Mp2 (PIntO2), that can increase *M. persicae* fecundity on Arabidopsis [501] as well as Mp10, that induces chlorosis in *N. benthamiana* and suppresses flg22-elicited ROS production [277]. Further evidence in support of Mp10's effector function comes from recent experiments showing that it can suppress aphid-extract induced ROS bursts, whilst reducing expression of the gene via RNAi reduces *M. persicae* fecundity [502]. Furthermore, Mp55 has been identified as an effector, with heterologous expression in Arabidopsis suppressing production of ROS, 4MI3M and callose, and abolishing expression of the effector reduces aphid fecundity [503]. Two effector candidates from *M. euphorbiae*, Me10 and Me23 were recently identified and shown to promote aphid fecundity; although no evidence for plant defence suppression was provided [504]. The plant target of aphid effectors has remained elusive. They might share similarity with the targets of pathogen effectors, or have a completely novel function.

R-genes and ETI

The second layer of plant defence, ETI, is activated by the plant perception of effectors during incompatible interactions. This perception is mediated by plant R-genes that recognise effectors in a gene-for-gene manner [505]. Many R-gene-effector combinations are now known [312, 506]. Detection of effectors by R-genes activates a second wave of defence that includes many of the same responses as PTI, including ion fluxes, kinase activation, ROS production, hormone biosynthesis and secondary metabolite production [420, 486, 507-512]. Indeed, R-genes appear to mediate a biphasic Ca^{2+} signature during ETI to incompatible pathogens [379, 509, 513]. ETI against pathogens often results in programmed cell death (HR) that is designed to limit the spread of the pathogen [312].

The best characterised insect R-gene is *Mi-1* from *S. lycopersicum*. *Mi-1* was first used in the 1940s to create more resistant varieties of cultivated tomatoes [514] and confers resistance to nematodes [515], potato aphids [516], whiteflies [517] and psyllids [518]. *Mi-1*-mediated aphid resistance appears to be based on altered SA production, as the SA-responsive gene *PR1* is more highly upregulated in *Mi-1* lines [519] and knocking out SA production from *Mi-1* lines abolishes resistance [398]. This signalling also requires *SOMATIC EMBRYOGENESIS RECEPTOR-LIKE KINASE 1* (*SERK1*) [520].

Another well-established R-gene effective against aphids is *Vat*, a gene from *Cucumis melo* (melon) that confers resistance to *Aphis gossypii* (cotton aphid) [521, 522]. *Vat* prevents virus transmission by both *A. gossypii* and *M. persicae*, implying that it inhibits successful salivation [523].

Other potential aphid R-genes include *RESISTANCE TO ACYRTHOSIPHON PISUM 1* (*RAP1*) from *M. truncatula* that confers resistance to *A. pisum* and induces an HR-like effect around stylet penetration sites [524]. Various genes and quantitative trait loci that enhance aphid resistance have been identified across crop species [525], and isolation of the R-genes underlying these phenotypes has the potential to significantly enhance resistance to aphids in the field.

1.3.6 Systemic signalling during stress

When a stress is perceived, signals can travel from tissue of perception systemically throughout the plant. In response to abiotic stimuli this is termed systemic acquired acclimation (SAA), whilst in response to biotic threats it is termed systemic acquired resistance (SAR). SAR benefits the fitness of a plant [526] by priming defences in systemic tissue [527]. Various signals involved in SAA and SAR have been identified. These include hydraulic signals [528], hormones [529, 530], RNA [531] and peptides [532]. Furthermore, SAR responses are SA-dependent [529, 533, 534]. An ion that has been well-demonstrated to perform this role in the context of abiotic signalling is Ca^{2+}. It is hypothesised that a wave-like propagation of CICR-mediated $[Ca^{2+}]_{cyt}$ elevations, in co-ordination with ROS and electrical signals, might account for the rapid systemic responses observed during SAA and SAR [535-537] (Figure 1.11).

Choi et al. [7] used a YCNano-65 cameleon sensor to visualise a bi-directional root-to-shoot Ca^{2+} signal in Arabidopsis upon application of salt stress. This signal

travelled through the root at a speed of 400 μm/s. In a separate study, the speed of the signal between the root and the shoot showed high variability, from 50 to 500 μm/s [538]. Using AEQ, Kiep et al. [123] demonstrated that wounding and herbivory of leaves results in a long-distance leaf-to-leaf Ca^{2+} signal, but only if the midrib is wounded. The signal travelled to neighbouring leaves with direct vascular connections within a few min.

However, the systemic Ca^{2+} signals are not driven by changes in $[Ca^{2+}]$ alone. In order to explain their speed, a ROS component must be added [121]. ROS allows propagation of the signal cell-to-cell through the apoplast, with localised $[Ca^{2+}]_{cyt}$ fluxes propagating the signal within cells [119, 121, 539]. This hypothesis is outlined in Figure 1.11, whereby an unknown ROS-activated PM Ca^{2+}-permeable channel and TPC1 mediate the $[Ca^{2+}]_{cyt}$ flux, and RBOHD, which is Ca^{2+}-activated via CPK5 [119], mediates ROS production in the apoplast [121]. Indeed loss of either TPC1 [7, 123] or RBOHD [121] significantly attenuates the systemic Ca^{2+} signal, and a RBOHD-dependent systemic ROS signal has been observed in responce to wounding [413]. Interestingly, CPK5 activity increases in response to H_2O_2 [119], suggesting there might also be positive feedback within ROS signalling, much like with CICR. Furthermore, the spread of Ca^{2+} and ROS signals within leaves are mediated by plasmodesmata, as the *PLASMODESMATA-LOCATED PROTEIN 1* (*PDLP1*) mutant *pdko3* shows significantly less Ca^{2+} release in response to Lepidopteran OS [540].

The spread of the Ca^{2+} signal to neighbouring leaves during wounding mirrors that which is seen with long-distance electrical signals. Using surface electrodes, Mousavi et al. [103] recorded electrical signals travelling at around 400 μm/s within the wounded leaf, and with speeds of up to 1500 μm/s between leaves [103]. A similar trend is seen with Ca^{2+}, with midrib signals travelling up to 10 times faster than those in the surrounding tissue [538]. *Pieris brassicae* (cabbage butterfly) larvae were shown to induce similar systemic electrical signals. As with Ca^{2+}, feeding from the midvein of the leaf was required for systemic spread [541]. Thus, the vasculature appears to be the primary conduit of this signal. The discrepancy between the speeds measured by Choi et al. [7] and Kiep et al. [123] could be due to the different stresses used, the different tissues examined, or because Ca^{2+} might not be the primary ion responsible for the wound-induced electrical signal. Again, systemic electrical signalling is dependent on plasmodesmata, as membrane depolarisation and K^+ channel activity is almost completely abolished in the *pdko3* mutant [540]

It is interesting that whilst long-distance Ca^{2+} signalling is TPC1-dependent [7, 123], *TPC1* expression has no effect on systemic electrical signalling (Edward Farmer, University of Lausanne, personal communication). Instead systemic electrical signalling is dependent on *GLR3.3* and *GLR3.6* [103]. However, the two signals are clearly linked and various Ca^{2+}-permeable channels, including TPC1, are voltage-gated [112, 114, 115, 542].

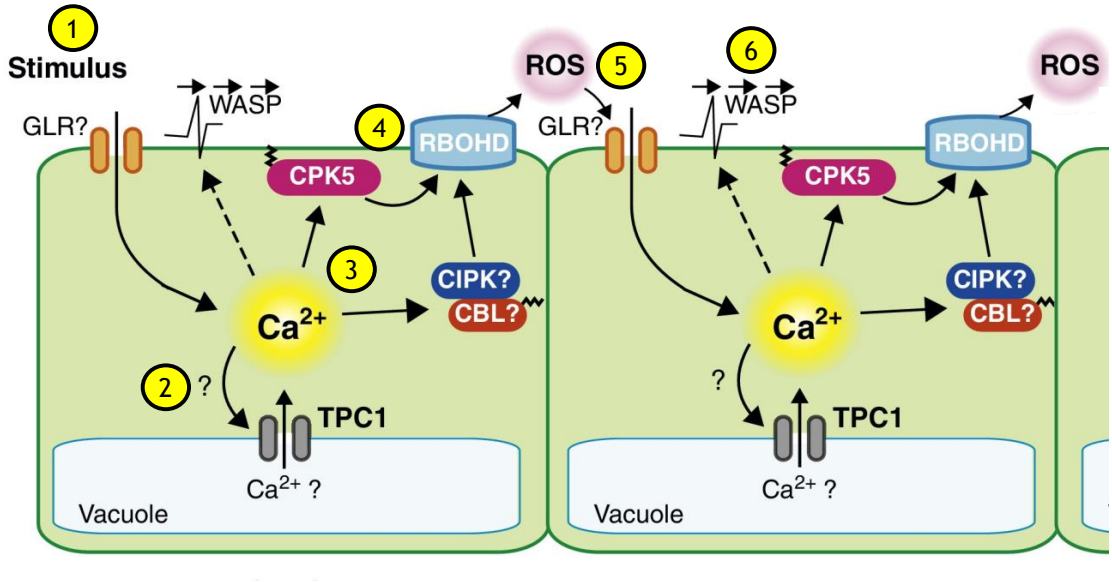

Figure 1.11: Ca^{2+}, ROS and electrical signals all participate in systemic signalling during stress.

(1) Upon stimulation by abiotic or biotic stress, Ca^{2+} is released into the cytosol from the apoplast through an unknown PM channel, possibly the GLRs. **(2)** This rise in $[Ca^{2+}]_{cyt}$ activates TPC1, which in turn releases further Ca^{2+} from the vacuole, amplifying the signal. **(3)** The rise in $[Ca^{2+}]_{cyt}$ activates Ca^{2+} decoders, including CDPKs and CIPKs, such as CPK5. **(4)** CPK5 phosphorylates RBOHD, a ROS-producing enzyme in the PM. **(5)** ROS is released into the apoplast, where it diffuses to activate PM Ca^{2+}-permeable channels in adjacent cells, propagating the Ca^{2+} signal systemically. **(6)** During wounding, wound-activated surface potentials (WASPs) also travel between cells as an electrical signal. This signal is dependent on GLR3.3 and GLR3.6. Figure adapted from Steinhorst & Kudla [535] based on data from Choi et al., [7], Dubiella et al. [119], Evans et al. [121] and Mousavi et al. [103].

The output of wounding and herbivory is accumulation of JA in the systemic tissues [543, 544] and this can occur within 30 s of wounding [545]. Indeed, JA is one of the best characterised systemic signals in biotic interactions. Local JA accumulation is dependent on *LIPOXYGENASE 2* (*LOX2*) [544], whilst systemic accumulation is dependent on *12-OXO-PHYTODIENOIC ACID REDUCTASE 3* (*OPR3*) [546] and LOX6 [545]. Thus, it might be that JA or its derivatives are acting directly as a systemic signal in the phloem [530]. However, as the JA accumulation pattern overlays almost exactly the pattern of systemic electrical signals, and expression of the JA marker genes *JASMONATE-ZIM-DOMAIN PROTEIN 10* (*JAZ10*) is lost when these electrical signals are abolished [103]. It is therefore possible that JA accumulation is regulated by systemic ion fluxes. It is worth noting *M. persicae* feeding does not appear to result in systemic JA production [308] and that SAR might not be occurring during the Arabidopsis-*M. persicae* interaction [431, 464].

1.4 This project

1.4.1 Aims of the project

Aphids, including *M. persicae,* trigger defences in plants comparable to PTI. One of the first events in PTI is a Ca^{2+} influx into the cytosol; however the mechanisms underlying this are unknown. The Sanders and Miller labs (John Innes Centre - JIC) have uncovered several of the channels and transporters that underlie ion homeostasis and signalling in plants, including TPC1. The Hogenhout lab (JIC) has identified several components of aphid-induced PTI, including a Ca^{2+}-dependent ROS burst elevation upon application of aphid extract [349]. However, an aphid-induced plant Ca^{2+} signal has yet to be demonstrated *in vivo*.

Recently, rapid improvement and optimisation of genetically-encoded Ca^{2+} sensors has revolutionised our understanding of plant Ca^{2+} signalling. Single-FP sensors have not been fully exploited in plants and present a novel tool with which to study this phenomenon in more detail than was previously possible. The Gilroy lab (University of Wisconsin-Madison) has stably expressed GCAMP3 in Arabidopsis. This has provided a unique opportunity to measure Ca^{2+} signals with tissue-level resolution *in vivo* in response to aphid attack. As such, the main goal of the current work was to

investigate aphid-induced Ca^{2+} signals and characterise the molecular mechanisms involved if present.

1.4.2 Overview of thesis contents

Chapter 3: *M. persicae* elicits rapid BAK1-dependent Ca^{2+} bursts in Arabidopsis

To establish if GCAMP3 is a viable tool for use in plant-aphid interactions, Arabidopsis plants expressing 35S::GCAMP3 were exposed to *M. persicae*. A repeatable and robust single-leaf assay for Ca^{2+} measurements during aphid feeding resulted in the identification of rapid $[Ca^{2+}]_{cyt}$ elevations around the feeding site that occurred within minutes of the aphid settling. Interestingly, no systemic signals could be identified. This tissue-level imaging was not possible with the FRET cameleon YCNano-65. To correlate the Ca^{2+} burst with the aphid feeding behaviour, EPG was used on single leaves and this showed that the Ca^{2+} burst most likely occurs during the pathway phase. In agreement with these findings, a Ca^{2+} burst in the phloem could not be detected a phloem-localised version of GCAMP3. This suggests that Ca^{2+} plays a role in the early stages of the plant-aphid interaction whilst the aphid probes the epidermal and mesophyll cells.

To determine if the $[Ca^{2+}]_{cyt}$ elevations were elicited by damage (DAMPs) or directly by aphid HAMPs, 35S::GCAMP3 was crossed with the *BAK1* null mutant *bak1-5*. The $[Ca^{2+}]_{cyt}$ elevations were not detectable in these plants, showing that they are elicited as a part of HAMP-triggered PTI. Furthermore, to investigate if the aphid is directly modulating this pathway, the assay was repeated with aphids with reduced expression of the effector *Mp10*. Such aphids elicited a slightly larger Ca^{2+} burst than the control group, indicating that the aphid is actively suppressing Ca^{2+} and supporting the hypothesis this signal is relevant to defence.

Chapter 4: Aphid-induced Ca^{2+} bursts are mediated by TPC1 and GLRs 3.3 and 3.6

To identify the plant proteins responsible for generating the aphid-induced $[Ca^{2+}]_{cyt}$ elevations, Arabidopsis ion channel mutants were investigated. Plants lacking *TPC1* transcription (*tpc1-2*) exhibited a significantly reduced Ca^{2+} burst, suggesting that vacuolar Ca^{2+} is released during the plant-aphid interaction. Induction of MAPK

and camalexin marker genes was also compromised in the *tpc1-2* mutant, suggesting this channel may be involved in downstream defence activation against aphids.

EPG revealed that aphids feeding on such plants have problems with phloem acceptance, but that there are no significant differences in pathway behaviours. As such, the *TPC1* phenotype is based on plant physiology and not aphid behaviour. Conversely, overexpression of *TPC1* did not affect the $[Ca^{2+}]_{cyt}$ elevations, but did result in an amplified ROS burst to aphid extract. Furthermore, over-activation of TPC1 (*fou2)* resulted in aberrant Ca^{2+} signalling and a strong defence phenotype that reduced *M. persicae* and *A. pisum* performance. Thus, TPC1 plays a role both in generating the Ca^{2+} burst and in plant defence.

Small $[Ca^{2+}]_{cyt}$ elevations were still observed in plants lacking *TPC1*. As such, it was hypothesised that other Ca^{2+} channels were also involved. Therefore $[Ca^{2+}]_{cyt}$ elevations in the GLR double mutant *glr3.3/gl3.6* were measured and demonstrated to be undetectable relative to untreated control leaves. This suggests that the initial Ca^{2+} release is from the extracellular environment, and this is required for aphid-induced $[Ca^{2+}]_{cyt}$ elevations. It is proposed that this then activates TPC1 to release further Ca^{2+} from the vacuole.

Chapter 5: Investigating the role of CIPKs in plant-aphid interactions

Finally, the role of downstream Ca^{2+} decoders in plant-aphid interactions was investigated. RNA-seq identified several Ca^{2+} decoders that were induced by infestation with the incompatible aphid *A. pisum*. However, in response to the compatible species *M. persicae*, many fewer genes were differentially regulated. As such, it appears that *M. persicae* is avoiding detection by the plant, including components of Ca^{2+} signalling. However, *CIPK3* was differentially regulated by both aphid species. Therefore it is proposed that *CIPK3* might play a role in host compatibility. However, abolishing *CIPK3* transcription or constructively activating the protein had no effect on aphid performance.

This finding lead to a study of redundancy between the Clade I CIPKs, revealing that *M. persicae* performance was significantly reduced on the *cipk9/23* double mutant, suggesting that *CIPK9* and *CIPK23* might play a role in defence against aphids downstream of the Ca^{2+} burst. Aphid performance was further reduced on the cipk3/*9/23/26* quadruple mutant, which also exhibited greater ROS production in

response to aphid extract. This suggests that all four CIPKs might have a role in negatively regulating defence against aphids.

1.4.3 Contributions to thesis

All experiments in this thesis were conducted by me (T.V.) unless otherwise acknowledged. Several undergraduate students contributed to this work under my supervision. Marieta Avramova (M.A.) was a year-in-industry student from the University of York (UK), James Canham (J.C.) and Magda Steele (M.S.) were students at the University of East Anglia (UK), Peter Higgins (P.H.) was a predoctoral scientist at the JIC and Natasha Bilkey (N.B.) was a student at the University of Wisconsin-Madison (USA) who undertook a summer project at the JIC. All experimental work performed by others and incorporated into this thesis is appropriately and fully acknowledged in the legends pertaining to display items (figures and tables). Further contributions of collaborators, including plant material and primers, are acknowledged in Chapter 2.

Chapter 2: Materials & Methods

2.1 Plant maintenance

2.1.1 Arabidopsis growth conditions

Arabidopsis plants for use in aphid performance assays (section 2.9), ROS burst assays (section 2.10) and RNA-seq (section 2.11) were germinated and maintained on Scotts Levington F2 compost (Scotts, Ipswich, UK). Seeds were vernalised for one week at 4-6°C before being transferred to a controlled environment room (CER) maintained at 22°C and with a photoperiod of 10 h light (90 µmol $m^{-2} s^{-1}$) and 14 h dark. Plants were grown in cell trays (each cell: base 3.5 x 3.5 cm, top 5.5 x 5.5 cm, height 5.5 cm). Plants for the majority of assays were used at 4 weeks post-germination (ages specified in experimental methods).

Plants for use in microscopy (section 2.8) and single leaf EPG (section 2.9.7) were grown on 100 mm^2 square plastic plates (R & L Slaughter Ltd, Upminster, UK) on ¼ strength Murashige and Skoog (MS) medium (recipe: 1.1 g Murashige and Skoog medium, 7.5 g sucrose, 10 g Formedium agar, 1 L de-ionised water) [547] and vernalised for three days in the dark (8°C). They were then grown in a CER with a 16 h day and 8 h night, at a constant temperature of 23°C. Plants were then used at 16-18 days old.

2.1.2 Arabidopsis lines

Many of the Arabidopsis lines used in this study were kind gifts from other researchers. Table 2.1 provides details on those used in this study. Corresponding wildtype controls, Columbia-0 (Col-0) or Wassilewskija-0 (Ws-0), were also provided with each mutant line.

2.1.3 *Vicia faba* growth conditions

V. faba (broad bean) plants were grown in Scotts Levington F2 (Scotts) compost in a glasshouse with a 14 h day (90 mol m^{-2} s^{-1} at 18°C) and a 10 h night (15°C) photoperiod. Plants were grown in circular plastic pots (10 cm diameter, 8 cm depth) and covered in aluminium foil until germination had taken place. The plants were attached to stakes for support as they grew.

Table 2.1: Arabidopsis lines used in this study.

[a] Arabidopsis gene identification number. [b] Arabidopsis background ecotype.

Line	Gene ID [a]	Source	B/G [b]	Reference
35S:: GCAMP3	-	Masatsugu Toyota (University of Wisconsin, USA)	Col-0	Unpublished as of Sept 2016
35S::YCNano-65	-	Won-Gyu Choi (University of Wisconsin, USA)	Col-0	Choi et al. [7]
SUC2:: GCAMP3	-	Masatsugu Toyota (University of Wisconsin, USA)	Col-0	Unpublished as of Sept 2016
bak1-5	AT4G33430	Ben Schwessinger (The Sainsbury Lab, Norwich)	Col-0	Schwessinger et al. [548]
35S::dsGFP	-	David Prince (JIC, Norwich)	Col-0	Pitino et al. [549]
35s::dsMp10 2-5	-	David Prince (JIC, Norwich)	Col-0	Unpublished as of Sept 2016
35S::dsMp10 2-2	-	David Prince (JIC, Norwich)	Col-0	Unpublished as of Sept 2016
tpc1-2	AT4G03560	Dale Sanders (JIC, Norwich)	Col-0	Peiter et al. [15]
35S:: GCAMP3 x *tpc1-2*	AT4G03560	Masatsugu Toyota (University of Wisconsin, USA)	Col-0	Unpublished as of Sept 2016
35S::TPC1 5.6	AT4G03560	Dale Sanders (JIC, Norwich)	Col-0	Peiter et al. [15]
35S:: GCAMP3 x 35S::TPC1 5.6	AT4G03560	Masatsugu Toyota (University of Wisconsin, USA)	Col-0	Unpublished as of Sept 2016
35S::TPC1 10.21	AT4G03560	Dale Sanders (JIC, Norwich)	Col-0	Peiter et al. [15]
fou2	AT4G03560	Aurore Lenglet (University of Lausanne, CHE)	Col-0	Bonadventure et al. [550]
35S:: GCAMP3 x *fou2*	AT4G03560	Masatsugu Toyota (University of Wisconsin, USA)	Col-0	Unpublished as of Sept 2016

Line	Gene ID [a]	Source	B/G [b]	Reference
aos	AT5G42650	Aurore Lenglet (University of Lausanne, CHE)	Col-0	Park et al. [551]
fou2/aos	AT4G03560 AT5G42650	Aurore Lenglet (University of Lausanne, CHE)	Col-0	Bonadventure et al. [552]
glr3.3/ glr3.6	AT1G42540 AT3G51480	Edward Farmer (University of Lausanne, CHE)	Col-0	Mousavi et al. [103]
35S:: GCAMP3 *x glr3.3/ glr3.6*	AT1G42540 AT3G51480	Masatsugu Toyota (University of Wisconsin, USA)	Col-0	Unpublished as of Sept 2016
cipk3-1	AT2G26980	Girdhar Pandey (University of Delhi, IND)	Ws-0	Kim et al., [175]
cipk3-101	AT2G26980	SAIL Arabidopsis Library	Col-0	SAIL_449_B12
cipk3-102	AT2G26980	SALK Arabidopsis Library	Col-0	SALK_064491
cipk3-103	AT2G26980	SAIL Arabidopsis Library	Col-0	SAIL_409_A04 Tang et al. [165]
cipk3-104	AT2G26980	SALK Arabidopsis Library	Col-0	SALK_137779.25.20.X
abf2 (AK218)	AT1G45249	Soo Young Kim (Chonnam National University, KOR)	Col-0	Kim et al. [553]
pp2ca-1	AT3G11410	Julian Schroeder (University of California, San Diego, USA)	Col-0	Kuhn et al. [554]
cipk3/26	AT2G26980 AT5G21326	Renjie Tang (University of California, Berkeley, USA)	Col-0	Tang et al., [165]
cipk9/23	AT1G01140 AT1G30270	Renjie Tang (University of California, Berkeley, USA)	Col-0	Tang et al. [165]
cipk3/9/23/26	AT2G26980 AT1G01140 AT1G30270 AT5G21326	Renjie Tang (University of California, Berkeley, USA)	Col-0	Tang et al. [165]

2.2 Insect maintenance

2.2.1 *M. persicae* stock colony

A stock colony of *M. persicae* (clone US1L, Mark Stevens, Brooms Barn) [277], was reared continuously on Chinese cabbage (*Brasica rapa,* subspecies *chinensis*) in cages (52 cm x 52 cm x 50 cm) with a 16 h day (90 µmol $m^{-2} s^{-1}$ at 22ºC) and 8 h night (20ºC) photoperiod.

2.2.2 Aged *M. persicae*

For use in experiments *M. persicae* individuals of a set age were used. These were produced by placing 5-15 mixed instar adults from the stock colony onto four-week old Arabidopsis (Col-0) grown in a CER with a 16 h day (90 µmol $m^{-2} s^{-1}$ at 22°C) and 9 h night (20°C) photoperiod, in pots (13.5 cm diameter, 9 cm depth) and caged inside clear plastic tubing (10 cm x 15 cm) with a plastic lid. These adults were removed after 24-48 h, leaving nymphs of the same age. Once adult, these individuals were used in experiments (ages specified in experimental methods).

2.2.3 *A. pisum* stock colony

A stock colony of *A. pisum* (Rothamsted Research), was reared continuously on *V. faba* plants in cages (52 cm x 52 cm x 50 cm) with a photoperiod of 16 h day (90 µmol $m^{-2} s^{-1}$ at 23°C) and 8 h night (20°C).

2.2.4 Aged *A. pisum*

Aged *A. pisum* were used in experiments as detailed in Prince et al. [555]. Briefly, 50 adults from the stock colonies were transferred to new four-week old *V. faba* plants, grown at 22°C with a 16 h day (90 µmol $m^{-2} s^{-1}$) and 8 h night photoperiod, contained in plastic pots (10 cm diameter, 8 cm depth). After 24 h, these adults were removed leaving a population of aged nymphs. This population was returned to the CER and adults were used once they were 10 days old.

2.3 DNA methods

2.3.1 DNA extraction

For genotyping, leaf DNA was extracted from plants grown in either soil or on MS plates (as specified in section 2.1.1). Leaves were frozen in liquid nitrogen and ground using disposable pellet pestles (Sigma-Aldrich, St. Louis, MO, USA) in a 1.5 ml Eppendorf tube. DNA extraction was performed using the QIAGEN DNAeasy plant mini kit (Qiagen, Hilden, Germany) according to the manufacturer's instructions.

2.3.2 Genotyping PCR

Diagnostic genotyping polymerase chain reaction (PCR) was carried out in one of two ways:

i) GoTaq Green polymerase (Promega, Madison, WI, USA) was used in 25 µL reactions. Each reaction contained 0.2 µL GoTaq enzyme, 4 µL of GoTaq Green 4X buffer, 0.5 µL 10 mM dNTPs, 0.5 µL of each primer (10 µM), 2 µL $MgCl_2$, 12.3 µL distilled water and 5 µL of DNA (100 ng/µL). The primers used for genotyping are listed in Table 2.2. PCR was carried out in GS1 thermocycler (G-Storm, Somerton, UK) and the conditions used were as follows: 30 s at 96°C, followed by 35 cycles of 30 s at 96°C, 40 s at 54°C, 90 s at 72°C, and a final cycle of 5 min at 72°C. This genotyping was performed to validate the *TPC1*, *dsMp10*, *bak1-5* and *CIPK3* lines.

ii) Copy number analysis of the *CIPK3* transgenic lines created in this study was performed by iDNA Genetics (Norwich, UK) allowing identification of single copy T1 and homozygous T2 plants. This procedure used quantitative real-time PCR (qRT-PCR) to estimate the numbers of transgene copies in individual Arabidopsis plants, similar to the approach taken in *H. vulgare* by Bartlett et al. [556]. An amplicon from the hygromycin resistance gene (with a FAM reporter) and an amplicon from an Arabidopsis internal positive control (IPC, with a VIC reporter) were amplified together in a multiplex reaction (15 min denaturation, then 40 cycles of 15 s 95°C and 60 s 60°C) in an ABI7900 real-time thermocycler (Thermofisher Scientific, Loughborough, UK). Fluorescence from the FAM and VIC fluorochromes was measured during each 60°C step and the cycle threshold (C_t) values obtained. The difference between the C_t values for the hygromycin gene and the IPC (ΔC_t) was used to allocate the assayed samples into groups with the same gene copy number.

Table 2.2: Primers used for DNA genotyping

Gene name	Primer name	Sequence (5' – 3')	Source
BAK1	BAK1_dCAPS_F	AAGAGGGCTTGCGTATTTACATGATCAGT	Schwessinger et al. [548]
	BAK1_dCAPS_R	GAGGCGAGCAAGATCAAAAG	
Mp10	Mp10-GW-F	AAAAAGCAGGCTCCATGGCGCCGCAAAAAGATGCTGTG	Jorunn Bos (Hogenhout lab, JIC, UK)
	Mp10-GW-R	AGAAAGCTGGGTCTTAAAATTTGACAACACCTTTTTTC	
TPC1	AtTPCfwd	ATGGAAGACCCGTTGATTGGTAG	Furuichi et al. [111]
	AtTPC1rev	TTATGTGTCAGAAGTGGAACACTC	
-	LBb1.3	ATTTTGCCGATTTCGGAAC	Sam Mugford
-	SAIL LB2	GCTTCCTATTATATCTTCCCAAATTACCAATACA	Sam Mugford
CIPK3	cipk3-101sail F	CAGATTAGAAGAGAGATAGC	Sam Mugford
	cipk3-101sail R	AGGCAGACCTCAGGAGCAACG	
CIPK3	cipk3-102salk F	GGAGGACAGTTGAATTCACCAG	Sam Mugford
	cipk3-102salk R	AACAGCTTATACATGCTGTGGAC	
CIPK3	cipk3-103sail F	CAAGGACTCTGAGGTGTGGATAG	Sam Mugford
	cipk3-103sail R	CAAACCATCATCTCTGCTTAGCTC	
CIPK3	cipk3-104salk F	AGCGTGTAACACCGCAAGAGG	Sam Mugford
	cipk3-104salk R	CCTTTCGACTTCGATACTTGAACC	
GFP	eGFP F	TCTCGTTGGGGTCTTTGCTC	Giles Oldroyd Lab, JIC, UK
	eGFP R	GGCAAGCTGACCCTGAAGTT	

2.3.3 DNA sequencing

DNA sequencing was performed by Eurofins Genomics (Ebersberg, Germany) value read service. Primers used for sequencing are listed in Table 2.3.

Table 2.3: Primers used for DNA sequencing

Gene name	Primer name	Sequence (5' – 3')	Source
-	LBb1.3	ATTTTGCCGATTTCGGAAC	Sam Mugford
-	SAIL LB2	GCTTCCTATTATATCTTCCCAAATTACCAATACA	Sam Mugford
-	GoldenG seqF2	ACCAGAGTGTCGTGCTCCACCAT	Giles Oldroyd Lab, JIC, UK
-	GoldenG seqR2	GGCGGAGCCTATGGAAAAACGC	Giles Oldroyd Lab, JIC, UK
-	GoldenG seqF3	CGCAAGAATTCAAGCTTAGC	Giles Oldroyd Lab, JIC, UK
CIPK3	CIPK3 qPCR F1	GCGAATGAGATCATCGAGAAG	Thomas Vincent
CIPK3	CIPK3 LV1 CDSseq	CGAGAAGATAGAAGAAGCTGC	Thomas Vincent
CIPK3	CIPK3 101/2 RT F	GAAGAACAATTGGAGAAGGAAC	Thomas Vincent
CIPK3	CIPK3 F5	TGGCTGAACAGATTAGAAGAGAGATAG	Thomas Vincent
CIPK3	CIPK3 Seq Pro F	CGACCTCTGTCTCTTCGACTCTC	Thomas Vincent
CIPK3	CIPK3 Seq Term R	CACACAAAGTAGCCGGTAAAGC	Thomas Vincent
CIPK3	CIPK3 seq gen F1	GCAGGTGATGGCAAGTAAGACG	Thomas Vincent
CIPK3	CIPK3 seq gen F2	GGTTCTCAATGATAGAGGCTATGATG	Thomas Vincent
CIPK3	CIPK3 seq gen F3	GCGTGTAACACCGCAAGAGG	Thomas Vincent

2.4 RNA methods

2.4.1 RNA extraction

Leaf and aphid samples were frozen in liquid nitrogen and ground using disposable pellet pestles (Sigma-Aldrich) in a 1.5 ml Eppendorf tube. RNA was extracted using 1 ml Tri Reagent (Sigma-Aldrich) per 100 mg of tissue. 1-bromo 3-chloropropane (Sigma-Aldrich) and isopropanol (Sigma-Aldrich) were used to precipitate the RNA. RNA was then treated with the RQ1 DNase (Promega). RNA quality was assessed by agarose gel electrophoresis and concentration was measured on a NanoDrop 2000 spectrophotometer (ThermoFisher Scientific).

2.4.2 cDNA synthesis

cDNA was synthesised in 20 µL reactions with 100-500 ng mRNA using the M-MLV-RT Kit (Invitrogen, Carlsbad, CA, USA) with oligo-dT primers, performed according to the manufacturer's instructions.

2.4.3 RNAi silencing

For silencing of the aphid effector *Mp10*, aged nymphs (section 2.2.2) were cultured on dsMp10 and dsGFP plants [557] for 9-11 days. Silencing of *Mp10* was verified by qPCR with primers listed in Table 2.5 (Section 2.5.2).

2.5 Real Time PCR

2.5.1 RT-PCR

cDNA was diluted 1:10 for use in RT-PCR with GoTaq Green polymerase (Promega) in 25 µL reactions. Each reaction contained 4 µL of GoTaq Green 4X buffer, 0.5 µL 10mM dNTPs, 0.5 µL of each primer (10 µM), 2 µL $MgCl_2$, 0.2 µL GoTaq enzyme, 12.3 µL distilled water, and 5 µL of cDNA. The primers used for RT-PCR are listed in Table 2.4. The reactions were performed in GS thermocycler (G-Storm) using the following programme: 30 s at 96°C, followed by 35 cycles of 30 s at 96°C, 40 s at 54°C, 90 s at 72°C, and a final cycle of 5 min at 72°C.

Table 2.4: Primers used for RT-PCR

Gene name	Primer name	Sequence (5' – 3')	Source
TPC1	AtTPC1-F2	CTACCTTCATAACTCCAGACGAGAAT	Bonadventure et al. [550]
	AtTPC1-R2	AGCCAATTCGGTTTCAAAGAGCTTT	
CIPK3	CIPK3-101/2-RT F	GGAGAACCTGTTGCTCTCAAG	Thomas Vincent
	CIPK3-101/2-RT R	CCACACGATGTATGCAAGAGTCC	
CIPK3	CIPK3-103/4-RT F	AACATGGACGATATTGATGCTG	Thomas Vincent
	CIPK3-103/4-RT R	CTTGAACCATATGAAGACTTGGCGC	
CIPK3	103/104-DS F	GAGGCTTGAGAATGTGAAGGCTGG	Thomas Vincent
	103/104-DS R	CGTCCAGACTACTTGCTCC	
CIPK3	101/102-US F	GAAGAACAATTGGAGAAGGAAC	Thomas Vincent
	101/102-US R	CTCCTCCTGTAACATACTCC	
CIPK3	gCIPK3_Pand F	GGAGAACCTGTTGCTCTCAAGATTCTT	Pandey et al. [176]
	gCIPK3_Pand R	TTGAGGTTTCCATAGGAGTCCAATAG	
ACTIN2	ACTIN2-RTF	GGAAGGATCTGTACGGTAAC	Tang et al. [165]
	ACTIN2-RTR	GGACCTGCCTCATCATAC	

2.5.2 qRT-PCR

cDNA was diluted 1:10 for qRT-PCR for use with SYBR Green JumpStart Taq ReadyMix (Sigma-Aldrich) in 20 µL reactions on 96-well plates (white ABgene PCR plate – ThermoFisher Scientific). Each reaction consisted of the following: 10 µL SYBR Green master mix, 5 µL cDNA, 1 µL of each primer (10 µM) and 3 µL of distilled water. Primers used in qRT-PCR analysis are listed in Table 2.5. All reference gene primers used had been previously validated by others in the Hogenhout lab (JIC, specific sources in Table 2.5). Reactions were combined in one or more plates, with each biological sample and primer combination represented in every plate. Reactions were carried out in a C1000^{TM} Touch thermocycler (Biorad, Hercules, CA, USA). The following PCR programme was used: 3 min at 95°C, followed by 40 cycles of 30 s at 94°C, 30 s at 60°C, 30 s at 72°C, followed by one cycle of 30 s at 50°C, followed by melt curve analysis (65°C to 95°C, increments of 0.5°C) with a plate read throughout.

In order to calculate the expression of the genes of interest relative to the reference genes, the mean C_t value from 3-4 technical replicates of primer-sample pairs was converted into relative expression values according to the equation (efficiency of primer pair)$^{-\Delta Ct}$ [558]. Two reference genes were used per experiment, and within each biological sample the geometric mean of the reference gene C_t values was used to normalize between them [559]. The reference genes used in this study were as follows: *Actin* and *L-27* for *M. persicae* and *Actin* and *PEX4* for Arabidopsis (Table 2.5). Data was analysed using classical linear regression within a generalised linear model (GLM), assuming independent data points with a normal distribution and a linear relationship between the dependent and independent variables. Pairwise comparisons between treatments were conducted within this model using a t-test. Statistical analysis was conducted with Genstat v.18 (VSN International, Hemel Hempstead, UK). To display the data, mean expression values were rescaled such that the relative expression of the control group was equal to one.

Table 2.5: Primers used for qRT-PCR.

Mp = *M. persicae*, *At* = Arabidopsis.

Gene name	Primer name	Sequence (5' – 3')	Source
Mp10 (Mp)	Mp10 F	GGTCGGAGCGCCGCAAAAAG	David Prince (Hogenhout Lab)
	Mp10 R	TTGGAACCCAAAACTTGGTCGATGT	
Actin (Mp)	ACT2 F	GGTGTCTCACACACAGTGCC	Pitino et al. [549]
	ACT2 R	CGGCGGTGGTGGTGAAGCTG	
L-27 (Mp)	L-27 F	CCGAAAAGCTGTCATAATGAAGAC	Pitino et al. [549] and Coleman [560]
	L-27 R	CCGAAAAGCTGTCATAATGAAGAC	
FRK1 (At)	FRK1F	ATCTTCGCTTGGAGCTTCTC	Segonzac et al. [561]
	FRK1 R	TGCAGCGCAAGGACTAGAG	
CYP81F2 (At)	CP81F2 F	AATGGAGAGAGCAACACAATG	Kettles et al. [306]
	CP81F2 F	ATACTGAGCATGAGCCCTTTG	
PAD3 (At)	PAD3 F	TGCTCCCAAGACAGACAATG	Chassot et al. [562]
	PAD3 R	GTTTTGGATCACGACCCATC	
Actin (At)	ACT2 F	GATGAGGCAGGTCCAGGAATC	Czechowski et al. [563]
	ACT2 R	GTTTGTCACACACAAGTGCATC	
PEX4 (At)	PEX4 F	TGCAACCTCCTCAAGTTCG	Czechowski et al. [563]
	PEX4 R	CACAGACTGAAGCGTCCAAG	

2.6 Gene Synthesis and cloning

2.6.1 Gene synthesis

In order to generate the *CIPK3* transgenic lines used in Chapter 5, the coding regions, promoters and 3' UTRs were synthesised by the GeneART™ service from ThermoFisher Scientific. All synthesised modules were sequence-verified by the company. The sequence details for each of the modules can be found in Appendix A.

2.6.2 Site-directed mutagenesis

For the creation of the CIPK3 constitutive-activation lines (CIPK3T183D), site-directed mutagenesis was performed on the genomic copy of CIPK3, previously synthesised by ThermoFisher Scientific (section 2.6.1). This was performed using the QuikChange Lightning site-directed mutagenesis kit (Agilent Technologies, Santa Clara, CA, USA) according to the manufacturer's instructions. The primers used for this reaction can be found in Table 2.6. Successful mutagenesis was confirmed by extraction of DNA from positive *Escherichia coli* clones and sequencing using the CIPK3 F5 primer (Table 2.3)

Table 2.6: Primers used for site-directed mutagenesis

Gene name	Primer name	Sequence (5' – 3')	Source
CIPK3	CIPK3T183D F2	CTTGCATACATCGTGTGGTGACCCAAACTACGTT GCTCCTG	Thomas Vincent
	CIPK3T183D R2	CAGGAGCAACGTAGTTTGGGTCACCACACGATG TATGCAAG	

2.6.3 DNA sequencing

DNA sequencing was performed by Eurofins Genomics value read service. Primers used for sequencing are listed in Table 2.3.

2.6.4 GoldenGate cloning

The components synthesised in Section 2.6.1 (level 0 components) were combined into full genetic units (level 1 components – promoter, CDS, terminator) according to the Golden Gate DNA assembly protocol. This protocol uses single tube 15 µL reactions produce the level 1 units. Each reaction contained 100 ng of the level 1 vector backbone, 100 ng of each level 0 assembly piece, 100X Bovine Serum Albumin (New England Biolabs, Ipswich, MA, USA), Bsa1 (New England Biolabs) and NEB T4 Ligase and buffer (New England Biolabs). The assembly reaction was carried out in a GS1 thermocycler (G-Storm) using the following conditions: 3 min at 37°C and 4 min at 16°C (25 cycles), 5 min at 50°C, 5 min at 80°C [564]. These plasmids were cloned into *Escherichia coli* (section 2.6.5) and verified by sequencing (Section 2.3.3) with the following primers: CIPK3 LV1 CDseq and eGFP (Table 2.3)

The level 1 components were then cloned into the final level 2 constructs containing the plant selection marker *HYG* (hygromycin resistance gene) according to the same procedure as above, except BpiI (ThermoFisher Scientific) was also added to the reaction mixture. Again, these plasmids were cloned into *E. coli* (section 2.6.5) verified by sequencing (Section 2.3.3) using the following primers: GoldenG seqF2, GoldenG seqR2, GoldenG seq F3 (Table 2.3). Details on the golden gate modules and vectors used in this study can be found in Appendix B.

2.6.5 Cloning into *E. coli*

For cloning of constructs into *E. coli*, 2 µL of the assembly reaction from Section 2.6.4 was transformed into 20 µL of competent bacteria (strain DH5α, maintained in the Sanders/Miller lab) in a single tube using the following procedure: 20 min on ice, 30 s at 42°C and 2 min on ice. 0.5 ml of liquid Super Optimal Broth with Catabolite repression (SOC) medium [565] was then added and the reactions and left at 37°C for 1 h. They were then plated on Lysogeny broth (LB) [566, 567] agar

with the appropriate antibiotic. DNA from positive colonies was extracted using the PureYield™ plasmid miniprep system (Promega) used according to manufacturer's instructions, and verified by sequencing using combinations of the primers detailed in Section 2.3.3. The mutation required to generate the *CIPK3T183D* lines was verified with CIPK3 F5 (Table 2.3).

2.6.6 Electroporation of *Agrobacterium tumefaciens*

Electro-competent *Agrobacterium tumefaciens* (strain GV3101::pMP90, maintained in the Giles Oldroyd Lab, JIC, Norwich, UK) in 50 µL aliquots were thawed on ice, to which 1-5 µg of plasmid DNA was added. The mixture was transferred to a pre-chilled electroporation cuvette (Biorad) and incubated on ice for at least 5 min. Electroporation was then carried out using a Gene Pulser™ (Biorad) under the following conditions: capacitance: 25 µF, voltage: 2.4 kV, resistance: 200 Ohm, pulse length: 5 msec. Immediately after electroporation, 1 ml of SOC media was added to the cuvette and the mixture was transferred to a 15 ml falcon tube (StarLab, Hamburg, Germany) and incubated for 2 h at 28°C with vigorous agitation (250 rpm). The mixture was then plated on LB agar containing the appropriate antibiotic and incubated for 2-3 days at 28°C.

2.6.7 Colony PCR

Agrobacterium positive clones were verified by colony PCR through amplification of the gene of interest. This was performed in a thermocycler using GoTaq Green polymerase (Promega) in 20 µL reactions using under following conditions: 30 s at 96°C, followed by 35 cycles of 30 s at 96°C, 40 s at 54°C, 90 s at 72°C, and a final cycle of 5 min at 72°C. Each reaction contained 0.2 µL GoTaq enzyme, 4 µL of GoTaq Green 4X buffer, 0.5 µL 10 mM dNTPs, 0.5 µL of each primer, 2 µL MgCl2, and 12.3 µL distilled water. The primers used for colony PCR were CIPK3 qPCR F1 / GG seqR2 (Table 2.3) and eGFP F / eGFP R (Table 2.2). DNA from positive colonies was then extracted with the PureYield™ plasmid miniprep system (Promega) according to the manufacturer's instructions, and verified by sequencing using combinations of the primers detailed in Table 2.3 in Section 2.3.3.

2.6.8 Restriction Digestion

In addition to colony PCR and sequencing, DNA from the positive *Agrobacterium* colonies was verified by restriction digestion followed and visualisation by agarose gel electrophoresis containing 1% ethidium bromide. This was performed by incubating the constructs with EcoR1 and Xba1 or Pvu1 (Roche, Basel, Switzerland) at 37°C for 2-3 h.

2.7 Plant Transformation & Crossing

2.7.1 Floral dipping of Arabidopsis

Arabidopsis were grown in a long day CER at a constant temperature of 22°C with a 16 h day (Hydrargyrum quartz iodide (HQI) lighting), 8 h night photoperiod. The first bolt was clipped using sharp scissors to encourage a greater amount of flower production. Six days after clipping, Agrobacterium containing the construct of interest was grown in LB medium along with kanamycin (gene of interest plasmid marker), Rifampicin (agrobacterium marker) and gentamycin (Ti plasmid marker). 100 µM acetosyringone (Sigma Aldrich) was added and the culture was pelleted by centrifugation at 3700 g for 15 min. The pellet was then re-suspended in 250 ml of 5% (w/v) sucrose (ThermoFisher Scientific) and Silwett-L77 surfactant (De Sangosse, Cambridge, UK) was added at final concentration of 0.04% (v/v).

Before dipping, the flowering Arabidopsis were transferred to a containment glasshouse with 16 h daylight (supplemental lighting provided by 600 w sodium lamps). The aboveground parts of the plants, including all inflorescences, were submerged in the Agrobacterium solution for 10 s with gentle agitation. Plants were then placed in autoclave bags and covered by black plastic sheeting for 24 h. After this period, the plants were uncovered and grown in the glasshouse, with seeds from the transformed plants harvested two months later. Successful T1 transformants were identified by resistance to hygromycin (plant selection marker) when plated on ¼ strength MS (ingredients specified in section 2.1.1) and then transferred to soil in a glasshouse (16 h daylight, supplemental lighting provided by 600 w sodium lamps) over subsequent generations. T1 plants were assessed for single copies of the gene of interest and T2 plants were screened for homozygosity, using the iDNA genetics genotyping service (section 2.3.2).

2.7.2 Crossing Arabidopsis

Crossing was conducted with 4-week old Arabidopsis plants, grown in a CER at a constant temperature of 22°C with a 16 h day (HQI lighting), 8 h night photoperiod. Two unopened buds per stalk were selected and the remaining buds were removed. The sepals, petals and stamens were removed from the selected buds, leaving a single carpel. Stamens from the other crossing partner were dissected and pollen transfer between the two was achieved by brushing the stamen against the carpel of the selected mutant. Dissections were carried out with a pair of sharp tweezers. Pollinated carpels were covered in 74 mm x 41 mm paper bags (Global Polythene, Preston, UK), sealed with tape and allowed to mature.

After four weeks, seeds from these crosses were collected and plated on ¼ strength MS (ingredients specified in section 2.1.1) containing 50 µg/ml kanamycin on 100 mm^2 square plates (R & L Slaughter) in order to identify T1 mutants heterozygous for 35S::GCAMP3. These plants were then transferred to Scotts Levington F2 compost (Scotts), grown in a glasshouse (16 h daylight, supplemental lighting provided by 600 w sodium lamps) and left to self-fertilise.

T2 plants were grown in the same conditions as the T1 generation. Single leaves were dissected and DNA was extracted as outlined in section 2.3.1. Plants were genotyped for the presence of the mutation of interest (*bak1-5*) using the BAK1_dCAPS-F and BAK1_dCAPS_R primers (Table 2.2). The subsequent amplicon was then cut with the restriction enzyme Rsa1 (Roche) and the restriction pattern used to identify plants homozygous for *bak1-5* [548]. T3 plants homozygous for *bak1-5* were then plated on ¼ strength MS (ingredients specified in section 2.1.1) on 100 mm^2 square plates (R & L Slaughter) with 50 µg/ml kanamycin to assess the 35S::GCAMP3 copy number. Plants homozygous for 35S::GCAMP3 were screened under a Leica M205FA stereo microscope (Leica Microsystems, Milton Keynes, UK) to identify seedlings with strong GFP fluorescence. GFP was excited using a 450 nm – 490 nm metal halide lamp, and fluorescent emission was captured between 500 nm and 550 nm. From this screen, the 35S::GCAMP3 x *bak1-5* line with the greatest fluorescent yeild, homozygous for both genes, was selected for use in experiments.

2.8 Microscopy

2.8.1 Plant sample preparation

Arabidopsis expressing the Ca^{2+} sensor of choice were grown on MS plates as detailed in section 2.1.1. Leaves from these plants were then dissected using sharp scissors, and placed in wells of a clear 96-well Microtitre™ plate (ThermoFisher Scientific) with 300 µL of distilled water, abaxial surface facing up. These plates were then covered in clear plastic wrap (SC Johnson & Son, Racine, WI, USA) and aluminium foil (Wrap Film Systems, Telford, UK) and left at room temperature overnight to allow the stress of the wounding to subside. Microscopy was carried out using these leaves the following day.

2.8.2 Insect preparation

Aged *M. persicae* colonies were created as outlined in section 2.2.2 and were left to mature to adulthood for 8-10 days in an 8 h day (90 µmol $m^{-2} s^{-1}$ at 18°C) and 16 h night (16°C) photoperiod.

2.8.3 Fluorescence microscopy

Analysis of the FRET from the YCNano-65 construct [7] was conducted on a Zeiss Lumar V12 stereo microscope (Zeiss, Oberkochen, Germany). CFP was excited using a 426 nm – 446 nm metal halide lamp, and YFP was excited using a 490 nm – 510 nm metal halide lamp. Fluorescent emission was captured between 460 nm and 500 nm (CFP) and 520 nm and 550 nm (YFP). The exposure was kept at 8 s for all experiments, with images taken every 30 s. Leaves were imaged in pairs, under a magnification of 6.4 X. Cold water treatment was performed by adding 40 µL ice-cold water to the leaf, whilst aphid treatment involved the transfer of one adult aphid to the leaf. The second leaf of the pair was left untreated as a control. The wounding treatment was performed by crushing the leaf with a pair of forceps.

To visualise fluorescence from the 35S::GCAMP3 construct, a Leica M205FA stereo microscope (Leica Microsystems) was used. GFP was excited using a 450 nm – 490 nm metal halide lamp, and fluorescent emission was captured between 500 nm and 550 nm. The exposure was kept constant within experiments (between 1 and 2.5

s depending on the fluorescent yield of the mutant line) and images were captured every 5 s with a gain of 3.5 using Leica Application Suite v3.2.0 (Leica Microsystems). Leaves were imaged in groups of four, two leaves per genotype, at a 7.8 X magnification and a focus of -127.833 mm. One adult aphid was added to a leaf of each genotype, with the other leaf left un-infested as a control. Images were captured for 50-60 min after aphid application, with the 96-well plate covered in cling film to prevent aphid escape. Images were exported as Tagged Image File Format (TIFF) files for analysis. For cold water treatments, 40 µL ice-cold water was added to the leaf using a pipette (Gilson, Middleton, WI, USA) and wounding treatments were carried out using forceps.

2.8.4 Aphid behaviour analysis

Aphid settling behaviour was recorded for each sample by analysing the microscopy images, and this was used to assess if samples were to be included in the fluorescent signal analysis. Ca^{2+} signal analysis was performed for aphids during their first period of settling greater than 5 min in length. Settling was defined as the aphid remaining stationary in one place on the leaf. Samples in which the aphid never settled, or settled in a location that could not be imaged, were discarded. The length and timing of every aphid settle was recoded for all samples. Aphid settling behaviour was compared using a two-way Student's t-test between the treatments within Genstat v18 (VSN International).

2.8.5 Fluorescent signal analysis

For both 35S::YCNano-65 and 35S::GCAMP3, TIFF files were imported into Fiji (Image J) v1.48a (National Institutes of Health, USA) and converted into 32-bit images for fluorescent signal analysis. Fluorescence was analysed over time for various regions of interest (ROIs) using the Fiji plugin Time Series Analyser v2 (University of California, Los Angeles, CA, USA). For aphid treatments, circular ROIs with a 50 pixel (0.65 mm) diameter were selected in three locations; at the feeding site, on the midrib systemic to the aphid feeding site, and in the tissue besides the midrib ('lateral tissue'). These ROIs are demonstrated in Figure 2.1. For whole plant analysis, the ROIs are displayed in Figure 3.2 (Chapter 3). For cold water treatments, a ROI was drawn around the entire leaf.

To analyse the images, the raw florescence values (F) were exported into Microsoft Office Excel (Microsoft, Redmond, WA, USA) for further analysis. For 35S::YCNano-65, the FRET ratio (R) was calculated according as F^{CFP}/F^{YFP} [568]. For 35S::GCAMP3, normalised fluorescence values (ΔF/F) were calculated according to the equation $\Delta F/F = (F - F_0)/F_0$, where F_0 is the average baseline fluorescence calculated from the average of F over the first 60 frames of the recording before the aphid settled [219]. Samples in which the controls showed large Ca^{2+} bursts ($\Delta F/F > 0.2$) were discarded. Ca^{2+} signals were analysed using classical linear regression within a generalised linear model (GLM), assuming independent data points with a normal distribution and a linear relationship between the dependent and independent variables. Pairwise comparisons between treatments were conducted within this model using a t-test in Genstat v18 (VSN International).

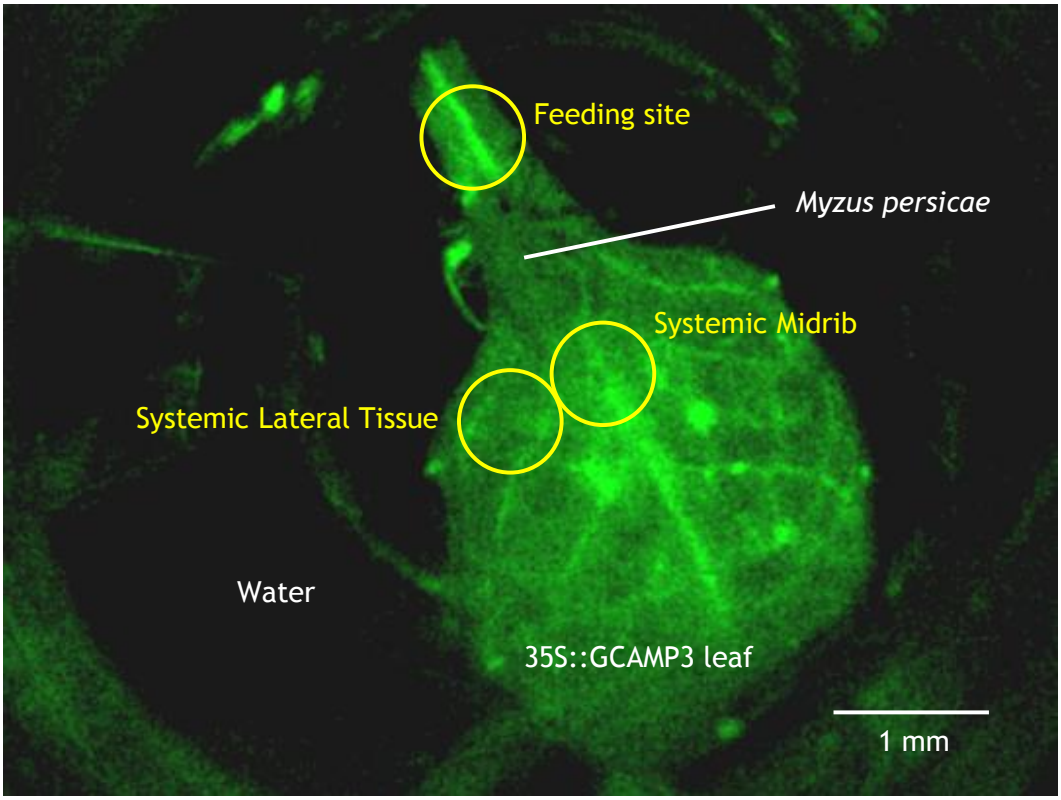

Figure 2.1: The ROIs used in the Ca^{2+} signal analysis.
Each ROI was 0.65 mm in diameter and placed relative to the head of the aphid.

The area of the aphid-induced Ca^{2+} burst was estimated using the Fiji freehand selection tool to draw around the maximum visible ('recordable' – R) burst and the area of this shape was calculated within Fiji. For analysis of the speed of the wave front, the Fiji plugin MTrackJ v 1.5.1 [569] was used. Representative videos of the aphid-induced Ca^{2+} bursts were created by converting the raw F values to heat maps using the NucMed_Image LUTs plugin for Fiji (J.A. Parker, IEEE.org). Time information was added using the Time Stamper plugin (W. Rasband, National Institutes of Health, USA). Area and seed data were analysed using a two-way t-test in Genstat v18 (VSN International), assuming a normal distribution, intendent data points, homogeneity of variance and a linear relationship between the dependent and independent variables.

2.9 Aphid performance assays

2.9.1 *M. persicae* fecundity assay

M. persicae fecundity was assessed as previously described by Pitino et al. [549]. The experiment was conducted with four-week old Arabidopsis grown in plastic pots (13 cm diameter, 10.5 cm depth) containing Scotts Levington F2 compost (Scotts, Ipswitch, UK) in a CER with a 8 h day (90 µmol m^{-2} s^{-1} at 18°C) and 16 h night (16°C) photoperiod. Five adult aphids from the stock colony (section 2.2.1) were added to each plant at the beginning of the experiment, and the plant was covered by Jetran Tubing (13 cm diameter, 10 cm tall - Bell Packaging, Luton, UK) capped with a white gauze-covered lid. After 48 h all adults were removed from these plants (day 0). After a further 72 h (day 3), any excess nymphs were removed, to leave five nymphs per plant. The number of offspring produced by these aphids was counted on day 11 and day 14 of the experiment, as was the final number of adult aphids. In order to assess fecundity, the number of offspring produced on day 11 and day 14 was summed per plant, and divided by the number of adults per plant. Six plants were used per treatment per experiment, and all experiments were repeated at least three times. Statistical analysis was performed in Genstat v18 (VSN International) using a classical linear regression within a GLM. The model took into account the experimental replicates as an additional factor, assuming independent data points with a Poisson distribution.

2.9.2 *M. persicae trans-generational fecundity assay*

The experiment was conducted with four four-week old Arabidopsis, potted together in black plastic trays (30cm x 45cm x 5cm) containing Scotts Levington F2 compost (Scotts, Ipswitch, UK) in a CER with an 8 h day (90 µmol $m^{-2} s^{-1}$ at 18°C) and 16 h night (16°C) photoperiod. A single 24 h-old nymph was added to each plant. The total number of offspring was then counted after four weeks. Four plants were used per treatment per experiment, and all experiments were repeated at least three times. Statistical analysis was performed in Genstat v18 (VSN International) using a classical linear regression within a GLM. The model took into account the experimental replicates as an additional factor, assuming independent data points with a Poisson distribution. Pairwise comparisons between treatments were conducted with a t-test within this model. This protocol was modified from Coleman et al. [560].

2.9.3 *M. persicae* choice assay

Two four-week old Arabidopsis plants were placed in Scotts Levington F2 soil (Scotts, Ipswich, UK) together in a plastic pot (13.5 cm diameter, 9 cm depth). A 50 mm diameter petri dish (R & L Slaughter) was placed between the two plants, and 30 randomly-selected adults from the stock colony (section 2.2.1) were added to this dish. The plants were then covered in plastic tubing (section 2.9.1) and placed in a CER with an 8 h day (90 µmol $m^{-2} s^{-1}$ at 18°C) and 16 h night (16°C) photoperiod. After 24 h, the number of adult aphids settled on each plant was assessed. Statistical analysis was performed in Genstat v18 (VSN International) using a pairwise Student's t-test assuming a normal distribution of variances and independent data points.

2.9.4 *M. persicae* induced resistance assay

Arabidopsis induced resistance (IR) to *M. persicae* was assessed by an assay modified from De Vos and Jander [464] using live aphids. The experiment was conducted with four-week old Arabidopsis plants in plastic pots (base 3.5 x 3.5 cm, top 5.5 x 5.5 cm, height 5.5 cm) grown in a CER with an 8 h day (90 µmol $m^{-2} s^{-1}$ at 18°C) and 16 h night (16°C) photoperiod. From the stock colony 50 mixed instar aphids (section 2.2.1) were then added to the first fully-expanded leaf of the plant

and confined within a clip cage (Figure 2.2). These aphids acted as a pre-treatment to induce Arabidopsis defence. As a control treatment an empty clip cage was used. Aphids were then removed 24 h later. An 11-day old aphid (section 2.2.2) was then added to the leaf inside a clip cage. After 10 days, the number of nymphs produced by this aphid was counted. For systemic induced resistance experiments, leaves were numbered from oldest to youngest, and the adult aphid was added to leaf n+5, where n = the leaf used for pre-treatment [103]. All experiments were repeated at least three times. Statistical analysis was performed in Genstat v18 (VSN International) using a classical linear regression within a GLM. The model took into account the experimental replicates as an additional factor, assuming independent data points with a Poisson distribution. Pairwise comparisons between treatments were conducted with a t-test within this model.

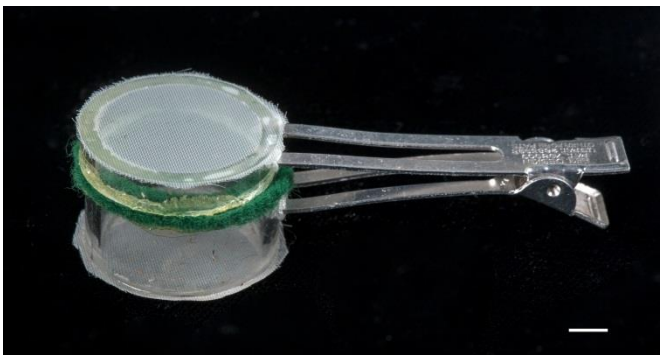

Figure 2.2: A clip cage.
Composed of a metal double prong hair clip (50 mm long), two pieces of plastic tube (10 and 5 mm high, 2 mm thick, 25 mm diameter), two circles of felt (25 mm diameter, 4 mm across, 1 mm thick), and two pieces of fine gauze (25 mm diameter). Scale bar = 5 mm. Figure taken from Prince et al [555].

2.9.5 *A. pisum* survival assay

Survival assays with *A. pisum* were carried out as described in Prince et al. [555]. The experiment was performed with 7-week old Arabidopsis in plastic pots (base 3.5 x 3.5 cm, top 5.5 x 5.5 cm, height 5.5 cm) in a CER with an 8 h day (90 µmol m^{-2} s^{-1} at 18°C) and 16 h night (16°C) photoperiod. Five 10-day old aphids (section 2.2.4) were added to the youngest fully expanded leaf, contained within a clip cage. The number alive adults (visible movement) was counted on two to seven days post-treatment. When aphid survival on the wildtype plants reached 50 %, the

percentage survival on all genotypes was averaged over the two days either side of this cut-off. Statistical analysis was performed in Genstat v18 (VSN International) using a classical linear regression within a GLM. The model took into account the experimental replicates as an additional factor, assuming independent data points with a Poisson distribution. Pairwise comparisons between treatments were conducted with a t-test within this model.

2.9.6 Whole plant EPG

EPG experiments were conducted as described by Tjallingi [263]. Adult 13-15 day old *M. persicae* (section 2.2.2) were starved in a sealed petri dish for one h prior to the start of the experiment. These aphids were then attached to the Giga-8 EPG system (EPG Systems, Wageningen, Netherlands) using 12.5 µm gold wire (EPG Systems) and silver glue (EPG Systems) and then placed on 4-week old Arabidopsis. The plants were kept in plastic pots (base 3.5 x 3.5 cm, top 5.5 x 5.5 cm, height 5.5 cm) for the entire experiment. The experiment was contained inside a Faraday cage to minimise electrical interference. Feeding behaviour was recorded for 8 h using Stylet+d (EPG Systems). Each EPG track was then analysed blind in Stylet+a (EPG Systems) to annotate different feeding behaviour types and durations. The timing of aphid settling relative to the beginning of probing was also documented. Relevant EPG parameters were calculated using the Microsoft Excel spreadsheet developed by Dr Edgar Schliephake (Julius Kuhn Institute, Germany) [570]. Comparisons of behaviours between treatments were performed using a Mann-Whitney U test in R v3.0 (Free Software Foundation, Boston, MA, USA) assuming equal distributions of independent data points.

2.9.7 Single leaf EPG

Single-leaf EPG was performed using a modified version of the set-up described in section 2.9.6. Leaves were taken from plate-grown plants, grown as detailed in section 2.1.1 and floated in 300 µL of water in 96-well plates as described in section 2.8.1. A small piece of copper wire was attached to the EPG ground electrode, and this was inserted into the well (Figure 2.3). Nine to eleven-day old *M. persicae* were then added to these leaves and the experiment was conducted and analysed as outlined in section 2.9.6 above.

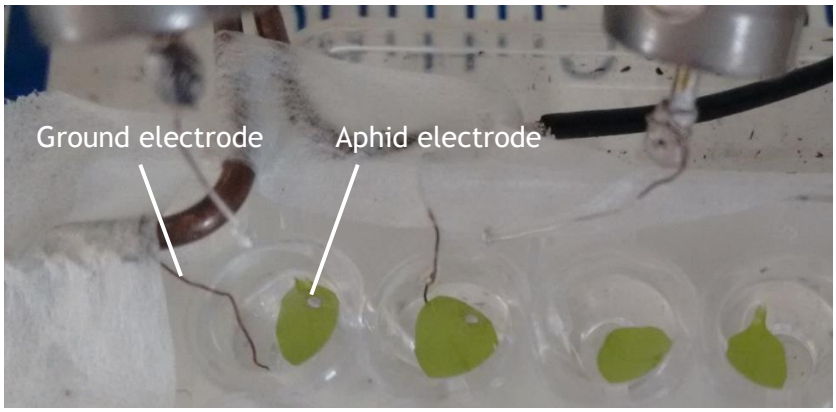

Figure 2.3: Single leaf EPG.
Arabidopsis leaves were floated in 300 µL of water with a single aphid connected to the circuit by gold wire and silver glue (aphid electrode). The Copper wire functioned as a ground electrode, submerged in the water. Photo credit: P.H.

2.10 Arabidopsis assays

2.10.1 Aphid extract collection

Aphid extract was prepared from mixed instar stock colony aphids (Section 2.2.1). Aphids were snap frozen in liquid nitrogen and ground to a fine powder using a mortar and pestle. This powder was then re-suspended in distilled water at a concentration of 5 mg/ml.

2.10.2 ROS assay

Leaf disks were taken from the two youngest fully-expanded leaves of 4-week old Arabidopsis using a cork borer (diameter: 4 mm), and floated in 200 µL of distilled water overnight in white 96-well plates (Grenier Bio-One, Kremsmünster, Austria). Eight leaf disks were used per treatment per experiment. Before beginning the experiment, the water was removed from the wells and replaced with 100 µL of the assay solution. This solution was composed of the following: 100 µg/ml horseradish peroxidase (HRP) (Sigma-Aldritch) and 21 nM of the luminol probe L-012 (8-amino-5-chloro-7- phenylpyrido [3,4-d] pyridazine-1,4(2H,3H) dione) (Wako, Osaka, Japan) [571], alongside 5 mg/ml aphid extract. Control assay solutions

contained distilled water instead of aphid extract. After addition of the assay solution, the 96-well plate was placed under a Photek camera (Photek, St Leonards on Sea, UK) to record the luminescence generated by the reaction between H_2O_2 and L-012 [406] catalysed by HRP [349]. Luminescence data were extracted using the Photek built-in software and analysed in Microsoft Excel (Microsoft). Statistical analysis was performed in Genstat v18 (VSN International) using a classical linear regression within a GLM taking into account the experimental replicates as an additional factor, assuming independent data points with a normal distribution and a linear relationship between the dependent and independent variables. Pairwise comparisons between treatments were conducted within this model using a t-test in Genstat v18 (VSN International).

2.10.3 Defence gene induction assay

Leaf disks were taken from the two youngest fully-expended leaves of 4-week old plants using a cork borer (diameter: 4 mm), and floated in 200 µL of distilled water overnight in white 96-well plates (Grenier Bio-One). Before beginning the experiment, the water was removed from the wells and replaced with 100 µL of aphid extract (5 mg/ml) or water as a control for 1 h. Eight leaf disks were pooled for each biological replicate. RNA extraction (Section 2.4.1), cDNA synthesis (Section 2.4.2) and qRT-PCR (Section 2.5.2) were then carried out on these samples. Statistical analysis was performed in Genstat v18 (VSN International) using a classical linear regression within a GLM taking into account the experimental replicates as an additional factor, assuming independent data points with a normal distribution and a linear relationship between the dependent and independent variables. Pairwise comparisons between treatments were conducted within this model using a t-test in Genstat v18 (VSN International).

2.10.4 Germination assay

To assess seedling germination, Arabidopsis seeds were grown on ¼ strength MS media (ingredients specified in section 2.1.1) in 100 mm^2 square plates (R & L Slaughter), 100 seeds per plate. For treatment plates, 150 mM NaCl was added to the media. The plates were then vernalised for four days in the dark (8°C), before being moved to a CER with a constant temperature of 23°C with a 16 h day and 8 h night

photoperiod. Three days after transfer to 23°C, the number of germinated seedlings, defined by emergence of the radical, was assessed using a light microscope (Leica Microsystems). Statistical analysis was performed in Genstat v18 (VSN International) using a classical linear regression within a GLM taking into account the experimental replicates as an additional factor, assuming independent data points with a normal distribution and a linear relationship between the dependent and independent variables. Pairwise comparisons between treatments were conducted within this model using a t-test in Genstat v18 (VSN International).

2.11 RNA-seq

2.11.1 Sample preparation

Four-week old Col-0 Arabidopsis were grown in pots as detailed in section 2.1.1 and then transferred to a new CER for the experiment with an 8 h day (90 µmol $m^{-2} s^{-1}$), 16 h night photoperiod at a constant temperature of 22°C. Two leaves from each plant were then placed in a clip cage (Figure 2.2) containing either 10 mixed instar adult *M. persicae* individuals (section 2.2.1), or 10 mixed instar adult *A. pisum* individuals (section 2.2.3). Insects were left on the plants for 48 h before being removed and the leaves frozen in liquid nitrogen. Five plants were treated with each insect, with 2 clip cages per plant.

RNA was extracted from the leaves contained within each clip cage using Trizol (section 2.4.1), and purified using Qiagen RNeasy with on column DNAse digestion (Qiagen). Illumina Truseq libraries were prepared from 1 ug RNA according to the manufacturer's protocol (Illumina, San Diego, CA, USA), and sequenced on a HiSeq 2000 (Illumina), with 4 barcoded libraries pooled per lane.

2.11.2 Sample analysis

Samples were mapped to the TAIR10 transcriptome (TAIR10_cdna_20101214_updated.fa) using the bowtie software [572]. Counts for each transcript were then calculated using RSEM [573]. Differential expression was computed using DEseq [574]. DEseq was used to determine significant differences in expression between treatments, with a cut-off of a 2-fold expression change together with a 5% false discovery rate (adjusted p-value, padj <0.05).

Chapter 3: *M. persicae* elicits rapid *BAK1*-dependent Ca^{2+} bursts in Arabidopsis

3.1 Introduction

3.1.1 YCNano-65 and GCAMP3 are highly-optimised tools for measuring Ca^{2+}

Ca^{2+} sensors such as FRET cameleons and single-FP sensors revolutionised the analysis of Ca^{2+} dynamics. Cameleons are dual fluorophore molecules where the binding of Ca^{2+} results in FRET between the fluorophores (Section 1.1.7, Chapter 1). Blue fluorescent protein (BFP) was originally used as the donor fluorophore; however this was soon replaced by CFP as a result of issues with low light production and instability in living cells [204]. Further optimisation of cameleons resulted in sensors less affected by cellular pH [575, 576] and a 5-fold increase in signal strength through the use of circularly permutated YFP [205, 577, 578]. In addition, redesigning the CaM-M13 binding interface to make it more specific for Ca^{2+}, as well as to reduce interference by endogenous CaM has also significantly improved cameleons. [579, 580].

Single-FP sensors are based on the discovery that specific insertions of Ca^{2+}-binding cassettes into GFP does not abolish florescence [578]. This allowed a CaM/M13 insertion in GFP to create the GCAMP range of sensors [209]. Upon Ca^{2+} binding, the CaM-M13 interaction results in ionisation of GFP and a change in fluorescence [211] (Section 1.1.7, Chapter 1). Such sensors typically display much greater signal strengths than cameleons and collecting data from a single fluorophore offers several technical advantages, including increased temporal resolution and simpler experimental design [212]. These attributes make single-FP sensors well-suited for recording dynamic measurements.

One important attribute of Ca^{2+} sensors is their dynamic range; the ratio between the minimum and maximum fluorescence. Whilst single-FP sensors have a dramatically increased dynamic range relative to traditional cameleons such as YC3.6, more recent cameleons such as YCNano-65 are comparable to GCAMPs (Table 3.1). Furthermore, YCNano-65 has a lower K_d, meaning that it can produce a measureable fluorescent output at a lower $[Ca^{2+}]$ [195, 206, 216]. As such, YCNano-65 is more sensitive to $[Ca^{2+}]$ (Table 3.1). Conversely, GCAMP3 offers superior responsiveness to changes in $[Ca^{2+}]$. This is because GCAMP3 boasts a higher Hill

coefficient, a measure of the cooperativity of binding each subsequent Ca^{2+}, and dissociation of Ca^{2+} from the sensor is much more rapid [195, 206, 216] (Table 3.1).

Table 3.1 Properties of some popular genetically-encoded Ca^{2+} sensors.

[a] D = dynamic range, ratio between the minimum and maximum fluorescence. [b] n = the Hill coefficient, the degree of cooperativity of binding of each subsequent Ca^{2+} ion. [c] T= time taken for one Ca^{2+} ion to dissociate from the sensor and at room temperature. [d] $[Ca^{2+}]$ = the $[Ca^{2+}]$ range that the sensor can report as a result of its inherent properties. Data taken from Koldenkova & Nagai [195].

Sensor	D[a]	K_d (μM)	n[b]	T (ms)[c]	$[Ca^{2+}]$[d]
AEQ	-	2.6-13	-	700	μM
YC3.6	6.6	0.22-0.78	1.7-3.6	2940	>100 nM
YCNano-65	14	0.06 – 1.4	1.6-1.8	3030	>10 nM
GCAMP3	12.3	0.41-0.5	2.1-2.7	700	>100 nM

3.1.2 Ca^{2+} signalling is important during plant-aphid interactions

$[Ca^{2+}]_{cyt}$ elevations are one of the first PTI-mediated responses to pathogen attack [200, 201, 219, 371, 509, 581, 582] (Section 1.3.3, Chapter 1) and several lines of evidence suggest that Ca^{2+} signalling is also relevant in plant-aphid interactions. Firstly, aphid extract and GroEL from the aphid symbiont *B. aphidicola* can induce ROS production [277, 349, 350]. Ca^{2+} lies upstream of this ROS, since the Ca^{2+} chelator EDTA significantly attenuates aphid extract-induced ROS production [502]. Furthermore, the aphid extract-induced ROS burst is dependent on *RBOHD* [349], a crosstalk node between ROS and Ca^{2+} signalling [119, 121].

Secondly, the vast majority of transcriptomic studies performed with aphids reveal a significant over-representation of Ca^{2+} signalling-related transcripts, most of which display upregulation (reviewed in [583]). In response to *M. persicae*, several of these genes are differentially regulated in Arabidopsis around 6 to 24 h post-infestation. These gene products include five ACAs, five CDPKs and several EF-hand containing proteins [442]. Furthermore, Jaouannet et al. [283] found that *M. persicae* induces differential regulation of several uncharacterised EF-hand containing proteins at 24 h post-infestation. Examples from other plant-aphid interactions include *M. euphorbiae* that induces several Ca^{2+}-related genes in *S. lycopersicum* [433 293], *A. glycines* that induces a 1.5-fold increase in several

Glycine max (soybean) CDPKs [402] and *B. brassicae* that upregulates several Arabidopsis Ca^{2+} channels, transporters and decoders within 6 h of feeding [304].

The third line of evidence comes from direct measurements of $[Ca^{2+}]$ using Ca^{2+} sensors. Feeding by lepidopteran larvae results in $[Ca^{2+}]_{cyt}$ increases measurable by Ca^{2+} dyes [369, 540], AEQ [123, 369, 370, 407], and YC3.6 [376]. It should be noted that chewing insects cause much larger amounts of cellular damage than *M. persicae*, and therefore the aphid-induced $[Ca^{2+}]_{cyt}$ elevation is likely to exhibit distinct characteristics. Ren et al. [584] used Ca^{2+}-selective microelectrodes to measure a significant Ca^{2+} flux out of the extracellular space into *Nicotiana tabacum* (tobacco) mesophyll cells after 2 h, 15 h and 5 d of incubation with *M. persicae*. In addition, both *M. persicae* and *S. littoralis* induce PM depolarisations when feeding [365, 369, 407], although these depolarisations appear to be independent of $[Ca^{2+}]$ elevations and based on K^+ channel activity [540]. Nevertheless, $[Ca^{2+}]_{cyt}$ elevations may be associated with changes in V_m, as seen in guard cells [48] and in response to lepidopteran herbivory [104, 369].

3.1.3 Phloem occlusion is Ca^{2+}-dependent

The phloem, specifically the SEs, acts as the main conduit for metabolite transport in the plant [285-287]. The SEs are also the location from which aphids establish long-term feeding [220, 284, 585]. Upon wounding, the flow of photo-assimilates in the phloem is blocked to prevent the loss of phloem sap and the invasion of pathogens, a process termed occlusion [287, 456, 586, 587]. In order for this feeding to be successful, aphids must overcome SE occlusion.

Occlusion is mediated by two mechanisms, including the formation of proteinaceous plugs by P-proteins [288, 291, 588, 589] and callose production [289, 295, 590, 591], both of which are suggested to be Ca^{2+}-regulated. Callose synthesis is regulated by Ca^{2+} in Arabidopsis, *N. tabacum* and *G. max* cells [293, 592, 593]. However, this was not observed in *Daucus carota* (carrot), where Ca^{2+} chelators have no effect on callose synthesis [294]. The Fabaceae have a unique set of P-proteins called forisomes, the dispersal of which plugs the sieve plates [290, 291]. Forisomes disperse upon Ca^{2+} application, the threshold for which is around 50 µM Ca^{2+}, and this leads to occlusion [291, 594, 595]. However, the average $[Ca^{2+}]$ in *V. faba* SEs during a Ca^{2+} burst is less than 1 µM, which means forisome dispersal is probably only

activated in Ca^{2+} hotspots [596] such as around clusters of Ca^{2+}-permeable channels [595].

Occlusion can also be triggered by electrical signals within the plant, and these signals are associated with the influx of Ca^{2+} [596]. It has been suggested that Ca^{2+} mediates occlusion during the propagation of electrical waves, however this conclusion was inferred using forisome dispersal as a proxy for [Ca^{2+}] changes [597]. In addition, Ca^{2+} regulation of P-proteins outside the Fabaceae is lacking [296]. Nevertheless, there is a clear link between Ca^{2+} and the mechanisms that underlie occlusion.

3.1.4 Prevention of occlusion during aphid feeding may involve Ca^{2+}

A thin glass capillary comparable in size to an aphid stylet can induce occlusion [287]. This suggests that in order to feed successfully, aphids may inhibit occlusion. Indeed, in the *A. pisum-V. faba* model system aphid feeding does not induce forisome dispersal [598]. Moreover, leaf burning induces occlusion and alters aphid feeding behaviour [599, 600]. However, a direct link between occlusion and feeding was not established, with the change in aphid behaviour potentially a result of the activation of other plant defences.

It has been proposed that aphids alter [Ca^{2+}] in SEs in order to prevent occlusion (Figure 3.1). Application of aphid watery saliva to forisomes results in a contraction comparable to that seen with the Ca^{2+} chelator EDTA, indicating that aphid saliva may be chelating Ca^{2+} in order to prevent occlusion [599]. Indeed, watery saliva contains Ca^{2+}-binding proteins [273, 599, 601] and is thought to be secreted into plant cells during the E1 phase of phloem feeding [270, 284] (Figure 3.1). Furthermore, free Ca^{2+} is depleted in artificial diets whilst aphids feed (Freddy Tjallingii, EPG Systems, personal communication). However, no demonstration of Ca^{2+} binding or depletion *in planta* has yet been provided. It has also been suggested that aphid sheath saliva contributes to blocking Ca^{2+} entry by preventing Ca^{2+} leakage into cells during stylet punctures (Figure 3.1) [296], although again *in vivo* evidence of this has not been forthcoming.

Adding further doubt to the role of aphid saliva in suppressing occlusion is the recent finding that aphid treatment does not reverse phloem plugging *in vivo*, despite a close proximity between the aphid stylets and forisomes [598, 602].

Furthermore, the loss of key proteins required for p-protein plugging in Arabidopsis did not significantly alter *M. persicae* fecundity [588]. Indeed, the role of occlusion itself may be more complex than previously thought, with confocal microscopy revealing that aggregations of P-proteins do not necessarily alter phloem translocation [603].

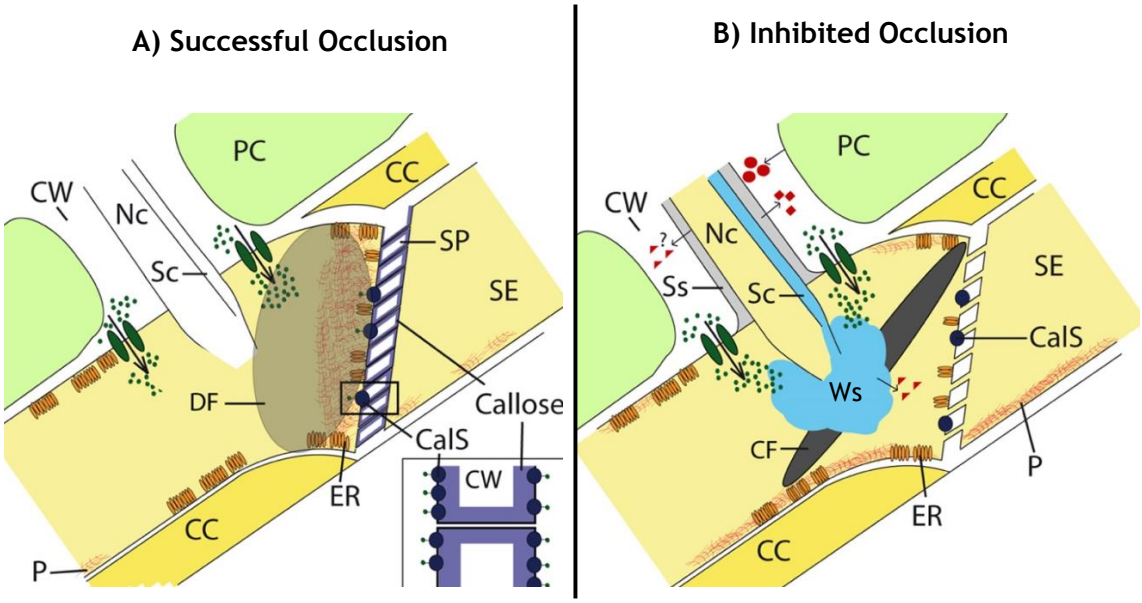

Figure 3.1: Aphids avoid phloem occlusion, possibly through inhibition of plant Ca^{2+}.
A) Successful occlusion is a result of P-protein plugging (P – red) and dispersal of forisomes (DF, grey) near the sieve pore (SP) of SEs. Occlusion also involves callose deposition (purple, inset) by the enzyme callose synthase (CalS). Occlusion should be induced by penetration of the SE by the aphid stylet (white), which is hypothesised to result in Ca^{2+} influx from the apoplast through Ca^{2+} channels (green). **B)** The secretion of sheath saliva (Ss – grey) and watery saliva (Ws – blue) through the salivary canal (Sc) is hypothesised to block Ca^{2+}-mediated occlusion, inhibiting P-proteins, condensing forisomes (CF) and preventing callose deposition. Aphid effectors (red squares) also suppress plant defence that is activated by perception of HAMPs (red triangles) and DAMPs (red circles). CC = companion cell. CW = cell wall, Nc = nutrition channel. Adapted from Will et al. [604].

3.1.5 SAR in plant-aphid interactions

The induction of systemic defence during pathogen attack, SAR, is well documented (Section 1.3.6, Chapter 1) [534, 605]. Ca^{2+} is implicated in SAR, with Ca^{2+} acting as a systemic signal between leaves during wounding and lepidopteran feeding [123]. Moreover, systemic signalling in response to flg22 is mediated by CPK5 [119]. The phloem acts as the primary conduit of systemic electrical and Ca^{2+} signals [103, 123, 606, 607], and thus it is reasonable to suggest aphids may trigger SAR.

Infestation of *Apium graveolens* (celery) with *M. persicae* results in the differential regulation of various phloem transcripts [608] and *M. persicae* infestation of Arabidopsis results in the differential regulation of transcripts in systemic leaves from 6 to 24 h post-infestation, including Ca^{2+} transporters and Ca^{2+} binding proteins [442]. Feeding by *M. persicae* also induces the local and systemic production of SA [609], a key mediator of SAR.

Supporting a role for SAR in plant-aphid interactions, *B. brassicae* feeding on *Brassica oleracea* (broccoli) exhibited less probing and phloem feeding after pre-treatment with aphids on systemic leaves [610]. *M. persicae* feeding was also negatively affected by systemic aphid pre-treatment of *Solanum tuberosum* (potato) [611], although this study also found enhancement of feeding locally, contrary to the negative impacts of local infestation seen with other studies [349, 464, 502]. Furthermore, SAR induced by *P. fluorescens* negatively affects *M. persicae* fecundity [612].

However, evidence supporting a significant role for SAR in defence against aphids is still lacking. Pre-treatment of leaves with *M. persicae* leads to a significant reduction in performance of aphids that subsequently feed from these leaves, a phenomenon known as induced resistance (IR) [464]. However, *M. persicae* pre-treatment does not appear to result in IR in systemic leaves of Arabidopsis [464] and the potential role of SAR in plant-aphid interactions is still unclear.

3.1.6 *M. persicae* induces plant defence through a BAK1-mediated pathway

BAK1 is a defence co-receptor that is required for full FLS2- and EFR-mediated PTI against bacterial pathogens [360, 361] (Section 1.3.2). In Arabidopsis, BAK1 positively regulates both ROS production and MAPK activity during this response [351]. Upon perception of flg22, BAK1 forms a complex with the PAMP-binding receptor FLS2 [360], and this results in the phosphorylation of BOTRYTIS-INDUCED KINASE1 (BIK1), a protein essential for the transduction of the PTI signal [613] and PAMP-induced $[Ca^{2+}]_{cyt}$ elevations [614].

BAK1 also mediates the defence response to chewing insects. Loss of BAK1 significantly decreases JA accumulation in response to *M. sexta* chewing, however this is independent of MAPK or SA involvement [424]. This suggests that although BAK1 functions as a common defence signalling component, there is a degree of specificity in the response to different threats. In addition, the *S. lycopersicum* homologue of BIK1 acts as a positive regulator of defence against *M. sexta*, with RNAi knock-down of the gene significantly increasing plant susceptibility [615]. However these results may be confounded by pleiotropic growth phenotypes associated with silencing *BAK1* [616] and to a lesser extent *BIK1* [617].

Multiple lines of evidence now suggest aphid-induced PTI is BAK1-dependent. *M. persicae*-induced ROS production, callose deposition and IR are all compromised in *bak1-5* mutants [349, 502]. The putative HAMP GroEL also stimulates these responses in a BAK1-dependent manner [350]. Interestingly, *FLS2* is not required for aphid-induced PTI [349], and as such the PRR that pairs with BAK1 in plant-aphid interactions remains elusive. Furthermore, loss of *BIK1* negatively affects *M. persicae* performance, implying it is a negative regulator of defence during this interaction [618], the opposite of that observed in plant-pathogen systems. Consequently, *M. persicae* induces many of the same PTI components as bacterial pathogens, however there are clear differences between the two, with many of the components involved in the aphid response yet to be identified.

3.1.7 *M. persicae* uses the effector Mp10 to suppress BAK1-mediated plant defence

Pathogens use effector molecules to suppress PTI, as do aphids (Section 1.3.5, Chapter 1). These effectors are secreted into the plant in the aphid watery saliva [272, 273] and thus they are introduced into plant tissues during the early stages of feeding [619]. The first identified aphid effector was C002 from *A. pisum*, which is secreted into the plant and is required for aphid survival and successful feeding [276, 500]. This effector is also present in *M. persicae* (MpC002), with overexpression of *MpC002* enhancing fecundity [277, 501] and reducing expression having the opposite effect [549, 560].

In addition to MpC002, Mp10 has also been identified as a putative *M. persicae* effector. *Mp10* is expressed in the salivary gland of *M. persicae* and heterologous overexpression of *Mp10* in *N. benthamiana* blocks flg22-induced ROS production, implying a role in suppressing plant defence [277]. Interestingly, this overexpression also reduces aphid fecundity, possibly as a result of ETI activation [277]. Further confirmation of Mp10's role as an effector comes from evidence showing that it can suppress aphid extract-induced ROS production in *N. benthamiana* and that it promotes aphid colonisation of Arabidopsis [502]. In addition, reducing *Mp10* expression through plant-mediated RNAi significantly reduces aphid fecundity. This phenotype is not observed on *bak1-5* mutants, suggesting Mp10 acts through the suppression of BAK1-mediated signalling [502]. Furthermore, Mp10 appears to have a role in the suppression of Ca^{2+}, as heterologous expression in *N. benthamiana* results in the suppression of flg22-induced Ca^{2+} bursts, as measured with AEQ [502]. Finally, immunogold labelling studies detected Mp10 inside the cytoplasm of mesophyll cells adjacent to the aphid stylets, but not systemically from the feeding site [279]. Thus, Mp10 may have a role in the suppression of plant defence responses early in the aphid feeding process during the pathway phase.

3.1.8 Aims of this chapter

This chapter describes work investigating the role of Ca^{2+} in plant-aphid interactions using the fluorescent sensor GCAMP3. A fluorescence microscopy approach was developed to measure $[Ca^{2+}]_{cyt}$ *in vivo* in real time during aphid feeding. The location and timing of these Ca^{2+} bursts were investigated using a

combination of phloem-localised GCAMP3 and comparisons to aphid feeding behaviour, measured through EPG. In addition, because Arabidopsis BAK1 and the *M. persicae* effector Mp10 are known modulators of plant PTI to aphids, the role of the aphid-induced rises in $[Ca^{2+}]_{cyt}$ during PTI was assessed through the use of Arabidopsis mutant *bak1-5* and dsMp10 *M. persicae*, which have reduced *Mp10* expression levels. The aim was to identify and characterise an aphid-induced plant Ca^{2+} burst and place it the context of plant defence.

3.1.9 Materials and methods

The methods used in his chapter are detailed in Chapter 2. Information on the the microscopy assay can be found in Section 2.8, induced resistance in Section 2.9.4, EPG in Section 2.9.6 and Section 2.9.7 and RNAi knockdown in Section 2.4.3.

3.2 Results

3.2.1 GCAMP3 can be used to measure Ca^{2+} dynamics during aphid feeding

In order to assess whether GCAMP3 could be used to visualise whole-tissue Ca^{2+} signals *in vivo,* 35S::GCAMP3 plants were grown on MS plates and imaged under a stereo microscope. Upon treatment with *M. persicae*, a burst of GFP fluorescence was detectable around the feeding site (Figure 3.2, Video 3.1, Video 3.2). Fluorescent bursts comparable to those seen at the feeding site were not obvious in the midrib, nor if fluorescence was averaged across the entire leaf (Figure 3.2b). However, there was a gradual increase in fluorescence over time in all locations (Figure 3.2b) and additional areas of high fluorescence were observable in areas systemic to the feeding site (Video 3.1 & Video 3.2).

3.2.2 Aphids induce rapid localised Ca^{2+} bursts in isolated Arabidopsis leaves

Due to the high variability in Ca^{2+} dynamics with plate-grown plants, as well as infrequent aphid settling, a single-leaf microscopy assay was developed. 35S::GCAMP3 leaves were excised 24 h before the experiment and floated in water in a 96-well plate (Section 2.8.1, Chapter 2). Untreated leaves showed more stable Ca^{2+} dynamics across the course of the experiment than was previously observed with whole plants, and a large biphasic $[Ca^{2+}]_{cyt}$ elevation could be observed when they were treated with cold water (Figure 3.3, Video 3.3).

Treatment of these isolated leaves with a single *M. persicae* individual resulted in a rapid increase in GFP fluorescence around the feeding site within 2 min of the aphid settling (Figure 3.4a and 3.4b, Video 3.4) that decreased to the level of the no-aphid controls after 7 min (Figure 3.4b and 3.4c). The average area of the Ca^{2+} burst was 111 μm^2 and the leading wave front of this burst travelled at 5.92 μm/s from its centre (Table 3.2). Several settling behavioural characteristics of the aphids were also measured (Table 3.2).

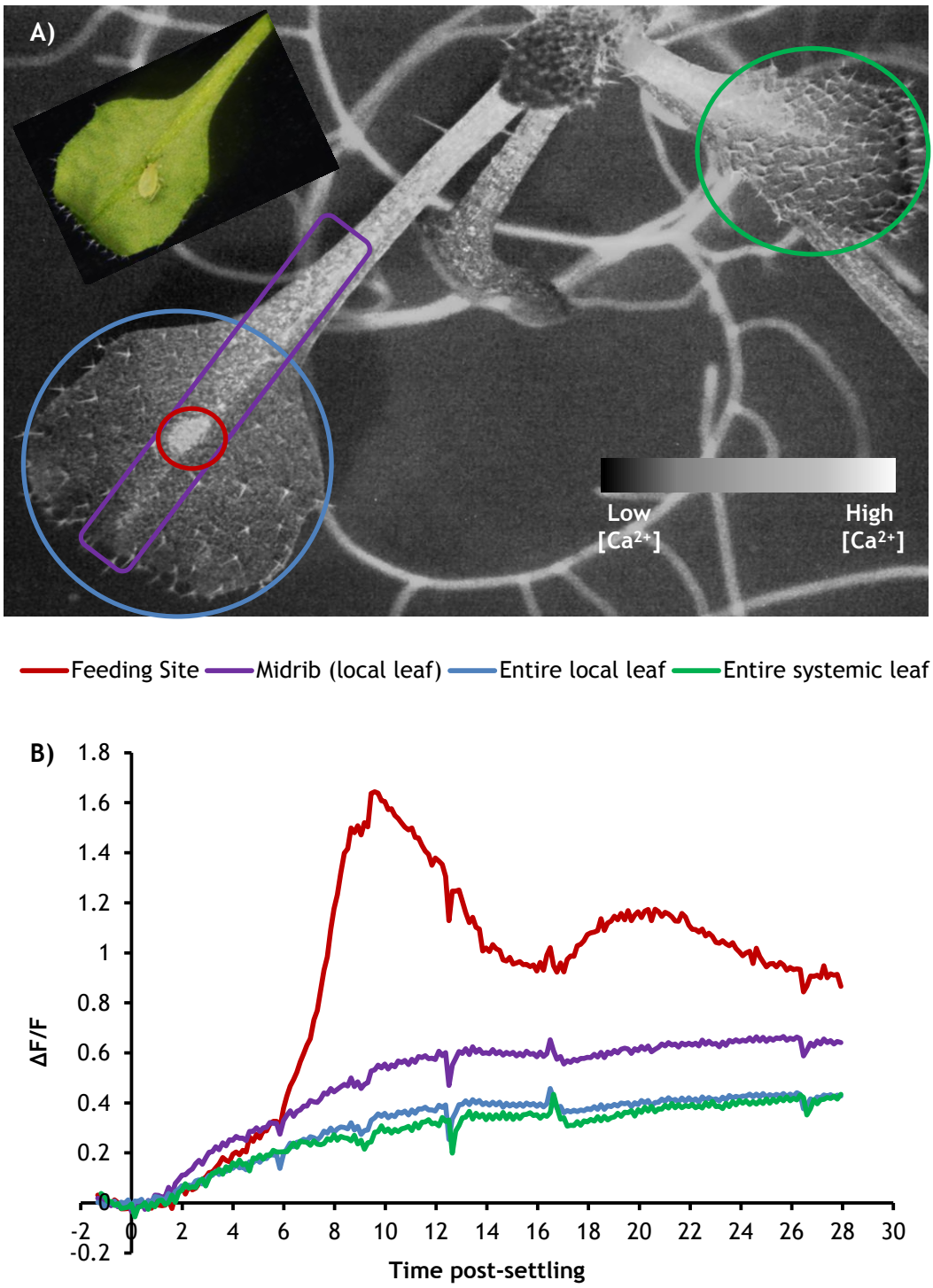

Figure 3.2: GCAMP3 can be used to detect *M. persicae*-induced Ca^{2+} signals around the feeding site in whole Arabidopsis plants.

Normalised GFP fluorescence (ΔF/F) of a representative sample shown. **A)** GFP fluorescence snapshot of the adaxial surface of 35S::GCAMP3 plants being fed on by *M. persicae*. Inset: Abaxial leaf surface under bright field showing location of aphid settling. Image brightness represents GFP fluorescence intensity. **B)** Normalised GFP expression measured over time for various regions of interest (ROIs - displayed on figure).

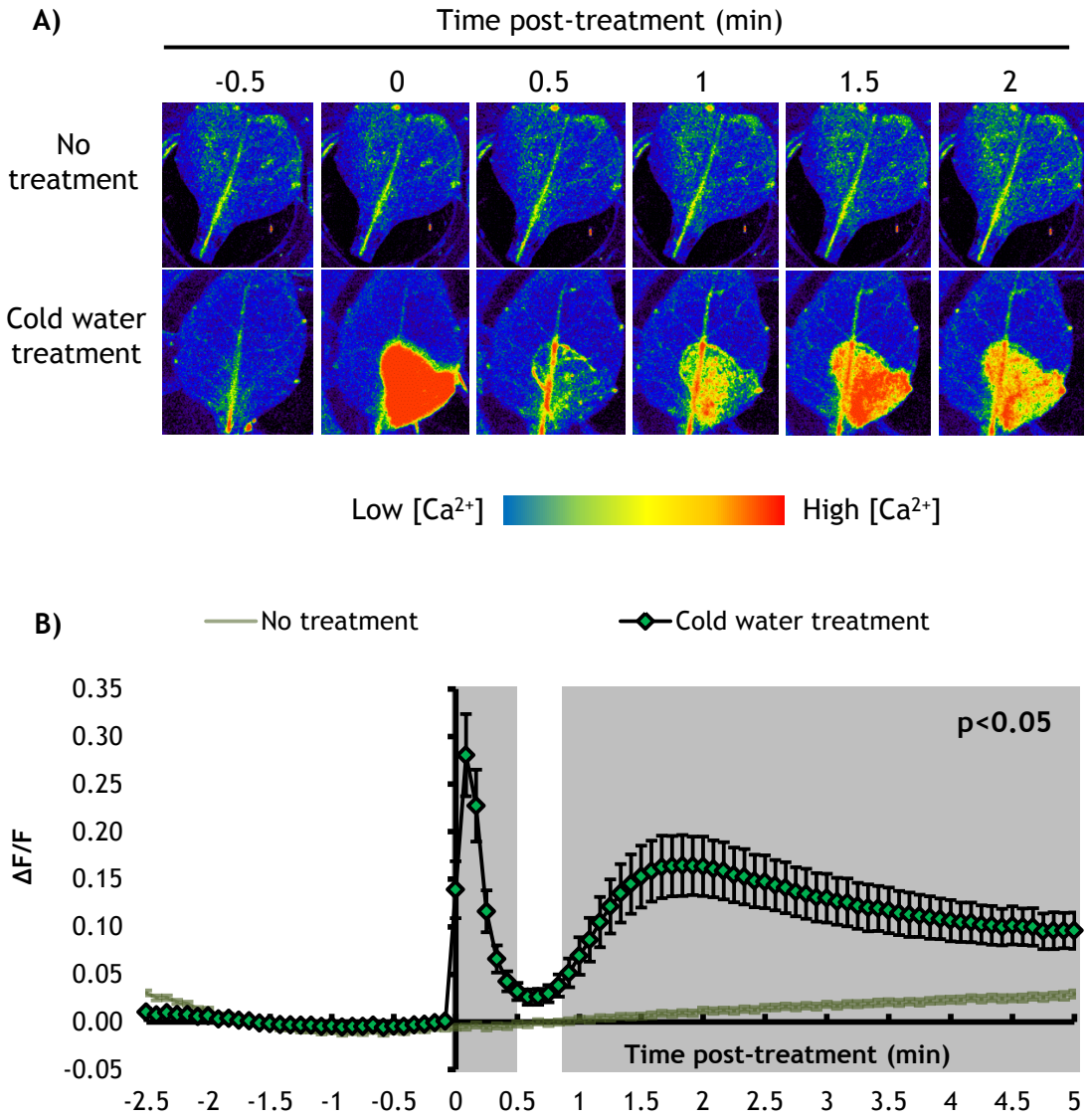

Figure 3.3: Cold water treatment induces a large biphasic Ca^{2+} burst in isolated 35S::GCAMP3 leaves.

A) GFP fluorescence represented as a heat map across a 2.5 min period. Representative sample shown. **B)** Normalised GFP fluorescence (ΔF/F) was averaged across the entire leaf. Error bars represent standard error of the mean (SEM, n=34). Grey shading indicates significant difference between treatments (Student's t-test within GLM at $p<0.05$). Experiment conceived and designed by T.V and performed by M.A. under supervision of T.V.

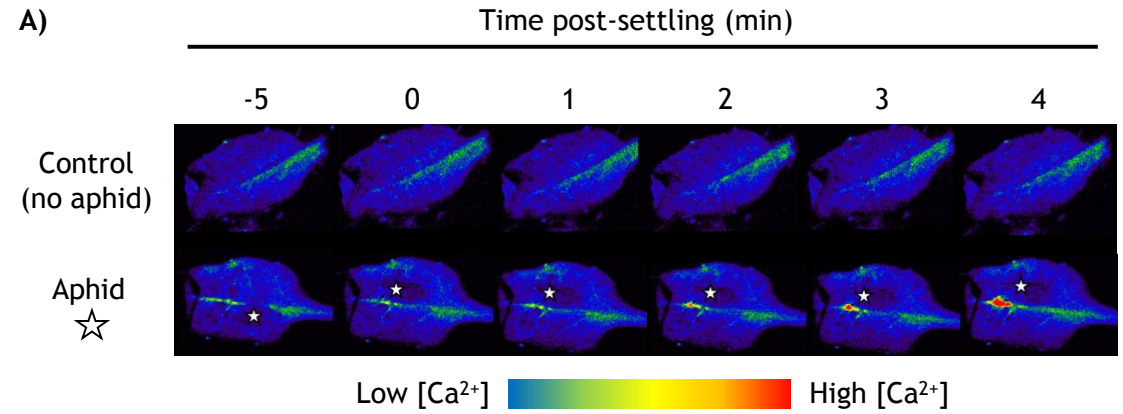
A)
Time post-settling (min)
-5
0
1
2
3
4
Control
(no aphid)
Aphid
Low [Ca2+]
High [Ca2+]

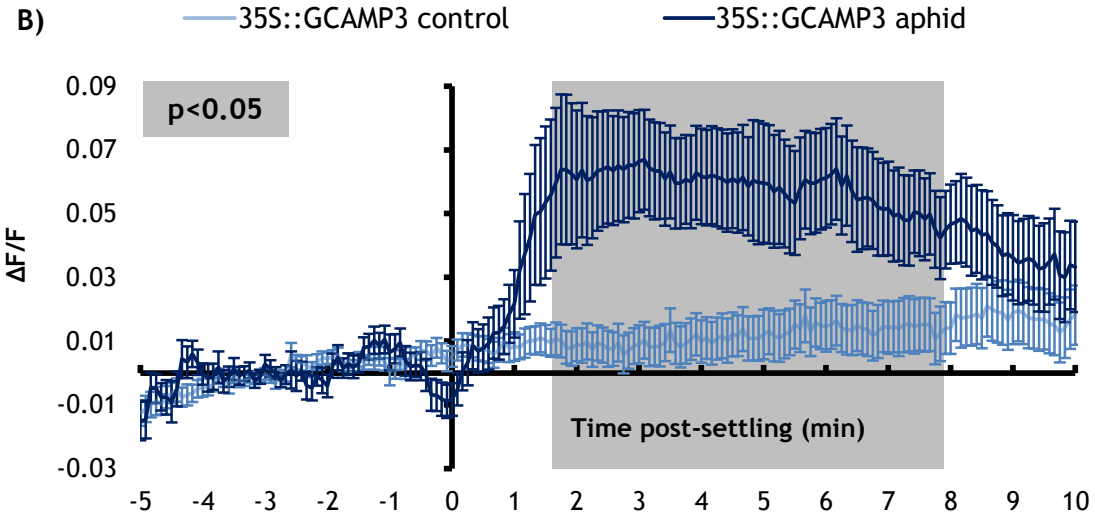
B)
35S::GCAMP3 control
35S::GCAMP3 aphid
p<0.05
ΔF/F
0.09
0.07
0.05
0.03
0.01
-0.01
-0.03
Time post-settling (min)
-5
-4
-3
-2
-1
0
1
2
3
4
5
6
7
8
9
10

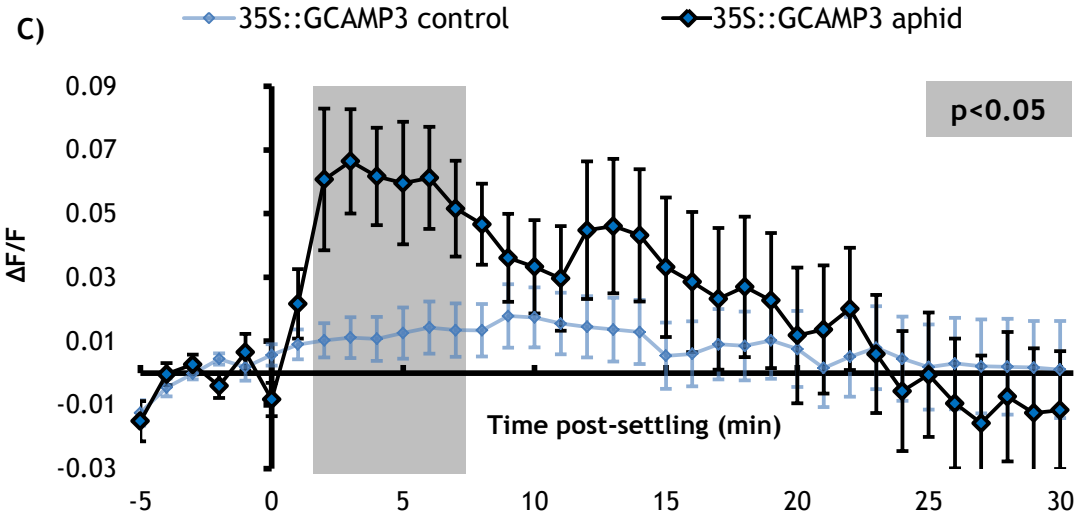
C)
35S::GCAMP3 control
35S::GCAMP3 aphid
p<0.05
ΔF/F
0.09
0.07
0.05
0.03
0.01
-0.01
-0.03
Time post-settling (min)
-5
0
5
10
15
20
25
30

Figure 3.4: GCAMP3 can be used to detect *M. persicae*-induced Ca^{2+}signals at the feeding site in isolated leaves.

A) GFP fluorescence represented as a heat map during aphid settling. Point of settling = 0. Aphid location represented by a star. Representative sample shown **B)** Quantification of normalised fluorescence (ΔF/F) around the feeding site from 5 min before settling to 10 min post-settling, displaying measurements every five seconds. **C)** Quantification of normalised fluorescence around the feeding site from 5 min before settling to 30 min post-settling, displaying measurements every one minute. Error bars represent SEM (n=34). Grey shading indicates significant difference between treatments (Student's t-test within GLM at $p<0.05$).

Table 3.2: Ca^{2+} signalling and aphid behaviour parameters during the GCAMP3 imaging.

[a] Speed of the visible signal from the point of initiation to the furthest point of spread. [b] Length of settling period used for Ca^{2+} signal analysis. [c] Length of time between the beginning of imaging and the first aphid settle.

Parameter	Average (± SEM)
Ca^{2+} signal	
Speed of wave front (μm/s)[a]	5.9 (± 0.6)
Maximum area of visible burst (μm^2)	111 (± 18)
Aphid Behaviour	
Number of settles (>5 min)	2.0 (±0.1)
Total number of settles	3.8 (± 0.4)
Time settled for imaging (min)[b]	20 (± 2)
Time until first settle (min)[c]	11 (± 1)
Percentage of total time spent settled (%)	62 (±3)

3.2.3 YCNano-65 could not detect an aphid-induced Ca^{2+} burst

To determine if the FRET sensor YCNano-65 [206] could be used to detect an aphid-induced Ca^{2+} signal in Arabidopsis, plants expressing this sensor were also analysed under a stereo microscope. Whilst wounding of the plants appeared to generate a FRET ratio change (Figure 3.5, Video 3.5), a detectable FRET ratio change was not produced in response to cold water (Figure 3.6, Video 3.6), contrary to the response seen with GCAMP3 (Figure 3.3, Video 3.3). Furthermore, upon aphid treatment no visible fluorescent bursts could be observed around the 35S::YCNano-65 feeding site (Figure 3.7, Videos 3.7 and 3.8).

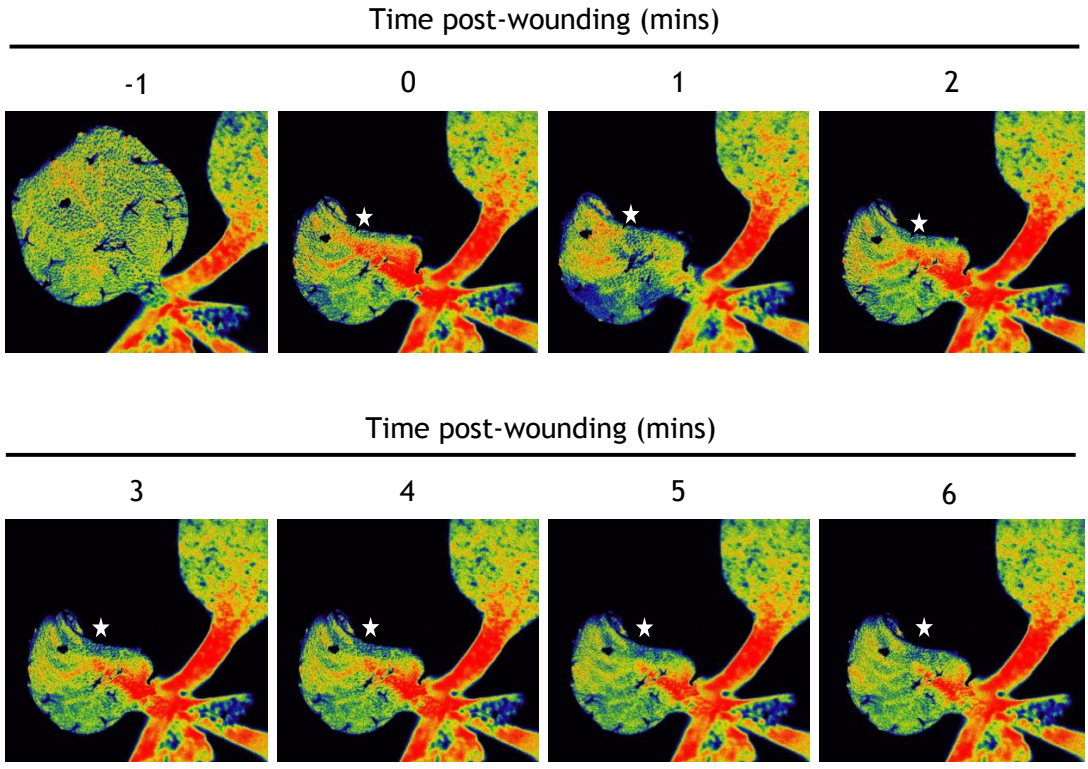

<u>Figure 3.5:</u> YCNano-65 can be used to detect wound-induced Ca^{2+} signals in whole Arabidopsis plants.

FRET ratio in 35S::YCNano-65 plants represented as a heat map across a 7 min period. Top-left leaf wounded with forceps at time 0, with the location of the wound represented by a star.

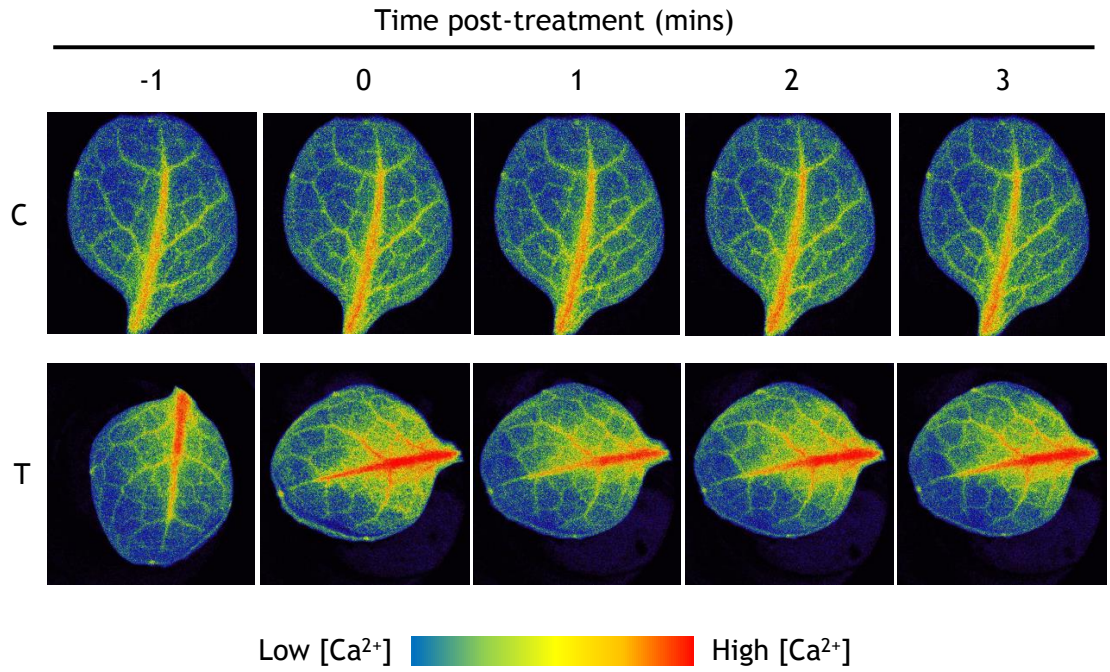

Figure 3.6: 35S::YCNano-65 isolated leaves treated with ice-cold water did not show large changes in FRET ratio.

FRET ratio represented as a heat map across a 5 min period. T = treatment, C= no treatment control. Representative sample shown (n=9).

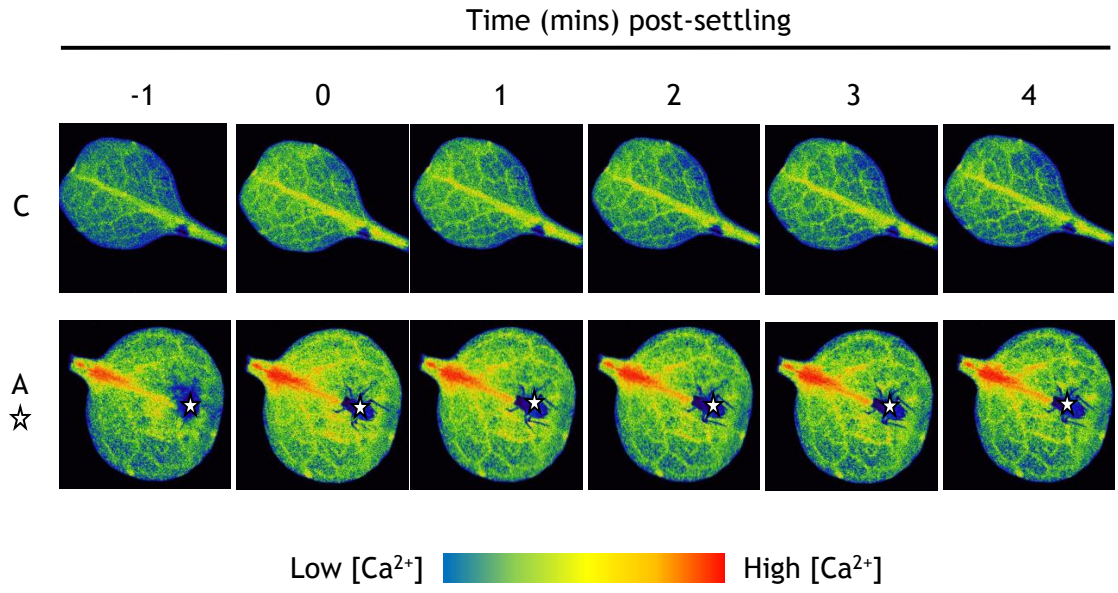

Figure 3.7: 35S::YCNano-65 isolated leaves treated with *M. persicae* did not exhibit changes in FRET ratio around the feeding site

FRET ratio represented as a heat map across a 6 min period. C= no aphid control, A = aphid treatment. Aphid location represented by a star. Experiment conceived and designed by T.V and conducted by T.V and Michael Giolai (Earlham Institute, Norwich). Representative sample shown (n=6).

3.2.4 *M. persicae* does not induce systemic Ca^{2+} signals or SAR in Arabidopsis

In order to investigate whether there was a systemic element to the aphid-induced $[Ca^{2+}]_{cyt}$ elevation, GFP fluorescence was analysed in systemic regions of the leaf as aphids fed (Figure 2.1, Chapter 2) in the midrib (Figure 3.8a) and in the lateral tissue beside the midrib (Figure 3.8b). No detectable increase in fluorescence was seen in either location.

To explore the role of systemic signalling in plant-aphid interactions further, IR to *M. persicae* was assessed in local and systemic leaves. Pre-treatment of the local leaf with 50 live aphids successfully activated IR against subsequent *M. persicae* attack (Figure 3.9). However, this resistance did not travel systemically (Figure 3.9).

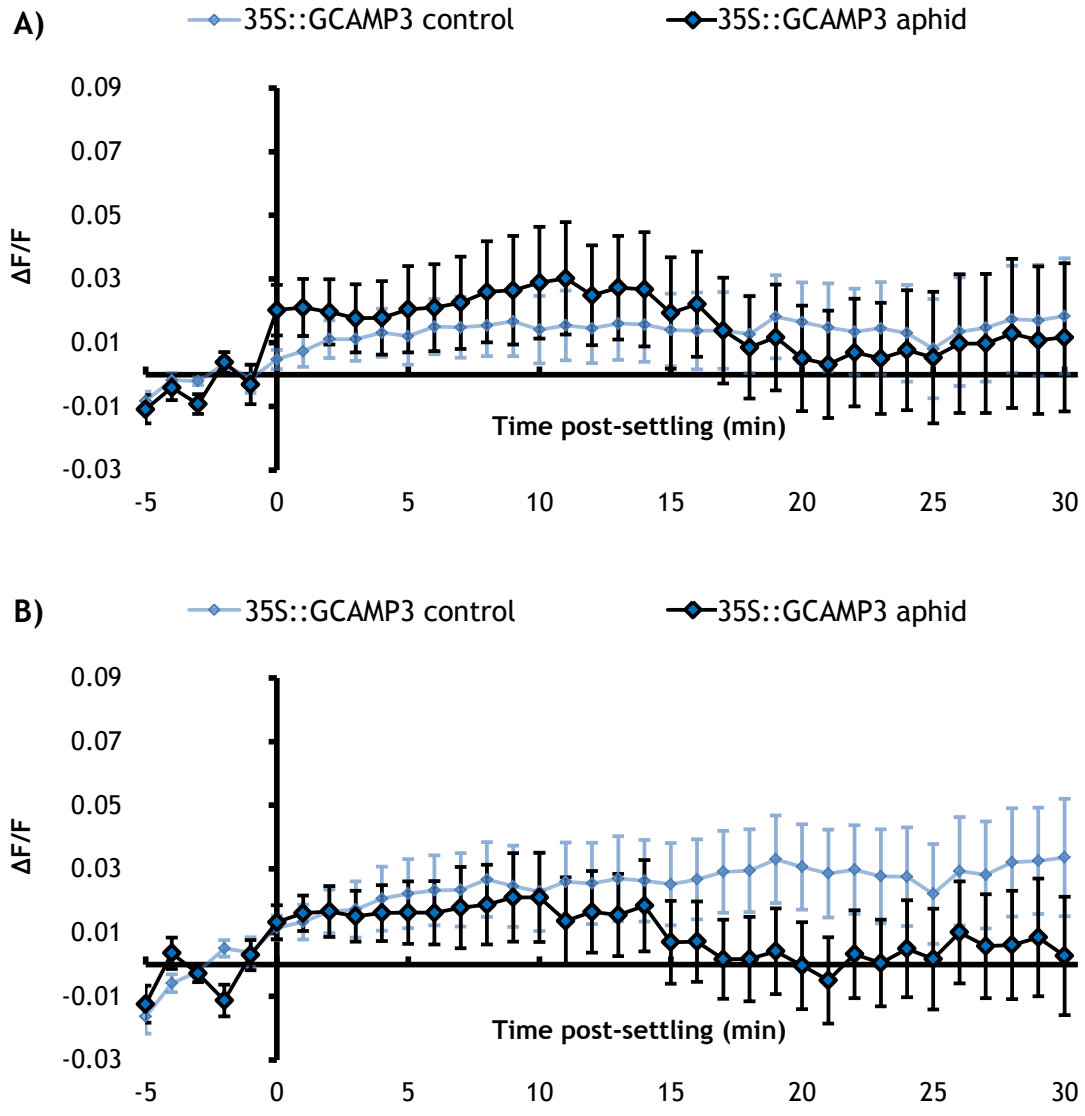

Figure 3.8: Ca^{2+} bursts in response to *M. persicae* cannot be detected systemically.
Normalised GFP fluorescence (ΔF/F) in 35S::GCAMP3 Arabidopsis upon *M. persicae* settling in two systemic locations. **A)** Midrib tissue. **B)** Lateral tissue (besides midrib). Error bars represent SEM (n=34).

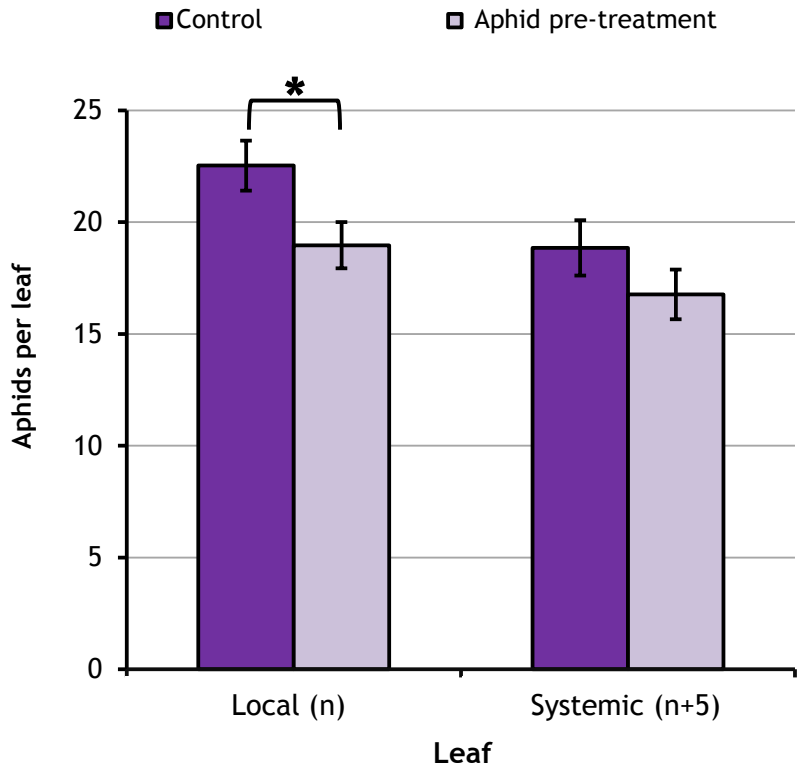

Figure 3.9: IR against *M. persicae* cannot be detected systemically
Local leaves (n) were pre-treated with 50 adult *M. persicae* individuals to activate IR. After removal of the initial infestation, the fecundity of a single adult feeding from the pre-treated leaves was measured. Pre-treatment with an empty clip cage was used as a control. Error bars represent SEM of 13-20 biological replicates from 5 independent experiments. * indicates significant difference between treatments (Student's t-test within GLM at $p<0.05$).

3.2.5 Aphid feeding begins rapidly upon settling and the phloem is not reached for several minutes

The EPG technique was used to compare aphid feeding behaviour to the timing of the Ca^{2+} burst and aphid settling behaviour. On soil-grown whole plants, the first potential drop (cell puncture) in the pathway phase occurred within 31 s of probing and it took the aphids an average of 24 min to reach the phloem (Figure 3.10a). Furthermore, an adapted version of the EPG technique was developed to assess feeding behaviour on isolated 35S::GCAMP3 leaves floating in water, in a set-up comparable to the microscopy assay. This assay revealed that the timing of the pathway and phloem phases on isolated 35S::GCAMP3 leaves was comparable to soil-grown plants, with the pathway phase lasting for 15-25 min (Figure 3.10b). In both assays, the pathway phase began almost instantly upon settling (Figure 3.10).

3.2.6 Aphid-induced Ca^{2+} signals could not be detected in the phloem

In order to assess whether a $[Ca^{2+}]_{cyt}$ elevation could be detected in the phloem, GCAMP3 was expressed under the companion cell (CC)-specific *SUCROSE-PROTON SYMPORTER 2* (*SUC2*) promoter [620]. In contrast to the 35S::GCAMP3 aphid-induced Ca^{2+} burst (Figure 3.11a), the phloem-specific sensor could not detect an aphid-induced signal, although there was a gradual increase in fluorescence over time that was aphid-independent (Figure 3.11b, Video 3.9). Systemic signals in the phloem were also not detected (Figures C1 and C2 - Appendix C).To verify whether the SUC2-localised GCAMP3 could produce a visible GFP readout upon stress treatment, wounding of SUC2::GCAMP3 plants was performed with forceps. Both 35S:GCAMP3 and SUC2::GCAMP3 plants exhibited rapid and systemic Ca^{2+} signals upon such wounding (Figure 3.12, Video 3.10).

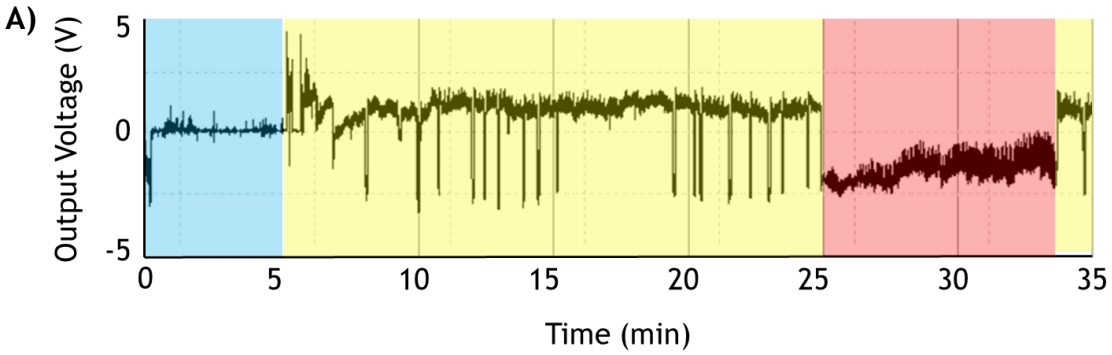

Behaviour	Average (±SEM)
Time until first cell puncture	31 s (± 11)
Time until first phloem phase (E1)	24 min (±3)

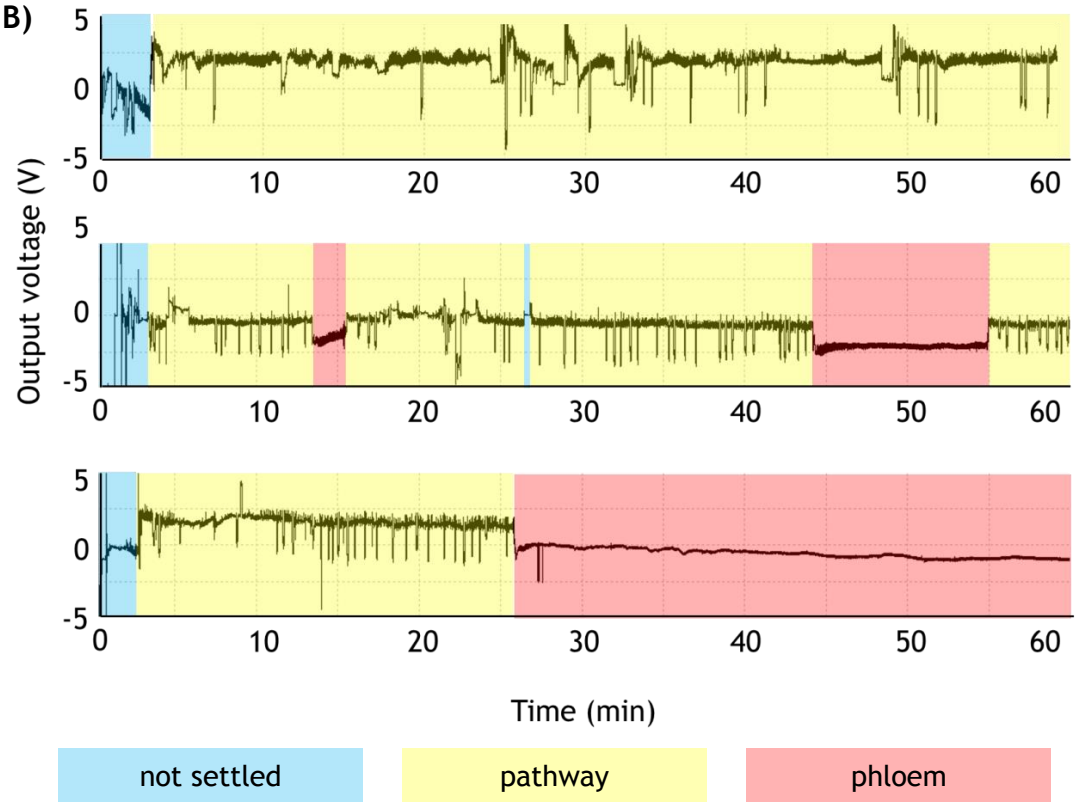

Figure 3.10: Representative EPG traces from *M. persicae* feeding on Arabidopsis.

A) Representative EPG trace from an aphid feeding on a whole Col-0 Arabidopsis plant. Average time until the first cell puncture and phloem phase once feeding begun are given below (n=22). **B)** Representative EPG traces from aphids feeding on isolated 35S::GCAMP3 leaves (n=6). Feeding phases represented by coloured shading. Experiment conceived and designed by T.V and conducted by P.H. under supervision of T.V.

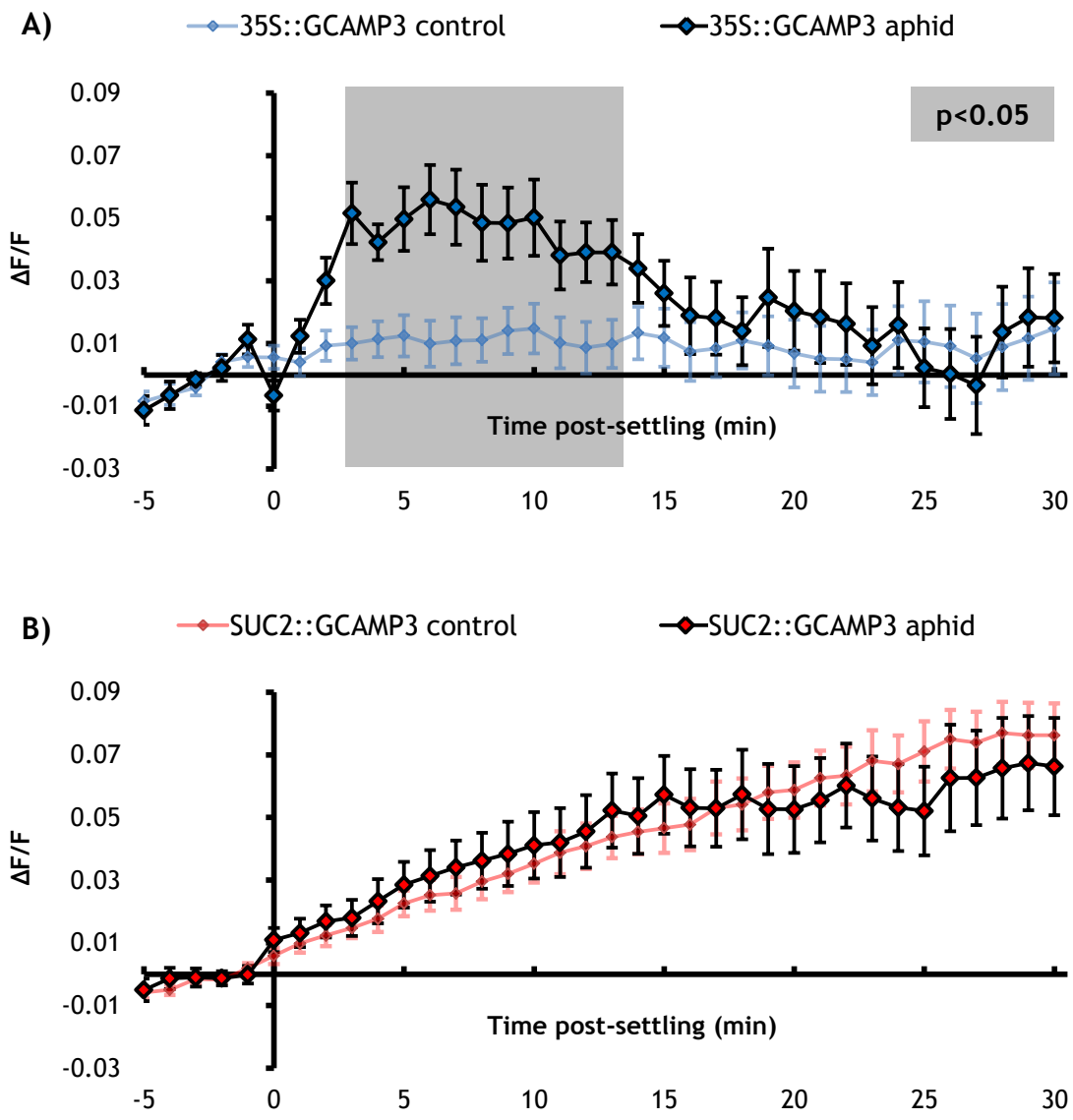

Figure 3.11: Normalised GFP fluorescence (ΔF/F) around the feeding site in 35S::GCAMP3 and SUC2::GCAMP3 Arabidopsis upon *M. persicae* settling.

A) 35S::GCAMP3 control (no aphid treatment) vs aphid treatment. **B)** SUC2::GCAMP3 control (no aphid treatment) vs aphid treatment. Error bars represent SEM (35S::GCAMP3 n=31, SUC2::GCAMP3 n=34). Grey shading indicates significant difference between treatments (Student's t-test within GLM at $p<0.05$). Experiment conceived and designed by T.V and conducted by T.V. and M.A.

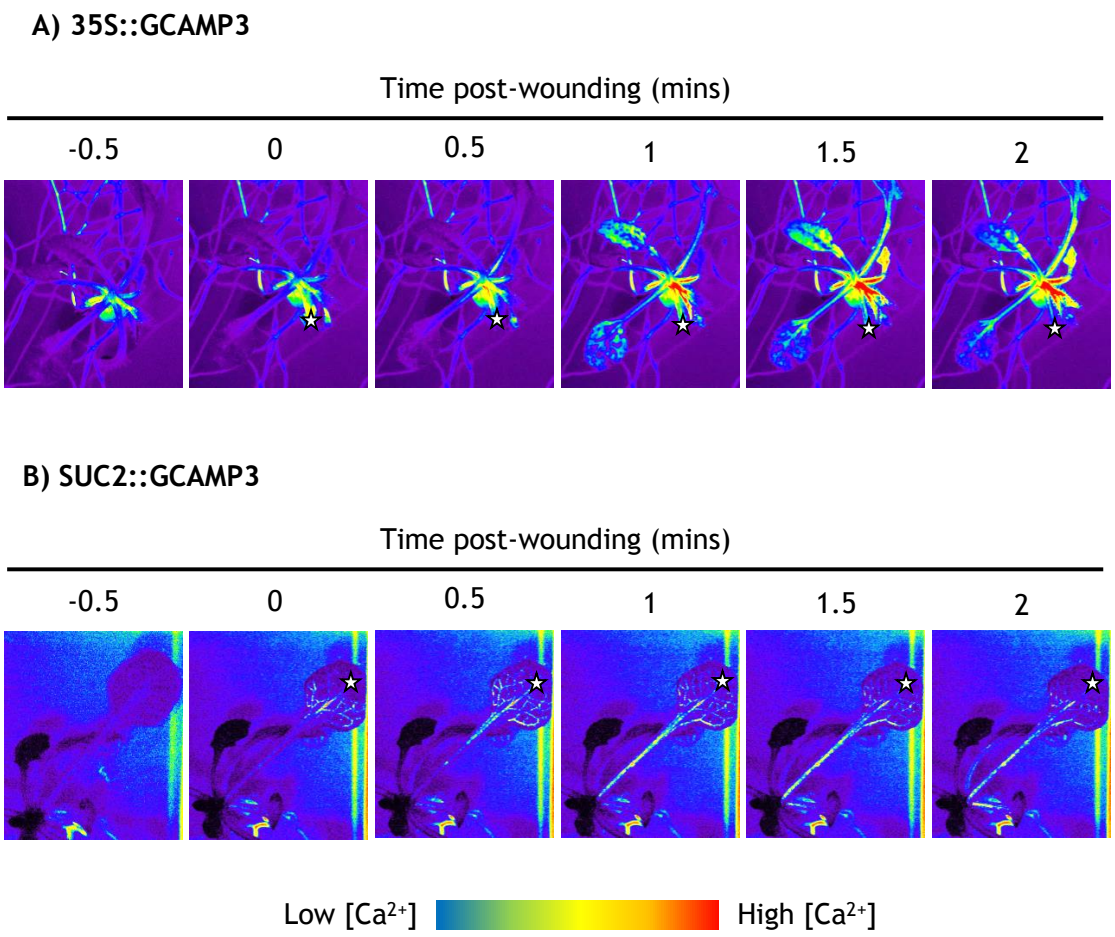

Figure 3.12: Wounding to Arabidopsis expressing *GCAMP3* results in systemic Ca^{2+} signals. GFP fluorescence represented as a heat map. Plants were wounded at time 0 using forceps, and the location of wound is represented by a star. **A)** 35S::GCAMP3. **B)** SUC2::GCAMP3. Representative samples shown (n=6 per genotype). Experiment conceived and designed by T.V and conducted by M.A. under the supervision of T.V.

3.2.7 Aphid-induced Ca^{2+} signals are significantly reduced in the *bak1-5* mutant

To investigate whether the aphid-induced $[Ca^{2+}]_{cyt}$ elevation was linked to BAK1, GCAMP3 was crossed with the *BAK1* null mutant *bak1-5*. The *bak1-5* mutant was selected as it only displays defects in immune signalling, but not in brassinosteroid signalling as seen with other *BAK1* mutants [548]. In 35S::GCAMP3 x *bak1-5* plants the aphids did not induce a significant Ca^{2+} burst around the feeding site compared to the no aphid control leaves (Figure 3.13b). As such, the amplitude of the feeding site Ca^{2+} burst was significantly reduced relative to 35S::GCAMP3 (Figure 3.13a, Figure 3.13c, Video 3.11). In samples that displayed visually recordable (R) GFP fluorescence changes around the feeding site, the maximal area of spread and the speed of the wave front were also assessed. The average area (Figure 3.14a) and speed (Figure 3.14b) of the signal were not significantly different between genotypes. Since fewer GCAMP3 x *bak1-5* samples displayed recordable (R) Ca^{2+} bursts (Figure 3.14), it is possible that the feeding site Ca^{2+} burst is a discrete 'on' or 'off' response, with the greater number of 'off' signals in the GCAMP3 x *bak1-5* line accounting for the significantly reduced amplitude of the Ca^{2+} burst (Figure 3.13). To address this, the amplitude of the burst at 7 min post-settling was analysed for each individual sample. This revealed a continuous spread of amplitudes across samples, rather than discrete populations of 'on' or 'off' responses (Figure 3.15).

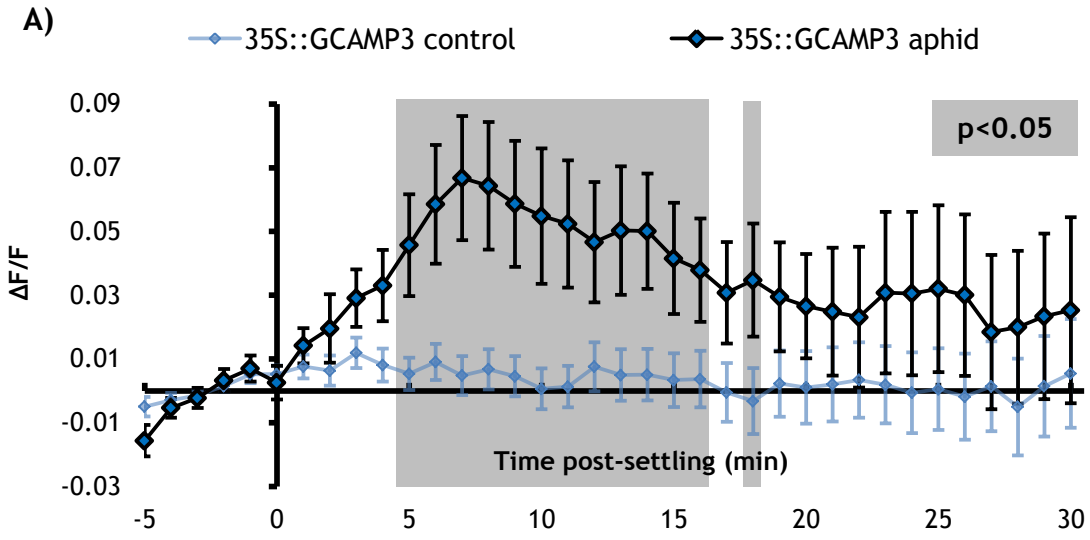
A)
35S::GCAMP3 control
35S::GCAMP3 aphid
p<0.05
ΔF/F
0.09
0.07
0.05
0.03
0.01
-0.01
-0.03
Time post-settling (min)
-5
0
5
10
15
20
25
30

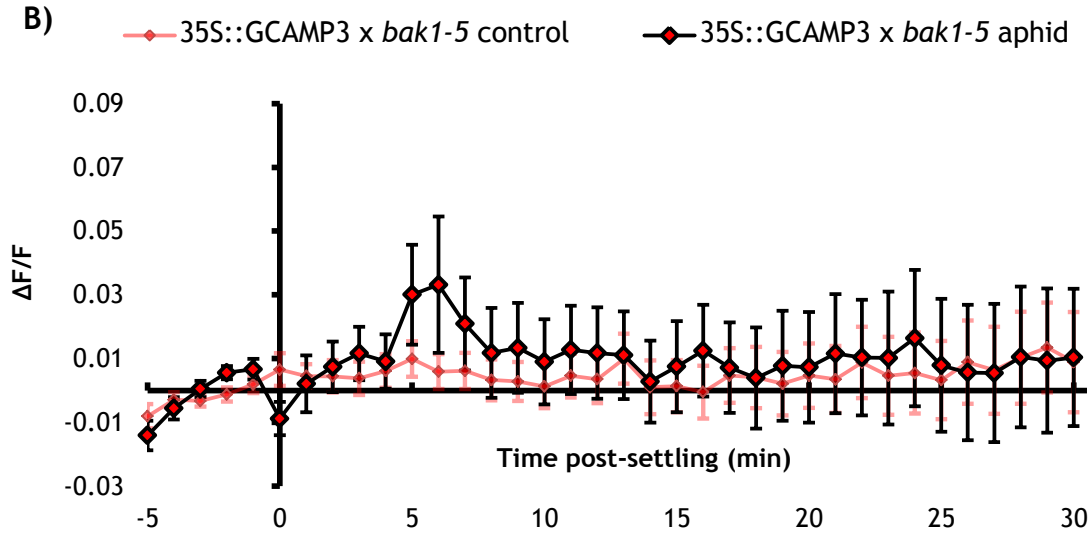
B)
35S::GCAMP3 x bak1-5 control
35S::GCAMP3 x bak1-5 aphid
ΔF/F
0.09
0.07
0.05
0.03
0.01
-0.01
-0.03
Time post-settling (min)
-5
0
5
10
15
20
25
30

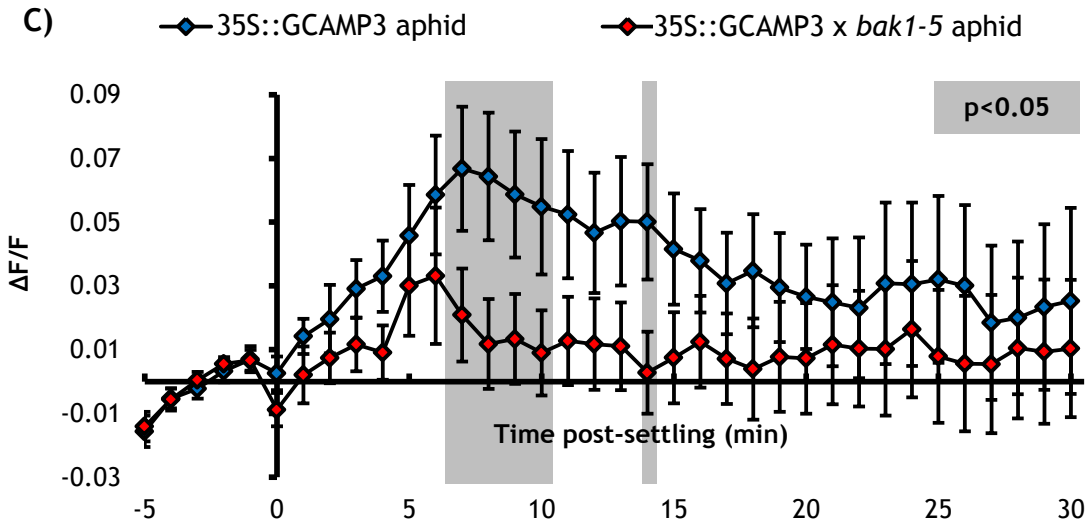
C)
35S::GCAMP3 aphid
35S::GCAMP3 x bak1-5 aphid
p<0.05
ΔF/F
0.09
0.07
0.05
0.03
0.01
-0.01
-0.03
Time post-settling (min)
-5
0
5
10
15
20
25
30

Figure 3.13: Normalised GFP fluorescence (ΔF/F) around the feeding site in 35S::GCAMP3 and 35S::GCAMP3 x *bak1-5* Arabidopsis upon *M. persicae* settling.

A) 35S::GCAMP3 control (no aphid treatment) vs aphid treatment. **B)** 35S::GCAMP3 x *bak1-5* control (no aphid treatment) vs aphid treatment. **C)** 35S::GCAMP3 aphid treatment vs 35S::GCAMP3 x *bak1-5* aphid treatment. Error bars represent SEM (35S::GCAMP3 n=30, 35S::GCAMP3 x *bak1-5* n=30). Grey shading indicates significant difference between treatments (Student's t-test within GLM at $p<0.05$). Experiment conceived and designed by T.V and conducted by T.V. and M.A.

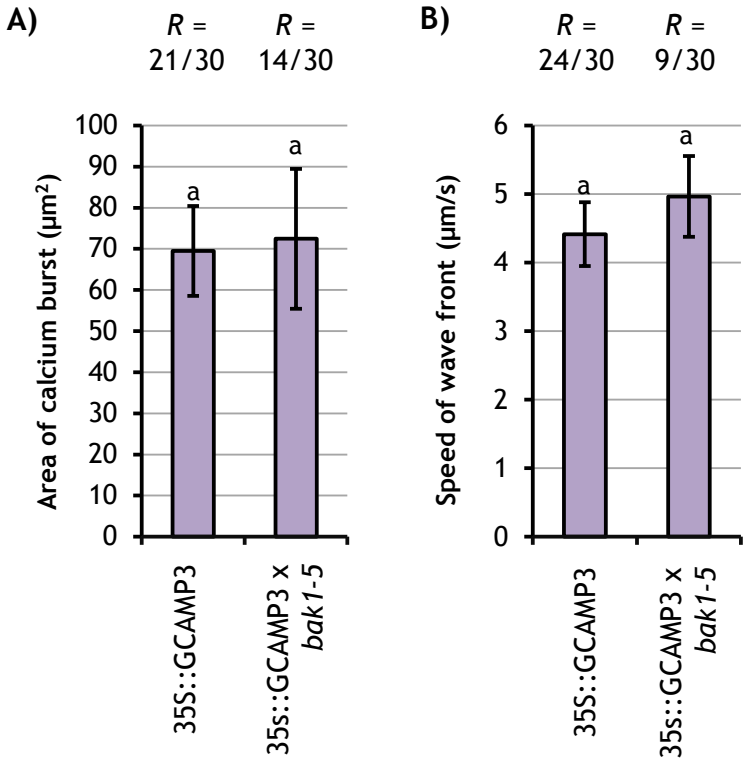

Figure 3.14: Properties of the *M. persicae*-induced Ca^{2+} burst around the feeding site in 35S::GCAMP3 and 35S::GCAMP3 x *bak1-5* leaves.

Comparing properties of the Ca^{2+} burst in all recordable samples (R), i.e. samples in which a feeding site GFP burst was visible by eye. **A)** Area of the Ca^{2+} burst. **B)** Speed of the Ca^{2+} wave front. Letters indicate no significant difference between genotypes (Student's t-test $p<0.05$) Error bars represent SEM. Experiment conceived and designed by T.V and conducted by T.V. and M.A.

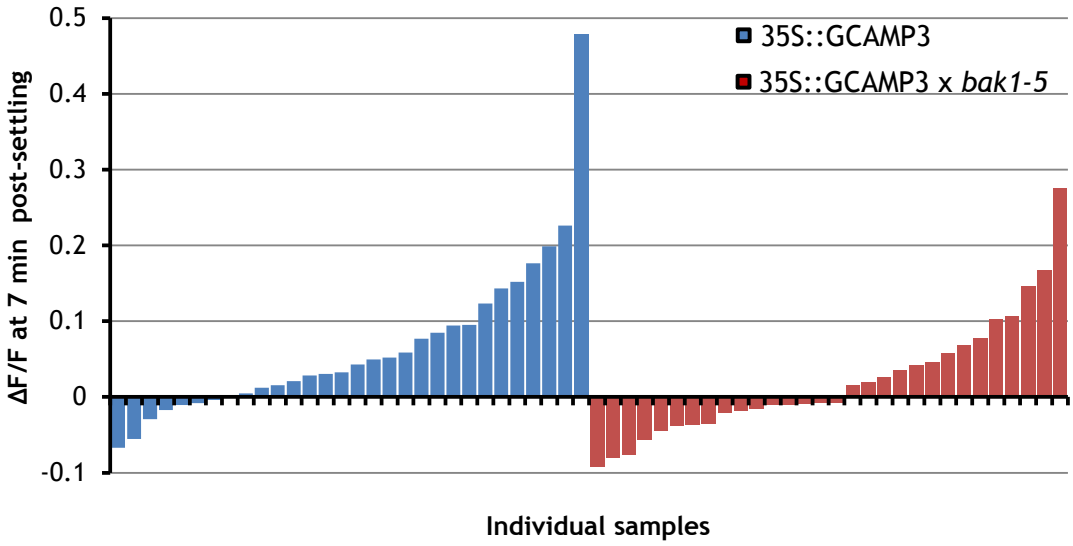

Figure 3.15: Normalised florescence (ΔF/F) around the *M. persicae* feeding site at 7 min post-settling 35S::GCAMP3 and 35S::GCAMP3 x *bak1-5* leaves.

Raw ΔF/F value for each leaf sample plotted. Experiment conceived and designed by T.V and conducted T.V. and M.A.

3.2.8 Phloem feeding is reduced on the *bak1-5* mutant

Under the microscope, there was no difference in the settling behaviour of *M. persicae*, either in terms of the number of settles, time until the first settle or length of settling on the *bak1-5* mutant (Figure 3.16). In addition, EPG was conducted on the *bak1-5* mutant. Whole plant EPG was used because EPG on leaf disks has been shown to be less sensitive at detecting behavioural changes due to plant-mediated resistance [621]. Pathway behaviours were first analysed across only the first h of recording to identify behavioural characteristics that might be occurring during the time period of the microscopy assay. No differences were found between Col-0 and *bak1-5* (Table 3.3). Total pathway behaviours were also assessed across the full 8 h recording, with no significant differences in the *bak1-5* mutant found (Figure 3.17, Table 3.3). However, analysis of phloem phase behaviours revealed that the duration of phloem ingestion (E2) is significantly reduced on the *bak1-5* mutant (Figure 3.17, Table 3.3 behaviour 33), whilst the minimum time to the reach first phloem phase was longer (Table 3.3 behaviour 36).

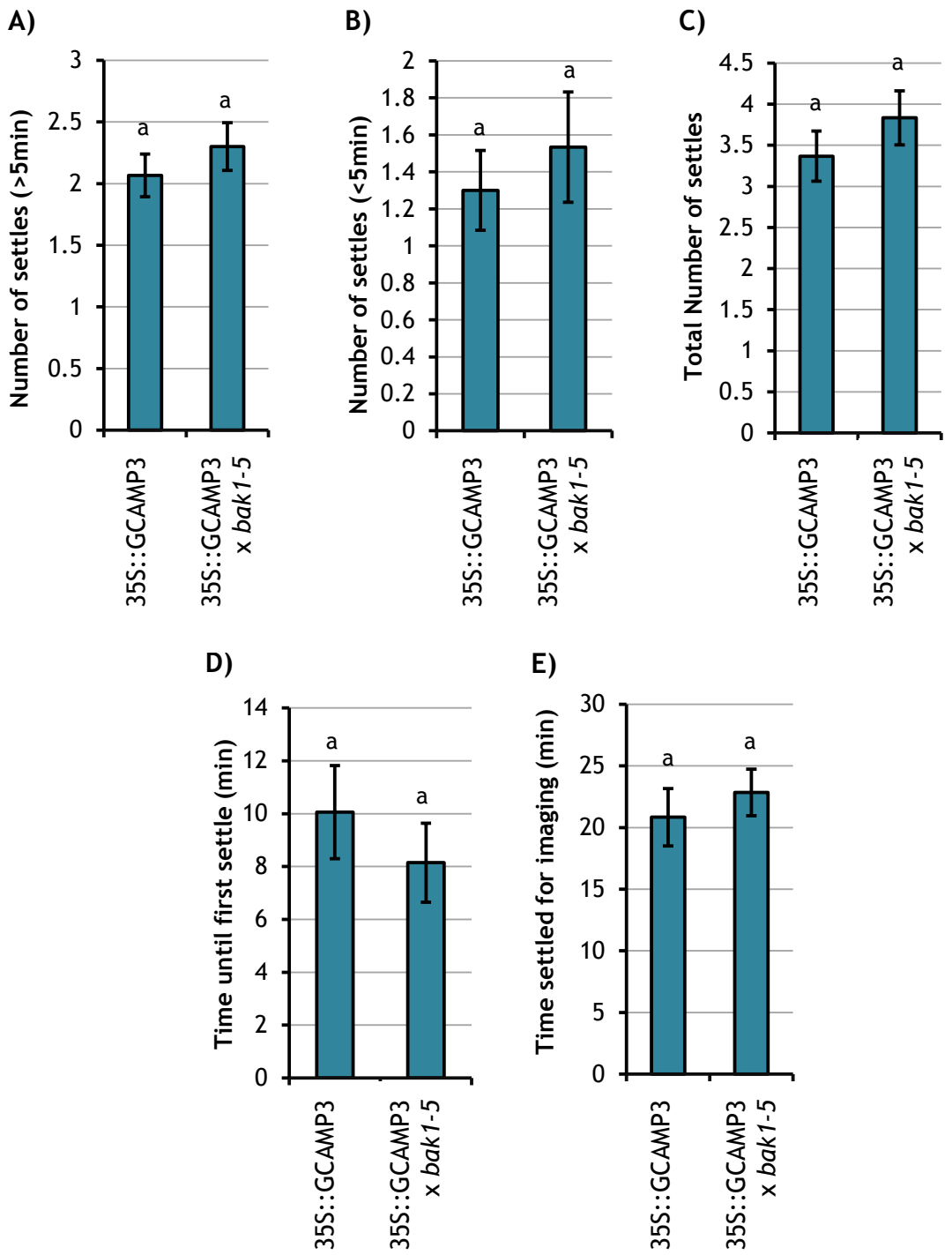

Figure 3.16: Settling behaviour of *M. persicae* on 35S::GCAMP3 and 35S::GCAMP3 x *bak1-5* leaves.

A) Number of settles greater than 5 min in length. **B)** Number of settles less than 5 min in length. **C)** Total number of settles. **D)** Time before first settle that lasted over 5 min. **E)** Time aphid spent settled during a settling event used to measure GCAMP3 fluorescence. Error bars represent SEM (35S::GCAMP3 n=34, 35S::GCAMP3 x *bak1-5* n=34). Letters indicate no significant difference between genotypes (Student's t-test $p<0.05$). Experiment conceived and designed by T.V and conducted by T.V. and M.A.

Table 3.3: EPG parameters for *M. persicae* feeding from Col-0 and *bak1-5* Arabidopsis.
Probe = feeding event, pd = potential drop (cell puncture), C = pathway phase, E1 = phloem salivation, E2 = phloem ingestion, sE2 = sustained E2 (>10 min), no = number. Duration recorded in s. P-values calculated using a Mann-Whitney U-test (Col-0 n= 24, *bak1-5* n= 22). Experiment conceived and designed by T.V and conducted by P.H. under supervision of T.V.

		Col-0		*bak1-5*		p-value
	Pathway behaviours (1st h)	**Mean**	**SEM**	**Mean**	**SEM**	
1	number of probes	8.5	1.0	9.2	1.1	0.68
2	average probe	420	160	260	78	0.55
3	sum of probing	1700	210	1400	200	0.43
4	duration of 1st probe	260	150	73	30	0.34
5	number of pd	23	3	21	3	0.73
6	average duration of pd	5	0.1	5.1	0.1	0.45
7	sum of pd	110	15	110	15	0.90
8	time to 1st pd (from start of 1st probe)	38	12	110	59	0.78
9	time to 1st pd in 1st probe with a pd	12	2	12	3	0.42
10	no. pd per min C	1.1	0.1	1.2	0.1	0.32
11	no. pd in 1st probe	2.1	0.7	2.8	1.3	0.84
12	duration of the first pd	6.2	0.4	6.0	0.4	0.94
13	mean duration of the first 5 pd	5.4	0.1	5.5	0.2	0.64
	Pathway behaviours (8 h)					
14	number of probes	29	4	31	4	0.54
15	average probe	1300	300	750	150	0.29
16	sum of probing	17000	1500	15000	1600	0.45
17	duration of 1st probe	800	680	73	29	0.18
18	number of pd	130	17	140	13	0.55
19	average duration of pd	4.9	0.1	4.8	0.0	0.72
20	sum of pd	640	83	680	64	0.53
21	time to 1st pd (from start of 1st probe)	31	11	110	59	0.87
22	time to 1st pd in 1st probe with a pd	12	1.8	12	3.3	0.42
23	no. pd per min C	0.9	0.1	1	0	0.13
24	no. pd in 1st probe	2.9	1.4	3.2	1.7	0.84
25	duration of the first pd	6.3	0.5	6.0	0.4	0.80
26	mean duration of the first 5 pd	5.4	0.1	5.4	0.2	0.85
27	time to 1st probe	300	120	650	190	0.13
	Phloem behaviours (8 h)					
28	number of single E1 (without E2) periods	0.2	0.1	0.4	0.1	0.33
29	sum of E1 (sgE1 and E1)	110	22	190	50	0.21
30	sum of E2	5600	1700	4200	1500	0.92

		Col-0		*bak1-5*		p-value
	Phloem behaviours (8 h) (cont.)	**Mean**	**SEM**	**Mean**	**SEM**	
31	maximum E2 period	6400	2000	3500	1300	0.24
32	number of sustained E2 (> 10 min)	0.8	0.2	1.1	0.3	0.52
33	mean duration of sE2	8200	2600	3400	1500	0.03
34	sum of duration of sE2	5100	1600	3800	1500	0.93
35	average time to 1st E within probes	1400	190	1300	58	0.94
36	minimum time to 1st E within probes	920	200	1100	82	0.04
37	number of probes before the 1st E	12	2.8	17	3.9	0.67

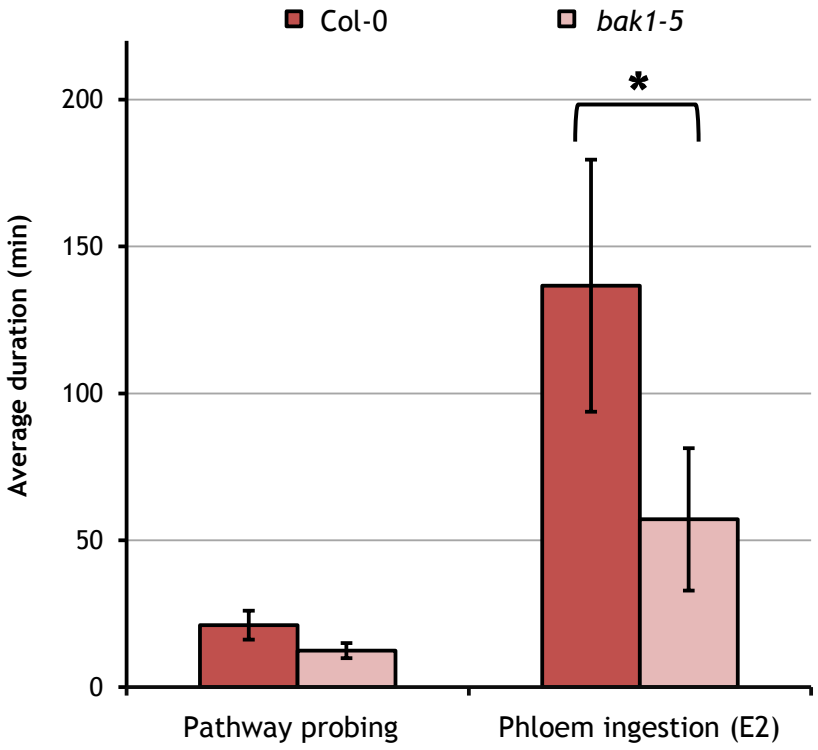

Figure 3.17: Average length of pathway and phloem ingestion (E2 phase) behaviours of *M. persicae* feeding on Col-0 and *bak1-5*.

Experiment run over 8 h. Error bars represent SEM (Col-0 n= 24, *bak1-5* n= 22). * indicates a significant difference between treatments (Mann-Whitney U-test $p<0.05$). Experiment conceived and designed by T.V and conducted by P.H. under supervision of T.V.

3.2.9 Reduced expression of *Mp10* alters the aphid-induced Ca^{2+} signal

In order to assess whether *M. persicae* attempts to suppress the Arabidopsis Ca^{2+} burst *in vivo*, aphids were reared on plants expressing RNAi targeted against the effector *Mp10* (dsMp10) or *GFP* as a control (dsGFP). Aphids reared on dsMp10 plants had a 80% reduction in *Mp10* expression (Figure 3.18). Feeding by both dsGFP (Figure 3.19a) and dsMp10 (Figure 3.19b) aphids resulted in Ca^{2+} bursts around the feeding site. When compared directly, the dsMp10 elicited a slightly higher amplitude Ca^{2+} burst (Figure 3.19c, Video 3.12). No differences in the Ca^{2+} signal area or speed were detected between dsGFP and dsMp10 aphids (Figure 3.20). Aphid settling behaviour was also not significantly altered between the two genotypes (Figure C7, Appendix C).

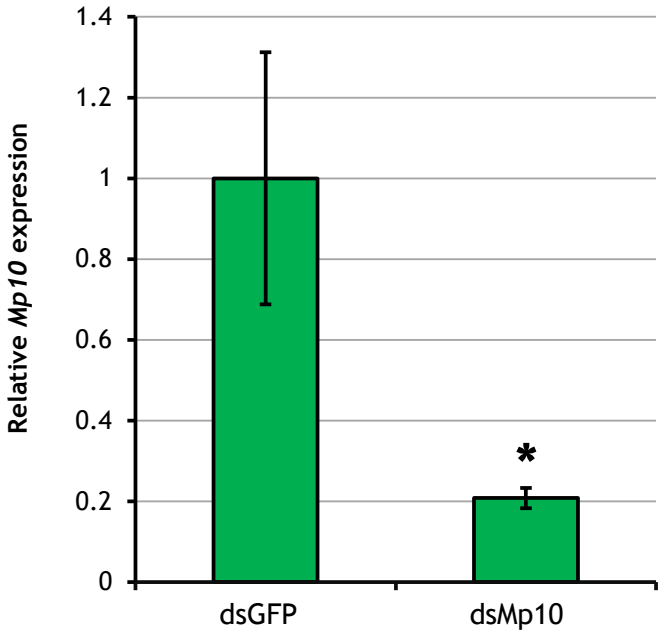

Figure 3.18: Relative expression of *Mp10* in dsGFP and dsMp10 *M. persicae*.
Error bars represent SEM (n=18). * indicates a significant difference between genotypes (Student's t-test $p<0.05$). Experiment conceived and designed by T.V and conducted by M.A. under supervision of T.V.

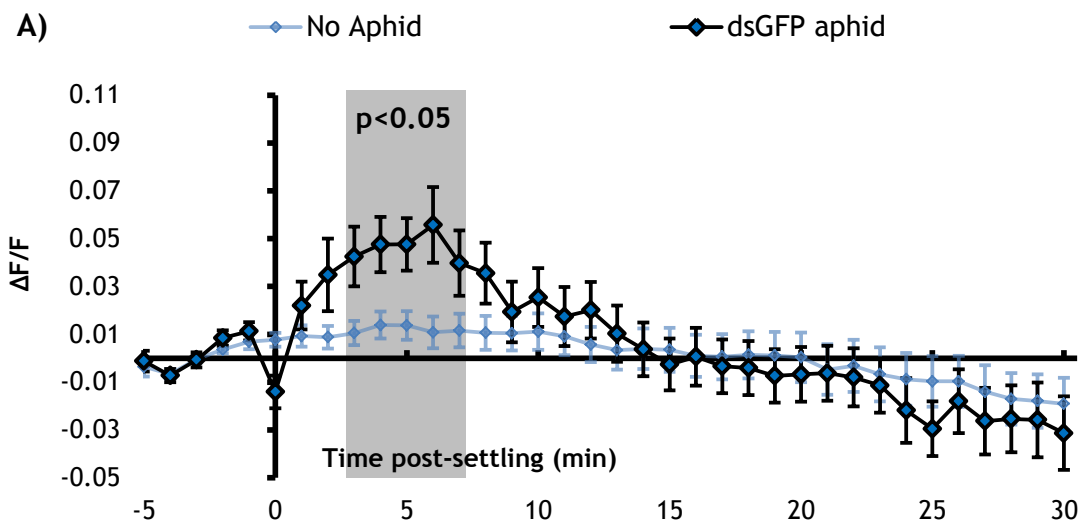
A)
No Aphid
dsGFP aphid
p<0.05
ΔF/F
Time post-settling (min)
0.11
0.09
0.07
0.05
0.03
0.01
-0.01
-0.03
-0.05
-5
0
5
10
15
20
25
30

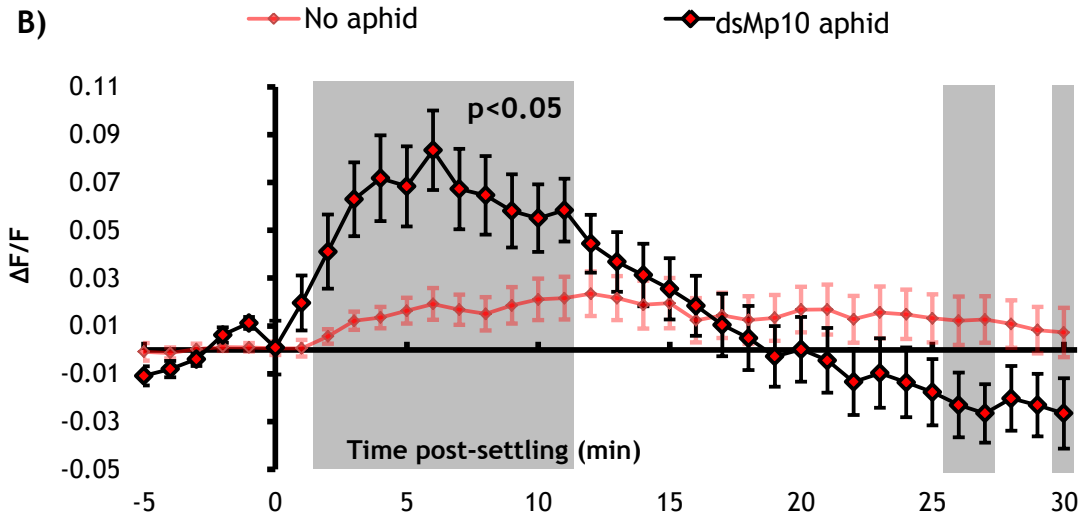
B)
No aphid
dsMp10 aphid
p<0.05
ΔF/F
Time post-settling (min)
0.11
0.09
0.07
0.05
0.03
0.01
-0.01
-0.03
-0.05
-5
0
5
10
15
20
25
30

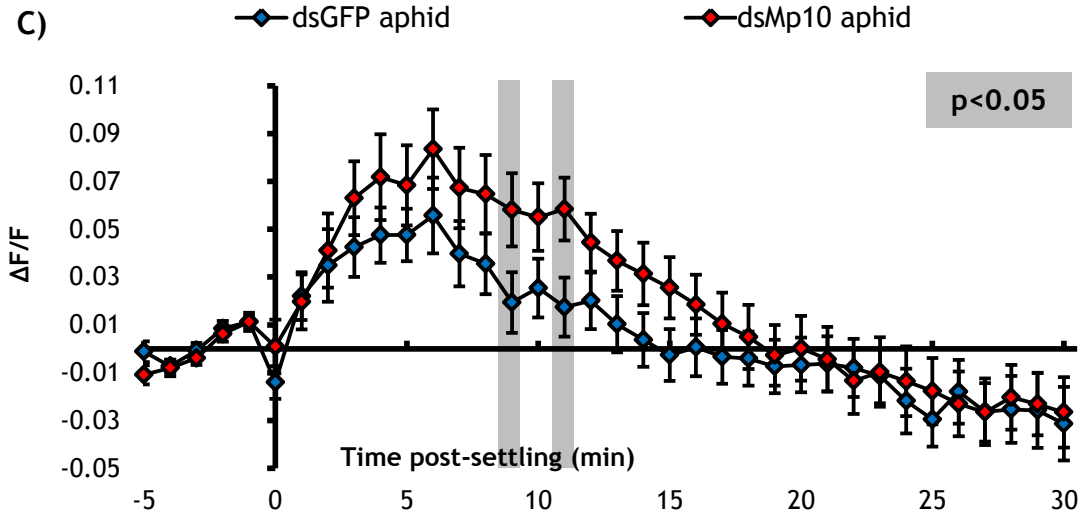
C)
dsGFP aphid
dsMp10 aphid
p<0.05
ΔF/F
Time post-settling (min)
0.11
0.09
0.07
0.05
0.03
0.01
-0.01
-0.03
-0.05
-5
0
5
10
15
20
25
30

Figure 3.19: Normalised GFP fluorescence (ΔF/F) around the feeding site in 35S::GCAMP3 Arabidopsis upon *M. persicae* settling.

A) No aphid control vs dsGFP aphid treatment. **B)** No aphid control vs dsMp10 aphid treatment. **C)** dsGFP aphid treatment vs dsMp10 aphid treatment. Error bars represent SEM (dsGFP n=34, dsMpP10 n=34). Grey shading indicates significant difference between treatments (Student's t-test within GLM at $p<0.05$). Experiment conceived and designed by T.V and conducted by T.V. and M.A.

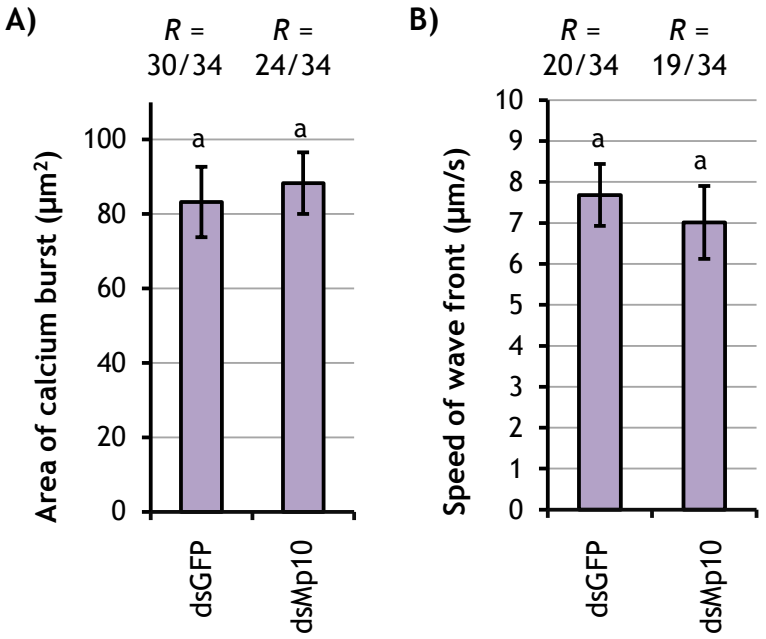

Figure 3.20: Properties of the *M. persicae*-induced Ca^{2+} burst around the feeding site in 35S::GCAMP3 plants treated with dsGFP and dsMp10 aphids.

Comparing properties of the Ca^{2+} burst in all recordable samples (R), i.e. samples in which a feeding site GFP burst was visible by eye. **A)** Area of the Ca^{2+} burst. **B)** Speed of the Ca^{2+} wave front. Error bars represent SEM. Letters indicate no significant difference between genotypes (Student's t-test $p<0.05$). Experiment conceived and designed by T.V and conducted by T.V. and M.A.

3.3 Discussion

3.3.1 GCAMP3 allows whole-tissue imaging of Ca^{2+} dynamics during aphid attack

Under the stereo microscope 35S::GCAMP3 emitted a strong GFP signal that allowed whole-tissue imaging of plant $[Ca^{2+}]_{cyt}$ (Videos B1 and B2). This strong signal, combined with the use of a single fluorophore, allowed measurements to be taken once every 5 s. As such, it was possible to image *in vivo* with exceptional temporal resolution. When aphids were added to the 35S:GCAMP3 plants, small bursts of fluorescence were observed around the site of settling (Figure 3.2, Video 3.1), specifically around the head of the aphid (Video 3.2) and were attributed to aphid feeding.

The $[Ca^{2+}]_{cyt}$ was highly dynamic in systemic regions, with a general increase in fluorescence being seen over time in all tissues (Figure 3.2b). However, a clear aphid-induced signal was not easy to distinguish. It is possible that the $[Ca^{2+}]_{cyt}$ changes in systemic regions were a result of plant stress caused by the microscopy assay. Indeed, blue light is known to induce Ca^{2+} signals [10, 11, 14, 622]. In addition, the high intensity light might have also resulted in temperature and osmotic stresses, both of which also induce Ca^{2+} signalling [6, 7, 177]. Furthermore, the difference in fluorescence between tissues could have been a result of variable expression of the GCAMP3 sensor.

Furthermore, *M. persicae* did not settle regularly on the 35S::GCAMP3 plants. Again this may have been due to the intense blue light used to excite the sensor. Vision in *M. persicae* is governed by three photoreceptors, including one with a peak sensitivity of 490 nm [623], within the range of the GFP excitation light (450-490 nm). When the aphids did settle, this was on the abaxial surface of the leaf (Video 3.1), a common preference seen for aphids [258, 624, 625]. Thus, the aphids were hidden from the view of the microscopy lens, making the position and timing of settling events difficult to determine.

3.3.2 Aphids induce a rapid and highly localised burst around the feeding site

In order to combat the aphid settling issues experienced on the whole plants, a single-leaf assay was developed. This involved the excision of 35S::GCAMP3 leaves the day prior to microscopy to allow wound-induced Ca^{2+} signals to dissipate. Single leaves or leaf disks have been successfully used previously for the study of both ROS [349] and Ca^{2+} [122, 538] signals. The leaves were floated in water to reduce osmotic stress and to prevent the escape of the aphids. To validate this assay, cold water treatments were used to elicit large cold-induced $[Ca^{2+}]_{cyt}$ rises (Figure 3.3, Video 3.3). These rises were biphasic and extremely rapid, making them comparable to established literature [6, 50, 626]. Thus, the single-leaf assay was capable of reporting Ca^{2+} elevations in response to stress.

In response to aphids, a rapid Ca^{2+} burst was seen around the feeding site that was not observed in un-infested control leaves (Figure 3.4a, Video 3.4). This burst was extremely rapid, occurring within 95 s and remaining significantly above the control for 6 min (Figure 3.4b). The decrease in signal after 6 min was unlikely to be the result of fluorophore bleaching as signals were still seen in other locations on the leaf after this time point.

The *Phytophthora sojae* PAMP Pep13 induces a change in $[Ca^{2+}]_{cyt}$ within 40 s in *Petroselinum crispum* (parsley) cell cultures [371], whilst 1 μM flg22 and elf18 can both induce rapid $[Ca^{2+}]_{cyt}$ elevations that peak within 2–3 min in Arabidopsis leaves [122], and 100 nM flg22 can induce $[Ca^{2+}]_{cyt}$ oscillations in epidermal and stomatal guard cells within 5 min [219]. Furthermore, the fungal PAMP cryptogein induces $[Ca^{2+}]_{cyt}$ elevations in *Nicotiana plumbaginifolia* cells that peak at 5 min post-treatment [372], whilst chitin induces Ca^{2+} bursts in Arabidopsis roots within 2 min of application [219]. Consequently, the *M. persicae*-elicited Ca^{2+} burst represents one of the most rapidly induced PAMP-triggered $[Ca^{2+}]_{cyt}$ elevations documented so far.

Unlike cold shock, the aphid feeding site burst was not biphasic and no further bursts were detected within 30 min of the aphid settling (Figure 3.4c). Biphasic signatures are common in response to PAMPs [371, 372] with the second sustained burst linked to successful defence induction in PTI [371] and ETI [509]. It is therefore possible that the single Ca^{2+} bursts observed in response to *M. persicae* may not fully activate defence (further discussion in Chapter 4).

Other parameters of the Ca^{2+} burst were also measured. The burst was highly localised and restricted to an area of 111 μm^2 (Table 3.2). This is significantly different to the large, systemic Ca^{2+} signals observed in response to chewing insects [123]. In addition, the Ca^{2+} wave front travelled radially from a central point of initiation (Video 3.4) at around 6 µm/s (Table 3.2). This speed is significantly slower than the systemically-propagating Ca^{2+} signals seen in the roots during salt stress, or the electrical signals within leaves during wounding, both of which travel at around 400 µm/s [7, 103]. The comparatively restricted area and slow speed of the aphid-induced burst might be linked the low quantity of tissue damage caused during phloem feeding [296], as well as active suppression by the aphid through effectors. Indeed, caterpillar OS are capable of suppressing systemic Ca^{2+} wound signals [123].

Furthermore, aphid settling behaviour on 35S::GCAMP3 leaves was recorded (Table 3.2). On average the aphids spent around 10 min exploring the leaf before a successful settling event (> 5 min) was established. The aphids spent around 60% of the experiment settled, and the aphids used for $[Ca^{2+}]_{cyt}$ measurements settled for an average length of 20 min. As such, the aphids were not deterred from settling on the isolated leaves and Ca^{2+} bursts occurred whilst the aphids were settled in their original location.

3.3.3 YCNano-65 could not be used to detect aphid-induced Ca^{2+} signals

The possibility of using a FRET cameleon to record aphid-induced Ca^{2+} signals was also explored. Wounding with forceps of 35S::YCNano-65 plants resulted in changes in the FRET ratio (Figure 3.5, Video 3.5), indicative of Ca^{2+} release. However, this fluorescence change was smaller than that observed with GCAMP3 upon wounding (Figure 3.12 Video 3.10). Cold water application did not result in large FRET changes in 35S::YCNano-65 leaves (Figure 3.6, Video 3.6), unlike the large fluorescence changes seen with 35S::GCAMP3 (Figure 3.3, Video 3.3). Upon aphid application, the feeding site burst was not visible with 35S::YCNano-65 in any of the leaves tested (Figure 3.7, Video 3.7 and Video 3.8). Also notable was the lack of background $[Ca^{2+}]_{cyt}$ dynamics visible with 35S::YCNano-65, indicating that these small background events were not detectable by YCNano-65 (Video 3.7 and Video 3.8). Furthermore, due to the low fluorescent yield of 35S::YCNano-65 under the microscope, the exposure had to be increased 8-fold relative to the GCAMP3

experiments. Thus in summary, under the stereo microscope 35S::YCNano-65 did not produce large fluorescence changes detectable at the tissue level and could not achieve the same $[Ca^{2+}]_{cyt}$ temporal resolution as GCAMP3.

GCAMP3 and YCNano-65 have similar dynamic ranges (Table 3.1) [195, 206, 213, 217] and YCNano-65 has been used successfully in plants to measure Ca^{2+} signals previously [7]. However, in the current study GCAMP3 clearly exhibited a greater fluorescent yield under the microscope. A probable reason for this was a technical limitation with the stereo microscope system used. The microscope excited and recorded CFP and YFP emission separately and therefore YFP was being excited by the microscope light source rather than by FRET from CFP. This meant that the YFP emission stayed constant and was independent of $[Ca^{2+}]_{cyt}$. As a result, only changes in CFP emission, which decreases upon Ca^{2+} binding due to FRET, could be used to measure $[Ca^{2+}]_{cyt}$. The fluorescent yield of CFP is half that of GFP [628], and decreases in this due to FRET are significantly harder to detect than the 12-fold increases in GFP fluorescence possible with GCAMP3 (Table 3.1) [195, 216]. This explains why in the present study YCNano-65 fluorescent yield was inferior to GCAMP3, reducing the resolution of the imaging and subsequently the measurement of aphid-induced Ca^{2+} signals.

3.3.4 No evidence for systemic signalling or defence against *M. persicae* could be identified

MeSA is a key signal in SAR to pathogens [529]. *M. persicae* induces SA-related genes [308] and SA accumulates in both local and systemic leaves within a few days post-treatment with numbers of *M. persicae* comparable to those used in the present study [609]. In addition, aphids prefer to settle on systemic leaves from plants naïve to aphids, as opposed to systemic leaves from plant pre-infested with aphids [610]. As such, it is reasonable to suggest that *M. persicae* may induce systemic defence. However, Ca^{2+} bursts were not observed distally from the feeding site, either in the midrib or lateral tissue (Figure 3.8). Xiong et al. [538] could still detect systemic Ca^{2+} signals within the vasculature of detached leaves in response to salt stress, and this suggests that systemic signals can be detected in single leaf assays if present. Therefore, *M. persicae* does not appear to elicit systemic Ca^{2+} signalling, unlike salt stress [538], lepidopteran feeding [123] and the wounding tests performed in this study (Figure 3.12, Video 3.10).

Furthermore, pre-treatment of leaves with a large number of aphids (50 adults) resulted in IR in the treated leaf, with the performance of subsequent infestations of aphids significantly reduced (Figure 3.9). De Vos et al. [464] previously found no systemic component to IR against *M. persicae*. In order to corroborate this result, in the present study the systemic leaf was strictly defined based on the plant vascular system. This was because systemic electrical [103] and Ca^{2+} (Simon Gilroy, University of Wisconsin, personal communication) signals travel preferentially to leaves with direct vascular connections. However, even in these leaves systemic IR did not occur (Figure 3.9). This agrees with observations that glucosinolate production in response to *M. persicae* is also observed around feeding sites, and not systemically [469]. Therefore, it appears that systemic Ca^{2+} signalling and induction of systemic defence does not occur in response to *M. persicae*.

The lack of a systemic Ca^{2+} signal and SAR might be due to the low amount of tissue damage caused by aphid feeding relative to other stresses such as chewing insects and wounding. However, SAR has been extensively documented in response to pathogens that cause less damage than *M. persicae* [534, 605, 629]. It is also possible that systemic signals are being actively suppressed by aphid effectors. Indeed, aphid saliva is capable of moving systemically between cells [630]. If this is occurring, it might not involve Mp10 as knocking-down transcription of *Mp10* does not restore systemic Ca^{2+} signals (Figures C5 and C6 – Appendix C). Furthermore, SAR is primarily activated during ETI rather than during PTI, through the recognition of pathogen effectors [631-633]. The compatibility between *M. persicae* and Arabidopsis implies that successful ETI is not established in this interaction, and this may account for the lack of systemic signalling and SAR.

3.3.5 The aphid-induced Ca^{2+} burst most likely occurs during pathway phase and cannot be detected in the phloem

EPG revealed that on soil-grown Col-0 Arabidopsis *M. persicae* punctures the first plant cell within 31 s of feeding (Figure 3.10a). Since the Ca^{2+} burst was detectable from 95 s post-settling (Figure 3.4b), there is only 64 s between the first cell puncture and a signal detectable by GCAMP3. In addition, *M. persicae* does not enter phloem phase feeding until 24 min post-settling (Figure 3.10a). This is shorter than observed for the *M. persicae*-Arabidopsis interaction in other EPG studies (68 min [634], 86 min [627], 150 min [635]), although comparisons between separate

studies are difficult due to the high variability of EPG-recorded behaviours in different experimental conditions.

A similar feeding pattern was seen with isolated 35S::GCAMP3 leaves, with the earliest phloem phase occurring 13 min post-settling, and several traces showing no phloem feeding within the first hour (Figure 3.10b). Feeding began almost instantly upon settling (Figure 3.10b), demonstrating that settling is a suitable proxy for aphid feeding. These data, combined with the whole-plant EPG, suggest that the Ca^{2+} burst observed in response to aphids occurs during the pathway phase.

To investigate this further, GCAMP3 was localised to the phloem, specifically to the CCs, using the *SUC2* promoter. No feeding site Ca^{2+} burst was seen in response to *M. persicae* with this reporter (Figure 3.11b, Video 3.9). In order to verify that SUC2::GCAMP3 was capable of producing a fluorescent output under the current experimental conditions, wounding treatments were used as a control. Clear wound-induced systemic Ca^{2+} signals could be seen travelling through the phloem in both 35S::GCAMP3 and SUC2::GCAMP3 plants (Figure 3.12, Video 3.10), suggesting that SUC2::GCAMP3 was capable of reporting changes in phloem $[Ca^{2+}]_{cyt}$. However, the SUC2::GCAMP3 sensor suffered from drift over time independently of aphid treatment (Figure 3.11b). The increase CC $[Ca^{2+}]_{cyt}$ over time may have been related to abiotic stress caused by the microscopy, as both temperature and salt can induce systemic Ca^{2+} signals [538, 636].

Together, the timing of the burst relative to aphid feeding behaviour and the lack of a detectable Ca^{2+} burst in the phloem suggest that the feeding site $[Ca^{2+}]_{cyt}$ elevation occurs during the pathway phase. Therefore, the signal is generated in epidermal and mesophyll cells probed by the aphid as it feeds [266, 267]. *M. persicae* has been shown to induce voltage changes in mesophyll cells upon feeding [365], and such electrical signals may be related to Ca^{2+}. Consistent with this, pathway probing still occurs with incompatible aphids [281, 282], indicating that factors present in these cells mediate aphid acceptance of plants and thus plant defence. The relevance of epidermal and mesophyll cells during ETI to aphids is also being uncovered, with R-gene transcripts having been discovered in these cells [637].

It is also possible that phloem-based Ca^{2+} signalling may be suppressed by the aphids, as suggested by the occlusion literature [273, 296, 599, 601] (Section 3.1.4). In order to test this further it would be interesting to compare if incompatible aphids, or compatible aphids deficient in effector molecules, can elicit a phloem-based $[Ca^{2+}]_{cyt}$ elevations. Indeed, the lack of phloem-based Ca^{2+} signal, together

with other data, supports the hypothesis that *M. persicae* does not induce systemic signalling or defence (section 3.3.4). It is worthy of note that the *SUC2* promoter localises GCAMP3 specifically to the CCs, whilst long term feeding by aphids occurs from the SEs [261], and this may partly account for the lack of a response. However, as there are high clusters of Ca^{2+} channels at the SE/CC interface [595], as well as a large amount of macromolecule trafficking between the two [607], it is likely that CC and SE Ca^{2+} dynamics are highly interconnected. For further investigation of SE $[Ca^{2+}]_{cyt}$ dynamics, localisation of GCAMP3 specifically to these cells might be archived by expressing the sensor under a SE-specific promoter such as *SUC3* [638].

3.3.6 BAK1 mediates the pathway phase Ca^{2+} burst as well as feeding from the phloem

Wounding is sufficient to induce Ca^{2+} signalling [123, 369, 400, 401, 424] (Figure 3.5 and Figure 3.12) and as such it is possible that tissue damage from stylet probes causes the Ca^{2+} burst independently of PTI or ETI. However, the Ca^{2+} burst is not detectable in the *bak1-5* mutant (Figure 3.13, Video 3.11), suggesting that the burst is generated as a part of BAK1-mediated PTI. Ca^{2+} acts upstream of ROS production mediated by RBOHD [119, 121, 639], and therefore the loss of Ca^{2+} in response to aphids in *bak1-5* may explain why aphid-induced ROS is also decreased in this mutant [349]. Furthermore, IR to aphids is lost in *bak1-5* mutants [349], suggesting Ca^{2+} may also act upstream of IR.

Interestingly, some *bak1-5* mutant samples did show a visible Ca^{2+} burst around the feeding site, allowing measurement of the area and speed of this signal to be calculated. Neither area nor speed were significantly altered by *BAK1* expression (Figure 3.14). However, only samples that could be recorded by eye ('recordable' samples – R) were used for these analyses, of which there were fewer in 35S::GCAMP x *bak1-5* compared to 35S::GCAMP3 (Figure 3.14). Consequently, it could be argued the Ca^{2+} response may be binary, divided between samples that showed a response and those that did not, and thus the 35S::GCAMP3 x *bak1-5* phenotype (Figure 3.13) is the result of a greater number of non-responding samples in this genotype. However, as the Ca^{2+} burst displayed a continuous range of amplitudes across samples (Figure 3.15), the binary response hypothesis does not hold true. These results also indicate that there may be some level of aphid-induced Ca^{2+} release that is independent of BAK1. In the case of *M. persicae*, a BAK1-independent pathway was

recently discovered that is mediated by ARABIDOPSIS G-PROTEIN BETA SUBUNIT (AGB1) that has a role in aphid-induced ROS and camalexin production [502], and has yet to be teased for a role in Ca^{2+} signalling.

Pathway phase feeding behaviour was not altered in the *bak1-5* mutants (Figure 3.17, Table 3.3), implying that BAK1-mediated PTI has no or little effect on *M. persicae* during the initial feeding phase. This is contrary to *Mi*- and *Vat*-mediated ETI, in *S. lycopersicum* and *C. melo* respectively, both of which have an effect on pathway behaviours [281, 302, 640]. The lack of an effect on pathway behaviours during BAK1-mediated PTI might be a result of the latency between aphid perception and plant defence induction, which can be several hs [283, 349, 350, 442]. One might therefore expect it more likely that altered defence would affect phloem feeding, which, like plant defence, might not be initiated until hs after the first feeding event [627, 634, 635] (Figure 3.10). These data also suggest that the difference in the pathway phase Ca^{2+} burst is due to plant physiology and not altered aphid feeding behaviour.

Surprisingly, phloem ingestion (E2) was significantly reduced in the *bak1-5* mutant. (Figure 3.17, Table 3.3 behaviour 33). Aphid fecundity is not altered in this mutant, despite *BAK1*'s role in aphid recognition and defence [349]. Thus, BAK1-mediated immunity is most likely suppressed by *M. persicae*. Moreover, reducing expression of the aphid effector *Mp10* significantly reduces aphid fecundity, most likely due to inadequacy at suppressing plant defence responses [277, 502]. However, fecundity is not compromised if these *Mp10* aphids are feeding on the *bak1-5* mutant [29], implying Mp10-mediated suppression of defence is BAK1-dependent. Consequently, one explanation for the resulted collected in the present study is that the BAK1 pathway acts as an entry point for aphid effectors into the plant defence network. This network is composed of several interconnected pathways (Section 1.3, Chapter 1) and in the *bak1-5* mutant these other pathways are still active, but BAK1-mediated suppression of the network is not. Alternatively, the aphid may perceive the defence status of the plant, and alterations to this may perturb normal feeding behaviour. Aphids are sensitive to several chemical cues in the environment and in the plant [255, 256, 259]. These cues can have effects on behaviour [282, 298, 627, 641-643]. Therefore, removal of the BAK1 pathway may significantly alter such cues [349, 350, 362], and as result alter feeding behaviour.

3.3.7 The aphid effector Mp10 modulates the plant Ca^{2+} burst

RNAi is a commonly-used method to decrease expression of genes in insects [644], including aphids [500, 549, 560, 645]. This technique was utilised in the present study to investigate the role of the *M. persicae* effector Mp10 on the plant Ca^{2+} burst. Rearing of *M. persicae* on Arabidopsis expressing dsRNA can result in around a 50% reduction in expression of aphid genes [549], including *Mp10* [502]. Furthermore, this reduced expression can persist for up to 4 days [560]. Indeed, rearing aphids for Ca^{2+} imaging on dsMp10 plants reduced the average level of *Mp10* expression by 80% (Figure 3.18).

Feeding by dsMp10 aphids induced slightly larger amplitude Ca^{2+} burst than the control group (dsGFP) (Figure 3.19, Video 3.12). Therefore, reduced *Mp10* expression results in a larger $[Ca^{2+}]_{cyt}$ elevation, suggesting that *Mp10* suppresses the aphid-induced Ca^{2+} burst in the epidermal and mesophyll cells. In accord with this interpretation, aphid watery saliva containing effector molecules [272-274, 276-278, 500] is injected into plant tissues almost immediately upon aphid feeding during the pathway phase [268, 619]. Indeed, Mp10 was recently demonstrated to be delivered preferentially into the cytosol of mesophyll cells and was not detectable in the vasculature [279]. Furthermore, Mp10 has been shown to inhibit the flg22-mediated Ca^{2+} burst [502], clearly demonstrating that Mp10 it does have Ca^{2+}-suppressive functions.

However, the change in $[Ca^{2+}]_{cyt}$ caused by reduced *Mp10* expression is relatively subtle. This could be because the remaining *Mp10* in the dsMp10 aphids was sufficient to suppress Ca^{2+}. Alternatively, it suggests that Mp10 has only marginal effects on Ca^{2+} *in vivo*. Indeed, multiple effectors often act redundantly [646, 647] and thus other putative *M. persicae* effectors, such as MpC002 [277], Mp1 [501], Mp2 [501] and Mp55 [503], might play a role. Although not yet tested, these effectors could have Ca^{2+}-suppressive qualities, with strong suppression of Ca^{2+} bursts in Arabidopsis requiring a combination of them delivered together in the saliva. Nevertheless, Mp10 acts in the BAK1 pathway to suppress PTI (see section 3.3.6). and therefore it appears that Mp10, BAK1 and $[Ca^{2+}]_{cyt}$ elevations are all connected as part of the same PTI pathway that is activated during aphid probing of the epidermal and mesophyll cells.

This page is intentionally left blank

Chapter 4: Aphid-induced Ca^{2+} bursts are mediated by *TPC1*, *GLR3.3* and *GLR3.6*

4.1 Introduction

4.1.1 The vacuole is a major store of intracellular Ca^{2+}

The vacuole is by far the largest store of Ca^{2+} inside mature plant cells, occupying up to 90% of the total cell volume [648] and containing mM concentrations of Ca^{2+} [649-651]. This organelle is therefore a candidate source of intracellular Ca^{2+}-release during stress, including in response to aphids. Localisation of AEQ to the tonoplast indicates that cold and hyperosmotic stress can induce $[Ca^{2+}]_{cyt}$ elevations around this membrane [652, 653] and that the second phase of the biphasic Ca^{2+} response to hypo-osmotic stress is linked to internal stores of Ca^{2+} [654]. In addition, Ca^{2+} release in response to flg22 is suggested to be mediated by intracellular stores, as inhibition of the $InsP_3$ pathway attenuates this response [378]. In addition, there is evidence that the $[Ca^{2+}]_{cyt}$ elevation in response to elf18 and chitin can be perturbed by pharmacological inhibitors of intracellular Ca^{2+} release [201]. Signalling may also be occurring within the vacuole, for example the vacuolar-localised CaM15 regulates the tonoplast antiporter NA+/H+ EXCHANGER 1 (NHX1) [655].

However, conclusive evidence for the role of vacuolar Ca^{2+} in signalling can only be obtained once the molecular identities of the tonoplast Ca^{2+}-permeable channels are uncovered. Although there is evidence of voltage- and ligand-gated vacuolar channels that may be permeable to Ca^{2+}, TPC1 is the only characterised Arabidopsis vacuolar Ca^{2+}-permeable channel to date [15, 648] (Section 1.1.4, Chapter 1).

4.1.2 TPC1 is regulated by a combination of Ca^{2+}, ROS, kinases and electrical signals

TPC1 is a tonoplast-localised [15, 112, 122] Ca^{2+}-permeable [15, 108-111] channel whose activity is regulated by voltage [112, 114, 115, 542] and Ca^{2+} [112, 114, 115]. In Arabidopsis TPC1 is a dimer, with each subunit housing 6 transmembrane domains and two pore domains responsible for ion conductance [114, 115] (Figure 1.2, Chapter 1). However, ion conductance is not restricted to Ca^{2+}; TPC1 is also permeable to Na^+ and K^+ [112, 113]. This lack of specificity has led to scepticism over the role of TPC1 in Ca^{2+} signalling [117, 656, 657] and it has been

suggested that TPC1 does not significantly affect $[Ca^{2+}]_{cyt}$ [122, 658]. However, fluorescent Ca^{2+} sensors can clearly visualise a TPC1-dependent $[Ca^{2+}]_{cyt}$ elevation in Arabidopsis [7, 123]. Furthermore, TPC1 contains two Ca^{2+}-binding EF-hand domains, one of which is highly selective for Ca^{2+} [112, 116] and binding of Ca^{2+} to this domain is required for full channel activation [114, 115]. Thus, TPC1 is linked to Ca^{2+} signalling irrespective of the channel's ion selectivity.

The Ca^{2+}-dependent activation of TPC1 means this channel, along with RBOHD and an unknown PM Ca^{2+}-permeable channel play a role in CICR (Figure 1.11, Chapter 1) [119, 121, 536, 537]. This model has been validated *in vivo*, with the demonstration of a TPC1- and RBOHD-dependent systemic Ca^{2+} signal in Arabidopsis roots [7, 121, 123] Moreover, extracellular ROS production is compromised in the TPC1 knock-out mutant *tpc1-2* [121].

TPC1 has two voltage-sensing domains (VSDs), although voltage-activation of the channel is mediated by VSD2 alone [114, 115]. This raises the possibility of electrical-regulation of TPC1. As with CICR, a positive feedback mechanism might be involved, as TPC1 ion release might alter the electrical potential of the cell [107, 122]. In addition, there are two phosphorylation sites close the EF-hand domains of TPC1, indicating there might be additional regulation by kinases [109, 115]. TPC1 also appears to mediate MAPK activity in *Oryza sativa* (rice) [659]. Thus, TPC1 has the capacity to regulate and be regulated by Ca^{2+}, ROS, electrical signals and kinase activity and the channel may represent a crosstalk node between these signalling pathways.

4.1.3 TPC1 mediates Ca^{2+} signalling during biotic and abiotic stress

The physiological role of TPC1 has been the subject of much debate. The Arabidopsis *tpc1-2* mutant is defective in Ca^{2+}-induced stomatal closure [15, 660] and ABA-induced inhibition of germination [15], although this ABA phenotype has been questioned [122]. Also in Arabidopsis, the endomembrane channel (and TPC1 [661]) inhibitor ruthenium red can significantly reduce the $[Ca^{2+}]_{cyt}$ increase in response to oxidative stress [662] touch [663] and cold shock [664]. However, the exact target and mechanism of this inhibitor is not known.

Ranf et al. [122] tested a range of possible elicitors on the *tpc1-2* mutant, and found no involvement for the channel in ABA or CO_2-mediated stomatal closure, or in

$[Ca^{2+}]_{cyt}$ elevations in response to cold shock, NaCl, H_2O_2, $CaCl_2$, flg22, elf18. Furthermore, expression of the SA defence marker *PR1* was not altered in *TPC1* mutants, nor was flg22- or elf18- ROS production. In addition, Bonaventure et al., [552] could find no role for *TPC1* in defence against *B. cinerea*. However, these studies investigated local application of stress. Research focused on systemic signalling has begun to elucidate a biological role for TPC1.

Application of 100 mM NaCl results in a Ca^{2+} signal that propagates along the Arabidopsis root at 400 µm/s [7]. This signal is attenuated in the *tpc1-2* mutant, where the speed is reduced to 16 µm/s [7]. Induction of various salt stress-related genes was also lost in the mutant, and overexpression of *TPC1* resulted in more salt-tolerant plants [7]. Moreover, wounding can induce leaf-to-leaf Ca^{2+} signals that can be visualised by AEQ, and these are also lost in the *tpc1-2* mutant [123]. Supporting a primarily systemic role for TPC1, these signals were comparable to wildtype within the local (wounded) leaf. Interestingly, TPC1 protein levels are significantly increased upon wounding [416] whilst the mRNA levels are not [416, 550], implying that post-translational mechanisms may be regulating TPC1 in response to stress.

TPC1 is ubiquitous across plant species [665], including *Physcomitrella patens* (moss) [666], *N. tabacum* [582], *O. sativa* [667] and wheat [667, 668]. Consequently, TPC1-mediated Ca^{2+} signalling is potentially relevant to many different systems. In *N. tabacum*, two TPC1 homologues have been identified, TPC1A and TPC1B, and these appear to mediate local Ca^{2+} release in response to the fungal elicitor cryptogein [582], SA [669] and H_2O_2 [670], as well as in response to sucrose [582] and hypo-osmotic shock [670]. In *O. sativa*, TPC1 mediates Ca^{2+} influx in response to fungal xylanases [671].

4.1.4 Over-activation of TPC1 enhances jasmonic acid production

In addition to being regulated by $[Ca^{2+}]_{cyt}$, TPC1 is also regulated by $[Ca^{2+}]_{vac}$, which in contrast to $[Ca^{2+}]_{cyt}$ inhibits channel activation [114, 656]. This $[Ca^{2+}]_{vac}$ sensitivity is conferred by four negatively-charged residues on the luminal side of the protein [672], but can be abolished by a single substitution (aspartic acid to asparagine - D454N) between the IIS1-IIS2 loop (Figure 1.2, Chapter 1) [550]. Residue D454 forms part of a critical region for $[Ca^{2+}]_{vac}$ sensitivity [114], and thus D454N gives rise to a gain-of-function allele named *fou2* that lacks this inhibition [550, 656]. Consequently, the *fou2* mutation results in increased TPC1 channel opening [550].

The *fou2* mutation also results in two-fold increase in basal JA levels and in LOX activity [550], placing the effect of this mutation at the very start of JA synthesis (Figure 4.1). As a result, a variety of stress- and JA-induced transcripts are upregulated in the *fou2* mutant [552]. The exact link between TPC1 and JA is not known. Animal LOX proteins have a Ca^{2+} binding domain [673], and Arabidopsis LOXs contain similar domains [550]. Although evidence of Ca^{2+} binding to LOXs in plants is scarce (e.g. [674]), LOX activity is regulated by kinases that are themselves regulated by Ca^{2+}, such as MPK3 and MPK6 [675]. Loss of JA perception by mutating *CORONATINE INSENSITIVE 1* (*COI1*) [676, 677] or JA synthesis by mutating *ALLENE OXIDE SYNTHASE* (*AOS*) [551] (Figure 4.1) abolishes the enhanced LOX activity and the growth inhibition exhibited in *fou2* mutants [550, 552]. Thus, the observed *fou2* phenotype is based solely on JA upregulation, and involves positive feedback between COI1 and AOS and LOX proteins [678, 679].

Loss of *TPC1* does not affect $[Ca^{2+}]_{cyt}$ elevations [660] or defence gene induction [552] elicited by methyl jasmonate (MeJA). Furthermore, abolishing transcription of *TPC1* does not affect JA production [550], and overexpression of *TPC1* does not mimic the *fou2* phenotype [15]. Thus, *TPC1* expression does not regulate wildtype JA production. Higher levels of Ca^{2+} are accumulated in the vacuole of *fou2* mesophyll cells [656], which combined with the increased probability of channel opening [550] has the potential to result in a large Ca^{2+} efflux from the vacuole. Conversely, abolishing TPC1 transcription significantly reduces $[Ca]_{vac}$ in epidermal cells, but has no effect on $[Ca]_{vac}$ in mesophyll cells [650].

There are several links between Ca^{2+} signalling and JA. MeJA elicits $[Ca^{2+}]_{cyt}$ elevations in stomata [84, 680], as well as *COI1*-dependent cation currents [681]. Furthermore, MeJA-induced stomatal closure is blocked by CaM and Ca^{2+} channel inhibitors [84, 680, 682, 683] and loss of *CNGC2* [84] or *CPK6* [684] abolishes MeJA-elicited $[Ca^{2+}]_{cyt}$ elevations. Moreover, in *N. tabacum* CDPK4 and CDPK5 are negative regulators of JA production [424]. These components are therefore candidates for crosstalk between Ca^{2+} and JA that may work independently of, or in combination with, TPC1-mediated Ca^{2+} signalling.

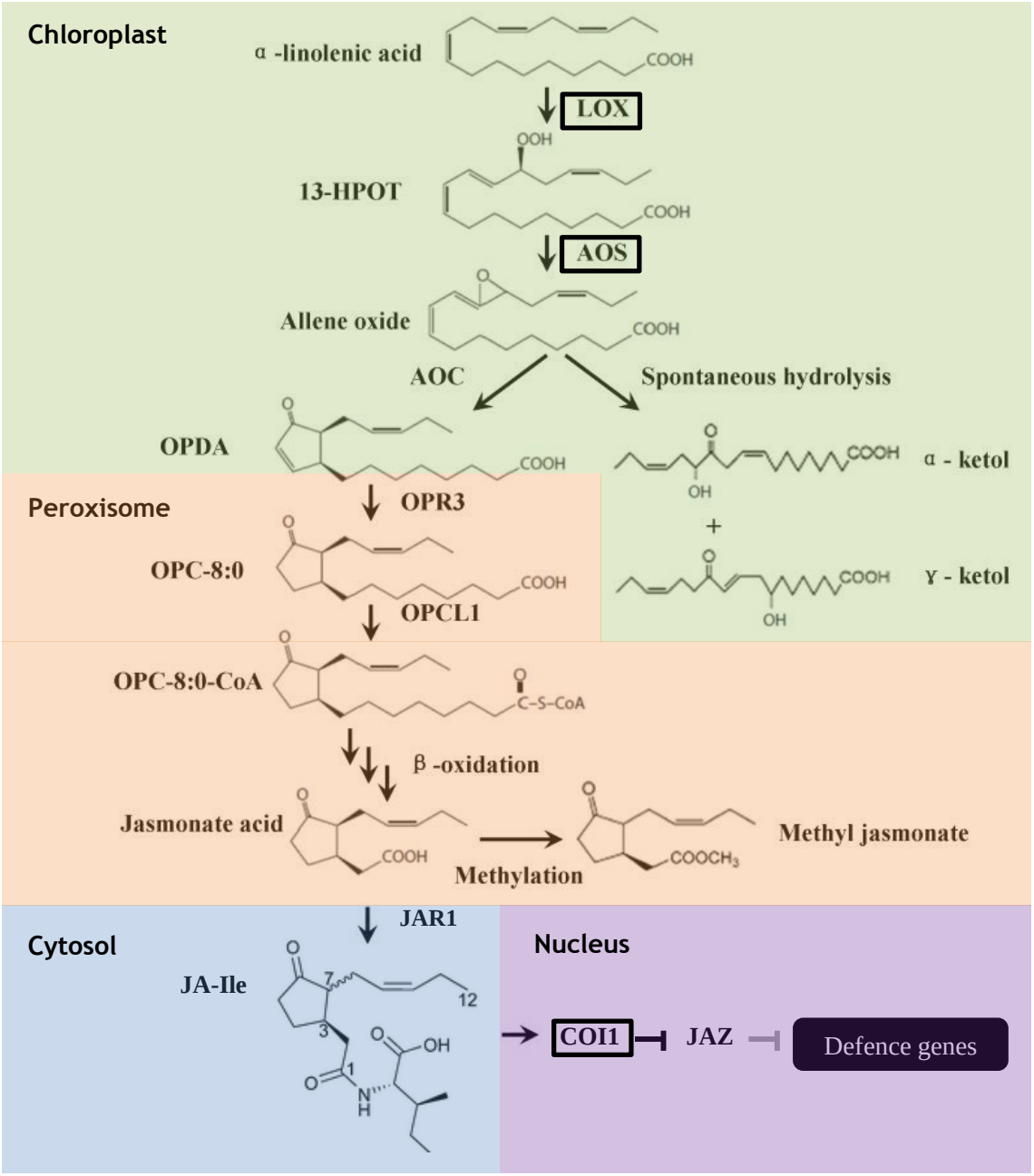

Figure 4.1: The jasmonate biosynthesis pathway.

The JA precursor α-linolenic acid is converted to active jasmonate (JA-Ile) through a series of enzymatic steps in the chloroplast (green shading), peroxisome (orange shading) and cytosol (blue shading). In the presence of JA-Ile, nuclear JAZ (jasmonate-zim-domain) proteins are targeted for degradation by COI1. This relieves JAZ repression of JA-responsive genes, including those involved in plant defence. 13-HPOT = 13-hydroperoxy linolenic acid, LOX = 13-lipoxygenase, OPDA = (9S, 13S)-12-oxo-phytodienoic acid, OPR3 = OPDA reductase, OPC-8:0 = 3-oxo-2(2'-[Z]-pentenyl)cyclopentane-1-octanoic acid, OPCL1 = OPC-8:0 CoA ligase 1, JAR1 = jasmonate resistant 1. Proteins relevant to the present study are boxed. Figure adapted from Lu et al.[685] and Jimenez-Aleman et al. [686].

4.1.5 JA is a key component of plant defence

JA accumulation is a well characterised response to wounding [392, 395, 416], herbivory [308, 332, 334, 335, 417-420] and pathogens [421, 552] (Section 1.3.4, Chapter 1). It is also detrimental to aphid performance [307, 426, 428, 429], and in agreement with this *B. brasssicae* fecundity is halved in the *fou2* mutant [430]. Furthermore, the *fou2* mutation results in the constitutive upregulation of several plant defence genes, including *PDF1.2*, *PR1*, *PR4*, *CYP79B2*, and *VSP2* [430, 552] and shows enhanced resistance to *B. cinerea* [550]. Interestingly, aphid infestation rarely results in strong differential regulation of JA-related genes [426, 427], however it has been suggested that upregulation of the SA pathway by aphids [304, 308, 433] is used to antagonise JA signalling as a part of successful colonisation of the plant [426, 427, 434-436].

4.1.6 GLR3.3 and GLR3.6 mediate wound signalling in plants

GLRs are Ca^{2+}-permeable channels [85, 91, 92] that are presumed to be localised to the PM [88, 95, 96, 105]. The Arabidopsis genome encodes 20 GLRs [83] and these can join in different combinations to form heteromers [84], the composition of which can effect biological function [99]. GLRs have an extracellular ligand-binding domain (Figure 1.2, Chapter 1) [104], and several amino acids including glutamate may act as GLR ligands [76, 92, 356], as seen with the animal GLR homologs, the iGluRs [82]. In accord with a physiological role for glutamate, glutamate application results in $[Ca^{2+}]_{cyt}$ elevations [99, 100, 687] that are attenuated in the *glr3.3* mutant [97]. Moreover, the extracellular ligand binding domain of GLRs suggests they are involved in the perception of stimuli from outside the cell. Concurring with this, GLR3.3 plays a role in $[Ca^{2+}]_{cyt}$ elevations and ROS production in response to oligogalacturonide DAMPs and *glr3.3* mutant lines exhibit compromised resistance to the oomycete *Hyaloperonospora arabidopsidis* [688]. Furthermore, antagonists of animal iGluRs can reduce the $[Ca^{2+}]_{cyt}$ elevation induced by flg22, elf18 and chitin in Arabidopsis [201].

Specific roles for *GLR3.6* in plants are not well characterised, although this gene has been linked to primary and lateral root growth [689]. However, recent work has identified that *GLR3.3* and *GLR3.6* act together to mediate wound signalling in Arabidopsis. Leaf-to-leaf electrical signals in response to wounding are significantly

attenuated in *glr3.3* and *glr3.6* mutants, and this signal is completely abolished if both are mutated (*glr3.3/3.6*) [103]. These GLR-dependent signals appear to travel systemically in the SE [541] and are composed of a brief action potential followed by a *GLR3.6*-mediated long potential [104]. Furthermore, such wounding induces JA signalling, detected through increased *JASMONATE-ZIM-DOMAIN PROTEIN 10* (*JAZ10*) expression. Interestingly, loss of *GLR3.3* or *GLR3.6* significantly reduces systemic *JAZ10* expression, but the induction in the local leaves remains the same [103]. This suggests that, as with TPC1, the primary role of the GLRs might be in systemic signalling, acting as crosstalk nodes between electrical signals, Ca^{2+} and JA. However, it is important to note that electrical signals in the local (wounded) leaf were also attenuated in both *GLR* mutants [103]. Thus, investigations to date position GLR3.3 and GLR3.6 as mediators of damage-induced signals in plants.

4.1.7 ROS and MAPKs are involved in defence against insects and are dependent on Ca^{2+} signalling

Plant defence against aphids involves several responses, including ROS production [316-318, 353, 354, 360, 371, 406, 407], MAPK activation [354, 387, 391-395] and secondary metabolite biosynthesis [296, 297, 319, 456, 457]. Incubating leaves with *M. persicae* extract results in the gradual production of H_2O_2 over several hours [349], and ROS is also produced in response to *A. pisum* [408] or *Diuraphis noxia* (Russian wheat aphid) [690] infestation, as well as to GroEL application [350]. Furthermore, infestation of Arabidopsis with *R. padi*, *M. cerasi*, or *M. persicae* results in the upregulation of genes related to ROS signalling [283], and disrupting this signalling by mutating *RBOHD* significantly increases *M. persicae* performance [413] whilst disrupting *RBOHF* expression benefits all three species [283]. Conversely, infestation with *B. brassicae* leads to a decrease in the expression of ROS-related transcripts including *RBOHD* [304]. Extracellular ROS production is dependent on TPC1 [121], RBOHD is activated by CPK5 [119] and RBOHF is regulated by CBL1, CBL9 and CIPK26 [691, 692], suggesting that ROS production lies downstream of Ca^{2+} signalling. However, there is feedback between the systems as ROS can also induce Ca^{2+} elevations [47, 120-122, 662].

MAPK activation is observed upon *M. sexta* herbivory [397], and is amplified by the presence of HAMPs in the saliva [386]. Wounding alone can also induce MAPK activation [390, 392, 393, 396] and this is linked to downstream JA signalling [392,

394, 395] and defence gene induction [393]. The role of MAPKs in plant-aphid interactions is less clear, although their involvement is likely given the role of PTI and ETI in these interactions. Indeed, silencing MAPKs in tomato significantly reduced resistance to *M. euphorbiae* [398], whilst extract from several other aphid species, including *M. persicae* and *A. pisum*, induces expression of the MAPK marker gene *FRK1* [349]. FRK1 is a PTI-activated a receptor kinase whose activity is partially regulated by the MAPK pathway [151]. *FRK1* is also significantly upregulated in plants heterologously expressing GroEL, further suggesting a role for this gene in PTI against aphids [350]. Like ROS production, MAPK activation is also dependent on Ca^{2+} signalling, as evidenced by inhibition of MAPKs by ion channel blockers [372, 693, 694]. MAPK activation is also linked to Ca^{2+} signalling through interdependence on the CDPKs [152, 386, 695].

4.1.8 Plant defence against insects culminates with the production of toxic secondary metabolites

Indole glucosinolates and camalexin are two tryptophan-derived secondary metabolites that play a crucial role in plant defence against insects. The indole glucosinolates are synthesised from indole-3-acetaldoxime (IAOx) by CYTOCHROME P450, FAMILY 81, SUBFAMILY F, POLYPEPTIDE 2 (CYP81F2) (Figure 4.2), and loss of the CYP81F2 pathway reduces the production of the anti-aphid compound 4MI3M and increases susceptibility to *M. persicae* [305]. Interestingly, this is aphid-specific, with *CYP81F2* expression appearing to have no effect on four lepidopteran species [305]. In addition, loss of enzymes upstream of IAOx synthesis, such as CYP79B2 and CYP79B3 (Figure 4.2) also results in plants more susceptible to aphid attack [470]. The plant glucosinolate response to aphids is rapid, with application of *M. persicae*, *A. pisum*, *B. brassicae* and *S. avenae* (English grain aphid) extract resulting in upregulation of *CYP81F2* within an hour [349].

Ca^{2+} signalling is implicated in glucosinolate production; with the CaM-binding protein IQ-DOMAIN 1 (IQD1) mediating the expression of several *CYPs* and overexpression of *IQD* resulting in reduced *M. persicae* fecundity [696]. ROS are also implicated in this pathway, with induction of *CYP81F2* significantly reduced if ROS production is compromised [697]. Furthermore, the production of 4MI3M is also dependent on MAPK signalling via *MPK3* and *MPK6* [698].

Camalexin biosynthesis from IAOx is mediated by the enzyme PAD3 (Figure 4.2) [455, 459]. Like 4MI3M, camalexin production is detrimental to aphid performance, with abolition of the *PAD3* transcript resulting in plants more susceptible to aphids [304, 306, 349]. Production of camalexin is upregulated by whole-body extracts from various aphids, including *M. persicae* [349], as well as by aphid saliva [464] and live feeding [304, 308]. A direct link between Ca^{2+} signalling and camalexin production has not been established, however both are important in plant defence against pathogens and aphids. As with 4MI3M, camalexin production in response to fungi is dependent on *MPK3* and *MPK6* in Arabidopsis [699].

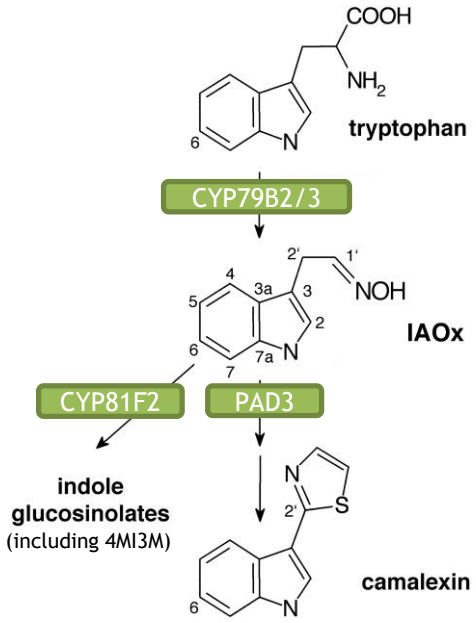

Figure 4.2: Tryptophan-derived secondary metabolites represent key anti-insect molecules.

Glucosinolates and camalexin are produced in plants during herbivory and reduce insect fitness. Proteins key in the production of each metabolite are shown in green boxes. Adapted from Glawischnig et al. [700].

4.1.9 Aims of this chapter

This chapter outlines experiments designed to identify the mechanisms behind the aphid-induced Ca^{2+} burst in Arabidopsis. Ca^{2+} signalling in plants lacking the Ca^{2+}-permeable channels TPC1 and GLR3.3/3.6 was investigated using the GCAMP3 sensor, as was the signalling in *TPC1* overexpression and *fou2* over-activation lines. These mutants were also assessed for a role in plant defence induction, including ROS production, MAPK activation and secondary metabolite pathways, as well as for altered aphid feeding behaviour and fitness. Consequently, this chapter also links the Ca^{2+} burst identified in Chapter 3 to downstream defence responses in the plant, as well as exploring connections between Ca^{2+} and other plant signalling pathways.

4.1.10 Materials and methods

The methods used in his chapter are detailed in Chapter 2. Information on the microscopy assay can be found in Section 2.8, aphid performance assays (including fecundity, survival, choice tests, EPG and IR) in Section 2.9, and Arabidopsis ROS and defence gene induction assays in Section 2.10.

4.2 Results

4.2.1 *TPC1* expression affects the amplitude and speed of the aphid-induced Ca^{2+} burst

In order to assess whether TPC1 plays a role in aphid-induced Ca^{2+} bursts, GFP fluorescence in 35::GCAMP3 x *tpc1-2* and 35S::GCAMP3 x 35S::TPC1 5.6 lines was assessed. In comparison to 35S::GCAMP3 (Figure 4.3a), the feeding site burst was significantly reduced (Figure 4.3c), although not abolished (Figure 4.3b), in 35S::GCAMP3 x *tpc1-2* (Video 4.1). In 35S::GCAMP3 x *tpc1-2* samples that produced a recordable measurement (R), the area of spread and the speed of the Ca^{2+} burst were not significantly altered (Figure 4.4). As observed previously (Figure 3.15, Chapter 3), the Ca^{2+} burst in 35S::GCAMP3 and 35S::GCAMP3 x *tpc1-2* lines was not the result of a discreet 'on' or 'off' response (Figure D1, Appendix D). In 35S::GCAMP3 x 35S::TPC1 5.6 plants, the amplitude of the burst was not significantly different from the control plants (Figure 4.5, Video 4.2), nor was the area of spread (Figure 4.6a). However, the speed of propagation was significantly increased (Figure 4.6b).

Analysis of systemic Ca^{2+} dynamics revealed that in the midrib of 35S::GCAMP3 x *tpc1-2* leaves treated with aphids, a significant rise in GFP fluorescence was observed relative to the un-infested control leaves (Figure D2, Appendix D). This was not seen in the lateral tissue (Figure D3, Appendix D). No systemic signals were seen in the 35S::GCAMP3 x 35S::TPC1 5.6 line (Figure D5 and D6, Appendix D). In addition, no differences in aphid settling behaviour were seen on either *TPC1* expression mutant (Figure D4 and D7, Appendix D).

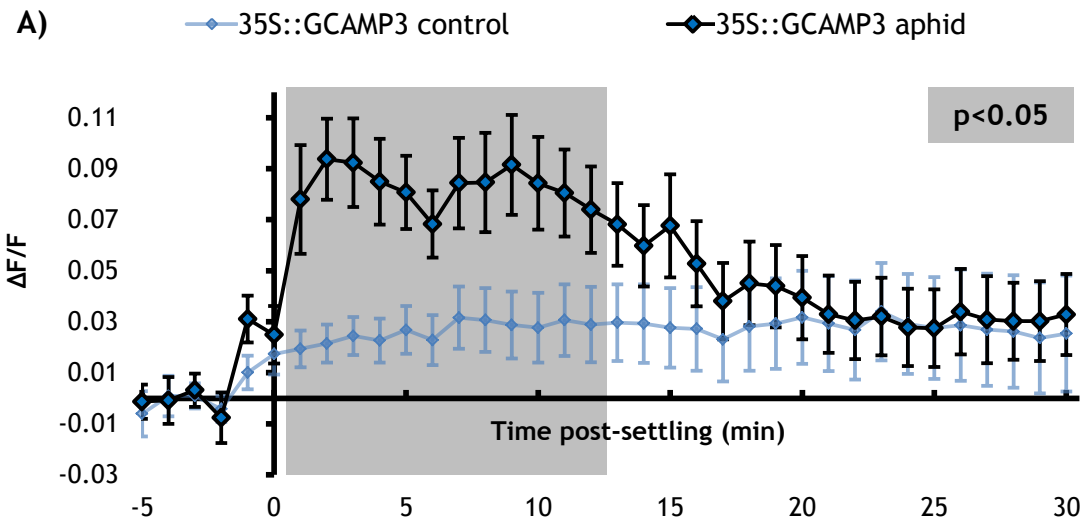
A)
35S::GCAMP3 control
35S::GCAMP3 aphid
p<0.05
ΔF/F
0.11
0.09
0.07
0.05
0.03
0.01
-0.01
-0.03
Time post-settling (min)
-5
0
5
10
15
20
25
30

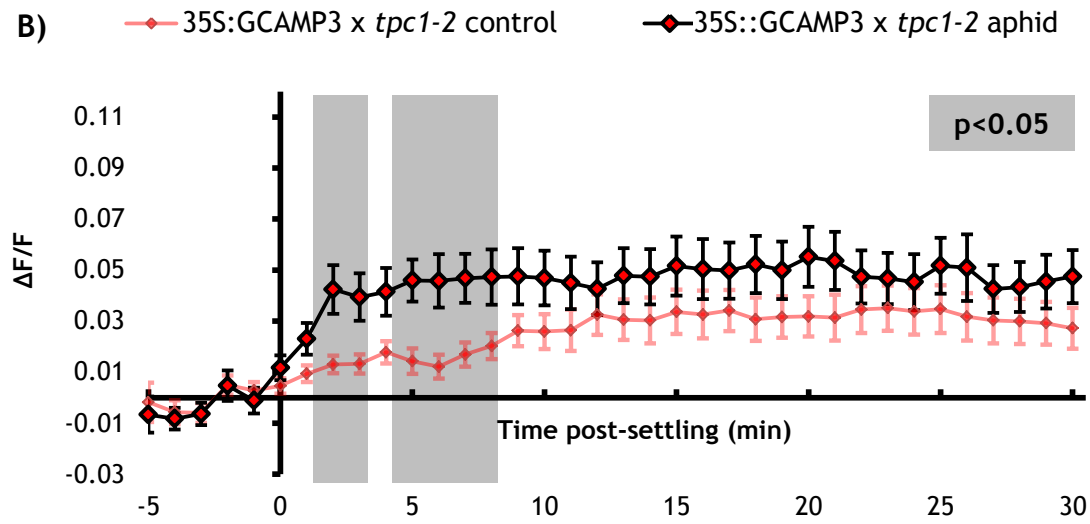
B)
35S:GCAMP3 x tpc1-2 control
35S::GCAMP3 x tpc1-2 aphid
p<0.05
ΔF/F
0.11
0.09
0.07
0.05
0.03
0.01
-0.01
-0.03
Time post-settling (min)
-5
0
5
10
15
20
25
30

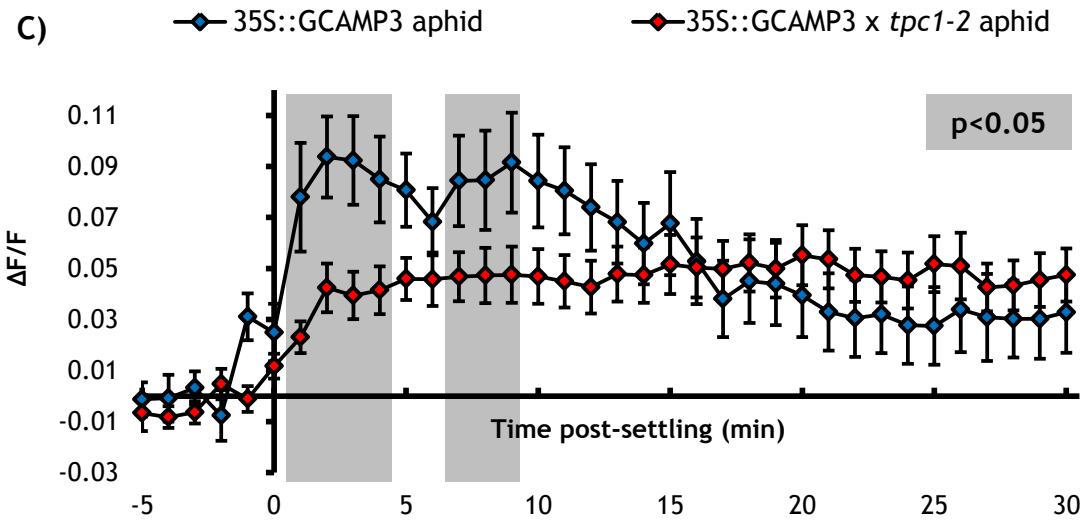
C)
35S::GCAMP3 aphid
35S::GCAMP3 x tpc1-2 aphid
p<0.05
ΔF/F
0.11
0.09
0.07
0.05
0.03
0.01
-0.01
-0.03
Time post-settling (min)
-5
0
5
10
15
20
25
30

Figure 4.3: Normalised GFP fluorescence (ΔF/F) around the feeding site in 35S:GCAMP3 and 35S:GCAMP3 x *tpc1-2* Arabidopsis upon *M. persicae* settling.

A) 35S:GCAMP3 control (no aphid treatment) vs aphid treatment. **B)** 35S:GCAMP3 x *tpc1-2* control (no aphid treatment) vs aphid treatment. **C)** 35S:GCAMP3 aphid treatment vs 35S:GCAMP3 x *tpc1-2* aphid treatment. Bars represent SEM (35S:GCAMP3 n=27, 35S:GCAMP3 x *tpc1-2* n=29). Grey shading indicates significant difference between treatments (Student's t-test within GLM at $p<0.05$). Experiment conceived and designed by T.V and conducted by T.V. and J.C.

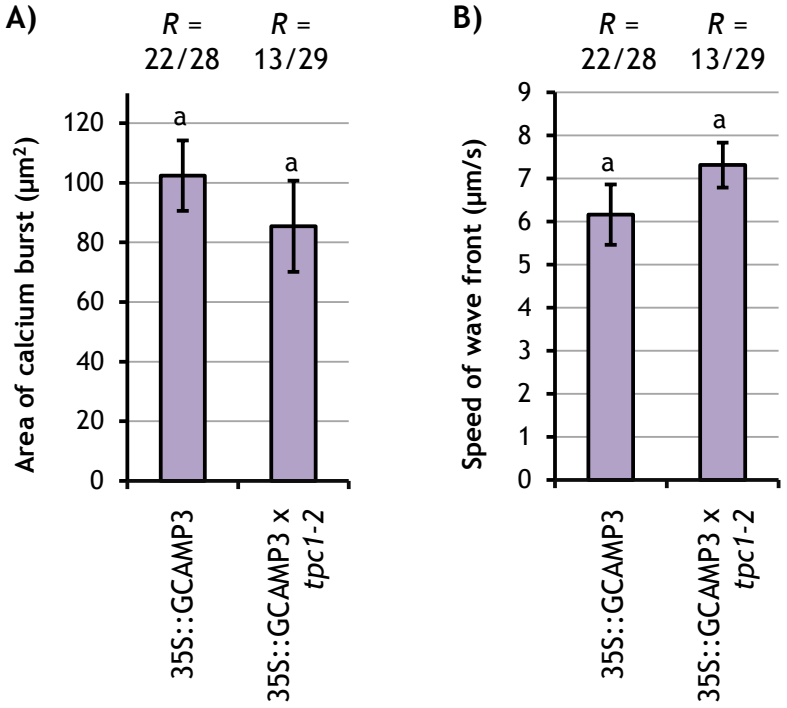

Figure 4.4: Properties of the *M. persicae*-induced Ca^{2+}burst around the feeding site in 35S::GCAMP3 and 35S::GCAMP3 x *tpc1-2* leaves.

Comparing properties of the Ca^{2+} burst only in recordable samples (R), i.e. samples in which a feeding site GFP burst was visible by eye. **A)** Area of the Ca^{2+} burst. **B)** Speed of the Ca^{2+} wave front. Bars represent SEM. Letters indicate no significant difference between genotypes (Student's t-test $p<0.05$). Experiment conceived and designed by T.V and conducted by T.V. and J.C.

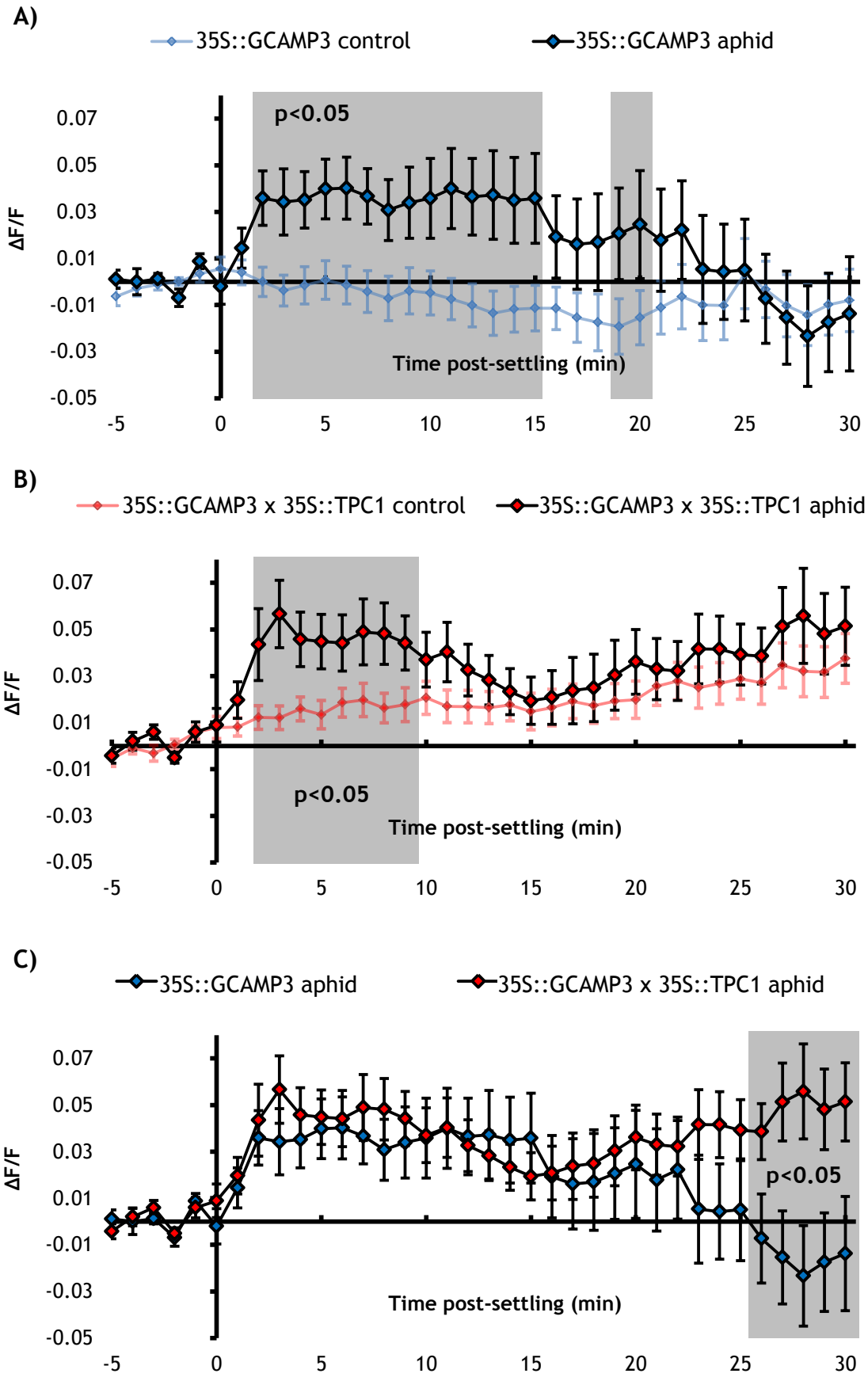
A)
35S::GCAMP3 control
35S::GCAMP3 aphid
p<0.05
ΔF/F
0.07
0.05
0.03
0.01
-0.01
-0.03
-0.05
Time post-settling (min)
-5
0
5
10
15
20
25
30
B)
35S::GCAMP3 x 35S::TPC1 control
35S::GCAMP3 x 35S::TPC1 aphid
p<0.05
ΔF/F
Time post-settling (min)
C)
35S::GCAMP3 aphid
35S::GCAMP3 x 35S::TPC1 aphid
p<0.05
ΔF/F
Time post-settling (min)

Figure 4.5: Normalised GFP fluorescence (ΔF/F) around the feeding site in 35S::GCAMP3 and 35S::GCAMP3 x 35S::TPC1 5.6 Arabidopsis upon *M. persicae* settling.

A) 35S::GCAMP3 control (no aphid treatment) vs aphid treatment. **B)** 35S::GCAMP3 x 35S::TPC1 5.6 control (no aphid treatment) vs aphid treatment. **C)** 35S::GCAMP3 aphid treatment vs 35S::GCAMP3 x 35S::TPC1 5.6 aphid treatment. Bars represent SEM (35S::GCAMP3 n=30, 35S::GCAMP3 x 35S::TPC1 5.6 n=29). Grey shading indicates significant difference between treatments (Student's t-test within GLM at $p<0.05$). Experiment conceived and designed by T.V and conducted by T.V. and M.A.

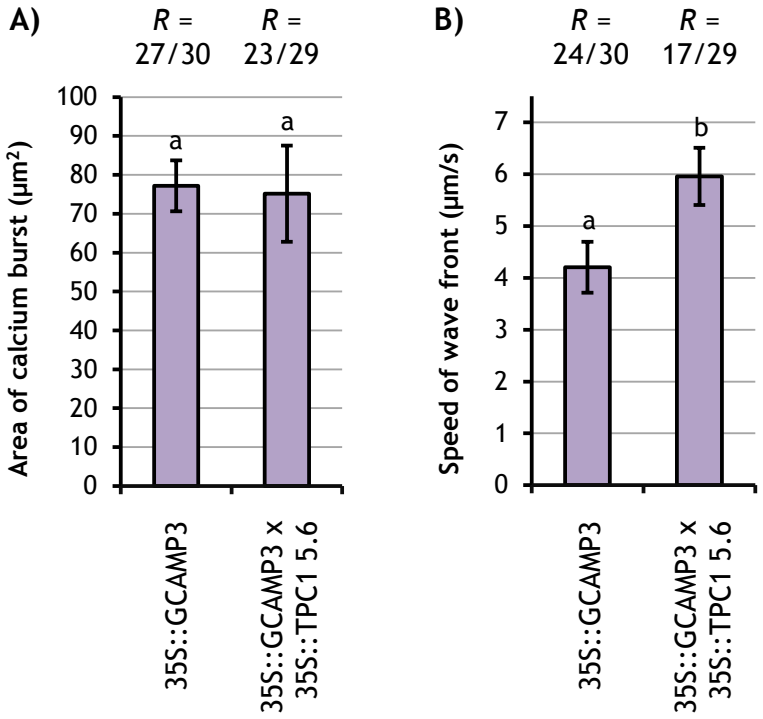

Figure 4.6: Properties of the *M. persicae*-induced Ca^{2+}burst around the feeding site in 35S::GCAMP3 and 35S::GCAMP3 x 35S::TPC1 5.6 leaves.

Comparing properties of the Ca^{2+} burst in recordable samples (R), i.e. samples in which a feeding site GFP burst was visible by eye. **A)** Area of the Ca^{2+} burst. **B)** Speed of the Ca^{2+} wave front. Bars represent SEM. Letters indicate a significant difference between genotypes (Student's t-test $p<0.05$). Experiment conceived and designed by T.V and conducted by T.V. and M.A.

4.2.2 Plant ROS production and IR is altered in 35S::TPC1 plants

To investigate if *TPC1* expression has an effect on plant defence, plant ROS production and IR was assessed. Application of aphid extract to leaf disks resulted in a ROS burst that peaked at around 200 min post-application (Figure 4.7a). This aphid extract-induced burst was significantly larger in 35S::TPC1 5.6 and 35S::TPC1 10.12 lines (Figure 4.7b and C5c), but not altered in the *tpc1-2* mutant (Figure 4.7d). Interestingly, the water controls also showed a ROS burst from 0-50 min (Figure 4.7a), as seen previously [349].

IR in response to local pre-treatment with aphids occurred on Col-0 as seen previously (Figure B5, Chapter 3). This also occurred with the *tpc1-2* mutant, but was compromised in the 35S::TPC1 5.6 line (Figure 4.8).

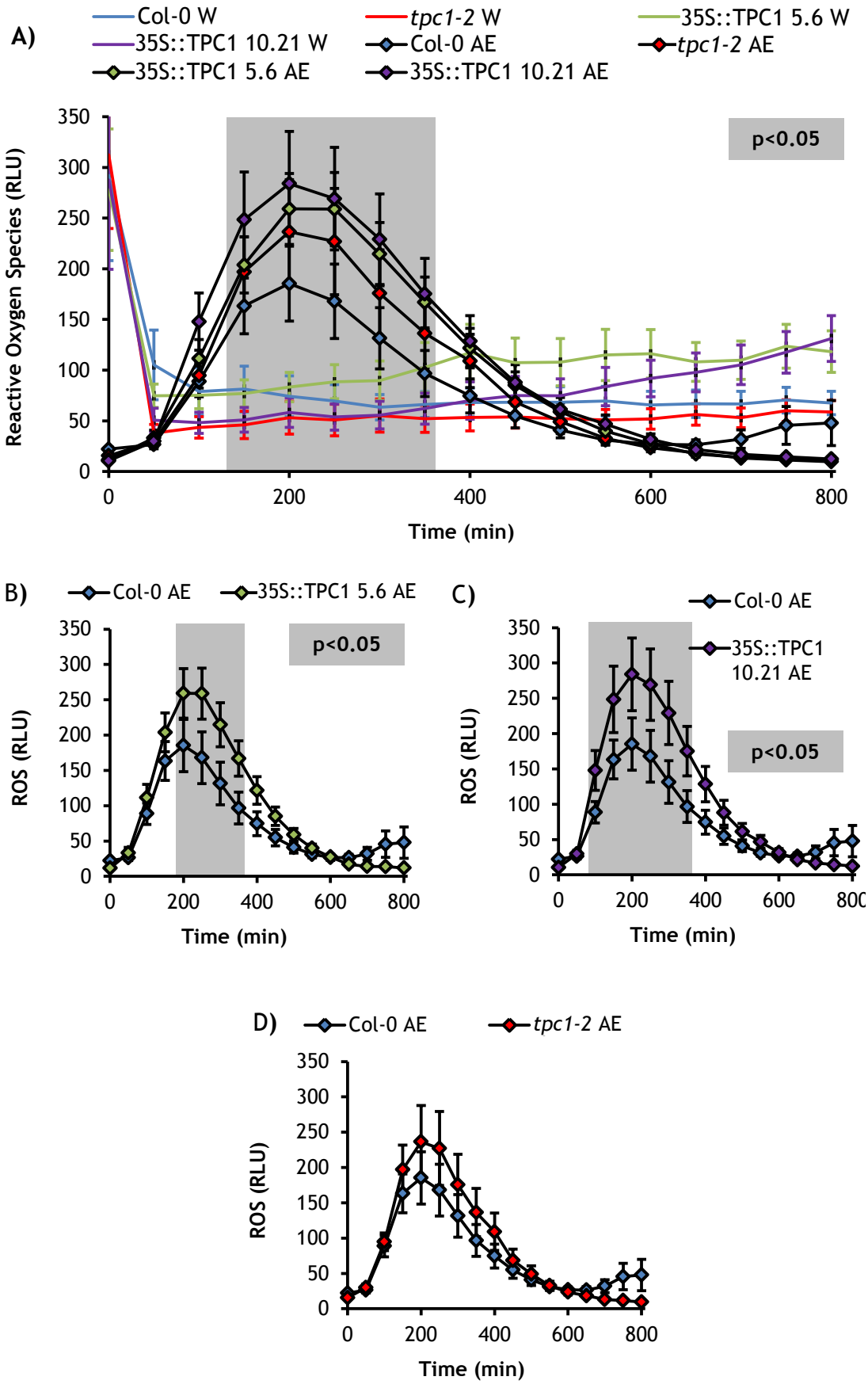
A)
Col-0 W
tpc1-2 W
35S::TPC1 5.6 W
35S::TPC1 10.21 W
Col-0 AE
tpc1-2 AE
35S::TPC1 5.6 AE
35S::TPC1 10.21 AE
Reactive Oxygen Species (RLU)
p<0.05
Time (min)
B)
Col-0 AE
35S::TPC1 5.6 AE
ROS (RLU)
p<0.05
Time (min)
C)
Col-0 AE
35S::TPC1 10.21 AE
ROS (RLU)
p<0.05
Time (min)
D)
Col-0 AE
tpc1-2 AE
ROS (RLU)
Time (min)

Figure 4.7: ROS production in Arabidopsis leaf disks upon application of *M. persicae* extract.

A) ROS production measured as relative light units (RLU) over time in all treatments. W= water. AE= aphid extract. Shading represents a significant difference between aphid extract and water treated leaf disks (within a genotype), shared across all four genotypes (Student's t-test within GLM at $p<0.05$). **B)** ROS production in 35S::TPC1 5.6 upon application of aphid extract compared to Col-0. **C)** ROS production over time upon application of aphid extract in 35S::TPC1 10.21 compared to Col-0. Shading represents a significant difference between genotypes (Student's t-test within GLM at $p<0.05$) **D)** ROS production over time upon application of aphid extract in *tpc1-2* compared to Col-0. Bars represent SEM of 24 biological replicates from 3 independent experiments. Shading represents a significant difference between genotypes (Student's t-test within GLM at $p<0.05$).

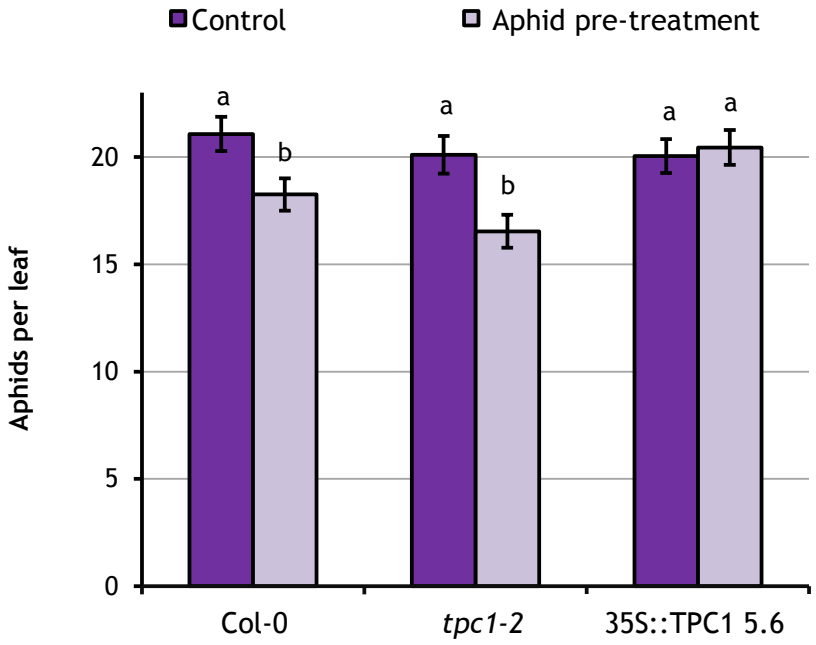

Figure 4.8: IR to *M. persicae* is lost on 35S::TPC1 5.6 Arabidopsis

Leaves were pre-treated with 50 adult *M. persicae* individuals to activate IR. After removal of the initial infestation, the fecundity of a single adult feeding from the pre-treated leaves was measured. Pre-treatment with an empty clip-cage was used as a control. Bars show SEM of 18 biological replicates from 6 independent experiments. Letters indicate significant difference between treatments (Student's t-test within GLM at $p<0.05$).

4.2.3 *TPC1* expression has an effect on aphid feeding behaviour

To test whether Ca^{2+} signalling mediated by TPC1 has an effect on aphid feeding behaviour, EPG was conducted on the *TPC1* lines. Comparing Col-0 and *tpc1-2*, no differences in pathway or the majority of phloem behaviours were found (Table 4.1). However, on the *tpc1-2* mutant phloem rejection behaviour was observed. This constituted salivations into the SE (E1) that were not followed by ingestion (E2), termed single phloem salivations (Table 4.1 behaviour 29, Figure 4.9a). This behaviour was absent from the wildtype (Figure 4.9a), but also present on the *TPC1* overexpression line (Figure 4.9b)

A comparison was also made between feeding behaviour of aphids on the *tpc1-2* mutant versus the 35S::TPC1 5.6 line. Again, no differences in pathway behaviours or most phloem behaviours were observed (Table 4.2, Figure 4.9c). However, the number of phloem ingestion phases (E2) was significantly higher in 35S::TPC1 5.6 relative to *tpc1-2* (Table 4.2, behaviour 32, Figure 4.9d). Interestingly, the sum of E1 behaviours on 35S::TPC1 5.6 was double that of *tpc1-2* (p=0.08, Table 4.2 behaviour 29).

Table 4.1: EPG data for Col-0 vs tpc1-2.

Probe = feeding event, pd = potential drop (cell puncture), C = pathway phase, E1 = phloem salivation, E2 = phloem ingestion, sE2 = sustained E2 (>10 min), no = number. Duration recorded in s. p-values calculated using a Mann-Whitney U-test (Col-0 n= 22, *tpc1-2* n= 23). Experiment conceived and designed by T.V and conducted by P.H. under supervision of T.V.

		Col-0		*tpc1-2*		p-value
	Pathway behaviours (1st h)	**Mean**	**SEM**	**Mean**	**SEM**	
1	number of probes	6.2	0.7	6.8	0.8	0.51
2	average probe	300	94	230	74	0.87
3	sum of probing	1200	200	1100	170	1.00
4	duration of 1st probe	160	110	97	35	0.76
5	number of pd	12	2	11	2	0.75
6	average duration of pd	6.3	0.3	6.1	0.2	0.35
7	sum of pd	74	10	68	9	0.58
8	time to 1st pd (from start of 1st probe)	180	111	180	110	0.85
9	time to 1st pd in 1st probe with a pd	12	2	17	3	0.21
10	no. pd per min C	1.0	0.1	0.9	0.1	0.35
11	no. pd in 1st probe	2.7	1.2	1.6	0.3	0.92

		Col-0		*tpc1-2*		p-value
	Pathway behaviours (8 h)	**Mean**	**SEM**	**Mean**	**SEM**	
12	duration of the first pd	26	2.2	25	2.7	0.73
13	mean duration of the first 5 pd	650	82	790	174	0.83
14	number of probes	14000	1100	13000	1000	0.55
15	average probe	160	110	97	35	0.76
16	sum of probing	130	13	120	11	1.00
17	duration of 1st probe	5.8	0.1	5.9	0.1	0.73
18	number of pd	750	70	720	66	1.00
19	average duration of pd	180	110	180	110	0.85
20	sum of pd	12	2.2	17	3	0.21
21	time to 1st pd (from start of 1st probe)	0.8	0.0	0.8	0.0	0.45
22	time to 1st pd in 1st probe with a pd	2.7	1.2	1.6	0.3	0.92
23	no. pd per min C	6.6	0.6	7.0	0.4	0.63
24	no. pd in 1st probe	6.5	0.3	6.3	0.2	0.36
25	duration of the first pd	1900	400	2800	810	0.60
26	mean duration of the first 5 pd	26	2.2	25	2.7	0.73
27	time to 1st probe	650	82	790	174	0.83
	Phloem behaviours (8 h)					
29	number of single E1 (without E2) periods	0.0	0.0	0.2	0.1	0.05
30	sum of E1 (sgE1 and E1)	68	13	110	26	0.34
31	sum of E2	2000	780	2000	740	0.97
32	maximum E2 period	1500	590	1700	660	0.78
33	number of sustained E2 (>10 min)	0.6	0.2	0.8	0.3	0.68
34	mean duration of sE2	2300	600	1700	370	0.35
35	sum of duration of sE2	1600	770	1600	720	0.73
36	average time to 1st E within probes	1700	220	1700	200	0.90
37	minimum time to 1st E within probes	1400	220	1300	210	0.84
38	number of probes before the 1st E	13	2.6	15	2.4	0.39

Table 4.2: EPG data for *tpc1-2* vs 35S:TPC1 5.6.

Probe = feeding event, pd = potential drop (cell puncture), C = pathway phase, E1 = phloem salivation, E2 = phloem ingestion, sE2 = sustained E2 (>10 min), no = number. Duration recorded in s. p-values calculated using a Mann-Whitney U-test (*tpc1-2* n= 25, 35S::TPC1 5.6 n= 30). Experiment conceived and designed by T.V and conducted by P.H. under supervision of T.V.

		tpc1-2		35S::TPC1 5.6		p-value
	Pathway behaviours (1st h)	**Mean**	**SEM**	**Mean**	**SEM**	
1	number of probes	7.2	0.8	7.0	0.8	0.92
2	average probe	350	120	350	140	0.97
3	sum of probing	1500	200	1500	200	1.00
4	duration of 1st probe	160	120	240	150	0.68
5	number of pd	21	2	21	3	0.98
6	average duration of pd	5.3	0.1	5.5	0.3	0.90
7	sum of pd	100	12	100	15	0.97
8	time to 1st pd (from start of 1st probe)	33	15	110	46	0.91
9	time to 1st pd in 1st probe with a pd	13	2	10	1	0.34
10	no. pd per min C	1.4	0.2	1.1	0.1	0.39
11	no. pd in 1st probe	3.4	2.0	5.5	3.1	0.54
12	duration of the first pd	6.4	0.4	6.1	0.5	0.74
13	mean duration of the first 5 pd	5.8	0.2	5.9	0.3	0.84
	Pathway behaviours (8 h)					
14	number of probes	27	3.4	26	2.5	0.86
15	average probe	2200	970	1000	170	0.68
16	sum of probing	17000	1200	19000	1100	0.34
17	duration of 1st probe	1000	950	290	200	0.59
18	number of pd	140	12	140	11	0.99
19	average duration of pd	4.8	0.0	4.9	0.1	0.80
20	sum of pd	690	57	700	52	0.82
21	time to 1st pd (from start of 1st probe)	33	15	270	170	0.90
22	time to 1st pd in 1st probe with a pd	13	2.3	9.8	1.3	0.29
23	no. pd per min C	1	0	1	0	0.35
24	no. pd in 1st probe	4	2.6	5.6	3	0.24
25	duration of the first pd	6.4	0.4	6.3	0.4	0.78
26	mean duration of the first 5 pd	5.8	0.2	5.7	0.2	0.59
27	time to 1st probe	1100	420	720	250	0.99

		tpc1-2		35S::TPC1 5.6		p-value
	Phloem behaviours (8 h)					
28	number of single E1 (without E2) periods	0.1	0.1	0.1	0.1	0.54
29	sum of E1 (sgE1 and E1)	110	18	270	97	0.08
30	sum of E2	6900	1500	8400	1400	0.33
31	maximum E2 period	6300	1500	6200	1300	0.56
32	number of sustained E2 (>10 min)	1	0.2	2.1	0.3	0.02
33	mean duration of sE2	6800	1500	5100	1300	0.39
34	sum of duration of sE2	6500	1500	7700	1400	0.36
35	average time to 1st E within probes	1400	130	1300	120	0.41
36	minimum time to 1st E within probes	1200	160	970	120	0.14
37	number of probes before the 1st E	13	2.1	11	2	0.59

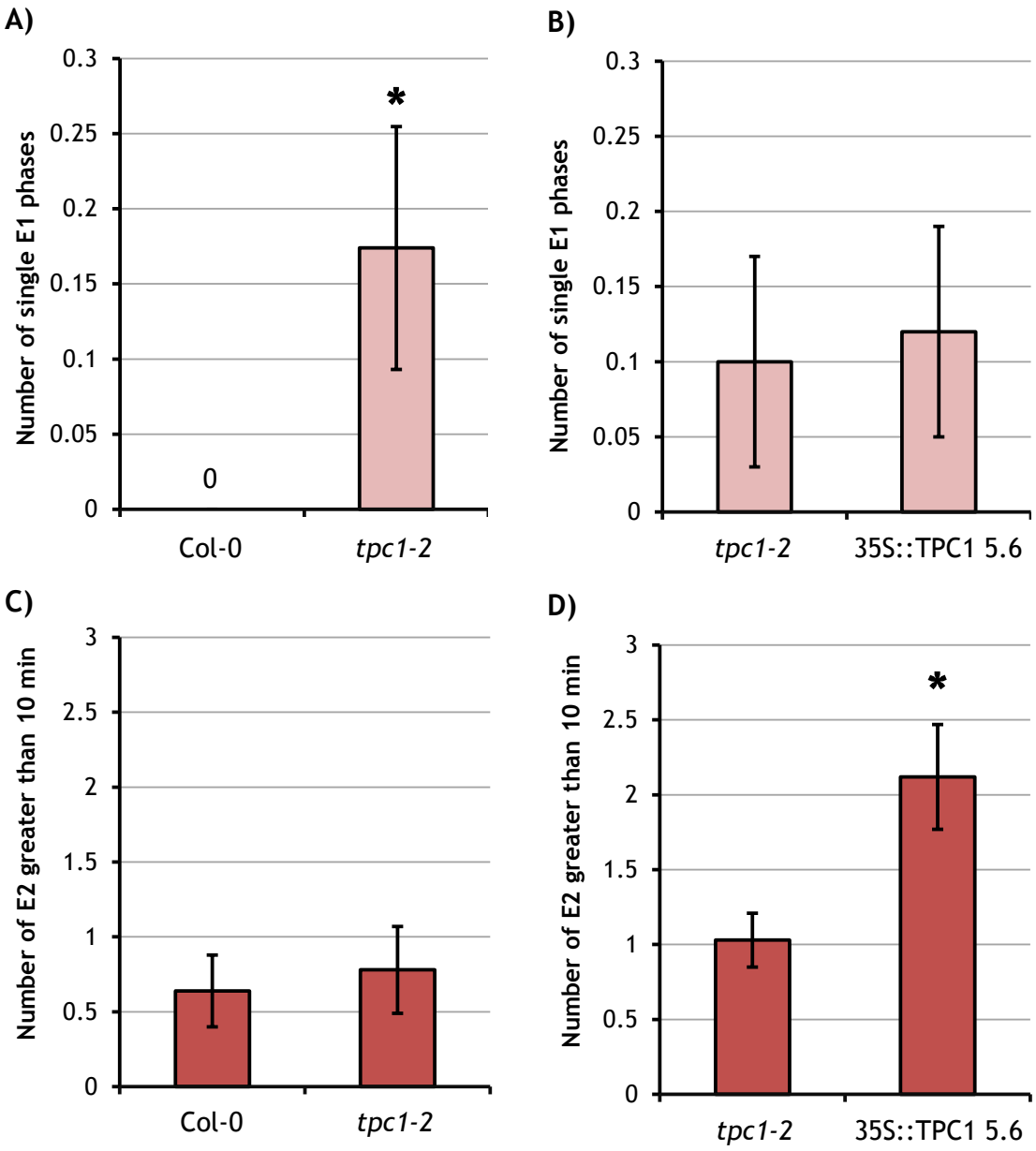

Figure 4.9: Altered *M. persicae* phloem phase behaviours in *TPC1* expression mutants.

A) Single phloem salivations (E1 without E2) in Col-0 vs *tpc1-2*. Error bars represent SEM (Col-0 n= 22, *tpc1-2* n= 23). **B)** Single phloem salivations (E1 without E2) in *tpc1-2* vs 35S::TPC1 5.6. Error bars represent SEM (*tpc1-2* n= 25, 35S::TPC1 5.6 n= 30). **C)** The number of sustained phloem ingestions (E2 > 10 min) in Col-0 vs *tpc1-2*. Error bars represent SEM (*tpc1-2* n= 25, 35S::TPC1 5.6 n= 30). **D)** The number of sustained phloem ingestions (E2 > 10 min) in *tpc1-2* vs 35S::TPC1 5.6. Error bars represent SEM (*tpc1-2* n= 25, 35S::TPC1 5.6 n= 30). * indicates a significant difference between treatments ($p<0.05$, Mann-Whitney U-test). Experiment conceived and designed by T.V and conducted by P.H. under supervision of T.V.

4.2.4 *TPC1* expression has no effect on aphid fecundity, host choice or survival

To assess whether *TPC1* expression has an effect on aphid fitness, the fecundity of *M. persicae* was assessed on these lines. Fecundity was not altered on the *tpc1-2* mutant (Figure 4.10a) or 35S::TPC1 5.6 (Figure 4.10b). Furthermore, when given a choice between the *tpc1-2* mutant and 35S::TPC1 5.6, *M. persicae* showed no host preference in a choice test (Figure 4.10c). In addition, the survival of *A. pisum* was not significantly different on *tpc1-2* or 35S::TPC1 5.6 (Figure 4.10d).

4.2.5 TPC1 over-activation (*fou2*) results in systemic aphid-induced Ca^{2+} bursts

In order to further assess the role of TPC1 in Ca^{2+} signalling during plant-aphid interactions, the *fou2* mutant was studied. The amplitude of the feeding site Ca^{2+} burst was not altered on 35S::GCAMP3 x *fou2* (Figure 4.11c), although it showed more variability relative to its no-aphid control (Figure 4.11b) than 35S::GCAMP3 (Figure 4.11a). The same large variability was seen in the area of the feeding site Ca^{2+} burst in 35S::GCAMP3 x *fou2* (Figure 4.12a), but not in the speed of its propagation (Figure 4.12b). In addition, a large systemic Ca^{2+} burst was seen in the 35S::GCAMP3 x *fou2* line (Video 4.3) that was detectable in the lateral tissue (Figure 4.13) but not the midrib (Figure 4.14). Aphid settling behaviour was not significantly altered on the 35S::GCAMP3 x *fou2* line (Figure D8, Appendix D).

4.2.6 TPC1 over-activation (*fou2*) significantly reduces aphid fecundity

In addition to the Ca^{2+} assays conducted on 35S::GCAMP3 x *fou2*, aphid performance was also assessed on the *fou2* mutant. *M. persicae* fecundity was significantly reduced on the *fou2* line. However, this was abolished on the JA-deficient double mutant *fou2*/*aos* (Figure 4.15a). Interestingly, *A. pisum* survival was also decreased on the *fou2* mutant and even further on the *fou2*/*aos* line (Figure 4.15b).

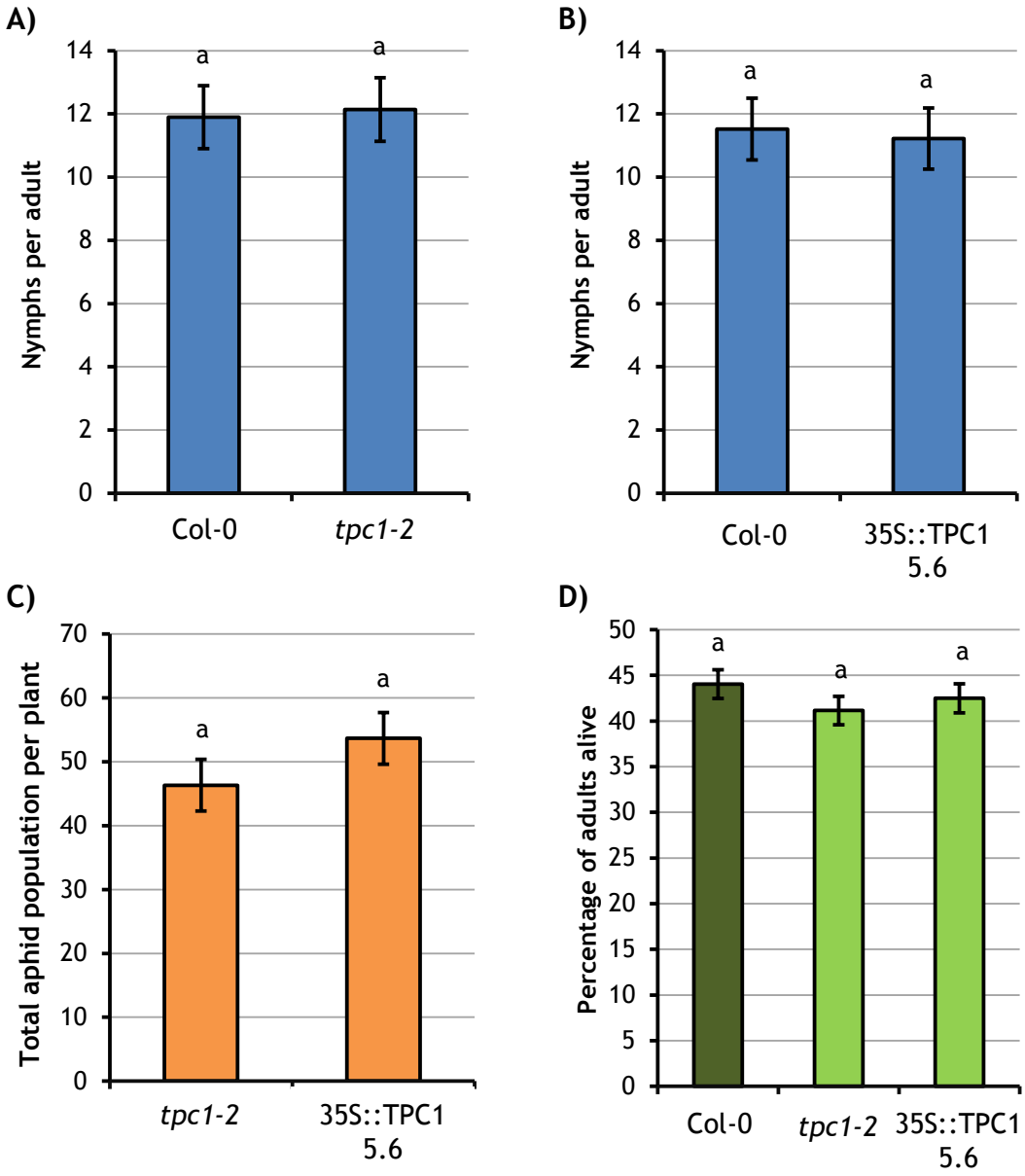

Figure 4.10: ***TPC1*** **expression does not affect aphid performance or host choice.**

A) *M. persicae* fecundity on *tpc1-2*. Bars show SEM of 12 biological replicates from 3 independent experiments. Experiment conducted by Marco Pitino (Hogenhout lab). **B)** *M. persicae* fecundity on 35S::TPC1 5.6. Bars show SEM of 12 biological replicates from 3 independent experiments. Experiment conducted by Marco Pitino (Hogenhout lab). **C)** *M. persicae* host choice preference between *tpc1-2* and 35S::TPC1 5.6. The percentage of the total aphid population settled on each plant after a 24-hour choice period is displayed. Bars show SEM of 20 biological replicates from 4 independent experiments. **D)** *A. pisum* survival on TPC1 mutants. Survival was averaged across the two days in which the control population (Col-0) decreased below 50% survival. Bars represent SEM of 18 biological replicates from 3 independent experiments. Letters indicate no significant difference between genotypes (Student's t-test within GLM, $p<0.05$).

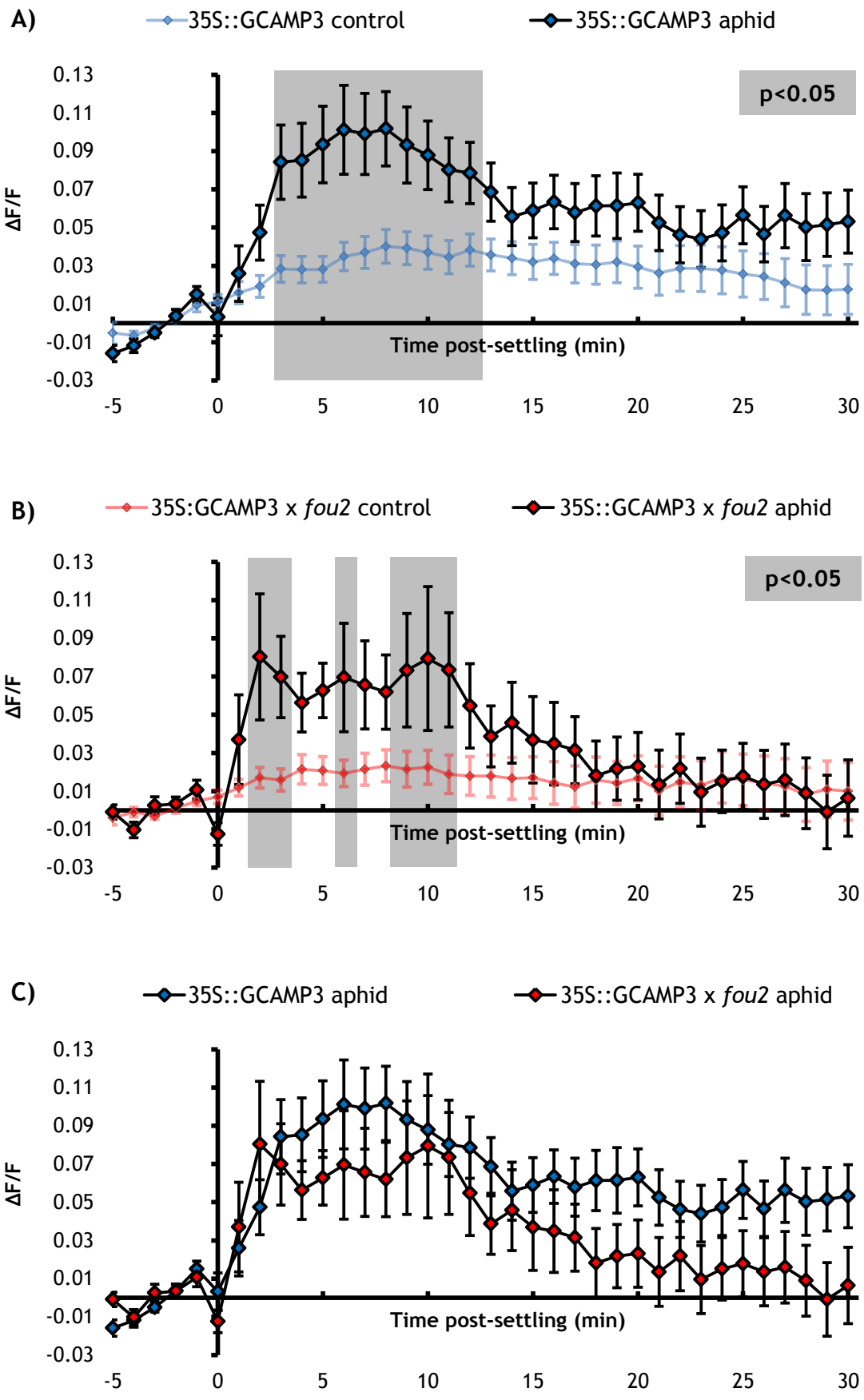
A)
35S::GCAMP3 control
35S::GCAMP3 aphid
p<0.05
ΔF/F
Time post-settling (min)
B)
35S:GCAMP3 x fou2 control
35S::GCAMP3 x fou2 aphid
p<0.05
ΔF/F
Time post-settling (min)
C)
35S::GCAMP3 aphid
35S::GCAMP3 x fou2 aphid
ΔF/F
Time post-settling (min)

Figure 4.11: Normalised GFP fluorescence (ΔF/F) around the feeding site in 35S:GCAMP3 and 35S:GCAMP3 x *fou2* Arabidopsis upon *M. persicae* settling.

A) 35S:GCAMP3 control (no aphid treatment) vs aphid treatment. **B)** 35S:GCAMP3 x *fou2* control (no aphid treatment) vs aphid treatment. **C)** 35S:GCAMP3 aphid treatment vs 35S:GCAMP3 x *fou2* aphid treatment. Bars represent SEM (35S:GCAMP3 n=28, 35S:GCAMP3 x *fou2* n=25). Grey shading indicates significant difference between treatments (Student's t-test within GLM at $p<0.05$). Experiment conceived and designed by T.V and conducted by T.V. and M.A.

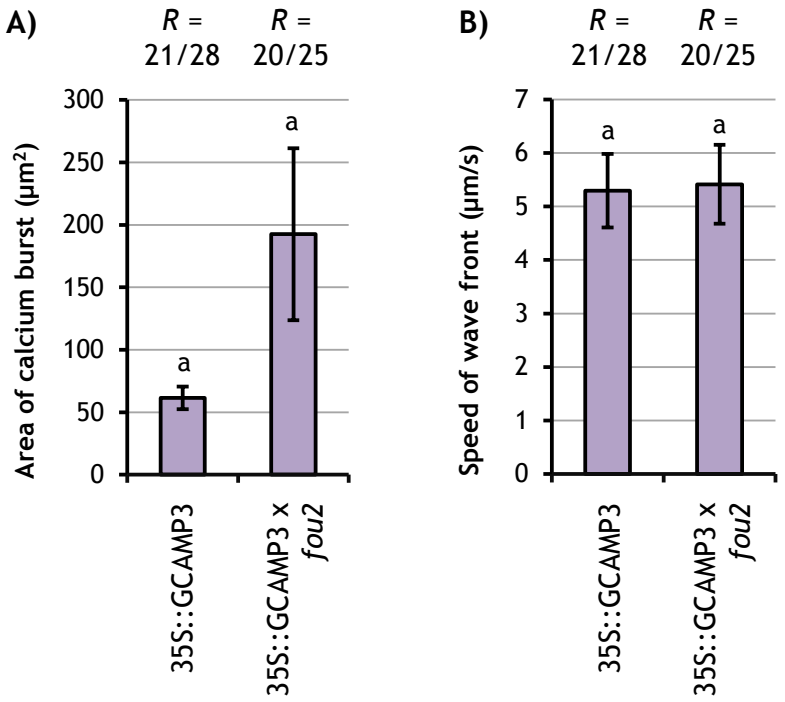

Figure 4.12: Properties of the *M. persicae*-induced Ca^{2+} burst around the feeding site in 35S::GCAMP3 and 35S::GCAMP3 x *fou2* leaves

Comparing properties of the Ca^{2+} burst in recordable samples (R), i.e. samples in which a feeding site GFP burst was visible by eye. **A)** Area of the Ca^{2+} burst. **B)** Speed of the Ca^{2+} wave front. Bars represent SEM. Letters indicate no significant difference between genotypes (Student's t-test $p<0.05$). Experiment conceived and designed by T.V and conducted by T.V. and M.A.

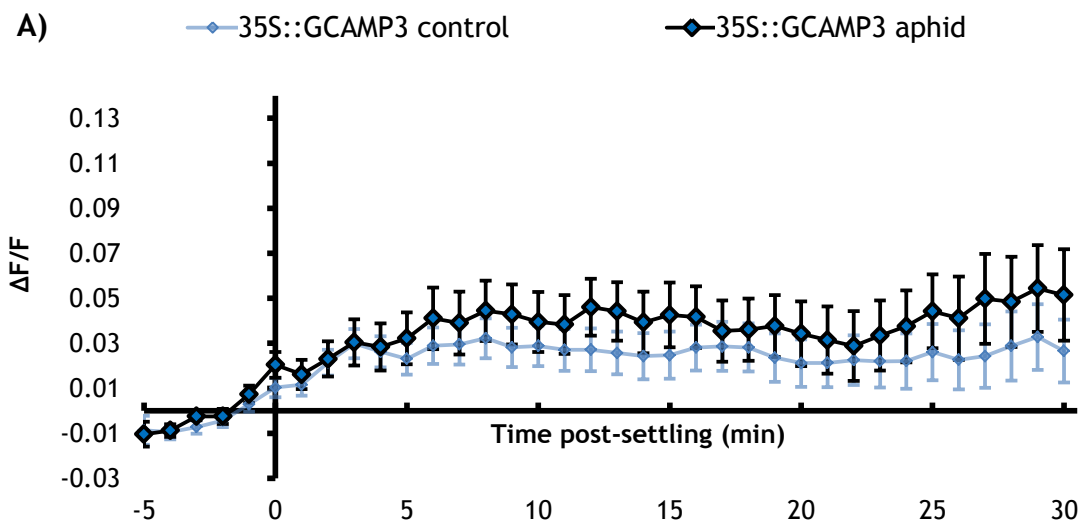
A)
35S::GCAMP3 control
35S::GCAMP3 aphid
ΔF/F
0.13
0.11
0.09
0.07
0.05
0.03
0.01
-0.01
-0.03
Time post-settling (min)
-5
0
5
10
15
20
25
30

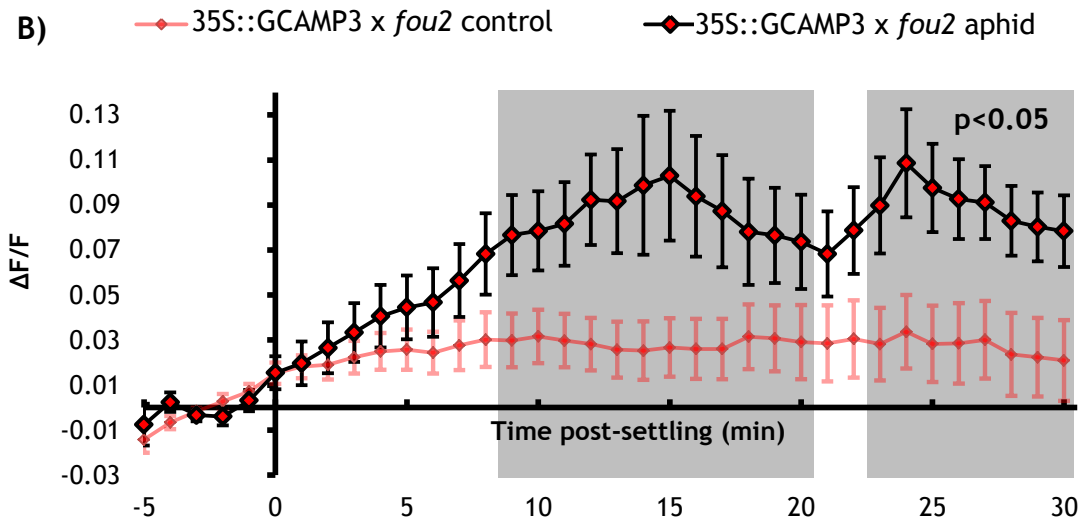
B)
35S::GCAMP3 x fou2 control
35S::GCAMP3 x fou2 aphid
p<0.05
ΔF/F
0.13
0.11
0.09
0.07
0.05
0.03
0.01
-0.01
-0.03
Time post-settling (min)
-5
0
5
10
15
20
25
30

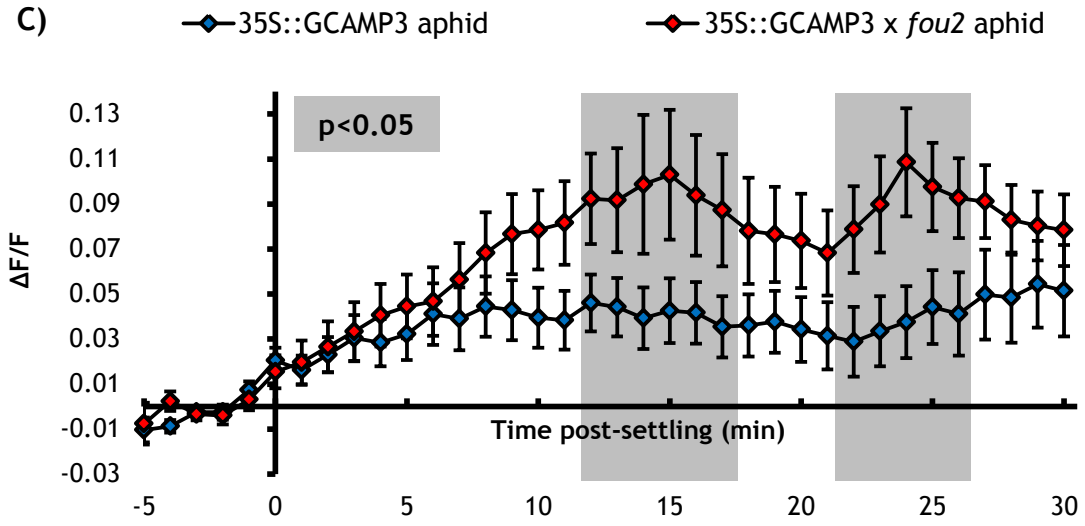
C)
35S::GCAMP3 aphid
35S::GCAMP3 x fou2 aphid
p<0.05
ΔF/F
0.13
0.11
0.09
0.07
0.05
0.03
0.01
-0.01
-0.03
Time post-settling (min)
-5
0
5
10
15
20
25
30

Figure 4.13: Normalised GFP fluorescence (ΔF/F) in the lateral tissue, systemic to the feeding site, in 35S::GCAMP3 and 35S::GCAMP3 x *fou2* Arabidopsis upon *M. persciae* settling.

A) 35S::GCAMP3 control (no aphid treatment) vs aphid treatment. **B)** 35S::GCAMP3 x *fou2* control (no aphid treatment) vs aphid treatment. **C)** 35S::GCAMP3 aphid treatment vs 35S::GCAMP3 x *fou2* aphid treatment. Bars represent SEM (35S::GCAMP3 n=28, 35S::GCAMP3 x *fou2* n=25). Grey shading indicates significant difference between treatments (Student's t-test within GLM at $p<0.05$). Experiment conceived and designed by T.V and conducted by T.V. and M.A.

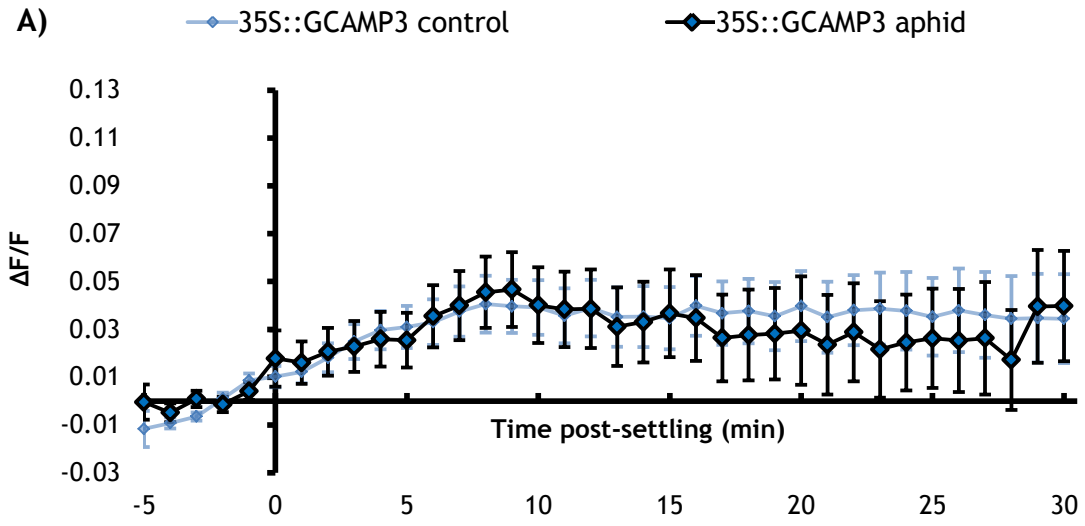
A)
35S::GCAMP3 control
35S::GCAMP3 aphid
ΔF/F
0.13
0.11
0.09
0.07
0.05
0.03
0.01
-0.01
-0.03
Time post-settling (min)
-5
0
5
10
15
20
25
30

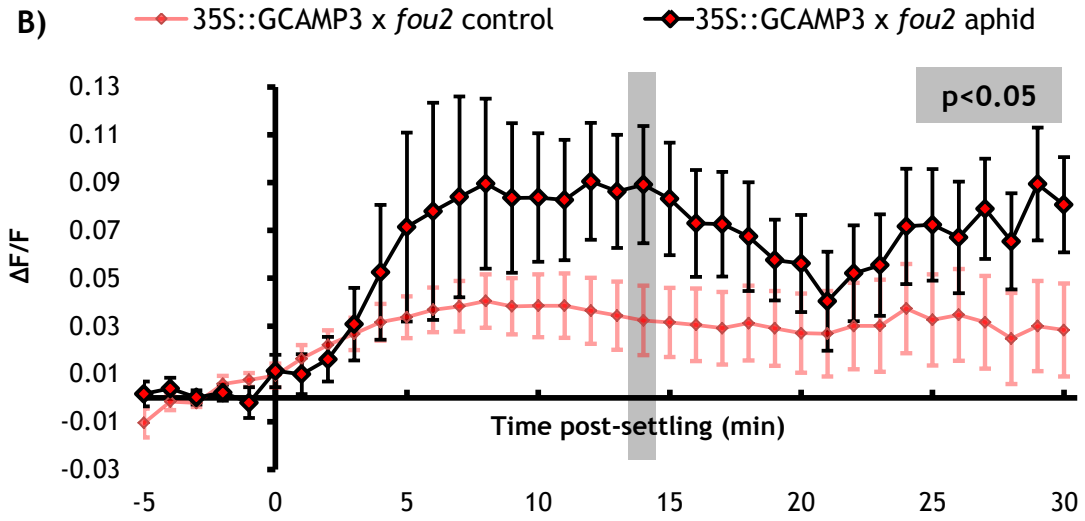
B)
35S::GCAMP3 x fou2 control
35S::GCAMP3 x fou2 aphid
p<0.05
ΔF/F
0.13
0.11
0.09
0.07
0.05
0.03
0.01
-0.01
-0.03
Time post-settling (min)
-5
0
5
10
15
20
25
30

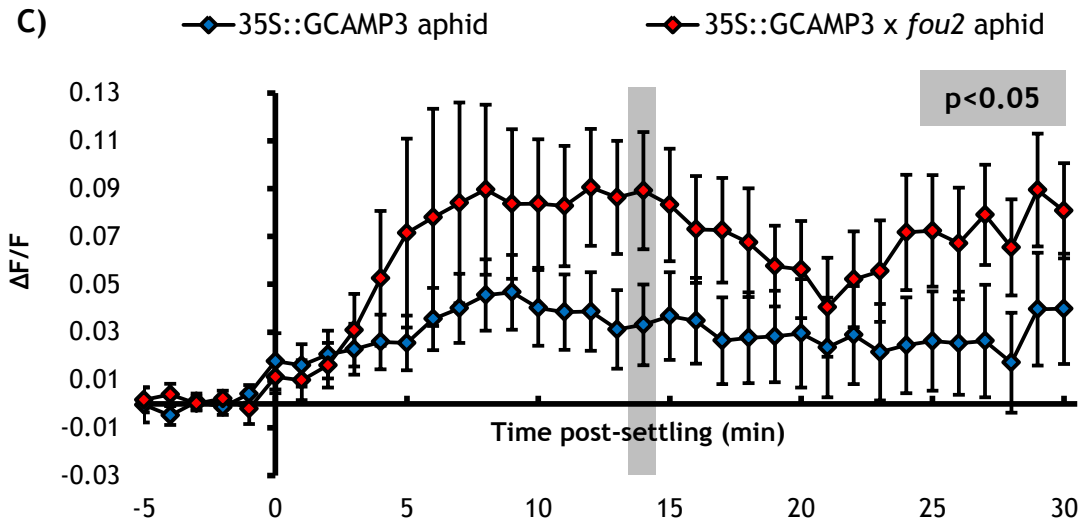
C)
35S::GCAMP3 aphid
35S::GCAMP3 x fou2 aphid
p<0.05
ΔF/F
0.13
0.11
0.09
0.07
0.05
0.03
0.01
-0.01
-0.03
Time post-settling (min)
-5
0
5
10
15
20
25
30

Figure 4.14: Normalised GFP fluorescence (ΔF/F) in the midrib, systemic to the feeding site, in 35S::GCAMP3 and 35S::GCAMP3 x *fou2* Arabidopsis upon *M. persicae* settling.
A) 35S::GCAMP3 control (no aphid treatment) vs aphid treatment. **B)** 35S::GCAMP3 x *fou2* control (no aphid treatment) vs aphid treatment. **C)** 35S::GCAMP3 aphid treatment vs 35S::GCAMP3 x *fou2* aphid treatment. Bars represent SEM (35S::GCAMP3 n=28, 35S::GCAMP3 x *fou2* n=25). Grey shading indicates significant difference between treatments (Student's t-test within GLM at $p<0.05$). Experiment conceived and designed by T.V and conducted by T.V. and M.A.

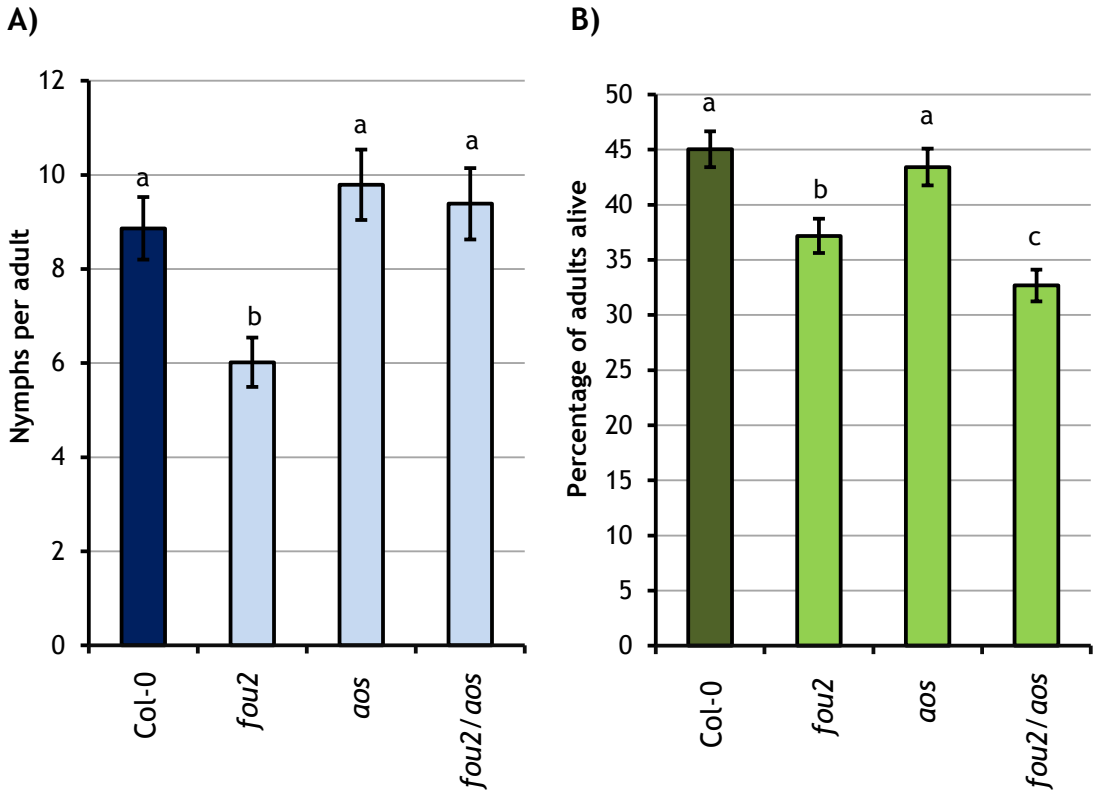

Figure 4.15: The *fou2* mutation significantly decreases aphid performance.
A) *M. persicae* fecundity on *fou2*. Bars show SEM of 16 biological replicates from 4 independent experiments. **B)** *A. pisum* survival. Survival was averaged across the two days in which the control population (Col-0) decreased below 50% survival. Bars represent SEM of 18 biological replicates from 3 independent experiments. Letters indicate significant differences between genotypes (Student's t-test within GLM, $p<0.05$).

4.2.7 Aphid-induced Ca^{2+} bursts are abolished in the *glr3.3/3.6* double mutant

Since the Ca^{2+} burst was not completely abolished on the *tpc1-2* mutant (Figure 4.3b), further Ca^{2+}-permeable channels were also investigated with respect to a possible role in producing the Ca^{2+} burst. This work focused on GLR3.3 and GLR3.6. Indeed, unlike the 35S::GCAMP3 line (Figure 4.16a), on the GLR double mutant 35S::GCAMP3 x *glr3.3/3.6* no feeding site Ca^{2+} burst was detectable relative to the untreated controls (Figure 4.16b, Figure 4.16c Video 4.4). Furthermore, in the three 35S::GCAMP3 x *glr3.3/3.6* samples that did display a recordable burst (R), there was a high variation in signal propagation speeds (Figure 4.17). As seen previously, these three samples did not represent a discrete group of responding samples (Figure D9, Appendix D). Interestingly, systemic aphid-induced signals could be detected in the 35S::GCAMP3 line in the midrib (Figure D10, Appendix D) and the lateral tissue (Figure D11, Appendix D) that were not observed in the 35S::GCAMP3 x *glr3.3/3.6* line. Aphid settling behaviour was not altered by the *glr3.3/3.6* mutation (Figure D12, Appendix D). Investigating the role of extracellular Ca^{2+} was also attempted through incubation of the leaves with EDTA or Lanthanide ions (La^{3+}), however these inhibitors had strong negative effects on both the leaf viability and aphid performance, making the assay not feasible.

4.2.8 Aphid fecundity and plant ROS production are not altered in the *glr3.3/3.6* double mutant

In order to assess if the *GLR* mutations also resulted in a plant defence or aphid performance phenotype, a plant ROS assay and *M. persicae* fecundity assay were performed with the *glr3.3/3.6* double mutant. In response to aphid extract, whilst ROS production was significantly reduced in the *bak1-5* mutant, no significant effect on ROS production was seen for *glr3.3/3.6* (Figure 4.18a). *M. persicae* fecundity was also not altered (Figure 4.18b).

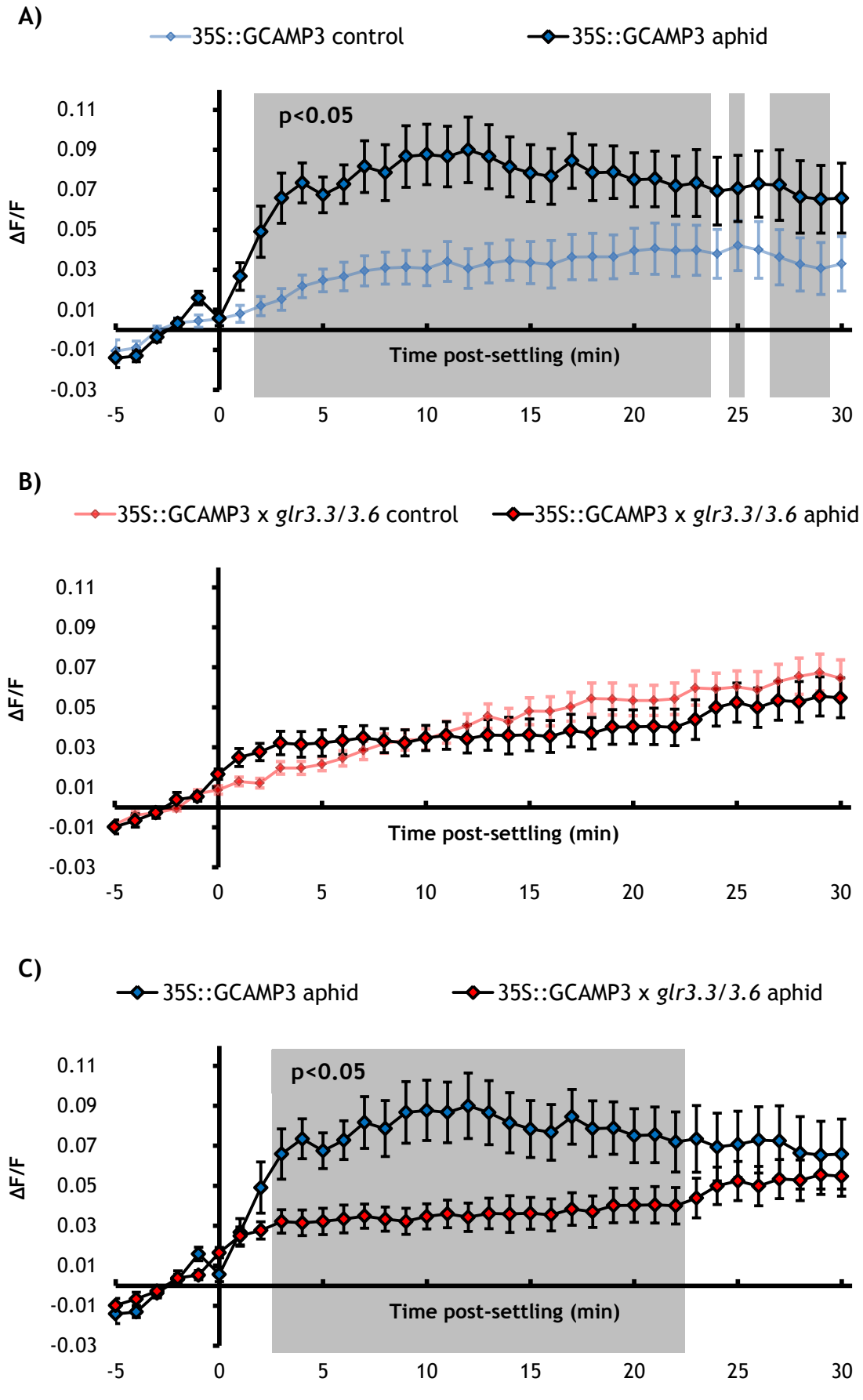
A)
35S::GCAMP3 control
35S::GCAMP3 aphid
p<0.05
ΔF/F
Time post-settling (min)
B)
35S::GCAMP3 x glr3.3/3.6 control
35S::GCAMP3 x glr3.3/3.6 aphid
ΔF/F
Time post-settling (min)
C)
35S::GCAMP3 aphid
35S::GCAMP3 x glr3.3/3.6 aphid
p<0.05
ΔF/F
Time post-settling (min)

Figure 4.16: Normalised GFP fluorescence (ΔF/F) around the feeding site in 35S::GCAMP3 and 35S::GCAMP3 x *glr3.3/glr3.6* Arabidopsis upon *M. persicae* settling.

A) 35S::GCAMP3 control (no aphid treatment) vs aphid treatment. **B)** 35S::GCAMP3 x *glr3.3/glr3.6* control (no aphid treatment) vs aphid treatment. **C)** 35S::GCAMP3 aphid treatment vs 35S::GCAMP3 x *glr3.3/glr3.6* aphid treatment. Bars represent SEM (35S::GCAMP3 n=34, 35S::GCAMP3 x *glr3.3/glr3.6* n=37). Grey shading indicates significant difference between treatments (Student's t-test within GLM at $p<0.05$). Experiment conceived and designed by T.V and conducted by T.V. and M.A.

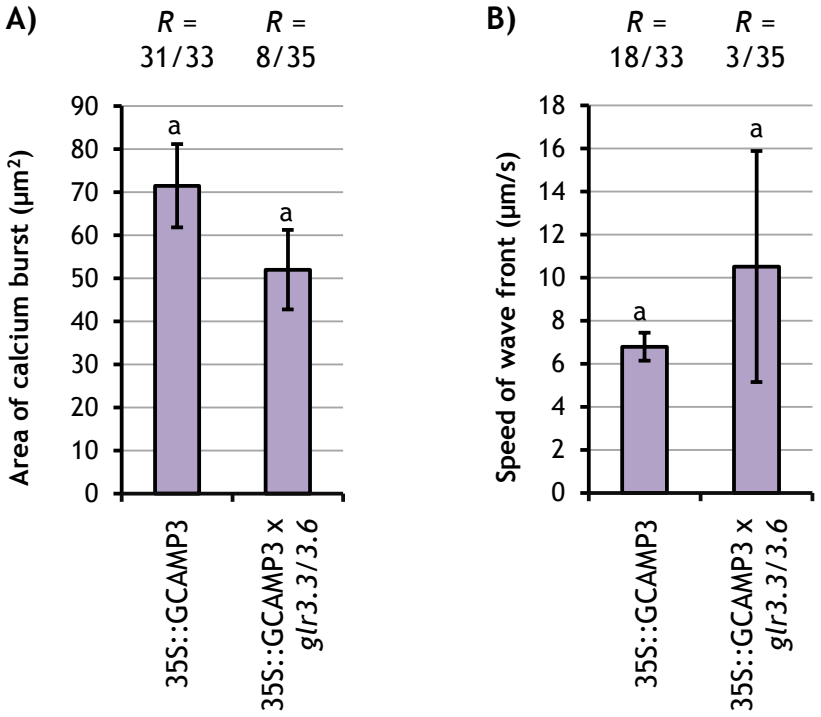

Figure 4.17: Properties of the *M. pericae*-induced Ca^{2+} burst around the feeding site in 35S::GCAMP3 and 35S::GCAMP3 x *glr3.3/3.6* leaves.

Comparing properties of the Ca^{2+} burst in recordable samples (R), i.e. samples in which a feeding site GFP burst was visible by eye. A) Area of the Ca^{2+} burst. **B)** Speed of the Ca^{2+} wave front. Letters indicate no significant difference between genotypes (Student's t-test $p<0.05$). Experiment conceived and designed by T.V and conducted by T.V. and M.A.

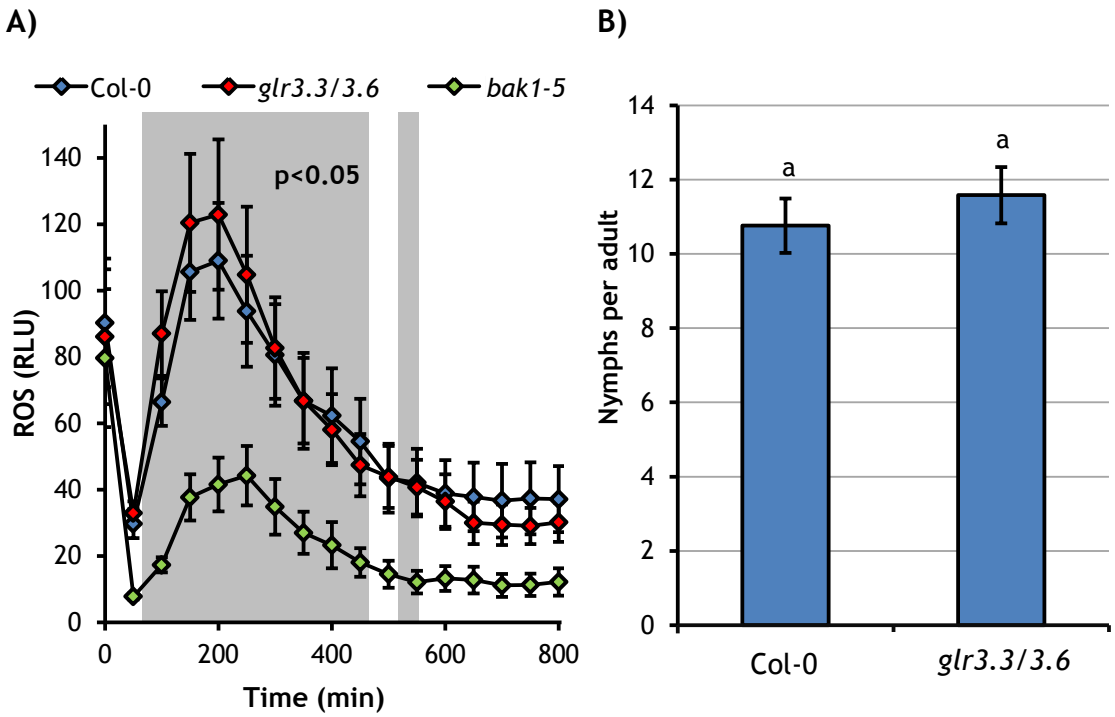

Figure 4.18: ROS production and susceptibility to *M. persicae* is not altered on the *glr3.3/glr3.6* double mutant.

A) ROS production in Col-0, *bak1-5 and glr3.3/glr3.6* leaf disks upon application of *M. persicae* extract. ROS measured as relative light units (RLU). Error bars represent SEM of 24 biological replicates from from 3 independent experiments. Shading indicates significant difference between Col-0 and *bak1-5* (Student's t-test within GLM at $p<0.05$). Experiment conceived and designed by T.V and conducted by T.V. and M.A. **B)** *M. persicae* fecundity on *glr3.3/3.6* Bars show SEM of 24 biological replicates from 4 independent experiments. Letters indicate no significant difference between genotypes (Student's t-test $p<0.05$). Experiment conceived and designed by T.V and conducted by T.V. and M.S.

4.2.9 Induction of *FRK1*, *CYP81F2* and *PAD3* is altered in the *bak1-5*, *tpc1-2* and *fou2*/*aos* mutants

To assess whether Ca^{2+} signalling has an effect on plant defence downstream of the initial perception by BAK1, the expression of three defence markers (*FRK1*, *CYP81F2* and *PAD3*) in the *bak1-5, tpc1-2* and *glr3.3*/*3.6* lines in response to aphid extract was investigated. Incubation of leaf disks with aphid extract for 1 h strongly induced expression of *FRK1*, *CYP81F2* and *PAD3* relative to water-incubated controls (Figure 4.19). Induction of *FRK1* was reduced in the *tpc1-2* mutant but was not significantly altered in *bak1-5* or *glr3.3*/*3.6* mutants (Figure 4.19a). *CYP81F2* induction was reduced in the *bak1-5* mutant but not in the other lines (Figure 4.19b), whilst *PAD3* expression was significantly attenuated in both *bak1-5* and *tpc1-2* mutants (Figure 4.19c).

The same assay was repeated with the *aos* and *fou2*/*aos* mutants to assess the effect of JA and JA-independent TPC1 over-activation on these pathways (Figure 4.20). Application of aphid extract induced *FRK1* expression in all genotypes, with no significant difference detected between them (Figure 4.20a). *CYP81F2* induction by aphid-extract was the same as wildtype in the *aos* mutant, but was compromised in the *fou2*/*aos* mutant (Figure 4.20b). *PAD3* expression was induced by aphid extract to the same level in all three genotypes (Figure 4.20c).

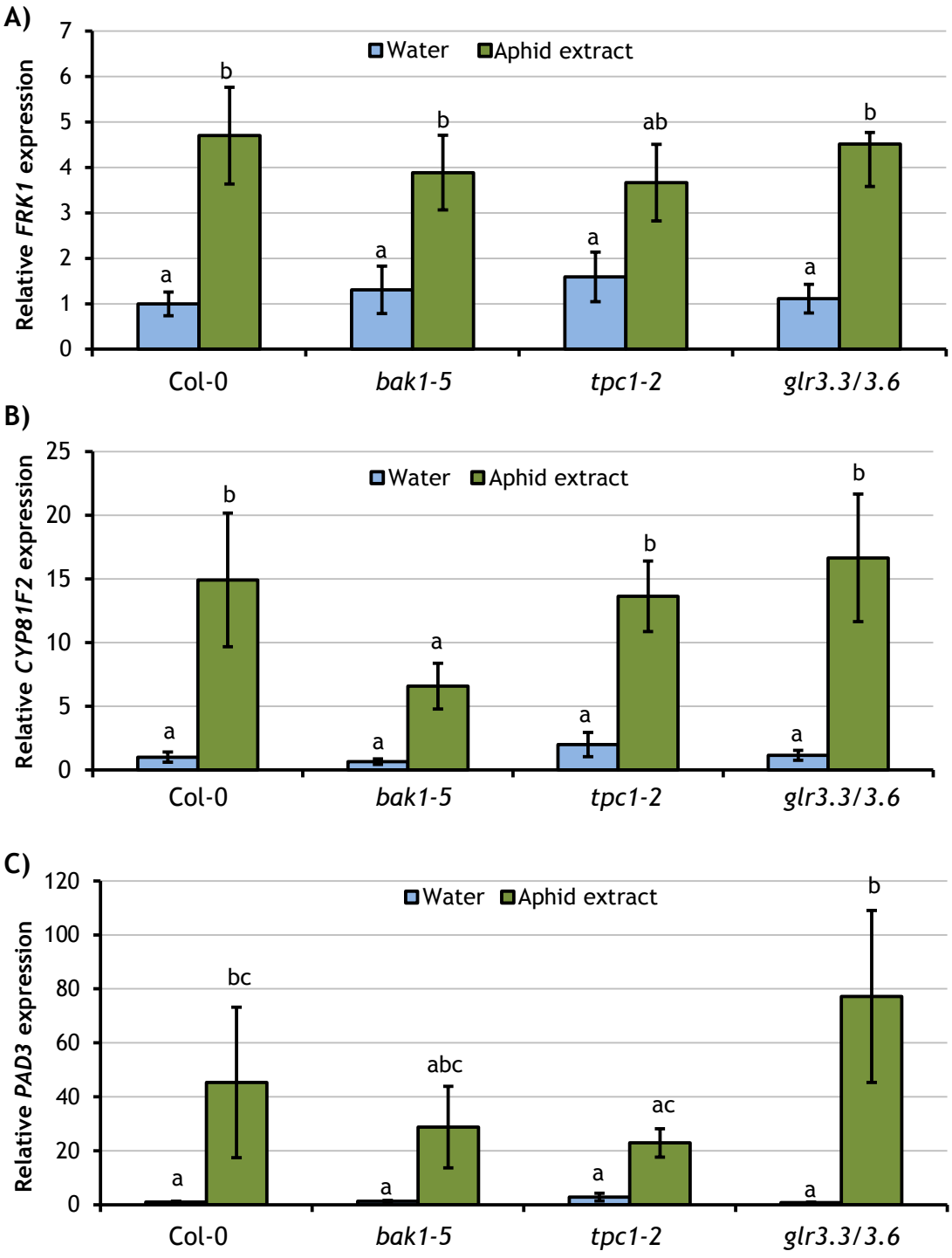

Figure 4.19: Defence gene induction in Col-0, *bak1-5*, *tpc1-2* and *glr3.3/3.6* leaf disks incubated with *M. persicae* extract (aphid extract) for 1 h.

Expression relative to water-treated Col-0 leaf disks. **A)** Relative *FRK1* expression**. B)** Relative *CYP81F2* expression. **C)** Relative *PAD3* expression. Bars show SEM of 9 biological replicates from from 3 independent experiments. Different letters indicate averages that are significantly different from one another (Student's t-probabilities calculated within GLM at P <0.05). Experiment conceived and designed by T.V and conducted by N.B. under supervision of T.V.

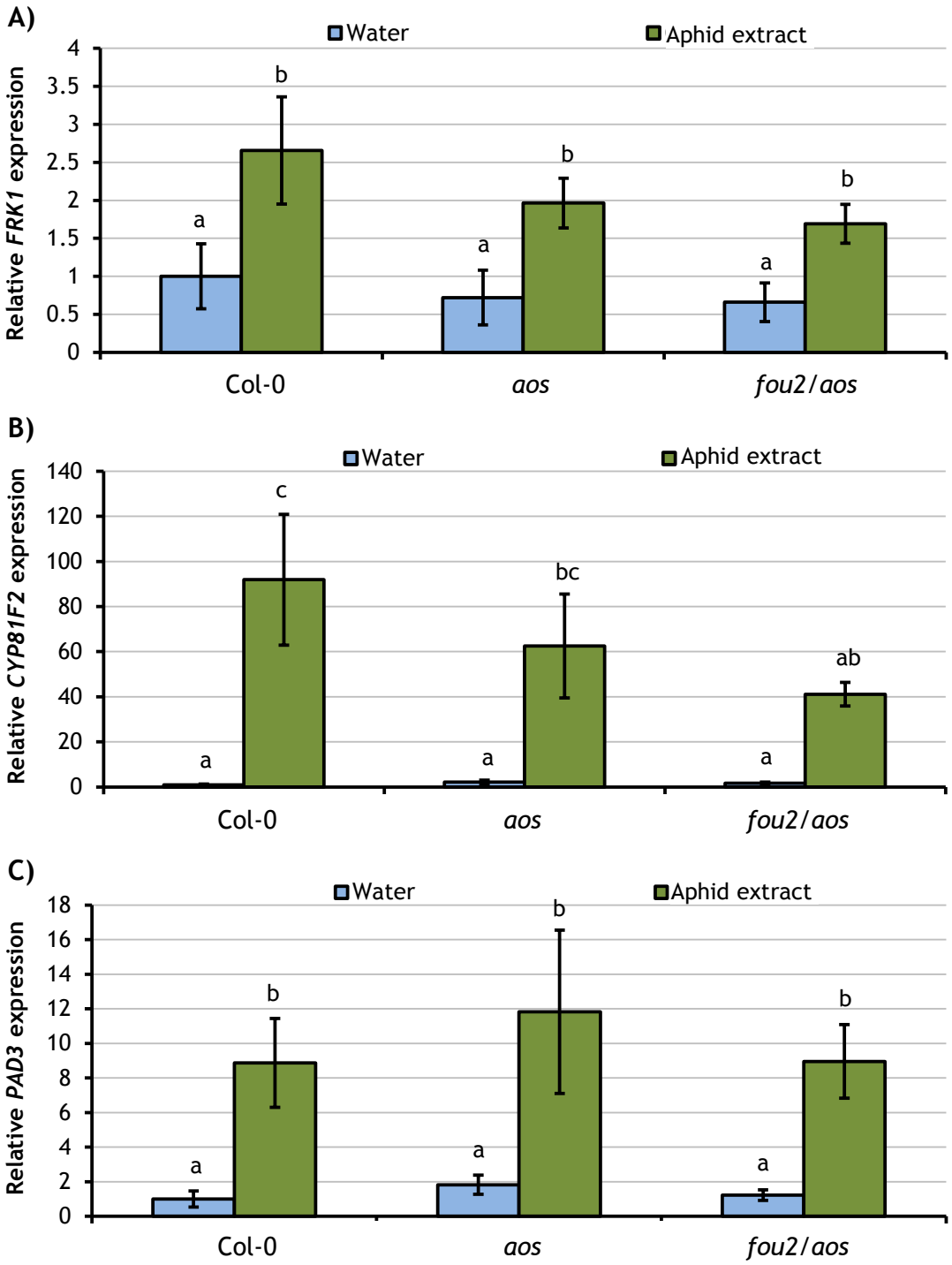

Figure 4.20: Defence gene induction in Col-0, *aos* and *fou2/aos* Arabidopsis leaf disks incubated with *M. persicae* extract (aphid extract) for 1 h.

Expression relative to water-treated Col-0 leaf disks. **A)** Relative *FRK1* expression. **B)** Relative *CYP81F2* expression. **C)** Relative *PAD3* expression. Bars show SEM of 9 biological replicates from 3 independent experiments. Different letters indicate averages that are significantly different from one another (Student's t-probabilities calculated within GLM at $P < 0.05$). Experiment conceived and designed by T.V and conducted by N.B. under supervision of T.V.

4.3 Discussion

4.3.1 Aphid feeding results in vacuolar Ca^{2+} release mediated by TPC1

The Ca^{2+} burst around the feeding site was significantly reduced in the *tpc1-2* mutant (Figure 4.3, Video 4.1), showing that vacuolar Ca^{2+} release via TPC1 is involved in this signal. Previously, the role of intracellular Ca^{2+} in plant defence has been inferred indirectly through the use of pharmacological inhibitors [201, 378] and wounding has been show to stimulate systemic TPC1-mediated Ca^{2+} release [123]. Indeed, TPC1's role appears to be mainly in systemic signalling [7, 121, 123], a phenomenon that appears to be less important in relation to *M. persicae* attack. Examples of systemic signalling in response to aphids were observed in the present chapter; however this was not a consistent response and occurred in the minority of cases (Figure D3, D10, D11, Appendix D).

Furthermore, local application of the bacterial PAMPs flg22 and elf18 can induce Ca^{2+} bursts detectable by AEQ that are not altered in the *tpc1-2* mutant [122]. Therefore, the role of TPC1 might be aphid-specific. It is also possible that the enhanced sensitivity of GCAMP3 compared to AEQ may also have contributed to the detection of the aphid TPC1 phenotype, as single-FP sensors allow measurements of PAMP-induced Ca^{2+} signals that were not previously detectable [219].

Overexpression of *TPC1* did not significantly alter the feeding site Ca^{2+} burst (Figure 4.5c, Video 4.2), suggesting that wildtype levels of *TPC1* are sufficient to generate the maximal signal. There does appear to be an increase in $[Ca^{2+}]_{cyt}$ after 25 min in 35S::GCAMP3 x 35S::TPC5.6 that was not observed in the wildtype (Figure 4.5c) that may represent a second burst as a result of overexpressing TPC1. However, this burst was not aphid-specific as only the initial Ca^{2+} burst in 35S::GCAMP3 x 35S::TPC1 5.6 was significantly higher than the no-aphid control (Figure 4.5b).

TPC1 expression had no effect on the spread of the Ca^{2+} burst within the leaf (Figure 4.4a). However, overexpression of *TPC1* did increase the speed of the aphid-induced Ca^{2+} wave front by a third, from 4 µm/s to 6µm/s (Figure 4.4b). This is very similar to the proportional increase in Ca^{2+} signal speed in response to salt-stress when TPC1 is overexpressed, which increases from 400 µm/s in Col-0 to 680 µm/s in 35S::TPC1 [7]. Interestingly, in *tpc1-2* plants that did exhibit a measurable Ca^{2+} signal

in response to aphids, the speed of the signal was unchanged (Figure 4.4b), suggesting that TPC1 is not required for the propagation of the signal, but is capable of enhancing it. Indeed, it is hypothesised that *TPC1* acts in CICR to propagate Ca^{2+} signals cell to cell [7, 121, 537, 539], and a similar mechanism might be applicable in the plant-aphid context. As with *bak1-5* (Figure B9, Chapter 3) production of visible Ca^{2+} bursts around the feeding site of some 35S::GCAMP3 x *tpc1-2* plants (Figure 4.17) suggests that there is some *TPC1*-independent signalling occurring.

The role of TPC1 in the aphid-induced Ca^{2+} burst further supports the hypothesis that this burst occurs in the epidermal and mesophyll cell layers, as mature SEs do not contain vacuoles [701]. Arabidopsis spongy mesophyll cells represent a large pool of stored Ca^{2+} available for signalling, with higher $[Ca]_{vac}$ than most other cell types [651, 702] and $[Ca]_{vac}$ in *tpc1-2* mesophyll cells is not significantly altered [650]. Consequently, the reduced Ca^{2+} burst in the *tpc1-2* mutant is not related to reduced vacuolar storage of Ca^{2+}.

4.3.2 *TPC1* expression alters ROS production, MAPK activity and camalexin biosynthesis during plant-aphid interactions

ROS production is a hallmark of PTI, including against aphids. Incubating Arabidopsis leaf disks with *M. persicae* extract resulted in a burst of H_2O_2 that peaked at around 200 min post-application and was significantly higher than disks incubated with water (Figure 4.7a). This fits well with the ROS response to aphid extract seen previously [349]. The water-incubated leaf disks did display a high level of initial ROS (Figure 4.7a), which has also been seen previously [349]. This is likely a result of the wounding required to harvest the leaf disks [413], but may also suggest that aphid extract is capable of suppressing this burst. Loss of the *TPC1* transcript had no effect on ROS production in response to aphid extract (Figure 4.7d). This agrees with previous work showing that ROS production in response to plant hormones (ABA and MeJA [660]) and bacteria (elf18 and *P. syringae* [122]) are also not altered in *tpc1-2* mutant leaves. However, *TPC1* is required for ROS production in roots in response to salt stress [121], and heterologous expression of *AtTPC1* in *N. tabacum* BY-2 cells showed that H_2O_2-induced $[Ca^{2+}]_{cyt}$ elevations may also involve *TPC1* [670]. Furthermore, plant redox status might influence TPC1 activity [703]. Thus, although the function of TPC1 is interconnected with ROS production, the biological relevance of this might be limited to specific tissues and/or systemic signalling.

Interestingly, overexpression of *TPC1* resulted in a larger ROS burst in both the 35S::TPC1 lines tested (Figure 4.7b and c), despite TPC1 not being required for aphid extract-induced ROS production (Figure 4.7d). It is also aphid-extract specific, as no difference in ROS production was observed in the 35S::TPC1 lines treated with water (Figure 4.7a). A similar increase in ROS production in response to a fungal elicitor can be achieved in *O. sativa* by overexpressing *OsTPC1* [659], although a comparable result cannot be achieved by overexpressing *TPC1* in Arabidopsis during bacterial infection [122]. *TPC1* overexpression has no effect on the feeding site Ca^{2+} burst during aphid attack (Figure 4.5), although it is worth noting that Ca^{2+} was not analysed in response to aphid extract nor over several hours, as was conducted for ROS. Given the considerable positive feedback between Ca^{2+}, TPC1 and ROS [119, 121, 691, 692] it is not surprising that overexpression of *TPC1* could result in enhanced ROS accumulation in response to stress.

In addition to ROS production, defence marker gene induction after aphid extract application was also assed. *FRK1* is a marker gene for early defence signalling [151] and the MAPK pathway [201, 394]. Incubation of leaf disks with aphid extract for 1 h resulted in significant upregulation of this gene in Col-0 plants (Figure 4.19a) as seen previously [349]. However, this induction was compromised in the *tpc1-2* mutant (Figure 4.19a), suggesting that TPC1 and intracellular Ca^{2+} signalling may be required for full MAPK activation during plant-aphid interactions. Indeed, MAPK activation in response to the fungal elicitor xylanase is significantly reduced in *O. sativa* if *OsTPC1* transcription is abolished [659]. Furthermore, MAPK activation in *P. crispum* in response to *Phytophthora sojae* is promoted by ion fluxes [693] and pharmacological inhibition of Ca^{2+} flux decreases MAPK activation in response to oomycetes [694] and fungi [372].

Loss of the *TPC1* transcript also significantly attenuated aphid-induced *PAD3* induction (Figure 4.19c), suggesting that TPC1 might also play a role in camalexin biosynthesis. Conversely, *TPC1* expression has no effect on *CYP81F2* and therefore the glucosinolate pathway (Figure 4.19b). A connection between Ca^{2+} and camalexin production has not been established to the authors knowledge, however camalexin production in response to fungi is MAPK-dependent [704], and given the considerable involvement of MAPKs in PTI [354, 360, 387-391] it is possible the altered MAPK activation in *tpc1-2* may result in altered *PAD3* induction. Furthermore, in cultured *O. sativa* cells phytoalexin accumulation is suppressed if *OsTPC1* transcription is abolished [671]. Given the anti-aphid role of camalexin [304, 306, 349], the data

collected in the present study suggest the *TPC1* expression might have an effect on the final toxicity status of the plant.

4.3.3 *TPC1* promotes phloem feeding but has no effect on most aphid feeding behaviours

The vast majority of aphid feeding behaviours were not altered in the *TPC1* expression mutants (Table 4.1, Table 4.2). This included all pathway behaviours, again demonstrating that the aphid-induced Ca^{2+} burst is not related to altered feeding behaviour. Interestingly, aphids on the *tpc1-2* mutant exhibited a behaviour not seen on the wildtype: instances of single phloem salivations (E1) not followed by phloem ingestion (E2). Such behaviour suggests that the aphid cannot successfully establish feeding, despite the potential release of effectors into the phloem [282, 297, 705], and is often observed during incompatible interactions [300-303]. Such problems with phloem acceptance are sometimes the result of R-gene recognition and ETI [281, 640, 706]. However, single phloem salivations were also observed in the 35S::TPC1 5.6 line (Figure 4.9b), suggesting that any perturbation in *TPC1* expression alters this behaviour. Furthermore, this behaviour was also seen in the wildtype plants during the BAK1 EPG experiment (Table B2, behaviour 28, Chapter 3). Consequently, the significance of this behaviour is likely to be small.

The number of sustained (>10 min) phloem ingestions was significantly higher on 35S::TPC1 5.6. These data imply that despite the potential role of Ca^{2+} and TPC1 in activation of plant defence, *TPC1* expression may be beneficial to the aphid. This unexpected result is similar to that observed with the *bak1-5* mutant, where loss of *BAK1* appeared to be beneficial to phloem feeding (Figure 3.17, Chapter 3). Both *BAK1* and *TPC1* are required for the aphid-induced Ca^{2+} burst, and might even act in the same pathway. As such, it is conceivable that the hypothesis outlined in Chapter 3 (Section 3.3.6), whereby the aphid is monitoring or suppressing the plant defence network via this pathway, might also involve TPC1. A result of this might be that disruption of this pathway (e.g. loss of *BAK1* or *TPC1*) is detrimental to *M. persicae*, whilst enhancement (e.g. overexpression of *TPC1*) is beneficial. It remains to be tested whether TPC1 lies within the BAK1 pathway, or whether effectors such as Mp10 are acting in a TPC1-dependent manner.

Alternatively, Ca^{2+} signalling via TPC1 could be a negative regulator of plant defence against aphids. Indeed, loss of the PM Ca^{2+} channel *CNGC2* leads to

constitutive defence activation [79, 377]. However, this is contrary to the *tpc1-2* and 35S::TPC1 phenotypes outlined in Section 4.3.2, where *TPC1* expression appears to promote defence activation. It could also be argued that the EPG data show that *TPC1* expression has very little effect on aphid feeding, consistent with the lack of an effect on aphid fecundity (Figure 4.10a and b). The total and average time spent feeding from the phloem was the same in all lines despite the altered number of occurrences (Table 4.1 and Table 4.2 behaviours 30, 31, 33 and 34). This hypothesis is further strengthened by the lack of a difference in basal resistance to aphids seen on the *TPC1* expression lines (Section 4.3.4– see below).

4.3.4 *TPC1* expression affects IR but not basal resistance to aphids

Despite the role of TPC1 in aphid-induced Ca^{2+} bursts (Section 4.3.1) and defence induction in response to aphid extract (Section 4.3.2), *TPC1* expression has little effect on aphid performance. *M. persicae* fecundity was not significantly altered on the *tpc1-2* (Figure 4.10a) or 35S::TPC1 5.6 (Figure 4.10b) lines, and the aphids showed no host preference for plants based on *TPC1* expression (Figure 4.10c). Therefore, the altered defence signalling mediated by TPC1 had no effect on basal resistance to aphids. *M. persicae* is compatible with Arabidopsis, feeding successfully from the plant, and this compatibility is most likely mediated by effectors [276, 277, 500-502, 549, 560]. Thus, during the *M. persicae*-Arabidopsis interaction plant defence is already suppressed, and therefore experiential disruption of defence signalling will most likely have little effect. Indeed, despite BAK1's role in perception of aphids, abolishing *BAK1* transcription has no effect on *M. persicae* fecundity [349]. This might also explain the lack of a strong feeding behaviour phenotype on the *tpc1-2* mutant (Section 4.3.3).

To counter this issue, the performance of an incompatible aphid, *A. pisum*, was also assessed on the *TPC1* expression lines. Use of incompatible aphids can help identify components of non-host resistance in Arabidopsis. For example, the incompatible species *R. padi* induces a larger plant ROS burst than *M. persicae* [283]. *A. pisum* extract application to Arabidopsis leaf disks results in induction of *FRK1*, *CYP81F2* and *PAD3* comparable to *M. persicae* extract [349], however *A. pisum* cannot survive on Arabidopsis [555]. This survival is increased significantly on the *bak1-5* mutant, although the aphid still remains incompatible [349]. Thus non-host

resistance is partly regulated by BAK1. To test if the same was true for TPC1, the same survival assay was conducted on the *tpc1-2* and 35S::TPC1 5.6 lines. However, no difference in *A. pisum* survival was observed (Figure 4.10d). This suggests that signalling mediated by TPC1 is not significantly regulating successful plant defence against non-host aphids. Alternatively, it is conceivable that like *M. persicae*, *A. pisum* is capable of suppressing Ca^{2+} signalling successfully and non-host resistance against this species might be Ca^{2+}-independent.

Since basal resistance to aphids was not altered on the *TPC1* expression lines, IR to *M. persicae* was also investigated. Previous exposure to a pest can lead to priming of plant defence against future challenge [527, 534, 629, 632]. This is the case for both pathogens [438, 526, 533, 634] and insects [464, 473, 474, 707], with the IR capable of being very broad-spectrum [431]. IR to *M. persicae* extract is dependent on aphid-perception by *BAK1* [349]. Furthermore, the camalexin biosynthesis pathway is also required for successful IR against *M. persicae*, as abolishing transcription of *CYP79B2*/*CYP79B3* or *PAD3* also abolishes IR [349]. Pre-treatment of leaves with 50 *M. persicae* adults resulted in IR in Col-0 local leaves (Figure 4.8) as seen previously (Figure 3.9, Chapter 3 [464]). The IR in *tpc1-2* mutants was equal to wildtype (Figure 4.8), demonstrating that Ca^{2+} signalling via *TPC1* is not required for IR to *M. persicae*. However, overexpression of *TPC1* abolished IR (Figure 4.8). This agrees with the hypothesis outlined in Section 4.3.3; that *TPC1* expression is beneficial to the aphid. This appears to be independent of the increased ROS production in the 35S::TPC1 lines (Figure 4.7b and Figure 4.7c). It might be that *TPC1* overexpression has an effect on other signalling pathways important in IR, such as JA [473, 474, 529, 530, 708-710], however the lack detectable phenotypes in 35S::TPC1 plants, combined with the lack of knowledge surrounding the mechanism that regulates IR against aphids, mean that further experiments are required to investigate this phenomenon.

4.3.5 Over-activating TPC1 significantly alters the plant Ca^{2+} signal

Over-activation of TPC1 by the *fou2* mutation did not significantly affect the amplitude of the feeding site Ca^{2+} burst (Figure 4.11c), however the burst exhibited greater variability (Figure 4.11b) than the wildtype (Figure 4.12a). Unlike overexpression of *TPC1*, over-activation did not affect the speed of the signal (Figure 4.12b). However, large systemic aphid-induced signals were detected in 35S::GCAMP3 x *fou2* lateral tissue (Figure 4.13c, Video 4.3). Thus, whilst TPC1 abundance affects the speed of signal propagation (Figure 4.6b, [7]), alterations to ion channel activity result in systemic signalling in response *M. persicae*. This fits with the theory that TPC1 regulation during stress is mainly post-transcriptional [416].

Ions including Ca^{2+} are thought to underlie systemic stress signalling in plants [7, 103, 121, 123]. Thus, if *M. persicae* is suppressing systemic Ca^{2+} release as part of its successful colonisation of the plant, then over-activation of TPC1 might counter-act this. To test this hypothesis, it would be interesting to investigate whether a non-adapted aphid such as *A. pisum* induces systemic Ca^{2+} bursts in Arabidopsis. In addition, it is worth noting that the JA-dependent phenotype of *fou2* does not occur within the first 2 weeks of growth, with LOX activity and physical appearance comparable to wildtype plants during this period [550]. Therefore, despite JA's role in systemic signalling, [530, 543-546] the Ca^{2+} phenotype observed in the 9-11 day old 35S::GCAMP3 seedlings used in the present study is likely to be independent of JA and might represent the first non-JA *fou2* phenotype.

4.3.6 Over-activating TPC1 enhances plant resistance to *M. persicae* through a JA-dependent mechanism

Over-activation of TPC1 resulted in a significant negative effect on *M. persicae* fecundity (Figure 4.15a). This phenotype was due to the upregulated JA production in the *fou2* mutant [550], as fecundity was rescued on the *fou2*/*aos* double mutant (Figure 4.15a). The *fou2* mutation has been shown to reduce fecundity of the Brassicaceae specialist aphid *B. brassicae* [430], although the role of JA was not explicitly investigated through use of the *fou2*/*aos* line. This *fou2* phenotype agrees with evidence in the literature suggesting that JA is detrimental to

aphids. *LOX2* transcription is increased 2-fold by *M. persicae* infestation [499] and *M. persicae* fecundity is significantly reduced on the JA-overproduction mutant *cev1*. Furthermore, application of MeJA to wildtype plants also reduces aphid performance [307, 429]. The *fou2* mutation induces several defence-related transcripts in a JA-dependent manner [552], and this results in constitutive defence activation [430, 550]. It is therefore not surprising that *M. persicae* performance is compromised on this mutant. Interestingly, despite the significant reduction in *B. brassicae* fecundity observed on the *fou2* mutant, the feeding behaviour of this aphid is not altered [430], casting doubt on the use of feeding behaviour as a measure of aphid success.

Contrary to the *fou2* phenotype, abolition of JA signalling in the *coi1* mutant appears to increase *M. persicae* and *B. brassicae* fecundity [307]. However, abolishing *AOS* transcription had no effect on *M. persicae* fecundity in the current study (Figure 4.15a), nor on the fecundity of *B. brassicae* [430], despite the number of defence-related transcripts that are compromised in the *aos* mutant. The disparity between the *coi1* and *aos* phenotypes may be due to an additional mutation in the *coi1-6* mutant line used by Ellis et al., [307] that alters callose production [711], a key anti-aphid defence [430]. Indeed, rearing *M. persicae* a *COI1* mutant free of this pleiotropic effect (*coi1-35*) or the *jar1* mutant (Figure 4.1) [712] results in no effect on aphid fecundity [306]. These results suggest either that JA biosynthesis is not one of the main determinants of *M. persicae* success, or that *M. persicae* successfully downregulates JA in wildtype plants to a level comparable to the *aos* mutant.

4.3.7 Induction of MAPKs, camalexin and glucosinolates by *M. persicae* is independent of JA

FRK1 induction in response to *M. persicae* extract was not significantly altered on the *aos* or *fou2*/*aos* lines (Figure 4.20a), indicating that neither JA nor JA-independent TPC1 over-activation have an effect on MAPK activation in response to *M. persicae*. MAPK activation lies upstream of JA production in response to wounding [392] and herbivory [397], and the results of the present study indicate that during plant-aphid interactions there is not significant feedback on MAPKs by JA signalling. Again this could be because of the relatively low induction of JA signalling by aphids, or the suppression of this pathway by the insect. It is also worth noting that *FRK1* induction is only a marker for the MAPK pathway, MAPK activation itself in response to *M. persicae* was not tested.

Aphid extract-induced expression of *PAD3* was also not altered in the *aos* or *fou2*/*aos* lines (Figure 4.20c), suggesting that camalexin production is JA-independent and not affected by JA-independent TPC1 over-activation. This is interesting given the role of *TPC1* expression in *PAD3* induction (Figure 4.19c), and implies that if camalexin production is partially *TPC1*-dependent, it might already be at its maximal level in wildtype plants. Camalexin production in response to the fungus *B. cinerea* is dependent on JA and compromised in *aos, coi1* and *aos*/*coi1* mutants, and *PAD3* induction is also lower in *coi1* [713]. However, whilst JA may play a role in the accumulation of camalexin in some defence contexts, this does not appear to be the case in the *M. persicae*-Arabidopsis interaction.

CYP81F2 expression was also not compromised in the *aos* mutant (Figure 4.20b), suggesting glucosinolate production in response to aphids is also JA-independent. This agrees with work by Mewis et al. [428], who observed that the levels of aliphatic and indolyl glucosinolates induced by *M. persicae* are not altered in the *coi1* mutant. However, *CYP81F2* induction was significantly attenuated in the *fou2*/aos line (Figure 4.20b). This implies that TPC1 over-activation, independently of JA, is capable of suppressing this response, despite *TPC1* itself not being required for glucosinolate production (Figure 17b). Consequently, it could be hypothesised that increasing ion flux through TPC1 might have an effect on JA-independent pathways upstream of glucosinolate production, potentially involving those based on Ca^{2+} [696], ROS [697] and MAPKs [698].

4.3.8 TPC1 over-activation reduces *A. pisum* survival independently of JA

To test the role of TPC1 activity and JA in non-host resistance, survival of the Arabidopsis-incompatible species *A. pisum* was assessed on the *fou2* and *aos* lines. As with the compatible generalist *M. persicae* (Section 4.3.6) and the compatible specialist *B. brassicae* [430], over-activation of TPC1 by the *fou2* mutation significantly reduced *A. pisum* performance, whilst abolition of JA production (*aos*) had no effect (Figure 4.15b). Thus, although JA plays a role in non-host resistance to microbial pathogens [714-717], the same may not be true for aphids. Further highlighting the independence of *A. pisum* performance and JA, aphid survival was also compromised on *fou2*/*aos* (Figure 4.15b), suggesting that the reduction in survival mediated by *fou2* is JA-independent. Interestingly, this reduction in survival

is greater than the reduction observed on the *fou2* single mutant. This implies that JA may be beneficial to the aphid when there is increased ion flux through TPC1.

In summary, over-activation of TPC1 increases Arabidopsis resistance against this aphid species - another gain-of-function role for the *fou2* mutation. Altered ion flux through TPC1 could be affecting various pathways related to non-host resistance, including Ca^{2+} [718], ROS [719-721], MAPKs [722], and SA [721, 723, 724] and ET [725], all of which have an effect on defence. Dissection of the mechanism by which *fou2* mediates non-host resistance will involve specific analysis of these pathways in response to *A. pisum* on the *fou2* and *fou2/aos* lines.

4.3.9 GLR3.3 and GLR3.6 mediate extracellular Ca^{2+} release during aphid feeding

An aphid-induced Ca^{2+} burst is still detectable in the *tpc1-2* mutant relative to untreated control leaves (Figure 4.3b), which implies that an additional mechanism of Ca^{2+} release is involved. Extracellular Ca^{2+} represents a large pool of Ca^{2+} in plants, with release into the cytosol mediated by CNGCs and GLRs [1, 2]. Since *GLR3.3* and *GLR3.6* have been implicated in the response to herbivory [103, 541], their role in plant-aphid interactions was addressed. Abolishing transcription of both *GLRs* in the 35S::GCAMP3 x *glr3.3/glr3.6* line abolished the aphid-induced Ca^{2+} burst (Figure 4.16b). This suggests that TPC1-mediated Ca^{2+} release in response to aphids lies downstream of extracellular Ca^{2+} influx, and is dependent on *GLR3.3* and *GLR3.6*. This agrees with work showing TPC1 is activated by increased $[Ca^{2+}]_{cyt}$ [112, 114, 115] and its suggested role in CICR [119, 121, 536, 537]. The data presented by the current study points to the GLRs as potential mediators of the extracellular Ca^{2+} influx during this process. Both GLR3.3 and GLR3.6 are good candidates for having a role in CICR, as like TPC1 they mediate systemic signalling in response to wounding [103, 104] and the PM channels involved in CICR still unknown.

An influx of Ca^{2+} from the extracellular space occurs during plant-pathogen interactions [371, 373] that can blocked by PM-channel inhibitors [17, 54, 372]. Ren et al. [584] measured net Ca^{2+} flux in the extracellular space of *N. tabacum* leaf disks after *M. persicae* feeding using Ca^{2+}-selective microelectrodes. They found that there was a net Ca^{2+} influx into cells pre-treated with aphids verses non-treated leaf disks, agreeing with the finding of the present study that extracellular Ca^{2+} influx is involved in this interaction.

In addition to its role in wound-induced signalling, *GLR3.3* also mediates DAMP perception [688], and it is therefore tempting to speculate that damage caused by aphid probing, including the release of glutamate, may activate a GLR-mediated Ca^{2+} burst. However, the loss of a feeding site Ca^{2+} burst distinguishable from untreated control leaves in the 35S::GCAMP3 x *glr3.3/3.6* line mirrors the phenotype in the 35S::GCAMP3 x *bak1-5* line (Figure 3.13, Chapter 3). This implies that aphid perception and PTI activation by BAK1 also lies upstream of TPC1-mediated Ca^{2+} release. The loss of the Ca^{2+} signal in both the *glr3.3/3.6* and *bak1-5* mutants suggests that they do not function in independent pathways and that BAK1 might lie upstream of $[Ca^{2+}]_{cyt}$ elevations and GLR activation. Thus, aphid-induced Ca^{2+} release is most likely stimulated by aphid HAMP perception. GLRs have been previously implicated in PAMP perception, with iGluR inhibitors attenuating flg22- elg18- and chitin-induced $[Ca^{2+}]_{cyt}$ elevations [201]. Furthermore, it is possible that glutamate itself is released from cells in response to PAMPs or HAMPs. The fungal PAMP cryptogein induces an extracellular rise in glutamate that is driven by exocytosis, demonstrated through the use of the exocytosis inhibitors brefeldin A and cytochalasin [726]. Moreover, these inhibitors also block the $[Ca^{2+}]_{cyt}$ elevation in response to the PAMP [726], suggesting that glutamate release from the cell is downstream of PAMP perception [92]. This might provide a mechanism by which BAK1-mediated aphid HAMP perception could stimulate GLR activation; however to the author's knowledge no direct link between BAK1 and GLRs or glutamate has yet been established in the literature.

4.3.10 *GLR3.3/3.6* expression has no effect on plant defence responses or aphid fecundity

ROS production (Figure 4.18a) and induction of *FRK1* (Figure 4.19a), *CYP81F2* (Figure 4.19b) and *PAD3* (Figure 4.19c) in response to aphid extract was unaltered in the *glr3.3/3.6* mutant. Therefore the GLR-mediated Ca^{2+} burst to aphid feeding might not have an effect on downstream defence induction. Nevertheless, ROS production in response to *M. persicae* extract can be blocked by PM Ca^{2+} channel inhibitors [502], implying extracellular Ca^{2+} entry does play a role. These unidentified channels may also generate the BAK1/GLR/TPC1 independent Ca^{2+} signals that can be observed in some samples upon aphid feeding (Figure 3.14, Chapter 3, Figure 4.4, Figure 4.17).

GLR3.3 is involved in DAMP-elicited ROS production and transcription of *RBOHD* and the defence marker *PR1* [688]. Whilst extracellular Ca^{2+} has been implicated in the plant response to fungal attack [372], cryptogein-elicited ROS production is not affected by iGluR antagonists that abolish cryptogein-elicited $[Ca^{2+}]_{cyt}$ elevations [726]. Thus, GLR involvement in ROS production may be DAMP-specific. Conversely, aphid extract, which contains HAMPs, but will not elicit DAMP production, induces BAK1-mediated ROS production (Figure 4.18a, [349]) and is therefore HAMP-specific. This agrees with the hypothesis that plant defence against aphids is based on HAMP not DAMP perception. This can only be demonstrated unequivocally once ROS production in response to live aphid feeding has been assessed in GLR and DAMP perception mutants.

FRK1 induction in response to flg22, elf18 and chitin can be attenuated by iGluR antagonists [201], suggesting that GLRs might play a role in MAPK activation during anti-microbial defence. However, the specific GLRs involved were not identified, and the results of the present study indicate that GLR3.3 and GLR3.6 are not involved in aphid-induced MAPK activation. The successful induction of *PAD3* and *CYP81F2* in the *glr3.3/glr3.6* mutant suggests that secondary metabolite production is not altered by the aphid-induced Ca^{2+} burst. Indeed, a sustained Ca^{2+} burst is required for phytoalexin production in response to pathogens [371], whilst the aphid-induced Ca^{2+} burst appears to be more transient. The results of the present study also imply that intracellular Ca^{2+} release mediated by TPC1 plays a role in *FRK1* and *PAD3* induction (Figure 4.19a and 4.19c), but extracellular Ca^{2+} entry via through GLRs does not.

In addition, *M. persicae* fecundity was unaltered on *glr3.3/glr3.6* (Figure 4.18b). The *glr3.3* mutant is more susceptible to biotrophic pathogens than necrotrophic pathogens, and defence against biotrophs is believed to be mediated by SA [688]. Thus one might expect SA signalling and therefore *M. persicae* fecundity to be compromised in the *glr3.3* mutant. However, as this is not the case these results further emphasise that the *M. persicae*-elicited GLR/TPC1-mediated Ca^{2+} burst characterised in this study does not affect aphid fitness. Again, this is not surprising given that Arabidopsis is a compatible host and suggests that plant susceptibility to *M. persicae* cannot be further increased by loss of the Ca^{2+} signal.

4.3.11 *BAK1* is involved in phytoalexin production in response to aphids

Analysis of the defence gene induction in the *bak1-5* mutant also presented some interesting findings. Firstly, *FRK1* induction after 1 h was not attenuated in this mutant, which suggests MAPK activation in response to *M. persicae* is independent of *BAK1*, whilst being modulated downstream in defence by *TPC1* (Figure 4.19a). This is contrary to the observation that *FRK1* induction is *BAK1*-dependent in response to a range of bacterial PAMPs [481]. However, it is in agreement with experiments showing that fungal and oomycete PAMPs induce *FRK1* independently of BAK1 [481] and that caterpillar-induced MAPK activation in *N. tabacum* is also independent of *BAK1* [362]. Interestingly, live *M. persicae* feeding induces a downregulation of *FRK1* after 5 h [365], suggesting that over time the initial induction of *FRK1* is suppressed by compatible aphid species. This difference might be the result of using of live feeding as opposed to aphid extract. Indeed, *B. brassicae* extract induces *CYP81F2* expression [349], whilst infestation with live *B. brassicae* actually reduces glucosinolate levels in leaves [304].

PAD3 and *CYP81F2* induction was attenuated on the *bak1-5* mutant (Figure 4.19b and 4.19c). This is contrary to the previous observation that *PAD3* induction in response to *M. persicae* extract is unaltered in the *bak1-5* mutant [349, 502]. However, in the current study *PAD3* expression in response to aphid extract in the *bak1-5* mutant was still 30-fold higher relative to the mock-treated controls (Figure 4.19c), and therefore there is clearly still some level of *PAD3* induction occurring. However, these findings do suggest a role for the BAK1 pathway in phytoalexin production in response to aphids. In agreement with this, glucosinolate production as a result of nematode feeding is *BAK1*-dependent [727], with use of the *bak1-5* mutant in both that study and the current one demonstrating that this phenotype is not related to brassinosteroid regulation of glucosinolates [728]. Furthermore, the wildtype level of *CYP81F2* induction in the *tpc1-2* and *glr3.3*/*glr3.6* mutants (Figure 4.19b) suggests that the BAK1-mediated regulation of glucosinolates is independent of Ca^{2+} signalling.

The difference in the dependency of Ca^{2+} release and defence gene induction on the GLRs, TPC1 and BAK1 could also be a result of the different systems used to study them. The Ca^{2+} bursts were characterised in response to live aphid feeding, whilst ROS and defence gene induction was assessed in relation to aphid extract

application. Thus, the two were addressing slightly different questions. It will be interesting to see how live aphid feeding modulates defence in the mutants characterised in this study.

This page is intentionally left blank

Chapter 5: Investigating the role of CIPKs in plant-aphid interactions

5.1 Introduction

5.1.1 CIPKs act downstream of Ca^{2+} release

Downstream of Ca^{2+} release, several different families of proteins are responsible for sensing the rise in $[Ca^{2+}]_{cyt}$ and translating it into a physiologically-relevant signal. Amongst these are the CIPKs (reviewed in [167]). In order to investigate whether Ca^{2+} acts as a signal in plant-aphid interactions, an RNA-seq screen conducted in the Hogenhout lab (JIC) to identify aphid-responsive genes implicated in Ca^{2+} signalling. Many differentially regulated transcripts were detected upon infestation with aphids, and this included *CIPK3*. There are five splice variants of *CIPK3* (Figure 5.1) and *CIPK3.2* was of particular interest because expression was regulated in opposite directions depending on the species of aphid feeding on the plant.

CIPKs are a group of serine/threonine protein kinases that specifically interact with the CBLs through the CIPK NAF domain [159] (Figure 5.1). An interaction between the NAF domain and the kinase activation domain render CIPKs auto-inhibitory, with phosphorylation and/or CBL binding required to relieve this [160]. CBLs have no inherent activity of their own [136, 155, 167]. As a result, CBLs and CIPKs work as partners, with CBLs acting as the Ca^{2+}-sensing half of the partnership [156] and the CIPK transducing this signal through phosphorylation of target proteins [157, 158]. CBLs and CIPKs are inherently promiscuous and can act together in a variety of partnerships, giving rise to a wide range of responses [729] and functional redundancy [164-166]. Currently, CIPK3 has been demonstrated to interact physically with CBL2, CBL3 and CBL9 [165, 166, 176].

5.1.2 CIPK3 functions in the ABA-mediated plant response to stress

The function of CIPK3 has only been studied by a handful of groups. The first reported role of CIPK3 was in response to abiotic stress (including cold, drought and salt) as well as wounding, which result in accumulation of the *CIPK3* transcript [175]. Furthermore, seedlings of the Arabidopsis mutant *cipk3-1*, which has abolished *CIPK3* expression, exhibit reduced germination under osmotic stress, and showed reduced

expression of the abiotic stress markers *KINASE 1* (*KIN1*), *KIN2* and *RESPONSIVE TO DESICCATION 29A* (*RD29A*) [175, 176].

There is considerable evidence that CIPK3 acts in the ABA pathway. Seedlings of *cipk3-1* mutants are hypersensitive to high levels of ABA, a plant hormone critical for many plant stress responses. The ABA synthesis inhibitor norflurazon can rescue the *cipk3-1* osmotic stress phenotype, demonstrating that this phenotype is ABA-dependent [175]. Furthermore, expression of *ABA REPRESSOR 1* (*ABR1*) is significantly reduced in *cipk3-1* mutants [730] and there appears to be a direct interaction between CIPK3 and ABF2 [731], a protein involved in the activation of ABA-inducible genes [732]. The ABA pathway is not only common to abiotic stresses, but also may play a role during wounding [172, 173] and pathogen defence [432, 439, 440] . Thus, like Ca^{2+}, ABA acts a common signalling molecule connecting a range of plant stress responses.

In ABA-induced stomatal closure, there are Ca^{2+}-independent components mediated by OPEN STOMATA 1 (OST1) and a Ca^{2+}-dependent pathway mediated by CDPKs including Ca^{2+}-DEPENDENT PROTEIN KINASE 6 (CPK6) (Figure 5.1) [733]. Furthermore, ABA stimulates $[Ca^{2+}]_{cyt}$ elevations in guard cells [47, 48, 734-738], thought to be mediated through a priming of Ca^{2+} channel and decoders [169] . As a result, there is a close association between the ABA and Ca^{2+} signalling pathways. The *cipk3-1* phenotype implies that CIPK3 is a negative regulator of ABA accumulation (Figure 5.2), suggesting CIPK3 may act as another protein involved in crosstalk between ABA and Ca^{2+}. However, the link between Ca^{2+} and ABA in non-stomatal cells during biotic interactions is still unclear.

CIPKs are characterised by several domains, including the NAF domain (see above) and a protein phosphatase interacting (PPI) domain, responsible for binding type 2c protein phosphatases (PP2Cs) [739] (Figure 5.1). PP2Cs have been suggested to act as inhibitors of CIPKs, with CBLs hypothesised to bind PP2Cs in order to inactivate them and rescue CIPK activity [161]. PP2Cs are both negative regulators of ABA [740, 741] and negatively regulated by ABA [742]. This places PP2Cs as additional components in the CIPK-CBL network, and provides another link between this network and ABA signalling (Figure 5.2).

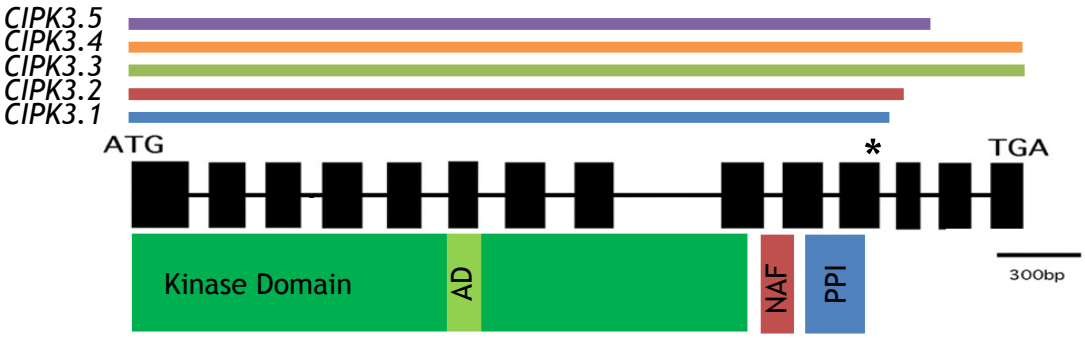

Figure 5.1: ***CIPK3*** **domains and gene models.**

Exons (solid boxes) and introns (lines) of the full length gene (*CIPK3.3*) are indicated. AD = kinase activation domain. NAF = NAF domain, required for interaction with CBLs. PPI = protein phosphatase interaction domain, required for interaction with PP2Cs. An additional 18 nucleotides in *CIPK3.2* (denoted by *) lead to a premature stop codon. Adapted from Kim et al. [175].

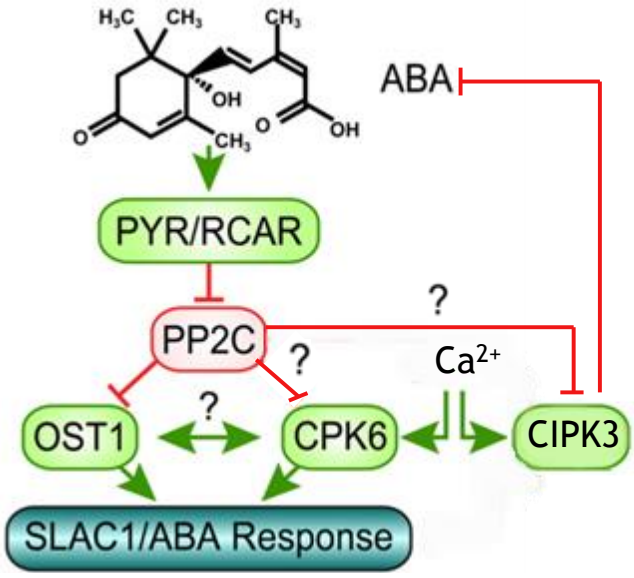

Figure 5.2: The Arabidopsis ABA pathway has Ca^{2+}-independent and Ca^{2+}-dependent components.

ABA is perceived by PYRABACTIN RESISTANCE 1/REGULATORY COMPONENTS OF ABA RECEPTORS (PYR/RCARs) that inhibit PP2Cs. This relieves PP2C repression of OST1 and promotes ABA-mediated responses, independently of Ca^{2+}. In addition, Ca^{2+} activates CPK6 that in turn activates ABA-mediated responses. In both cases the responses are partially governed by SLOW ANION CHANNEL-ASSOCIATED 1 (SLAC1). CIPK3 acts as a negative regulator of ABA accumulation. PP2Cs are hypothesised to inhibit CPK6 and CIPK3, but there is no direct experimental evidence for this (represented by a ?). Adapted from Laanemets et al. [733].

5.1.3 ABA is implicated in the plant response to aphid attack

ABA, along with several other phytohormones, is believed to act in the regulation of plant-aphid interactions. It is hypothesised that in a compatible interaction such as *M. persicae* and Arabidopsis, the aphid induces an increase in ABA and SA that antagonises JA, a hormone known to have a detrimental effect on aphids [307, 427, 428, 435, 743]. Supporting this, *M. persicae* infestation causes an accumulation of ABA [437], and *M. persicae* fecundity is lower on the ABA synthesis mutants *ABA DEFICIENT 1* (*aba1*) [437] and *aba2* [442]. Furthermore, *M. persicae* avoids *aba1* and *aba2* as hosts if given a choice [437].

Conversely, ABA has been suggested to promote JA production via the JA signalling transcription factor JASMONATE INSENSITIVE 1 (JIN1) [744]. In addition, abolishing transcription of the ABA signalling repressor and CIPK-interacting protein *ABA INSENSITIVE 1* (*ABI1*) results in lower *M. persicae* fecundity, and disrupting the ABA signalling network through mutation of *ABI4* increases *M. persicae* fecundity [442]. It is also worth noting that ABA is involved in production of ROS [745, 746] and the deposition of callose [747], both of which are part of the plant defence response to aphids [349].

Consequently, the role of ABA in plant-aphid interactions is far from clear. Indeed, ABA signalling-related genes are both activated and repressed by aphid infestation [442, 748]. Furthermore, it may be that ABA plays a different role in compatible vs incompatible plant-aphid interactions, with further exploration into what contributes to non-host resistance in plant-aphid interactions still required [749].

5.1.4 CIPK3 may act independently of ABA

CIPK3 might also play a role in the response to stress independently of ABA. Indeed, in Arabidopsis there is an ABA-independent salt stress response mediated through DRE-BINDING PROTEIN 2A (DREB2A) [750-752]. Furthermore, *RD29A*, a cold stress marker gene known to be ABA-independent [753] exhibits altered expression in *cipk3-1* [175]. It is therefore possible that *CIPK3* acts as cross talk node between Ca^{2+}, ABA-dependent, and ABA-independent pathways [175].

5.1.5 CIPK3 is part of a four-member family of CIPKs

Phylogenetically, CIPK3 lies within clade I of the CIPK family, along with CIPK9, CIPK23 and CIPK26 (Figure 5.3), which together act in the regulation of Mg^{2+} sequestration (Figure 1.4, Chapter 1) [165, 166]. These genes act redundantly in this response, as only in double, triple and quadruple mutants can a phenotype be observed [165, 166]. Additionally, all four proteins interact with CBL2 and CBL3, which recruits them to the tonoplast membrane [165]. As a result, the role of CIPK3 may be closely associated with that of CIPK9, CIPK23 and CIPK26.

Individually, these clade I CIPKs are involved in a multitude of plant processes. CIPK9 and CIPK23 have been implicated in potassium homeostasis and drought tolerance [183, 187, 754]. CIPK23 is also thought to act in nitrogen sensing [189]. CIPK26 has been implicated in ABA signalling through interactions with ABI1, ABI2 and ABI5 [166, 755] as well as in ROS production [691, 692]. The interplay and inter-dependence between CIPKs in these processes is still being unravelled.

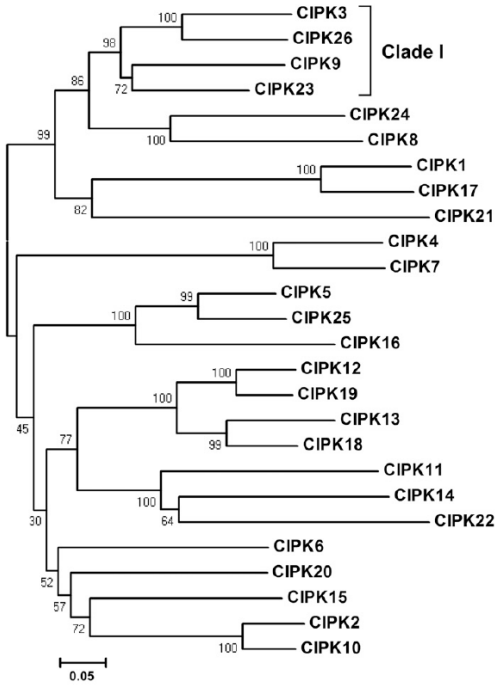

Figure 5.3: Phylogenetic grouping of the 26 CIPKs in Arabidopsis based on amino acid sequence.

CIPK3, 9, 23 and 26 form a monophyletic CIPK group named clade I. Taken from Tang et al. [165].

5.1.6 Aims of this chapter

This chapter will outline work investigating the downstream components of Ca^{2+} signalling in plant-aphid interactions, specifically the role of CIPK3 and related genes CIPK9, CIPK23 and CIPK26. This investigation was conducted using a combination of aphid performance and plant physiological assays. The aim was to complement the work that characterised an aphid-induced Ca^{2+} burst in Arabidopsis (Chapters 3 and 4) by investigating the biological relevance of Ca^{2+} decoding mechanisms in defence against aphids.

5.1.7 Materials and methods

The methods used in his chapter are detailed in Chapter 2. Information on the RNAseq can be found in Section 2.11, gene synthesis and cloning in Section 2.6, aphid performance assays (including fecundity, survival, choice tests) in Section 2.9, and Arabidopsis ROS and germination assays in Section 2.10.

5.2 Results

5.2.1 *CIPK3.2* is differentially expressed in response to feeding by different aphid species

RNA-seq was conducted on aphid-infested Arabidopsis leaves (accession: Col-0) in order to identify genes that were differentially regulated upon aphid attack. These leaves were not detached from the plant, as in Chapters 3 & 4, so as to avoid confounding factors associated with wounding. Two species of aphid were used, *A. pisum* and *M. persicae*. This screen identified several aphid-responsive genes that are involved in Ca^{2+} signalling. After treatment with *A. pisum*, expression of various putative cation-permeable channels was altered 48 h post-infestation. These included CNGCs and GLRs, the majority of which were significantly upregulated in response to *A. pisum* (Table 5.1). Several downstream components of the Ca^{2+} network were also revealed to be responsive to *A. pisum* infestation, including CIPKs, CDPKs and CaM-related proteins (Table 5.1). Conversely, *M. persicae* infestation results in differential expression of far fewer genes, however the proportion of those related to Ca^{2+} signalling was similar to *A. pisum* (Figure 5.4). Only one channel, *CNGC12*, and one downstream component of the Ca^{2+} signal, *CIPK3*, were differentially expressed in response to *M. persicae* (Table 5.1).

CIPK3 was of particular interest because out of the 33,603 genes analysed, *CIPK3* splice variant 2 (*CIPK3.2*) was the only gene that showed an opposite expression pattern in response to the two aphid species. Upon application of *A. pisum*, *CIPK3.2* was significantly downregulated, as was *CIPK3.3*. Conversely, treatment with *M. persicae* resulted in a significant upregulation of *CIPK3.2* (Figure 5.5). *CIPK3.2* differs from the full-length gene (*CIPK3.3*) as a result of an additional 18 nucleotides in exon 11, resulting in a frame shift that creates a premature stop codon. This results in CIPK3.2 having a truncated C-terminal region relative to *CIPK3.3* (Figure 5.1).

Table 5.1: Differential expression of Ca^{2+} signalling-related transcripts in response to infestation with two species of aphid (*M. persicae* and *A. pisum*) for 48 h.

[a] Arabidopsis gene identification number. [b] Expression ratios were calculated in comparison to uninfested plants (empty cages). Numbers reported represent genes that were significantly differentially expressed (two-fold change, padj<0.05). ns = non-significant. [c] Database annotation of the protein product as listed on The Arabidopsis Information Resource (TAIR). Experiment conceived and conducted by Sam Mugford (Hogenhout Lab, JIC). Table compiled by T.V

.

AGI[a]	Expression ratio relative to control plant[b]		TAIR annotation[c]
	A. pisum	*M. persicae*	
AT5G15410.1	0.42	ns	DND1, ATCNGC2, CNGC2 | Cyclic nucleotide-regulated ion channel family protein
AT2G46430.2	1.71	ns	ATCNGC3, CNGC3, CNGC3.C | cyclic nucleotide gated channel 3
AT2G46450.2	2.71	ns	CNGC12 | cyclic nucleotide-gated channel 12
AT2G46450.3	ns	0.40	CNGC12 | cyclic nucleotide-gated channel 12
AT1G05200.2	2.03	ns	ATGLR3.4, GLR3.4, GLUR3 | glutamate receptor 3.4
AT2G32390.1	5.75	ns	ATGLR3.5, GLR3.5, GLR6 | glutamate receptor 3.5
AT4G35290.2	2.73	ns	GLUR2, GLR3.2, ATGLR3.2, ATGLUR2 | glutamate receptor 2
AT5G57110.1	0.23	ns	ACA8, AT-ACA8 | autoinhibited Ca2+ -ATPase, isoform 8
AT2G26980.2	0.14	5.69	CIPK3 | CBL-interacting protein kinase 3
AT2G26980.3	0.14	ns	CIPK3 | CBL-interacting protein kinase 3

Table 5.1 (cont.)

AGI[a]	Expression ratio relative to control plant[b]		TAIR annotation[c]
	A. pisum	*M. persicae*	
AT3G23000.1	2.40	ns	CIPK7, SnRK3.10, PKS7, ATSRPK1, ATSR2 | CBL-interacting protein kinase 7
AT5G45820.1	3.21	ns	CIPK20, SnRK3.6, PKS18 | CBL-interacting protein kinase 20
AT4G14580.1	0.25	ns	CIPK4, SnRK3.3 | CBL-interacting protein kinase 4
AT5G10930.1	14.0	ns	CIPK5, SnRK3.24 | CBL-interacting protein kinase 5
AT5G01810.1	0.14	ns	CIPK15, ATPK10, PKS3, SNRK3.1, SIP2 | CBL-interacting protein kinase 15
AT5G04870.1	0.38	ns	CPK1, ATCPK1 | Ca^{2+}-dependent protein kinase 1
AT2G17290.1	0.41	ns	CPK6, ATCDPK3, ATCPK6 | Ca^{2+}-dependent protein kinase family protein 6
AT1G74740.1	0.47	ns	CPK30, CDPK1A, ATCPK30 | Ca^{2+}-dependent protein kinase 30
AT2G41110.1	0.27	ns	CAM2, ATCAL5 | calmodulin 2
AT2G22300.2	0.49	ns	CAMTA3, SR1 | signal responsive 1

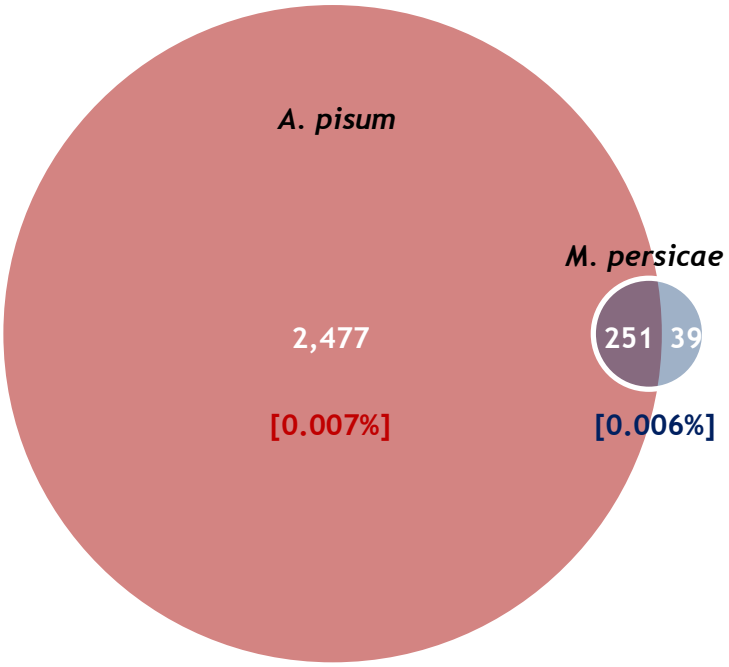

Figure 5.4: Total genes differentially regulated upon infestation with two species of aphid (*M. persicae* or *A. pisum*) for 48 h.

Number of Ca^{2+} signalling-related genes differentially regulated is reported in square brackets as a proportion of the total genes differentially regulated by each species. DEseq was used to determine differential expression between controls and aphid-treated samples, with a 5% false discovery rate (padj<0.05) and >two-fold change (n=10). Experiment conceived and conducted by Sam Mugford (Hogenhout Lab, JIC). Figure compiled by T.V.

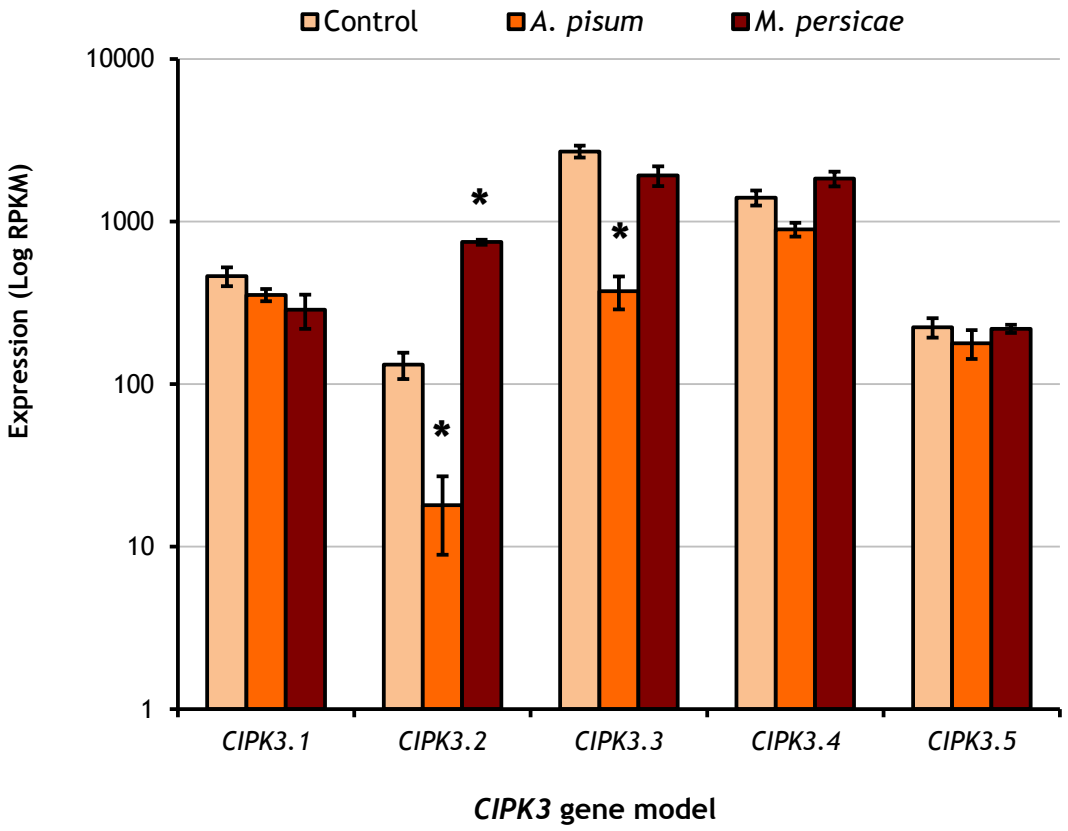

Figure 5.5: Absolute gene expression of *CIPK3* splice variants in response to treatment with *M. persicae*, *A. pisum* or an empty clip cage (control).

Expression is represented as the log to the base 10 of the reads per kilobase of transcript per million mapped reads (RPKM), as detected by RNA-seq. DEseq was used to determine differential expression between controls and aphid treatments (asterisks), with a 5% false discovery rate (padj<0.05) and >two-fold change (n=10). Error bars show SEM. Experiment conceived and conducted by Sam Mugford (Hogenhout Lab, JIC). Figure compiled by T.V.

5.2.2 Aphid performance and plant ROS production is not altered on *cipk3-1*

In order to determine the biological relevance of altered *CIPK3* expression, *CIPK3(.2)* expression was assessed in relation to beneficial or detrimental effects on either aphid species. For this, the *cipk3-1* null mutant [175, 176] was used in aphid performance assays. In addition, the *cipk3-1* mutant was complemented with a full-length genomic version of *CIPK3* (Figure 5.6a). However, *M. persicae* fecundity was not altered on these lines (Figure 5.6b). In addition, the *cipk3-1* mutant was complemented with the coding sequence of *CIPK3.2* (Figure 5.7a), in order to produce plants expressing only this splice variant. Again, *M. persicae* fecundity was not altered on these lines (Figure 5.7b).

To examine more subtle effects on fecundity, the trans-generational fecundity of *M. persicae* was analysed over a four-week period [560]. Again, no difference on the *cipk3-1* mutant was observed (Figure 5.8a). In addition, no host preference was found for *cipk3-1* over the wildtype (Figure 5.8b). To assess whether *CIPK3* expression had an effect on downstream defences elicited by *M. persicae*, ROS production in response to aphid extract was assessed on the mutant. No difference in the aphid extract-elicited burst could be detected (Figure 5.8c).

As infestation with *A. pisum* resulted in significant decreases in *CIPK3.2* and *CIPK3.3* expression (Figure 5.5), the performance of this species on *cipk3-1* was also investigated. No difference in *A. pisum* survival was found between *cipk3-1* and wildtype (Figure 5.8d).

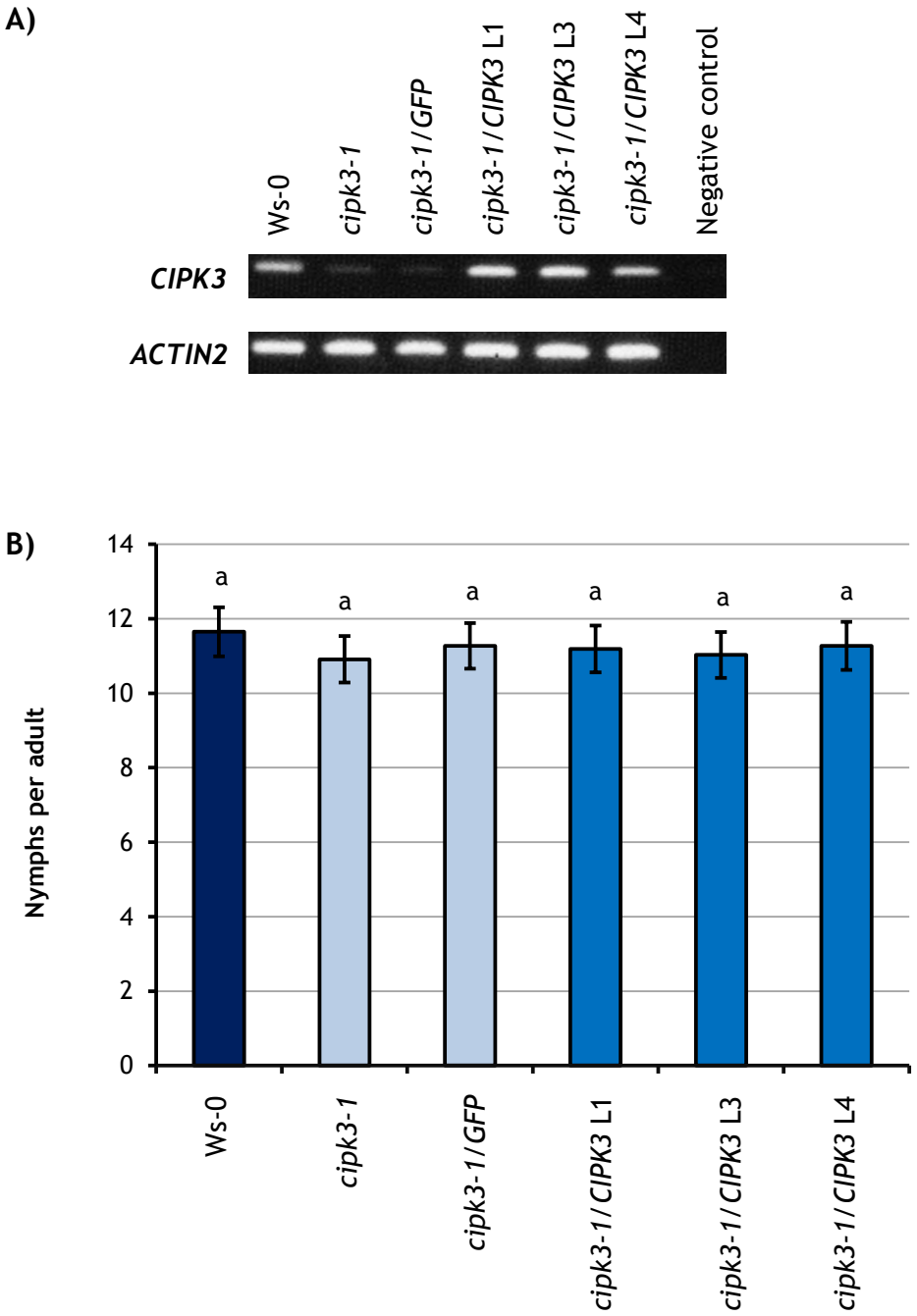

Figure 5.6: *M. persicae* fecundity is not altered on *cipk3-1* and *cipk3-1* complementation lines.

A) *cipk3-1* complemented with a genomic copy of *CIPK3* expressed under its native promoter. *ACTIN2* expression was used as a control. Primers: ACTIN2-RT and gCIPK3_Pand (Table 2.4). **B)** *M. persicae* fecundity over 14 days on *cipk3-1* and complemented lines. L= line. Letters indicate no significant different between genotypes (Student's t-test within GLM at $p<0.05$). Error bars show SEM of 24 biological replicates from 4 independent experiments.

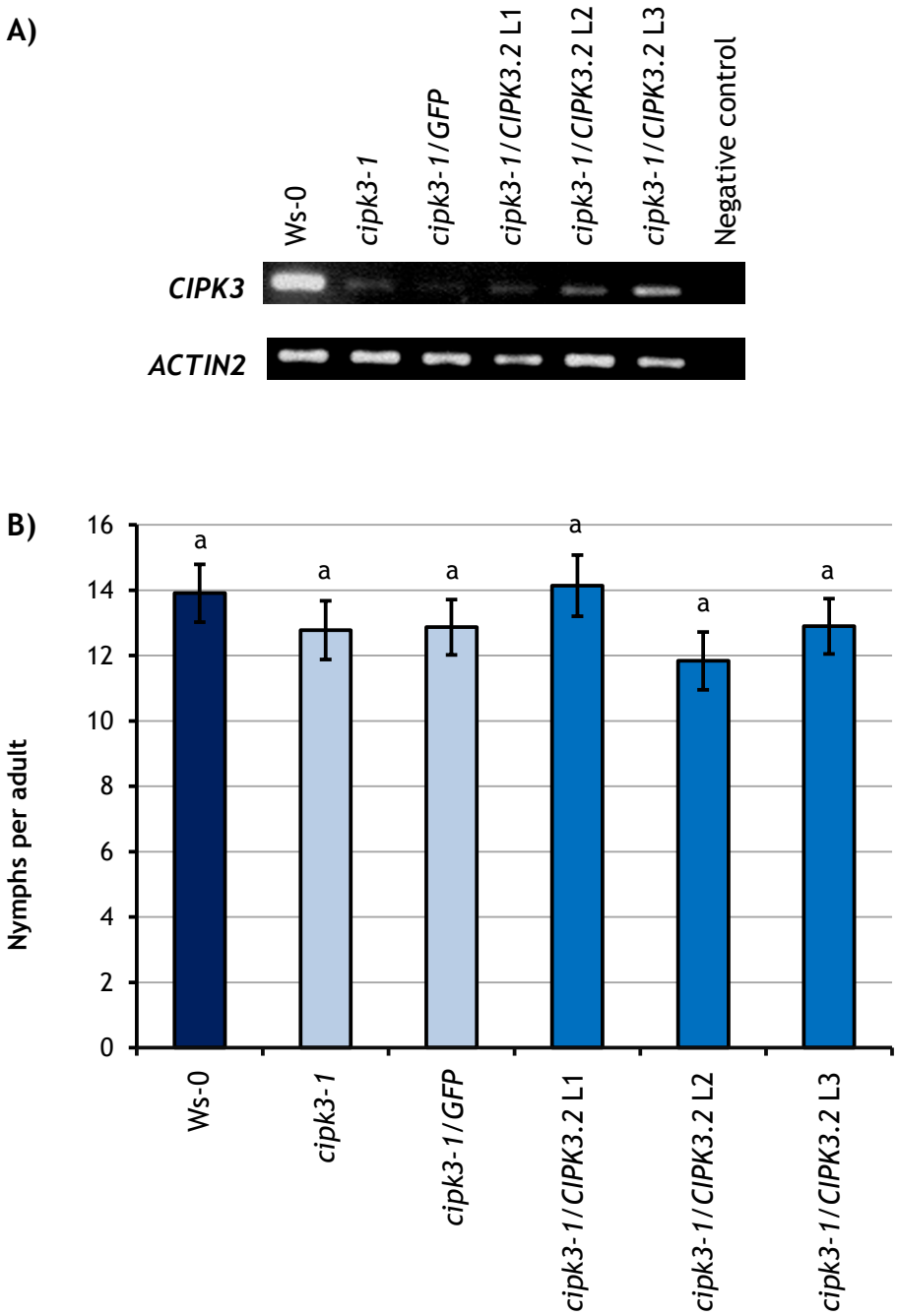

Figure 5.7: *M. persicae* fecundity is not altered on *CIPK3.2* complementation lines.

A) *cipk3-1* complemented with the coding sequence of *CIPK3.2*. *ACTIN2* expression was used as a control. Primers: ACTIN2-RT and gCIPK3_Pand (Table 2.4). **B)** *M. persicae* fecundity over 14 days on *CIPK3.2* complemented lines. L= line. Letters indicate no significant different between genotypes (Student's t-test within GLM at $p<0.05$). Error bars show SEM of 18 biological replicates from 3 independent experiments.

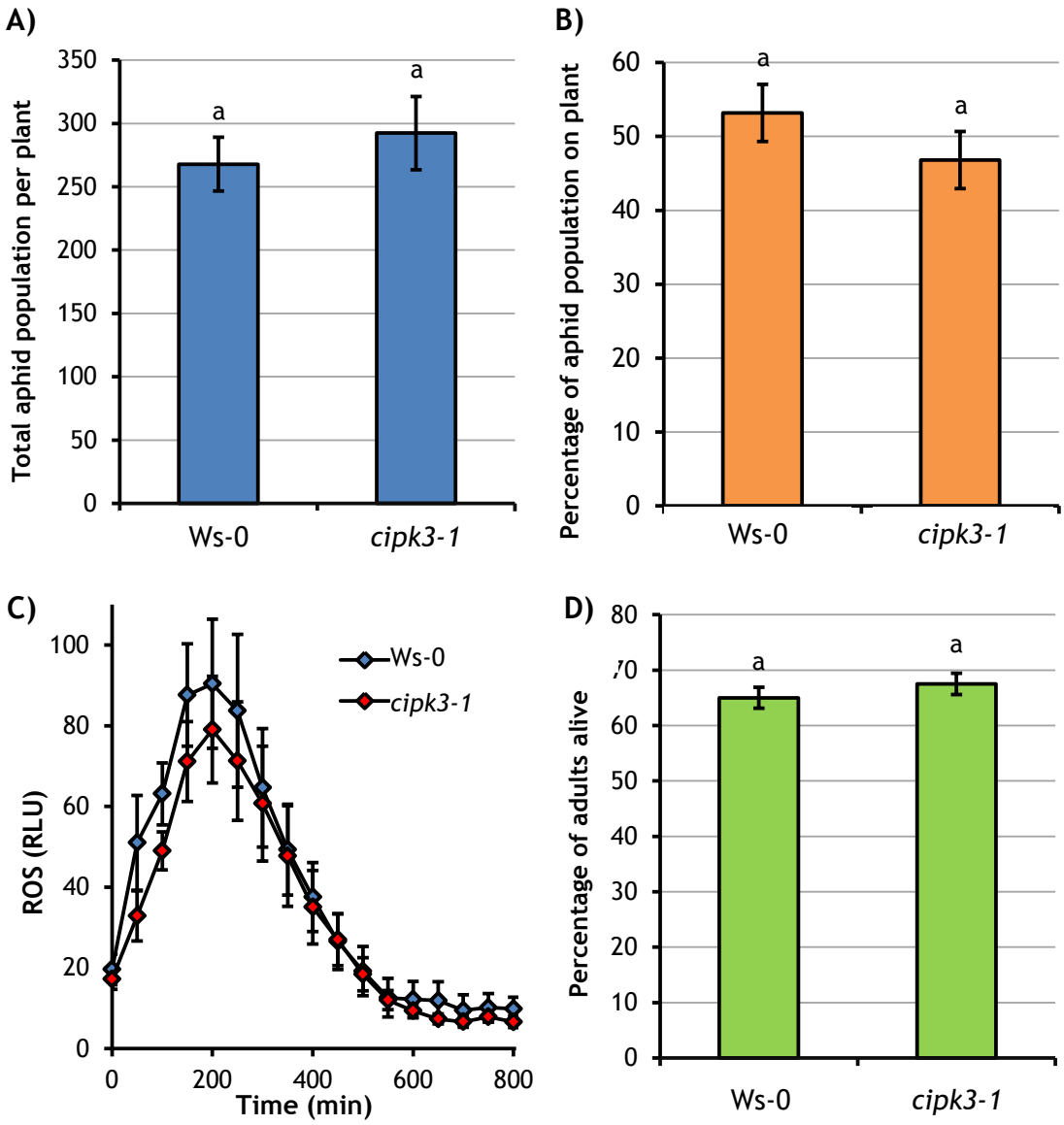

Figure 5.8: Aphid performance, host choice and plant ROS production are not altered on the *cipk3-1* mutant.

A) Trans-generational fecundity of *M. persicae*. Total aphid population per plant after 4 weeks is displayed. Error bars show SEM of 24 biological replicates from 4 independent experiments. **B)** *M. persicae* host choice. The percentage of the total aphid population settled on each plant after a 24-hour choice period is displayed. Error bars show SEM of 24 biological replicates from 4 independent experiments. **C)** ROS production (RLU) over time in response to *M. persicae* extract. Error bars show SEM of 24 biological replicates from 3 independent experiments. **D)** *A. pisum* survival. Survival was averaged across the two days in which the control population (Ws-0) decreased below 50% survival. Error bars show SEM of 18 biological replicates from 3 independent experiments. Letters indicate no significant difference between genotypes (Student's t-test within GLM at $p<0.05$).

5.2.3 Constitutive activation of *CIPK3* had no effect on *M. persicae* fecundity

In order to test whether CIPK3 activity had an effect on aphid performance, the *cipk3-1* mutant was complemented with a constitutively-active version of the enzyme (*CIPK3T183D*). By mutating a Threonine residue (Thr183) to an Aspartate (Asp183) a 9-fold increase in kinase activity can be achieved [756]. The mutated version of CIPK3 was transformed into the *cipk3-1* mutant by agro-infiltration (Figure 5.9a). Out of the three independent *CIPK3T183D* lines generated, only *cipk3-1/CIPK3T183D* line 3 showed a significant reduction in *M. persicae* fecundity (Figure 5.9b). However, the *cipk3-1/CIPK3* line 3 plants were severely stunted (Figure 5.9c) and this was not seen in the other two lines.

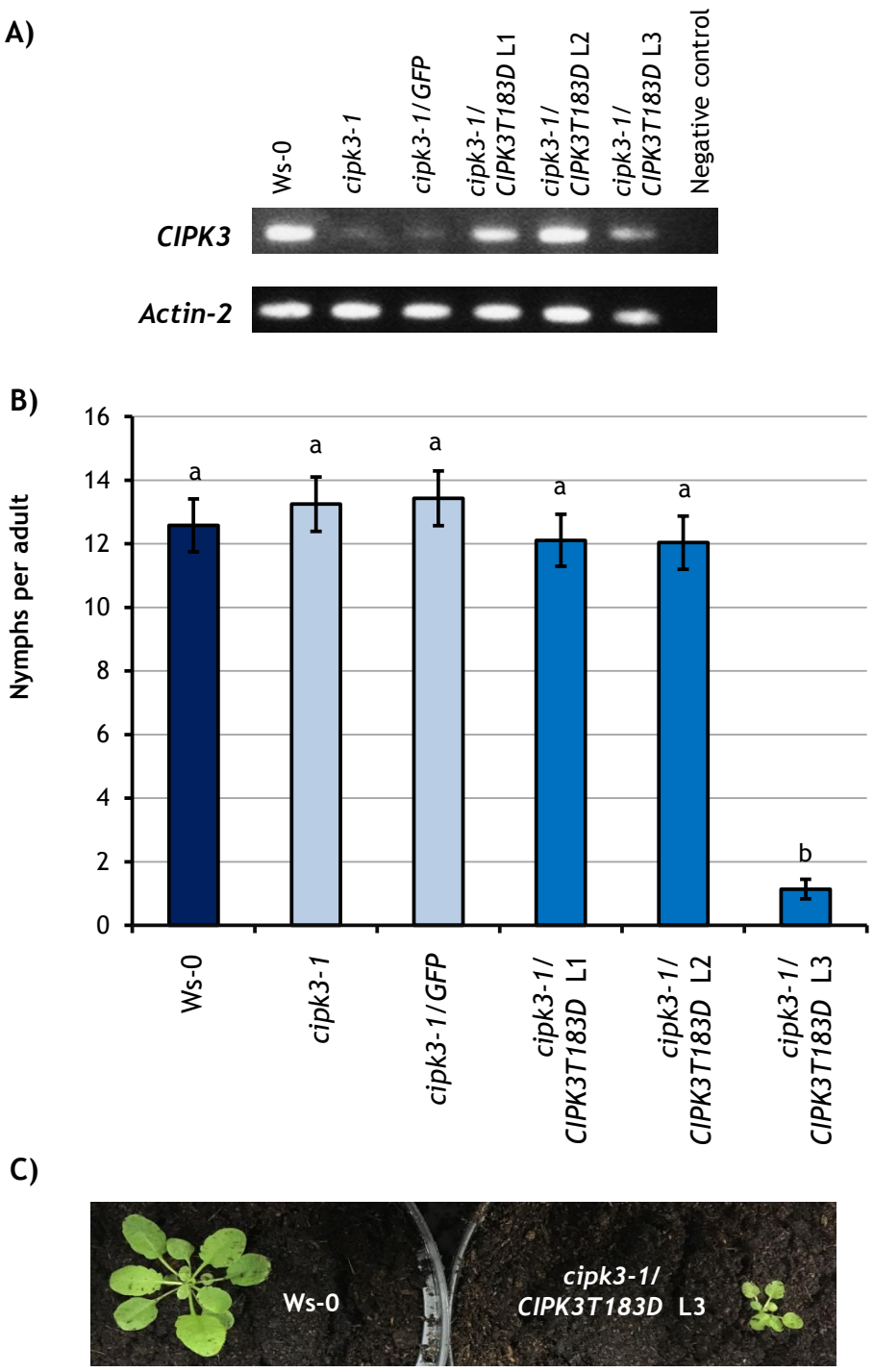

Figure 5.9: Constitutive activation of *CIPK3* (*CIPK3T183D*) did not have a consistent effect on *M. persicae* fecundity

A) RT-PCR of *CIPK3T183D* lines. L = line. *ACTIN 2* was used as a control. Primers: ACTIN2-RT and gCIPK3_Pand (Table 2.4). **B)** *M. persicae* fecundity over 14 days on *CIPK3T183D* lines. Error bars show SEM of 18 biological replicates from 3 independent experiments. Letters indicate a significant difference between genotypes (Student's t-test within GLM at $p<0.05$). **C)** *cipk3-1/ CIPK3T183D L3* displays a severe growth phenotype. L= line.

5.2.4 Aphid performance is not altered on an alternative *CIPK3* mutant, *cipk3-103*

The established mutant *cipk3-1* was identified in the Wassilewskija (Ws) Arabidopsis ecotype [175]. However, the transcriptomic screen presented in section 5.2.1 was conducted with the Columbia (Col-0) ecotype. Thus, for consistency aphid performance was tested on a *cipk3* null mutant in the Col-0 background. Several candidates were identified from the SALK and SAIL libraries, based on T-DNA insertions within *CIPK3*. These were named *cipk3-101* (SAIL_449_B12), *cipk3-102* (SALK_064491), *cipk3-103* (SAIL_409_A04) and *cipk3-104* (SALK_137779.25.20.X) and the position of the insertion was identified through sequencing with Lbb1.3, SAIL LB2 and CIPK3-specific primers (Table 2.3) (Figure 5.10a).

In order to assess whether the candidate mutants lacked transcription of *CIPK3*, RT-PCR was conducted on plants homozygous for the insertions, using primers specific to different regions along the gene (Figure 5.10a). Of these, c*ipk3-103 and cipk3-104* lacked transcription around the insertion site but not at other locations, whilst cipk3-102 lacked all transcription downstream of the T-DNA insertion (Figure 5.10b). *cipk3-101* had no detectible alteration in *CIPK3* transcription (Figure 5.10b). From this it was concluded that the *cipk3-102, cipk3-103* and *cipk3-104* mutants cannot produce a full-length transcript.

These candidate mutants were assessed in a phenotypic assay, based on the reduced germination seen in *cipk3-1* during osmotic stress [175, 176]. However, when grown on media containing 150 mM NaCl, none exhibited reduced germination as seen for *cipk3-1* (Figure 5.11). Surprisingly, one candidate, *cipk3-104*, exhibited increased germination (Figure 5.11).

Nevertheless, from the identified *CIPK3* mutants, *cipk3-103* was selected for screening aphid performance as this was the only candidate with a T-DNA insertion in an exon (Figure 5.10a). This mutant has been subsequently published by Tang et al. [165]. However, as with the *cipk3-1* mutant, neither *M. persicae* fecundity (Figure 5.12a) nor *A. pisum* survival (Figure 5.12b) was altered on *cipk3-103*.

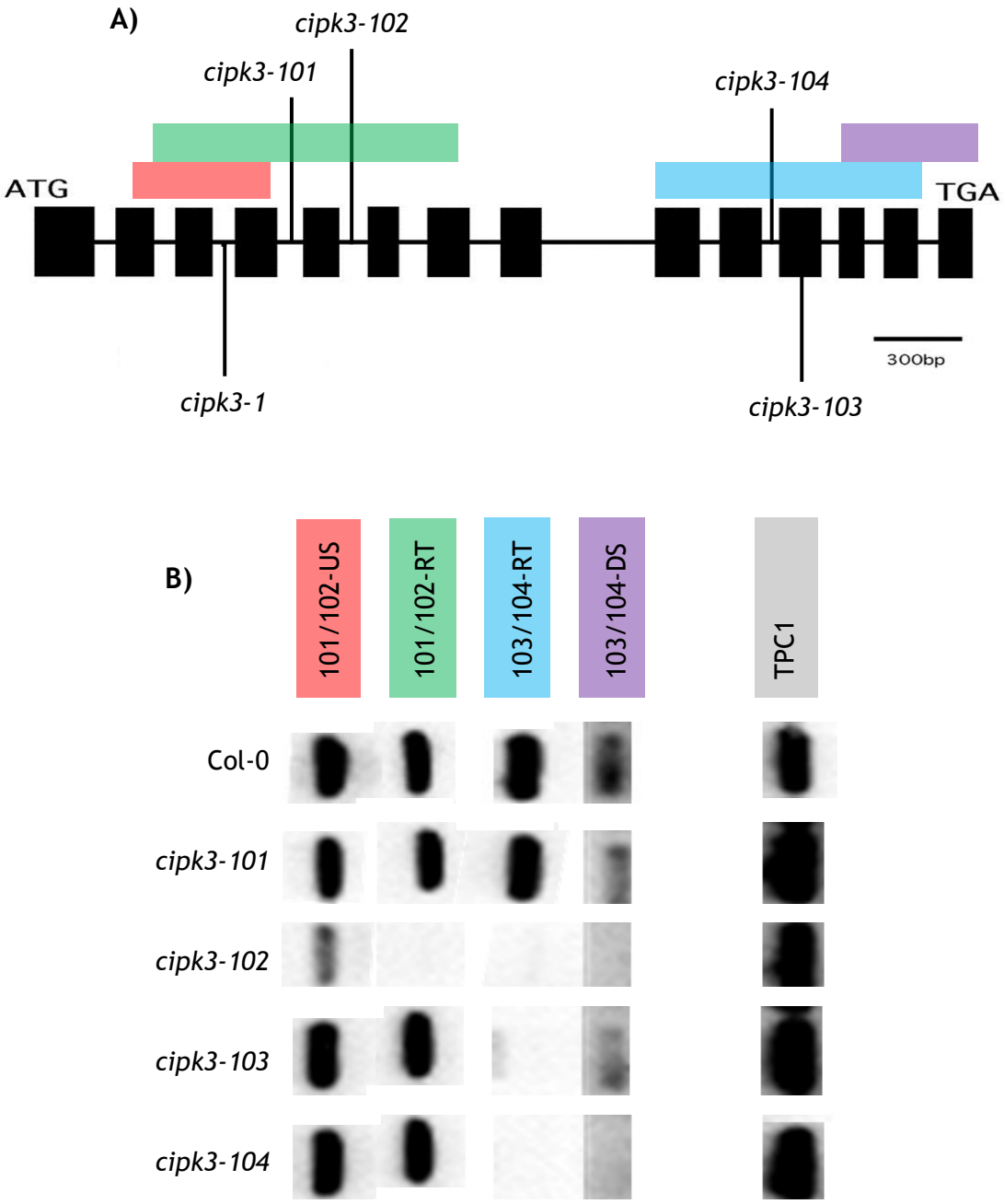

Figure 5.10: Identifying *CIPK3* T-DNA insertion mutants in the Col-0 ecotype

A) Scheme of the *Arabidopsis CIPK3* gene. Exons (solid boxes) and introns (lines) are indicated. The position of the original Ws-0 insertion is shown (*cipk3-1*), along with the position of the Col-0 insertions identified through DNA sequencing using *CIPK3*-specific primers (Table 2.3). Coloured boxes indicate the position of the amplicons generated by different primer pairs used to genotype the insertion mutants (red = 101/102-US, green = 101/102-RT, blue = 103/104-RT and purple = 101/102-DS, details in Table 2.4). Adapted from Kim et al [175]. **B)** RT-PCR of *CIPK3* insertion mutants using the *CIPK3*-specific primers, and *TPC1* as a control gene (AtTPC1-F2 & R2, Table 2.4). Full gel provided in Figure E1 (Appendix E).

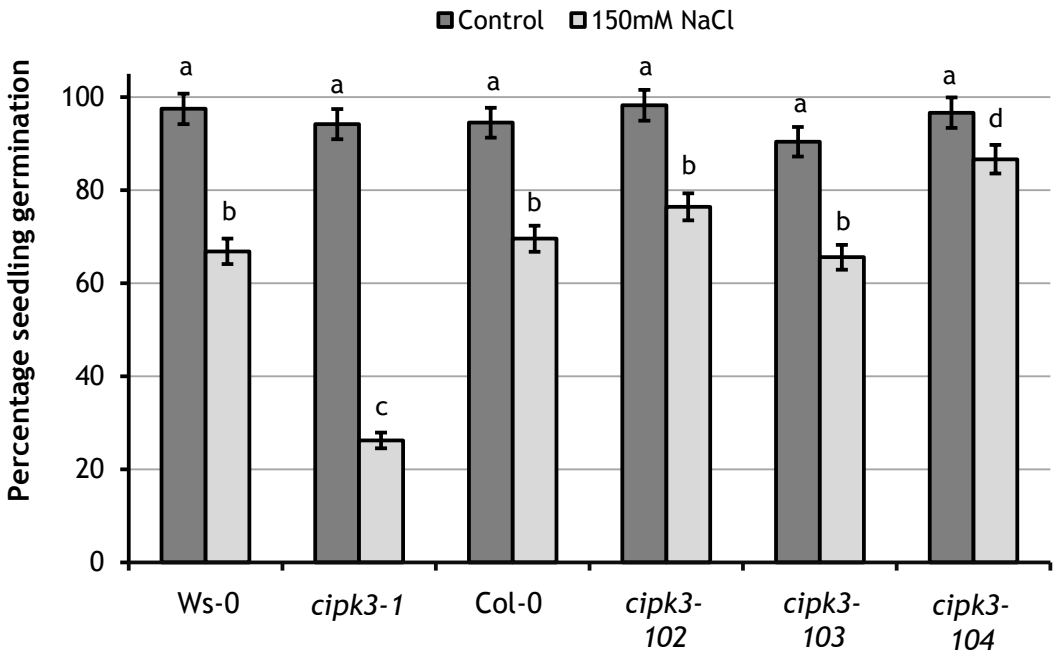

Figure 5.11: Germination success of 3-day old Arabidopsis *CIPK3* candidate mutants on salt-stressed media.

Number of germinated seedlings on ¼ strength MS medium (control) and ¼ strength MS medium supplemented with 150 mM NaCl. Error bars show SEM of 9 biological replicates from 3 independent experiments. Letters indicate significant differences (Student's t-probabilities calculated within GLM at $p<0.05$). Experiment conceived and designed by T.V and conducted by J.C. under supervision of T.V.

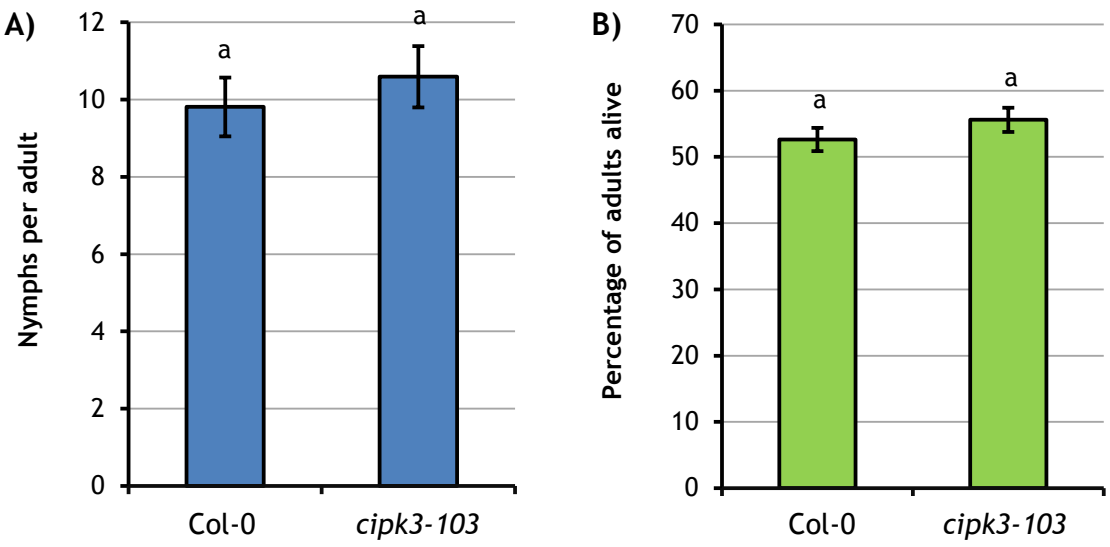

Figure 5.12: Aphid performance is not altered on *cipk3-103*.
A) *M. persicae* fecundity over 14 days. Error bars show SEM of 18 biological replicates from 3 independent experiments. **B)** *A. pisum* survival. Survival is averaged over the two days in which the control population (Ws-0) decreased below 50% survival. Letters indicate no significant differences between genotypes (Student's t-test within GLM at $p<0.05$). Error bars show SEM of 18 biological replicates from 3 independent experiments.

5.2.5 Abolishing transcription of a combination of clade I CIPKs negatively affects aphid fecundity

The possible roles of other genes in the CIPK3 pathway on plant-aphid interactions was also investigated. *M. persicae* fecundity was assessed on null mutants of *ABF2* and *PP2CA*, and was not significantly different to wildtype in either case (Figure 5.13a). Furthermore, in order to determine whether *CIPK3* acts redundantly with other closely-related CIPKs, *M. persicae* fecundity on Arabidopsis mutants lacking a combination of *CIPK3*, *CIPK9*, *CIPK23* and *CIPK26* was assessed. Mutation of *CIPK26* in addition to *CIPK3* had no effect on aphid fecundity. However, on plants lacking both *CIPK9* and *CIPK23* transcription, *M. persicae* fecundity was significantly reduced. In the quadruple mutant *cipk3/9/23/26* this negative effect on fecundity was even stronger (Figure 5.13b).

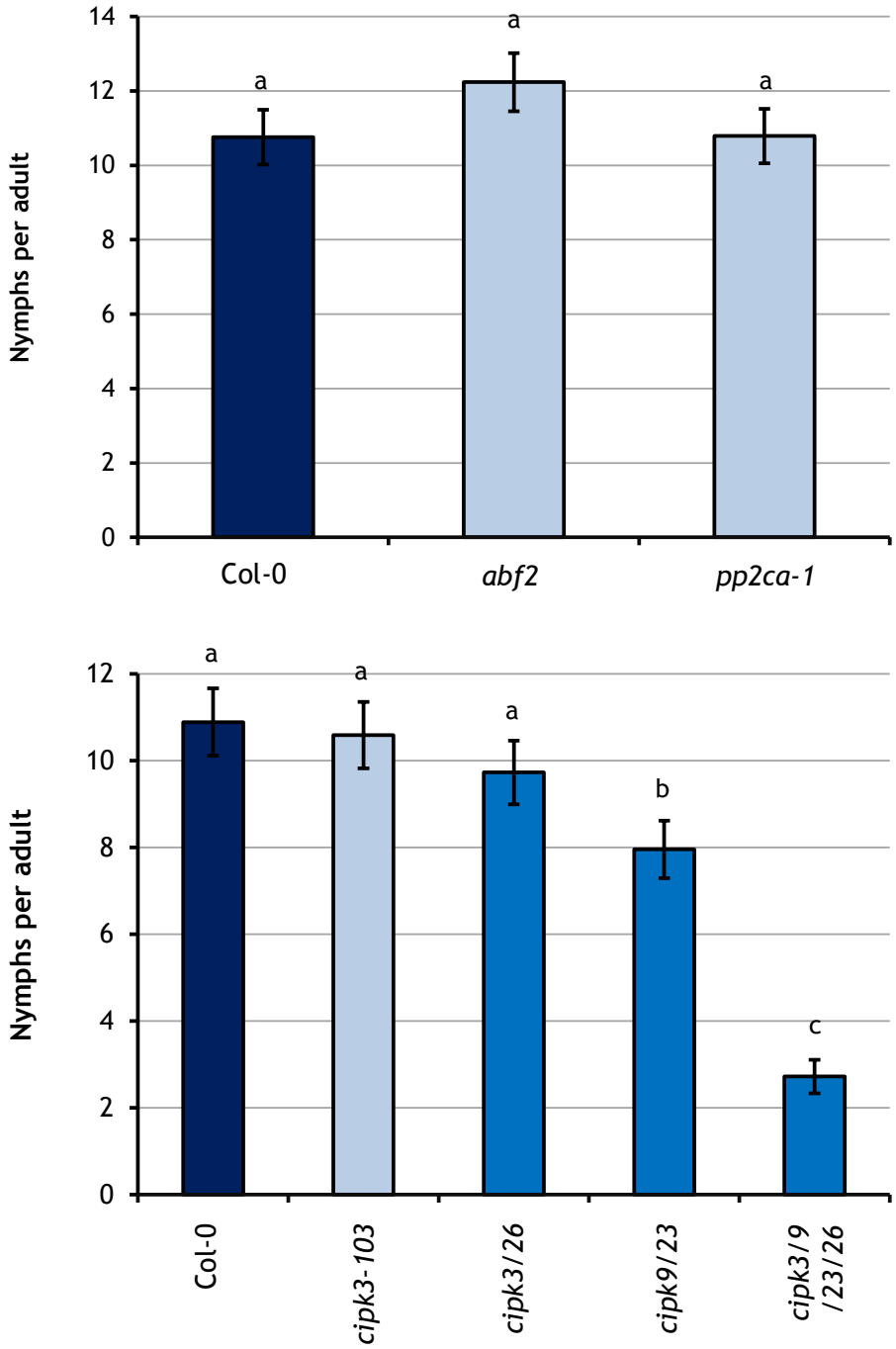

Figure 5.13: ***M. persicae*** **fecundity on** ***CIPK3*****-related mutants.**

Fecundity assessed after a 14-day period**. A)** Putative genes downstream of CIPK3. Error bars show SEM of 24 biological replicates from 4 independent experiments. Experiment conceived and designed by T.V conducted by T.V. and M.S. **B)** Other Clade I CIPKs. Letters indicate a significant difference between genotypes (Student's t-test within GLM at $p<0.05$). Error bars show SEM of 19 biological replicates from 3 independent experiments.

5.2.6 Abolishing transcription of all four clade I CIPKs significantly increases ROS production in response to *M. persicae*

As a result of the altered aphid fecundity on the clade I CIPK mutants, the plant defence response to aphids was investigated. *M. persicae* extract-elicited ROS was significantly reduced on *bak1-5*, as previously demonstrated (Chapter 3, Figure C16b). However, it was not altered on *cipk3-103* (Figure 5.14c), agreeing with the results obtained with *cipk3-1* (Section 5.2.2). ROS was also unaltered on the *cipk3/26* (Figure 5.14d) or *cipk9/23* (Figure 5.14e) mutants. However, on the *cipk3/9/23/26* quadruple mutant, aphid extract elicited a significantly larger ROS burst relative to wildtype (Figure 5.14f).

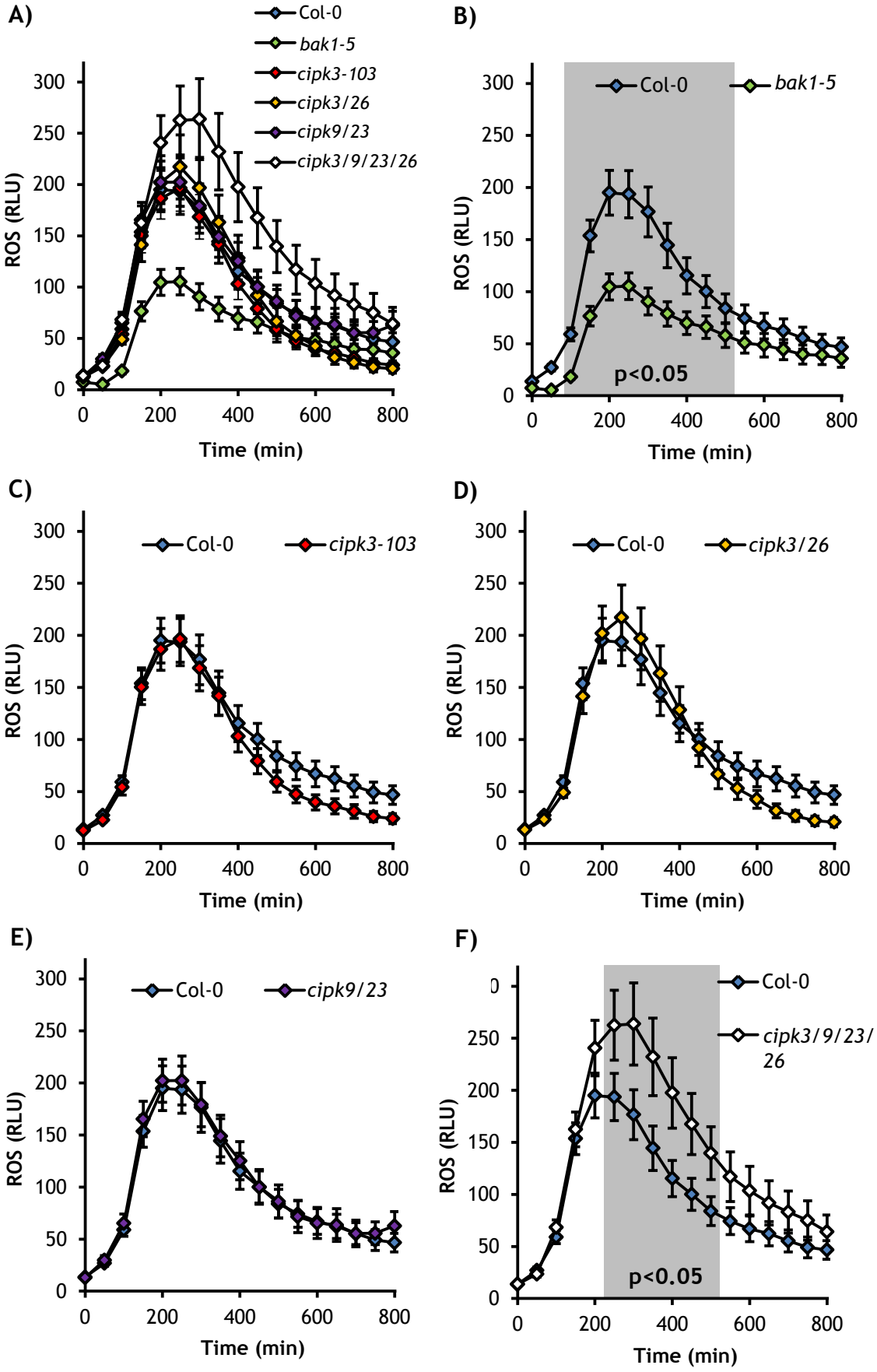
A)
Col-0
bak1-5
cipk3-103
cipk3/26
cipk9/23
cipk3/9/23/26
ROS (RLU)
Time (min)
B)
Col-0
bak1-5
p<0.05
ROS (RLU)
Time (min)
C)
Col-0
cipk3-103
ROS (RLU)
Time (min)
D)
Col-0
cipk3/26
ROS (RLU)
Time (min)
E)
Col-0
cipk9/23
ROS (RLU)
Time (min)
F)
Col-0
cipk3/9/23/26
p<0.05
ROS (RLU)
Time (min)

Figure 5.14: ROS production in response to *M. persicae* extract in clade I *CIPK3* mutants. **A)** ROS production measured as relative light units (RLU) over time in all treatments. **B)** ROS production in *cipk3-103* compared to Col-0. **C)** ROS production in *cipk3/26* compared to Col-0. **D)** ROS production in *cipk9/23* compared to Col-0. **E)** ROS production in *cipk3/9/23/26* compared to Col-0. Bars represent SEM of 24 biological replicates from 3 independent experiments. Shading represents a significant difference between genotypes (Student's t-test within GLM at $p<0.05$). Experiment conceived and designed by T.V and conducted by M.A. under supervision of T.V.

5.3 Discussion

5.3.1 *A. pisum* infestation alters the expression of several Ca^{2+}-related genes in Arabidopsis

Aphid feeding alters the expression of a variety of plant genes, including several related to Ca^{2+} signalling (Table 5.1). Feeding by *A. pisum,* a legume specialist incompatible with Arabidopsis [221], resulted in an expression change for several Ca^{2+}-related genes. This included *CNGC2*, a cAMP-activated channel [757] capable of conducting various ions including Ca^{2+} [65, 67]. The *CNGC2* mutant *dnd1* exhibits constitutive defence activation, including constitutively high SA production and expression of pathogenesis-related genes [377]. Hence, *CNGC2* may act as negative regulator of defence, with the downregulation in response to *A. pisum* suggesting it may also act in defence against aphids. Conversely, *CNGC3* and *CNGC12* were upregulated by *A. pisum* infestation. A specific role for *CNGC3* in defence has not been established [59], however *CNGC12* acts as a positive regulator of defence against the mould *Hyaloperonospora parasitica* [374]. Three GLRs were also upregulated by *A. pisum*, including *GLR3.5,* a gene recently linked to systemic wound signalling [104].

The expression of various downstream Ca^{2+} sensors was also altered upon *A. pisum* infestation. This included downregulation of *CDPK1*, a positive regulator of SA [404] and *CDPK6*, which has been linked to defence through its modulation of ABA (Figure 5.2) [758], MeJA [684] and ET [444]. In addition, *A. pisum* feeding resulted in downregulation of *CALMODULIN-BINDING TRANSCRIPTION ACTIVATOR 3* (*CAMTA3*) which mediates the plant general stress response through modulation of SA/JA crosstalk [381, 759, 760], including during insect attack [382]. Together, these results highlight various links between Ca^{2+} signalling and the plant response to infestation with *A. pisum*.

5.3.2 *CIPK3* is one of the few Arabidopsis Ca^{2+} signalling genes responsive to *M. persicae*

In response to *M. persicae*, far fewer genes were differentially regulated compared to *A. pisum* (Figure 5.4). This agrees with previous work showing that *M. persicae* effects a very small number of Arabidopsis transcripts [464, 761], and suggests that during this interaction *M. persicae* avoids or actively suppresses detection. Despite this, Ca^{2+} signalling-related genes are often over-represented in response to phloem-feeding insects, however most of these studies investigated significantly longer periods of infestation than the 48 h used in the present study [583].

Differentially-regulated transcripts after 48 h of *M. persicae* infestation included *CNGC12* and *CIPK3*, which both responded in an opposite direction to when plants were infested with *A. pisum* (Table 5.1). This was especially interesting given the opposing compatibilities of these species on Arabidopsis. Consequently, it may be that these genes are related to the response of a plant to hosts vs non-hosts. Since this chapter is focused on investigating the downstream components of the Ca^{2+} burst characterised in Chapters 3 and 4, *CIPK3* was explored further. In addition, other groups have also observed that feeding by *M. persicae* results in an upregulation of *CIPK3* [308], as does infiltration with *M. persicae* saliva [464]. Moreover, the specialist *B. brassicae* also induces an upregulation of the *CIPK3* transcript [304].

5.3.3 *CIPK3* expression alone is not sufficient to alter the plant defence response to aphids

Aphids, including both *M. persicae* and *A. pisum*, will probe non-host plants before determining compatibility [762-764]. Therefore, the plant responses that mediate this compatibility are most likely responsive to aphid probing and occur during or after the Ca^{2+} burst characterised in Chapters 3 and 4. As probing by the incompatible species *A. pisum* resulted in downregulation of *CIPK3.2* and *CIPK3.3* (Figure 5.5), this might represent part of the basal plant defence response. Conversely, the upregulation of *CIPK3.2* during *M. persicae* feeding might represent a direct manipulation of the plant by the aphid to allow sucessful colonisation. CIPK3 appears to be negative regulator of ABA [175] (Figure 5.2) and although evidence for ABA's role in aphid defence is contradictory, it clearly plays a role in these

interactions [442, 748]. Consequently, differential regulation of *CIPK3.2* and *CIPK3.3* might be a result of the modulation of ABA signalling during aphid feeding.

The fitness of *M. persicae* on *cipk3-1* was assessed in a fecundity assay, with no effect on knocking out *CIPK3* observed (Figure 5.6). However, as a successful generalist adapted to Arabidopsis, the effect of abolishing expression of a single gene on *M. persicae* fecundity might be relatively subtle. Indeed, rearing *M. persicae* on mutant lines over multiple generations can produce fecundity phenotypes not seen with single generations, for example whilst aphid fecundity was not altered over a 2-week period on the *cyp81f2* mutant [306], it was significantly reduced on *cyp81f2* mutants after 6.5 weeks [305]. However, the trans-generational fecundity of *M. persicae* was not altered on the *cipk3-1* mutant (Figure 5.8a), although this assay was only carried out over 4 weeks. Furthermore, plant defence status can also modulate host choice [259], but *CIPK3* had no effect on this behaviour (Figure 5.8b).

The production of ROS is a key part of the plant defence response to *M. persicae* [349, 413] and this production is closely linked to Ca^{2+} signals [121, 414, 415]. Based on this evidence, ROS production in the *cipk3-1* mutant in response to aphids was assessed. Application of aphid extract to Arabidopsis leaf disks results in the gradual production of ROS over a period of hours, peaking around 150-250 minutes post-application [349], and this finding was repeated in the present work (Figure 5.8c). However, ROS production in response to aphid extract was not altered in the *cipk3-1* mutant (Figure 5.8c), in accord with the unaltered aphid performance on this mutant.

As a compatible host of *M. persicae*, scope for further reductions in plant defence may be restricted, given that host defences are likely to already be suppressed. Indeed, this was implied by the small number of genes differentially regulated by *M. persicae* (Figure 5.4). As such, non-host resistance was assessed using *A. pisum* survival [555]. However, the *cipk3-1* mutant had no effect on this species either (Figure 5.8d).

For completeness, an additional *CIPK3* mutant was identified, *cipk3-103,* in the Col-0 background as was used for the RNA-seq experiment. The *cipk3-103* mutant lacked wildtype transcription of *CIPK3* (Figure 5.10), but again this had no effect on *M. persicae* or *A. pisum* performance (Figure 5.12), or the plant ROS response to aphid extract (Figure 5.14c). Interestingly, this mutant did not show the established osmotic stress hypersensitivity found with *cipk3-1* (Figure 5.11) [175]. The *cipk3-103* insertion is at the C-terminal end of the protein (Figure 5.10a), after the NAF and PPI

domains (Figure 5.1). In addition, upstream transcription of *CIPK3* still occurred in the *cipk3-103* mutant (Figure 5.10b) and therefore in the remote possibility that a functional protein was produced [765], it would hypothetically contain all the key CIPK functional domains. Alternatively, it may be that a wildtype CIPK3 protein was still produced in *cipk3-103*, or that salt tolerance mediated by CIPK3 is ecotype-dependent.

Unexpectedly, *cipk3-104* showed increased tolerance to salt (Figure 5.11). The *cipk3-104* t-DNA insertion is within the PPI domain, and thus if a functional protein was produced it may be disrupted specifically in its interactions with protein phosphatases [161, 739] which may affect the plants response to abiotic stress [740-742]. However, as with the *cipk3-103* the more likely situation is that there is an ecotype-specific effect occurring, or a background mutation present in the *cipk3-104* line.

5.3.4 A truncated version of *CIPK3*, *CIPK3.2*, had no effect on aphid performance

It was hypothesised that there may be functional relevance relating to the C-terminal truncated product produced by *CIPK3.2* (Figure 5.1). Although this truncation does not affect the PPI domain [739], alterations in the C-terminal end of CIPK6 result in altered interactions with PP2CA [161]. Thus, *CIPK3.2* may encode a functionally distinct product compared to the full-length gene. In order to test if *CIPK3.2* alone played a role in plant-aphid interactions, this *CIPK3* variant was expressed in the absence of the other four (Figure 5.7a). However, this had no effect on *M. persicae* fecundity (Figure 5.7b).

5.3.5 Constitutive activation of CIPK3 had no effect on aphid performance

The possibility that the kinase activity of CIPK3 had an effect on plant-aphid interactions was also tested. Constitutive activation of protein kinases can be achieved by mutating conserved residues in the activation domain, as has been exploited previously with SOS2/CIPK24 [766-768] and CIPK3 [176, 756]. Constitutive activation of CIPK3 has been shown to rescue the ABA and osmotic hypersensitivity of *cbl9* plants [176]. However, the ability of *CIPK3T183D* to alter or rescue the *cipk3-1*

phenotype was not tested. The constitutively-active version (*CIPK3T183D*) was transformed into the *cipk3-1* mutant (Figure 5.9a), however *CIPK3T183D* had no consistent effect on *M. persicae* fecundity (Figure 5.9b). One line, *cipk3-1/CIPK3T183D* line 3 did show reduced fecundity (Figure 5.9b), however this line also exhibited a severe growth impairment phenotype (Figure 5.9c). Interestingly, this type of phenotype is often a feature of constitutive defence activation as a result of trade-off between the growth and defence [769-771]. However, since this phenotype was only observed in one of the three lines, was concluded that it is CIPK3-independent, most probably the result of a pleotropic effect(s) generated by the transgenic insertion.

5.3.6 Altered *CIPK3* expression might be irrelevant to plant-aphid interactions

Taken together, the results gathered in this chapter appear to rule out a singular role for CIPK3 in plant-aphid interactions. The differential *CIPK3* transcriptional responses to the two aphid species relative to the empty clip cage control (Figure 5.5) suggests that this change in expression is being mediated specifically by aphid feeding, rather than as an artefact of the experimental design. This response might be a non-specific effect, not relevant to plant defence, generated by other changes in the plant upon aphid treatment. Alternatively, it might be that although CIPK3 has no direct effect on aphids, changes in *CIPK3* expression are the result of upstream events in the defence response against these insects. *CIPK3* is wound-responsive [175] and thus might be induced by the damage caused by stylet penetration, especially if this damage produces a rise in $[Ca^{2+}]_{cyt}$ [123]. Indeed, ABA is implicated in plant-aphid interactions [437, 442], and application of 100 μM ABA can induce *CIPK3* expression [175]. However, based on the present work showing *CIPK3* expression and activity have no effect on aphid performance or plant ROS production, it is not possible to differentiate between these hypotheses.

Indeed, despite induction of *CIPK3* during drought, no physiological effect of this stress can be seen adult *cipk3-1* mutant plants [175]. It is also worthy of note that the established *cipk3-1* seedling phenotype in the presence of ABA or salt was not observed in adult plants [176]. As a result, the role of CIPK3 in stress responses might be primarily during early development.

5.3.7 *CIPK9* and *CIPK23* have a significant effect on aphid performance that might be mediated by plant nutrient homeostasis

CIPK3 might act redundantly in plant-aphid interactions, as occurs with Mg^{2+} stress [165, 166]. In order to assess this hypothesis, aphid performance on Arabidopsis mutants of additional genes related to the CIPK3 pathway was assessed. Neither *ABF2* nor *PP2CA* expression appeared to have an effect on *M. persicae* performance (Figure 5.13a), ruling out a role for these ABA-signalling genes in successful defence against *M. persicae*. Loss of *CIPK26* transcription had no effect on *M. persicae* fecundity (Figure 5.13b) or on aphid-induced ROS production (Figure 5.14d), despite its role in the regulation of RBOHF [692]. However, a significant effect on *M. persicae* fecundity was observed on *cipk9/23* and *cipk3/9/23/26* plants (Figure 5.13b). This implies that CIPK9 and/or CIPK23 might play a direct role in plant defence against aphids, and that all four CIPKs might be acting with some redundancy in this response. Moreover, this is the first demonstration to the author's knowledge of a role for Arabidopsis CIPKs in biotic stress, although CIPKs in other species have been linked to PTI against fungi [385] and ETI against *P. syringae* [772].

CIPK23 acts in nitrogen homeostasis in Arabidopsis, phosphorylating NITROGEN TRANSPORTER 1.1 (NRT1.1) during low nitrogen conditions to modulate nitrogen sensing and uptake [189]. Plant nitrogen is key to the nutritional content of the plant, and although few studies have explicitly investigated the role of nitrogen in plant-aphid interactions, it is clear that the nutritional quality of the host has an effect on insect performance [773-776] and more widely on plant defence [777]. Increased amounts of essential amino acids in the phloem results in a higher assimilation of such amino acids by *M. persicae* [778], and *R. padi* reproduction is decreased on *H. vulgare* grown in nitrogen-deficient soil [779]. It has therefore been speculated that plant nitrogen status is a contributing factor to aphid performance [780] In addition, CIPK23 has a role in K^+ uptake in roots, and loss of this protein leads to ABA hypersensitivity and drought tolerant plants as a result of reduced transpiration [183]. Moreover, CBL1 and CBL9 are required for CIPK23 action, presumably by localising the protein to the PM [183], where it activates K+ TRANSPORTER 1 (AKT1) to enhance K^+ uptake into the cell [163, 186].

The only reported singular role for CIPK9 so far is also in K^+ homeostasis. However, there is conflicting evidence regarding this role, with the same *cipk9*

mutant showing both increased tolerance to low K^+, as well as hypersensitivity to K^+ [182, 754]. CIPK9 is recruited to the tonoplast by CBL3 [165], and cannot interact with AKT1 [754], implying it might act in a separate pathway. It might be that CIPK9 is involved in vacuolar K^+ sequestration, as it for Mg^{2+} [165, 166].

Furthermore, ROS production in response to aphid extract was not altered on the *cipk9/23* double mutant (Figure 5.14e). Taken together, these results suggest there might be a link between the potassium status of the plant and aphid performance, and that this may be independent of PTI. Most evidence so far points to potassium deficiency as being beneficial to aphids [781-784], potentially by increasing the plant nitrogen availability in the shoots [784, 785]. Although this hypothesis agrees with the reduced aphid fecundity on *cipk9/23* (Figure 5.13b), without dissection of the individual roles played by CIPK9 and CIPK23 in plant resistance to aphids, it is impossible to attribute their individual roles in nitrogen or potassium homeostasis to this reduced fecundity.

5.3.8 The clade I CIPKs act as a hub to negatively regulate plant defence

M. persicae fecundity was reduced beyond that observed on *cipk9/23* when feeding on the *cipk3/9/23/26* mutant, implying that there may be additional redundancy in this system, as seen for Mg^{2+} homeostasis [165, 166]. Furthermore, aphid extract-induced ROS production was greater in this mutant (Figure 5.14f). ROS forms a key part of PTI against pathogens and aphids [331, 349, 360, 413] and the increased ROS production in the *cipk3/9/23/26* mutant might be partially responsible for the enhanced aphid resistance of this mutant. CIPK26 has been implicated in ROS signalling through a direct interaction with RESPIRATORY BURST OXIDASE HOMOLOG F (RBOHF) [691, 692]. However, since aphid extract-induced ROS production was higher in the *cipk3/9/23/26* mutant, and not significantly altered in the *cipk3/26* mutant, positive regulation of RBOHF by CIPK26 does not appear to be occurring in this context. The role of CIPKs in biotic stress are unexplored in Arabidopsis. However, there is a precedent for negative regulation of ROS by CIPKs in wheat, where overexpression of *CIPK29* reduces accumulation of H_2O_2 [786]. Conversely, heterologous expression of *S. lycopersicum CIPK6* in *N. benthamiana* leaves results in the accumulation of ROS [772].

Since the enhanced aphid resistance and increased ROS production is the result of abolishing all four CIPKs, it appears that these proteins act as a hub to negatively regulate defence. This agrees with observations of these CIPKs acting as a hub to regulate Mg^{2+} sequestration [165, 166] and that Ca^{2+} signalling can suppress defence as well as activate it [375]. However, necrotic lesions, reminiscent of HR, can be observed on *cipk3/9/23/26* leaves [165, 166], suggesting a possible role for these CIPKs in ETI, as seen for *CIPK6* in *S. lycopersicum* [772]. Loss of Ca^{2+}-ATPases can result in similar HR lesions in Arabidopsis [787], implicating disrupted ion homeostasis in this phenotype.

However, the author cannot exclude pleiotropic effects in the *cipk3/9/23/26* mutant from affecting aphid performance. The growth phenotype of this mutant [165, 166] may be a result of such effects, or due to enhanced defence activation [769-771]. Reduced early growth can impact aphid populations [236], however a dwarfing phenotype *per se* does not affect *M. persicae* fecundity [306]. The ABA sensitivity of this mutant is similar to that of the wild type [166], implying that altered ABA signalling is probably not the cause of the *cipk9/23* and *cipk3/9/23/26* phenotypes.

Nevertheless, it is clear that the clade I CIPKs modulate a range of plant responses. It is impossible to dissect their exact role in plant-aphid interactions without first identifying the individual role of each of these genes and how they may combine to effect aphid performance. To that end, the suite of double and triple mutants presented by Mogami et al. [166] represent a highly useful tool for further investigations. In this chapter evidence has been presented that rules out a unilateral role for CIPK3 in plant-aphid interactions. However, it has also been demonstrated that CIPK3, in combination with its close homologues CIPK9, CIPK23 and CIPK26, may play a role in mediating aphid success on plants. Consequently, these CIPKs might act as vital components, downstream of the Ca^{2+} signal, in the plant response to *M. persicae*.

This page is intentionally left blank

Chapter 6: General Discussion

6.1 Summary of research findings

The proposed role of Ca^{2+} signalling in plant-aphid interactions, as investigated in the current study, is outlined in Figure 6.1.

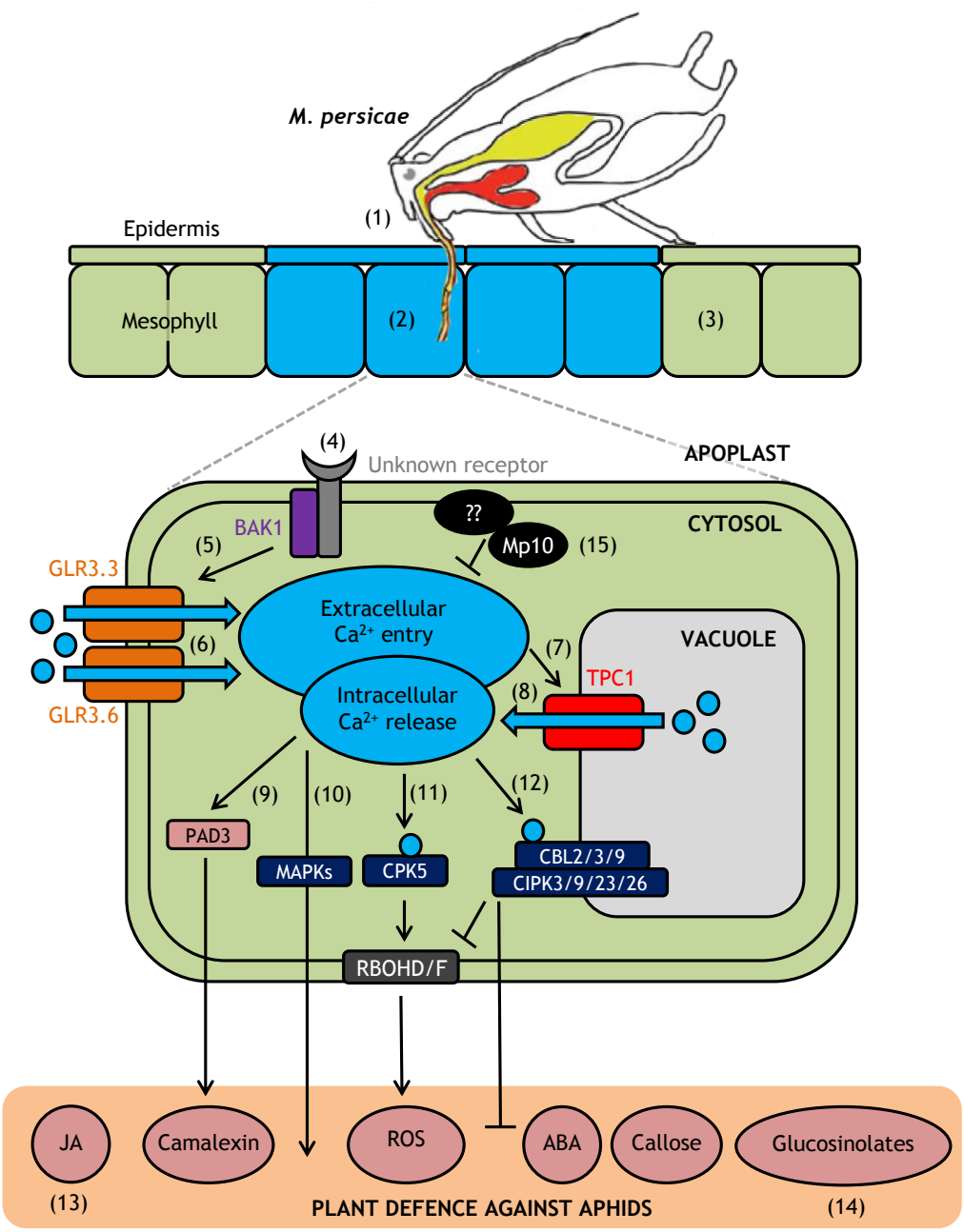

Figure 6.1: Proposed role of Ca^{2+} signalling during the *M. persicae*-Arabidopsis interaction
(1) Aphids probe epidermal and mesophyll cell layers within a minute of feeding (Chapter 3). **(2)** An aphid-induced Ca^{2+} burst can be detected around the feeding site within a few minutes of settling (Chapter 3). **(3)** This Ca^{2+} burst is restricted to the feeding site and cannot be detected systemically (Chapter 3). **(4)** BAK1 and an unknown PRR perceive aphid HAMPs, resulting in aphid-induced Ca^{2+} bursts (Chapter 3). **(5)** Perception of aphid HAMPs by BAK1 leads to activation of GLR3.3/GLR3.6, potentially through the intracellular release of glutamate [726]. **(6)** GLR3.3/GLR3.6 mediate extracellular Ca^{2+} influx into the cell within minutes of the aphid settling (Chapters 4). **(7)** The increase in $[Ca^{2+}]_{cyt}$ results in activation of TPC1 [112, 114, 115]. **(8)** TPC1 mediates release of intracellular Ca^{2+} from the vacuole into the cytosol in response to *M. persicae* (Chapter 4). **(9)** The rise in $[Ca^{2+}]_{cyt}$ mediated by TPC1 contributes to camalexin production via PAD3 (Chapter 4). **(10)** The rise in $[Ca^{2+}]_{cyt}$ mediated by TPC1 contributes to MAPK activation (Chapter 4). **(11)** The rise in $[Ca^{2+}]_{cyt}$ mediated by GLR3.3, GLR3.6 and TPC1 results extracellular ROS production most likely through activation of RBOHD and RBOHF [283,349] (Chapter 4). **(12)** Ca^{2+} binds CBL2, 3 and 9, leading to activation of CIPK3, 9, 23 and 26 which negatively regulate defence, partially through suppression of ROS (Chapter 5). **(13)** Accumulation of JA is detrimental to aphids, but is not required for effective defence against *M. persicae* or *A. pisum* (Chapter 4). **(14)** Glucosinolate production is mediated through a TPC1/GLR-independent pathway that involves a contribution from BAK1 (Chapter 4). **(15)** *M. persicae* suppresses Arabidopsis defence responses using effectors, including Mp10 that partially suppresses the Ca^{2+} burst (Chapter 3). Ca^{2+} represented by blue circles. Aphid image taken from Hogenhout and Bos [275].

6.1.1 *M. persicae* elicits a rapid, localised Ca^{2+} burst in the upper cell layers of Arabidopsis

This study identified a rapid Ca^{2+} burst in Arabidopsis around the feeding site of *M. persicae*. Recordings from the EPG show that penetration of the epidermal and mesophyll cells layers occurred within a minute of feeding, whilst the microscopy assay demonstrated that a $[Ca^{2+}]_{cyt}$ elevation, distinguishable at the tissue level, occurred within 2 min of settling (Chapter 3). This burst occurred as single transient release of Ca^{2+}, unlike the sustained biphasic or oscillatory signatures produced by other stresses such as cold shock [50, 626, 652] DAMPs [371] or PAMPs [17, 219]. The rise in $[Ca^{2+}]_{cyt}$ also appeared to be restricted to the region of the feeding site (Figure 6.1) (Chapters 3 & 4), with small signals bring detected systemically on occasion but not reliably (Appendices C & D).

The variability in systemic signalling in response to *M. persicae* might be a result of the variability in the number of neighbouring cells the aphid stylets penetrate on their way to the phloem. In addition, the systemic ROIs were defined relative to the aphid and therefore represented a different location on the leaf for each sample (Chapter 2). As such, optimisation of the Ca^{2+} analysis is required to investigate systemic signalling further. The absence of reliable systemic signals puts the aphid-induced Ca^{2+} burst in sharp contrast to other abiotic [7, 538] and biotic [103, 123] stresses. For systemic Ca^{2+} signals to occur it is assumed that $[Ca^{2+}]_{cyt}$ or ROS concentration in the apoplast must reach a threshold value in order to successfully activate subsequent components in the chain [121] and cellular penetrations by the *M. persicae* stylets might not cause enough damage [296] to reach this threshold. Alternatively, the insect may be actively suppressing systemic Ca^{2+} signals [123, 502]. The use of isolated leaves for the assay might also have had an effect on systemic signalling, although systemic Ca^{2+} signals [538] and defence activation against aphids [469] have been observed previously in isolated leaves. The absence of a consistent systemic signal agrees with the lack of SAR observed in response to *M. persicae* (Chapter 3, [308, 464]). Systemic signals could be re-constituted by over-activation of TPC1 (Chapter 4), a channel already implicated in systemic signalling during salt stress and wounding [7, 123].

The timing and area of the burst indicated that the Ca^{2+} release measured in 35S::GCAMP3 occurred primarily in the epidermal and mesophyll cell layers. Indeed, aphid feeding from the phloem does not usually occur within the same time-frame,

and whilst localisation of GCAMP3 to phloem could detect signals in response to wounding, aphid-induced signals could not be detected in this tissue (Chapter 3). The aphid-induced Ca^{2+} signals propagate relatively slowly, around 100-fold slower compared to other stresses [7, 536, 538], which is likely to be related to the lack of phloem and systemic components involved in the signal [103, 123, 538]. However, the speed of the aphid-induced burst is comparable to rates of Ca^{2+} wave propagation in cultured animal cells and tissues [788]. Furthermore, the partial requirement for vacuolar Ca^{2+} release for this burst (Chapter 4) makes a SE-elicited signal less likely given the lack of vacuoles in these cells [701]. This separates the characterised Ca^{2+} burst from phloem-based resistance mechanisms such as occlusion, and agrees with work showing that resistance to phloem feeders is also mediated by factors in the mesophyll [637, 789].

6.1.2 BAK1, GLR3.3, GLR3.6 and TPC1 mediate Ca^{2+} release in response to *M. persicae*

The feeding site burst is dependent on BAK1, with complete abolition of the signal in the *bak1-5* mutant (Chapter 3). BAK1's role early in PTI against aphids [349, 350] suggests this co-receptor is one of the first molecular components involved in the generation of the Ca^{2+} burst, along with an as-yet uncharacterised HAMP receptor [277]. The involvement of PTI in this response suggests this is not a damage-meditated response as seen with chewing insects such as Lepidoptera [123]. This is not surprising given the effort aphids invest in minimising wounding, for example through the use of gelling saliva to plug damage sites [270, 271, 789]. It would be interesting to analyse Ca^{2+} dynamics response to wounding by a stylet-mimic, such as a thin glass capillary [287], in order to dissect the potential role of wounding in this response.

The perception of the aphid via BAK1 leads to an influx of Ca^{2+} from the apoplast and from intracellular stores. The extracellular component is mediated by GLR3.3 and GLR3.6, with a vacuole-derived contribution from TPC1 (Chapter 4). The complete abolition of the signal in the *glr3.3/3.6* mutant and a small but reduced signal in the *tpc1-2* mutant implies that extracellular Ca^{2+} release lies upstream of intracellular release.

The abolition of Ca^{2+} burst in *bak1-5* and *glr3.3/glr3.6* mutants implies GLR3.3/3.6 and BAK1 lie in the same pathway (Chapters 3 & 4). The link between

BAK1 perception and GLR opening is unclear. Glutamate is proposed to be a ligand of the GLRs [76, 92, 356], and can function as a physiological signal in plants that generates a GLR-mediated Ca^{2+} burst [97, 99, 100, 687]. Furthermore, release of glutamate into the extracellular space is facilitated by exocytosis downstream of cryptogein perception, implying this amino acid may function in PTI [726]. It is therefore possible that PTI-triggered release of glutamate into the apoplast binds the extracellular ligand-binding domain of GLR3.3/GLR3.6 and elicits a Ca^{2+} burst. Alternatively, activation of the GLRs may occur independently of glutamate, and involves one of the other BAK1-regulated signalling pathways. Given the promiscuity of BAK1 during plant defence [360, 361], and the wide range of potential GLR agonists and antagonists [92], it is difficult to select a specific signalling pathway for investigation. However, a good place to start would be to check if glutamate-elicited Ca^{2+} signals still occur in the *bak1-5* mutant.

TPC1 also mediates Ca^{2+} release in response to *M. persicae* (Chapter 4) and these results add to the growing amount of literature implicating this channel and vacuolar Ca^{2+} as components involved in the plant response to stress [7, 121, 123]. A small $[Ca^{2+}]_{cyt}$ elevation can be seen in the *tpc1-2* mutant, suggesting that GLR-facilitated Ca^{2+} entry is still occurring, and that TPC1 is required to amplify this signal. Indeed, TPC1 is Ca^{2+}-activated [112, 114, 115], can be regulated by CaMs [790-792] and has a hypothesised role in CICR [7, 121, 537, 539], allowing for a model whereby GLR-mediated Ca^{2+} influx leads to TPC1 channel opening and a second release of Ca^{2+} (Figure 6.1). It is also possible that GLR or BAK1-mediated signalling activates TPC1 independently of Ca^{2+}. TPC1 activity can also be modulated by phosphorylation status [109, 114, 115, 793] and owing to the considerable role of protein kinases and phosphatases in PTI, it is possible that TPC1 opening is mediated by these pathways. Furthermore, CIPKs are known to regulate ion channels [161, 163, 167, 186, 794], and the tonoplast-localisation of CIPKs 3, 9, 23 and 26 by CBL2 and CBL3 [165] do not exclude CIPK-based regulation of TPC1 as a possibility.

6.1.3 Activation of plant defence is modulated by BAK1 and Ca^{2+} signalling

To prove that Ca^{2+} is a physiologically relevant signal in plant-aphid interactions, at least two lines of evidence need to be demonstrated. Firstly, loss of the signal should result in an alteration of the downstream response, and secondly

Ca^{2+}-sensitive elements should be present in the system [795]. Loss of *BAK1* is already established to be beneficial to aphids [349], and in this study it was linked to having a role in camalexin and glucosinolate production during plant-aphid interactions (Chapter 4). However, this is not direct evidence of a role for Ca^{2+} in this system.

Abolition of *TPC1* expression attenuated the expression of marker genes implicated in MAPK activation (*FRK1*) and camalexin biosynthesis (*PAD3*) in response to aphid extract, suggesting a role for Ca^{2+} signalling in these processes (Chapter 4) (Figure 6.1). This defence gene induction was GLR-independent, whilst loss of *TPC1* or *GLR3.3/3.6* did not result in a significant effect on aphid-induced ROS production (Chapter 4). This suggests that the activation of these pathways is distinct from the Ca^{2+} burst measured with GCAMP3. This might be a result of using aphid extract for these assays as opposed to live insects. As a result, it will be interesting to measure marker gene expression and ROS production in mutant leaves infested with live aphids. Nevertheless, overexpression of *TPC1* and loss of *CIPK3/9/23/26* resulted in significant effects on aphid-elicited ROS production and aphid performance (Chapters 4 & 5), implicating Ca^{2+} in aphid-elicited ROS production and fitting with observations of substantial interplay between Ca^{2+}, TPC1 and ROS [119, 121, 691, 692]. Furthermore, the timing of defence marker induction in the mutants was not explored and might be affected by Ca^{2+} signalling.

Several Ca^{2+}-sensitive elements are present in Arabidopsis during aphid attack. Of the genes that directly bind or allow transport of Ca^{2+}, only *CNGC12* and *CIPK3* were differentially regulated after 48 h of *M. persicae* infestation (Chapter 5). However, several genes with an established role in plant-aphid interactions have connections to Ca^{2+} signalling, including the MAPKs [152, 372, 386, 693-695] and those involved in ROS production (e.g. *RBOHD* [119, 349, 350]). Furthermore, loss of the Ca^{2+} decoders *CIPK9* and *CIPK23* significantly reduced *M. persicae* fecundity, and fecundity was even further reduced on the *cipk3/9/23/26* quadruple mutant (Chapter 5). The CIPKs have been linked to regulation of PTI responses in *O. sativa* [385] wheat [786], and tomato [772], but this is the first reported role for Arabidopsis CIPKs in biotic interactions to the author's knowledge. The alterations in plant and aphid responses upon loss of the aphid-induced Ca^{2+} burst, in combination with the modulation of several Ca^{2+}-sensitive elements during this interaction, provides supports the hypothesis that the Ca^{2+} burst is acting as a physiologically relevant signal in plant-aphid interactions.

6.1.4 *M. persicae* suppresses BAK1-mediated PTI and Ca^{2+} signalling

Despite the role of GLR3.3/GLR3.6 and TPC1 in the aphid-induced Ca^{2+} burst, *M. persicae* fecundity on *tpc1-2* or *glr3.3/3.6* mutants was unaffected (Chapter 4). The same is seen with the *bak1-5* mutant [349], suggesting that PTI elicited by *M. persicae* has a limited effect on the aphid. This is not surprising given compatibility of *M. persicae* with Arabidopsis, which implies that basal immunity in this plant species is not sufficient to affect aphid performance. As a result, further reductions in this defence by attenuation of the Ca^{2+} signal might have a limited effect. However, this assumes that Ca^{2+} signalling is a positive regulator of defence against aphids, and the increased aphid resistance observed in the *cipk3/9/23/26* mutant (Chapter 5) suggests that this is not necessarily the case.

Small effects on aphid feeding behaviour were observed in the *BAK1* and *TPC1* mutants (Chapters 3 & 4). In both cases pathway behaviour was unaffected, demonstrating that there is latency between BAK1-mediated Ca^{2+} signalling, defence activation and an effect on aphid feeding. Indeed, secondary metabolite production is not induced for several hours or even days post-feeding [78, 159]. Surprisingly, loss of *BAK1* or *TPC1* expression disturbed phloem feeding, whilst *TPC1* overexpression enhanced it. Whilst this fits with established literature showing that the main effects of plant defence are experienced by aphids when they are feeding from the phloem [301, 796, 797], it appears to contradict the hypothesis that BAK1-mediated Ca^{2+} signalling forms a part of PTI. However, the feeding phenotypes are relatively subtle, only occurring as differences in single behaviours that are not consistent between EPG experiments. Consequently, it is hypothesised that *M. persicae* targets BAK1-mediated Ca^{2+} signalling during its successful colonisation of the plant and loss of this pathway disturbs the aphid manipulation of its host, resulting in feeding disruption.

M. persicae uses a suite of effectors to suppress plant defence [275, 501], and this might explain the relatively small number of Arabidopsis genes differentially regulated by *M. persicae* attack (Chapter 5). These effectors include Mp10 that acts in the BAK1 pathway [277, 502]. Mp10 is capable of partially suppressing the feeding site Ca^{2+} burst (Chapter 3), as well as flg22-elicited Ca^{2+} bursts [502]. Thus, Mp10 has a role in the BAK1 Ca^{2+} signalling pathway. Indeed, Mp10 is delivered preferentially into the mesophyll tissue [279], the very location of the feeding site Ca^{2+} burst. Therefore, it is possible that BAK1/GLR/TPC1 pathway is one that *M. persicae*

monitors and manipulates in order to modulate the plant defence network (Figure 6.1). In order to test this hypothesis, analysis of the feeding behaviour of dsMp10 aphids on the *bak1-5* mutant should be conducted. Reducing expression of *C002* in *A. pisum* results in a considerable increase in pathway phase probing and almost complete loss of phloem feeding [276], highlighting the role of the epidermal and mesophyll cells in PTI and effector function and agreeing with the role of these processes in phloem acceptance. One might also predict the fecundity penalty suffered by dsMp10 *M. persicae* on Col-0 will be abolished on *tpc1-2* and *glr3.3/3.6* mutants, as seen on the *bak1-5* mutant [502], if Mp10 is required to manipulate this Ca^{2+} signalling pathway.

It is also important to consider that other *M. persicae* effectors might be modulating BAK1-mediated Ca^{2+} signalling. It is possible that effectors are delivered into the apoplast, along with the watery [619] or sheath [267] saliva. Recent results from the Hogenhout lab indicate that Mp1 [501] is associated with aphid salivary sheath [279] and it reasonable to suggest such apoplast effectors might target extracellular Ca^{2+} influx. The involvement of other effectors in the suppression of Ca^{2+} signalling would explain the relatively subtle effects of reducing expression of *Mp10* alone (Chapter 3), and therefore testing the role of these other effectors, or combinations of them, on the Ca^{2+} signal could potentially identify additional components involved in the suppression of defence. Furthermore, it would also be intriguing to use aphid extract from effector knock-down aphids in ROS and defence gene assays to test the role of effectors in these defence responses.

6.2 Open questions

6.2.1 The role of Ca^{2+} signalling in non-host resistance

The lack of a significant *M. persicae* fitness penalty on the mutants investigated in this study is suggested to be the result of using an aphid species compatible with Arabidopsis. This implies that exploring the role of Ca^{2+} signalling in incompatible interactions, where it might play a role in non-host resistance, would be informative. Indeed, *A. pisum* has a greater survival rate on *bak1-5* mutants [349], suggesting the BAK1 pathway contributes to non-host resistance. However, the aphids still cannot complete their life cycle on this mutant, demonstrating that BAK1-independent pathways are also at play during plant defence against aphids.

One might predict that disturbance of Ca^{2+} signalling could result in enhanced susceptibility to incompatible insects. Several Arabidopsis Ca^{2+}-binding proteins and channels are differentially regulated by *A. pisum* infestation (Chapter 5), implying that such signalling may play a role in resistance to this aphid. Non-host resistance to *P. syringae* can be affected by altered plant Ca^{2+} dynamics [798] and the same may true in aphid resistance. Incompatible aphid species might also induce larger feeding site Ca^{2+} bursts, or even systemic signals and it will be revealing to analyse Ca^{2+} dynamics in response to *A. pisum* using GCAMP3. This analysis might also reveal if Arabidopsis resistance to this species is mediated by PTI or ETI, given the biphasic nature of Ca^{2+} signal one might expect during ETI [379, 509, 513].

Abolition of *TPC1* transcription alone is not sufficient to alter *A. pisum* survival on Arabidopsis (Chapter 4). However, Ca^{2+} signalling mediated by other genes, including the GLRs, is still occurring in the *tpc1-2* mutant (Chapter 4). It will therefore be informative to study the survival of *A. pisum* on the *glr3.3/3.6* mutant to fully investigate the role of the feeding site Ca^{2+} burst in non-host resistance.

In combination with this, analysis of the downstream Arabidopsis defence response will also be enlightening. Arabidopsis ROS production is greater in response to the incompatible aphid *R. padi* [283], and the same may be true for *A. pisum*. This could be analysed in the existing aphid extract-based assay (Chapters 4 & 5) or to make it more comparable to the Ca^{2+} assay, live ROS imaging could be attempted *in vivo* during aphid feeding using a fluorescent redox probe such as roGFP [799-801]. Interestingly, *FRK1*, *CYP81F2* and *PAD3* induction is comparable between *M. persicae* and *A. pisum* when aphid extract is applied to leaf disks for 1 h [349], however the same might not be true for live aphid infestation of a leaf.

6.2.2 The role of other Ca^{2+} stores and Ca^{2+}-related genes in plant-aphid interactions

The aphid-elicited $[Ca^{2+}]_{cyt}$ elevation documented in this study is an early event in the plant-aphid interaction, however *M. persicae* and other aphids can feed from a plant for hours (Chapter 3 & 4) or even days [270]. Ca^{2+} signalling may still be playing a role during this time, and this may involve additional proteins and/or pools of Ca^{2+} not investigated in this study.

Whole tissue imaging does not necessarily reflect signalling at the single cell level [802], and thus in the future confocal microscopy might help to uncover the

characteristics of the signal at the subcellular level. Direct targeting of fluorescent Ca^{2+} sensors to the vacuole has been underutilised [648], but tonoplast-localised Ca^{2+} sensors may provide finer detail on the dynamics of Ca^{2+} release from this compartment. This could be attempted with existing FRET sensors such as TP-D3cpv [803], or new ratiometric single-FP sensors such as GEM-GECO1 [213]. The same is true for other subcellular compartments, including the nucleus and the ER. Indeed, nuclear-localised CaM-binding protein IQD1 positively regulates defence against *M. persicae* [696], suggesting that Ca^{2+} in this compartment also plays a role in plant-aphid interactions. Concurrent imaging of several cellular compartments could also be achieved using the GECO suite of Single-FP sensors. Furthermore, fluorescence sensors have been incorporated within transporters to allow analysis of ion flux in yeast [804], and a similar method could be developed in plants to analyse transporter or channel activity *in vivo*.

Aphid-induced Ca^{2+} bursts are observable in some *bak1-5* and *glr3.3/3.6* samples but once the data were compiled the rarity of these Ca^{2+} bursts made it impossible to distinguish such events from the no-aphid controls (Chapter 3 & 4). These bursts might be mediated by additional Ca^{2+}-permeable channels, candidates of which include CNGC2, which already has an established defence phenotype [79, 84, 377] and CNGC17, which is co-expressed *in vivo* and interacts *in vitro* with BAK1 [805]. Furthermore, analysis of Ca^{2+} signalling in the *pepr1/2* mutant may reveal a role for DAMPs in the aphid-elicited Ca^{2+} burst [757]. Consequently, transformation of GCAMP3 into additional mutants may uncover additional regulators of the signal.

The role of Ca^{2+} export systems and decoders in this interaction should also be considered. Ca^{2+}-ATPases in have been implicated in altered Ca^{2+} signatures during cryptogein-elicited PTI in *N. tabacum* [798] and loss of *ACA4* or *ACA11* in Arabidopsis leads to HR-like symptoms [787]. Furthermore, in addition to the CIPKs (Chapter 5), CDPKs and CMLs are also differentially regulated during aphid attack [134, 402].

6.2.3 The role of other ions in plant-aphid interactions

None of the characterised Ca^{2+}-permeable channels in plants are specific for Ca^{2+}. This includes the GLRs and TPC1, which are also permeable to Na^{+} and K^{+} [88, 95, 96, 112, 113]. As a result, other ions may contribute to the observed GLR and TPC1 phenotypes. Furthermore, Ca^{2+} signalling is interlinked with electrical signals and both have been observed to follow similar patterns of spread in response to

wounding [103, 104, 123], with the wound-induced electrical signal, thought to be based on K^+ channel activity [540]. Furthermore, TPC1 is voltage activated [114, 115] and is regulated by Na^+ and Mg^{2+} concentrations inside the vacuole [658]. Conversely, Ca^{2+} can also regulate K^+ channel activity [1, 806], demonstrating the level of interplay between Ca^{2+} and electrical signalling pathways. Indeed, the changes in tonoplast voltage in the *fou2* mutant may have activated additional ion channels that might have contributed to the aberrant signalling seen in this mutant (Chapter 4).

In addition, the K^+ [182, 183, 754] and Mg^{2+} [165, 166] homeostasis genes CIPK9 and CIPK23 negatively regulate defence against *M. persicae* (Chapter 5). This provides a link between ion homeostasis and aphid performance. Moreover, *M. persicae* elicits a membrane depolarisation in infested leaves that can be detected by intracellular electrodes [365]. Taken together, these data suggest that K^+ might play an important role in plant-aphid interactions. However, it will be important to decipher the difference between altered host nutritional quality and altered plant defence.

6.2.4 The role of plant hormones in plant-aphid interactions

Loss of JA biosynthesis has no effect on *M. persicae* performance or plant defence gene induction, suggesting that this hormone is not responsible for defending Arabidopsis against *M. persicae* (Chapter 4). This agrees with a body of evidence suggesting that JA does not play a significant role in plant-aphid interactions [306, 430], in accord with the relatively low number of differentially regulated JA-related genes caused by aphid infestation [426, 427]. This result is in sharp contrast to the plant response to chewing insects such as Lepidoptera, which relies heavily on JA-mediated wound signalling [308, 332, 334, 335, 417-420], hypothetically regulated by *BAK1* [362]. It has been argued that SA-upregulation during aphid infestation [304, 308, 433] might antagonise JA production in order to increase plant susceptibility [426, 427, 434-436], whilst the increased aphid resistance seen on the *fou2* mutant (Chapter 4) clearly shows that JA is detrimental to *M. persicae*. Therefore, whilst basal levels of JA have no effect on aphids, it might be that aphids induce an increased level of JA that reduces aphid performance. This effect would be masked during compatible interactions by effectors that suppress defence but during incompatible interactions an increase in JA might represent a factor contributing to successful resistance. However, this hypothesis is not

supported by the results collected in the present study, with JA biosynthesis having no effect on *A. pisum* survival on Arabidopsis (Chapter 4).

ABA has also been implicated in plant-aphid interactions, with accumulation of this hormone occurring upon *M. persicae* feeding [437]. ABA and JA are highly interlinked, with JA-upregulation in the *fou2* mutant dependent on ABA biosynthesis [552] and both JA and ABA being regulated by the PP2Cs [740, 741, 807]. It is not clear whether ABA is beneficial or detrimental to aphids, with conflicting reports on the matter [437, 442]. However, ABA is related to Ca^{2+} signalling and forms a possible link between links TPC1 and CIPK3, with both *tpc1-2* and *cipk3-1* mutants showing ABA hypersensitivity phenotypes [15, 175]. Furthermore, BAK1 directly interacts with and modulates OST1 and ABI1 during the regulation of ABA-induced stomatal closure [808], a pathway implicated in ROS production via RBOHF [809]. As a result, it is possible that ABA may play a role in PTI against aphids.

6.3 Implications of the research findings

The work outlined in this thesis contributes significantly to our understanding of the role of Ca^{2+} signalling in plant-aphid interactions. The molecular mechanisms that underlie defence against phloem-feeding insects are less well characterised than those of plant pathogens, which is surprising given that such insects can cause large amounts of damage to crop species around the world. The traditionally ecological understanding of plant-aphid interactions is now being complemented with molecular characterisation, to which the current study offers a significant contribution.

The role of TPC1 in plants has been a controversial issue, however the present work adds to the growing body of evidence in support of TPC1's role in Ca^{2+} signalling. Moreover, the role of Ca^{2+} signalling in plant defence against pathogens is well-established but lacks mechanistic detail. Given the common mechanisms utilised by plants to protect themselves from various biotic threats, including signalling via BAK1, it is possible that the work included in this thesis can inform the wider plant defence field.

The vast host range and ecological success of aphids such as *M. persicae* make them a huge threat to world agriculture [238-240]. In order to breed crops more resistant to aphids, the plant mechanisms that limit aphid success must be elucidated. One of the largest impact aphids have on agriculture is through their transmission of plant viruses during feeding. The work in this thesis has demonstrated

that one of the first plant responses to aphid probing is Ca^{2+} signalling, and therefore further investigation of such signalling may offer opportunities to disturb aphid feeding and virus transmission.

Consequently, the findings of this work enhance our fundamental understanding of Ca^{2+} signalling in plant defence against aphids and contribute to a growing collection of literature that might one day offer practical solutions for crop protection.

Appendix A: Synthesised genetic units

pL0M-SC-gCIPK3-73016

CACTCTGTGGTCTCAAATGATGTTGATCCCCAACAAAAAATTAAGGTTCTTTTTTGCTTTTTAAATAAGT
AATATATATATATATATATATATATATATATATATATATATATAAGATTGAGATATTCTCTGTCTTGCTTCTT
CTTTACCCTTTTCTTGTTTCCAATCAAATCCTCTAAAGTTTCGTTCTTTGTTCTAAGTTTTCTGAAGGAGT
GATATTTGTTTGTGGTGTGGTTAGAGAAATGAATCGGAGACAGCAAGTGAAACGTAGAGTAGGTAAATA
TGAAGTTGGAAGAACAATTGGAGAAGGAACGTTTGCTAAAGTTAAGTTTGCTAGAAACTCTGAAACTGG
AGAACCTGTTGCTCTCAAGATTCTTGATAAAGAGAAAGTTCTCAAGCATAAAATGGCTGAACAGGTTTTT
GTTATTATTGAATTATGGATACTCTGCTTTCGCATTGCGGTTTTTTATCGGTTGATTTTGATCTTGCTTG
TGTTTTTTTGTTGAATTTTACAGATTAGAAGAGAGATAGCTACTATGAAGTTGATAAAACATCCAAATGT
TGTTCAATTATATGAGGTAATTAACACTTCTTTAGATAAATGTGTTATTTGATTATGTACTATGTACTTG
GAAATTACTTACTTCGAAATTGTACTGGTTGTTGTTGTTGCAGGTGATGGCAAGTAAGACGAAAATATT
TATCATCTTGGAGTATGTTACAGGAGGAGAACTCTTTGATAAGATTGTAAGTTAGTTACCACAATTATAA
ATGGTTGTGATTCTGTGATGTCACATTATAGTTGTGAAATCTGATAGTGATAACTTATGAATGAAGGTA
AATGATGGGCGGATGAAAGAAGATGAGGCGCGGAGATATTTCCAACAGCTTATACATGCTGTGGACTAC
TGTCATAGCAGAGGGGTCTACCATAGAGATCTCAAGGTACATACATTGTTTTTATAGATGGTAGGACTG
AAACATGGTATATTGATAGAGAAGTTACCTATGCATATATTATGTGCAGTAAGCCAGTAATTGACTATTG
TAATGTGATTTTGCAGCCTGAAAATTTACTATTGGACTCCTATGGAAACCTCAAGATCTCAGATTTTGGA
TTAAGTGCTTTGTCCCAACAAGTCAGGGTAATGACCATCTGTTTCCATAAGTATTTTACTGTTCCAAGAA
GTGGTTTCATTTTTCCTAAGAACTTACGGATTTTGTTGTCAAAAATTATATACATATATCTATTCTTAAAC
ATGGTTTATATGCTTGGGGATATCAGGATGATGGACTCTTGCATACATCGTGTGGAACACCAAACTACG
TTGCTCCTGAGGTCTGCCTAAAACAAACATGATTTCTTTATATCTTATAATATTATCCTTTCATTTTACGT
CTTTATAACCGACATCTTTGCGGGTTTTAGGTTCTCAATGATAGAGGCTATGATGGAGCAACAGCTGAC
ATGTGGTCATGCGGTGTTGTACTCTATGTCCTGCTTGCAGGTTACTTACCTTTTGATGATTCTAATCTAA
TGAATCTTTATAAAAAAGTGAGCAACTCTTTTCTAAAATTCTCTCTTTTAGATGGAATCTTCCAGCAATGC
TTGTTTTAGGATTTTTATAACTCCCTTTCGGCATTTTTGTGGTTTGGTGCAGATATCATCTGGTGAATTC
AACTGTCCTCCGTGGCTCTCACTCGGAGCCATGAAACTCATCACTAGAATCTTAGATCCGAATCCGATGA
CTGTAAGTAATTTTTACATGCTCATATACCCCTCTAAATAAAAGGCATTTACTTGTCCACAACTGTTGGA
GCGAAAAGCTGTCCATTGCTAAGAATTTTCACACAAACATGAACTTTATGGCTTTTAAAAACCCTTGAGA
GTTGAGTAATGAGCTCTATATTCCTTCCTTTGCACCATGATTTATTGTACTACTCAACCATGTTTTCCATT
TTTCCAGCACAAAAGGGCTGGAGAAAAAAAGTTGAGGAACCTGTGTTATGCATAATAACATGTACAACT
CTATCTGCTTCATCTCTCATTTCATTGCACAGTTTCTGATTGTTCCCTTGTTTTTGGCAAAAATCAACCAC
TAGTTCTTGGTTAAGCATACTAATCGAATAAACATGTCTTTTGATTACCGGAGAATGAGGATCCTAAACA
CTCACTATTATTTAGATTGTTTGTTTCCTATGCAATTTGAAGAAACTGAGTTGATTTGGTTTTGTGTCAG
CGTGTAACACCGCAAGAGGTTTTCGAAGATGAATGGTTCAAGAAAGATTACAAGCCACCTGTTTTCGAG
GAGAGGGATGATTCAAACATGGACGATATTGATGCTGTTTTCAAGGACTCTGAGGTGTGGATAGTTTTT
CTTCTTCTTTTTCATTTTTTCTTAACAAGAGCATCACATAACGCATGTGATGATCATATACAGGAACATCT
TGTTACTGAGAAGAGAGAAGAACAGCCAGCGGCGATCAATGCCTTCGAGATCATTTCAATGTCAAGGGG
ACTTAACCTAGAGAATCTGTTTGATCCAGAACAGGTTTGTGTTCTGTTCCTATAAAAGACTGGCTCTCCT
GTCTCCATATTCTGAGATCGGAATATTTTATTTTGAAAACAGGAATTTAAGAGGGAAACAAGGATAACAT

TGAGAGGAGGCGCGAATGAGATCATCGAGAAGATAGAAGAAGCTGCAAAGCCTCTCGGTTTCGATGTT
CAAAAGAAGAACTACAAGGTTAGTGAAAACTCTGTAACGGAAATGAAATGAAATGAAAAGAATCAATAAC
TAAAGACGTCGTAGTACATTACTTGAAATCAGATGAGGCTTGAGAATGTGAAGGCTGGAAGAAAGGGGA
ATCTCAATGTAGCGACAGAGGTATGTTATATGAGACTGGACATTCAAGAAAGTGTTGGTGATGGTTTAT
TGAATCAGTGTGTTTTTTGTTTGTATGGTGTGACAACAAGCAGATATTCCAAGTAGCGCCAAGTCTCCA
TATGGTTCAAGTATCGAAGTCGAAAGGAGACACTCTCGAATTTCACAAGGTAAGTCAAATAGCTTGGTT
TCGACTATATGATAGGGTAATTAACTGGTTTATGAGCTAAGCAGAGATGATGGTTTGTTTGCAGTTCTA
TAAGAAGCTCTCTAATTCTCTGGAGCAAGTAGTCTGGACGAATAACGAAGTTAAGAAAGAAACAGCAAA
GTGAGCTTTGAGACCACGAAGTG

pL0M-SC-cCIPK3sv2-73017

CACTCTGTGGTCTCAAATGATGAATCGGAGACAGCAAGTGAAACGTAGAGTAGGTAAATATGAAGTTGG
AAGAACAATTGGAGAAGGAACGTTTGCTAAAGTTAAGTTTGCTAGAAACTCTGAAACTGGAGAACCTGT
TGCTCTCAAGATTCTTGATAAAGAGAAAGTTCTCAAGCATAAAATGGCTGAACAGATTAGAAGAGAGATA
GCTACTATGAAGTTGATAAAACATCCAAATGTTGTTCAATTATATGAGGTGATGGCAAGTAAGACGAAAA
TATTTATCATCTTGGAGTATGTTACAGGAGGAGAACTCTTTGATAAGATTGTAAATGATGGGCGGATGA
AAGAAGATGAGGCGCGGAGATATTTCCAACAGCTTATACATGCTGTGGACTACTGTCATAGCAGAGGGG
TCTACCATAGAGATCTCAAGCCTGAAAATTTACTATTGGACTCCTATGGAAACCTCAAGATCTCAGATTT
TGGATTAAGTGCTTTGTCCCAACAAGTCAGGGATGATGGACTCTTGCATACATCGTGTGGAACACCAAA
CTACGTTGCTCCTGAGGTTCTCAATGATAGAGGCTATGATGGAGCAACAGCTGACATGTGGTCATGCGG
TGTTGTACTCTATGTCCTGCTTGCAGGTTACTTACCTTTTGATGATTCTAATCTAATGAATCTTTATAAA
AAAATATCATCTGGTGAATTCAACTGTCCTCCGTGGCTCTCACTCGGAGCCATGAAACTCATCACTAGAA
TCTTAGATCCGAATCCGATGACTCGTGTAACACCGCAAGAGGTTTTCGAAGATGAATGGTTCAAGAAAG
ATTACAAGCCACCTGTTTTCGAGGAGAGGGATGATTCAAACATGGACGATATTGATGCTGTTTTCAAGG
ACTCTGAGGAACATCTTGTTACTGAGAAGAGAGAAGAACAGCCAGCGGCGATCAATGCCTTCGAGATCA
TTTCAATGTCAAGGGGACTTAACCTAGAGAATCTGTTTGATCCAGAACAGGAATTTAAGAGGGAAACAA
GGATAACATTGAGAGGAGGCGCGAATGAGATCATCGAGAAGATAGAAGAAGCTGCAAAGCCTCTCGGT
TTCGATGTTCAAAAGAAGAACTACAAGTACATTACTTGAGCTTTGAGACCACGAAGT

pL0M-SC-cCIPK3sv3-73018

CACTCTGTGGTCTCAAATGATGAATCGGAGACAGCAAGTGAAACGTAGAGTAGGTAAATATGAAGTTGG
AAGAACAATTGGAGAAGGAACGTTTGCTAAAGTTAAGTTTGCTAGAAACTCTGAAACTGGAGAACCTGT
TGCTCTCAAGATTCTTGATAAAGAGAAAGTTCTCAAGCATAAAATGGCTGAACAGATTAGAAGAGAGATA
GCTACTATGAAGTTGATAAAACATCCAAATGTTGTTCAATTATATGAGGTGATGGCAAGTAAGACGAAAA
TATTTATCATCTTGGAGTATGTTACAGGAGGAGAACTCTTTGATAAGATTGTAAATGATGGGCGGATGA
AAGAAGATGAGGCGCGGAGATATTTCCAACAGCTTATACATGCTGTGGACTACTGTCATAGCAGAGGGG
TCTACCATAGAGATCTCAAGCCTGAAAATTTACTATTGGACTCCTATGGAAACCTCAAGATCTCAGATTT
TGGATTAAGTGCTTTGTCCCAACAAGTCAGGGATGATGGACTCTTGCATACATCGTGTGGAACACCAAA

CTACGTTGCTCCTGAGGTTCTCAATGATAGAGGCTATGATGGAGCAACAGCTGACATGTGGTCATGCGG
TGTTGTACTCTATGTCCTGCTTGCAGGTTACTTACCTTTTGATGATTCTAATCTAATGAATCTTTATAAA
AAAATATCATCTGGTGAATTCAACTGTCCTCCGTGGCTCTCACTTGGAGCCATGAAACTCATCACTAGAA
TCTTAGATCCGAATCCGATGACTCGTGTAACACCGCAAGAGGTTTTCGAAGATGAATGGTTCAAGAAAG
ATTACAAGCCACCTGTTTTCGAGGAGAGGGATGATTCAAACATGGACGATATTGATGCTGTTTTCAAGG
ACTCTGAGGAACATCTTGTTACTGAGAAGAGAGAAGAACAGCCAGCGGCGATCAATGCCTTCGAGATCA
TTTCAATGTCAAGGGGACTTAACCTAGAGAATCTGTTTGATCCAGAACAGGAATTTAAGAGGGAAACAA
GGATAACATTGAGAGGAGGCGCGAATGAGATCATCGAGAAGATAGAAGAAGCTGCAAAGCCTCTCGGT
TTCGATGTTCAAAAGAAGAACTACAAGATGAGGCTTGAGAATGTGAAGGCTGGAAGAAAGGGGAATCTC
AATGTAGCGACAGAGATATTCCAAGTAGCGCCAAGTCTCCATATGGTTCAAGTATCGAAGTCGAAAGGA
GACACTCTCGAATTTCACAAGTTCTATAAGAAGCTCTCTAATTCTCTGGAGCAAGTAGTCTGGACGAATA
ACGAAGTTAAGAAAGAAACAGCAAAGTGAGCTTTGAGACCACGAAGTG

pL0M-T-CIPK3sv2-73019

CACTCTGTGGTCTCAGCTTAATCAGATGAGGCTTGAGAATGTGAAGGCTGGAAGAAAGGGGAATCTCAA
TGTAGCGACAGAGATATTCCAAGTAGCGCCAAGTCATCATATGGTTCAAGTATCGAAGTCGAAAGGAGA
CACTCTCGAATTTCACAAGTTCTATAAGAAGCTCTCTAATTCTCTGGAGCAAGTAGTCTGGACGAATAAC
GAAGTTAAGAAAGAAACAGCAAAGTGATGTATGAGAGTTTTCTTTTGGGACAATTCTTGCTTTCTTTGT
GTATAAGAGCTTTTTTGCTTTACCGGCTACTTTGTGTGGATGATGAGAAAGGGAGTGGGATTGGTTTTG
TGTAAAAGAAAGGTGTAAATATGAACTGCATTACTCGATAAGGTGCTGCGATGCCAGTTATAAAGTCAT
ATCAAAGCTTGTTGGCTAAAAGTTTGAAAATGCCTCATTGCTCTATTTGTTATTCTGTGCCGGCGAAATT
TGTCTCGTTTCAAAAAAACTATCTGATCCGTTTTGTCTTTTCTTTTACAACTTGAAGATGGAACGTATCA
AAAATGTCATGATCGAAGGACTGCCTATTTCCACTCATAAGGAATTCAGTAACCTTACTATGACGGTTTC
AGATCATTATGATAGCTTCATGTCCATCCTGAAGTTATAAGTTTTTAGGGCTTTTCATTTTATATTTACTT
ATTCTTATTTATGTAAGTTAAGATTTTGTTTTGAGAAGCACCATGATTCAAAGATTTTAGTTTAAAATCAC
GCTTGAGACCACGAAGTG

pL0M-T-CIPK3sv3-73020

CACTCTGTGGTCTCAGCTTTGTATGAGAGTTTTCTTTTGGGACAATTCTTGCTTTCTTTGTGTATAAGAG
CTTTTTTGCTTTACCGGCTACTTTGTGTGGATGATGAGAAAGGGAGTGGGATTGGTTTTGTGTAAAAGA
AAGGTGTAAATATGAACTGCATTACTCGATAAGGTGCTGCGATGCCAGTTATAAAGTCATATCAAAGCTT
GTTGGCTAAAAGTTTGAAAATGCCTCATTGCTCTATTTGTTATTCTGTGCCGGCGAAATTTGTCTCGTTT
CAAAAAAACTATCTGATCCGTTTTGTCTTTTCTTTTACAACTTGAAGATGGAACGTATCAAAAATGTCAT
GATCGAAGGACTGCCTATTTCCACTCATAAGGAATTCAGTAACCTTACTATGACGGTTTCAGATCATTAT
GATAGCTTCATGTCCATCCTGAAGTTATAAGTTTTTAGGGCTTTTCATTTTATATTTACTTATTCTTATTT
ATGTAAGTTAAGATTTTGTTTTGAGAAGCACCATGATTCAAAGATTTTAGTTTAAAATCACGCTTGAGAC
CACGAAGTG

pL0M-PU-CIPK3-73021

CACTCTGTGGTCTCAGGAGCTTGGAAACCTCTCTTTTGGATAGATTTTGTGATTTGGCGTTGATTCTTT
GTGGATTATCTGTTTCTCTTCACATAGCTGGATTTGATGGAGTTTATAAACCACTTCAATGCCAAGAAAA
AGGATTTGAAACTTTTCTTCATTCTCATTTTTAAAATTGATTTCTTAACTTTGCAGCAACTAGATAGTAAT
TGCAAGCGATGGGTGATATGCACCGGAACTCTTACAAATAACGTGGATGTCTTTTTCGAGTAAGGTTAC
GACTATGAATATTAAAAGTGAAACAAATCTGAACAAGAAAATTAGGTTCGAATAATTTAATTAGCTTTTA
ATTTGTCAATCTTTCTGGATCTTTGCTTGTTGTTACACACTGGCCAGTGGGCCAGTTGCCACTGATTAAA
TTTTATAATAACCATTCAACTCAAAGTAAACTCTGCACTATAACTCTCATATATCAAATGTCAGTCAAGTT
GAGACTGTTAAAGCGAAGCTGCATAAAATGTGTTTGTCCATATAAAAATTGAACATTATTATATATAAAA
ATACAAACTTATCTGGTGGTATACCATCTAGATTAGATCCTAGTATTGTCCTTTTTTTTTTACAACAGATT
AGTATCTTTTACATGTTCAATCTTTTGTGGATGACAAAATTACTTAAATCGAAAAATCTTGTTAGTTATT
GTCACTATCAGTAAGTCAATAAACAAACATTCATCACAAAAACAAAAAAACAAAATCTTCACTAGTCACAA
CAAAATTCGCCCCAATTCTTTGATCCATTAAAAAAAACTAATATTATCATTTTTAATCATTATTATTTCAG
AATTGTTTGGCAAAAATAATTCAACATTAAAAAAAGAAATTTAATATCAAAATAAAATAAAAGAAAAGAAA
AGAGAAAACAGATCCGAATTGAGTTCATCATCTTAAAACTTTGAAATCGGTTACTGTGCCTTTTTTTTTT
TTTTTTTTTTTAGTGGTTACAAGTTACAAAACTCAAAAAAAGACCAAAGACAGCAATTAATTTTTGTTTCT
TTCTGTTCTAAGGATCTTTGTCTGCTACTGAAACTCCTTAAAGCAAAACTGTAACTTCTCACCAAAAACG
AATTTTTCCAACAAAAATTTAATAATCAAAATAAATCTTCTTCTTCTTCTTCATCGTTTATCACGACCTCT
GTCTCTTCGACTCTCTCAAAAGCCATTTTAAATCTCTCTCTTTCTCACTCAATCTCTCTGTAGCTATCAGA
TCTTCTCTTAATGTGAGACCACGAAGTG

pL0M-T-gCIPK3-73032

CACTCTGTGGTCTCAGCTTTGTATGAGAGTTTTCTTTTGGGACAATTCTTGCTTTCTTTGTGTATAAGAG
CTTTTTTGCTTTACCGGCTACTTTGTGTGGATGATGAGAAAGGGAGTGGGATTGGTTTTGTGTAAAAGA
AAGGTGTAAATATGAACTGCATTACTCGATAAGGTGCTGCGATGCCAGTTATAAAGTCATATCAAAGCTT
GTTGGCTAAAAGTTTGAAAATGCCTCATTGCTCTATTTGTTATTCTGTGCCGGCGAAATTTGTCTCGTTT
CAAAAAAACTATCTGATCCGTTTTGTCTTTTCTTTTACAACTTGAAGATGGAACGTATCAAAAATGTCAT
GATCGAAGGACTGCCTATTTCCACTCATAAGGAATTCAGTAACCTTACTATGACGGTTTCAGATCATTAT
GATAGCTTCATGTCCATCCTGAAGTTATAAGTTTTTAGGGCTTTTCATTTTATATTTACTTATTCTTATTT
ATGTAAGTTAAGATTTTGTTTTGAGAAGCACCATGATTCAAAGATTTTAGTTTAAAATCATGGCAACTAG
TTGGTGCTCTTAAGATGATCTCATCTTCCCTCTTCTGCCTTTCAGGAATTGTCTTGCCCAATTTGGGACT
TTAATTACCATTATTATAGCTAGGAACTATGGTTAACTATTTGATGATTTTATAATTGTCATTAGTTTAGT
TACAAGTTTGTAACCAAACTGTTTTTTTTTTTTTGTTTTTTTAATTGAAAATTCTTTGATGTAAGTTCCAA
AAATGACATGATAGTGTAGAAGAAATAGATGATAAGTAGATTGCGAACTTTGCTTAGTTATCCTCTTTCA
TGTTTTAATGACTGAATATTGGCAATTTTTAACTTTGTAATTTATTTTCCCATGGAATAACCAAACAAAAA
TTAAACCAACTCTACGGATATTATAACCGTTTAGGATGAGCTCGATTGGTGTAGAACATATAAGTGGACT
TACACTTTTTGTGAGCCAGTCATATTTTGTTATGTGAACTTCTAAGTGAGAAAGGTTCGAAGCATGCGA
ATCCATTGTTTTGATGTTAGATGTTTTGGGAGATGCATTCAATAAAGAAGCCTTCTTGATAAACAGAGAT
CCTTGTGAGTTTTGATGTTAGGCTTTAAACGTTCAACATCATTACAGCACCCGTTTTGTTTTGTCTTTTC

TTTTTACGATGAAGATCCTTTTGACACACAAAATAAATAAAATATTGAAGGAAGTTCCAAAAATGACATG
GATAGTCATGAAATTAATAGTCACAAATGGTTTCTTCTTCTTATTCTTCGTCTAATCTTTTAAGTCTTGAT
GAAGAAACAGATGATGGTATATTGTGAACTAATATATGGAATAAACAAAATGTTGACTGTCACACATGAA
TTTAAATTGTTATGGATTTATATCTACGAAACCAAAAGGGTGAATATCACATATGGATTAAGTTTGTCTT
AGATATCTATACAATGAAGTTTAATATATTTTAGCTCTTCTTGTCATCGTGTGTTTTTCTTTTACTTTCTT
ATAAATTTTTTTGGGTACATACAACGATATATGTGTTTTGTTGATCAATAAAAAGTTCACCTTATCTCGT
AGAGAACTAATCGAGTGATGGACGGCGTTTGTTATTTAATTTGTGGTTGAAATTTATCATCTACATGACT
ACATCATCTACAATACGCTTGAGACCACGAAGTG

Appendix B: Golden Gate modules and vectors

Table B1: **Level 0 Golden Gate modules.**

ENSA ID	ENSA Standard name	Description
73016	pL0M-SC-gCIPK3-73016	CIPK3 Genomic sequence
73017	pL0M-SC-cCIPK3sv2-73017	CIPK3 SV2 CDS
73018	pL0M-SC-cCIPK3sv3-73018	CIPK3 SV3 CDS
73019	pL0M-T-CIPK3sv2-73019	CIPK3 SV2 3'UTR
73020	pL0M-T-CIPk3sv3-73020	CIPK3 SV3 3'UTR
73021	pL0M-PU-CIPK3-73021	CIPK3 native promoter
73032	pL0M-T-gCIPK3-73032	Genomic CIPK3 3'UTR
15058	pLOM-PU-p35S(short)-15058	35S promoter
41414	pL0M-T-35S-1-41414	35S terminator
15112	pL0M-SC-eGFP-15112	eGFP CDS

Table B2: **Golden Gate level 2 modules.**

ENSA ID	ENSA Standard Name	Backbone	P/PU	S/SC/SC1	T
73029	pL1M-pCIPK3::gCIPK3-73029	pL1V-R2-47811	pL0M-PU-CIPK3-73021	pL0M-SC-gCIPK3-73016	pL0M-T-gCIPK3-73032
73024	pL1M-p35S::gCIPK3-73024	pL1V-R2-47811	pL0M-PU-p35S(short)-15058	pL0M-SC-gCIPK3-73016	pL0M-T-35S-1-41414
73025	pL1M-pCIPK3::cCIPK3sv2-73025	pL1V-R2-47811	pL0M-PU-CIPK3-73021	pL0M-SC-cCIPK3sv2-73017	pL0M-T-CIPK3sv2-73019
73026	pL1M-pCIPK3::cCIPK3sv3-73026	pL1V-R2-47811	pL0M-PU-CIPK3-73021	pL0M-SC-cCIPK3sv3-73018	pL0M-T-CIPK3sv3-73020
73027	pL1M-p35S::cCIPK3sv2-73027	pL1V-R2-47811	pL0M-PU-p35S(short)-15058	pL0M-SC-cCIPK3sv2-73017	pL0M-T-35S-1-41414
73028	pL1M-p35S::cCIPK3sv3-73028	pL1V-R2-47811	pL0M-PU-p35S(short)-15058	pL0M-SC-cCIPK3sv3-73018	pL0M-T-35S-1-41414
73033	pL1M-pCIPK3::GFP-73033	pL1V-R2-47811	pL0M-PU-CIPK3-73021	pL0M-SC-eGFP-15112	pL0M-T-gCIPK3-73032

Table B3: GoldenGate Level 2 modules.

ENSA ID	ENSA Standard name	Backbone vector	Position 1	Position 2	Position 3
73034	pL2B-CIPK3::CIPK3-73034	pL2V-HYG-15027	HYG	pL1M-pCIPK3::gCIPK3-73029	pL1M-ELE-2-41744
73035	pL2B-35S::CIPK3-73035	pL2V-HYG-15027	HYG	pL1M-p35S::gCIPK3-73024	pL1M-ELE-2-41744
73036	pL2B-CIPK3::CIPK3sv2-73036	pL2V-HYG-15027	HYG	pL1M-pCIPK3::cCIPK3sv2-73025	pL1M-ELE-2-41744
73037	pL2B-CIPK3::CIPK3sv3-73037	pL2V-HYG-15027	HYG	pL1M-pCIPK3::cCIPK3sv3-73026	pL1M-ELE-2-41744
73038	pL2B-35S::CIPK3sv2-73038	pL2V-HYG-15027	HYG	pL1M-p35S::cCIPK3sv2-73027	pL1M-ELE-2-41744
73039	pL2B-35S::CIPK3sv3-73039	pL2V-HYG-15027	HYG	pL1M-p35S::cCIPK3sv3-73028	pL1M-ELE-2-41744
73040	pL2B-CIPK3::GFP-73040	pL2V-HYG-15027	HYG	pL1M-pCIPK3::GFP-73033	pL1M-ELE-2-41744

Appendix C: Chapter 3 supplemental figures

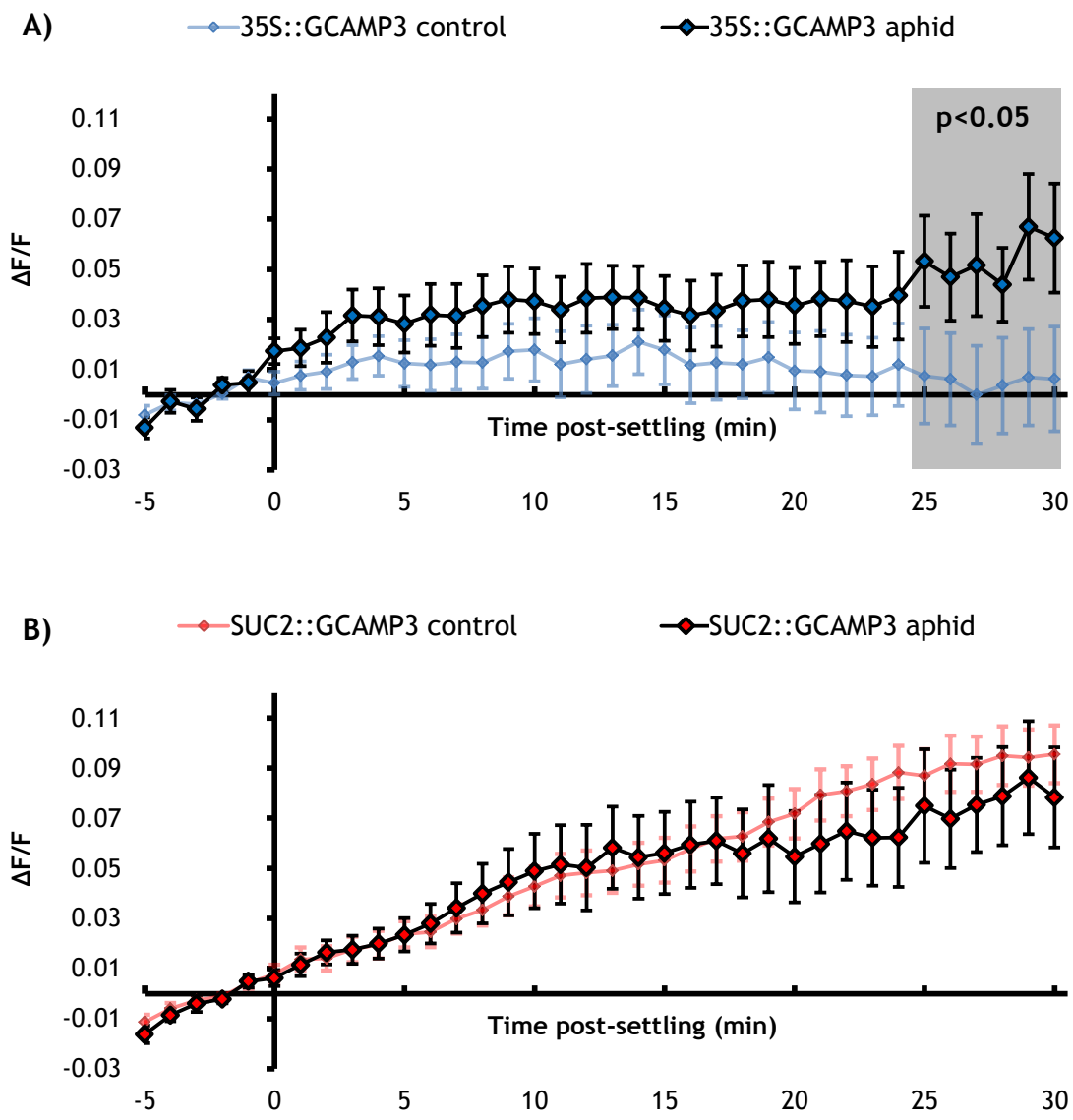

Figure C1: Normalised GFP fluorescence (ΔF/F) in the midrib, systemic to the feeding site, in 35S::GCAMP3 and SUC2::GCAMP3 Arabidopsis upon *M. persicae* settling.

A) 35S::GCAMP3 control (no aphid treatment) vs aphid treatment. **B)** SUC2::GCAMP3 control (no aphid treatment) vs aphid treatment. Error bars represent SEM (35S::GCAMP3 n=31, SUC2::GCAMP3 n=34). Grey shading indicates significant difference between treatments (Student's t-test within GLM at $p<0.05$). Experiment conceived and designed by T.V. and conducted by T.V. and M.A.

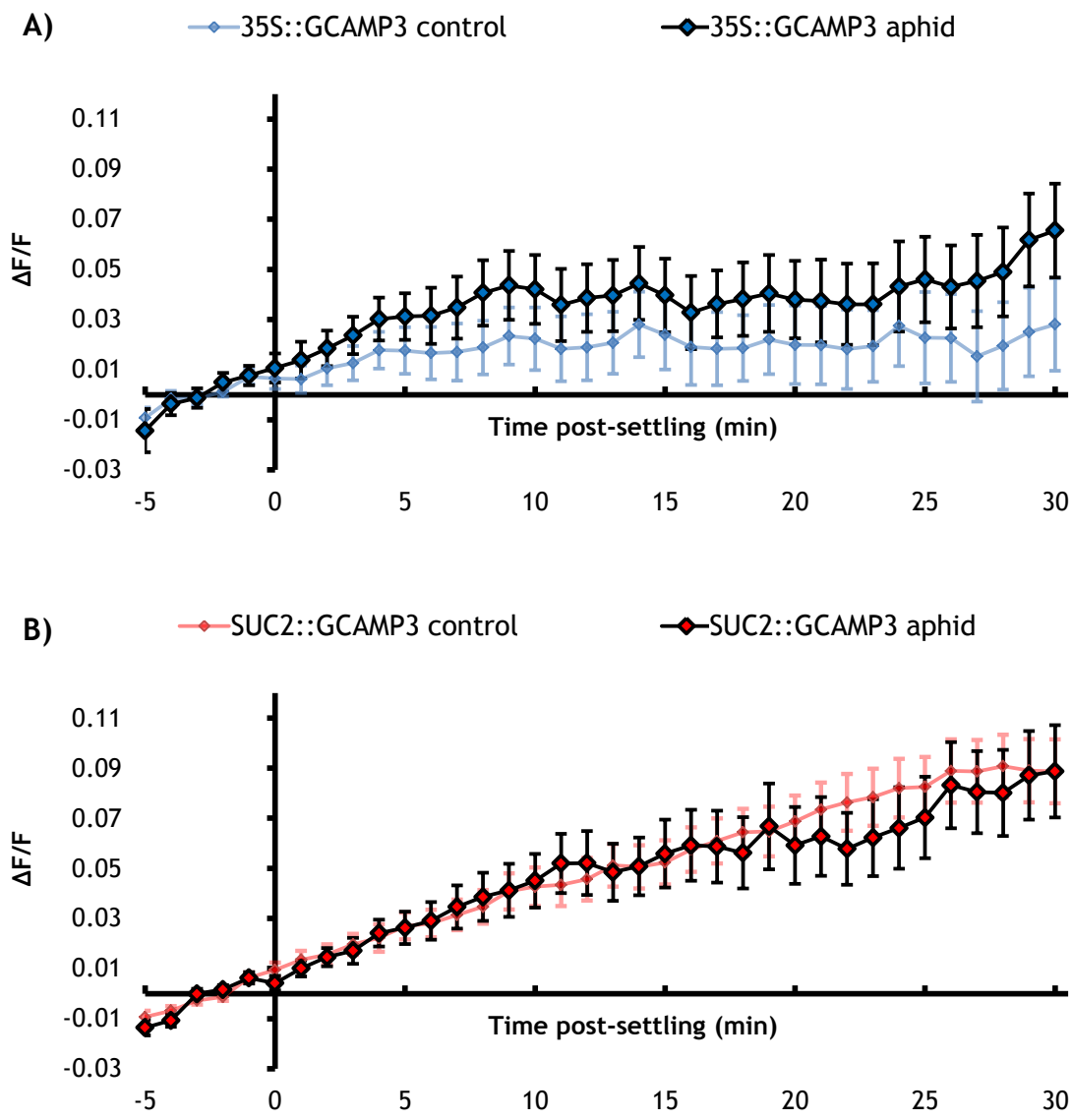

Figure C2: Normalised GFP fluorescence (ΔF/F) in the lateral tissue, systemic to the feeding site, in 35S::GCAMP3 and SUC2::GCAMP3 Arabidopsis upon *M. persicae* settling. **A)** 35S::GCAMP3 control (no aphid treatment) vs aphid treatment. **B)** SUC2::GCAMP3 control (no aphid treatment) vs aphid treatment. Error bars represent SEM (35S::GCAMP3 n=31, SUC2::GCAMP3 n=34). Grey shading indicates significant difference between treatments (Student's t-test within GLM at $p<0.05$). Experiment conceived and designed by T.V. and conducted by T.V. and M.A.

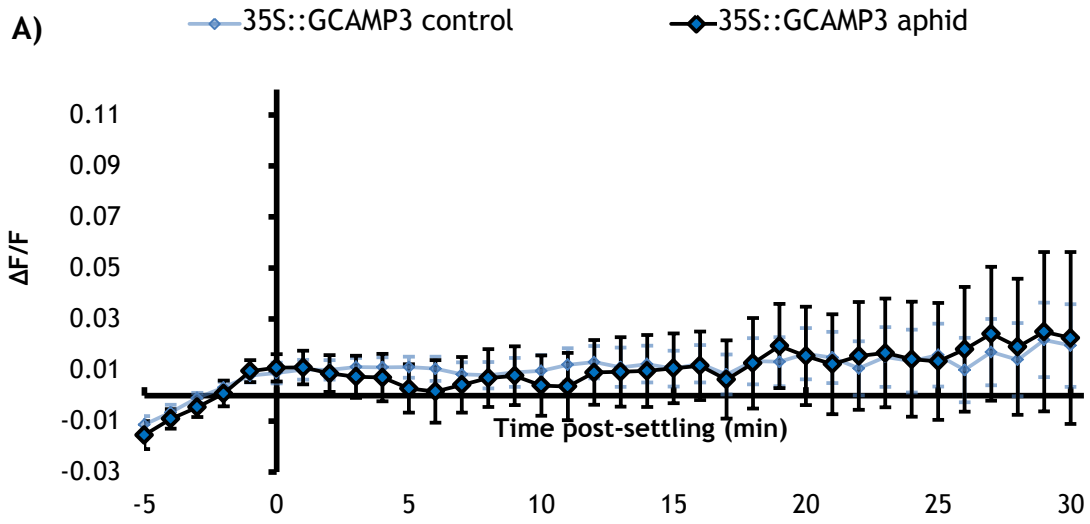
A)
35S::GCAMP3 control
35S::GCAMP3 aphid
ΔF/F
0.11
0.09
0.07
0.05
0.03
0.01
-0.01
-0.03
-5
0
5
10
15
20
25
30
Time post-settling (min)

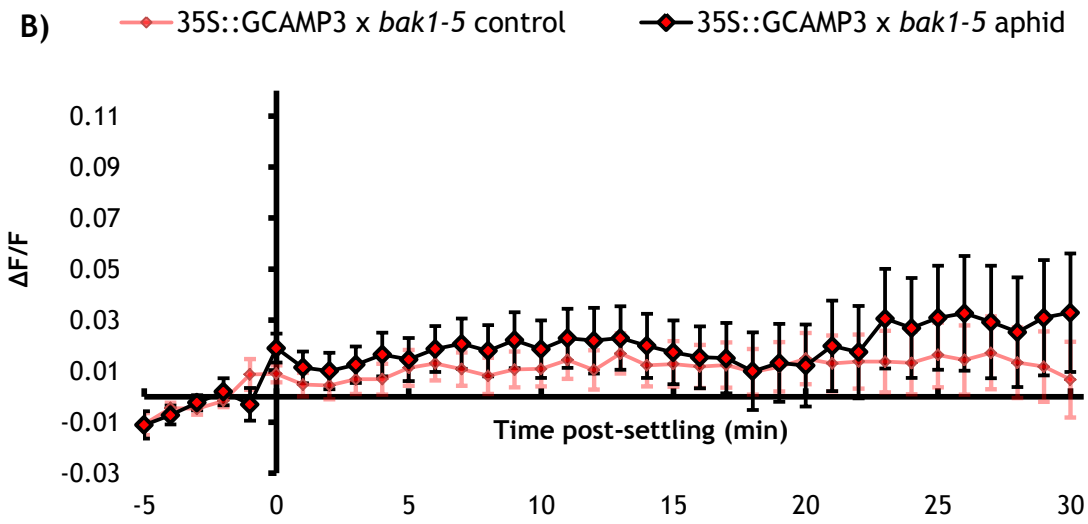
B)
35S::GCAMP3 x bak1-5 control
35S::GCAMP3 x bak1-5 aphid
ΔF/F
0.11
0.09
0.07
0.05
0.03
0.01
-0.01
-0.03
-5
0
5
10
15
20
25
30
Time post-settling (min)

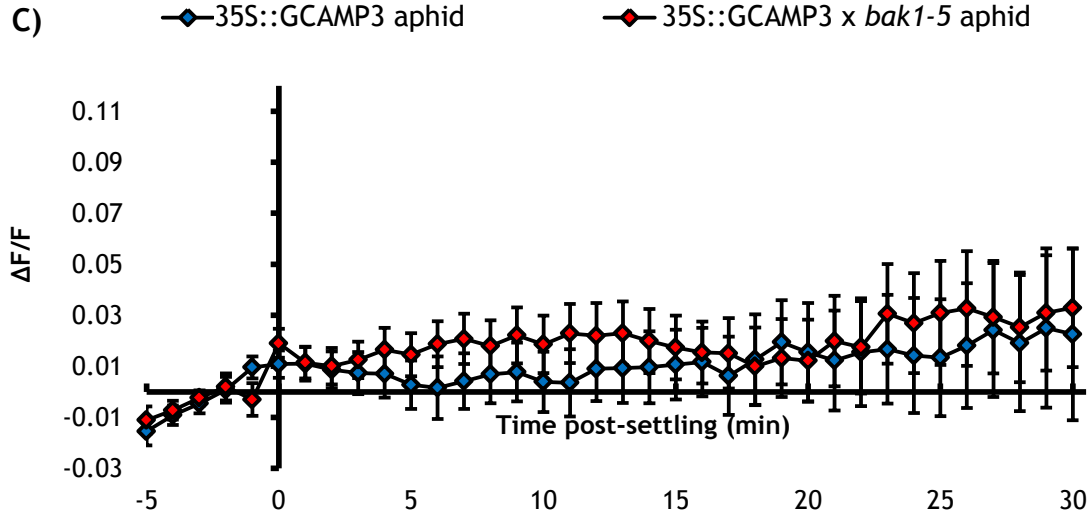
C)
35S::GCAMP3 aphid
35S::GCAMP3 x bak1-5 aphid
ΔF/F
0.11
0.09
0.07
0.05
0.03
0.01
-0.01
-0.03
-5
0
5
10
15
20
25
30
Time post-settling (min)

Figure C3: Normalised GFP fluorescence (ΔF/F) in the midrib, systemic to the feeding site, in 35S::GCAMP3 and 35S::GCAMP3 x *bak1-5* Arabidopsis upon *M. persicae* settling.
A) 35S::GCAMP3 control (no aphid treatment) vs aphid treatment. **B)** 35S::GCAMP3 x *bak1-5* control (no aphid treatment) vs aphid treatment. **C)** 35S::GCAMP3 aphid treatment vs 35S::GCAMP3 x *bak1-5* aphid treatment. Bars represent SEM (35S::GCAMP3 n=30, 35S::GCAMP3 x *bak1-5* n=30). Experiment conceived and designed by T.V. and conducted by T.V. and M.A.

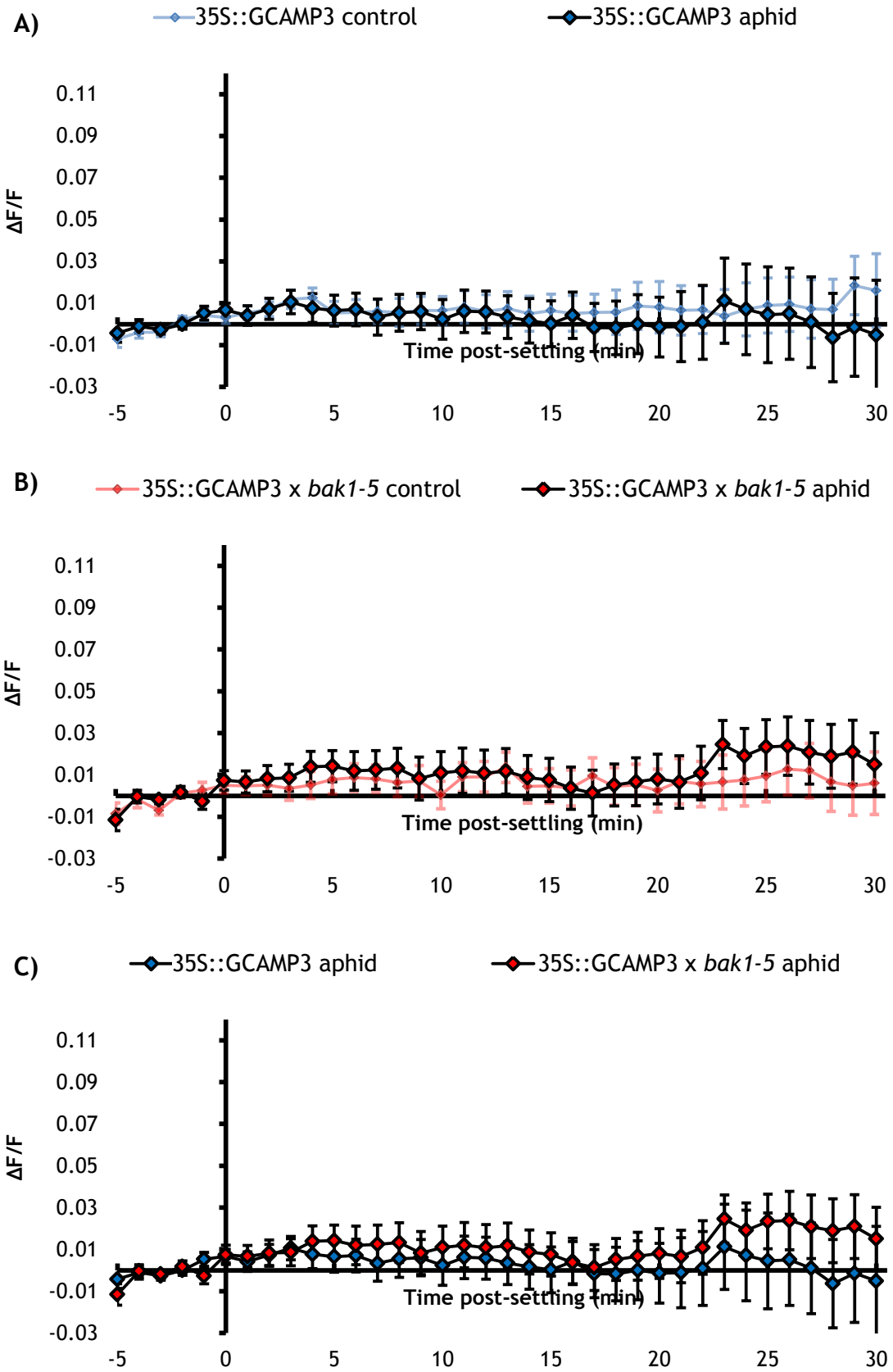
A)
35S::GCAMP3 control
35S::GCAMP3 aphid
ΔF/F
0.11
0.09
0.07
0.05
0.03
0.01
-0.01
-0.03
-5
0
5
10
15
20
25
30
Time post-settling (min)
B)
35S::GCAMP3 x bak1-5 control
35S::GCAMP3 x bak1-5 aphid
ΔF/F
Time post-settling (min)
C)
35S::GCAMP3 aphid
35S::GCAMP3 x bak1-5 aphid
ΔF/F
Time post-settling (min)

<u>Figure C4:</u> Normalised GFP fluorescence (ΔF/F) in the lateral tissue, systemic to the feeding site, in 35S::GCAMP3 and 35S::GCAMP3 x *bak1-5* Arabidopsis upon *M. persciae* settling.

A) 35S::GCAMP3 control (no aphid treatment) vs aphid treatment. **B)** 35S::GCAMP3 x *bak1-5* control (no aphid treatment) vs aphid treatment. **C)** 35S::GCAMP3 aphid treatment vs 35S::GCAMP3 x *bak1-5* aphid treatment. Bars represent SEM (35S::GCAMP3 n=30, 35S::GCAMP3 x *bak1-5* n=30). Experiment conceived and designed by T.V. and conducted by T.V. and M.A.

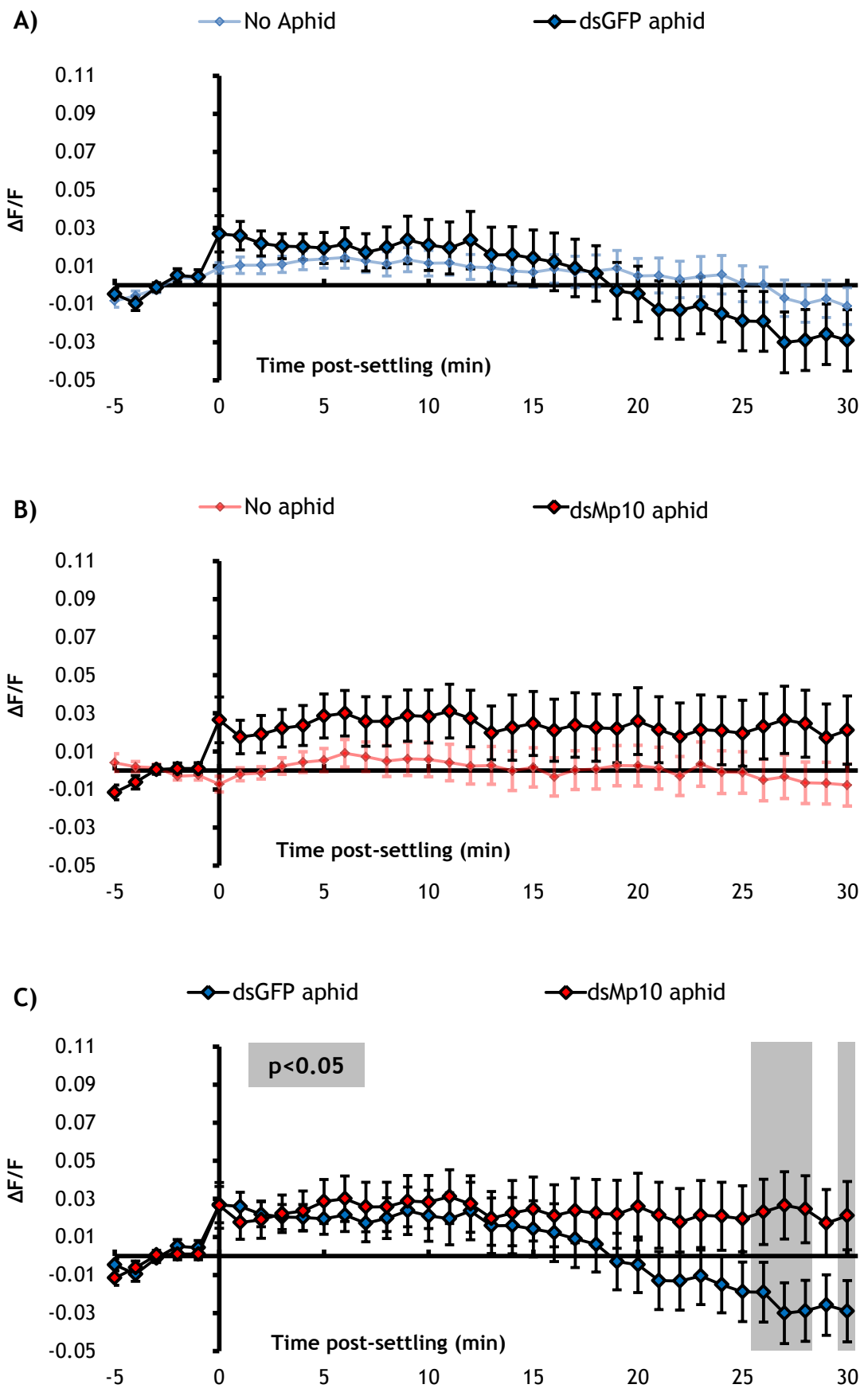
A)
No Aphid
dsGFP aphid
ΔF/F
0.11
0.09
0.07
0.05
0.03
0.01
-0.01
-0.03
-0.05
Time post-settling (min)
-5
0
5
10
15
20
25
30
B)
No aphid
dsMp10 aphid
ΔF/F
Time post-settling (min)
C)
dsGFP aphid
dsMp10 aphid
p<0.05
ΔF/F
Time post-settling (min)

<u>Figure C5:</u> Normalised GFP fluorescence (ΔF/F) around the midrib, systemic to the feeding site, in 35S::GCAMP3 Arabidopsis upon *M. persicae* settling.

A) No aphid control vs dsGFP aphid treatment. **B)** No aphid control vs dsMp10 aphid treatment. **C)** dsGFP aphid treatment vs dsMp10 aphid treatment. Bars represent SEM (dsGFP n=34, dsMp10 n=34). Grey shading indicates significant difference between treatments (Student's t-test within GLM at $p<0.05$). Experiment conceived and designed by T.V. and conducted by T.V. and M.A.

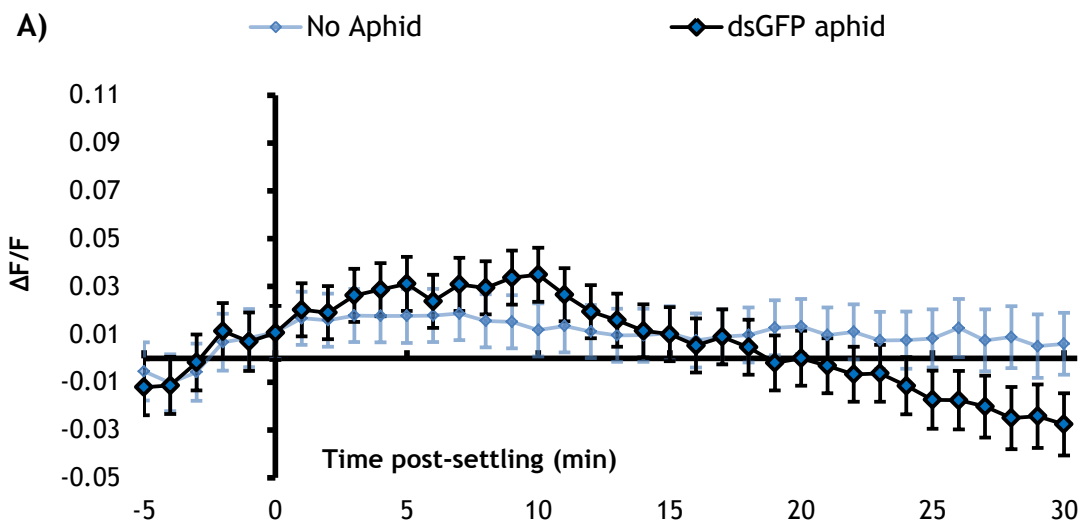
A)
No Aphid
dsGFP aphid
ΔF/F
0.11
0.09
0.07
0.05
0.03
0.01
-0.01
-0.03
-0.05
Time post-settling (min)
-5
0
5
10
15
20
25
30

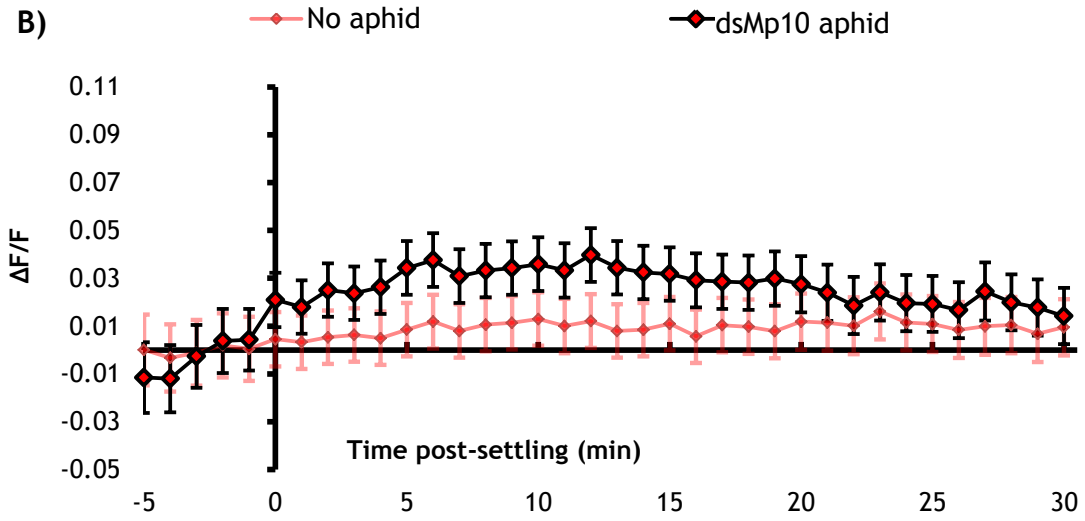
B)
No aphid
dsMp10 aphid
ΔF/F
0.11
0.09
0.07
0.05
0.03
0.01
-0.01
-0.03
-0.05
Time post-settling (min)
-5
0
5
10
15
20
25
30

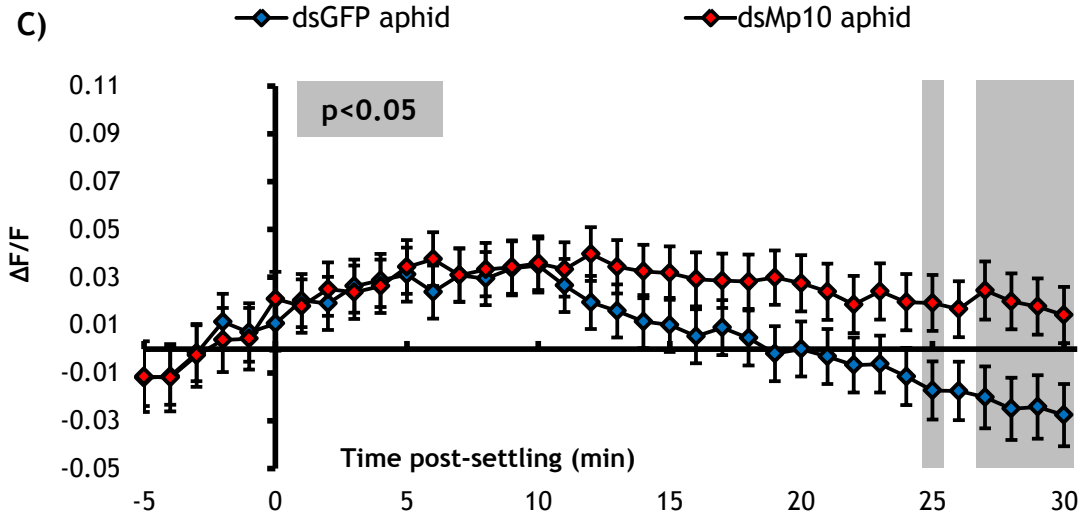
C)
dsGFP aphid
dsMp10 aphid
p<0.05
ΔF/F
0.11
0.09
0.07
0.05
0.03
0.01
-0.01
-0.03
-0.05
Time post-settling (min)
-5
0
5
10
15
20
25
30

Figure C6: Normalised GFP fluorescence (ΔF/F) around the lateral tissue, systemic to the feeding site, in 35S::GCAMP3 Arabidopsis upon *M. persicae* settling.

A) No aphid control vs dsGFP aphid treatment. **B)** No aphid control vs dsMp10 aphid treatment. **C)** dsGFP aphid treatment vs dsMp10 aphid treatment. Bars represent SEM (dsGFP n=34, dsMp10 n=34). Grey shading indicates significant difference between treatments (Student's t-test within GLM at $p<0.05$). Experiment conceived and designed by T.V. and conducted by T.V. and M.A.

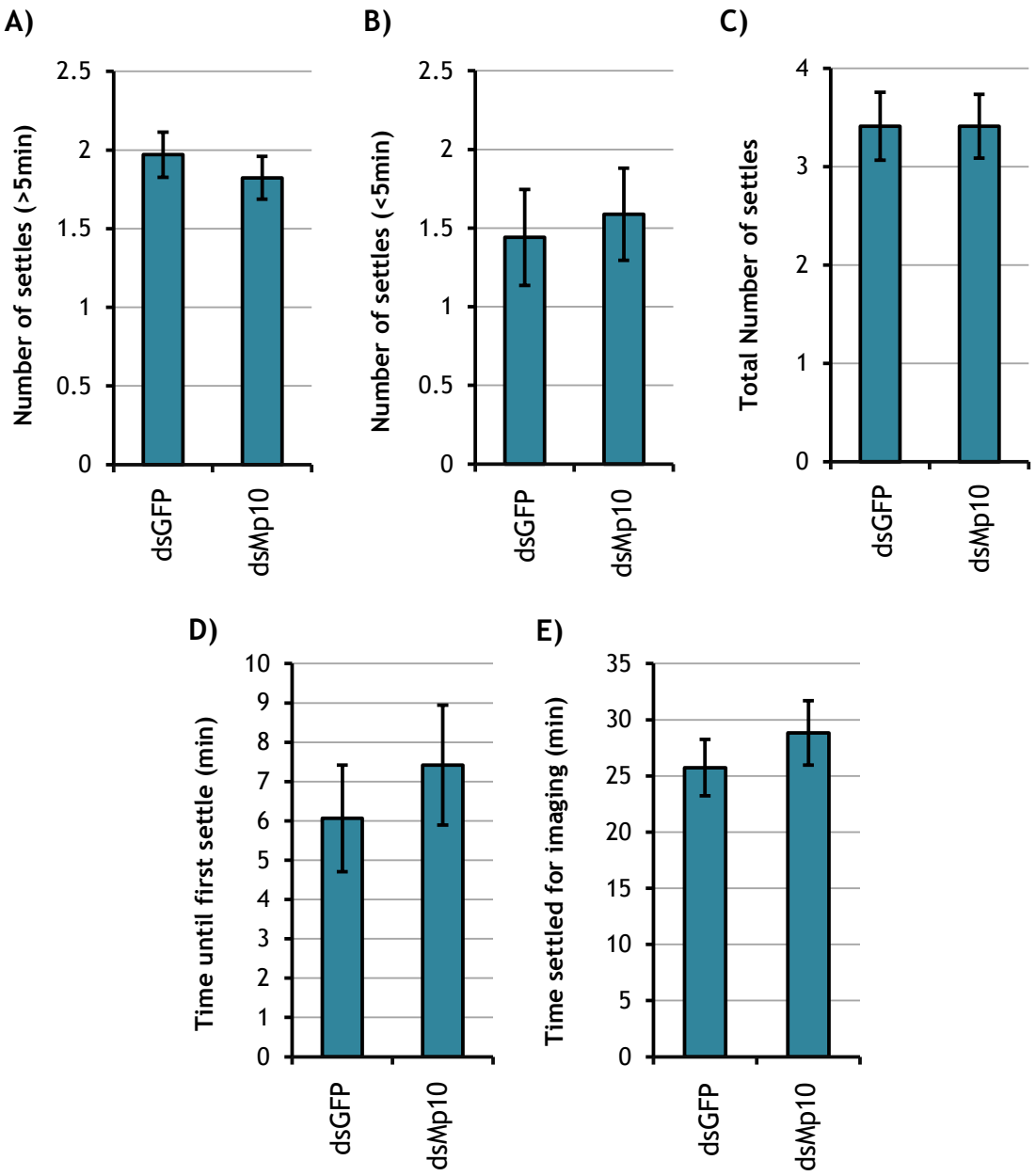

Figure C7: Settling behaviour of dsGFP and dsMp10 *M. persicae* on 35S::GCAMP3 leaves.
A) Number of settles greater than 5 min in length. **B)** Number of settles less than 5 min in length. **C)** Total number of settles. **D)** Time before first settle that lasted over 5 min. **E)** Time aphid spent settled during a settling event used to measure GCAMP3 fluorescence. Bars represent SEM (dsGFP n=34, dsMp10 n=34). Experiment conceived and designed by T.V. and conducted by T.V. and M.A.

Appendix D: Chapter 4 supplemental figures

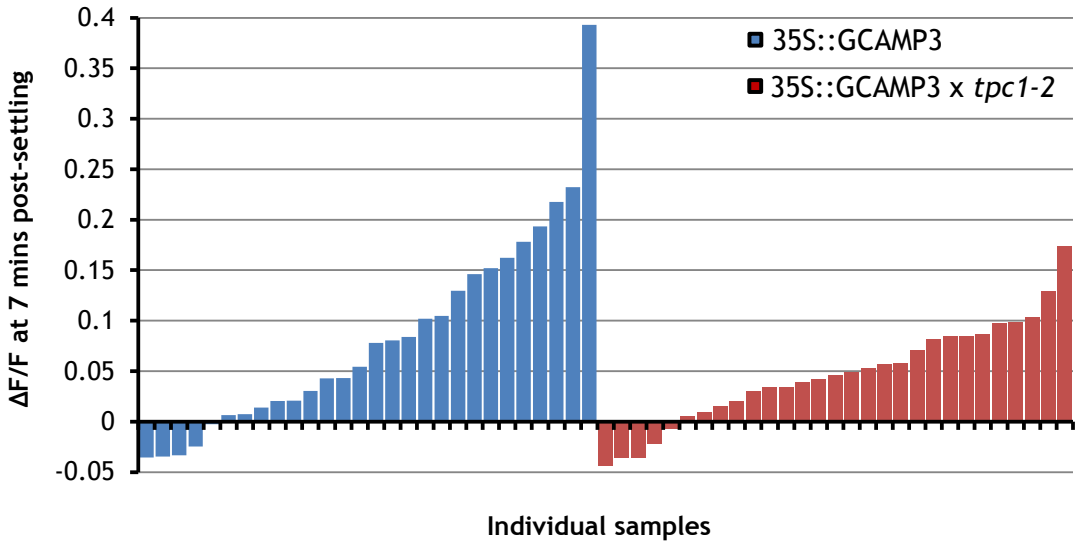

Figure D1: Normalised florescence (ΔF/F) around the *M. persicae* feeding site at 7 mins post-settling in 35S::GCAMP3 and 35S::GCAMP3 x *tpc1-2* leaves.

Raw ΔF/F value for each leaf sample plotted. Experiment conceived and designed by T.V. and conducted by T.V. and J.C.

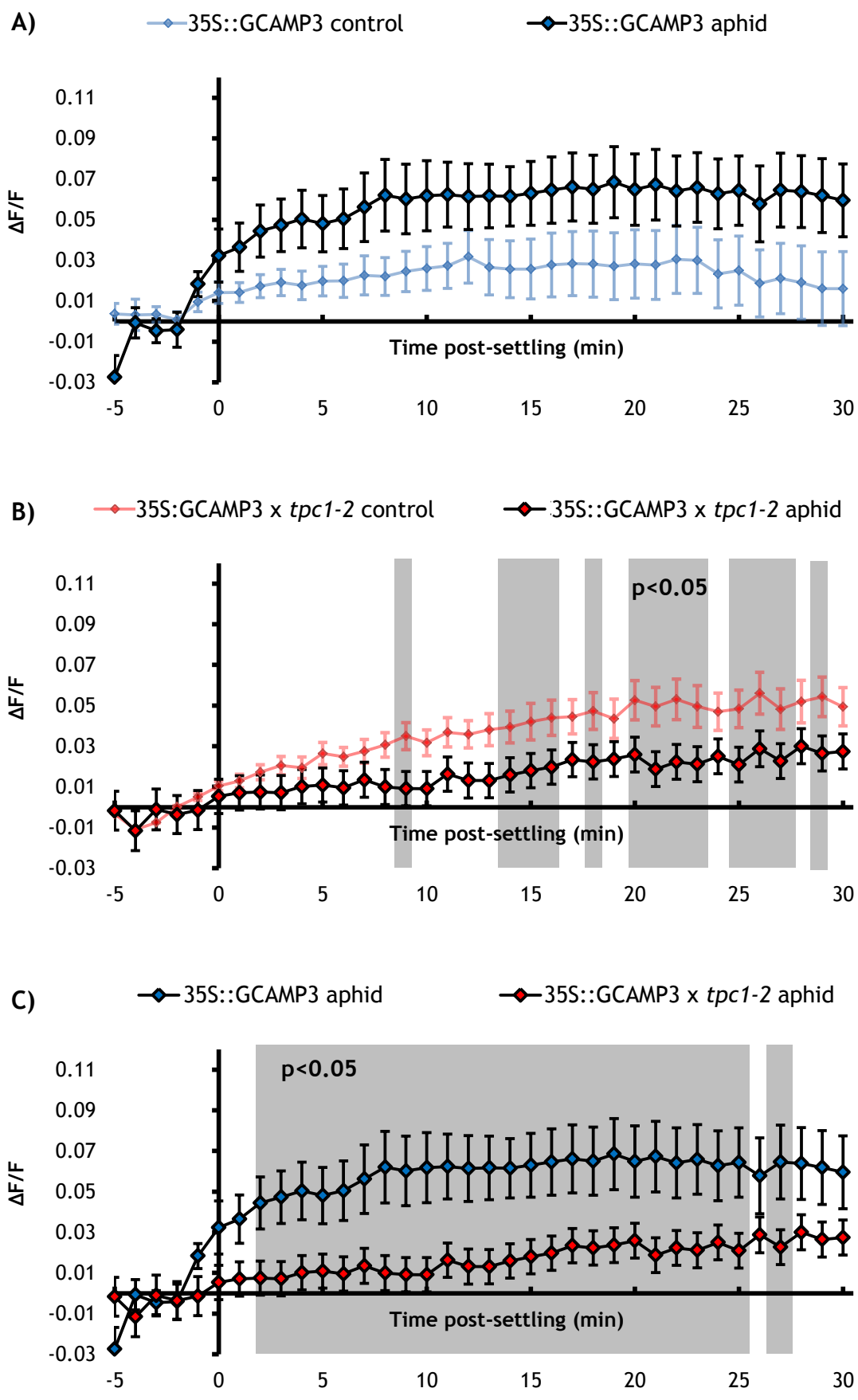
A)
35S::GCAMP3 control
35S::GCAMP3 aphid
ΔF/F
0.11
0.09
0.07
0.05
0.03
0.01
-0.01
-0.03
Time post-settling (min)
-5
0
5
10
15
20
25
30
B)
35S:GCAMP3 x tpc1-2 control
35S::GCAMP3 x tpc1-2 aphid
p<0.05
ΔF/F
Time post-settling (min)
C)
35S::GCAMP3 aphid
35S::GCAMP3 x tpc1-2 aphid
p<0.05
ΔF/F
Time post-settling (min)

<u>Figure D2:</u> Normalised GFP fluorescence (ΔF/F) in the midrib, systemic to the feeding site, in 35S::GCAMP3 and 35S::GCAMP3 x *tpc1-2* Arabidopsis upon *M. persicae* settling.

A) 35S::GCAMP3 control (no aphid treatment) vs aphid treatment. **B)** 35S::GCAMP3 x *tpc1-2* control (no aphid treatment) vs aphid treatment. **C)** 35S::GCAMP3 aphid treatment vs 35S::GCAMP3 x *tpc1-2* aphid treatment. Bars represent SEM (35S::GCAMP3 n=27, 35S::GCAMP3 x *tpc1-2* n=29). Grey shading indicates significant difference between treatments (Student's t-test within GLM at $p<0.05$). Experiment conceived and designed by T.V. and conducted by T.V. and J.C.

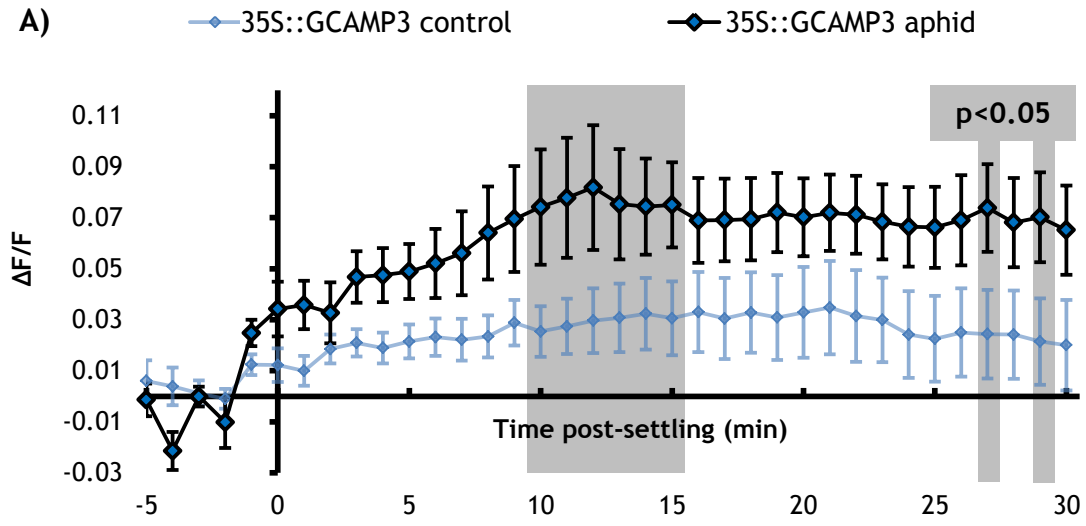
A)
35S::GCAMP3 control
35S::GCAMP3 aphid
p<0.05
ΔF/F
0.11
0.09
0.07
0.05
0.03
0.01
-0.01
-0.03
Time post-settling (min)
-5
0
5
10
15
20
25
30

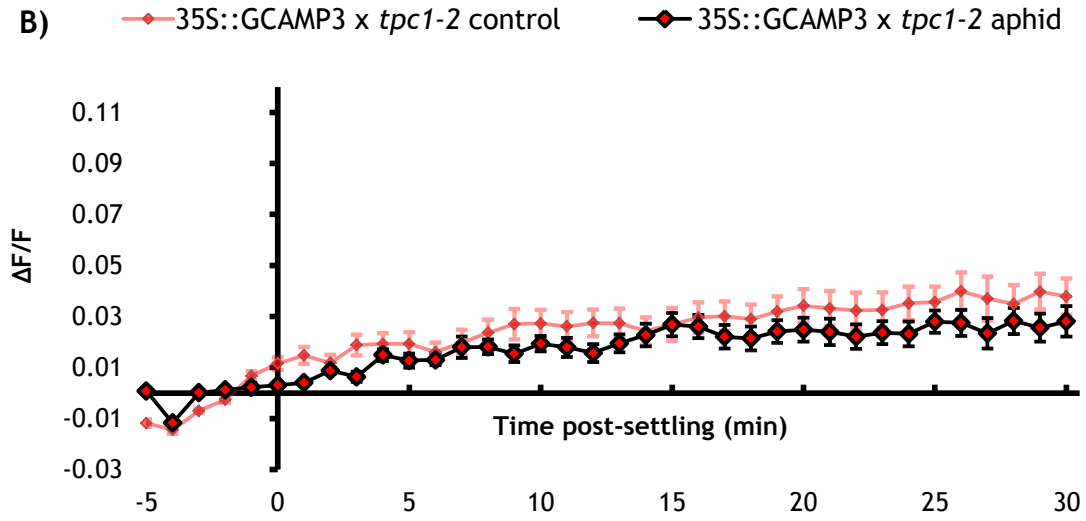
B)
35S::GCAMP3 x tpc1-2 control
35S::GCAMP3 x tpc1-2 aphid
ΔF/F
0.11
0.09
0.07
0.05
0.03
0.01
-0.01
-0.03
Time post-settling (min)
-5
0
5
10
15
20
25
30

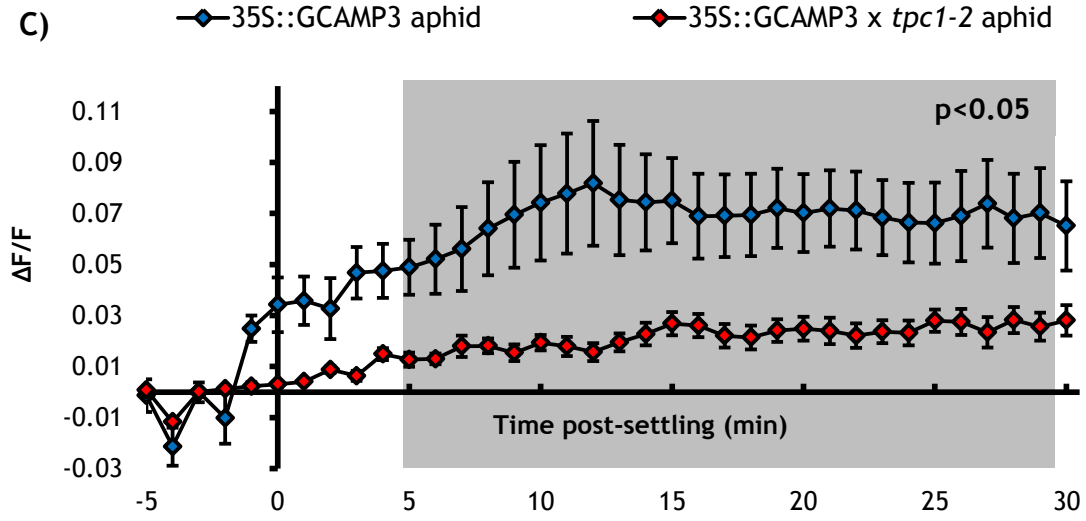
C)
35S::GCAMP3 aphid
35S::GCAMP3 x tpc1-2 aphid
p<0.05
ΔF/F
0.11
0.09
0.07
0.05
0.03
0.01
-0.01
-0.03
Time post-settling (min)
-5
0
5
10
15
20
25
30

<u>Figure D3:</u> Normalised GFP fluorescence (ΔF/F) in the lateral tissue, systemic to the feeding site, in 35S::GCAMP3 and 35S::GCAMP3 x *tpc1-2* Arabidopsis upon *M. persicae* settling.

A) 35S::GCAMP3 control (no aphid treatment) vs aphid treatment. **B)** 35S::GCAMP3 x *tpc1-2* control (no aphid treatment) vs aphid treatment. **C)** 35S::GCAMP3 aphid treatment vs 35S::GCAMP3 x *tpc1-2* aphid treatment. Bars represent SEM (35S::GCAMP3 n=27, 35S::GCAMP3 x *tpc1-2* n=29). Grey shading indicates significant difference between treatments (Student's t-test within GLM at $p<0.05$). Experiment conceived and designed by T.V. and conducted by T.V. and J.C.

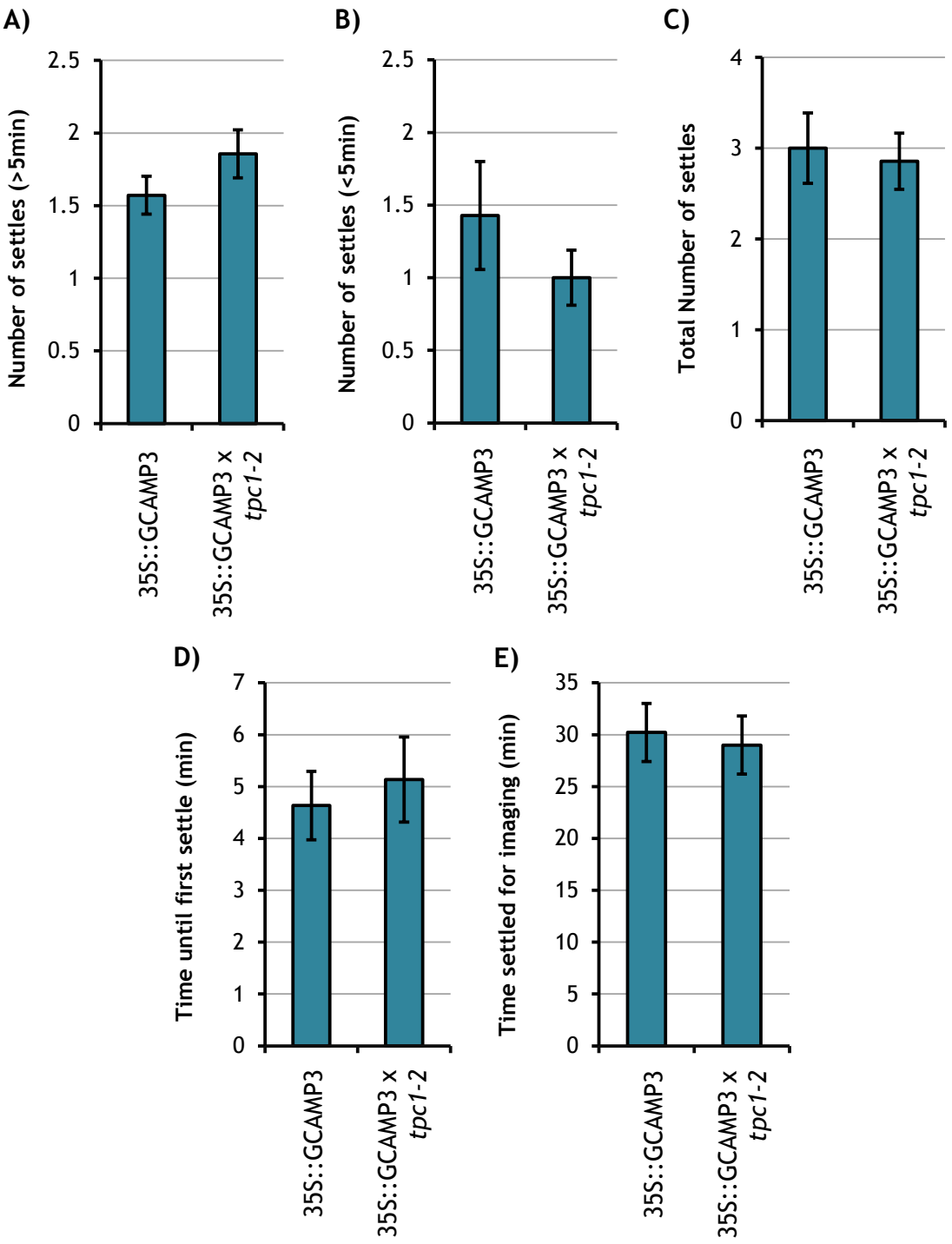

Figure D4: Settling behaviour of *M. persicae* on 35S::GCAMP3 and 35S::GCAMP3 x *tpc1-2* leaves.

A) Number of settles greater than 5 min in length. **B)** Number of settles less than 5 min in length. **C)** Total number of settles. **D)** Time before first settle that lasted over 5 min. **E)** Time aphid spent settled during a settling event used to measure GCAMP3 fluorescence. Bars represent SEM (35S::GCAMP3 n=28, 35S::GCAMP3 x *tpc1-2* n=29). Experiment conceived and designed by T.V. and conducted by T.V. and J.C.

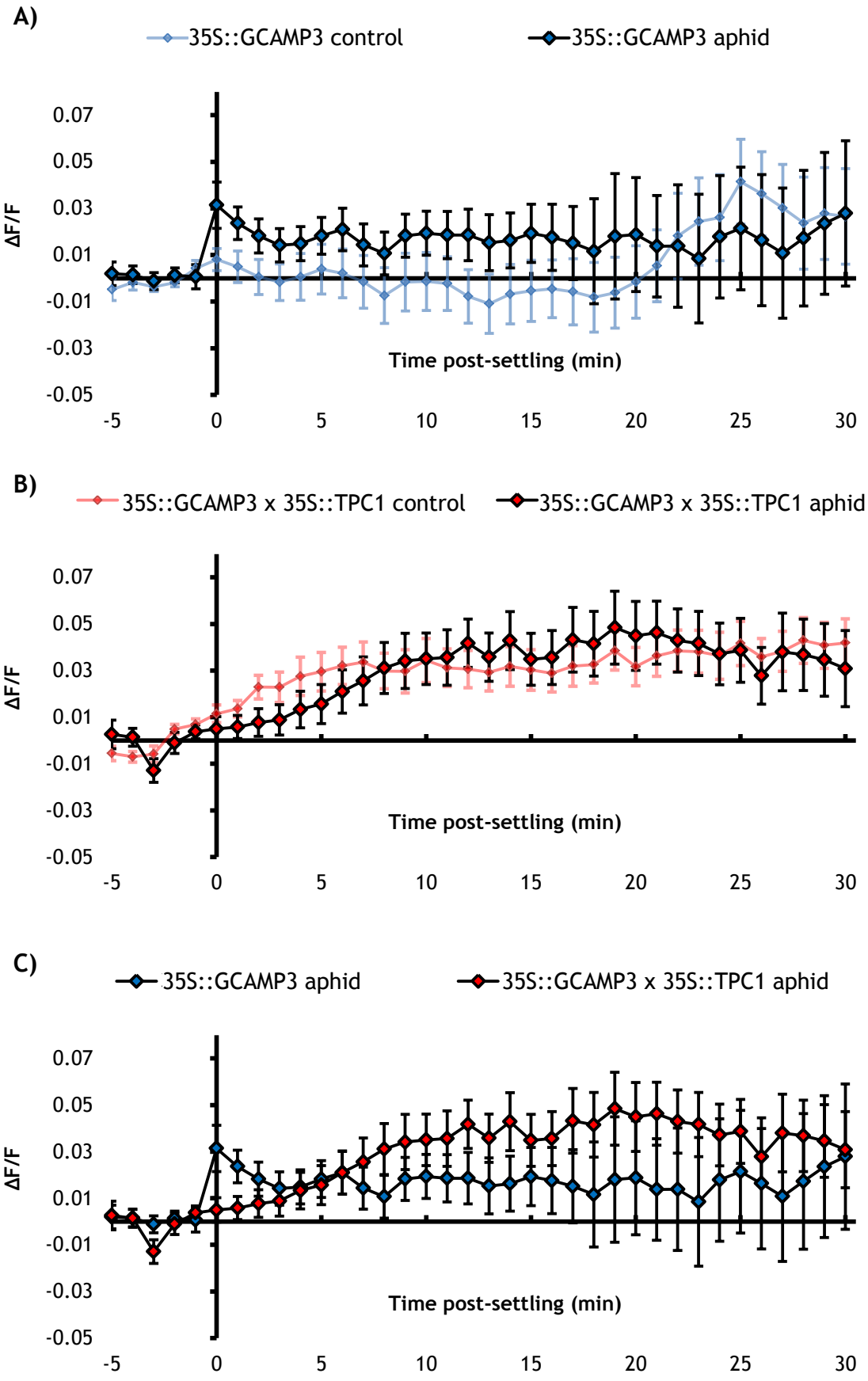
A)
35S::GCAMP3 control
35S::GCAMP3 aphid
ΔF/F
0.07
0.05
0.03
0.01
-0.01
-0.03
-0.05
Time post-settling (min)
-5
0
5
10
15
20
25
30
B)
35S::GCAMP3 x 35S::TPC1 control
35S::GCAMP3 x 35S::TPC1 aphid
ΔF/F
0.07
0.05
0.03
0.01
-0.01
-0.03
-0.05
Time post-settling (min)
-5
0
5
10
15
20
25
30
C)
35S::GCAMP3 aphid
35S::GCAMP3 x 35S::TPC1 aphid
ΔF/F
0.07
0.05
0.03
0.01
-0.01
-0.03
-0.05
Time post-settling (min)
-5
0
5
10
15
20
25
30

Figure D5: Normalised GFP fluorescence (ΔF/F) in the midrib, systemic to the feeding site, in 35S::GCAMP3 and 35S::GCAMP3 x 35S::TPC1 5.6 Arabidopsis upon *M. persicae* settling. **A)** 35S::GCAMP3 control (no aphid treatment) vs aphid treatment. **B)** 35S::GCAMP3 x 35S::TPC1 5.6 control (no aphid treatment) vs aphid treatment. **C)** 35S::GCAMP3 aphid treatment vs 35S::GCAMP3 x 35S::TPC1 5.6 aphid treatment. Bars represent SEM (35S::GCAMP3 n=30, 35S::GCAMP3 x 35S::TPC1 5.6 n=29). Experiment conceived and designed by T.V. and conducted by T.V. and M.A.

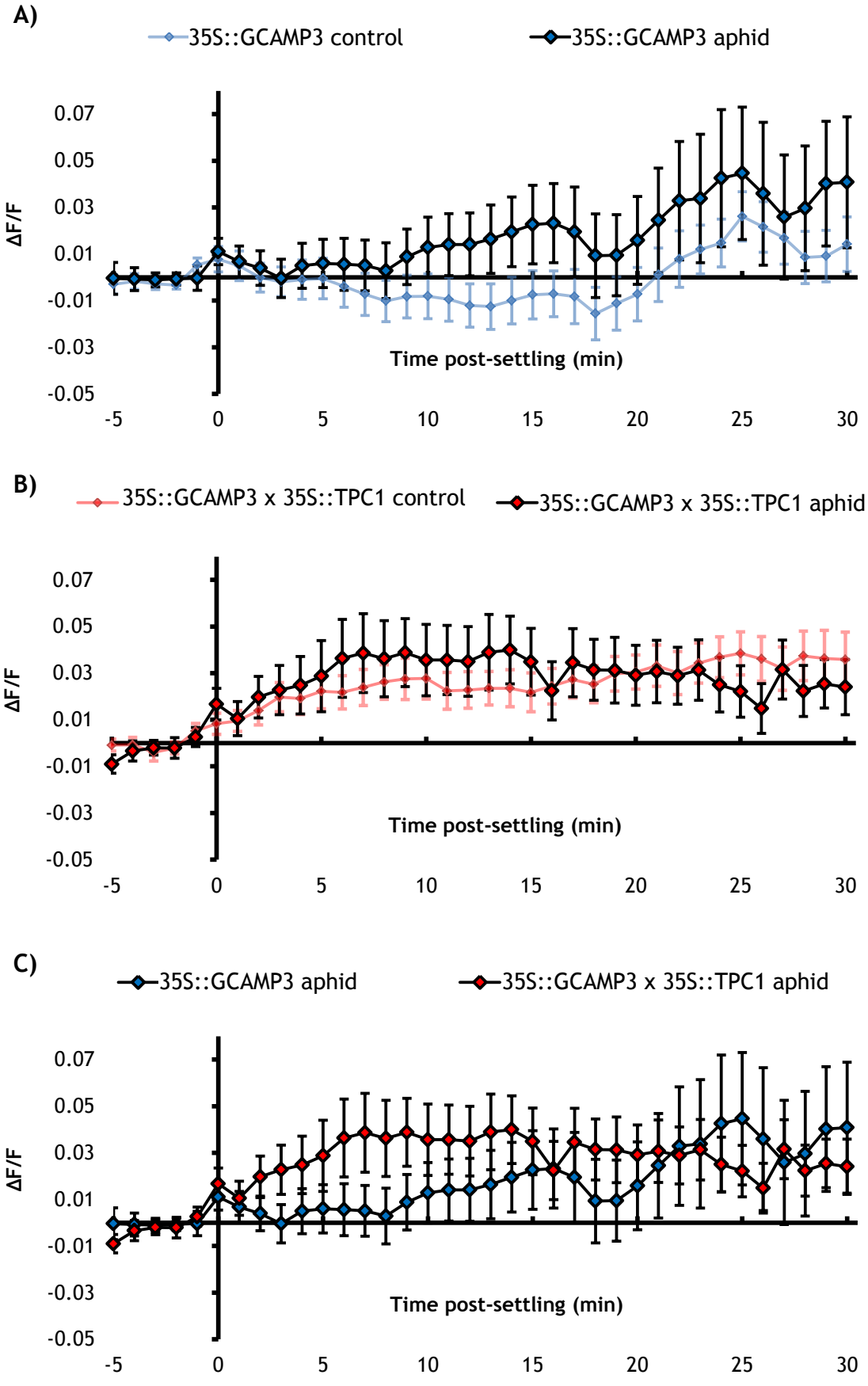
A)
35S::GCAMP3 control
35S::GCAMP3 aphid
ΔF/F
0.07
0.05
0.03
0.01
-0.01
-0.03
-0.05
Time post-settling (min)
-5
0
5
10
15
20
25
30
B)
35S::GCAMP3 x 35S::TPC1 control
35S::GCAMP3 x 35S::TPC1 aphid
ΔF/F
0.07
0.05
0.03
0.01
-0.01
-0.03
-0.05
Time post-settling (min)
-5
0
5
10
15
20
25
30
C)
35S::GCAMP3 aphid
35S::GCAMP3 x 35S::TPC1 aphid
ΔF/F
0.07
0.05
0.03
0.01
-0.01
-0.03
-0.05
Time post-settling (min)
-5
0
5
10
15
20
25
30

Figure D6: Normalised GFP fluorescence (ΔF/F) in the lateral tissue, systemic to the feeding site, in 35S::GCAMP3 and 35S::GCAMP3 x 35S::TPC1 5.6 Arabidopsis upon *M. persicae* settling.

A) 35S::GCAMP3 control (no aphid treatment) vs aphid treatment. **B)** 35S::GCAMP3 x 35S::TPC1 5.6 control (no aphid treatment) vs aphid treatment. **C)** 35S::GCAMP3 aphid treatment vs 35S::GCAMP3 x 35S::TPC1 5.6 aphid treatment. Bars represent SEM (35S::GCAMP3 n=30, 35S::GCAMP3 x 35S::TPC1 5.6 n=29). Experiment conceived and designed by T.V. and conducted by T.V. and M.A.

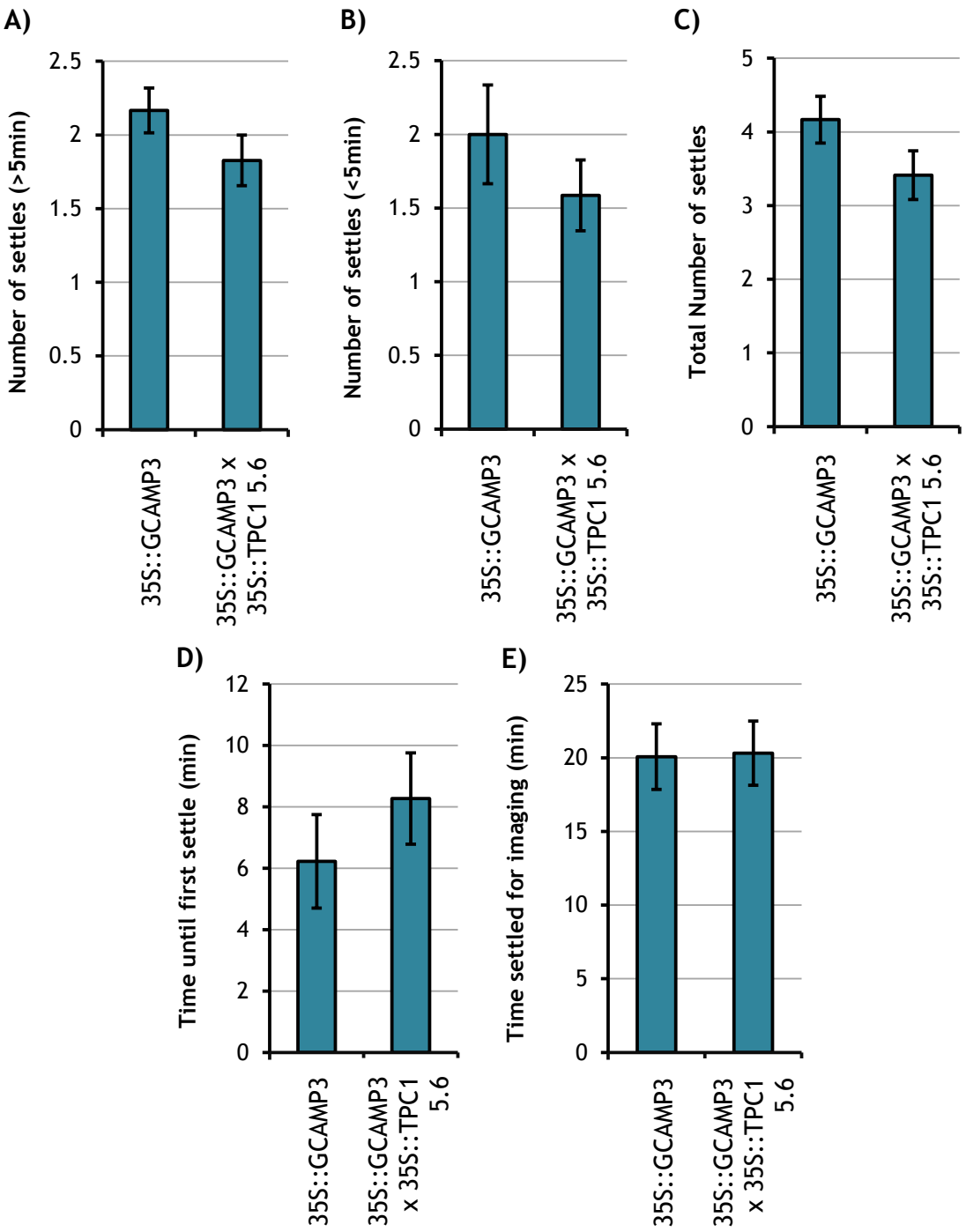

Figure D7: Settling behaviour of *M. persicae* on 35S::GCAMP3 and 35S::GCAMP3 x 35S::TPC1 5.6 leaves.

A) Number of settles greater than 5 min in length. **B)** Number of settles less than 5 min in length. **C)** Total number of settles. **D)** Time before first settle that lasted over 5 min. **E)** Time aphid spent settled during a settling event used to measure GCAMP3 fluorescence. Bars represent SEM (35S::GCAMP3 n=30, 35S::GCAMP3 x 35S::TPC1 5.6 n=29). Experiment conceived and designed by T.V. and conducted by T.V. and J.C.

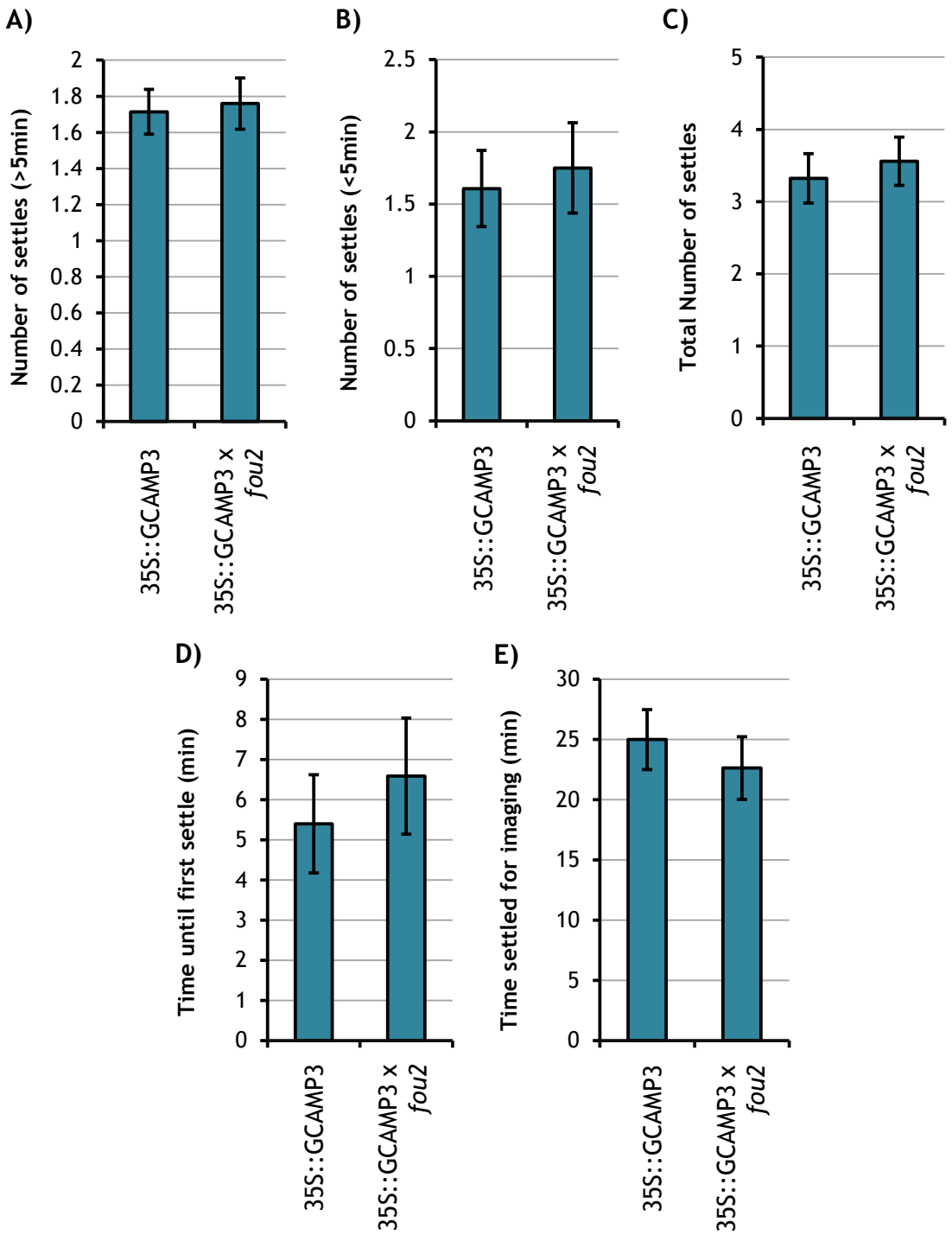

<u>Figure D8:</u> Settling behaviour of *M. persicae* on 35S::GCAMP3 and 35S::GCAMP3 x *fou2* leaves.

A) Number of settles greater than 5 min in length. **B)** Number of settles less than 5 min in length. **C)** Total number of settles. **D)** Time before first settle that lasted over 5 min. **E)** Time aphid spent settled during a settling event used to measure GCAMP3 fluorescence. Bars represent SEM (35S::GCAMP3 n=28, 35S::GCAMP3 x *fou2* n=26). Experiment conceived and designed by T.V. and conducted by T.V. and M.A.

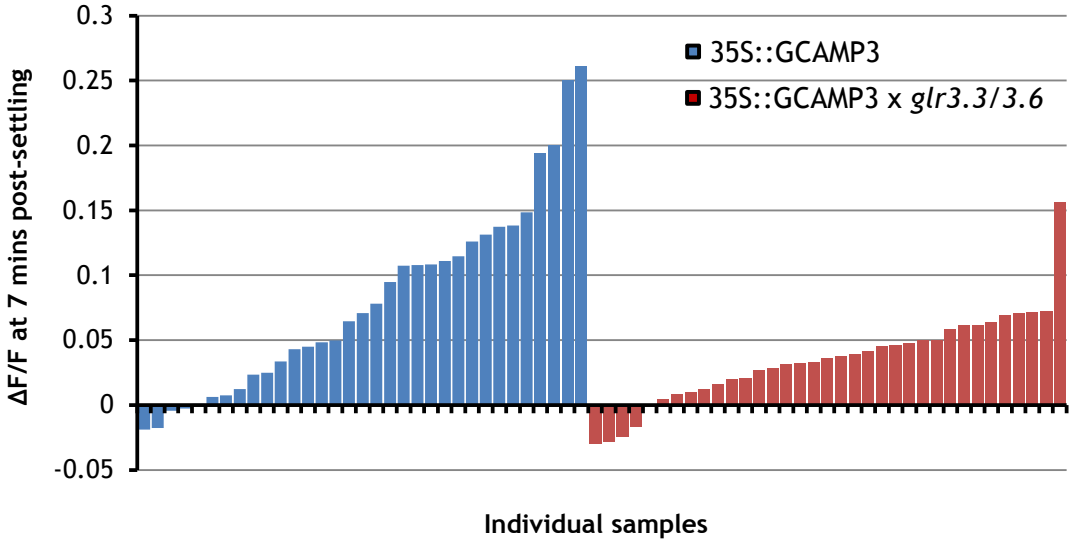

Figure D9: Normalised florescence (ΔF/F) around the *M. persicae* feeding site at 7 mins post-settling in 35S::GCAMP3 and 35S::GCAMP3 x *glr3.3/3.6* leaves.

Raw ΔF/F value for each leaf sample plotted. Experiment conceived and designed by T.V. and conducted by T.V. and M.A.

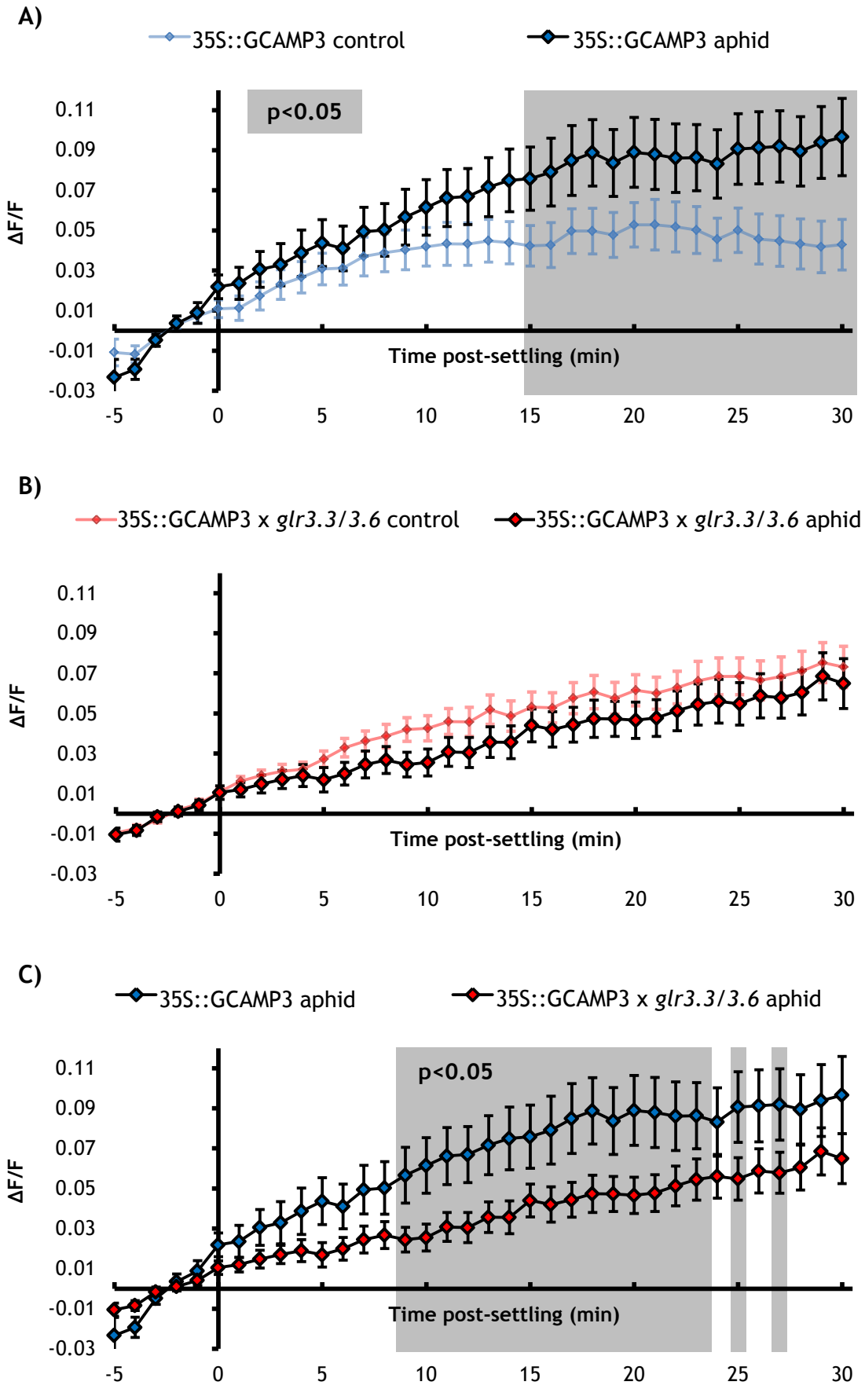
A)
35S::GCAMP3 control
35S::GCAMP3 aphid
p<0.05
ΔF/F
0.11
0.09
0.07
0.05
0.03
0.01
-0.01
-0.03
-5
0
5
10
15
20
25
30
Time post-settling (min)
B)
35S::GCAMP3 x glr3.3/3.6 control
35S::GCAMP3 x glr3.3/3.6 aphid
ΔF/F
Time post-settling (min)
C)
35S::GCAMP3 aphid
35S::GCAMP3 x glr3.3/3.6 aphid
p<0.05
ΔF/F
Time post-settling (min)

<u>Figure D10:</u> Normalised GFP fluorescence (ΔF/F) in the midrib, systemic to the feeding site, in 35S::GCAMP3 and 35S::GCAMP3 x *glr3.3/glr3.6* Arabidopsis upon *M. persicae* settling.

A) 35S::GCAMP3 control (no aphid treatment) vs aphid treatment. **B)** 35S::GCAMP3 x *glr3.3/glr3.6* control (no aphid treatment) vs aphid treatment. **C)** 35S::GCAMP3 aphid treatment vs 35S::GCAMP3 x *glr3.3/glr3.6* aphid treatment. Bars represent SEM (35S::GCAMP3 n=34, 35S::GCAMP3 x *glr3.3/glr3.6* n=37). Grey shading indicates significant difference between treatments (Student's t-test within GLM at $p<0.05$). Experiment conceived and designed by T.V. and conducted by T.V. and M.A.

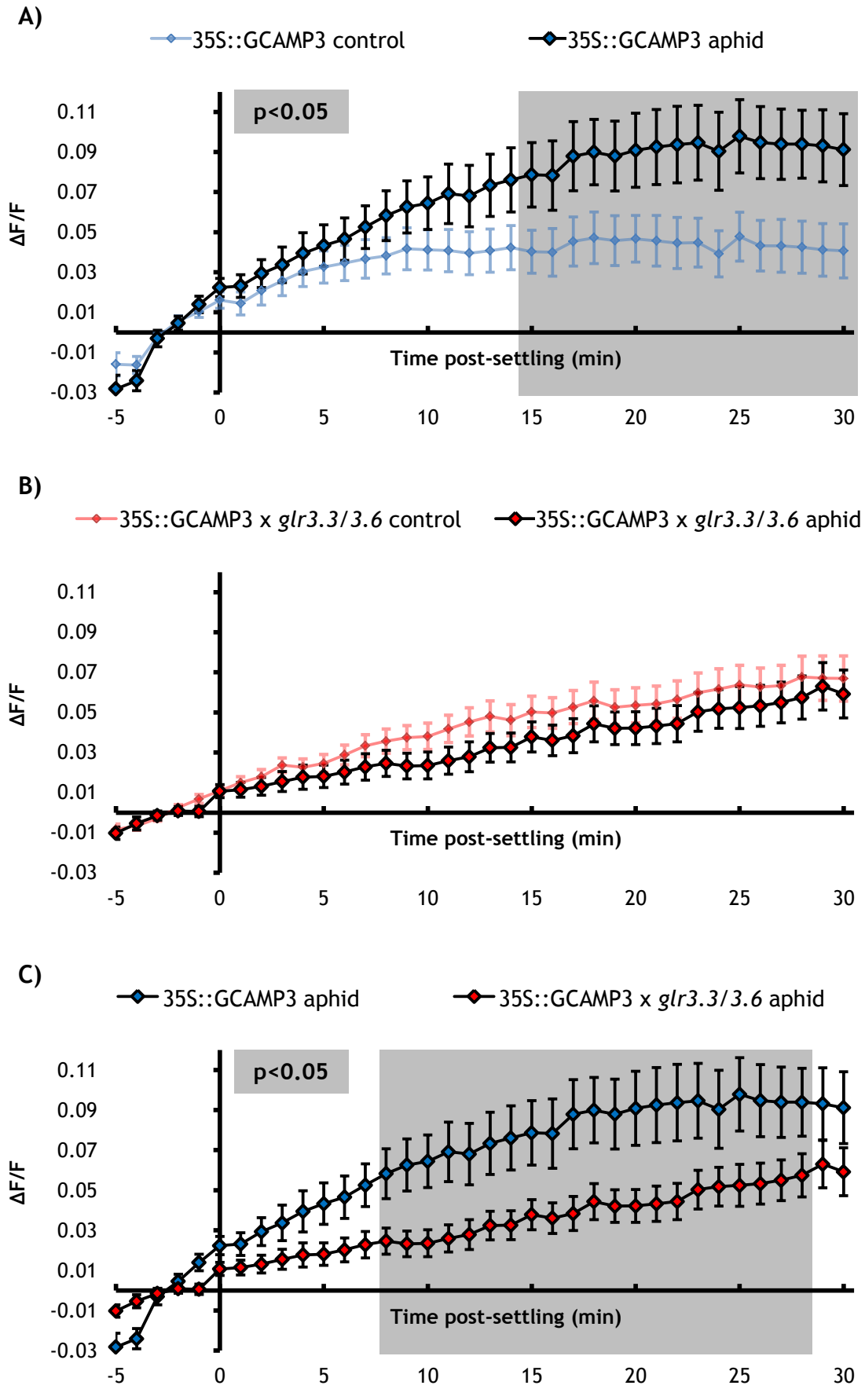
A)
35S::GCAMP3 control
35S::GCAMP3 aphid
p<0.05
ΔF/F
0.11
0.09
0.07
0.05
0.03
0.01
-0.01
-0.03
-5
0
5
10
15
20
25
30
Time post-settling (min)
B)
35S::GCAMP3 x glr3.3/3.6 control
35S::GCAMP3 x glr3.3/3.6 aphid
ΔF/F
Time post-settling (min)
C)
35S::GCAMP3 aphid
35S::GCAMP3 x glr3.3/3.6 aphid
p<0.05
ΔF/F
Time post-settling (min)

Figure D11: Normalised GFP fluorescence (ΔF/F) in the lateral tissue, systemic to the feeding site, in 35S::GCAMP3 and 35S::GCAMP3 x *glr3.3/glr3.6* Arabidopsis upon *M. persciae* settling.

A) 35S::GCAMP3 control (no aphid treatment) vs aphid treatment. **B)** 35S::GCAMP3 x *glr3.3/glr3.6* control (no aphid treatment) vs aphid treatment. **C)** 35S::GCAMP3 aphid treatment vs 35S::GCAMP3 x *glr3.3/glr3.6* aphid treatment. Bars represent SEM (35S::GCAMP3 n=34, 35S::GCAMP3 x *glr3.3/glr3.6* n=37). Grey shading indicates significant difference between treatments (Student's t-test within GLM at $p<0.05$). Experiment conceived and designed by T.V. and conducted by T.V. and M.A.

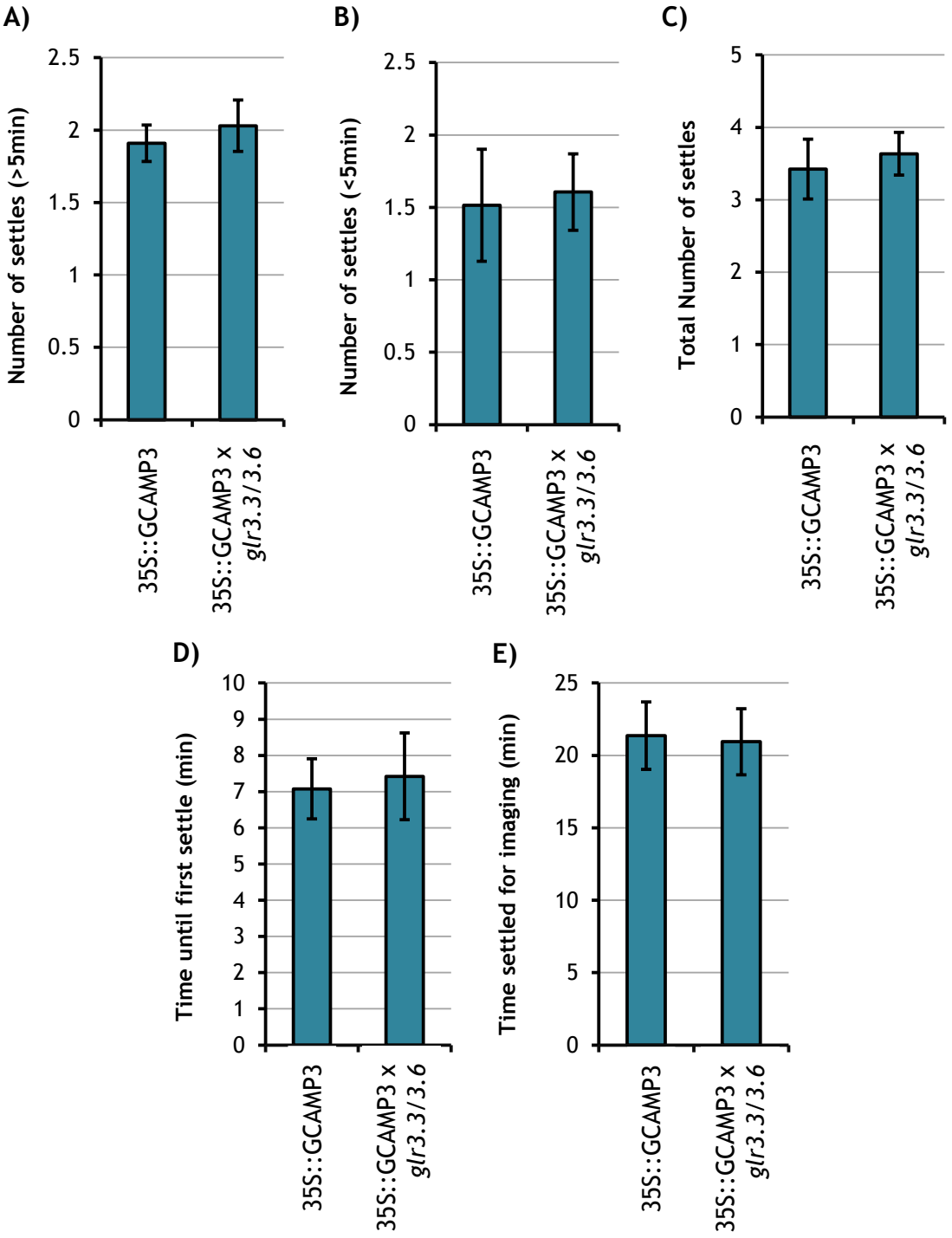

Figure D12: Settling behaviour of *M. persicae* on 35S::GCAMP3 and 35S::GCAMP3 x *glr3.3/3.6* leaves.

A) Number of settles greater than 5 min in length. **B)** Number of settles less than 5 min in length. **C)** Total number of settles. **D)** Time before first settle that lasted over 5 min. **E)** Time aphid spent settled during a settling event used to measure GCAMP3 fluorescence. Bars represent SEM (35S::GCAMP3 n=33, 35S::GCAMP3 x *glr3.3/3.6* n=33). Experiment conceived and designed by T.V. and conducted by T.V. and M.A.

Appendix E: Chapter 5 supplemental figures

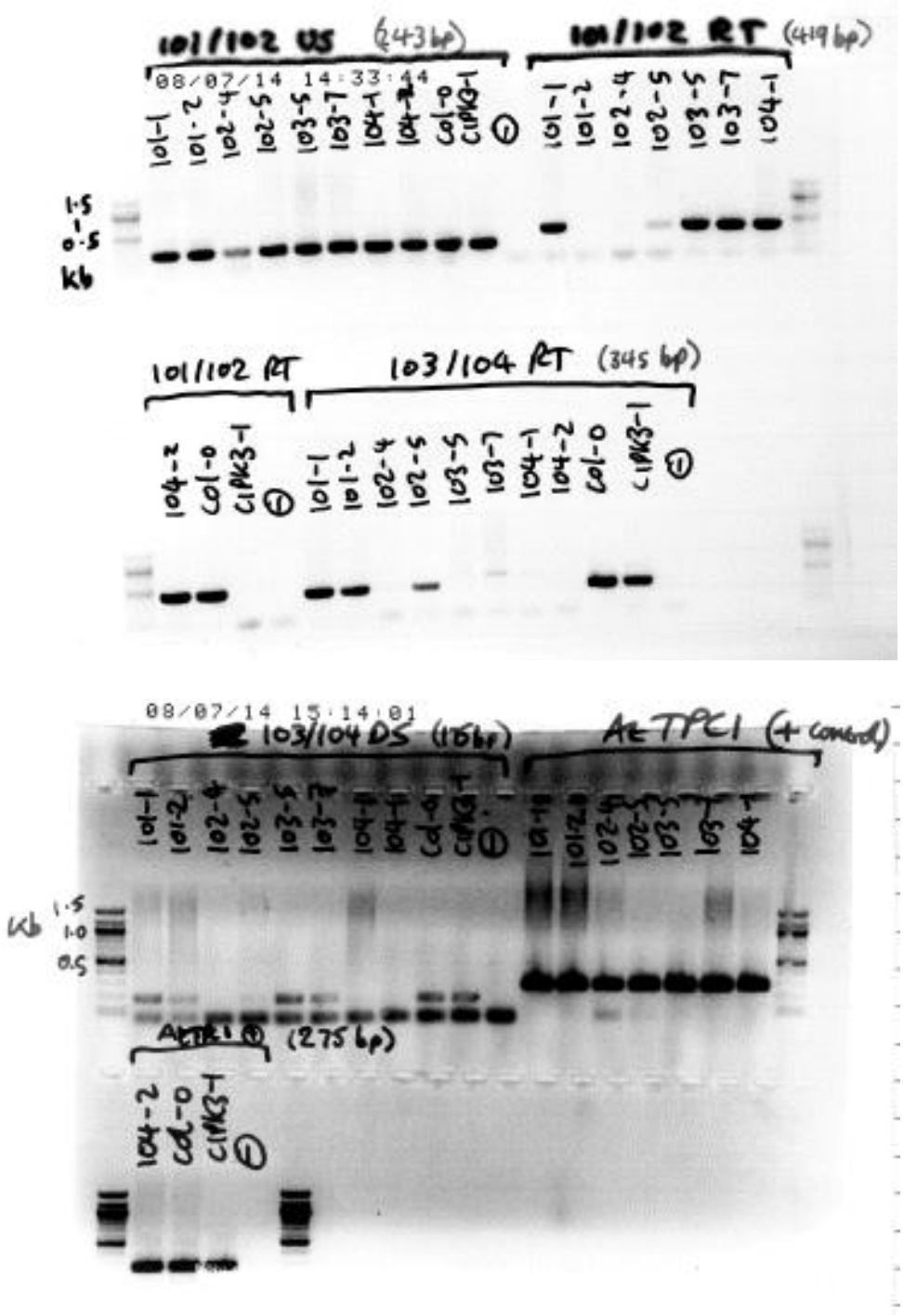

Figure E1: Full electrophoresis gel of *CIPK3* candidate mutant RT-PCR

PCR conducted using *CIPK3*-specific primers, and *TPC1* as a control gene (AtTPC1-F2 & R2, Table 2.4).

Bibliography

1. **Dodd AN, Kudla J, Sanders D**. (2010). The language of calcium signaling. *Annu Rev Plant Biol*; **61**:593-620.

2. **Sanders D, Pelloux J, Brownlee C, Harper JF**. (2002). Calcium at the crossroads of signaling. *Plant Cell*; **14**:S401-S17.

3. **Allen GJ, Chu SP, Harrington CL, Schumacher K, Hoffman T, Tang YY, et al.** (2001). A defined range of guard cell calcium oscillation parameters encodes stomatal movements. *Nature*; **411**:1053-7.

4. **Mcainsh MR, Webb AaR, Taylor JE, Hetherington AM**. (1995). Stimulus-induced oscillations in guard-cell cytosolic-free calcium. *Plant Cell*; **7**:1207-19.

5. **Allen GJ, Chu SP, Schumacher K, Shimazaki CT, Vafeados D, Kemper A, et al.** (2000). Alteration of stimulus-specific guard cell calcium oscillations and stomatal closing in Arabidopsis *det3* mutant. *Science*; **289**:2338-42.

6. **Kiegle E, Moore CA, Haseloff J, Tester MA, Knight MR**. (2000). Cell-type-specific calcium responses to drought, salt and cold in the Arabidopsis root. *Plant J*; **23**:267-78.

7. **Choi WG, Toyota M, Kim SH, Hilleary R, Gilroy S**. (2014). Salt stress-induced Ca^{2+} waves are associated with rapid, long-distance root-to-shoot signaling in plants. *Proc Natl Acad Sci U S A*.

8. **Kosuta S, Hazledine S, Sun J, Miwa H, Morris RJ, Downie JA, et al.** (2008). Differential and chaotic calcium signatures in the symbiosis signaling pathway of legumes. *P Natl Acad Sci USA*; **105**:9823-8.

9. **Logan DC, Knight MR**. (2003). Mitochondrial and cytosolic calcium dynamics are differentially regulated in plants. *Plant Physiol*; **133**:21-4.

10. **Johnson CH, Knight MR, Kondo T, Masson P, Sedbrook J, Haley A, et al.** (1995). Circadian oscillations of cytosolic and chloroplastic free calcium in plants. *Science*; **269**:1863-5.

11. **Johnson CH, Sai JQ, Knight MR, Olivari C, Kondo T, Masson P, et al.** (1997). Circadian oscillations of cytosolic and chloroplastic free calcium in transgenic luminous plants. *Plant Physiol*; **114**:1408-.

12. **Gilroy S, Fricker MD, Read ND, Trewavas AJ**. (1991). Role of calcium in signal transduction of commelina guard-cells. *Plant Cell*; **3**:333-44.

13. **Ng CKY, Mcainsh MR, Gray JE, Hunt L, Leckie CP, Mills L, et al.** (2001). Calcium-based signalling systems in guard cells. *New Phytol*; **151**:109-20.

14. **Baum G, Long JC, Jenkins GI, Trewavas AJ**. (1999). Stimulation of the blue light phototropic receptor NPH1 causes a transient increase in cytosolic Ca^{2+}. *P Natl Acad Sci USA*; **96**:13554-9.

15. **Peiter E, Maathuis FJM, Mills LN, Knight H, Pelloux J, Hetherington AM, et al.** (2005). The vacuolar Ca^{2+}-activated channel TPC1 regulates germination and stomatal movement. *Nature*; **434**:404-8.

16. **Muir SR, Sanders D**. (1997). Inositol 1,4,5-trisphosphate-sensitive Ca^{2+} release across nonvacuolar membranes in cauliflower. *Plant Physiol*; **114**:1511-21.

17. **Lecourieux D, Lamotte O, Bourque S, Wendehenne D, Mazars C, Ranjeva R, et al.** (2005). Proteinaceous and oligosaccharidic elicitors induce different calcium signatures in the nucleus of tobacco cells. *Cell Calcium*; **38**:527-38.

18. **Tracy FE, Gilliham M, Dodd AN, Webb AaR, Tester M**. (2008). NaCl-induced changes in cytosolic free Ca^{2+} in *Arabidopsis thaliana* are heterogeneous and modified by external ionic composition. *Plant Cell Environ*; **31**:1063-73.

19. **Mcainsh MR, Pittman JK**. (2009). Shaping the calcium signature. *New Phytol*; **181**:275-94.

20. **Toyoshima C, Nakasako M, Nomura H, Ogawa H**. (2000). Crystal structure of the calcium pump of sarcoplasmic reticulum at 2.6 angstrom resolution. *Nature*; **405**:647-55.

21. **Boursiac Y, Harper JF**. (2007). The origin and function of calmodulin regulated Ca^{2+} pumps in plants. *J Bioenerg Biomembr*; **39**:409-14.

22. **Hsieh WL, Pierce WS, Sze H**. (1991). Calcium-pumping atpases in vesicles from carrot cells - stimulation by calmodulin or phosphatidylserine, and formation of a 120 kilodalton phosphoenzyme. *Plant Physiol*; **97**:1535-44.

23. **Baxter I, Tchieu J, Sussman MR, Boutry M, Palmgren MG, Gribskov M, et al.** (2003). Genomic comparison of P-type ATPase ion pumps in Arabidopsis and rice. *Plant Physiol*; **132**:618-28.

24. **Hong BM, Ichida A, Wang YW, Gens JS, Pickard BC, Harper JF**. (1999). Identification of a calmodulin-regulated Ca^{2+}-ATPase in the endoplasmic reticulum. *Plant Physiol*; **119**:1165-75.

25. **Bonza MC, Morandini P, Luoni L, Geisler M, Palmgren MG, De Michelis MI**. (2000). At-ACA8 encodes a plasma membrane-localized calcium-ATPase of Arabidopsis with a calmodulin-binding domain at the N terminus. *Plant Physiol*; **123**:1495-505.

26. **Harper JF, Hong BM, Hwang ID, Guo HQ, Stoddard R, Huang JF, et al.** (1998). A novel calmodulin-regulated Ca^{2+}-ATPase (ACA2) from Arabidopsis with an N-terminal autoinhibitory domain. *J Biol Chem*; **273**:1099-106.

27. **Geisler M, Frangne N, Gomes E, Martinoia E, Palmgren MG**. (2000). The ACA4 gene of arabidopsis encodes a vacuolar membrane calcium pump that improves salt tolerance in yeast. *Plant Physiol*; **124**:1814-27.

28. **Wu ZY, Liang F, Hong BM, Young JC, Sussman MR, Harper JF, et al.** (2002). An endoplasmic reticulum-bound Ca^{2+}/Mn^{2+} pump, ECA1, supports plant growth and confers tolerance to Mn^{2+} stress. *Plant Physiol*; **130**:128-37.

29. **Li XY, Chanroj S, Wu ZY, Romanowsky SM, Harper JF, Sze H**. (2008). A distinct endosomal Ca^{2+}/Mn^{2+} pump affects root growth through the secretory process. *Plant Physiol*; **147**:1675-89.

30. **Mills RF, Doherty ML, Lopez-Marques RL, Weimar T, Dupree P, Palmgren MG, et al.** (2008). ECA3, a Golgi-localized P-2A-type ATPase, plays a crucial role in manganese nutrition in Arabidopsis. *Plant Physiol*; **146**:116-28.

31. **Schiott M, Palmgren MG**. (2005). Two plant Ca^{2+} pumps expressed in stomatal guard cells show opposite expression patterns during cold stress. *Physiol Plant*; **124**:278-83.

32. **Cerana M, Bonza MC, Harris R, Sanders D, De Michelis MI**. (2006). Abscisic acid stimulates the expression of two isoforms of plasma membrane Ca^{2+}-ATPase in Arabidopsis thaliana seedlings. *Plant Biol*; **8**:572-8.

33. **Wang F, Chen Z-H, Liu X, Colmer TD, Zhou M, Shabala S**. (2016). Tissue-specific root ion profiling reveals essential roles of the CAX and ACA calcium transport systems in response to hypoxia in Arabidopsis. *J Exp Bot*; **67**:3747-62.

34. **Bartsch M, Gobbato E, Bednarek P, Debey S, Schultze JL, Bautor J, et al.** (2006). Salicylic acid-independent ENHANCED DISEASE SUSCEPTIBILITY1 signaling in Arabidopsis immunity and cell death is regulated by the monooxygenase FMO1 and the nudix hydrolase NUDT7. *Plant Cell*; **18**:1038-51.

35. **Sze H, Liang F, Hwang I, Curran AC, Harper JF**. (2000). Diversity and regulation of plant Ca2+ pumps: insights from expression in yeast. *Annu Rev Plant Physiol Plant Mol Biol*; **51**:433-62.

36. **Hirschi KD, Zhen RG, Cunningham KW, Rea PA, Fink GR**. (1996). CAX1, an H^+/Ca^{2+} antiporter from Arabidopsis. *P Natl Acad Sci USA*; **93**:8782-6.

37. **Manohar M, Shigaki T, Hirschi KD**. (2011). Plant cation/H^+ exchangers (CAXs): biological functions and genetic manipulations. *Plant Biol*; **13**:561-9.

38. **Shigaki T, Hirschi KD**. (2006). Diverse functions and molecular properties emerging for CAX cation/H^+ exchangers in plants. *Plant Biol*; **8**:419-29.

39. **Pittman JK, Sreevidya CS, Shigaki T, Ueoka-Nakanishi H, Hirschi KD**. (2002). Distinct N-terminal regulatory domains of Ca^{2+}/H^+ antiporters. *Plant Physiol*; **130**:1054-62.

40. **Pittman JK, Shigaki T, Marshall JL, Morris JL, Cheng NH, Hirschi KD**. (2004). Functional and regulatory analysis of the *Arabidopsis thaliana* CAX2 cation transporter. *Plant Mol Biol*; **56**:959-71.

41. **Cheng NH, Hirschi KD**. (2003). Cloning and characterization of CXIP1, a novel PICOT domain-containing Arabidopsis protein that associates with CAX1. *J Biol Chem*; **278**:6503-9.

42. **Catala R, Santos E, Alonso JM, Ecker JR, Martinez-Zapater JM, Salinas J**. (2003). Mutations in the $Ca^{2+}/^{H+}$ transporter CAX1 increase CBF/DREB1 expression and the cold-acclimation response in Arabidopsis. *Plant Cell*; **15**:2940-51.

43. **Hirschi KD**. (1999). Expression of Arabidopsis CAX1 in tobacco: altered calcium homeostasis and increased stress sensitivity. *Plant Cell*; **11**:2113-22.

44. **Shigaki T, Hirschi K**. (2000). Characterization of CAX-like genes in plants: implications for functional diversity. *Gene*; **257**:291-8.

45. **Cheng NH, Pittman JK, Barkla BJ, Shigaki T, Hirschi KD**. (2003). The Arabidopsis *cax1* mutant exhibits impaired ion homeostasis, development, and hormonal responses and reveals interplay among vacuolar transporters. *Plant Cell*; **15**:347-64.

46. **Gelli A, Blumwald E**. (1997). Hyperpolarization-activated Ca^{2+}-permeable channels in the plasma membrane of tomato cells. *J Membr Biol*; **155**:35-45.

47. **Pei ZM, Murata Y, Benning G, Thomine S, Klusener B, Allen GJ, et al.** (2000). Calcium channels activated by hydrogen peroxide mediate abscisic acid signalling in guard cells. *Nature*; **406**:731-4.

48. **Grabov A, Blatt MR**. (1998). Membrane voltage initiates Ca^{2+} waves and potentiates Ca^{2+} increases with abscisic acid in stomatal guard cells. *P Natl Acad Sci USA*; **95**:4778-83.

49. **Thion L, Mazars C, Thuleau P, Graziana A, Rossignol M, Moreau M, et al.** (1996). Activation of plasma membrane voltage-dependent calcium-permeable channels by disruption of microtubules in carrot cells. *FEBS Lett*; **393**:13-8.

50. **Kiegle E, Gilliham M, Haseloff J, Tester M**. (2000). Hyperpolarisation-activated calcium currents found only in cells from the elongation zone of *Arabidopsis thaliana* roots. *Plant J*; **21**:225-9.

51. **Swarbreck SM, Colaco R, Davies JM**. (2013). Plant calcium-permeable channels. *Plant Physiol*; **163**:514-22.

52. **White PJ**. (2000). Calcium channels in higher plants. *Bba-Biomembranes*; **1465**:171-89.

53. **Maathuis FJM, Sanders D**. (2001). Sodium uptake in Arabidopsis roots is regulated by cyclic nucleotides. *Plant Physiol*; **127**:1617-25.

54. **Zimmermann S, Nurnberger T, Frachisse JM, Wirtz W, Guern J, Hedrich R, et al.** (1997). Receptor-mediated activation of a plant Ca^{2+}-permeable ion channel involved in pathogen defense. *P Natl Acad Sci USA*; **94**:2751-5.

55. **Chiu J, Desalle R, Lam HM, Meisel L, Coruzzi G**. (1999). Molecular evolution of glutamate receptors: A primitive signaling mechanism that existed before plants and animals diverged. *Mol Biol Evol*; **16**:826-38.

56. **Schuurink RC, Shartzer SF, Fath A, Jones RL**. (1998). Characterization of a calmodulin-binding transporter from the plasma membrane of barley aleurone. *P Natl Acad Sci USA*; **95**:1944-9.

57. **Maser P, Thomine S, Schroeder JI, Ward JM, Hirschi K, Sze H, et al.** (2001). Phylogenetic relationships within cation transporter families of Arabidopsis. *Plant Physiol*; **126**:1646-67.

58. **Arazi T, Kaplan B, Fromm H**. (2000). A high-affinity calmodulin-binding site in a tobacco plasma-membrane channel protein coincides with a characteristic element of cyclic nucleotide-binding domains. *Plant Mol Biol*; **42**:591-601.

59. **Gobert A, Park G, Amtmann A, Sanders D, Maathuis FJM**. (2006). *Arabidopsis thaliana* cyclic nucleotide gated channel 3 forms a non-selective ion transporter involved in germination and cation transport. *J Exp Bot*; **57**:791-800.

60. **Urquhart W, Gunawardena AHLaN, Moeder W, Ali R, Berkowitz GA, Yoshioka K**. (2007). The chimeric cyclic nucleotide-gated ion channel ATCNGC11/12 constitutively induces programmed cell death in a Ca^{2+} dependent manner. *Plant Mol Biol*; **65**:747-61.

61. **Tunc-Ozdemir M, Rato C, Brown E, Rogers S, Mooneyham A, Frietsch S, et al.** (2013). Cyclic nucleotide gated channels 7 and 8 are essential for male reproductive fertility. *Plos One*; **8**.

62. **Chang F, Yan A, Zhao LN, Wu WH, Yang ZB**. (2007). A putative calcium-permeable cyclic nucleotide-gated channel, CNGC18, regulates polarized pollen tube growth. *J Integr Plant Biol*; **49**:1261-70.

63. **Yuen CCY, Christopher DA**. (2013). The group IV-A cyclic nucleotide-gated channels, CNGC19 and CNGC20, localize to the vacuole membrane in *Arabidopsis thaliana*. *Aob Plants*; **5**.

64. **Charpentier M, Sun JH, Martins TV, Radhakrishnan GV, Findlay K, Soumpourou E, et al.** (2016). Nuclear-localized cyclic nucleotide-gated channels mediate symbiotic calcium oscillations. *Science*; **352**:1102-5.

65. **Leng Q, Mercier RW, Yao WZ, Berkowitz GA**. (1999). Cloning and first functional characterization of a plant cyclic nucleotide-gated cation channel. *Plant Physiol*; **121**:753-61.

66. **Balague C, Lin BQ, Alcon C, Flottes G, Malmstrom S, Kohler C, et al.** (2003). HLM1, an essential signaling component in the hypersensitive response, is a member of the cyclic nucleotide-gated channel ion channel family. *Plant Cell*; **15**:365-79.

67. **Leng Q, Mercier RW, Hua BG, Fromm H, Berkowitz GA**. (2002). Electrophysiological analysis of cloned cyclic nucleotide-gated ion channels. *Plant Physiol*; **128**:400-10.

68. **Zagotta WN, Siegelbaum SA**. (1996). Structure and function of cyclic nucleotide-gated channels. *Annu Rev Neurosci*; **19**:235-63.

69. **Craven KB, Zagotta WN**. (2006). CNG and HCN channels: two peas, one pod. *Annu Rev Physiol*; **68**:375-401.

70. **Gao F, Han XW, Wu JH, Zheng SZ, Shang ZL, Sun DY, et al.** (2012). A heat-activated calcium-permeable channel - Arabidopsis cyclic nucleotide-gated ion channel 6 - is involved in heat shock responses. *Plant J*; **70**:1056-69.

71. **Kingston EE, Beynon JH, Newton RP**. (1984). The identification of cyclic-nucleotides from living systems using collision-induced dissociation of ions generated by fast atom bombardment mass-spectrometry. *Biomed Mass Spectrom*; **11**:367-74.

72. **Richards H, Das S, Smith CJ, Pereira L, Geisbrecht A, Devitt NJ, et al.** (2002). Cyclic nucleotide content of tobacco BY-2 cells. *Phytochemistry*; **61**:531-7.

73. **Ludidi N, Gehring C**. (2003). Identification of a novel protein with guanylyl cyclase activity in *Arabidopsis thaliana*. *J Biol Chem*; **278**:6490-4.

74. **Kwezi L, Meier S, Mungur L, Ruzvidzo O, Irving H, Gehring C**. (2007). The *Arabidopsis thaliana* brassinosteroid receptor (AtBRI1) contains a domain that functions as a guanylyl cyclase *in vitro*. *Plos One*; **2**.

75. **Chin K, Moeder W, Yoshioka K**. (2009). Biological roles of cyclic-nucleotide-gated ion channels in plants: what we know and don't know about this 20 member ion channel family. *Botany*; **87**:668-77.

76. **Dietrich P, Anschutz U, Kugler A, Becker D**. (2010). Physiology and biophysics of plant ligand-gated ion channels. *Plant Biol*; **12**:80-93.

77. **Sunkar R, Kaplan B, Bouche N, Arazi T, Dolev D, Talke IN, et al.** (2000). Expression of a truncated tobacco NtCBP4 channel in transgenic plants and disruption of the homologous Arabidopsis CNGC1 gene confer Pb^{2+} tolerance. *Plant J*; **24**:533-42.

78. **Guo KM, Babourina O, Christopher DA, Borsics T, Rengel Z**. (2008). The cyclic nucleotide-gated channel, AtCNGC10, influences salt tolerance in Arabidopsis. *Physiol Plant*; **134**:499-507.

79. **Clough SJ, Fengler KA, Yu IC, Lippok B, Smith RK, Bent AF**. (2000). The Arabidopsis *dnd1* "defense, no death" gene encodes a mutated cyclic nucleotide-gated ion channel. *P Natl Acad Sci USA*; **97**:9323-8.

80. **Frietsch S, Wang YF, Sladek C, Poulsen LR, Romanowsky SM, Schroeder JI, et al.** (2007). A cyclic nucleotide-gated channel is essential for polarized tip growth of pollen. *P Natl Acad Sci USA*; **104**:14531-6.

81. **Kugler A, Kohler B, Palme K, Wolff P, Dietrich P**. (2009). Salt-dependent regulation of a CNG channel subfamily in Arabidopsis. *BMC Plant Biol*; **9**.

82. **Borsics T, Webb D, Andeme-Ondzighi C, Staehelin LA, Christopher DA**. (2007). The cyclic nucleotide-gated calmodulin-binding channel AtCNGC10 localizes to the plasma membrane and influences numerous growth responses and starch accumulation in *Arabidopsis thaliana*. *Planta*; **225**:563-73.

83. **Christopher DA, Borsics T, Yuen CYL, Ullmer W, Andeme-Ondzighi C, Andres MA, et al.** (2007). The cyclic nucleotide gated cation channel AtCNGC10 traffics from the ER via Golgi vesicles to the plasma membrane of Arabidopsis root and leaf cells. *BMC Plant Biol*; **7**.

84. **Lu M, Zhang YY, Tang SK, Pan JB, Yu YK, Han J, et al.** (2016). AtCNGC2 is involved in jasmonic acid-induced calcium mobilization. *J Exp Bot*; **67**:809-19.

85. **Dingledine R, Borges K, Bowie D, Traynelis SF**. (1999). The glutamate receptor ion channels. *Pharmacol Rev*; **51**:7-61.

86. **Lacombe B, Becker D, Hedrich R, Desalle R, Hollmann M, Kwak JM, et al.** (2001). The identity of plant glutamate receptors. *Science*; **292**:1486-7.

87. **Turano FJ, Muhitch MJ, Felker FC, Mcmahon MB**. (2002). The putative glutamate receptor 3.2 from *Arabidopsis thaliana* (AtGLR3.2) is an integral membrane peptide that accumulates in rapidly growing tissues and persists in vascular-associated tissues. *Plant Sci*; **163**:43-51.

88. **Vincill ED, Bieck AM, Spalding EP**. (2012). Ca^{2+} conduction by an amino acid-gated ion channel related to glutamate receptors. *Plant Physiol*; **159**:40-6.

89. **Vincill ED, Clarin AE, Molenda JN, Spalding EP**. (2013). Interacting glutamate receptor-like proteins in phloem regulate lateral root initiation in Arabidopsis. *Plant Cell*; **25**:1304-13.

90. **Price MB, Kong D, Okumoto S**. (2013). Inter-subunit interactions between glutamate-like receptors in Arabidopsis. *Plant signaling & behavior*; **8**:e27034.

91. **Roy SJ, Gilliham M, Berger B, Essah PA, Cheffings C, Miller AJ, et al.** (2008). Investigating glutamate receptor-like gene co-expression in *Arabidopsis thaliana*. *Plant Cell Environ*; **31**:861-71.

92. **Weiland M, Mancuso S, Baluska F**. (2016). Signalling via glutamate and GLRs in *Arabidopsis thaliana*. *Funct Plant Biol*; **43**:1-25.

93. **Chiu JC, Brenner ED, Desalle R, Nitabach MN, Holmes TC, Coruzzi GM**. (2002). Phylogenetic and expression analysis of the glutamate-receptor-like gene family in *Arabidopsis thaliana*. *Mol Biol Evol*; **19**:1066-82.

94. **Nagata T, Iizumi S, Satoh K, Ooka H, Kawai J, Carninci P, et al.** (2004). Comparative analysis of plant and animal calcium signal transduction element using plant full-length cDNA data. *Mol Biol Evol*; **21**:1855-70.

95. **Tapken D, Hollmann M**. (2008). *Arabidopsis thaliana* glutamate receptor ion channel function demonstrated by ion pore transplantation. *J Mol Biol*; **383**:36-48.

96. **Ni J, Yu Z, Du G, Zhang Y, Taylor JL, Shen C, et al.** (2016). Heterologous expression and functional analysis of rice GLUTAMATE RECEPTOR-LIKE family indicates its role in glutamate triggered calcium flux in rice roots. *Rice*; **9**:(8 March 2016).

97. **Qi Z, Stephens NR, Spalding EP**. (2006). Calcium entry mediated by GLR3.3, an Arabidopsis glutamate receptor with a broad agonist profile. *Plant Physiol*; **142**:963-71.

98. **Forde BG, Lea PJ**. (2007). Glutamate in plants: metabolism, regulation, and signalling. *J Exp Bot*; **58**:2339-58.

99. **Stephens NR, Qi Z, Spalding EP**. (2008). Glutamate receptor subtypes evidenced by differences in desensitization and dependence on the GLR3.3 and GLR3.4 genes. *Plant Physiol*; **146**:529-38.

100. **Meyerhoff O, Muller K, Roelfsema MR, Latz A, Lacombe B, Hedrich R, et al.** (2005). AtGLR3.4, a glutamate receptor channel-like gene is sensitive to touch and cold. *Planta*; **222**:418-27.

101. **Kang JM, Turano FJ**. (2003). The putative glutamate receptor 1.1 (AtGLR1.1) functions as a regulator of carbon and nitrogen metabolism in *Arabidopsis thaliana*. *P Natl Acad Sci USA*; **100**:6872-7.

102. **Kang JM, Mehta S, Turano FJ**. (2004). The putative glutamate receptor 1.1 (AtGLR1.1) in *Arabidopsis thaliana* regulates abscisic acid biosynthesis and signaling to control development and water loss. *Plant Cell Physiol*; **45**:1380-9.

103. **Mousavi SA, Chauvin A, Pascaud F, Kellenberger S, Farmer EE**. (2013). GLUTAMATE RECEPTOR-LIKE genes mediate leaf-to-leaf wound signalling. *Nature*; **500**:422-6.

104. **Salvador-Recatala V**. (2016). New roles for the GLUTAMATE RECEPTOR-LIKE 3.3, 3.5, and 3.6 genes as on/off switches of wound-induced systemic electrical signals. *Plant signaling & behavior*; **11**:e1161879.

105. **Lam HM, Chiu J, Hsieh MH, Meisel L, Oliveira IC, Shin M, et al.** (1998). Glutamate-receptor genes in plants. *Nature*; **396**:125-6.

106. **Stael S, Wurzinger B, Mair A, Mehlmer N, Vothknecht UC, Teige M**. (2012). Plant organellar calcium signalling: an emerging field. *J Exp Bot*; **63**:1525-42.

107. **Hedrich R, Flugge UI, Fernandez JM**. (1986). Patch-clamp studies of ion-transport in isolated plant vacuoles. *FEBS Lett*; **204**:228-32.

108. **Ward JM, Schroeder JI**. (1994). Calcium-activated K^+ channels and calcium-induced calcium-release by slow vacuolar ion channels in guard-cell vacuoles implicated in the control of stomatal closure. *Plant Cell*; **6**:669-83.

109. **Allen GJ, Sanders D**. (1995). Calcineurin, a type 2b protein phosphatase, modulates the Ca^{2+}-permeable slow vacuolar ion-channel of stomatal guard-cells. *Plant Cell*; **7**:1473-83.

110. **Pottosin II, Dobrovinskaya OR, Muniz J**. (2001). Conduction of monovalent and divalent cations in the slow vacuolar channel. *J Membr Biol*; **181**:55-65.

111. **Furuichi T, Cunningham KW, Muto S**. (2001). A putative two pore channel AtTPC1 mediates Ca^{2+} flux in Arabidopsis leaf cells. *Plant Cell Physiol*; **42**:900-5.

112. **Hedrich R, Neher E**. (1987). Cytoplasmic calcium regulates voltage-dependent ion channels in plant vacuoles. *Nature*; **329**:833-6.

113. **Ivashikina N, Hedrich R**. (2005). K^+ currents through SV-type vacuolar channels are sensitive to elevated luminal sodium levels. *Plant J*; **41**:606-14.

114. **Guo J, Zeng W, Chen Q, Lee C, Chen L, Yang Y, et al.** (2016). Structure of the voltage-gated two-pore channel TPC1 from *Arabidopsis thaliana*. *Nature*; **531**:196-201.

115. **Kintzer AF, Stroud RM**. (2016). Structure, inhibition and regulation of two-pore channel TPC1 from *Arabidopsis thaliana*. *Nature*; **531**:258-62.

116. **Schulze C, Sticht H, Meyerhoff P, Dietrich P**. (2011). Differential contribution of EF-hands to the Ca^{2+}-dependent activation in the plant two-pore channel TPC1. *The Plant journal : for cell and molecular biology*; **68**:424-32.

117. **Pottosin II, Tikhonova LI, Hedrich R, Schonknecht G**. (1997). Slowly activating vacuolar channels can not mediate Ca^{2+}-induced Ca^{2+} release. *Plant J*; **12**:1387-98.

118. **Pottosin I, Martinez-Estevez M, Dobrovinskaya O, Muniz J, Schonknecht G**. (2004). Mechanism of luminal Ca^{2+} and Mg^{2+} action on the vacuolar slowly activating channels. *Planta*; **219**:1057-70.

119. **Dubiella U, Seybold H, Durian G, Komander E, Lassig R, Witte CP, et al.** (2013). Calcium-dependent protein kinase/NADPH oxidase activation circuit is required for rapid defense signal propagation. *P Natl Acad Sci USA*; **110**:8744-9.

120. **Richards SL, Laohavisit A, Mortimer JC, Shabala L, Swarbreck SM, Shabala S, et al.** (2014). Annexin 1 regulates the H_2O_2-induced calcium signature in *Arabidopsis thaliana* roots. *Plant J*; **77**:136-45.

121. **Evans MJ, Choi WG, Gilroy S, Morris RJ**. (2016). A ROS-assisted calcium wave dependent on atrbohd and tpc1 propagates the systemic response to salt stress in Arabidopsis roots. *Plant Physiol*; **171**:1771-84.

122. **Ranf S, Wunnenberg P, Lee J, Becker D, Dunkel M, Hedrich R, et al.** (2008). Loss of the vacuolar cation channel, AtTPC1, does not impair Ca^{2+} signals induced by abiotic and biotic stresses. *Plant J*; **53**:287-99.

123. **Kiep V, Vadassery J, Lattke J, Maass JP, Boland W, Peiter E, et al.** (2015). Systemic cytosolic Ca^{2+} elevation is activated upon wounding and herbivory in Arabidopsis. *The New phytologist*; **207**:996-1004.

124. **Hamilton ES, Schlegel AM, Haswell ES**. (2015). United in diversity: mechanosensitive ion channels in plants. *Annu Rev Plant Biol*; **66**:113-37.

125. **Laohavisit A, Mortimer JC, Demidchik V, Coxon KM, Stancombe MA, Macpherson N, et al.** (2009). *Zea mays* Annexins modulate cytosolic free Ca^{2+} and generate a Ca^{2+}-permeable conductance. *Plant Cell*; **21**:479-93.

126. **Allen GJ, Sanders D**. (1994). Two voltage-gated, calcium-release channels coreside in the vacuolar membrane of broad bean guard-cells. *Plant Cell*; **6**:685-94.

127. **Allen GJ, Muir SR, Sanders D**. (1995). Release of Ca^{2+} from individual plant vacuoles by both $InsP_3$ and cyclic ADP-ribose. *Science*; **268**:735-7.

128. **Krinke O, Novotna Z, Valentova O, Martinec J**. (2007). Inositol trisphosphate receptor in higher plants: is it real? *J Exp Bot*; **58**:361-76.

129. **Navazio L, Bewell MA, Siddiqua A, Dickinson GD, Galione A, Sanders D**. (2000). Calcium release from the endoplasmic reticulum of higher plants elicited by the NADP metabolite nicotinic acid adenine dinucleotide phosphate. *P Natl Acad Sci USA*; **97**:8693-8.

130. **Navazio L, Mariani P, Sanders D**. (2001). Mobilization of Ca_{2+} by cyclic ADP-ribose from the endoplasmic reticulum of cauliflower florets. *Plant Physiol*; **125**:2129-38.

131. **Kudla J, Batistic O, Hashimoto K**. (2010). Calcium signals: the lead currency of plant information processing. *Plant Cell*; **22**:541-63.

132. **Hashimoto K, Kudla J**. (2011). Calcium decoding mechanisms in plants. *Biochimie*; **93**:2054-9.

133. **Mccormack E, Braam J**. (2003). Calmodulins and related potential calcium sensors of Arabidopsis. *New Phytol*; **159**:585-98.

134. **Mccormack E, Tsai YC, Braam J**. (2005). Handling calcium signaling: Arabidopsis CaMs and CMLs. *Trends Plant Sci*; **10**:383-9.

135. **Kawasaki H, Nakayama S, Kretsinger RH**. (1998). Classification and evolution of EF-hand proteins. *BioMetals*; **11**:277-95.

136. **Luan S, Kudla J, Rodriguez-Concepcion M, Yalovsky S, Gruissem W**. (2002). Calmodulins and calcineurin B-like proteins: calcium sensors for specific signal response coupling in plants. *Plant Cell*; **14**:S389-S400.

137. **Reddy VS, Safadi F, Zielinski RE, Reddy ASN**. (1999). Interaction of a kinesin-like protein with calmodulin isoforms from Arabidopsis. *J Biol Chem*; **274**:31727-33.

138. **Kohler C, Neuhaus G**. (2000). Characterisation of calmodulin binding to cyclic nucleotide-gated ion channels from *Arabidopsis thaliana*. *FEBS Lett*; **471**:133-6.

139. **Finkler A, Ashery-Padan R, Fromm H**. (2007). CAMTAs: calmodulin-binding transcription activators from plants to human. *FEBS Lett*; **581**:3893-8.

140. **Zeng HQ, Xu LQ, Singh A, Wang HZ, Du LQ, Poovaiah BW**. (2015). Involvement of calmodulin and calmodulin-like proteins in plant responses to abiotic stresses. *Frontiers in Plant Science*; **6**.

141. **Hrabak EM, Chan CWM, Gribskov M, Harper JF, Choi JH, Halford N, et al.** (2003). The Arabidopsis CDPK-SnRK superfamily of protein kinases. *Plant Physiol*; **132**:666-80.

142. **Harmon AC, Yoo BC, Mccaffery C**. (1994). Pseudosubstrate inhibition of CDPK, a protein-kinase with a calmodulin-like domain. *Biochemistry-Us*; **33**:7278-87.

143. **Lu SX, Hrabak EM**. (2002). An Arabidopsis calcium-dependent protein kinase is associated with the endoplasmic reticulum. *Plant Physiol*; **128**:1008-21.

144. **Dammann C, Ichida A, Hong BM, Romanowsky SM, Hrabak EM, Harmon AC, et al.** (2003). Subcellular targeting of nine calcium-dependent protein kinase isoforms from Arabidopsis. *Plant Physiol*; **132**:1840-8.

145. **Geiger D, Scherzer S, Mumm P, Marten I, Ache P, Matschi S, et al.** (2010). Guard cell anion channel SLAC1 is regulated by CDPK protein kinases with distinct Ca^{2+} affinities. *P Natl Acad Sci USA*; **107**:8023-8.

146. **Hwang I, Sze H, Harper JF**. (2000). A calcium-dependent protein kinase can inhibit a calmodulin-stimulated Ca^{2+} pump (ACA2) located in the endoplasmic reticulum of Arabidopsis. *P Natl Acad Sci USA*; **97**:6224-9.

147. **Kobayashi M, Ohura I, Kawakita K, Yokota N, Fujiwara M, Shimamoto K, et al.** (2007). Calcium-dependent protein kinases regulate the production of reactive oxygen species by potato NADPH oxidase. *Plant Cell*; **19**:1065-80.

148. **Choi HI, Park HJ, Park JH, Kim S, Im MY, Seo HH, et al.** (2005). Arabidopsis calcium-dependent protein kinase AtCPK32 interacts with ABF4, a transcriptional regulator of abscisic acid-responsive gene expression, and modulates its activity. *Plant Physiol*; **139**:1750-61.

149. **Zhu SY, Yu XC, Wang XJ, Zhao R, Li Y, Fan RC, et al.** (2007). Two calcium-dependent protein kinases, CPK4 and CPK11, regulate abscisic acid signal transduction in Arabidopsis. *Plant Cell*; **19**:3019-36.

150. **Ishida S, Yuasa T, Nakata M, Takahashi Y**. (2008). A tobacco calcium-dependent protein kinase, CDPK1, regulates the transcription factor REPRESSION OF SHOOT GROWTH in response to gibberellins. *Plant Cell*; **20**:3273-88.

151. **Asai T, Tena G, Plotnikova J, Willmann MR, Chiu WL, Gomez-Gomez L, et al.** (2002). MAP kinase signalling cascade in Arabidopsis innate immunity. *Nature*; **415**:977-83.

152. **Ludwig AA, Saitoh H, Felix G, Freymark G, Miersch O, Wasternack C, et al.** (2005). Ethylene-mediated cross-talk between calcium-dependent protein kinase and MAPK signaling controls stress responses in plants. *P Natl Acad Sci USA*; **102**:10736-41.

153. **Singh S, Parniske M**. (2012). Activation of calcium- and calmodulin-dependent protein kinase (CCaMK), the central regulator of plant root endosymbiosis. *Curr Opin Plant Biol*; **15**:444-53.

154. **Gleason C, Chaudhuri S, Yang TB, Munoz A, Poovaiah BW, Oldroyd GED**. (2006). Nodulation independent of rhizobia induced by a calcium-activated kinase lacking autoinhibition. *Nature*; **441**:1149-52.

155. **Shi JR, Kim KN, Ritz O, Albrecht V, Gupta R, Harter K, et al.** (1999). Novel protein kinases associated with calcineurin B-like calcium sensors in Arabidopsis. *Plant Cell*; **11**:2393-405.

156. **Kudla J, Xu Q, Harter K, Gruissem W, Luan S**. (1999). Genes for calcineurin B-like proteins in Arabidopsis are differentially regulated by stress signals. *P Natl Acad Sci USA*; **96**:4718-23.

157. **Liu JP, Ishitani M, Halfter U, Kim CS, Zhu JK**. (2000). The *Arabidopsis thaliana* SOS2 gene encodes a protein kinase that is required for salt tolerance. *P Natl Acad Sci USA*; **97**:3730-4.

158. **Halfter U, Ishitani M, Zhu JK**. (2000). The Arabidopsis SOS2 protein kinase physically interacts with and is activated by the calcium-binding protein SOS3. *P Natl Acad Sci USA*; **97**:3735-40.

159. **Albrecht V, Ritz O, Linder S, Harter K, Kudla J**. (2001). The NAF domain defines a novel protein-protein interaction module conserved in Ca^{2+}-regulated kinases. *EMBO J*; **20**:1051-63.

160. **Chaves-Sanjuan A, Sanchez-Barrena MJ, Gonzalez-Rubio JM, Moreno M, Ragel P, Jimenez M, et al.** (2014). Structural basis of the regulatory mechanism of the plant CIPK family of protein kinases controlling ion homeostasis and abiotic stress. *Proc Natl Acad Sci U S A*.

161. **Lan WZ, Lee SC, Che YF, Jiang YQ, Luan S**. (2011). Mechanistic analysis of AKT1 regulation by the CBL-CIPK-PP2CA interactions. *Mol Plant*; **4**:527-36.

162. **Weinl S, Kudla J**. (2009). The CBL-CIPK Ca^{2+}-decoding signaling network: function and perspectives. *New Phytol*; **184**:517-28.

163. **Xu J, Li HD, Chen LQ, Wang Y, Liu LL, He L, et al.** (2006). A protein kinase, interacting with two calcineurin B-like proteins, regulates K^+ transporter AKT1 in Arabidopsis. *Cell*; **125**:1347-60.

164. **Tang RJ, Liu H, Yang Y, Yang L, Gao XS, Garcia VJ, et al.** (2012). Tonoplast calcium sensors CBL2 and CBL3 control plant growth and ion homeostasis through regulating V-ATPase activity in Arabidopsis. *Cell Res*; **22**:1650-65.

165. **Tang RJ, Zhao FG, Garcia VJ, Kleist TJ, Yang L, Zhang HX, et al.** (2015). Tonoplast CBL-CIPK calcium signaling network regulates magnesium homeostasis in Arabidopsis. *Proc Natl Acad Sci U S A*.

166. **Mogami J, Fujita Y, Yoshida T, Tsukiori Y, Nakagami H, Nomura Y, et al.** (2015). Two distinct families of protein kinases are required for plant growth under high external Mg^{2+} concentrations in Arabidopsis. *Plant Physiol*.

167. **Luan S**. (2009). The CBL-CIPK network in plant calcium signaling. *Trends Plant Sci*; **14**:37-42.

168. **Manik SMN, Shi S, Mao J, Dong L, Su Y, Wang Q, et al.** (2015). The Calcium Sensor CBL-CIPK Is Involved in Plant's Response to Abiotic Stresses. *International journal of genomics*; **2015**:493191.

169. **Young JJ, Mehta S, Israelsson M, Godoski J, Grill E, Schroeder JI**. (2006). CO_2 signaling in guard cells: calcium sensitivity response modulation, a Ca^{2+}-independent phase, and CO_2 insensitivity of the *gca2* mutant. *P Natl Acad Sci USA*; **103**:7506-11.

170. **Zhang J, Jia W, Yang J, Ismail AM**. (2006). Role of ABA in integrating plant responses to drought and salt stresses. *Field Crops Res*; **97**:111-9.

171. **Larkindale J, Hall JD, Knight MR, Vierling E**. (2005). Heat stress phenotypes of Arabidopsis mutants implicate multiple signaling pathways in the acquisition of thermotolerance. *Plant Physiol*; **138**:882-97.

172. **Hildmann T, Ebneth M, Penacortes H, Sanchezserrano JJ, Willmitzer L, Prat S**. (1992). General roles of abscisic and jasmonic acids in gene activation as a result of mechanical wounding. *Plant Cell*; **4**:1157-70.

173. **Suttle JC, Lulai EC, Huckle LL, Neubauer JD**. (2013). Wounding of potato tubers induces increases in ABA biosynthesis and catabolism and alters expression of ABA metabolic genes. *J Plant Physiol*; **170**:560-6.

174. **Allen GJ, Kwak JM, Chu SP, Llopis J, Tsien RY, Harper JF, et al.** (1999). Cameleon calcium indicator reports cytoplasmic calcium dynamics in Arabidopsis guard cells. *Plant J*; **19**:735-47.

175. **Kim KN, Cheong YH, Grant JJ, Pandey GK, Luan S**. (2003). CIPK3, a calcium sensor-associated protein kinase that regulates abscisic acid and cold signal transduction in Arabidopsis. *Plant Cell*; **15**:411-23.

176. **Pandey GK, Grant JJ, Cheong YH, Kim BG, Li LG, Luan S**. (2008). Calcineurin-B-like protein CBL9 interacts with target kinase CIPK3 in the regulation of ABA response in seed germination. *Mol Plant*; **1**:238-48.

177. **Plieth C, Hansen UP, Knight H, Knight MR**. (1999). Temperature sensing by plants: the primary characteristics of signal perception and calcium response. *Plant J*; **18**:491-7.

178. **Knight MR, Campbell AK, Smith SM, Trewavas AJ**. (1991). Transgenic plant aequorin reports the effects of touch and cold-shock and elicitors on cytoplasmic calcium. *Nature*; **352**:524-6.

179. **Quiles-Pando C, Rexach J, Navarro-Gochicoa MT, Camacho-Cristobal JJ, Herrera-Rodriguez MB, Gonzalez-Fontes A**. (2013). Boron deficiency increases

the levels of cytosolic Ca^{2+} and expression of Ca^{2+}-related genes in *Arabidopsis thaliana* roots. *Plant Physiol Biochem*; **65**:55-60.

180. **Boudsocq M, Sheen J**. (2013). CDPKs in immune and stress signaling. *Trends Plant Sci*; **18**:30-40.

181. **Cutler SR, Rodriguez PL, Finkelstein RR, Abrams SR**. (2010). Abscisic acid: emergence of a core signaling network. *Annu Rev Plant Biol*; **61**:651-79.

182. **Pandey GK, Cheong YH, Kim KN, Grant JJ, Li LG, Hung W, et al.** (2004). The calcium sensor calcineurin B-Like 9 modulates abscisic acid sensitivity and biosynthesis in Arabidopsis. *Plant Cell*; **16**:1912-24.

183. **Cheong YH, Pandey GK, Grant JJ, Batistic O, Li L, Kim BG, et al.** (2007). Two calcineurin B-like calcium sensors, interacting with protein kinase CIPK23, regulate leaf transpiration and root potassium uptake in Arabidopsis. *Plant J*; **52**:223-39.

184. **D'angelo C, Weinl S, Batistic O, Pandey GK, Cheong YH, Schultke S, et al.** (2006). Alternative complex formation of the Ca^{2+}-regulated protein kinase CIPK1 controls abscisic acid-dependent and independent stress responses in Arabidopsis. *Plant J*; **48**:857-72.

185. **Pandey GK, Kanwar P, Singh A, Steinhorst L, Pandey A, Yadav AK, et al.** (2015). CBL-interacting protein kinase, CIPK21, regulates osmotic and salt stress responses in Arabidopsis. *Plant Physiol*:pp.00623.2015.

186. **Li LG, Kim BG, Cheong YH, Pandey GK, Luan S**. (2006). A Ca^{2+} signaling pathway regulates a K^+ channel for low-K response in Arabidopsis. *P Natl Acad Sci USA*; **103**:12625-30.

187. **Pandey GK, Cheong YH, Kim BG, Grant JJ, Li L, Luan S**. (2007). CIPK9: a calcium sensor-interacting protein kinase required for low-potassium tolerance in Arabidopsis. *Cell Res*; **17**:411-21.

188. **Ren XL, Qi GN, Feng HQ, Zhao S, Zhao SS, Wang Y, et al.** (2013). Calcineurin B-like protein CBL10 directly interacts with AKT1 and modulates K^+ homeostasis in Arabidopsis. *Plant J*; **74**:258-66.

189. **Ho CH, Lin SH, Hu HC, Tsay YF**. (2009). CHL1 functions as a nitrate sensor in plants. *Cell*; **138**:1184-94.

190. **Brownlee C, Wood JW**. (1986). A gradient of cytoplasmic free calcium in growing rhizoid cells of fucus-serratus. *Nature*; **320**:624-6.

191. **Miller AJ, Sanders D**. (1987). Depletion of cytosolic free calcium induced by photosynthesis. *Nature*; **326**:397-400.

192. **Ridgway EB, Ashley CC**. (1967). Calcium transients in single muscle fibers. *Biochem Biophys Res Commun*; **29**:229.

193. **Kanchiswamy CN, Malnoy M, Occhipinti A, Maffei ME**. (2014). Calcium imaging perspectives in plants. *Int J Mol Sci*; **15**:3842-59.

194. **Cranfill PJ, Sell BR, Baird MA, Allen JR, Lavagnino Z, De Gruiter HM, et al.** (2016). Quantitative assessment of fluorescent proteins. *Nat Methods*; **13**:557-62.

195. **Koldenkova VP, Nagai T**. (2013). Genetically encoded Ca^{2+} indicators: properties and evaluation. *Bba-Mol Cell Res*; **1833**:1787-97.

196. **Gifford JL, Walsh MP, Vogel HJ**. (2007). Structures and metal-ion-binding properties of the Ca^{2+}-binding helix-loop-helix EF-hand motifs. *Biochem J*; **405**:199-221.

197. **Shimomura O, Johnson FH, Saiga Y**. (1962). Extraction, purification and properties of aequorin, a bioluminescent protein from *Luminous Hydromedusan, Aequorea*. *J Cell Compar Physl*; **59**:223-&.

198. **Plieth C**. (2001). Plant calcium signaling and monitoring: pros and cons and recent experimental approaches. *Protoplasma*; **218**:1-23.

199. **Campbell AK, Trewavas AJ, Knight MR**. (1996). Calcium imaging shows differential sensitivity to cooling and communication in luminous transgenic plants. *Cell Calcium*; **19**:211-8.

200. **Mithofer A, Mazars C**. (2002). Aequorin-based measurements of intracellular Ca^{2+}-signatures in plant cells. *Biological Procedures Online*; **4**:105-18.

201. **Kwaaitaal M, Huisman R, Maintz J, Reinstadler A, Panstruga R.** (2011). Ionotropic glutamate receptor (iGluR)-like channels mediate MAMP-induced calcium influx in *Arabidopsis thaliana*. *Biochem J*; **440**:355-65.

202. **Ranf S, Eschen-Lippold L, Pecher P, Lee J, Scheel D**. (2011). Interplay between calcium signalling and early signalling elements during defence responses to microbe- or damage-associated molecular patterns. *Plant J*; **68**:100-13.

203. **Zhu XH, Feng Y, Liang GM, Liu N, Zhu JK**. (2013). Aequorin-based luminescence imaging reveals stimulus- and tissue-specific Ca^{2+} dynamics in Arabidopsis plants. *Mol Plant*; **6**:444-55.

204. **Miyawaki A, Llopis J, Heim R, Mccaffery JM, Adams JA, Ikura M, et al.** (1997). Fluorescent indicators for Ca^{2+} based on green fluorescent proteins and calmodulin. *Nature*; **388**:882-7.

205. **Nagai T, Yamada S, Tominaga T, Ichikawa M, Miyawaki A**. (2004). Expanded dynamic range of fluorescent indicators for Ca^{2+} by circularly permuted yellow fluorescent proteins. *P Natl Acad Sci USA*; **101**:10554-9.

206. **Horikawa K, Yamada Y, Matsuda T, Kobayashi K, Hashimoto M, Matsu-Ura T, et al.** (2010). Spontaneous network activity visualized by ultrasensitive Ca^{2+} indicators, yellow cameleon-nano. *Nat Methods*; **7**:729-U88.

207. **Choi J, Tanaka K, Cao YR, Qi Y, Qiu J, Liang Y, et al.** (2014). Identification of a plant receptor for extracellular ATP. *Science*; **343**:290-4.

208. **Nagai T, Sawano A, Park ES, Miyawaki A**. (2001). Circularly permuted green fluorescent proteins engineered to sense Ca^{2+}. *P Natl Acad Sci USA*; **98**:3197-202.

209. **Nakai J, Ohkura M, Imoto K**. (2001). A high signal-to-noise Ca^{2+} probe composed of a single green fluorescent protein. *Nat Biotechnol*; **19**:137-41.

210. **Tsien RY**. (1998). The green fluorescent protein. *Annu Rev Biochem*; **67**:509-44.

211. **Akerboom J, Rivera JDV, Guilbe MMR, Malave ECA, Hernandez HH, Tian L, et al.** (2009). Crystal structures of the GCaMP calcium sensor reveal the mechanism of fluorescence signal change and aid rational design. *J Biol Chem*; **284**:6455-64.

212. **Okumoto S**. (2012). Quantitative imaging using genetically encoded sensors for small molecules in plants. *Plant J*; **70**:108-17.

213. **Zhao YX, Araki S, Jiahui WH, Teramoto T, Chang YF, Nakano M, et al.** (2011). An expanded palette of genetically encoded Ca^{2+} indicators. *Science*; **333**:1888-91.

214. **Ohkura M, Matsuzaki M, Kasai H, Imoto K, Nakai J**. (2005). Genetically encoded bright Ca^{2+} probe applicable for dynamic Ca^{2+} imaging of dendritic spines. *Anal Chem*; **77**:5861-9.

215. **Tallini YN, Ohkura M, Choi BR, Ji GJ, Imoto K, Doran R, et al.** (2006). Imaging cellular signals in the heart *in vivo*: cardiac expression of the high-signal Ca^{2+} indicator GCaMP2. *P Natl Acad Sci USA*; **103**:4753-8.

216. **Tian L, Hires SA, Mao T, Huber D, Chiappe ME, Chalasani SH, et al.** (2009). Imaging neural activity in worms, flies and mice with improved GCaMP calcium indicators. *Nat Methods*; **6**:875-U113.

217. **Akerboom J, Chen TW, Wardill TJ, Tian L, Marvin JS, Mutlu S, et al.** (2012). Optimization of a GCaMP calcium indicator for neural activity imaging. *J Neurosci*; **32**:13819-40.

218. **Pedelacq JD, Cabantous S, Tran T, Terwilliger TC, Waldo GS**. (2006). Engineering and characterization of a superfolder green fluorescent protein. *Nat Biotechnol*; **24**:79-88.

219. **Keinath NF, Waadt R, Brugman R, Schroeder JI, Grossmann G, Schumacher K, et al.** (2015). Live cell imaging with R-GECO1 sheds light on flg22- and chitin-induced transient $[Ca^{2+}]_{cyt}$ patterns in Arabidopsis. *Mol Plant*; **8**:1188-200.

220. **Dixon A**. (1998) *Aphid Ecology: An Optimization Approach*. London: Springer.

221. **Blackman RL, Eastop VF**. (2000) *Aphids on the world's crops: an identification and information guide*. Chichester, UK: John Wiley & Sons, Ltd.

222. **Mathers TC, Chen Y, Kaithakottil G, Legeai F, Mugford ST, Baa-Puyoulet P, et al.** (2016). A clonally reproducing generalist aphid pest colonises diverse host plants by rapid transcriptional plasticity of duplicated gene clusters. *bioRxiv*.

223. **Schuett W, Dall SRX, Baeumer J, Kloesener MH, Nakagawa S, Beinlich F, et al.** (2011). "Personality" variation in a clonal insect: the pea aphid, *Acyrthosiphon pisum*. *Dev Psychobiol*; **53**:631-40.

224. **Leather SR**. (1992). Aspects of aphid overwintering (Homoptera, Aphidinea, Aphididae). *Entomol Gen*; **17**:101-13.

225. **Buchner P**. (1965) *Endosymbioses of animals with plant microorganisms*. Chichester, UK: John Wiley. 31-8 p.

226. **Douglas AE**. (1993). The nutritional quality of phloem sap utilized by natural aphid populations. *Ecol Entomol*; **18**:31-8.

227. **Douglas AE**. (1988). Sulfate utilization in an aphid symbiosis. *Insect Biochem*; **18**:599-605.

228. **Febvay G, Rahbe Y, Rynkiewicz M, Guillaud J, Bonnot G**. (1999). Fate of dietary sucrose and neosynthesis of amino acids in the pea aphid, *Acyrthosiphon pisum*, reared on different diets. *J Exp Biol*; **202**:2639-52.

229. **Shigenobu S, Watanabe H, Hattori M, Sakaki Y, Ishikawa H**. (2000). Genome sequence of the endocellular bacterial symbiont of aphids *Buchnera* sp *APS*. *Nature*; **407**:81-6.

230. **Gunduz EA, Douglas AE**. (2009). Symbiotic bacteria enable insect to use a nutritionally inadequate diet. *P R Soc B*; **276**:987-91.

231. **Wilson ACC, Ashton PD, Calevro F, Charles H, Colella S, Febvay G, et al.** (2010). Genomic insight into the amino acid relations of the pea aphid, *Acyrthosiphon pisum*, with its symbiotic bacterium *Buchnera aphidicola*. *Insect Mol Biol*; **19**:249-58.

232. **Price DRG, Duncan RP, Shigenobu S, Wilson ACC**. (2011). Genome expansion and differential expression of amino acid transporters at the aphid/buchnera symbiotic interface. *Mol Biol Evol*; **28**:3113-26.

233. **Capinera JL**. (2001) *Myzus persicae* (Sulzer) (Insecta: Hemiptera: Aphididae) updated October 2005. [Available from: http://entnemdept.ufl.edu/creatures/veg/aphid/green_peach_aphid.htm#life].

234. **Davidson RH, Lyon WF**. (1979) *Insect Pests of Farm, Garden, and Orchard*. New York: John Wiley and Sons.

235. **Cabi**. (2015) Invasive speices compendium
CABI. [Available from: http://www.cabi.org/isc/datasheet/35642].

236. **Zust T, Joseph B, Shimizu KK, Kliebenstein DJ, Turnbull LA**. (2011). Using knockout mutants to reveal the growth costs of defensive traits. *P R Soc B*; **278**:2598-603.

237. **Kennedy JS, Day MF, Eastop VF**. (1962) *A Conspectus of Aphids as Vectors of Plant Viruses*.

238. **Petitt FL, Smilowitz Z**. (1982). Green peach aphid (Homoptera, Aphididae) feeding damage to potato in various plant-growth stages. *J Econ Entomol*; **75**:431-5.

239. **Sexson DL**. (2005) Chapter 5: Potato. In: **Foster R, Flood BR,** editors. *Vegetable Insect Management*. OH, USA: Meister Media Worldwide. p. 93-106.

240. **Barbagallo S, Cocuzza G, Cravedi P, Komazaki S**. (2007) IPM case studies: deciduous fruit trees. In: **Van Emden HF, Harrington R,** editors. *Aphids as crop pests*: CAB International.

241. **Powell DM**. (1980). Control of the green peach aphid (Homoptera, Aphididae) on potatoes with soil systemic insecticides - preplant broadcast and planting time furrow applications, 1973-77. *J Econ Entomol*; **73**:839-43.

242. **Devonshire AL, Field LM, Foster SP, Moores GD, Williamson MS, Blackman RL**. (1998). The evolution of insecticide resistance in the peach-potato aphid, *Myzus persicae*. *Philos T R Soc B*; **353**:1677-84.

243. **Field LM, Devonshire AL**. (1998). Evidence that the E4 and FE4 esterase genes responsible for insecticide resistance in the aphid *Myzus persicae* (Sulzer) are part of a gene family. *Biochem J*; **330**:169-73.

244. **Bass C, Puinean AM, Zimmer CT, Denholm I, Field LM, Foster SP, et al.** (2014). The evolution of insecticide resistance in the peach potato aphid, *Myzus persicae*. *Insect Biochem Mol Biol*; **51**:41-51.

245. **Pesticideresistance.Org**. (2014) Arthropod pesticide resistance database: Michigan State University. [Available from: http://www.pesticideresistance.org/display.php?page=species&arId=384].

246. **Guinnessworldrecords.Com**. (2016) Most resistant insect: Guinness World Records. [Available from: http://www.guinnessworldrecords.com/world-records/most-resistant-insect/].

247. **Gilkeson LA, Hill SB**. (1987). Release rates for control of green peach aphid (Homoptera, Aphidae) by the predatory midge *Aphidoletes aphidimyza* (diptera, cecidomyiidae) under winter greenhouse conditions. *J Econ Entomol*; **80**:147-50.

248. **Tamaki G, Annis B, Weiss M**. (1981). Response of natural enemies to the green peach aphid in different plant cultures (Homoptera, Aphididae). *Environ Entomol*; **10**:375-8.

249. **Jansson RK, Smilowitz Z**. (1986). Influence of nitrogen on population parameters of potato insects - abundance, population-growth, and within-plant distribution of the green peach aphid, *Myzus persicae*. *Environ Entomol*; **15**:49-55.

250. **Beale MH, Birkett MA, Bruce TJA, Chamberlain K, Field LM, Huttly AK, et al.** (2006). Aphid alarm pheromone produced by transgenic plants affects aphid and parasitoid behavior. *P Natl Acad Sci USA*; **103**:10509-13.

251. **Bruce TJA, Aradottir GI, Smart LE, Martin JL, Caulfield JC, Doherty A, et al.** (2015). The first crop plant genetically engineered to release an insect pheromone for defence. *Sci Rep-Uk*; **5**.

252. **Kring JB**. (1972). Flight behavior of aphids. *Annu Rev Entomol*; **17**:461-+.

253. **Doering TF**. (2014). How aphids find their host plants, and how they don't. *Ann Appl Biol*; **165**:3-26.

254. **Heathcote GD**. (1957). The comparison of yellow cylindrical, flat and water traps, and of Johnson suction traps, for sampling aphids. *Ann Appl Biol*; **45**:133-9.

255. **Tuomi J**. (1992). Toward integration of plant defense theories. *Trends Ecol Evol*; **7**:365-7.

256. **Losel PM, Lindemann M, Scherkenbeck J, Campbell CaM, Hardie J, Pickett JA, et al.** (1996). Effect of primary-host kairomones on the attractiveness of the hop-aphid sex pheromone to *Phorodon humuli* males and gynoparae. *Entomol Exp Appl*; **80**:79-82.

257. **Keiser CN, Sheeks LE, Mondor EB**. (2013). The effect of microhabitat feeding site selection on aphid foraging and predation risk. *Arthropod-Plant Inte*; **7**:633-41.

258. **Hopkins GW, Dixon AFG**. (2000). Feeding site location in birch aphids (Sternorrhyncha : Aphididae): the simplicity and reliability of cues. *Eur J Entomol*; **97**:279-80.

259. **Smith CM, Chuang WP**. (2014). Plant resistance to aphid feeding: behavioral, physiological, genetic and molecular cues regulate aphid host selection and feeding. *Pest Manage Sci*; **70**:528-40.

260. **Howe GA, Jander G**. (2008). Plant immunity to insect herbivores. *Annu Rev Plant Biol*; **59**:41-66.

261. **Pollard DG**. (1973). Plant penetration by feeding aphids (Hemiptera, Aphidoidea). *Bull Entomol Res*; **62**:631-714.

262. **Mclean DL, Kinsey MG**. (1964). A technique for electronically recording aphid feeding and salivation. *Nature*; **202**:1358-9.

263. **Tjallingii WF**. (1978). Mechanoreceptors of the aphid labium. *Entomol Exp Appl*; **24**:731-&.

264. **Tjallingii WF**. (1985). Membrane-potentials as an indication for plant-cell penetration by aphid stylets. *Entomol Exp Appl*; **38**:187-93.

265. **Tjallingii WF**. (1988) *Electrical recording of stylet penetration activities. Aphids, their Biology, Natural Enemies and Control*. vol. 2B ed. Amsterdam, The Netherlands: Elsevier.

266. **Tjallingii WF**. (1985). lectrical nature of recorded signals during stylet penetration by aphids. *Entomol Exp Appl*; **38**:177-86.

267. **Tjallingii WF, Esch TH**. (1993). Fine-structure of aphid stylet routes in plant-tissues in correlation with EPG signals. *Physiol Entomol*; **18**:317-28.

268. **Martin B, Collar JL, Tjallingii WF, Fereres A**. (1997). Intracellular ingestion and salivation by aphids may cause the acquisition and inoculation of non-persistently transmitted plant viruses. *J Gen Virol*; **78**:2701-5.

269. **Powell G**. (2005). Intracellular salivation is the aphid activity associated with inoculation of non-persistently transmitted viruses. *J Gen Virol*; **86**:469-72.

270. **Tjallingii WF**. (2006). Salivary secretions by aphids interacting with proteins of phloem wound responses. *J Exp Bot*; **57**:739-45.

271. **Miles PW**. (1999). Aphid saliva. *Biol Rev Camb Philos Soc*; **74**:41-85.

272. **Harmel N, Letocart E, Cherqui A, Giordanengo P, Mazzucchelli G, Guillonneau F, et al.** (2008). Identification of aphid salivary proteins: a proteomic investigation of *Myzus persicae*. *Insect Mol Biol*; **17**:165-74.

273. **Carolan JC, Fitzroy CIJ, Ashton PD, Douglas AE, Wilkinson TL**. (2009). The secreted salivary proteome of the pea aphid *Acyrthosiphon pisum* characterised by mass spectrometry. *Proteomics*; **9**:2457-67.

274. **Carolan JC, Caragea D, Reardon KT, Mutti NS, Dittmer N, Pappan K, et al.** (2011). Predicted effector molecules in the salivary secretome of the pea aphid (*Acyrthosiphon pisum*): a dual transcriptomic/proteomic approach. *J Proteome Res*; **10**:1505-18.

275. **Hogenhout SA, Bos JIB**. (2011). Effector proteins that modulate plant-insect interactions. *Curr Opin Plant Biol*; **14**:422-8.

276. **Mutti NS, Louis J, Pappan LK, Pappan K, Begum K, Chen MS, et al.** (2008). A protein from the salivary glands of the pea aphid, *Acyrthosiphon pisum*, is essential in feeding on a host plant. *P Natl Acad Sci USA*; **105**:9965-9.

277. **Bos JI, Prince D, Pitino M, Maffei ME, Win J, Hogenhout SA**. (2010). A functional genomics approach identifies candidate effectors from the aphid species *Myzus persicae* (green peach aphid). *PLoS Genet*; **6**:e1001216.

278. **Naessens E, Dubreuil G, Giordanengo P, Baron OL, Minet-Kebdani N, Keller H, et al.** (2015). A secreted MIF cytokine enables aphid feeding and represses plant immune responses. *Curr Biol*; **25**:1898-903.

279. **Mugford ST, Barclay E, Drurey C, Findlay KC, Hogenhout SA**. (2016). An immuno-suppressive aphid saliva protein is delivered into the cytosol of plant mesophyll cells during feeding. *Mol Plant-Microbe Interact*; **29**:854-61.

280. **Harrington R, Katis N, Gibson RW**. (1986). Field assessment of the relative importance of different aphid species in the transmission of *potato virus-y. potato*. *Potato Res*; **29**:67-76.

281. **Chen JQ, Rahbe Y, Delobel B, Sauvion N, Guillaud J, Febvay G**. (1997). Melon resistance to the aphid *Aphis gossypii*: behavioural analysis and chemical correlations with nitrogenous compounds. *Entomol Exp Appl*; **85**:33-44.

282. **Sauge MH, Kervella J, Rahbe Y**. (1998). Probing behaviour of the green peach aphid *Myzus persicae* on resistant Prunus genotypes. *Entomol Exp Appl*; **89**:223-32.

283. **Jaouannet M, Morris JA, Hedley PE, Bos JI**. (2015). Characterization of arabidopsis transcriptional responses to different aphid species reveals genes that contribute to host susceptibility and non-host resistance. *PLoS Pathog*; **11**:e1004918.

284. **Prado E, Tjallingii WF**. (1994). Aphid activities during sieve element punctures. *Entomol Exp Appl*; **72**:157-65.

285. **Goeschl JD, Magnuson CE**. (1986). Physiological implications of the Munch-Horwitz theory of phloem transport - effects of loading rates. *Plant Cell Environ*; **9**:95-102.

286. **Magnuson CE, Goeschl JD, Fares Y**. (1986). Experimental tests of the Munch-Horwitz theory of phloem transport - effects of loading rates. *Plant Cell Environ*; **9**:103-9.

287. **Knoblauch M, Van Bel AJE**. (1998). Sieve tubes in action. *Plant Cell*; **10**:35-50.

288. **Ernst AM, Jekat SB, Zielonka S, Muller B, Neumann U, Ruping B, et al.** (2012). Sieve element occlusion (SEO) genes encode structural phloem proteins involved in wound sealing of the phloem. *P Natl Acad Sci USA*; **109**:E1980-E9.

289. **Aspinall GO, Kessler G**. (1957). The structure of callose from the grape vine. *Chem Ind-London*:1296-.

290. **Zee SY**. (1968). Ontogeny of cambium and phloem in epicotyl of *Pisum sativum*. *Aust J Bot*; **16**:419-&.

291. **Knoblauch M, Peters WS, Ehlers K, Van Bel AJE**. (2001). Reversible calcium-regulated stopcocks in legume sieve tubes. *Plant Cell*; **13**:1221-30.

292. **Kauss H**. (1987). Callose synthesis - regulation by induced Ca^{2+}-uptake in plant-cells. *Naturwissenschaften*; **74**:275-81.

293. **Singh A, Paolillo DJ**. (1990). Role of calcium in the callose response of self-pollinated brassica stigmas. *Am J Bot*; **77**:128-33.

294. **Messiaen J, Nerinckx F, Vancutsem P**. (1995). Callose synthesis in spirostanol treated carrot cells is not triggered by cytosolic calcium, cytosolic pH or membrane-potential changes. *Plant Cell Physiol*; **36**:1213-20.

295. **Nedukha OM**. (2015). Callose: localization, functions, and synthesis in plant cells. *Cytol Genet*; **49**:49-57.

296. **Will T, Van Bel AJE**. (2006). Physical and chemical interactions between aphids and plants. *J Exp Bot*; **57**:729-37.

297. **Will T, Tjallingii WF, Thonnessen A, Van Bel AJ**. (2007). Molecular sabotage of plant defense by aphid saliva. *Proc Natl Acad Sci U S A*; **104**:10536-41.

298. **Schwarzkopf A, Rosenberger D, Niebergall M, Gershenzon J, Kunert G**. (2013). To feed or not to feed: plant factors located in the epidermis, mesophyll, and sieve elements influence pea aphid's ability to feed on legume species. *Plos One*; **8**:e75298.

299. **Lu H, Yang PC, Xu YY, Luo L, Zhu JJ, Cui N, et al.** (2016). Performances of survival, feeding behavior, and gene expression in aphids reveal their different fitness to host alteration. *Sci Rep-Uk*; **6**.

300. **Vanhelden M, Tjallingii WF**. (1993). Tissue localization of lettuce resistance to the aphid *Nasonovia ribisnigri* using electrical penetration graphs. *Entomol Exp Appl*; **68**:269-78.

301. **Klingler J, Powell G, Thompson GA, Isaacs R**. (1998). Phloem specific aphid resistance in *Cucumis melo* line AR 5: effects on feeding behaviour and performance of *Aphis gossypii*. *Entomol Exp Appl*; **86**:79-88.

302. **Garzo E, Soria C, Gomez-Guillamon ML, Fereres A**. (2002). Feeding behavior of *Aphis gossypii* on resistant accessions of different melon genotypes (Cucumis melo). *Phytoparasitica*; **30**:129-40.

303. **Alvarez AE, Tjallingii WF, Garzo E, Vleeshouwers V, Dicke M, Vosman B**. (2006). Location of resistance factors in the leaves of potato and wild tuber-bearing Solanum species to the aphid *Myzus persicae*. *Entomol Exp Appl*; **121**:145-57.

304. **Kusnierczyk A, Winge P, Jorstad TS, Troczynska J, Rossiter JT, Bones AM**. (2008). Towards global understanding of plant defence against aphids-timing and dynamics of early Arabidopsis defence responses to cabbage aphid (*Brevicoryne brassicae*) attack. *Plant Cell Environ*; **31**:1097-115.

305. **Pfalz M, Vogel H, Kroymann J**. (2009). The gene controlling the indole glucosinolate modifier1 quantitative trait locus alters indole glucosinolate structures and aphid resistance in Arabidopsis. *Plant Cell*; **21**:985-99.

306. **Kettles GJ, Drurey C, Schoonbeek HJ, Maule AJ, Hogenhout SA**. (2013). Resistance of *Arabidopsis thaliana* to the green peach aphid, *Myzus persicae*, involves camalexin and is regulated by microRNAs. *The New phytologist*; **198**:1178-90.

307. **Ellis C, Karafyllidis L, Turner JG**. (2002). Constitutive activation of jasmonate signaling in an Arabidopsis mutant correlates with enhanced resistance to *Erysiphe cichoracearum*, *Pseudomonas syringae*, and *Myzus persicae*. *Mol Plant-Microbe Interact*; **15**:1025-30.

308. **De Vos M, Van Oosten VR, Van Poecke RMP, Van Pelt JA, Pozo MJ, Mueller MJ, et al.** (2005). Signal signature and transcriptome changes of Arabidopsis during pathogen and insect attack. *Mol Plant-Microbe Interact*; **18**:923-37.

309. **Aharoni A, Giri AP, Deuerlein S, Griepink F, De Kogel WJ, Verstappen FWA, et al.** (2003). Terpenoid metabolism in wild-type and transgenic Arabidopsis plants. *Plant Cell*; **15**:2866-84.

310. **Wu JQ, Baldwin IT**. (2010). New Insights into Plant Responses to the Attack from Insect Herbivores. *Annu Rev Genet*; **44**:1-24.

311. **Bidart-Bouzat MG, Kliebenstein D**. (2011). An ecological genomic approach challenging the paradigm of differential plant responses to specialist versus generalist insect herbivores. *Oecologia*; **167**:677-89.

312. **Jones JDG, Dangl JL**. (2006). The plant immune system. *Nature*; **444**:323-9.

313. **Cook DE, Mesarich CH, Thomma BP**. (2015). Understanding plant immunity as a surveillance system to detect invasion. *Annual review of phytopathology*; **53**:541-63.

314. **Zipfel C**. (2009). Early molecular events in PAMP-triggered immunity. *Curr Opin Plant Biol*; **12**:414-20.

315. **Mithofer A, Boland W**. (2008). Recognition of herbivory-associated molecular patterns. *Plant Physiol*; **146**:825-31.

316. **Clarke CR, Chinchilla D, Hind SR, Taguchi F, Miki R, Ichinose Y, et al.** (2013). Allelic variation in two distinct *Pseudomonas syringae* flagellin epitopes modulates the strength of plant immune responses but not bacterial motility. *The New phytologist*; **200**:847-60.

317. **Felix G, Duran JD, Volko S, Boller T**. (1999). Plants have a sensitive perception system for the most conserved domain of bacterial flagellin. *Plant J*; **18**:265-76.

318. **Kunze G, Zipfel C, Robatzek S, Niehaus K, Boller T, Felix G**. (2004). The N terminus of bacterial elongation factor Tu elicits innate immunity in Arabidopsis plants. *Plant Cell*; **16**:3496-507.

319. **Gomez-Gomez L, Felix G, Boller T**. (1999). A single locus determines sensitivity to bacterial flagellin in Arabidopsis thaliana. *Plant J*; **18**:277-84.

320. **Zipfel C, Robatzek S, Navarro L, Oakeley EJ, Jones JDG, Felix G, et al.** (2004). Bacterial disease resistance in Arabidopsis through flagellin perception. *Nature*; **428**:764-7.

321. **Ebel J, Ayers AR, Albersheim P**. (1976). Response of suspension-cultured soybean cells to elicitor isolated from phytophthora-megasperma var sojae, a fungal pathogen of soybeans. *Plant Physiol*; **57**:775-9.

322. **Shibuya N, Minami E**. (2001). Oligosaccharide signalling for defence responses in plant. *Physiol Mol Plant Pathol*; **59**:223-33.

323. **Wan J, Tanaka K, Zhang XC, Son GH, Brechenmacher L, Nguyen TH, et al.** (2012). LYK4, a lysin motif receptor-like kinase, is important for chitin signaling and plant innate immunity in Arabidopsis. *Plant Physiol*; **160**:396-406.

324. **Heil M**. (2009). Damaged-self recognition in plant herbivore defence. *Trends Plant Sci*; **14**:356-63.

325. **Darvill AG, Albersheim P**. (1984). Phytoalexins and their elicitors - a defense against microbial infection in plants. *Annu Rev Plant Physiol Plant Mol Biol*; **35**:243-75.

326. **Bergey DR, Orozco-Cardenas M, De Moura DS, Ryan CA**. (1999). A wound- and systemin-inducible polygalacturonase in tomato leaves. *P Natl Acad Sci USA*; **96**:1756-60.

327. **D'ovidio R, Mattei B, Roberti S, Bellincampi D**. (2004). Polygalacturonases, polygalacturonase-inhibiting proteins and pectic oligomers in plant-pathogen interactions. *Bba-Proteins Proteom*; **1696**:237-44.

328. **Kauss H, Fauth M, Merten A, Jeblick W**. (1999). Cucumber hypocotyls respond to cutin monomers via both an inducible and a constitutive H_2O_2-generating system. *Plant Physiol*; **120**:1175-82.

329. **Boller T**. (2005). Peptide signalling in plant development and self/non-self perception. *Curr Opin Cell Biol*; **17**:116-22.

330. **Huffaker A, Pearce G, Ryan CA**. (2006). An endogenous peptide signal in Arabidopsis activates components of the innate immune response. *P Natl Acad Sci USA*; **103**:10098-103.

331. **Boller T, Felix G**. (2009). A renaissance of elicitors: perception of microbe-associated molecular patterns and danger signals by pattern-recognition receptors. *Annu Rev Plant Biol*; **60**:379-406.

332. **Mccloud ES, Baldwin IT**. (1997). Herbivory and caterpillar regurgitants amplify the wound-induced increases in jasmonic acid but not nicotine in *Nicotiana sylvestris*. *Planta*; **203**:430-5.

333. **Halitschke R, Kessler A, Kahl J, Lorenz A, Baldwin IT**. (2000). Ecophysiological comparison of direct and indirect defenses in *Nicotiana attenuata*. *Oecologia*; **124**:408-17.

334. **Schmelz EA, Carroll MJ, Leclere S, Phipps SM, Meredith J, Chourey PS, et al.** (2006). Fragments of ATP synthase mediate plant perception of insect attack. *P Natl Acad Sci USA*; **103**:8894-9.

335. **Schmelz EA, Leclere S, Carroll MJ, Alborn HT, Teal PEA**. (2007). Cowpea chloroplastic ATP synthase is the source of multiple plant defense elicitors during insect herbivory. *Plant Physiol*; **144**:793-805.

336. **Halitschke R, Schittko U, Pohnert G, Boland W, Baldwin IT**. (2001). Molecular interactions between the specialist herbivore *Manduca sexta* (Lepidoptera, Sphingidae) and its natural host Nicotiana attenuata. III. Fatty acid-amino acid conjugates in herbivore oral secretions are necessary and sufficient for herbivore-specific plant responses. *Plant Physiol*; **125**:711-7.

337. **Alborn HT, Turlings TCJ, Jones TH, Stenhagen G, Loughrin JH, Tumlinson JH**. (1997). An elicitor of plant volatiles from beet armyworm oral secretion. *Science*; **276**:945-9.

338. **Pare PW, Alborn HT, Tumlinson JH**. (1998). Concerted biosynthesis of an insect elicitor of plant volatiles. *P Natl Acad Sci USA*; **95**:13971-5.

339. **Pohnert G, Jung V, Haukioja E, Lempa K, Boland W**. (1999). New fatty acid amides from regurgitant of lepidopteran (Noctuidae, Geometridae) caterpillars. *Tetrahedron*; **55**:11275-80.

340. **Spiteller D, Boland W**. (2003). N-(15,16-Dihydroxylinoleoyl)-glutamine and N-(15,16-epoxylinoleoyl)-glutamine isolated from oral secretions of lepidopteran larvae. *Tetrahedron*; **59**:135-9.

341. **Spiteller D, Oldham NJ, Boland W**. (2004). N-(17-phosphonooxylinolenoyl)glutamine and N-(17-phosphonooxylinoleoyl)glutamine from insect gut: the first backbone-phosphorylated fatty acid derivatives in nature. *J Org Chem*; **69**:1104-9.

342. **Gilardoni PA, Schuck S, Jungling R, Rotter B, Baldwin IT, Bonaventure G**. (2010). SuperSAGE analysis of the *Nicotiana attenuata* transcriptome after fatty acid-amino acid elicitation (FAC): identification of early mediators of insect responses. *BMC Plant Biol*; **10**:66.

343. **Truitt CL, Wei HX, Pare PW**. (2004). A plasma membrane protein from *Zea mays* binds with the herbivore elicitor volicitin. *Plant Cell*; **16**:523-32.

344. **Alborn HT, Hansen TV, Jones TH, Bennett DC, Tumlinson JH, Schmelz EA, et al.** (2007). Disulfooxy fatty acids from the American bird grasshopper *Schistocerca americana*, elicitors of plant volatiles. *P Natl Acad Sci USA*; **104**:12976-81.

345. **Schmelz EA, Engelberth J, Alborn HT, Tumlinson JH, Teal PEA**. (2009). Phytohormone-based activity mapping of insect herbivore-produced elicitors. *P Natl Acad Sci USA*; **106**:653-7.

346. **Schroder R, Forstreuter M, Hilker M**. (2005). A plant notices insect egg deposition and changes its rate of photosynthesis. *Plant Physiol*; **138**:470-7.

347. **Little D, Gouhier-Darimont C, Bruessow F, Reymond P**. (2007). Oviposition by pierid butterflies triggers defense responses in Arabidopsis. *Plant Physiol*; **143**:784-800.

348. **Mattiacci L, Dicke M, Posthumus MA**. (1995). Beta-glucosidase - an elicitor of herbivore-induced plant odor that attracts host-searching parasitic wasps. *P Natl Acad Sci USA*; **92**:2036-40.

349. **Prince DC, Drurey C, Zipfel C, Hogenhout SA**. (2014). The leucine-rich repeat receptor-like kinase BRASSINOSTEROID INSENSITIVE1-ASSOCIATED KINASE1 and the cytochrome P450 PHYTOALEXIN DEFICIENT3 contribute to innate immunity to aphids in Arabidopsis. *Plant Physiol*; **164**:2207-19.

350. **Chaudhary R, Atamian HS, Shen ZX, Brigg SP, Kaloshian I**. (2014). GroEL from the endosymbiont *Buchnera aphidicola* betrays the aphid by triggering plant defense. *P Natl Acad Sci USA*; **111**:8919-24.

351. **Chinchilla D, Bauer Z, Regenass M, Boller T, Felix G**. (2006). The Arabidopsis receptor kinase FLS2 binds flg22 and determines the specificity of flagellin perception. *Plant Cell*; **18**:465-76.

352. **Naito K, Taguchi F, Suzuki T, Inagaki Y, Toyoda K, Shiraishi T, et al.** (2008). Amino Acid sequence of bacterial microbe-associated molecular pattern flg22 is required for virulence. *Mol Plant-Microbe Interact*; **21**:1165-74.

353. **Gomez-Gomez L, Boller T**. (2000). FLS2: An LRR receptor-like kinase involved in the perception of the bacterial elicitor flagellin in Arabidopsis. *Mol Cell*; **5**:1003-11.

354. **Zipfel C, Kunze G, Chinchilla D, Caniard A, Jones JDG, Boller T, et al.** (2006). Perception of the bacterial PAMP EF-Tu by the receptor EFR restricts Agrobacterium-mediated transformation. *Cell*; **125**:749-60.

355. **Yamaguchi Y, Pearce G, Ryan CA**. (2006). The cell surface leucine-rich repeat receptor for AtPep1, an endoaenous peptide elicitor in Arabidopsis, is functional in transgenic tobacco cells. *P Natl Acad Sci USA*; **103**:10104-9.

356. **Forde BG, Roberts MR**. (2014). Glutamate receptor-like channels in plants: a role as amino acid sensors in plant defence? *Prime Rep*; **6**:37.

357. **Miya A, Albert P, Shinya T, Desaki Y, Ichimura K, Shirasu K, et al.** (2007). CERK1, a LysM receptor kinase, is essential for chitin elicitor signaling in Arabidopsis. *P Natl Acad Sci USA*; **104**:19613-8.

358. **Wan JR, Zhang XC, Neece D, Ramonell KM, Clough S, Kim SY, et al.** (2008). A LysM receptor-like kinase plays a critical role in chitin signaling and fungal resistance in Arabidopsis. *Plant Cell*; **20**:471-81.

359. **Aker J, De Vries SC**. (2008). Plasma membrane receptor complexes. *Plant Physiol*; **147**:1560-4.

360. **Chinchilla D, Zipfel C, Robatzek S, Kemmerling B, Nurnberger T, Jones JDG, et al.** (2007). A flagellin-induced complex of the receptor FLS2 and BAK1 initiates plant defence. *Nature*; **448**:497-U12.

361. **Heese A, Hann DR, Gimenez-Ibanez S, Jones AME, He K, Li J, et al.** (2007). The receptor-like kinase SERK3/BAK1 is a central regulator of innate immunity in plants. *P Natl Acad Sci USA*; **104**:12217-22.

362. **Yang DH, Hettenhausen C, Baldwin IT, Wu JQ**. (2011). BAK1 regulates the accumulation of jasmonic acid and the levels of trypsin proteinase inhibitors in *Nicotiana attenuata's* responses to herbivory. *J Exp Bot*; **62**:641-52.

363. **Zipfel C, Robatzek S**. (2010). Pathogen-Associated Molecular Pattern-Triggered Immunity: Veni, Vidi ... ? *Plant Physiol*; **154**:551-4.

364. **Ward JM, Pei ZM, Schroeder JI**. (1995). Roles of ion channels in initiation of signal-transduction in higher-plants. *Plant Cell*; **7**:833-44.

365. **Bricchi I, Bertea CM, Occhipinti A, Paponov IA, Maffei ME**. (2012). Dynamics of membrane potential variation and gene expression induced by *Spodoptera littoralis*, *Myzus persicae*, and *Pseudomonas syringae* in Arabidopsis. *Plos One*; **7**:e46673.

366. **Mithofer A, Ebel J, Felle HH**. (2005). Cation fluxes cause plasma membrane depolarization involved in beta-glucan elicitor-signaling in soybean roots. *Mol Plant-Microbe Interact*; **18**:983-90.

367. **Wendehenne D, Lamotte O, Frachisse JM, Barbier-Brygoo H, Pugin A**. (2002). Nitrate efflux is an essential component of the cryptogein signaling pathway leading to defense responses and hypersensitive cell death in tobacco. *Plant Cell*; **14**:1937-51.

368. **Bricchi I, Leitner M, Foti M, Mithofer A, Boland W, Maffei ME**. (2010). Robotic mechanical wounding (MecWorm) versus herbivore-induced responses: early signaling and volatile emission in lima bean (*Phaseolus lunatus L.*). *Planta*; **232**:719-29.

369. **Maffei M, Bossi S, Spiteller D, Mithofer A, Boland W**. (2004). Effects of feeding *Spodoptera littoralis* on lima bean leaves. I. Membrane potentials, intracellular calcium variations, oral secretions, and regurgitate components. *Plant Physiol*; **134**:1752-62.

370. **Maischak H, Grigoriev PA, Vogel H, Boland W, Mithofer A**. (2007). Oral secretions from herbivorous lepidopteran larvae exhibit ion channel-forming activities. *FEBS Lett*; **581**:898-904.

371. **Blume B, Nurnberger T, Nass N, Scheel D**. (2000). Receptor-mediated increase in cytoplasmic free calcium required for activation of pathogen defense in parsley. *Plant Cell*; **12**:1425-40.

372. **Lecourieux D, Mazars C, Pauly N, Ranjeva R, Pugin A**. (2002). Analysis and effects of cytosolic free calcium increases in response to elicitors in *Nicotiana plumbaginifolia* cells. *Plant Cell*; **14**:2627-41.

373. **Gelli A, Higgins VJ, Blumwald E**. (1997). Activation of plant plasma membrane Ca^{2+}-permeable channels by race-specific fungal elicitors. *Plant Physiol*; **113**:269-79.

374. **Yoshioka K, Moeder W, Kang HG, Kachroo P, Masmoudi K, Berkowitz G, et al.** (2006). The chimeric Arabidopsis CYCLIC NUCLEOTIDE-GATED ION CHANNEL11/12 activates multiple pathogen resistance responses. *Plant Cell*; **18**:747-63.

375. **Du LQ, Ali GS, Simons KA, Hou JG, Yang TB, Reddy ASN, et al.** (2009). Ca^{2+}/calmodulin regulates salicylic-acid-mediated plant immunity. *Nature*; **457**:1154-U116.

376. **Verrillo F, Occhipinti A, Kanchiswamy CN, Maffei ME**. (2014). Quantitative analysis of herbivore-induced cytosolic calcium by using a cameleon (YC 3.6) calcium sensor in *Arabidopsis thaliana*. *J Plant Physiol*; **171**:136-9.

377. **Yu IC, Parker J, Bent AF**. (1998). Gene-for-gene disease resistance without the hypersensitive response in Arabidopsis *dnd1* mutant. *P Natl Acad Sci USA*; **95**:7819-24.

378. **Ma Y, Walker RK, Zhao YC, Berkowitz GA**. (2012). Linking ligand perception by PEPR pattern recognition receptors to cytosolic Ca^{2+} elevation and downstream immune signaling in plants. *P Natl Acad Sci USA*; **109**:19852-7.

379. **Ma W, Berkowitz GA**. (2007). The grateful dead: calcium and cell death in plant innate immunity. *Cell Microbiol*; **9**:2571-85.

380. **Kang S, Kim HB, Lee H, Choi JY, Heu S, Oh CJ, et al.** (2006). Overexpression in Arabidopsis of a plasma membrane-targeting glutamate receptor from small radish increases glutamate-mediated Ca^{2+} influx and delays fungal infection. *Mol Cells*; **21**:418-27.

381. **Bjornson M, Benn G, Song X, Comai L, Franz AK, Dandekar AM, et al.** (2014). Distinct roles for mitogen-activated protein kinase signaling and CALMODULIN-BINDING TRANSCRIPTIONAL ACTIVATOR3 in regulating the peak time and amplitude of the plant general stress response. *Plant Physiol*; **166**:988-96.

382. **Qiu YJ, Xi J, Du LQ, Suttle JC, Poovaiah BW**. (2012). Coupling calcium/calmodulin-mediated signaling and herbivore-induced plant response through calmodulin-binding transcription factor AtSR1/CAMTA3. *Plant Mol Biol*; **79**:89-99.

383. **Romeis T, Herde M**. (2014). From local to global: CDPKs in systemic defense signaling upon microbial and herbivore attack. *Curr Opin Plant Biol*; **20C**:1-10.

384. **Monaghan J, Matschi S, Romeis T, Zipfel C**. (2015). The calcium-dependent protein kinase CPK28 negatively regulates the BIK1-mediated PAMP-induced calcium burst. *Plant signaling & behavior*; **10**.

385. **Kurusu T, Hamada J, Nokajima H, Kitagawa Y, Kiyoduka M, Takahashi A, et al.** (2010). Regulation of microbe-associated molecular pattern-induced hypersensitive cell death, phytoalexin production, and defense gene expression by calcineurin b-like protein-interacting protein kinases, osCIPK14/15, in rice cultured cells. *Plant Physiol*; **153**:678-92.

386. **Wu JQ, Hettenhausen C, Meldau S, Baldwin IT**. (2007). Herbivory rapidly activates MAPK signaling in attacked and unattacked leaf regions but not between leaves of *Nicotiana attenuata*. *Plant Cell*; **19**:1096-122.

387. **Nuhse TS, Peck SC, Hirt H, Boller T**. (2000). Microbial elicitors induce activation and dual phosphorylation of the *Arabidopsis thaliana* MAPK 6. *J Biol Chem*; **275**:7521-6.

388. **Suarez-Rodriguez MC, Adams-Phillips L, Liu YD, Wang HC, Su SH, Jester PJ, et al.** (2007). MEKK1 is required for flg22-induced MPK4 activation in Arabidopsis plants. *Plant Physiol*; **143**:661-9.

389. **Anderson JC, Bartels S, Besteiro MaG, Shahollari B, Ulm R, Peck SC**. (2011). Arabidopsis MAP Kinase Phosphatase 1 (AtMKP1) negatively regulates MPK6-mediated PAMP responses and resistance against bacteria. *Plant J*; **67**:258-68.

390. **Ichimura K, Casais C, Peck SC, Shinozaki K, Shirasu K**. (2006). MEKK1 is required for MPK4 activation and regulates tissue-specific and temperature-dependent cell death in Arabidopsis. *J Biol Chem*; **281**:36969-76.

391. **Sidonskaya E, Schweighofer A, Shubchynskyy V, Kammerhofer N, Hofmann J, Wieczorek K, et al.** (2016). Plant resistance against the parasitic nematode *Heterodera schachtii* is mediated by MPK3 and MPK6 kinases, which are controlled by the MAPK phosphatase AP2C1 in Arabidopsis. *J Exp Bot*; **67**:107-18.

392. **Seo S, Sano H, Ohashi Y**. (1999). Jasmonate-based wound signal transduction requires activation of WIPK, a tobacco mitogen-activated protein kinase. *Plant Cell*; **11**:289-98.

393. **Takabatake R, Seo S, Ito N, Gotoh Y, Mitsuhara I, Ohashi Y**. (2006). Involvement of wound-induced receptor-like protein kinase in wound signal transduction in tobacco plants. *Plant J*; **47**:249-57.

394. **Takahashi F, Yoshida R, Ichimura K, Mizoguchi T, Seo S, Yonezawa M, et al.** (2007). The mitogen-activated protein kinase cascade MKK3-MPK6 is an important part of the jasmonate signal transduction pathway in Arabidopsis. *Plant Cell*; **19**:805-18.

395. **Seo S, Katou S, Seto H, Gomi K, Ohashi Y**. (2007). The mitogen-activated protein kinases WIPK and SIPK regulate the levels of jasmonic and salicylic acids in wounded tobacco plants. *Plant J*; **49**:899-909.

396. **Seo S, Okamoto N, Seto H, Ishizuka K, Sano H, Ohashi Y**. (1995). Tobacco map kinase - a possible mediator in wound signal-transduction pathways. *Science*; **270**:1988-92.

397. **Kandoth PK, Ranf S, Pancholi SS, Jayanty S, Walla MD, Miller W, et al.** (2007). Tomato MAPKs LeMPK1, LeMPK2, and LeMPK3 function in the systemin-mediated defense response against herbivorous insects. *P Natl Acad Sci USA*; **104**:12205-10.

398. **Li Q, Xie QG, Smith-Becker J, Navarre DA, Kaloshian I**. (2006). Mi-1-mediated aphid resistance involves salicylic acid and mitogen-activated protein kinase signaling cascades. *Mol Plant-Microbe Interact*; **19**:655-64.

399. **Boudsocq M, Willmann MR, Mccormack M, Lee H, Shan LB, He P, et al.** (2010). Differential innate immune signalling via Ca^{2+} sensor protein kinases. *Nature*; **464**:418-U116.

400. **Szczegielniak J, Klimecka M, Liwosz A, Ciesielski A, Kaczanowski S, Dobrowolska G, et al.** (2005). A wound-responsive and phospholipid-regulated maize calcium-dependent protein kinase. *Plant Physiol*; **139**:1970-83.

401. **Szczegielniak J, Borkiewicz L, Szurmak B, Lewandowska-Gnatowska W, Statkiewicz M, Klimecka M, et al.** (2012). Maize calcium-dependent protein kinase (ZmCPK11): local and systemic response to wounding, regulation by touch and components of jasmonate signaling. *Physiol Plant*; **146**:1-14.

402. **Hettenhausen C, Sun GL, He YB, Zhuang HF, Sun T, Qi JF, et al.** (2016). Genome-wide identification of calcium-dependent protein kinases in soybean and analyses of their transcriptional responses to insect herbivory and drought stress. *Sci Rep-Uk*; **6**.

403. **Monaghan J, Matschi S, Shorinola O, Rovenich H, Matei A, Segonzac C, et al.** (2014). The calcium-dependent protein kinase CPK28 buffers plant immunity and regulates BIK1 turnover. *Cell Host Microbe*; **16**:605-15.

404. **Coca M, San Segundo B**. (2010). AtCPK1 calcium-dependent protein kinase mediates pathogen resistance in Arabidopsis. *Plant J*; **63**:526-40.

405. **Kanchiswamy CN, Takahashi H, Quadro S, Maffei ME, Bossi S, Bertea C, et al.** (2010). Regulation of Arabidopsis defense responses against Spodoptera littoralis by CPK-mediated calcium signaling. *BMC Plant Biol*; **10**.

406. **Keppler LD, Baker CJ, Atkinson MM**. (1989). Active oxygen production during a bacteria-induced hypersensitive reaction in tobacco suspension cells. *Phytopathology*; **79**:974-8.

407. **Maffei ME, Mithofer A, Arimura GI, Uchtenhagen H, Bossi S, Bertea CM, et al.** (2006). Effects of feeding *Spodoptera littoralis* on lima bean leaves. III. Membrane depolarization and involvement of hydrogen peroxide. *Plant Physiol*; **140**:1022-35.

408. **Mai VC, Bednarski W, Borowiak-Sobkowiak B, Wilkaniec B, Samardakiewicz S, Morkunas I**. (2013). Oxidative stress in pea seedling leaves in response to *Acyrthosiphon pisum* infestation. *Phytochemistry*; **93**:49-62.

409. **Torres MA, Dangl JL, Jones JDG**. (2002). Arabidopsis gp91(phox) homologues AtrbohD and AtrbohF are required for accumulation of reactive oxygen intermediates in the plant defense response. *P Natl Acad Sci USA*; **99**:517-22.

410. **Nuhse TS, Bottrill AR, Jones AME, Peck SC**. (2007). Quantitative phosphoproteomic analysis of plasma membrane proteins reveals regulatory mechanisms of plant innate immune responses. *Plant J*; **51**:931-40.

411. **Zhang J, Shao F, Cui H, Chen LJ, Li HT, Zou Y, et al.** (2007). A *Pseudomonas syringae* effector inactivates MAPKs to suppress PAMP-Induced immunity in plants. *Cell Host Microbe*; **1**:175-85.

412. **Torres MA, Jones JDG, Dangl JL**. (2005). Pathogen-induced, NADPH oxidase-derived reactive oxygen intermediates suppress spread of cell death in *Arabidopsis thaliana*. *Nat Genet*; **37**:1130-4.

413. **Miller G, Schlauch K, Tam R, Cortes D, Torres MA, Shulaev V, et al.** (2009). The plant NADPH oxidase RBOHD mediates rapid systemic signaling in response to diverse stimuli. *Science signaling*; **2**:ra45.

414. **Sagi M, Fluhr R**. (2006). Production of reactive oxygen species by plant NADPH oxidases. *Plant Physiol*; **141**:336-40.

415. **Foreman J, Demidchik V, Bothwell JH, Mylona P, Miedema H, Torres MA, et al.** (2003). Reactive oxygen species produced by NADPH oxidase regulate plant cell growth. *Nature*; **422**:442-6.

416. **Gfeller A, Baerenfaller K, Loscos J, Chetelat A, Baginsky S, Farmer EE**. (2011). Jasmonate controls polypeptide patterning in undamaged tissue in wounded Arabidopsis leaves. *Plant Physiol*; **156**:1797-807.

417. **Leitner M, Boland W, Mithofer A**. (2005). Direct and indirect defences induced by piercing-sucking and chewing herbivores in *Medicago truncatula*. *New Phytol*; **167**:597-606.

418. **Bodenhausen N, Reymond P**. (2007). Signaling pathways controlling induced resistance to insect herbivores in Arabidopsis. *Mol Plant-Microbe Interact*; **20**:1406-20.

419. **Wunsche H, Baldwin IT, Wu JQ**. (2011). S-Nitrosoglutathione reductase (GSNOR) mediates the biosynthesis of jasmonic acid and ethylene induced by feeding of the insect herbivore *Manduca sexta* and is important for jasmonate-elicited responses in *Nicotiana attenuata*. *J Exp Bot*; **62**:4605-16.

420. **Tian D, Peiffer M, Shoemaker E, Tooker J, Haubruge E, Francis F, et al.** (2012). Salivary glucose oxidase from caterpillars mediates the induction of rapid and delayed-induced defenses in the tomato plant. *Plos One*; **7**:e36168.

421. **Doares SH, Syrovets T, Weiler EW, Ryan CA**. (1995). Oligogalacturonides and chitosan activate plant defensive genes through the octadecanoid pathway. *P Natl Acad Sci USA*; **92**:4095-8.

422. **Bruinsma M, Van Broekhoven S, Poelman EH, Posthumus MA, Muller MJ, Van Loon JJA, et al.** (2010). Inhibition of lipoxygenase affects induction of both direct and indirect plant defences against herbivorous insects. *Oecologia*; **162**:393-404.

423. **Watanabe T, Seo S, Sakai S**. (2001). Wound-induced expression of a gene for 1-aminocyclopropane-1-carboxylate synthase and ethylene production are

regulated by both reactive oxygen species and jasmonic acid in *Cucurbita maxima*. *Plant Physiol Biochem*; **39**:121-7.

424. **Yang DH, Hettenhausen C, Baldwin IT, Wu JQ**. (2012). Silencing *Nicotiana attenuata* calcium-dependent protein kinases, CDPK4 and CDPK5, strongly up-regulates wound- and herbivory-induced jasmonic acid accumulations. *Plant Physiol*; **159**:1591-607.

425. **Kallenbach M, Alagna F, Baldwin IT, Bonaventure G**. (2010). *Nicotiana attenuata* SIPK, WIPK, NPR1, and fatty acid-amino acid conjugates participate in the induction of jasmonic acid biosynthesis by affecting early enzymatic steps in the pathway. *Plant Physiol*; **152**:1760-.

426. **Zhu-Salzman K, Salzman RA, Ahn JE, Koiwa H**. (2004). Transcriptional regulation of sorghum defense determinants against a phloem-feeding aphid. *Plant Physiol*; **134**:420-31.

427. **Walling LL**. (2008). Avoiding effective defenses: strategies employed by phloem-feeding insects. *Plant Physiol*; **146**:859-66.

428. **Mewis I, Tokuhisa JG, Schultz JC, Appel HM, Ulrichs C, Gershenzon J**. (2006). Gene expression and glucosinolate accumulation in *Arabidopsis thaliana* in response to generalist and specialist herbivores of different feeding guilds and the role of defense signaling pathways. *Phytochemistry*; **67**:2450-62.

429. **Gao LL, Anderson JP, Klingler JP, Nair RM, Edwards OR, Singh KB**. (2007). Involvement of the octadecanoid pathway in bluegreen aphid resistance in *Medicago truncatula*. *Mol Plant-Microbe Interact*; **20**:82-93.

430. **Kusnierczyk A, Tran DH, Winge P, Jorstad TS, Reese JC, Troczynska J, et al.** (2011). Testing the importance of jasmonate signalling in induction of plant defences upon cabbage aphid (*Brevicoryne brassicae*) attack. *BMC Genomics*; **12**:423.

431. **De Vos M, Van Zaanen W, Koornneef A, Korzelius JP, Dicke M, Van Loon LC, et al.** (2006). Herbivore-induced resistance against microbial pathogens in Arabidopsis. *Plant Physiol*; **142**:352-63.

432. **De Torres Zabala M, Bennett MH, Truman WH, Grant MR**. (2009). Antagonism between salicylic and abscisic acid reflects early host-pathogen conflict and moulds plant defence responses. *Plant J*; **59**:375-86.

433. **Coppola V, Coppola M, Rocco M, Digilio MC, D'ambrosio C, Renzone G, et al.** (2013). Transcriptomic and proteomic analysis of a compatible tomato-aphid interaction reveals a predominant salicylic acid-dependent plant response. *BMC Genomics*; **14**.

434. **Thompson GA, Goggin FL**. (2006). Transcriptomics and functional genomics of plant defence induction by phloem-feeding insects. *J Exp Bot*; **57**:755-66.

435. **Goggin FL**. (2007). Plant-aphid interactions: molecular and ecological perspectives. *Curr Opin Plant Biol*; **10**:399-408.

436. **Kazan K, Manners JM**. (2008). Jasmonate signaling: toward an integrated view. *Plant Physiol*; **146**:1459-68.

437. **Hillwig MS, Chiozza M, Casteel CL, Lau ST, Hohenstein J, Hernandez E, et al.** (2016). Abscisic acid deficiency increases defence responses against *Myzus persicae* in Arabidopsis. *Mol Plant Pathol*; **17**:225-35.

438. **Ton J, Mauch-Mani B**. (2004). Beta-amino-butyric acid-induced resistance against necrotrophic pathogens is based on ABA-dependent priming for callose. *Plant J*; **38**:119-30.

439. **Anderson JP, Badruzsaufari E, Schenk PM, Manners JM, Desmond OJ, Ehlert C, et al.** (2004). Antagonistic interaction between abscisic acid and jasmonate-ethylene signaling pathways modulates defense gene expression and disease resistance in Arabidopsis. *Plant Cell*; **16**:3460-79.

440. **Adie BaT, Perez-Perez J, Perez-Perez MM, Godoy M, Sanchez-Serrano JJ, Schmelz EA, et al.** (2007). ABA is an essential signal for plant resistance to pathogens affecting JA biosynthesis and the activation of defenses in Arabidopsis. *Plant Cell*; **19**:1665-81.

441. **Fan J, Hill L, Crooks C, Doerner P, Lamb C**. (2009). Abscisic acid has a key role in modulating diverse plant-pathogen interactions. *Plant Physiol*; **150**:1750-61.

442. **Kerchev PI, Karpinska B, Morris JA, Hussain A, Verrall SR, Hedley PE, et al.** (2013). Vitamin C and the abscisic acid-insensitive 4 transcription factor are important determinants of aphid resistance in Arabidopsis. *Antioxidants & redox signaling*; **18**:2091-105.

443. **Lund ST, Stall RE, Klee HJ**. (1998). Ethylene regulates the susceptible response to pathogen infection in tomato. *Plant Cell*; **10**:371-82.

444. **Gravino M, Savatin DV, Macone A, De Lorenzo G**. (2015). Ethylene production in *Botrytis cinerea*- and oligogalacturonide-induced immunity requires calcium-dependent protein kinases. *The Plant journal : for cell and molecular biology*; **84**:1073-86.

445. **Spanu P, Grosskopf DG, Felix G, Boller T**. (1994). The apparent turnover of 1-aminocyclopropane-1-carboxylate synthase in tomato cells is regulated by protein-phosphorylation and dephosphorylation. *Plant Physiol*; **106**:529-35.

446. **Argandona VH, Chaman M, Cardemil L, Munoz O, Zuniga GE, Corcuera LJ**. (2001). Ethylene production and peroxidase activity in aphid-infested barley. *J Chem Ecol*; **27**:53-68.

447. **Wu CJ, Avila CA, Goggin FL**. (2015). The ethylene response factor Pti5 contributes to potato aphid resistance in tomato independent of ethylene signalling. *J Exp Bot*; **66**:559-70.

448. **Dillwith JW, Berberet RC, Bergman DK, Neese PA, Edwards RM, Mcnew RW**. (1991). Plant biochemistry and aphid populations - studies on the spotted alfalfa aphid, *Therioaphis maculata*. *Arch Insect Biochem Physiol*; **17**:235-51.

449. **Miller HL, Neese PA, Ketring DL, Dillwith JW**. (1994). Involvement of ethylene in aphid infestation of barley. *J Plant Growth Regul*; **13**:167-71.

450. **Mantelin S, Bhattarai KK, Kaloshian I**. (2009). Ethylene contributes to potato aphid susceptibility in a compatible tomato host. *New Phytol*; **183**:444-56.

451. **Reymond P, Weber H, Damond M, Farmer EE**. (2000). Differential gene expression in response to mechanical wounding and insect feeding in Arabidopsis. *Plant Cell*; **12**:707-19.

452. **Grata E, Boccard J, Glauser G, Carrupt PA, Farmer EE, Wolfender JL, et al.** (2007). Development of a two-step screening ESI-TOF-MS method for rapid determination of significant stress-induced metabolome modifications in plant leaf extracts: The wound response in *Arabidopsis thaliana* as a case study. *J Sep Sci*; **30**:2268-78.

453. **Skibbe M, Qu N, Galis I, Baldwin IT**. (2008). Induced plant defenses in the natural environment: Nicotiana attenuata WRKY3 and WRKY6 coordinate responses to herbivory. *Plant Cell*; **20**:1984-2000.

454. **Maleck K, Levine A, Eulgem T, Morgan A, Schmid J, Lawton KA, et al.** (2000). The transcriptome of *Arabidopsis thaliana* during systemic acquired resistance. *Nat Genet*; **26**:403-10.

455. **Zhou N, Tootle TL, Glazebrook J**. (1999). Arabidopsis PAD3, a gene required for camalexin biosynthesis, encodes a putative cytochrome P450 monooxygenase. *Plant Cell*; **11**:2419-28.

456. **Ellinger D, Voigt CA**. (2014). Callose biosynthesis in arabidopsis with a focus on pathogen response: what we have learned within the last decade. *Ann Bot*; **114**:1349-58.

457. **Hao PY, Liu CX, Wang YY, Chen RZ, Tang M, Du B, et al.** (2008). Herbivore-induced callose deposition on the sieve plates of rice: an important mechanism for host resistance. *Plant Physiol*; **146**:1810-20.

458. **War AR, Paulraj MG, Ahmad T, Buhroo AA, Hussain B, Ignacimuthu S, et al.** (2012). Mechanisms of plant defense against insect herbivores. *Plant signaling & behavior*; **7**:1306-20.

459. **Schuhegger R, Nafisi M, Mansourova M, Petersen BL, Olsen CE, Svatos A, et al.** (2006). CYP71B15 (PAD3) catalyzes the final step in camalexin biosynthesis. *Plant Physiol*; **141**:1248-54.

460. **Thomma BPHJ, Nelissen I, Eggermont K, Broekaert WF**. (1999). Deficiency in phytoalexin production causes enhanced susceptibility of *Arabidopsis thaliana* to the fungus *Alternaria brassicicola*. *Plant J*; **19**:163-71.

461. **Ferrari S, Plotnikova JM, De Lorenzo G, Ausubel FM**. (2003). Arabidopsis local resistance to *Botrytis cinerea* involves salicylic acid and camalexin and requires EDS4 and PAD2, but not SID2, EDS5 or PAD4. *Plant J*; **35**:193-205.

462. **Rogers EE, Glazebrook J, Ausubel FN**. (1996). Mode of action of the *Arabidopsis thaliana* phytoalexin camalexin and its role in Arabidopsis-pathogen interactions. *Mol Plant-Microbe Interact*; **9**:748-57.

463. **Denoux C, Galletti R, Mammarella N, Gopalan S, Werck D, De Lorenzo G, et al.** (2009). Activation of defense response pathways by OGs and flg22 elicitors in Arabidopsis seedlings. *Mol Plant*; **2**:838-.

464. **De Vos M, Jander G**. (2009). *Myzus persicae* (green peach aphid) salivary components induce defence responses in *Arabidopsis thaliana*. *Plant Cell Environ*; **32**:1548-60.

465. **Bednarek P, Pislewska-Bednarek M, Svatos A, Schneider B, Doubsky J, Mansurova M, et al.** (2009). A Glucosinolate Metabolism Pathway in Living Plant Cells Mediates Broad-Spectrum Antifungal Defense. *Science*; **323**:101-6.

466. **Wittstock U, Halkier BA**. (2002). Glucosinolate research in the Arabidopsis era. *Trends Plant Sci*; **7**:263-70.

467. **Hopkins RJ, Van Dam NM, Van Loon JJA**. (2009). Role of glucosinolates in insect-plant relationships and multitrophic interactions. *Annu Rev Entomol*; **54**:57-83.

468. **Muller R, De Vos M, Sun JY, Sonderby IE, Halkier BA, Wittstock U, et al.** (2010). Differential effects of indole and aliphatic glucosinolates on lepidopteran herbivores. *J Chem Ecol*; **36**:905-13.

469. **Kim JH, Jander G**. (2007). *Myzus persicae* (green peach aphid) feeding on Arabidopsis induces the formation of a deterrent indole glucosinolate. *Plant J*; **49**:1008-19.

470. **Kim JH, Lee BW, Schroeder FC, Jander G**. (2008). Identification of indole glucosinolate breakdown products with antifeedant effects on *Myzus persicae* (green peach aphid). *Plant J*; **54**:1015-26.

471. **Turlings TCJ, Loughrin JH, Mccall PJ, Rose USR, Lewis WJ, Tumlinson JH**. (1995). How caterpillar-damaged plants protect themselves by attracting parasitic wasps. *P Natl Acad Sci USA*; **92**:4169-74.

472. **Allmann S, Baldwin IT**. (2010). Insects betray themselves in nature to predators by rapid isomerization of green leaf volatiles. *Science*; **329**:1075-8.

473. **Engelberth J, Alborn HT, Schmelz EA, Tumlinson JH**. (2004). Airborne signals prime plants against insect herbivore attack. *Proc Natl Acad Sci U S A*; **101**:1781-5.

474. **Kessler A, Halitschke R, Diezel C, Baldwin IT**. (2006). Priming of plant defense responses in nature by airborne signaling between *Artemisia tridentata* and *Nicotiana attenuata*. *Oecologia*; **148**:280-92.

475. **Ament K, Kant MR, Sabelis MW, Haring MA, Schuurink RC**. (2004). Jasmonic acid is a key regulator of spider mite-induced volatile terpenoid and methyl salicylate emission in tomato. *Plant Physiol*; **135**:2025-37.

476. **Halitschke R, Ziegler J, Keinanen M, Baldwin IT**. (2004). Silencing of hydroperoxide lyase and allene oxide synthase reveals substrate and defense signaling crosstalk in *Nicotiana attenuata*. *Plant J*; **40**:35-46.

477. **Matthes MC, Bruce TJA, Ton J, Verrier PJ, Pickett JA, Napier JA**. (2010). The transcriptome of cis-jasmone-induced resistance in *Arabidopsis thaliana* and its role in indirect defence. *Planta*; **232**:1163-80.

478. **Allmann S, Halitschke R, Schuurink RC, Baldwin IT**. (2010). Oxylipin channelling in *Nicotiana attenuata*: lipoxygenase 2 supplies substrates for green leaf volatile production. *Plant Cell Environ*; **33**:2028-40.

479. **Scala A, Mirabella R, Mugo C, Matsui K, Haring MA, Schuurink RC**. (2013). E-2-hexenal promotes susceptibility to *Pseudomonas syringae* by activating jasmonic acid pathways in Arabidopsis. *Frontiers in Plant Science*; **4**.

480. **Galan JE, Lara-Tejero M, Marlovits TC, Wagner S**. (2014). Bacterial type III secretion systems: specialized nanomachines for protein delivery into target cells. *Annu Rev Microbiol*; **68**:415-38.

481. **Shan LB, He P, Li JM, Heese A, Peck SC, Nurnberger T, et al.** (2008). Bacterial effectors target the common signaling partner BAK1 to disrupt multiple MAMP receptor-signaling complexes and impede plant immunity. *Cell Host Microbe*; **4**:17-27.

482. **Debroy S, Thilmony R, Kwack YB, Nomura K, He SY**. (2004). A family of conserved bacterial effectors inhibits salicylic acid-mediated basal immunity and promotes disease necrosis in plants. *P Natl Acad Sci USA*; **101**:9927-32.

483. **Gimenez-Ibanez S, Boter M, Fernandez-Barbero G, Chini A, Rathjen JP, Solano R**. (2014). The bacterial effector HopX1 targets JAZ transcriptional repressors to activate jasmonate signaling and promote infection in Arabidopsis. *PLoS Biol*; **12**.

484. **Giraldo MC, Valent B**. (2013). Filamentous plant pathogen effectors in action. *Nat Rev Microbiol*; **11**:800-14.

485. **Asai S, Shirasu K**. (2015). Plant cells under siege: plant immune system versus pathogen effectors. *Curr Opin Plant Biol*; **28**:1-8.

486. **Van Den Burg HA, Harrison SJ, Joosten MHaJ, Vervoort J, De Wit PJGM**. (2006). Cladosporium fulvum Avr4 protects fungal cell walls against hydrolysis by plant chitinases accumulating during infection. *Mol Plant-Microbe Interact*; **19**:1420-30.

487. **Marshall R, Kombrink A, Motteram J, Loza-Reyes E, Lucas J, Hammond-Kosack KE, et al.** (2011). Analysis of two *in planta* expressed LysM effector homologs from the fungus *Mycosphaerella graminicola* reveals novel functional properties and varying contributions to virulence on wheat. *Plant Physiol*; **156**:756-69.

488. **Mentlak TA, Kombrink A, Shinya T, Ryder LS, Otomo I, Saitoh H, et al.** (2012). Effector-mediated suppression of chitin-triggered immunity by *Magnaporthe oryzae* is necessary for rice blast disease. *Plant Cell*; **24**:322-35.

489. **Sanchez-Vallet A, Saleem-Batcha R, Kombrink A, Hansen G, Valkenburg DJ, Thomma BPHJ, et al.** (2013). Fungal effector Ecp6 outcompetes host immune receptor for chitin binding through intrachain LysM dimerization. *Elife*; **2**.

490. **Tian MY, Huitema E, Da Cunha L, Torto-Alalibo T, Kamoun S**. (2004). A Kazal-like extracellular serine protease inhibitor from *Phytophthora infestans* targets the tomato pathogenesis-related protease P69B. *J Biol Chem*; **279**:26370-7.

491. **Tian MY, Win J, Song J, Van Der Hoorn R, Van Der Knaap E, Kamoun S**. (2007). A *Phytophthora infestans* cystatin-like protein targets a novel tomato papain-like apoplastic protease. *Plant Physiol*; **143**:364-77.

492. **Song J, Win J, Tian MY, Schornack S, Kaschani F, Ilyas M, et al.** (2009). Apoplastic effectors secreted by two unrelated eukaryotic plant pathogens target the tomato defense protease Rcr3. *P Natl Acad Sci USA*; **106**:1654-9.

493. **Bozkurt TO, Schornack S, Win J, Shindo T, Ilyas M, Oliva R, et al.** (2011). *Phytophthora infestans* effector AVRblb2 prevents secretion of a plant immune protease at the haustorial interface. *P Natl Acad Sci USA*; **108**:20832-7.

494. **Schittko U, Hermsmeier D, Baldwin IT**. (2001). Molecular interactions between the specialist herbivore *Manduca sexta* (Lepidoptera, Sphingidae) and its natural host *Nicotiana attenuata*. II. Accumulation of plant mRNAs in response to insect-derived cues. *Plant Physiol*; **125**:701-10.

495. **Bede JC, Musser RO, Felton GW, Korth KL**. (2006). Caterpillar herbivory and salivary enzymes decrease transcript levels of *Medicago truncatula* genes encoding early enzymes in terpenoid biosynthesis. *Plant Mol Biol*; **60**:519-31.

496. **Hu YH, Leung DWM, Kang L, Wang CZ**. (2008). Diet factors responsible for the change of the glucose oxidase activity in labial salivary glands of *Helicoverpa armigera*. *Arch Insect Biochem Physiol*; **68**:113-21.

497. **Musser RO, Hum-Musser SM, Eichenseer H, Peiffer M, Ervin G, Murphy JB, et al.** (2002). Caterpillar saliva beats plant defences - a new weapon emerges in the evolutionary arms race between plants and herbivores. *Nature*; **416**:599-600.

498. **Eichenseer H, Mathews MC, Powell JS, Felton GW**. (2010). Survey of a salivary effector in caterpillars: glucose oxidase variation and correlation with host range. *J Chem Ecol*; **36**:885-97.

499. **Moran PJ, Cheng YF, Cassell JL, Thompson GA**. (2002). Gene expression profiling of *Arabidopsis thaliana* in compatible plant-aphid interactions. *Arch Insect Biochem Physiol*; **51**:182-203.

500. **Mutti NS, Park Y, Reese JC, Reeck GR**. (2006). RNAi knockdown of a salivary transcript leading to lethality in the pea aphid, *Acyrthosiphon pisum*. *J Insect Sci*; **6**.

501. **Pitino M, Hogenhout SA**. (2013). Aphid protein effectors promote aphid colonization in a plant species-specific manner. *Mol Plant-Microbe Interact*; **26**:130-9.

502. **Drurey C**. (2016) *The dynamics of molecular components that regulate aphid-plant interactions*. Norwich: University of East Anglia.

503. **Elzinga DA, De Vos M, Jander G**. (2014). Suppression of plant defenses by a *Myzus persicae* (green peach aphid) salivary effector protein. *Mol Plant-Microbe Interact*; **27**:747-56.

504. **Atamian HS, Chaudhary R, Dal Cin V, Bao E, Girke T, Kaloshian I**. (2013). *In Planta* expression or delivery of potato aphid *Macrosiphum euphorbiae* effectors Me10 and Me23 enhances aphid fecundity. *Mol Plant-Microbe Interact*; **26**:67-74.

505. **Van Der Biezen EA, Jones JDG**. (1998). Plant disease-resistance proteins and the gene-for-gene concept. *Trends Biochem Sci*; **23**:454-6.

506. **Dangl JL, Jones JDG**. (2001). Plant pathogens and integrated defence responses to infection. *Nature*; **411**:826-33.

507. **Blatt MR, Grabov A, Brearley J, Hammond-Kosack K, Jones JDG**. (1999). K^+ channels of Cf-9 transgenic tobacco guard cells as targets for Cladosporium fulvum Avr9 elicitor-dependent signal transduction. *Plant J*; **19**:453-62.

508. **Romeis T, Piedras P, Zhang SQ, Klessig DF, Hirt H, Jones JDG**. (1999). Rapid Avr9- and Cf-9-dependent activation of MAP kinases in tobacco cell cultures and leaves: convergence of resistance gene, elicitor, wound, and salicylate responses. *Plant Cell*; **11**:273-87.

509. **Grant M, Brown I, Adams S, Knight M, Ainslie A, Mansfield J**. (2000). The RPM1 plant disease resistance gene facilitates a rapid and sustained increase in cytosolic calcium that is necessary for the oxidative burst and hypersensitive cell death. *Plant J*; **23**:441-50.

510. **Romeis T, Tang SJ, Hammond-Kosack K, Piedras P, Blatt M, Jones JDG**. (2000). Early signalling events in the Avr9/Cf-9-dependent plant defence response. *Mol Plant Pathol*; **1**:3-8.

511. **Romeis T, Ludwig AA, Martin R, Jones JDG**. (2001). Calcium-dependent protein kinases play an essential role in a plant defence response. *EMBO J*; **20**:5556-67.

512. **Rowland O, Ludwig AA, Merrick CJ, Baillieul F, Tracy FE, Durrant WE, et al.** (2005). Functional analysis of Avr9/Cf-9 rapidly elicited genes identifies a protein kinase, ACIK1, that is essential for full Cf-9-dependent disease resistance in tomato. *Plant Cell*; **17**:295-310.

513. **Pike SM, Zhang XC, Gassmann W**. (2005). Electrophysiological characterization of the Arabidopsis avrRpt2-specific hypersensitive response in the absence of other bacterial signals. *Plant Physiol*; **138**:1009-17.

514. **Smith PG**. (1944). Embryo culture of a tomato species hybrid. *Proc Am Soc Hortic Sci*; **44**:413–6.

515. **Milligan SB, Bodeau J, Yaghoobi J, Kaloshian I, Zabel P, Williamson VM.** (1998). The root knot nematode resistance gene Mi from tomato is a member of the leucine zipper, nucleotide binding, leucine-rich repeat family of plant genes. *Plant Cell*; **10**:1307-19.

516. **Rossi M, Goggin FL, Milligan SB, Kaloshian I, Ullman DE, Williamson VM.** (1998). The nematode resistance gene Mi of tomato confers resistance against the potato aphid. *P Natl Acad Sci USA*; **95**:9750-4.

517. **Nombela G, Beitia F, Muniz M.** (2001). A differential interaction study of Bemisia tabaci Q-biotype on commercial tomato varieties with or without the Mi resistance gene, and comparative host responses with the B-biotype. *Entomol Exp Appl*; **98**:339-44.

518. **Casteel CL, Walling LL, Paine TD.** (2006). Behavior and biology of the tomato psyllid, *Bactericerca cockerelli*, in response to the *Mi-1.2* gene. *Entomol Exp Appl*; **121**:67-72.

519. **De Ilarduya OM, Xie QG, Kaloshian I.** (2003). Aphid-induced defense responses in Mi-1-mediated compatible and incompatible tomato interactions. *Mol Plant-Microbe Interact*; **16**:699-708.

520. **Mantelin S, Peng HC, Li BB, Atamian HS, Takken FLW, Kaloshian I.** (2011). The receptor-like kinase SlSERK1 is required for Mi-1-mediated resistance to potato aphids in tomato. *Plant J*; **67**:459-71.

521. **Klingler J, Kovalski I, Silberstein L, Thompson GA, Perl-Treves R.** (2001). Mapping of cotton-melon aphid resistance in melon. *J Am Soc Hort Sci*; **126**:56-63.

522. **Pauquet J, Burget E, Hagen L, Chovelon V, Menn A, Valot N, et al.** Map-based cloning of the vat gene from melon conferring resistance to both aphid colonization and aphid transmission of several viruses. Progress in cucurbit genetics and breeding research Proceedings of Cucurbitaceae 2004, the 8th EUCARPIA Meeting on Cucurbit Genetics and Breeding, Olomouc, Czech Republic, 12-17 July, 2004; Palacky University, Olomouc2004. p. 325–9.

523. **Martin B, Rahbe Y, Fereres A.** (2003). Blockage of stylet tips as the mechanism of resistance to virus transmission by *Aphis gossypii* in melon lines bearing the *Vat* gene. *Ann Appl Biol*; **142**:245-50.

524. **Stewart SA, Hodge S, Ismail N, Mansfield JW, Feys BJ, Prosperi JM, et al.** (2009). The RAP1 gene confers effective, race-specific resistance to the pea aphid in *Medicago truncatula* independent of the hypersensitive reaction. *Mol Plant-Microbe Interact*; **22**:1645-55.

525. **Dogimont C, Bendahmane A, Chovelon V, Boissot N.** (2010). Host plant resistance to aphids in cultivated crops: genetic and molecular bases, and interactions with aphid populations. *C R Biol*; **333**:566-73.

526. **Traw MB, Kniskern JM, Bergelson J.** (2007). SAR increases fitness of *Arabidopsis thaliana* in the presence of natural bacterial pathogens. *Evolution*; **61**:2444-9.

527. **Conrath U**. (2011). Molecular aspects of defence priming. *Trends Plant Sci*; **16**:524-31.

528. **Farmer EE, Gasperini D, Acosta IF**. (2014). The squeeze cell hypothesis for the activation of jasmonate synthesis in response to wounding. *The New phytologist*; **204**:282-8.

529. **Park SW, Kaimoyo E, Kumar D, Mosher S, Klessig DF**. (2007). Methyl salicylate is a critical mobile signal for plant systemic acquired resistance. *Science*; **318**:113-6.

530. **Koo AJK, Howe GA**. (2009). The wound hormone jasmonate. *Phytochemistry*; **70**:1571-80.

531. **Hong YG**. (2012). Non-coding RNAs in intercellular and systemic signaling. *Frontiers in Plant Science*; **3**.

532. **Notaguchi M, Okamoto S**. (2015). Dynamics of long-distance signaling via plant vascular tissues. *Frontiers in Plant Science*; **6**.

533. **Metraux JP, Signer H, Ryals J, Ward E, Wyssbenz M, Gaudin J, et al.** (1990). Increase in salicylic-acid at the onset of systemic acquired-resistance in cucumber. *Science*; **250**:1004-6.

534. **Ryals J, Uknes S, Ward E**. (1994). Systemic acquired-resistance. *Plant Physiol*; **104**:1109-12.

535. **Steinhorst L, Kudla J**. (2014). Signaling in cells and organisms - calcium holds the line. *Curr Opin Plant Biol*; **22C**:14-21.

536. **Choi WG, Hilleary R, Swanson SJ, Kim SH, Gilroy S**. (2016). Rapid, long-distance electrical and calcium signaling in plants. *Annual Review of Plant Biology, Vol 67*; **67**:287-307.

537. **Gilroy S, Bialasek M, Suzuki N, Gorecka M, Devireddy AR, Karpinski S, et al.** (2016). ROS, calcium, and electric signals: key mediators of rapid systemic signaling in plants. *Plant Physiol*; **171**:1606-15.

538. **Xiong TC, Ronzier E, Sanchez F, Corratge-Faillie C, Mazars C, Thibaud JB**. (2014). Imaging long distance propagating calcium signals in intact plant leaves with the BRET-based GFP-aequorin reporter. *Front Plant Sci*; **5**:43.

539. **Gilroy S, Suzuki N, Miller G, Choi W-G, Toyota M, Devireddy AR, et al.** (2014). A tidal wave of signals: calcium and ROS at the forefront of rapid systemic signaling. *Trends Plant Sci*.

540. **Bricchi I, Occhipinti A, Bertea CM, Zebelo SA, Brillada C, Verrillo F, et al.** (2013). Separation of early and late responses to herbivory in Arabidopsis by changing plasmodesmal function. *The Plant journal : for cell and molecular biology*; **73**:14-25.

541. **Salvador-Recatala V, Tjallingii WF, Farmer EE**. (2014). Real-time, *in vivo* intracellular recordings of caterpillar-induced depolarization waves in sieve elements using aphid electrodes. *The New phytologist*; **203**:674-84.

542. **Cang CL, Bekele B, Ren DJ**. (2014). The voltage-gated sodium channel TPC1 confers endolysosomal excitability. *Nat Chem Biol*; **10**:463-9.

543. **Glauser G, Grata E, Dubugnon L, Rudaz S, Farmer EE, Wolfender JL**. (2008). Spatial and temporal dynamics of jasmonate synthesis and accumulation in Arabidopsis in response to wounding. *J Biol Chem*; **283**:16400-7.

544. **Glauser G, Dubugnon L, Mousavi SaR, Rudaz S, Wolfender JL, Farmer EE**. (2009). Velocity estimates for signal propagation leading to systemic jasmonic acid accumulation in wounded Arabidopsis. *J Biol Chem*; **284**:34506-13.

545. **Chauvin A, Caldelari D, Wolfender JL, Farmer EE**. (2013). Four 13-lipoxygenases contribute to rapid jasmonate synthesis in wounded *Arabidopsis thaliana* leaves: a role for lipoxygenase 6 in responses to long-distance wound signals. *The New phytologist*; **197**:566-75.

546. **Koo AJK, Gao XL, Jones AD, Howe GA**. (2009). A rapid wound signal activates the systemic synthesis of bioactive jasmonates in Arabidopsis. *Plant J*; **59**:974-86.

547. **Murashige T, Skoog F**. (1962). A revised medium for rapid growth and bio assays with tobacco tissue cultures. *Physiol Plant*; **15**:473-97.

548. **Schwessinger B, Roux M, Kadota Y, Ntoukakis V, Sklenar J, Jones A, et al.** (2011). Phosphorylation-dependent differential regulation of plant growth, cell death, and innate immunity by the regulatory receptor-like kinase BAK1. *PLoS Genet*; **7**:e1002046.

549. **Pitino M, Coleman AD, Maffei ME, Ridout CJ, Hogenhout SA**. (2011). Silencing of aphid genes by dsRNA feeding from plants. *Plos One*; **6**.

550. **Bonaventure G, Gfeller A, Proebsting WM, Hortensteiner S, Chetelat A, Martinoia E, et al.** (2007). A gain-of-function allele of TPC1 activates oxylipin biogenesis after leaf wounding in Arabidopsis. *Plant J*; **49**:889-98.

551. **Park JH, Halitschke R, Kim HB, Baldwin IT, Feldmann KA, Feyereisen R**. (2002). A knock-out mutation in allene oxide synthase results in male sterility and defective wound signal transduction in Arabidopsis due to a block in jasmonic acid biosynthesis. *Plant J*; **31**:1-12.

552. **Bonaventure G, Gfeller A, Rodriguez VM, Armand F, Farmer EE**. (2007). The *fou2* gain-of-function allele and the wild-type allele of two pore channel 1 contribute to different extents or by different mechanisms to defense gene expression in Arabidopsis. *Plant Cell Physiol*; **48**:1775-89.

553. **Kim S, Kang J-Y, Cho D-I, Park JH, Kim SY**. (2004). ABF2, an ABRE-binding bZIP factor, is an essential component of glucose signaling and its overexpression affects multiple stress tolerance. *The Plant Journal*; **40**:75-87.

554. **Kuhn JM, Boisson-Dernier A, Dizon MB, Maktabi MH, Schroeder JI**. (2006). The protein phosphatase AtPP2CA negatively regulates abscisic acid signal transduction in Arabidopsis, and effects of abh1 on AtPP2CA mRNA. *Plant Physiol*; **140**:127-39.

555. **Prince DC, Mugford ST, Vincent TR, Hogenhout SA**. (2014). Pea aphid survival assays on *Arabidopsis thaliana*. *bio-protocol*; **4**.

556. **Bartlett JG, Alves SC, Smedley M, Snape JW, Harwood WA**. (2008). High-throughput Agrobacterium-mediated barley transformation. *Plant Methods*; **4**.

557. **Prince D**. (2012) *Dissecting the role of plant immunity in plant-aphid interactions*. Norwich: University of East Anglia.

558. **Pfaffl MW**. (2001). A new mathematical model for relative quantification in real-time RT-PCR. *Nucleic Acids Res*; **29**.

559. **Vandesompele J, De Preter K, Pattyn F, Poppe B, Van Roy N, De Paepe A, et al.** (2002). Accurate normalization of real-time quantitative RT-PCR data by geometric averaging of multiple internal control genes. *Genome Biol*; **3**.

560. **Coleman AD, Wouters RHM, Mugford ST, Hogenhout SA**. (2015). Persistence and transgenerational effect of plant-mediated RNAi in aphids. *J Exp Bot*; **66**:541-8.

561. **Segonzac C, Nimchuk ZL, Beck M, Tarr PT, Robatzek S, Meyerowitz EM, et al.** (2012). The Shoot apical meristem regulatory peptide CLV3 does not activate innate immunity. *Plant Cell*; **24**:3186-92.

562. **Chassot C, Buchala A, Schoonbeek HJ, Metraux JP, Lamotte O**. (2008). Wounding of Arabidopsis leaves causes a powerful but transient protection against Botrytis infection. *Plant J*; **55**:555-67.

563. **Czechowski T, Stitt M, Altmann T, Udvardi MK, Scheible WR**. (2005). Genome-wide identification and testing of superior reference genes for transcript normalization in Arabidopsis. *Plant Physiol*; **139**:5-17.

564. **Engler C, Gruetzner R, Kandzia R, Marillonnet S**. (2009). Golden gate shuffling: a one-pot dna shuffling method based on type II restriction enzymes. *Plos One*; **4**.

565. **Hanahan D**. (1983). Studies on transformation of *Escherichia coli* with plasmids. *J Mol Biol*; **166**:557-80.

566. **Bertani G**. (1951). Studies on lysogenesis .I. The mode of phage liberation by lysogenic *Escherichia coli*. *J Bacteriol*; **62**:293-300.

567. **Bertani G**. (2004). Lysogeny at mid-twentieth century: P1, P2, and other experimental, systems. *J Bacteriol*; **186**:595-600.

568. **Kardash E, Bandemer J, Raz E**. (2011). Imaging protein activity in live embryos using fluorescence resonance energy transfer biosensors. *Nat Protoc*; **6**:1835-46.

569. **Meijering E, Dzyubachyk O, Smal I**. (2012). Methods for cell and particle tracking. *Methods Enzymol*; **504**:183-200.

570. **Sarria E, Cid M, Garzo E, Fereres A**. (2009). Excel workbook for automatic parameter calculation of EPG data. *Comput Electron Agric*; **67**:35-42.

571. **Nishinaka Y, Aramaki Y, Yoshida H, Masuya H, Sugawara T, Ichimori Y**. (1993). A new sensitive chemiluminescence probe, l-012, for measuring the production of superoxide anion by cells. *Biochem Biophys Res Commun*; **193**:554–9.

572. **Langmead B, Trapnell C, Pop M, Salzberg SL**. (2009). Ultrafast and memory-efficient alignment of short DNA sequences to the human genome. *Genome Biol*; **10**.

573. **Li B, Dewey CN**. (2011). RSEM: accurate transcript quantification from RNA-Seq data with or without a reference genome. *BMC Bioinformatics*; **12**.

574. **Anders S, Huber W**. (2010). Differential expression analysis for sequence count data. *Genome Biol*; **11**.

575. **Miyawaki A, Griesbeck O, Heim R, Tsien RY**. (1999). Dynamic and quantitative Ca^{2+} measurements using improved cameleons. *P Natl Acad Sci USA*; **96**:2135-40.

576. **Griesbeck O, Baird GS, Campbell RE, Zacharias DA, Tsien RY**. (2001). Reducing the environmental sensitivity of yellow fluorescent protein - mechanism and applications. *J Biol Chem*; **276**:29188-94.

577. **Topell S, Hennecke J, Glockshuber R**. (1999). Circularly permuted variants of the green fluorescent protein. *FEBS Lett*; **457**:283-9.

578. **Baird GS, Zacharias DA, Tsien RY**. (1999). Circular permutation and receptor insertion within green fluorescent proteins. *P Natl Acad Sci USA*; **96**:11241-6.

579. **Palmer AE, Jin C, Reed JC, Tsien RY**. (2004). Bcl-2-mediated alterations in endoplasmic reticulum Ca^{2+} analyzed with an improved genetically encoded fluorescent sensor. *P Natl Acad Sci USA*; **101**:17404-9.

580. **Palmer AE, Giacomello M, Kortemme T, Hires SA, Lev-Ram V, Baker D, et al.** (2006). Ca^{2+} indicators based on computationally redesigned calmodulin-peptide pairs. *Chem Biol*; **13**:521-30.

581. **Nemchinov LG, Shabala L, Shabala S**. (2008). Calcium efflux as a component of the hypersensitive response of *Nicotiana benthamiana* to *Pseudomonas syringae*. *Plant Cell Physiol*; **49**:40-6.

582. **Kadota Y, Furuichi T, Ogasawara Y, Goh T, Higashi K, Muto S, et al.** (2004). Identification of putative voltage-dependent Ca^{2+}-permeable channels involved in cryptogein-induced Ca^{2+} transients and defense responses in tobacco BY-2 cells. *Biochem Biophys Res Commun*; **317**:823-30.

583. **Foyer CH, Verrall SR, Hancock RD**. (2015). Systematic analysis of phloem-feeding insect-induced transcriptional reprogramming in Arabidopsis highlights common features and reveals distinct responses to specialist and generalist insects. *J Exp Bot*; **66**:495-512.

584. **Ren GW, Wang XF, Chen D, Wang XW, Liu XD**. (2014). Effects of aphids *Myzus persicae* on the changes of Ca^{2+} and H_2O_2 flux and enzyme activities in tobacco. *J Plant Interact*; **9**:883-8.

585. **Kimmins FM, Tjallingii WF**. (1985). Ultrastructure of Sieve Element Penetration by Aphid Stylets during Electrical Recording. *Entomol Exp Appl*; **39**:135-41.

586. **Sjolund RD**. (1997). The phloem sieve element: a river runs through it. *Plant Cell*; **9**:1137-46.

587. **Van Bel AJE**. (2003). The phloem, a miracle of ingenuity. *Plant Cell Environ*; **26**:125-49.

588. **Anstead JA, Froelich DR, Knoblauch M, Thompson GA**. (2012). Arabidopsis p-protein filament formation requires both AtSEOR1 and AtSEOR2. *Plant Cell Physiol*; **53**:1033-42.

589. **Jekat SB, Ernst AM, Von Bohl A, Zielonka S, Twyman RM, Noll GA, et al.** (2013). P-proteins in Arabidopsis are heteromeric structures involved in rapid sieve tube sealing. *Frontiers in Plant Science*; **4**:9.

590. **Xie B, Hong Z**. (2011). Unplugging the callose plug from sieve pores. *Plant signaling & behavior*; **6**:491-3.

591. **Shi X, Han X, Lu TG**. (2016). Callose synthesis during reproductive development in monocotyledonous and dicotyledonous plants. *Plant signaling & behavior*; **11**:5.

592. **Kauss H, Kohle H, Jeblick W**. (1983). Proteolytic activation and stimulation by Ca^{2+} of glucan synthase from soybean cells. *FEBS Lett*; **158**:84-8.

593. **Aidemark M, Andersson CJ, Rasmusson AG, Widell S**. (2009). Regulation of callose synthase activity in situ in alamethicin-permeabilized Arabidopsis and tobacco suspension cells. *BMC Plant Biol*; **9**.

594. **Knoblauch M, Noll GA, Muller T, Prufer D, Schneider-Huther I, Scharner D, et al.** (2003). ATP-independent contractile proteins from plants. *Nat Mater*; **2**:600-3.

595. **Furch ACU, Van Bel AJE, Fricker MD, Felle HH, Fuchs M, Hafke JB**. (2009). Sieve element Ca^{2+} channels as relay stations between remote stimuli and sieve tube occlusion in *Vicia faba*. *Plant Cell*; **21**:2118-32.

596. **Hafke JB, Furch AC, Fricker MD, Van Bel AJ**. (2009). Forisome dispersion in *Vicia faba* is triggered by Ca^{2+} hotspots created by concerted action of diverse Ca^{2+} channels in sieve elements. *Plant signaling & behavior*; **4**:968-72.

597. **Furch ACU, Hafke JB, Schulz A, Van Bel AJE.** (2007). Ca^{2+}-mediated remote control of reversible sieve tube occlusion in *Vicia faba*. *J Exp Bot*; **58**:2827-38.

598. **Walker GP, Medina-Ortega KJ.** (2012). Penetration of faba bean sieve elements by pea aphid does not trigger forisome dispersal. *Entomol Exp Appl*; **144**:326-35.

599. **Will T, Tjallingii WF, Thonnessen A, Van Bel AJE.** (2007). Molecular sabotage of plant defense by aphid saliva. *P Natl Acad Sci USA*; **104**:10536-41.

600. **Furch ACU, Zimmermann MR, Will T, Hafke JB, Van Bel AJE.** (2010). Remote-controlled stop of phloem mass flow by biphasic occlusion in *Cucurbita maxima*. *J Exp Bot*; **61**:3697-708.

601. **Rao SaK, Carolan JC, Wilkinson TL.** (2013). Proteomic Profiling of cereal aphid saliva reveals both ubiquitous and adaptive secreted proteins. *Plos One*; **8.**

602. **Medina-Ortega KJ, Walker GP.** (2013). Does aphid salivation affect phloem sieve element occlusion *in vivo*? *J Exp Bot*; **64**:5525-35.

603. **Froelich DR, Mullendore DL, Jensen KH, Ross-Elliott TJ, Anstead JA, Thompson GA, et al.** (2011). Phloem ultrastructure and pressure flow: sieve-element-occlusion-related agglomerations do not affect translocation. *Plant Cell*; **23**:4428-45.

604. **Will T, Furch ACU, Zimmermann MR.** (2013). How phloem-feeding insects face the challenge of phloem-located defenses. *Frontiers in Plant Science*; **4.**

605. **Shah J.** (2009). Plants under attack: systemic signals in defence. *Curr Opin Plant Biol*; **12**:459-64.

606. **Van Bel AJE, Gaupels F.** (2004). Pathogen-induced resistance and alarm signals in the phloem. *Mol Plant Pathol*; **5**:495-504.

607. **Van Bel AJE, Furch ACU, Will T, Buxa SV, Musetti R, Hafke JB.** (2014). Spread the news: systemic dissemination and local impact of Ca^{2+} signals along the phloem pathway. *J Exp Bot*.

608. **Divol F, Vilaine F, Thibivilliers S, Amselem J, Palauqui JC, Kusiak C, et al.** (2005). Systemic response to aphid infestation by *Myzus persicae* in the phloem of *Apium graveolens*. *Plant Mol Biol*; **57**:517-40.

609. **Zhang X, Xue M, Zhao HP.** (2015). Species-specific effects on salicylic acid content and subsequent *Myzus persicae* (Sulzer) performance by three phloem-sucking insects infesting *Nicotiana tabacum L*. *Arthropod-Plant Inte*; **9**:383-91.

610. **Prado E, Tjallingii WF.** (2007). Behavioral evidence for local reduction of aphid-induced resistance. *J Insect Sci*; **7.**

611. **Dugravot S, Brunissen L, Létocart E, Tjallingii WF, Vincent C, Giordanengo P, et al.** (2007). Local and systemic responses induced by aphids in *Solanum tuberosum* plants. *Entomol Exp Appl*; **123**:271-7.

612. **De Vos M, Van Oosten VR, Jander G, Dicke M, Pieterse CM**. (2005). Plants under attack: multiple interactions with insects and microbes. *Plant signaling & behavior*; **2**:527-9.

613. **Lu DP, Wu SJ, Gao XQ, Zhang YL, Shan LB, He P**. (2010). A receptor-like cytoplasmic kinase, BIK1, associates with a flagellin receptor complex to initiate plant innate immunity. *P Natl Acad Sci USA*; **107**:496-501.

614. **Ranf S, Eschen-Lippold L, Frhlich K, Westphal L, Scheel D, Lee J**. (2014). Microbe-associated molecular pattern-induced calcium signaling requires the receptor-like cytoplasmic kinases, PBL1 and BIK1. *BMC Plant Biol*; **14**.

615. **Abuqamar S, Chai MF, Luo HL, Song FM, Mengiste T**. (2008). Tomato protein kinase 1b mediates signaling of plant responses to necrotrophic fungi and insect herbivory. *Plant Cell*; **20**:1964-83.

616. **Li J, Wen JQ, Lease KA, Doke JT, Tax FE, Walker JC**. (2002). BAK1, an Arabidopsis LRR receptor-like protein kinase, interacts with BRI1 and modulates brassinosteroid signaling. *Cell*; **110**:213-22.

617. **Veronese P, Nakagami H, Bluhm B, Abuqamar S, Chen X, Salmeron J, et al.** (2006). The membrane-anchored BOTRYTIS-INDUCED KINASE1 plays distinct roles in Arabidopsis resistance to necrotrophic and biotrophic pathogens. *Plant Cell*; **18**:257-73.

618. **Lei JX, Finlayson SA, Salzman RA, Shan LB, Zhu-Salzman K**. (2014). BOTRYTIS-INDUCED KINASE1 modulates arabidopsis resistance to green peach aphids via PHYTOALEXIN DEFICIENT4. *Plant Physiol*; **165**:1657-70.

619. **Moreno A, Garzo E, Fernandez-Mata G, Kassem M, Aranda MA, Fereres A**. (2011). Aphids secrete watery saliva into plant tissues from the onset of stylet penetration. *Entomol Exp Appl*; **139**:145-53.

620. **Stadler R, Sauer N**. (1996). The Arabidopsis thaliana AtSUC2 gene is specifically expressed in companion cells. *Bot Acta*; **109**:299-306.

621. **Kloth KJ, Ten Broeke CJM, Thoen MPM, Den Brink MHV, Wiegers GL, Krips OE, et al.** (2015). High-throughput phenotyping of plant resistance to aphids by automated video tracking. *Plant Methods*; **11**.

622. **Harada A, Shimazaki KI**. (2007). Phototropins and blue light-dependent calcium signaling in higher plants. *Photochem Photobiol*; **83**:102-11.

623. **Kirchner SM, Doring TF, Saucke H**. (2005). Evidence for trichromacy in the green peach aphid, *Myzus persicae* (Sulz.) (Hemiptera : Aphididae). *J Insect Physiol*; **51**:1255-60.

624. **Dixon A**. (1985) *Aphid Ecology*. Glasgow: Blackie and Sons.

625. **Karley AJ, Mitchell C, Brookes C, Mcnicol J, O'neill T, Roberts H, et al.** (2016). Exploiting physical defence traits for crop protection: leaf trichomes of *Rubus*

idaeus have deterrent effects on spider mites but not aphids. *Ann Appl Biol*; **168**:159-72.

626. **Knight H, Knight MR**. (2000). Imaging spatial and cellular characteristics of low temperature calcium signature after cold acclimation in Arabidopsis. *J Exp Bot*; **51**:1679-86.

627. **Zhang CL, Shi HJ, Chen L, Wang XM, Lu BB, Zhang SP, et al.** (2011). Harpin-induced expression and transgenic overexpression of the phloem protein gene AtPP2-A1 in Arabidopsis repress phloem feeding of the green peach aphid *Myzus persicae*. *BMC Plant Biol*; **11**.

628. **Shaner NC, Patterson GH, Davidson MW**. (2007). Advances in fluorescent protein technology. *J Cell Sci*; **120**:4247-60.

629. **Gao QM, Zhu SF, Kachroo P, Kachroo A**. (2015). Signal regulators of systemic acquired resistance. *Frontiers in Plant Science*; **6**.

630. **Madhusudhan VV, Miles PW**. (1998). Mobility of salivary components as a possible reason for differences in the responses of alfalfa to the spotted alfalfa aphid and pea aphid. *Entomol Exp Appl*; **86**:25-39.

631. **Fu ZQ, Yan SP, Saleh A, Wang W, Ruble J, Oka N, et al.** (2012). NPR3 and NPR4 are receptors for the immune signal salicylic acid in plants. *Nature*; **486**:228-+.

632. **Fu ZQ, Dong XN**. (2013). Systemic acquired resistance: turning local infection into global defense. *Annu Rev Plant Biol*; **64**:839-63.

633. **Breitenbach HH, Wenig M, Wittek F, Jorda L, Maldonado-Alconada AM, Sarioglu H, et al.** (2014). Contrasting roles of the apoplastic aspartyl protease APOPLASTIC, ENHANCED DISEASE SUSCEPTIBILITY1-DEPENDENT1 and LEGUME LECTIN-LIKE PROTEIN1 in arabidopsis systemic acquired resistance. *Plant Physiol*; **165**:791-809.

634. **Wittek F, Hoffmann T, Kanawati B, Bichlmeier M, Knappe C, Wenig M, et al.** (2014). Arabidopsis ENHANCED DISEASE SUSCEPTIBILITY1 promotes systemic acquired resistance via azelaic acid and its precursor 9-oxo nonanoic acid. *J Exp Bot*; **65**:5919-31.

635. **Coleman AD**. (2013) *Control of Turnip yellows virus: Assessing impact on oilseed rape quality traits and dissecting circulative transmission by aphids*. Norwich: Universtiy of East Anglia.

636. **Gorsuch PA, Sargeant AW, Penfield SD, Quick WP, Atkin OK**. (2010). Systemic low temperature signaling in Arabidopsis. *Plant Cell Physiol*; **51**:1488-98.

637. **Pallipparambil GR, Sayler RJ, Shapiro JP, Thomas JMG, Kring TJ, Goggin FL**. (2015). Mi-1.2, an R gene for aphid resistance in tomato, has direct negative effects on a zoophytophagous biocontrol agent, *Orius insidiosus*. *J Exp Bot*; **66**:549-57.

638. **Meyer S, Lauterbach C, Niedermeier M, Barth I, Sjolund RD, Sauer N**. (2004). Wounding enhances expression of AtSUC3, a sucrose transporter from Arabidopsis sieve elements and sink tissues. *Plant Physiol*; **134**:684-93.

639. **Dangl JL, Horvath DM, Staskawicz BJ**. (2013). Pivoting the plant immune system from dissection to deployment. *Science*; **341**:746-51.

640. **Pallipparambil GR, Reese JC, Avila CA, Louis JM, Goggin FL**. (2010). Mi-mediated aphid resistance in tomato: tissue localization and impact on the feeding behavior of two potato aphid clones with differing levels of virulence. *Entomol Exp Appl*; **135**:295-307.

641. **Shepherd T, Robertson GW, Griffiths DW, Birch ANE**. (1999). Epicuticular wax ester and triacylglycerol composition in relation to aphid infestation and resistance in red raspberry (Rubus idaeus L.). *Phytochemistry*; **52**:1255-67.

642. **Bergman DK, Dillwith JW, Zarrabi AA, Caddel JL, Berberet RC**. (1991). Epicuticular lipids of alfalfa relative to its susceptibility to spotted alfalfa aphids (Homoptera, Aphididae). *Environ Entomol*; **20**:781-5.

643. **Pegadaraju V, Louis J, Singh V, Reese JC, Bautor J, Feys BJ, et al.** (2007). Phloem-based resistance to green peach aphid is controlled by Arabidopsis PHYTOALEXIN DEFICIENT4 without its signaling partner ENHANCED DISEASE SUSCEPTIBILITY1. *Plant J*; **52**:332-41.

644. **Araujo RN, Santos A, Pinto FS, Gontijo NF, Lehane MJ, Pereira MH**. (2006). RNA interference of the salivary gland nitrophorin 2 in the triatomine bug *Rhodnius prolixus* (Hemiptera : Reduviidae) by dsRNA ingestion or injection. *Insect Biochem Mol Biol*; **36**:683-93.

645. **Jaubert-Possamai S, Le Trionnaire G, Bonhomme J, Christophides GK, Rispe C, Tagu D**. (2007). Gene knockdown by RNAi in the pea aphid *Acyrthosiphon pisum*. *BMC Biotechnol*; **7**.

646. **Kvitko BH, Park DH, Velasquez AC, Wei CF, Russell AB, Martin GB, et al.** (2009). Deletions in the repertoire of *Pseudomonas syringae* pv. tomato DC3000 yype III secretion effector genes reveal functional overlap among effectors. *PLoS Path*; **5**.

647. **Zheng XZ, Mclellan H, Fraiture M, Liu XY, Boevink PC, Gilroy EM, et al.** (2014). Functionally redundant RXLR effectors from *Phytophthora infestans* act at different steps to suppress early flg22-triggered immunity. . *PLoS Path*; **10**.

648. **Peiter E**. (2011). The plant vacuole: emitter and receiver of calcium signals. *Cell Calcium*; **50**:120-8.

649. **Karley AJ, Leigh RA, Sanders D**. (2000). Differential ion accumulation and ion fluxes in the mesophyll and epidermis of barley. *Plant Physiol*; **122**:835-44.

650. **Gilliham M, Athman A, Tyerman SD, Conn SJ**. (2011). Cell-specific compartmentation of mineral nutrients is an essential mechanism for optimal plant productivity-another role for TPC1? *Plant signaling & behavior*; **6**:1656-61.

651. **Conn SJ, Gilliham M, Athman A, Schreiber AW, Baumann U, Moller I, et al.** (2011). Cell-Specific vacuolar calcium storage mediated by CAX1 regulates apoplastic calcium concentration, gas exchange, and plant productivity in Arabidopsis. *Plant Cell*; **23**:240-57.

652. **Knight H, Trewavas AJ, Knight MR**. (1996). Cold calcium signaling in Arabidopsis involves two cellular pools and a change in calcium signature after acclimation. *Plant Cell*; **8**:489-503.

653. **Knight H, Trewavas AJ, Knight MR**. (1997). Calcium signalling in Arabidopsis thaliana responding to drought and salinity. *Plant J*; **12**:1067-78.

654. **Cessna SG, Chandra S, Low PS**. (1998). Hypo-osmotic shock of tobacco cells stimulates Ca^{2+} fluxes deriving first from external and then internal Ca^{2+} stores. *J Biol Chem*; **273**:27286-91.

655. **Yamaguchi T, Aharon GS, Sottosanto JB, Blumwald E**. (2005). Vacuolar Na^+/H^+ antiporter cation selectivity is regulated by calmodulin from within the vacuole in a Ca^{2+}- and pH-dependent manner. *P Natl Acad Sci USA*; **102**:16107-12.

656. **Beyhl D, Hortensteiner S, Martinoia E, Farmer EE, Fromm J, Marten I, et al.** (2009). The *fou2* mutation in the major vacuolar cation channel TPC1 confers tolerance to inhibitory luminal calcium. *Plant J*; **58**:715-23.

657. **Hedrich R, Marten I**. (2011). TPC1-SV channels gain shape. *Mol Plant*; **4**:428-41.

658. **Perez V, Wherrett T, Shabala S, Muniz J, Dobrovinskaya O, Pottosin I**. (2008). Homeostatic control of slow vacuolar channels by luminal cations and evaluation of the channel-mediated tonoplast Ca^{2+} fluxes *in situ*. *J Exp Bot*; **59**:3845-55.

659. **Kurusu T, Yagala T, Miyao A, Hirochika H, Kuchitsu K**. (2005). Identification of a putative voltage-gated Ca^{2+} channel as a key regulator of elicitor-induced hypersensitive cell death and mitogen-activated protein kinase activation in rice. *Plant J*; **42**:798-809.

660. **Islam MM, Munemasa S, Hossain MA, Nakamura Y, Mori IC, Murata Y**. (2010). Roles of AtTPC1, vacuolar Two Pore Channel 1, in Arabidopsis stomatal closure. *Plant Cell Physiol*; **51**:302-11.

661. **Pottosin II, Dobrovinskaya OR, Muniz J**. (1999). Cooperative block of the plant endomembrane ion channel by ruthenium red. *Biophys J*; **77**:1973-9.

662. **Price AH, Taylor A, Ripley SJ, Griffiths A, Trewavas AJ, Knight MR**. (1994). Oxidative signals in tobacco increase cytosolic calcium. *Plant Cell*; **6**:1301-10.

663. **Legue V, Blancaflor E, Wymer C, Perbal G, Fantin D, Gilroy S**. (1997). Cytoplasmic free Ca^{2+} in Arabidopsis roots changes in response to touch but not gravity. *Plant Physiol*; **114**:789-800.

664. **Knight MR, Smith SM, Trewavas AJ**. (1992). Wind-induced plant motion immediately increases cytosolic calcium. *P Natl Acad Sci USA*; **89**:4967-71.

665. **Hedrich R**. (2012). Ion channels in plants. *Physiol Rev*; **92**:1777-811.

666. **Koselski M, Trebacz K, Dziubinska H**. (2013). Cation-permeable vacuolar ion channels in the moss *Physcomitrella patens*: a patch-clamp study. *Planta*; **238**:357-67.

667. **Dadacz-Narloch B, Kimura S, Kurusu T, Farmer EE, Becker D, Kuchitsu K, et al.** (2013). On the cellular site of two-pore channel TPC1 action in the Poaceae. *The New phytologist*.

668. **Wang YJ, Yu JN, Chen T, Zhang ZG, Hao YJ, Zhang JS, et al.** (2005). Functional analysis of a putative Ca^{2+} channel gene TaTPC1 from wheat. *J Exp Bot*; **56**:3051-60.

669. **Lin C, Yu Y, Kadono T, Iwata M, Umemura K, Furuichi T, et al.** (2005). Action of aluminum, novel TPC1-type channel inhibitor, against salicylate-induced and cold-shock-induced calcium influx in tobacco BY-2 cells. *Biochem Biophys Res Commun*; **332**:823-30.

670. **Kawano T, Kadono T, Fumoto K, Lapeyrie F, Kuse M, Isobe M, et al.** (2004). Aluminium as a specific inhibitor of plant TPC1 Ca^{2+} channels. *Biochem Biophys Res Commun*; **324**:40-5.

671. **Hamada H, Kurusu T, Okuma E, Nokajima H, Kiyoduka M, Koyano T, et al.** (2012). Regulation of a proteinaceous elicitor-induced Ca^{2+} influx and production of phytoalexins by a putative voltage-gated cation channel, OsTPC1, in cultured rice cells. *J Biol Chem*; **287**:9931-9.

672. **Dadacz-Narloch B, Beyhl D, Larisch C, Lopez-Sanjurjo EJ, Reski R, Kuchitsu K, et al.** (2011). A novel calcium binding site in the slow vacuolar cation channel TPC1 senses luminal calcium levels. *Plant Cell*; **23**:2696-707.

673. **Oldham ML, Brash AR, Newcomer ME**. (2005). Insights from the X-ray crystal structure of coral 8R-lipoxygenase - calcium activation via a C2-like domain and a structural basis of product chirality. *J Biol Chem*; **280**:39545-52.

674. **Tatulian SA, Steczko J, Minor W**. (1998). Uncovering a calcium-regulated membrane-binding mechanism for soybean lipoxygenase-1. *Biochemistry-Us*; **37**:15481-90.

675. **Zhao YY, Zhou J, Xing D**. (2014). Phytochrome B-mediated activation of lipoxygenase modulates an excess red light-induced defence response in Arabidopsis. *J Exp Bot*; **65**:4907-18.

676. **Katsir L, Schilmiller AL, Staswick PE, He SY, Howe GA**. (2008). COI1 is a critical component of a receptor for jasmonate and the bacterial virulence factor coronatine. *P Natl Acad Sci USA*; **105**:7100-5.

677. **Yan JB, Zhang C, Gu M, Bai ZY, Zhang WG, Qi TC, et al.** (2009). The Arabidopsis CORONATINE INSENSITIVE1 protein is a jasmonate receptor. *Plant Cell*; **21**:2220-36.

678. **Sasaki Y, Asamizu E, Shibata D, Nakamura Y, Kaneko T, Awai K, et al.** (2001). Monitoring of methyl jasmonate-responsive genes in Arabidopsis by cDNA macroarray: self-activation of jasmonic acid biosynthesis and crosstalk with other phytohormone signaling pathways. *DNA Res*; **8**:153-61.

679. **Schaller F, Schaller A, Stintzi A**. (2004). Biosynthesis and metabolism of jasmonates. *J Plant Growth Regul*; **23**:179-99.

680. **Sun QP, Yu YK, Wan SX, Zhao FK, Hao YL**. (2010). Extracellular and intracellular calcium both involved in the jasmonic acid induced calcium mobilization in *Arabidopsis thaliana*. *Agr Sci China*; **9**:497-503.

681. **Munemasa S, Oda K, Watanabe-Sugimoto M, Nakamura Y, Shimoishi Y, Murata Y**. (2007). The coronatine-insensitive 1 mutation reveals the hormonal signaling interaction between abscisic acid and methyl jasmonate in arabidopsis guard cells. Specific impairment of ion channel activation and second messenger production. *Plant Physiol*; **143**:1398-407.

682. **Suhita D, Kolla VA, Vavasseur A, Raghavendra AS**. (2003). Different signaling pathways involved during the suppression of stomatal opening by methyl jasmonate or abscisic acid. *Plant Sci*; **164**:481-8.

683. **Suhita D, Raghavendra AS, Kwak JM, Vavasseur A**. (2004). Cytoplasmic alkalization precedes reactive oxygen species production during methyl jasmonate- and abscisic acid-induced stomatal closure. *Plant Physiol*; **134**:1536-45.

684. **Munemasa S, Hossain MA, Nakamura Y, Mori IC, Murata Y**. (2011). The Arabidopsis calcium-dependent protein kinase, CPK6, functions as a positive regulator of methyl jasmonate signaling in guard cells. *Plant Physiol*; **155**:553-61.

685. **Lu X, Zhang FY, Shen Q, Jiang WM, Pan QF, Lv ZY, et al.** (2014). Overexpression of Allene Oxide Cyclase Improves the Biosynthesis of Artemisinin in Artemisia annua L. *Plos One*; **9**.

686. **Jimenez-Aleman GH, Machado RaR, Gorls H, Baldwin IT, Boland W**. (2015). Synthesis, structural characterization and biological activity of two diastereomeric JA-Ile macrolactones. *Org Biomol Chem*; **13**:5885-93.

687. **Dennison KL, Spalding EP**. (2000). Glutamate-gated calcium fluxes in Arabidopsis. *Plant Physiol*; **124**:1511-4.

688. **Manzoor H, Kelloniemi J, Chiltz A, Wendehenne D, Pugin A, Poinssot B, et al.** (2013). Involvement of the glutamate receptor AtGLR3.3 in plant defense signaling and resistance to *Hyaloperonospora arabidopsidis*. *The Plant journal : for cell and molecular biology*:Accepted Article.

689. **Singh SK, Chien CT, Chang IF**. (2016). The Arabidopsis glutamate receptor-like gene GLR3.6 controls root development by repressing the kip-related protein gene KRP4. *J Exp Bot*; **67**:1853-69.

690. **Moloi MJ, Van Der Westhuizen AJ**. (2006). The reactive oxygen species are involved in resistance responses of wheat to the Russian wheat aphid. *J Plant Physiol*; **163**:1118-25.

691. **Drerup MM, Schlucking K, Hashimoto K, Manishankar P, Steinhorst L, Kuchitsu K, et al.** (2013). The calcineurin B-like calcium sensors CBL1 and CBL9 together with their interacting protein kinase CIPK26 regulate the Arabidopsis NADPH oxidase RBOHF. *Mol Plant*; **6**:559-69.

692. **Kimura S, Kawarazaki T, Nibori H, Michikawa M, Imai A, Kaya H, et al.** (2013). The CBL-interacting protein kinase CIPK26 is a novel interactor of Arabidopsis NADPH oxidase AtRbohF that negatively modulates its ROS-producing activity in a heterologous expression system. *J Biochem*; **153**:191-5.

693. **Ligterink W, Kroj T, Zurnieden U, Hirt H, Scheel D**. (1997). Receptor-mediated activation of a MAP kinase in pathogen defense of plants. *Science*; **276**:2054-7.

694. **Lebrun-Garcia A, Ouaked F, Chiltz A, Pugin A**. (1998). Activation of MAPK homologues by elicitors in tobacco cells. *Plant J*; **15**:773-81.

695. **Xie KB, Chen JP, Wang Q, Yang YO**. (2014). Direct phosphorylation and activation of a mitogen-activated protein kinase by a calcium-dependent protein kinase in rice. *Plant Cell*; **26**:3077-89.

696. **Levy M, Wang QM, Kaspi R, Parrella MP, Abel S**. (2005). Arabidopsis IQD1, a novel calmodulin-binding nuclear protein, stimulates glucosinolate accumulation and plant defense. *Plant J*; **43**:79-96.

697. **O'brien JA, Daudi A, Finch P, Butt VS, Whitelegge JP, Souda P, et al.** (2012). A peroxidase-dependent apoplastic oxidative burst in cultured Arabidopsis cells functions in MAMP-elicited defense. *Plant Physiol*; **158**:2013-27.

698. **Xu J, Meng J, Meng XZ, Zhao YT, Liu JM, Sun TF, et al.** (2016). Pathogen-responsive MPK3 and MPK6 reprogram the biosynthesis of indole glucosinolates and their derivatives in Arabidopsis immunity. *Plant Cell*; **28**:1144-62.

699. **Ren DT, Liu YD, Yang KY, Han L, Mao GH, Glazebrook J, et al.** (2008). A fungal-responsive MAPK cascade regulates phytoalexin biosynthesis in Arabidopsis. *P Natl Acad Sci USA*; **105**:5638-43.

700. **Glawischnig E, Hansen BG, Olsen CE, Halkier BA**. (2004). Camalexin is synthesized from indole-3-acetaldoxime, a key branching point between primary and secondary metabolism in Arabidopsis. *Proc Natl Acad Sci U S A*; **101**:8245-50.

701. **Esau K**. (1977) Phloem. *Anatomy of Seed Plants*
London: John Wiley and Sons.

702. **Conn SJ, Conn V, Tyerman SD, Kaiser BN, Leigh RA, Gilliham M**. (2011). Magnesium transporters, MGT2/MRS2-1 and MGT3/MRS2-5, are important for magnesium partitioning within *Arabidopsis thaliana* mesophyll vacuoles. *New Phytol*; **190**:583-94.

703. **Carpaneto A, Cantu AM, Gambale F**. (1999). Redox agents regulate ion channel activity in vacuoles from higher plant cells. *FEBS Lett*; **442**:129-32.

704. **Kishi-Kaboshi M, Okada K, Kurimoto L, Murakami S, Umezawa T, Shibuya N, et al.** (2010). A rice fungal MAMP-responsive MAPK cascade regulates metabolic flow to antimicrobial metabolite synthesis. *Plant J*; **63**:599-612.

705. **Dorschner K, W.** (1990) Aphid induced alteration of the availability and form of nitrogenous compounds in plants. In: **Campbell RK, Eikenbary RD,** editors. *Aphid-plant genotype interactions*. Amsterdam: Elsevier. p. 225–35.

706. **Marchetti E, Civolani S, Leis M, Chicca M, Tjallingii WF, Pasqualini E, et al.** (2009). Tissue location of resistance in apple to the rosy apple aphid established by electrical penetration graphs. *Bull Insectol*; **62**:203-8.

707. **Frost CJ, Mescher MC, Carlson JE, De Moraes CM**. (2008). Plant defense priming against herbivores: getting ready for a different battle. *Plant Physiol*; **146**:818-24.

708. **Meldau S, Baldwin IT, Wu J**. (2011). SGT1 regulates wounding- and herbivory-induced jasmonic acid accumulation and *Nicotiana attenuata's* resistance to the specialist lepidopteran herbivore *Manduca sexta*. *New Phytol*; **190**:809-.

709. **Buxdorf K, Rahat I, Gafni A, Levy M**. (2013). The epiphytic fungus *Pseudozyma aphidis* induces jasmonic acid- and salicylic acid/nonexpressor of PR1-independent local and systemic resistance. *Plant Physiol*; **161**:2014-22.

710. **Okada K, Abe H, Arimura G**. (2015). Jasmonates Induce both defense responses and communication in monocotyledonous and dicotyledonous plants. *Plant Cell Physiol*; **56**:16-27.

711. **Westphal L, Scheel D, Rosahl S**. (2008). The *coi1-16* mutant harbors a second site mutation rendering PEN2 nonfunctional. *Plant Cell*; **20**:824-6.

712. **Staswick PE, Su W, Howell SH**. (1992). Methyl jasmonate inhibition of root growth and induction of a leaf protein are decreased in an *Arabidopsis thaliana* mutant. *Proc Natl Acad Sci U S A*; **89**:6837-40.

713. **Rowe HC, Walley JW, Corwin J, Chan EKF, Dehesh K, Kliebenstein DJ**. (2010). Deficiencies in jasmonate-mediated plant defense reveal quantitative variation in *Botrytis cinerea* pathogenesis. *PLoS Path*; **6**.

714. **Zimmerli L, Stein M, Lipka V, Schulze-Lefert P, Somerville S**. (2004). Host and non-host pathogens elicit different jasmonate/ethylene responses in Arabidopsis. *Plant J*; **40**:633-46.

715. **Shafiei R, Hang C, Kang JG, Loake GJ**. (2007). Identification of loci controlling non-host disease resistance in Arabidopsis against the leaf rust pathogen *Puccinia triticina*. *Mol Plant Pathol*; **8**:773-84.

716. **Loehrer M, Langenbach C, Goellner K, Conrath U, Schaffrath U**. (2008). haracterization of nonhost resistance of Arabidopsis to the asian soybean rust. *Mol Plant-Microbe Interact*; **21**:1421-30.

717. **Ishiga Y, Ishiga T, Ikeda Y, Matsuura T, Mysore KS**. (2016). NADPH-dependent thioredoxin reductase C plays a role in nonhost disease resistance against

Pseudomonas syringae pathogens by regulating chloroplast-generated reactive oxygen species. *Peerj*; **4**.

718. **Christopher-Kozjan R, Heath MC**. (2003). Cytological and pharmacological evidence that biotrophic fungi trigger different cell death execution processes in host and nonhost cells during the hypersensitive response. *Physiol Mol Plant Pathol*; **62**:265-75.

719. **Bestwick CS, Brown IR, Mansfield JW**. (1998). Localized changes in peroxidase activity accompany hydrogen peroxide generation during the development of a nonhost hypersensitive reaction in lettuce. *Plant Physiol*; **118**:1067-78.

720. **Torres MA, Jones JDG, Dangl JL**. (2006). Reactive oxygen species signaling in response to pathogens. *Plant Physiol*; **141**:373-8.

721. **Rojas CM, Senthil-Kumar M, Wang K, Ryu CM, Kaundal A, Mysore KS**. (2012). Glycolate oxidase modulates reactive oxygen species-mediated signal transduction during nonhost resistance in *Nicotiana benthamiana* and Arabidopsis. *Plant Cell*; **24**:336-52.

722. **Takahashi Y, Bin Nasir KH, Ito A, Kanzaki H, Matsumura H, Saitoh H, et al.** (2007). A high-throughput screen of cell-death-inducing factors in *Nicotiana benthamiana* identifies a novel MAPKK that mediates INF1-induced cell death signaling and non-host resistance to *Pseudomonas cichorii*. *Plant J*; **49**:1030-40.

723. **An CF, Mou ZL**. (2012). Non-host defense response in a novel Arabidopsis-*Xanthomonas citri* subsp *citri* pathosystem. *Plos One*; **7**.

724. **Cheng YL, Zhang HC, Yao JN, Han QM, Wang XJ, Huang LL, et al.** (2013). Cytological and molecular characterization of non-host resistance in *Arabidopsis thaliana* against wheat stripe rust. *Plant Physiol Biochem*; **62**:11-8.

725. **Nasir KHB, Takahashi Y, Ito A, Saitoh H, Matsumura H, Kanzaki H, et al.** (2005). High-throughput in planta expression screening identifies a class II ethylene-responsive element binding factor-like protein that regulates plant cell death and non-host resistance. *Plant J*; **43**:491-505.

726. **Vatsa P, Chiltz A, Bourque S, Wendehenne D, Garcia-Brugger A, Pugin A**. (2011). Involvement of putative glutamate receptors in plant defence signaling and NO production. *Biochimie*; **93**:2095-101.

727. **Teixeira MA, Wei LH, Kaloshian I**. (2016). Root-knot nematodes induce pattern-triggered immunity in *Arabidopsis thaliana* roots. *New Phytol*; **211**:276-87.

728. **Guo RF, Qian HM, Shen WS, Liu LH, Zhang M, Cai CX, et al.** (2013). BZR1 and BES1 participate in regulation of glucosinolate biosynthesis by brassinosteroids in Arabidopsis. *J Exp Bot*; **64**:2401-12.

729. **Li RF, Zhang JW, Wei JH, Wang HZ, Wang YZ, Ma RC**. (2009). Functions and mechanisms of the CBL-CIPK signaling system in plant response to abiotic stress. *Prog Nat Sci*; **19**:667-76.

730. **Pandey GK, Grant JJ, Cheong YH, Kim BG, Li L, Luan S**. (2005). ABR1, an APETALA2-domain transcription factor that functions as a repressor of ABA response in Arabidopsis. *Plant Physiol*; **139**:1185-93.

731. **Edel K, Becker K, Scholz M, Köster P, Hippler M, Kudla J**. Ca^{2+} dependent phosphorylation activates the ABA responsive transcription factor ABF2. Plant Calcium Signalling 2014; Münster, Germany2014.

732. **Yoshida T, Fujita Y, Maruyama K, Mogami J, Todaka D, Shinozaki K, et al.** (2015). Four Arabidopsis AREB/ABF transcription factors function predominantly in gene expression downstream of SnRK2 kinases in abscisic acid signalling in response to osmotic stress. *Plant Cell Environ*; **38**:35-49.

733. **Laanemets K, Brandt B, Li JL, Merilo E, Wang YF, Keshwani MM, et al.** (2013). Calcium-dependent and -independent stomatal signaling network and compensatory feedback control of stomatal opening via Ca^{2+} sensitivity priming. *Plant Physiol*; **163**:504-13.

734. **Mcainsh MR, Brownlee C, Hetherington AM**. (1990). Abscisic acid-induced elevation of guard-cell cytosolic Ca^{2+} precedes stomatal closure. *Nature*; **343**:186-8.

735. **Staxen I, Pical C, Montgomery LT, Gray JE, Hetherington AM, Mcainsh MR**. (1999). Abscisic acid induces oscillations in guard-cell cytosolic free calcium that involve phosphoinositide-specific phospholipase C. *P Natl Acad Sci USA*; **96**:1779-84.

736. **Macrobbie EaC**. (2000). ABA activates multiple Ca^{2+} fluxes in stomatal guard cells, triggering vacuolar $K^+(Rb^+)$ release. *P Natl Acad Sci USA*; **97**:12361-8.

737. **Schroeder JI, Hagiwara S**. (1990). Repetitive increases in cytosolic Ca^{2+} of guard-cells by abscisic-acid activation of nonselective Ca^{2+} permeable channels. *P Natl Acad Sci USA*; **87**:9305-9.

738. **Hamilton DWA, Hills A, Kohler B, Blatt MR**. (2000). Ca^{2+} channels at the plasma membrane of stomatal guard cells are activated by hyperpolarization and abscisic acid. *P Natl Acad Sci USA*; **97**:4967-72.

739. **Ohta M, Guo Y, Halfter U, Zhu JK**. (2003). A novel domain in the protein kinase SOS2 mediates interaction with the protein phosphatase 2C ABI2. *Proc Natl Acad Sci U S A*; **100**:11771-6.

740. **Merlot S, Gosti F, Guerrier D, Vavasseur A, Giraudat J**. (2001). The ABI1 and ABI2 protein phosphatases 2C act in a negative feedback regulatory loop of the abscisic acid signalling pathway. *Plant J*; **25**:295-303.

741. **Umezawa T, Sugiyama N, Mizoguchi M, Hayashi S, Myouga F, Yamaguchi-Shinozaki K, et al.** (2009). Type 2C protein phosphatases directly regulate abscisic acid-activated protein kinases in Arabidopsis. *P Natl Acad Sci USA*; **106**:17588-93.

742. **Park SY, Fung P, Nishimura N, Jensen DR, Fujii H, Zhao Y, et al.** (2009). Abscisic acid inhibits type 2C protein phosphatases via the PYR/PYL family of START proteins. *Science*; **324**:1068-71.

743. **De Vos M, Kim JH, Jander G**. (2007). Biochemistry and molecular biology of Arabidopsis-aphid interactions. *Bioessays*; **29**:871-83.

744. **Abe H, Urao T, Ito T, Seki M, Shinozaki K, Yamaguchi-Shinozaki K**. (2003). Arabidopsis AtMYC2 (bHLH) and AtMYB2 (MYB) function as transcriptional activators in abscisic acid signaling. *Plant Cell*; **15**:63-78.

745. **Bartoli CG, Casalongue CA, Simontacchi M, Marquez-Garcia B, Foyer CH**. (2013). Interactions between hormone and redox signalling pathways in the control of growth and cross tolerance to stress. *Environ Exp Bot*; **94**:73-88.

746. **Xia XJ, Zhou YH, Shi K, Zhou J, Foyer CH, Yu JQ**. (2015). Interplay between reactive oxygen species and hormones in the control of plant development and stress tolerance. *J Exp Bot*; **66**:2839-56.

747. **Saheed SA, Larsson KaE, Delp G, Botha CEJ, Jonsson LMV, Bradley G**. (2007). Wound callose synthesis in response to Russian wheat aphid and bird cherry-oat aphid feeding on barley ev clipper. *S Afr J Bot*; **73**:310-.

748. **Studham ME, Macintosh GC**. (2013). Multiple phytohormone signals control the transcriptional response to soybean aphid infestation in susceptible and resistant soybean plants. *Mol Plant-Microbe Interact*; **26**:116-29.

749. **Jaouannet M, Rodriguez PA, Thorpe P, Lenoir CJG, Macleod R, Escudero-Martinez C, et al.** (2014). Plant immunity in plant-aphid interactions. *Frontiers in Plant Science*; **5**.

750. **Sakuma Y, Maruyama K, Qin F, Osakabe Y, Shinozaki K, Yamaguchi-Shinozaki K**. (2006). Dual function of an Arabidopsis transcription factor DREB2A in water-stress-responsive and heat-stress-responsive gene expression. *P Natl Acad Sci USA*; **103**:18822-7.

751. **Sakuma Y, Maruyama K, Osakabe Y, Qin F, Seki M, Shinozaki K, et al.** (2006). Functional analysis of an Arabidopsis transcription factor, DREB2A, involved in drought-responsive gene expression. *Plant Cell*; **18**:1292-309.

752. **Yoshida T, Mogami J, Yamaguchi-Shinozaki K**. (2014). ABA-dependent and ABA-independent signaling in response to osmotic stress in plants. *Curr Opin Plant Biol*; **21**:133-9.

753. **Yamaguchishinozaki K, Shinozaki K**. (1994). A novel cis-acting element in an Arabidopsis gene is involved in responsiveness to drought, low-temperature, or high-salt stress. *Plant Cell*; **6**:251-64.

754. **Liu LL, Ren HM, Chen LQ, Wang Y, Wu WH**. (2013). A protein kinase, calcineurin B-like protein-interacting protein kinase 9, interacts with calcium sensor calcineurin B-like protein 3 and regulates potassium homeostasis under low-potassium stress in Arabidopsis. *Plant Physiol*; **161**:266-77.

755. **Lyzenga WJ, Liu H, Schofield A, Muise-Hennessey A, Stone SL**. (2013). Arabidopsis CIPK26 interacts with KEG, components of the ABA signalling network and is degraded by the ubiquitin-proteasome system. *J Exp Bot*; **64**:2779-91.

756. **Gao P, Kolenovsky A, Cui YH, Cutler AJ, Tsang EWT**. (2012). Expression, purification and analysis of an Arabidopsis recombinant CBL-interacting protein kinase 3 (CIPK3) and its constitutively active form. *Protein Expression Purif*; **86**:45-52.

757. **Qi Z, Verma R, Gehring C, Yamaguchi Y, Zhao YC, Ryan CA, et al.** (2010). Ca^{2+} signaling by plant Arabidopsis thaliana Pep peptides depends on AtPepR1, a receptor with guanylyl cyclase activity, and cGMP-activated Ca^{2+} channels. *P Natl Acad Sci USA*; **107**:21193-8.

758. **Mori IC, Murata Y, Yang YZ, Munemasa S, Wang YF, Andreoli S, et al.** (2006). CDPKs CPK6 and CPK3 function in ABA regulation of guard cell S-type anion- and Ca^{2+}-permeable channels and stomatal closure. *PLoS Biol*; **4**:1749-62.

759. **Benn G, Wang CQ, Hicks DR, Stein J, Guthrie C, Dehesh K**. (2014). A key general stress response motif is regulated non-uniformly by CAMTA transcription factors. *Plant J*; **80**:82-92.

760. **Bouche N, Scharlat A, Snedden W, Bouchez D, Fromm H**. (2002). A novel family of calmodulin-binding transcription activators in multicellular organisms. *The Journal of biological chemistry*; **277**:21851-61.

761. **Couldridge C, Newbury HJ, Ford-Lloyd B, Bale J, Pritchard J**. (2007). Exploring plant responses to aphid feeding using a full Arabidopsis microarray reveals a small number of genes with significantly altered expression. *Bull Entomol Res*; **97**:523-32.

762. **Mclean DL**. (1971). Probing behavior of pea aphid, *Acyrthosiphon pisum* (Homoptera Aphididae) .Comparison of *Vicia faba*, *Pisum sativum*, and a chemically defined diet as food sources. *Ann Entomol Soc Am*; **64**:499-&.

763. **Troncoso AJ, Vargas RR, Tapia DH, Olivares-Donoso R, Niemeyer HM**. (2005). Host selection by the generalist aphid *Myzus persicae* (Hemiptera : Aphididae) and its subspecies specialized on tobacco, after being reared on the same host. *Bull Entomol Res*; **95**:23-8.

764. **Alvarez AE, Garzo E, Verbeek M, Vosman B, Dicke M, Tjallingii WF**. (2007). Infection of potato plants with potato leafroll virus changes attraction and feeding behaviour of Myzus persicae. *Entomol Exp Appl*; **125**:135-44.

765. **Wang YH**. (2008). How effective is T-DNA insertional mutagenesis in Arabidopsis? *J Biochem Tech*; **1**:11-20.

766. **Gong DM, Guo Y, Jagendorf AT, Zhu JK**. (2002). Biochemical characterization of the Arabidopsis protein kinase SOS2 that functions in salt tolerance. *Plant Physiol*; **130**:256-64.

767. **Gong DM, Zhang CQ, Chen XY, Gong ZZ, Zhu JK**. (2002). Constitutive activation and transgenic evaluation of the function of an Arabidopsis PKS protein kinase. *J Biol Chem*; **277**:42088-96.

768. **Guo Y, Halfter U, Ishitani M, Zhu JK**. (2001). Molecular characterization of functional domains in the protein kinase SOS2 that is required for plant salt tolerance. *Plant Cell*; **13**:1383-99.

769. **Coley PD, Bryant JP, Chapin FS**. (1985). Resource availability and plant antiherbivore defense. *Science*; **230**:895-9.

770. **Heil M, Baldwin IT**. (2002). Fitness costs of induced resistance: emerging experimental support for a slippery concept. *Trends Plant Sci*; **7**:61-7.

771. **Huot B, Yao J, Montgomery BL, He SY**. (2014). Growth-defense tradeoffs in plants: a balancing act to optimize fitness. *Mol Plant*; **7**:1267-87.

772. **De La Torre F, Gutierrez-Beltran E, Pareja-Jaime Y, Chakravarthy S, Martin GB, Del Pozo O**. (2013). The tomato calcium sensor CBL10 and its interacting protein kinase CIPK6 define a signaling pathway in plant immunity. *Plant Cell*; **25**:2748-64.

773. **Mattson WJ**. (1980). Herbivory in relation to plant nitrogen content. *Annu Rev Ecol Syst*; **11**:119-61.

774. **Mattson WJ**. (1993). Nitrogen - the driving element - a citation-classic commentary on herbivory in relation to plant nitrogen-content. *Cc/Agr Biol Environ*:8-.

775. **Liu YH, Kang ZW, Guo Y, Zhu GS, Shah MMR, Song Y, et al.** (2016). Nitrogen hurdle of host alternation for a polyphagous aphid and the associated changes of endosymbionts. *Sci Rep-Uk*; **6**.

776. **Weibull J**. (1987). Seasonal-changes in the free amino-acids of oat and barley phloem sap in relation to plant-growth stage and growth of *Rhopalosiphum padi*. *Ann Appl Biol*; **111**:729-37.

777. **Fagard M, Launay A, Clement G, Courtial J, Dellagi A, Farjad M, et al.** (2014). Nitrogen metabolism meets phytopathology. *J Exp Bot*; **65**:5643-56.

778. **Hunt EJ, Pritchard J, Bennett MJ, Zhu X, Barrett DA, Allen T, et al.** (2006). The *Arabidopsis thaliana*/*Myzus persicae* model system demonstrates that a single gene can influence the interaction between a plant and a sap-feeding insect. *Mol Ecol*; **15**:4203-13.

779. **Ponder KL, Pritchard J, Harrington R, Bale JS**. (2000). Difficulties in location and acceptance of phloem sap combined with reduced concentration of phloem amino acids explain lowered performance of the aphid *Rhopalosiphum padi* on nitrogen deficient barley (*Hordeum vulgare*) seedlings. *Entomol Exp Appl*; **97**:203-10.

780. **Pritchard J, Griffiths B, Hunt EJ**. (2007). Can the plant-mediated impacts on aphids of elevated CO_2 and drought be predicted? *Global Change Biol*; **13**:1616-29.

781. **Havlickova H, Smetankova M.** (1998). Effect of potassium and magnesium fertilization on barley preference by the bird cherry oat aphid *Rhopalosiphum padi* (L.). *Rost Vyroba*; **44**:379-83.

782. **Myers SW, Gratton C, Wolkowski RP, Hogg DB, Wedberg JL**. (2005). Effect of soil potassium availability on soybean aphid (Hemiptera:Aphididae) population dynamics and soybean yield. *J Econ Entomol*; **98**:113-20.

783. **Myers SW, Gratton C**. (2006). Influence of potassium fertility on soybean aphid, Aphis glycines Matsumura (Hemiptera : Aphididae), population dynamics at a field and regional scale. *Environ Entomol*; **35**:219-27.

784. **Walter AJ, Difonzo CD**. (2007). Soil potassium deficiency affects soybean phloem nitrogen and soybean aphid populations. *Environ Entomol*; **36**:26-33.

785. **Yamada S, Osaki M, Shinano T, Yamada M, Ito M, Permana AT**. (2002). Effect of potassium nutrition on current photosynthesized carbon distribution to carbon and nitrogen compounds among rice, soybean, and sunflower. *J Plant Nutr*; **25**:1957-73.

786. **Deng XM, Hu W, Wei SY, Zhou SY, Zhang F, Han JP, et al.** (2013). TaCIPK29, a CBL-Interacting protein kinase gene from wheat, confers salt stress tolerance in transgenic tobacco. *Plos One*; **8**.

787. **Boursiac Y, Lee SM, Romanowsky S, Blank R, Sladek C, Chung WS, et al.** (2010). Disruption of the vacuolar calcium-ATPases in Arabidopsis results in the activation of a salicylic acid-dependent programmed cell death pathway. *Plant Physiol*; **154**:1158-71.

788. **Jaffe LF**. (2010). Fast calcium waves. *Cell Calcium*; **48**:102-13.

789. **Walling LL**. (2000). The myriad plant responses to herbivores. *J Plant Growth Regul*; **19**:195-216.

790. **Weiser T, Blum W, Bentrup FW**. (1991). Calmodulin regulates the Ca^{2+}-dependent slow-vacuolar ion channel in the tonoplast of *Chenopodium rubrum* suspension cells. *Planta*; **185**:440-2.

791. **Bethke PC, Jones RL**. (1994). Ca^{2+}-calmodulin modulates ion-channel activity in storage protein vacuoles of barley aleurone cells. *Plant Cell*; **6**:277-85.

792. **Schulzlessdorf B, Hedrich R**. (1995). Protons and calcium modulate sv-type channels in the vacuolar-lysosomal compartment - channel interaction with calmodulin inhibitors. *Planta*; **197**:655-71.

793. **Bethke PC, Jones RL**. (1997). Reversible protein phosphorylation regulates the activity of the slow-vacuolar ion channel. *Plant J*; **11**:1227-35.

794. **Hashimoto K, Eckert C, Anschutz U, Scholz M, Held K, Waadt R, et al.** (2012). Phosphorylation of Calcineurin B-like (CBL) calcium sensor proteins by their CBL-interacting Protein Kinases (CIPKs) is required for full activity of CBL-CIPK complexes toward their target proteins. *J Biol Chem*; **287**:7956-68.

795. **Sanders D, Brownlee C, Harper JF**. (1999). Communicating with calcium. *Plant Cell*; **11**:691-706.

796. **Garzo EI, Fereres A, Gomez-Guillamon ML, Tjallingii WF**. (2005). Mechanism of phloem-based resistance in melon (TGR-1551) to the aphid *Aphis gossypii*. *Comp Biochem Phys A*; **141**:S231-S.

797. **Klingler J, Creasy R, Gao LL, Nair RM, Calix AS, Jacob HS, et al.** (2005). Aphid resistance in Medicago truncatula involves antixenosis and phloem-specific, inducible antibiosis, and maps to a single locus flanked by NBS-LRR resistance gene analogs. *Plant Physiol*; **137**:1445-55.

798. **Zhu XH, Caplan J, Mamillapalli P, Czymmek K, Dinesh-Kumar SP**. (2010). Function of endoplasmic reticulum calcium ATPase in innate immunity-mediated programmed cell death. *EMBO J*; **29**:1007-18.

799. **Meyer AJ, Brach T, Marty L, Kreye S, Rouhier N, Jacquot JP, et al.** (2007). Redox-sensitive GFP in *Arabidopsis thaliana* is a quantitative biosensor for the redox potential of the cellular glutathione redox buffer. *Plant J*; **52**:973-86.

800. **Morgan B, Sobotta MC, Dick TP**. (2011). Measuring E(GSH) and H_2O_2 with roGFP2-based redox probes. *Free Radic Biol Med*; **51**:1943-51.

801. **Aller I, Rouhier N, Meyer AJ**. (2013). Development of roGFP2-derived redox probes for measurement of the glutathione redox potential in the cytosol of severely glutathione-deficient *rml1* seedlings. *Front Plant Sci*; **4**:506.

802. **Dodd AN, Jakobsen MK, Baker AJ, Telzerow A, Hou SW, Laplaze L, et al.** (2006). Time of day modulates low-temperature Ca^{2+} signals in Arabidopsis. *Plant J*; **48**:962-73.

803. **Krebs M, Held K, Binder A, Hashimoto K, Den Herder G, Parniske M, et al.** (2012). FRET-based genetically encoded sensors allow high-resolution live cell imaging of Ca^{2+} dynamics. *Plant J*; **69**:181-92.

804. **Ast C, De Michele R, Kumke MU, Frommer WB**. (2015). Single-fluorophore membrane transport activity sensors with dual-emission read-out. *Elife*; **4**.

805. **Ladwig F, Dahlke RI, Stuhrwohldt N, Hartmann J, Harter K, Sauter M**. (2015). Phytosulfokine regulates growth in Arabidopsis through a response module at the plasma membrane that includes CYCLIC NUCLEOTIDE-GATED CHANNEL17, H+-ATPase, and BAK1. *Plant Cell*; **27**:1718-29.

806. **Schroeder JI, Hagiwara S**. (1989). Cytosolic calcium regulates ion channels in the plasma membrane of *Vicia faba* guard cells. *Nature*; **338**:427-30.

807. **Schweighofer A, Kazanaviciute V, Scheikl E, Teige M, Doczi R, Hirt H, et al.** (2007). The PP2C-type phosphatase AP2C1, which negatively regulates MPK4 and MPK6, modulates innate immunity, jasmonic acid, and ethylene levels in Arabidopsis. *Plant Cell*; **19**:2213-24.

808. **Shang Y, Dai C, Lee MM, Kwak JM, Nam KH**. (2016). BRI1-Associated Receptor Kinase 1 Regulates Guard Cell ABA Signaling Mediated by Open Stomata 1 in Arabidopsis. *Mol Plant*; **9**:447-60.

809. **Sirichandra C, Gu D, Hu HC, Davanture M, Lee S, Djaoui M, et al.** (2009). Phosphorylation of the Arabidopsis AtrbohF NADPH oxidase by OST1 protein kinase. *FEBS Lett*; **583**:2982-6.